
National Nanotechnology Infrastructure Network

Research Highlights 2012

Prof. Roger T. Howe

Stanford University

NNIN Director

Oct. 2012

Table of Contents

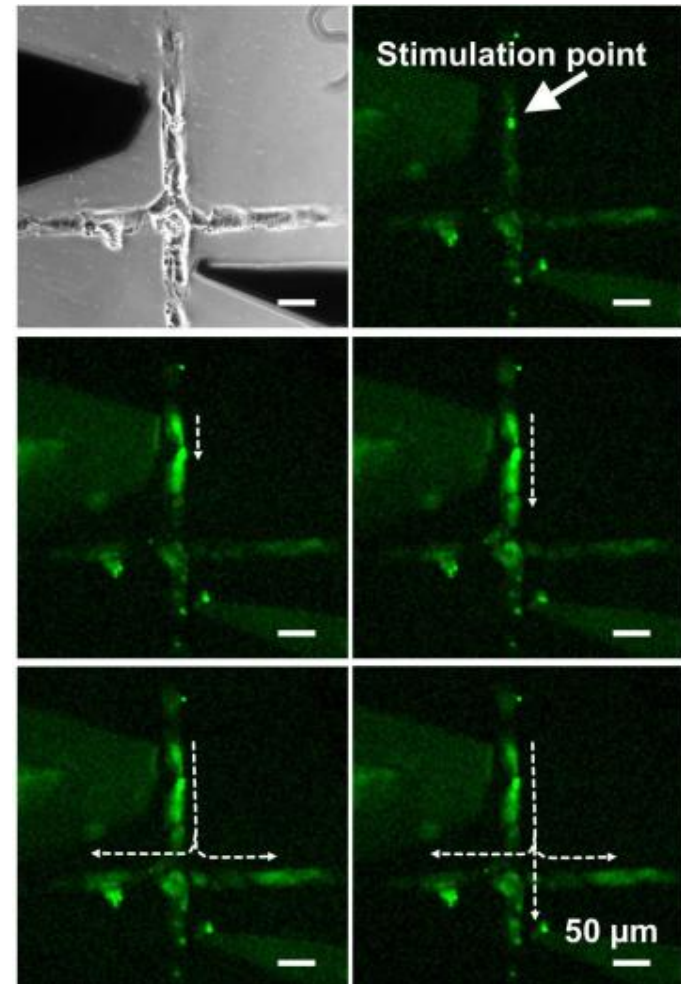
• Arizona State University	p.3
• Cornell University	p.26
• Georgia Tech	p.69
• Harvard University	p.100
• Howard University	p.136
• Stanford University	p. 146
• UCSB	p. 202
• University of Colorado	p .232
• University of Michigan	p. 245
• University of Minnesota	p. 293
• University of Texas	p. 310
• University of Washington	p. 321
• Washington University at St. Louis	p. 340

Arizona State University

Architecture Dependence of Intercellular Calcium Communication

Using a plasma lithography technology to engineer endothelial cell networks, the architecture dependence of mechanically stimulated intercellular calcium communication can be systematically investigated. Our results reveal that intracellular calcium signaling provides a robust mechanism for cell-cell communication in networks of endothelial cells despite the diversity of the microenvironmental inputs and complexity of the vascular networks. The cell patterning and mechanostimulation technologies used here may prove useful to future studies, as it allows systematic investigation of the architecture dependence of cell-cell communication.

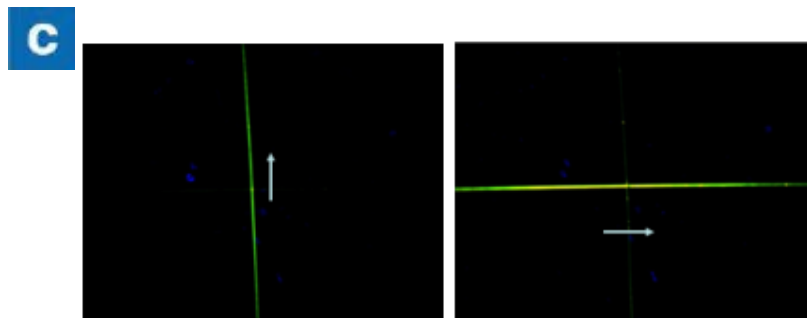
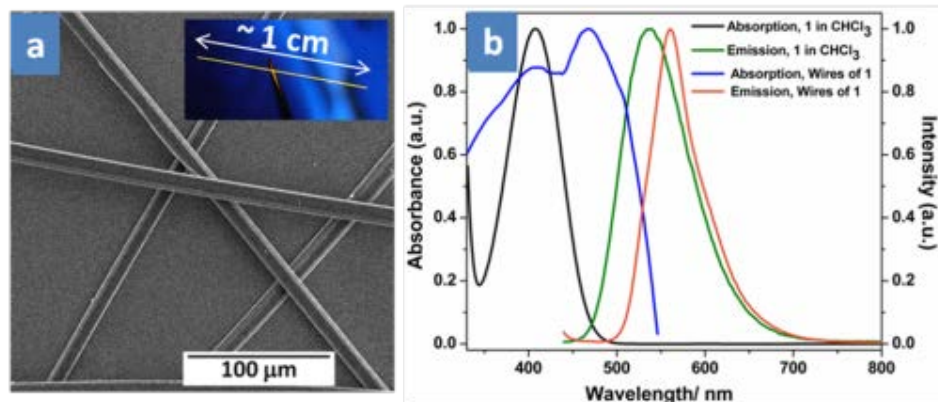
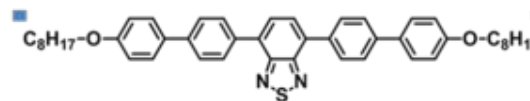
Pak Kin Wong,
University of Arizona, Tucson, AZ
Work performed at ASU NanoFab



Visualization of calcium wave propagation in micro-engineered endothelial cell networks with signal splitting.

Self Assembled Polarized Light Emitter

The purpose of the research is to develop high quantum efficiency polarized light emitters using bottom-up self-assembly of synthesized π -conjugated fluorescent molecules to create supramolecular 1D and 2D micro/nano-structures. The assembled structures are tested for electroluminescence at ASU.



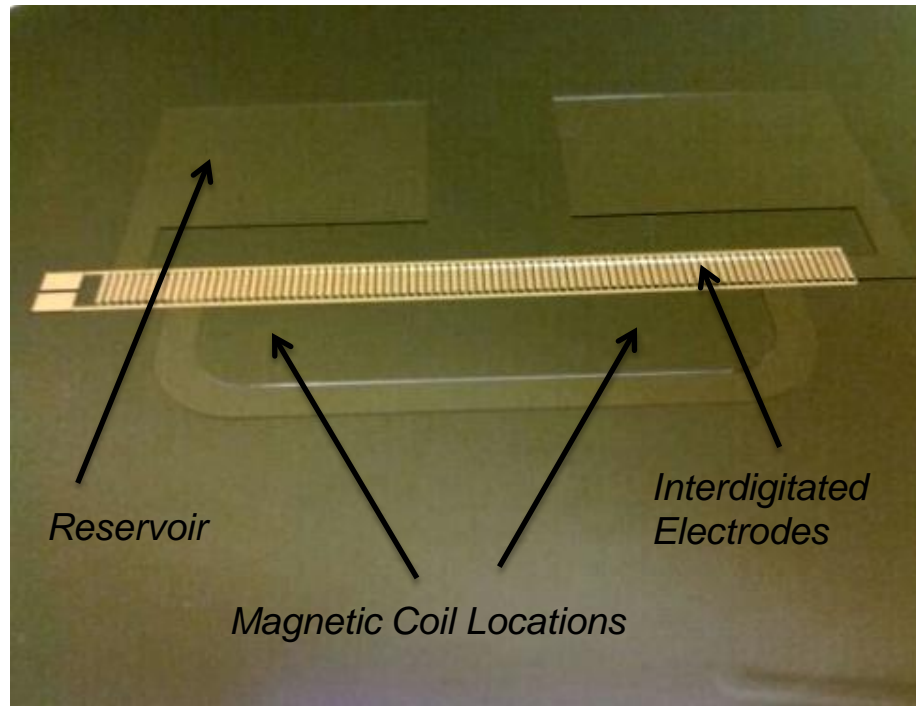
Stanley Pau,
University of Arizona, Tucson, AZ
Work performed at ASU NanoFab

Figure: Chemical structure of benzothiadiazole molecule. (a) SEM of self-assembled high aspect ratio microtubules. (b) emission and absorption spectrum in solution and microtubule state. (c) polarized light emission from microtubules.

Magneto-Electro-Hydrodynamic Microfluidic Device

The structure shown in the figure is part of a patented microfluidic device that is designed to operate based on the superposition of magnetic and electro-osmotic actuation. The device is intended to generate flow rates ranging from microliters per minute to milliliters per minute, in a continuous (not pulsing) flow.

The electro-osmotic actuation is controlled by the interdigitated electrodes shown while the magnetic actuation is controlled by an array of magnetic coils whose locations are indicated in the picture.



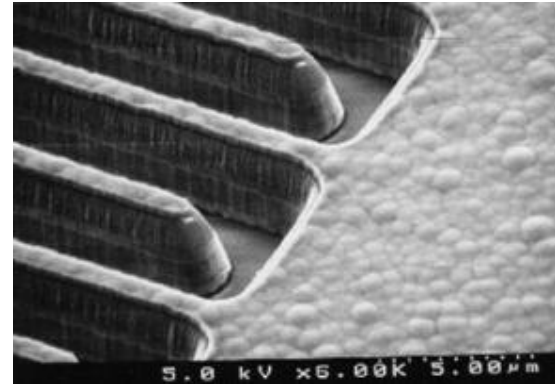
Microfluidic device with electrode array (pre-channel etch). Several magnetic coils will be added to the structure in the next phase.

Constantin Ciocanel,
Northern Arizona University, Flagstaff, AZ
Work performed at ASU NanoFab

In-situ Electrochemical Residue Sensor

The purpose of the project is to develop new sensor-based metrology technology that can significantly reduce water and related energy usage during semiconductor manufacturing. So far, the sensor-based real-time monitoring approach has shown 30% less water and energy used for ultra-clean chip production. The team's real-time monitoring approach is applicable to current cleaning processes for 300mm silicon wafers, and the gain is expected to be especially beneficial when the industry transitions to 450mm wafers. The sensors are currently fabricated using equipment and processes available at UA Micro/Nano Fab and the ASU NanoFab.

Farhang Shadman and Omid Mahdavi,
University of Arizona, Tucson, AZ
Semiconductor Research Corporation (SRC)
Work performed at ASU NanoFab & UA Micro/Nano Fab



In-situ monitors provide unprecedented control of water and chemical usage during surface preparation for silicon wafers. Highly sensitive sensors, like those shown in this micrograph of a sensing channel, can reduce the amount of resources needed for the cleaning of surfaces.



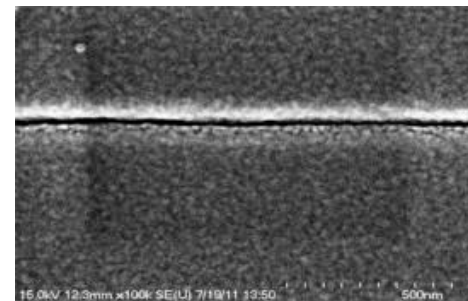
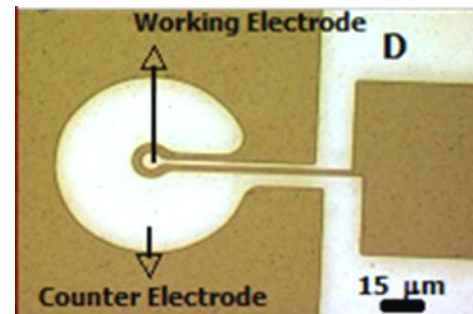
Sensor in action: Fabricated on a fused silica substrate it is making measurements in hot DI water tank.

Nano Patterned Sensor Array Project

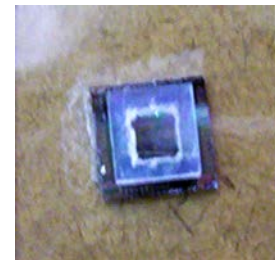
The purpose of the nano patterned sensor array project is to detect single nucleotide polymorphisms which is a powerful method for early diagnosis for a number of cardiac diseases. The ASU-NNIN fabricated components of this system have been the nano scale gold patterns on the base platform on which the remaining components of our sensor were assembled. Si wafers form the base substrate to enable the processing of the nanopatterns. The electrode leads are fabricated to connect to the microscale features on the substrate on to which the nano patterns were generated. The form factor of the entire assembled sensor array was 2 cm x 2cm.

Shalini Prasad,
Wichita State University, Wichita, KS
Work performed at ASU NanoFab

Microscale substrate on to which the nano pattern is assembled.



Nanopattern on the sensor substrate.

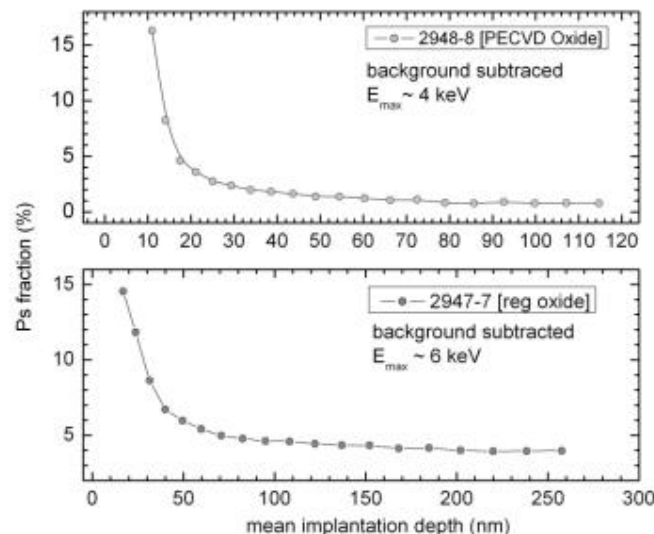


An assembled nano array sensor

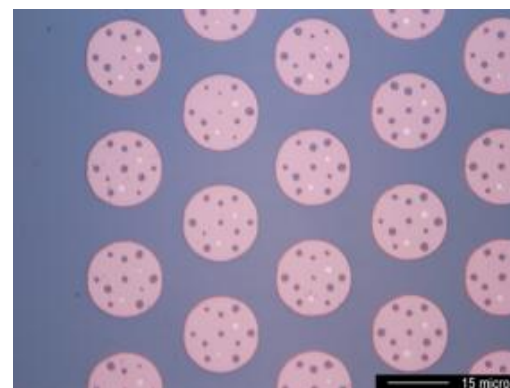
Positronium Test Structures

Second generation silica-based matter-antimatter (blister) test structure arrays have been designed by First Point Scientific Inc., fabricated at ASU and tested at the Positron Laboratory at the University of California, Riverside. Positronium is a short lived bound state of a positron and an electron. Preliminary positronium diffusion length measurements show differences based on the type of oxide used in the cavity structures. PECVD oxide structures exhibited much shorter diffusion lengths than the gate oxide based arrays. These results suggest differences in the density of traps/defects of the SiO_2 that interact with the positrons. The test structures have since been subjected to a passivation process and will undergo further measurements in the near future.

David Cassidy,
University of California, Riverside, CA.
John Bayless, First Point Scientific, Inc.
Work performed at ASU NanoFab



Positronium diffusion length measurements in silica test structures fabricated using gate oxide (sample 2947-7) versus PECVD oxide (sample 2948-8).

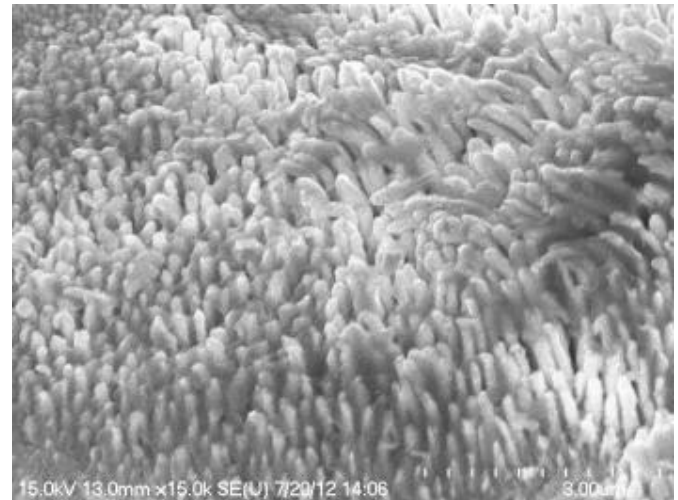


Optical micrograph of silica blister structures (pre-XeF2 etch) diameter 20 microns.

Nanotexturing for Neural Electrodes

In this study a nanoporous membrane was used as a template for electrochemical deposition of gold nanowires on electrodes to enhance neural recording from MEA (micro electrode arrays). The goal was to investigate the effect of the nanowires on the MEA by examining the impedance of the electrodes as well as the effect of nanotexturing on growth patterns of cortical neurons.

In addition a neural interface was created to allow for both recording and excitation of action potentials from a cockroach. This project was designed with the purposed of creating educational opportunities and to advance the study of neurophysiology. The work was completed as a summer research experience for five high school students.



FESEM image of gold nanorods grown on MEA



Neural interface for cockroach. Hardware from Backyard Brains and HexBug.

Dixie Kullman, Central Arizona College, Coolidge, AZ
Jennifer Blain Christen, Arizona State University
Work performed at ASU NanoFab Facility

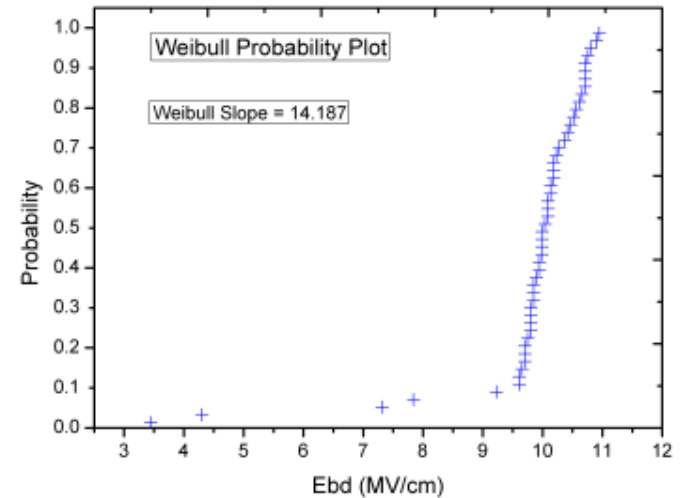
High-Quality Low-Temperature Photodiodes for Solar Cell Applications

Traditional implants and high-temperature anneals can be replaced with depositions and low-to-moderate temperature drive-ins for doping silicon¹. Our objective is to fabricate high-quality silicon photodiodes for solar cell applications with a low-temperature, low-defect process. The performance of the equipment set at ASU NanoFab is being evaluated for this purpose. Process monitoring of lithography, oxide uniformity and quality, metal deposition and etch uniformity are critical to reach this goal.

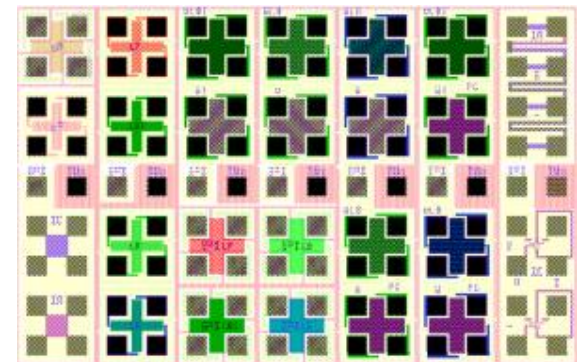
Preliminary results show that reliable photodiode experimentation can be performed in the ASU NanoFab by developing dedicated test structures and incorporating process monitoring procedures at critical points in the fabrication process.

1. A. Šakić, L. Qi, T.L.M. Scholtes, J. van der Cingel, L. K. Nanver. *Epitaxial Growth of Large-Area p+n Diodes at 400°C by Aluminum-Induced Crystallization*. Accepted for presentation at ESSDERC 2012, Bordeaux, France, 18-22 September, 2012.

Tom L.M. Scholtes,
Delft University of Technology, Delft, The Netherlands
Work performed at ASU NanoFab



Oxide quality control by the statistical analysis of the breakdown of electrically stressed oxide layers.



Test structure development for process monitoring.

Nano-sensors for Next Generation Diagnostics

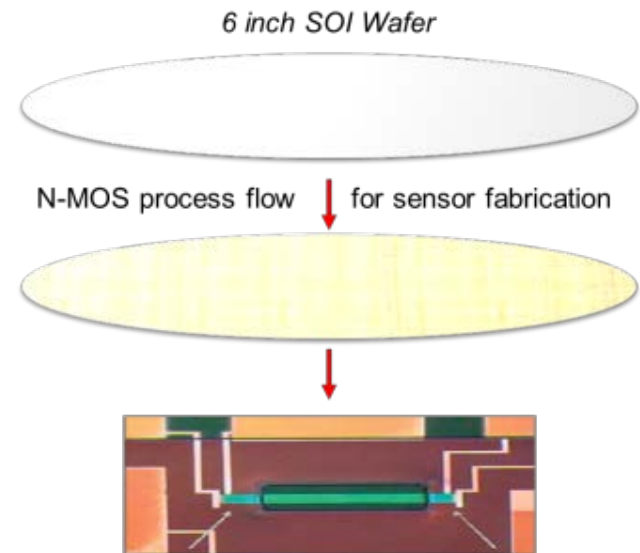
Highly sensitive biosensors that also provide high selectivity for molecular detection are required for high confidence disease diagnostics. Using nano-biosensors modified with biomarkers specific to diseases, it is possible to detect diseases in early stages, resulting in increased success of therapeutic interventions.

INanoBio is currently using the ASU NanoFab to fabricate CMOS-based FET sensor devices for chemical and biological sensing applications. After fabrication of core devices at NanoFab, special coatings of chemicals and biomolecules are applied at INanoBio Labs for specific sensing applications. One example of this is detection of insulin concentration in blood using DNA aptamers for diabetes Type-1 and Type-2 diagnosis. We are currently working on applied research for this and other similar applications, with the aim of offering low-cost, high-confidence biosensors for diagnostics.

Bharath Takulapalli and Mukilan Mohan, INanoBio LLC
Work performed at ASU NanoFab, Tempe AZ



6 inch wafer fabricated at ASU NanoFab; Image showing CMOS based FET nanowire sensors in different layouts.



Chip packaging and chemical, biomolecular coating for biosensor applications

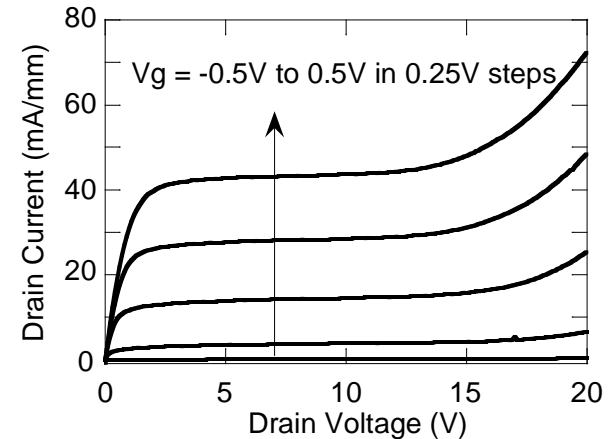
Enhanced Voltage SOI MESFETs for RF Power Amplifiers

Silicon-on-insulator (SOI) metal-semiconductor field-effect-transistors (MESFETs) fabricated using a commercial 45 nm SOI CMOS foundry demonstrate enhanced voltage capability compared to the baseline MOSFETs. An RF test board was designed for 900 MHz operation and populated with a single MESFET die and surface mount components to demonstrate Class AB amplifier operation.

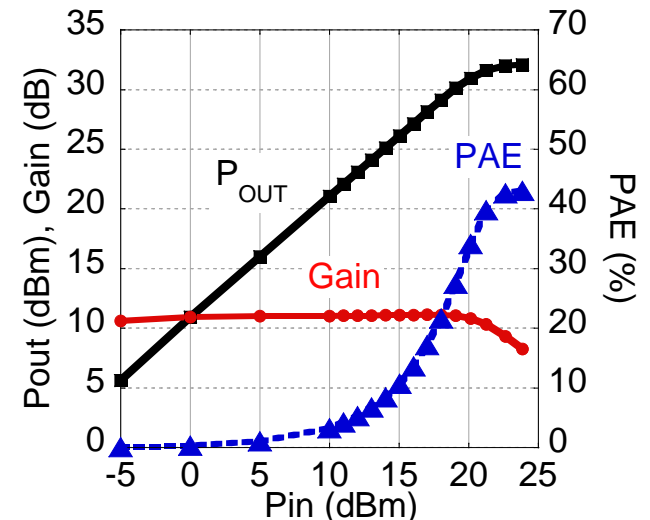
The supply voltage of the RF test board was set at 8V, allowing for wide voltage excursions up to 16V at the inductively coupled drain contact of the MESFET. The RF output power, gain and power-added-efficiency (PAE) were measured as a function of input power. A peak output power of 32 dBm was measured with a PAE of >40%. This is the highest RF output power demonstrated from a single die using such a highly scaled CMOS technology.

This work was supported by DARPA STTR contract number W31P4Q-10-C-0020.

Seth Wilk and William Lepkowski,
SJT Micropower Inc., Fountain Hills, AZ
Work performed at ASU NanoFab



The family of curves of a 300nm gate length MESFET with a breakdown voltage of >20V



A 900 MHz PA demonstrates 11 dB of gain with a peak output power of > 1.5 W from a single die.

Indium Gallium Arsenide Photodiodes

Laser Components DG Inc. uses the ASU NanoFab facilities to develop Indium Gallium Arsenide (InGaAs) photodiodes with different active area diameters and material configurations from lattice matched InGaAs to strained structures with sensitivity ranging from 1700nm to 2600nm.

InGaAs PIN photodiodes are near infrared (NIR) detectors that feature low noise, low terminal capacitance, high shunt resistance and high-speed response. When cooled with a thermoelectric cooler, InGaAs photodiodes exhibit very low dark current and deliver higher D^* (Detectivity).

InGaAs detectors are used for NIR spectroscopy, gas sensing, optical communication and other industrial applications.

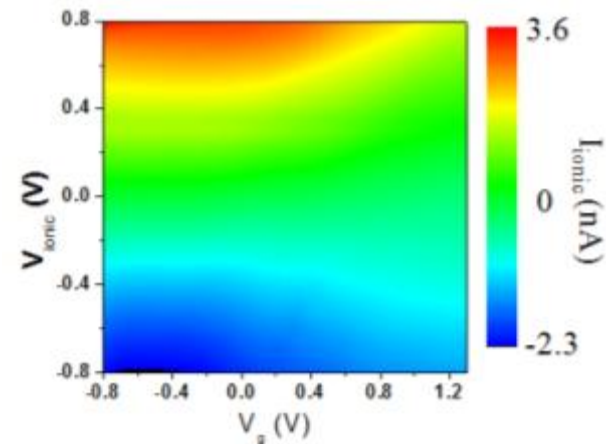
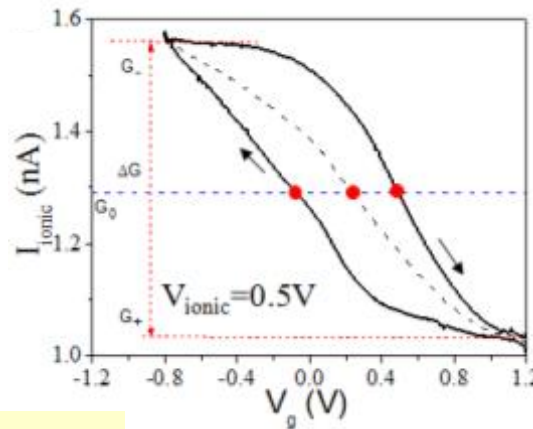
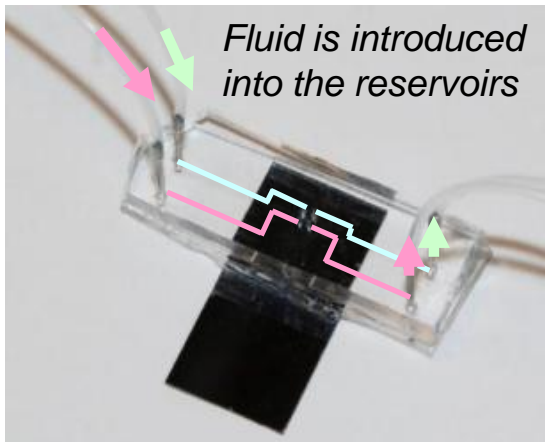
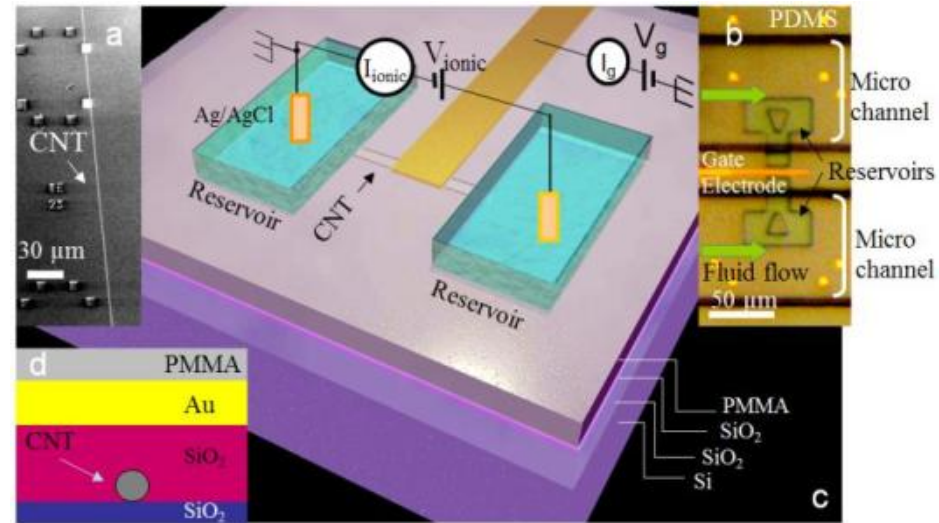


InGaAs photodiode in TO-46 housing.

Punarvasu Joshi, Dragan Grubisic,
Laser Components DG Inc. Tempe, AZ
Worked performed at ASU NanoFab

CNT Nanofluidic Device

Carbon nanotubes (CNTs) are of interest for applications in nanofluidics, owing to their atomically smooth and hydrophobic surface and high aspect ratio geometry. The purpose of this project is to fabricate CNT based nanofluidic devices, like a nanofluidic field-effect transistor, showing the charge carriers are cations, in the form of electroosmosis, when KCl electrolyte is used. This method provides a new probe to understand the mechanism of ionic flow inside the CNT, and also opens the doors to use CNT based nanofluidic devices for ion and molecule manipulation.



Pei Pang and Stuart Lindsay, ASU
 Predrag S. Krstić, Oak Ridge National Lab
 Work performed at ASU Nanofab Facilities

p-type ionic field-effect transistor characteristics

Neural Interfaces

Robotic brain implants - The overall goal of this NIH funded research is to develop a novel MEMS technology that will allow sensors to seek and monitor single neurons of interest in the brain over long periods of time. During the last 12 months we have demonstrated that electrothermal microactuators with peg drive were more reliable and performed better than chevron microactuators for brain implant applications.

Biochip for gene delivery -The overall goal of this project is to develop a technology for delivering genetic material to spatially restricted population of primary neurons in culture. We have successfully demonstrated targeted transfection of siRNAs and plasmids into neurons.

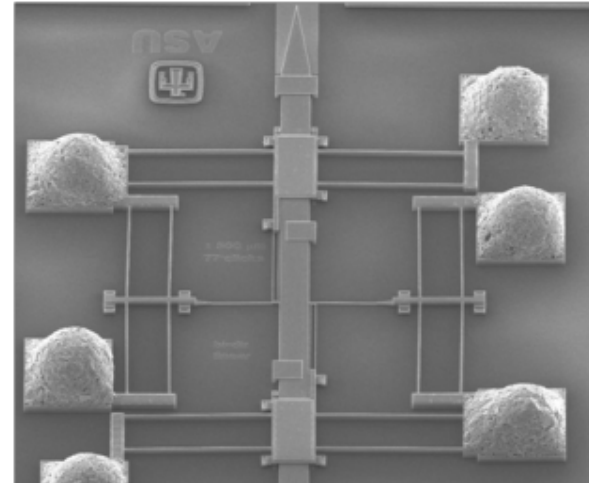
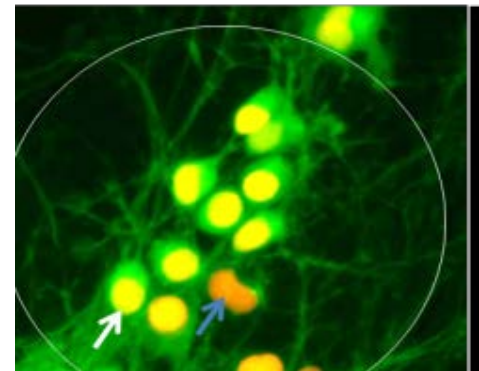


Image of an electrothermal peg drive microactuator with microbumps to facilitate flip-chip interconnects



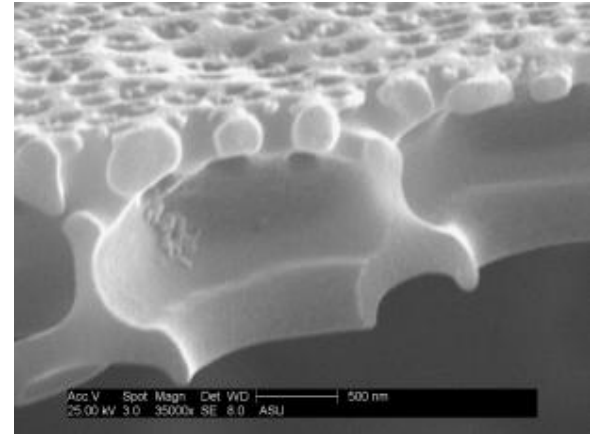
Neurons are alive and transfected with a dye on a 100 μ m diameter microelectrode.

Jit Muthuswamy, ASU, Tempe, AZ
Murat Okandan, Sandia National Laboratories, NM
Work performed at ASU Neural Microsystems lab, ASU
NanoFab, and Sandia National labs

NNIN is supported by NSF ECCS-0335765

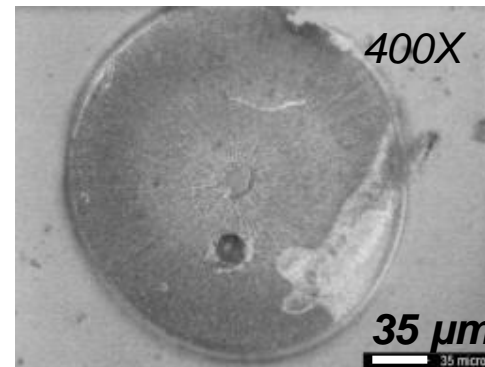
Nanoporous Diatom Shells on Silicon Chips

Biomaterialized Diatom shells exhibit impressive features, such as a hierarchical pore structure with the smallest pores having a diameter of 40 nm. This structure makes them extraordinarily mechanically stable, while allowing a short pore length. This makes them very attractive for nanoparticle filtration applications, the study of cell-cell-communication and ion channel sensors based on nanoscale bilayer lipid membranes.

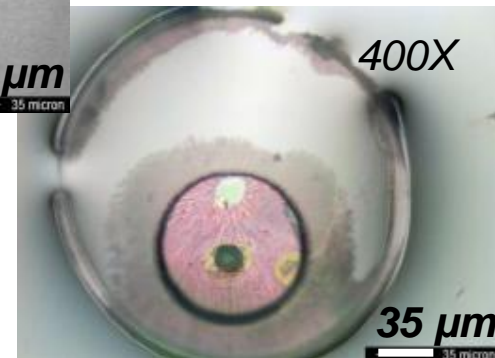


Scanning electron microscopy image of a cross section of a diatom frustule, mounted on a silicon substrate

Recently, we have developed a photolithographic process which allow us to permanently attach diatom frustules to micromachined silicon substrates, using SU-8 epoxy resist. This process ensures a fluidic seal around the diatom frustule perimeter, still maintaining free flow through the central nanopores. The epoxy resin is highly resilient to chemicals, allowing cleaning of the nanopores without risking detachment.



Optical microscope image of a diatom frustule on top of a silicon micropore before (left) and after SU-8 lithography (bottom).



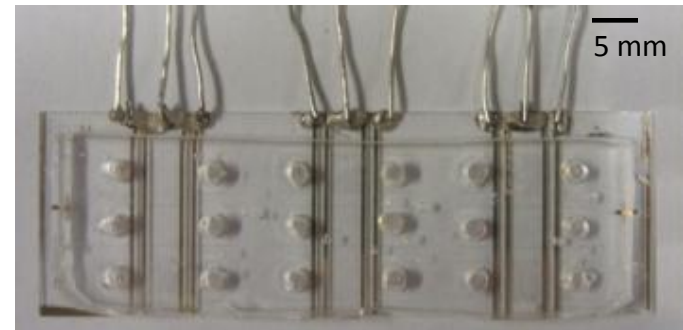
M. Goryll, B. L Ramakrishna, X. Wang and S.K. Dey,
Arizona State University
Melissa Gosse, REU student from Johns Hopkins University
Work performed at ASU NanoFab

Electrophoretic Exclusion on a Microchip

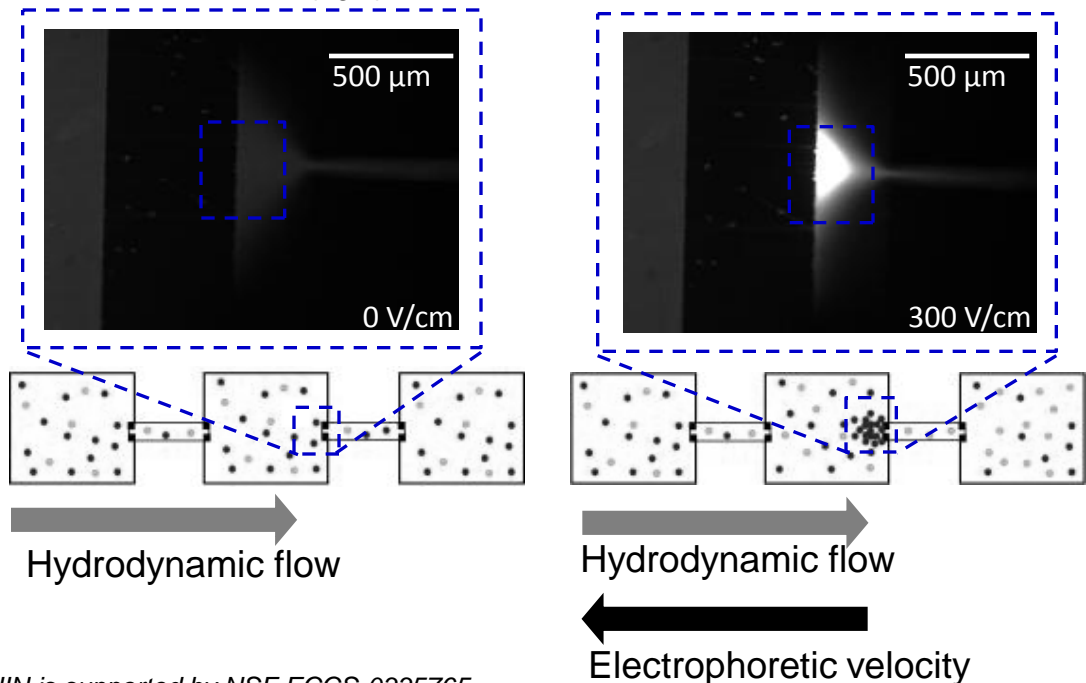
Isolating and concentrating low abundance species is essential when studying complex samples. Electrophoretic exclusion is a novel separations technique that differentiates species in bulk solution based upon their electrophoretic mobilities. Species are excluded in a reservoir, near a channel entrance, when the electrophoretic velocity of the analyte is greater than or equal to the opposing hydrodynamic flow through the system. Initial microchip studies indicate that small dye molecules and 1 μm polystyrene spheres can successfully be captured. Current research focuses on developing a device with several reservoirs and channels in series and parallel for addressing more complex samples.

Stacy Kenyon, Noah Weiss, and Mark Hayes
ASU, Department of Chemistry & Biochemistry
Fabrication performed using the ASU NanoFab

Photograph of the complete hybrid glass/PDMS chip with nine individual separation channels.



Exclusion of rhodamine dye from a channel entrance. Before the application of an electric field the dye travels with the hydrodynamic flow through the system (left). Once an electric field is induced the dye is excluded in the reservoir near the channel entrance (right).



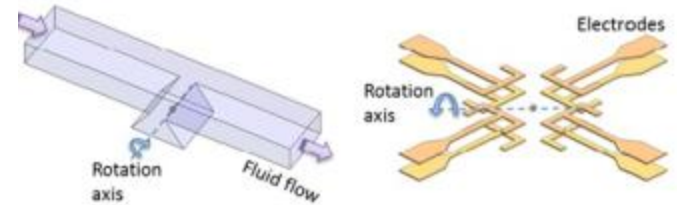
Single Cell Rotation using an Electrocage and a Hydrodynamic Microvortex

Single cell analysis has become increasingly important in understanding disease, especially when applied to cancer. Through the advent of single cell computerized tomography (Cell-CT), researchers now have the ability to obtain high resolution 3D reconstructions of single cells. Our efforts focus on imaging live cells rotated in a microchamber by one of two methods: Dielectrophoresis (DEP) or a Hydrodynamic Microvortex.

For the DEP method, we developed electrorotation (ROT) chips to trap and rotate single cells using electrokinetic forces. The ROT chip consists of a set of closely spaced metal electrodes that form a closed electric field cage (electrocage) when driven with appropriately phased, AC voltages. We flowed cells through a microchannel to the electrocage where they could be precisely trapped, levitated and rotated.

The second method uses a microfluidic chip to rotate live single cells in hydrodynamic microvortices about an axis parallel to the optical focal plane. A novel 3D microchamber design arranged beneath the main channel creates flow detachment into the chamber, producing recirculating flow conditions. We flowed single cells through the main channel, held them in the center of the microvortex by an optical trap, and rotated them by the tangential shear forces induced by the recirculating fluid flow.

Roger Johnson, Haixin Zhu and Deirdre Meldrum
Center for Biosignatures Discovery Automation
The Biodesign Institute at Arizona State University
Device fabrication performed at ASU NanoFab Facility



Schematic of the microvortex (L) and DEP (R) microchambers

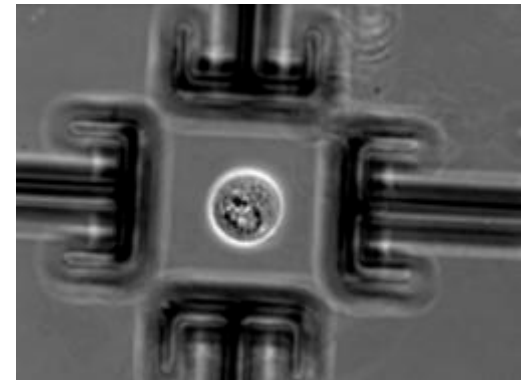
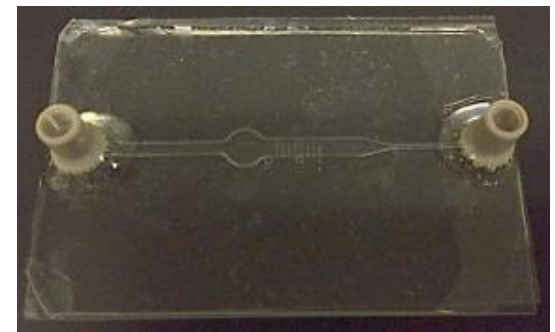


Image of K-562 cell rotating in the ROT chip



Channel and trapezoidal traps with nanoports for flowing cells in

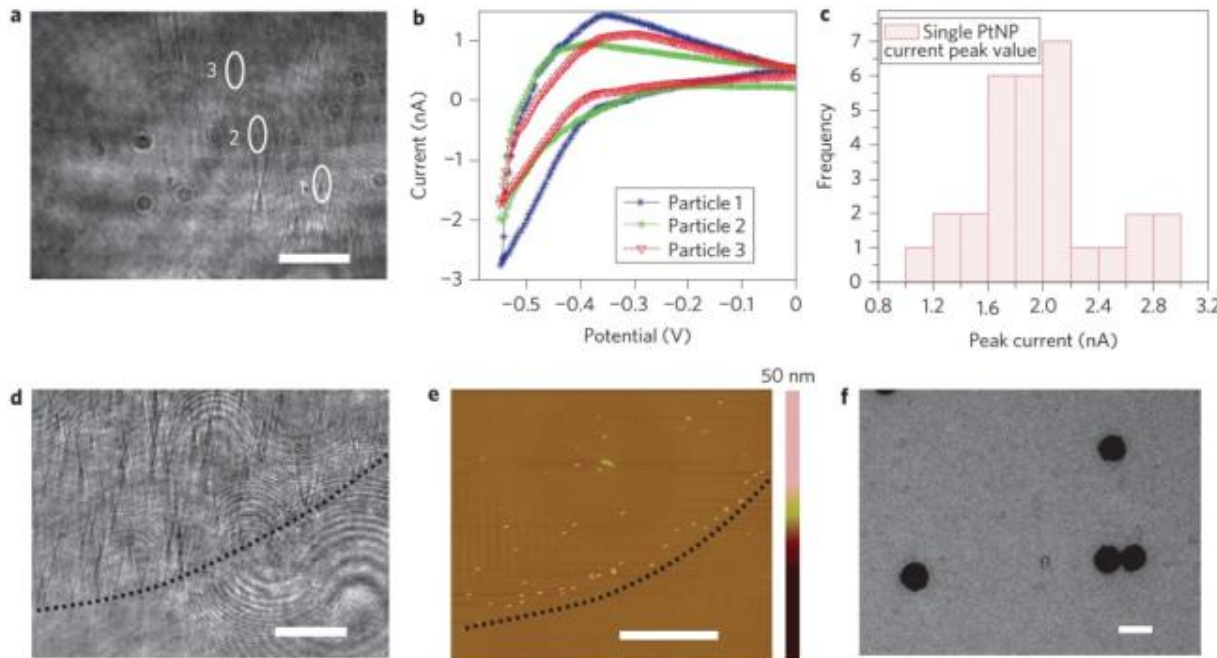
Imaging the Electrocatalytic Activity of Single Nanoparticles

The electrocatalytic properties of nanoparticles depend on their size, shape and composition. These properties are typically probed by measuring the total electrocatalytic reaction current of a large number of nanoparticles, but this approach is time-consuming and can only measure the average catalytic activity of the nanoparticles under study. However, the identification of new catalysts requires the ability to rapidly measure the properties of nanoparticles synthesized under various conditions and, ideally, to measure the electrocatalytic activity of individual nanoparticles.

We demonstrate that a plasmonic-based electrochemical current imaging technique can simultaneously image and quantify the electrocatalytic reactions of an array of 1.6×10^5 platinum nanoparticles printed on an electrode surface, which could facilitate high-throughput screening of the catalytic activities of nanoparticles. We also show that the approach can be used to image the electrocatalytic reaction current and measure the cyclic voltammograms of single nanoparticles.

(Published in *Nature Nanotechnology*, DOI: 10.1038/NNANO.2012.134)

Xiaonan Shan, N.J. Tao et.al.,
Biodesign Institute, ASU
Work performed at ASU NanoFab

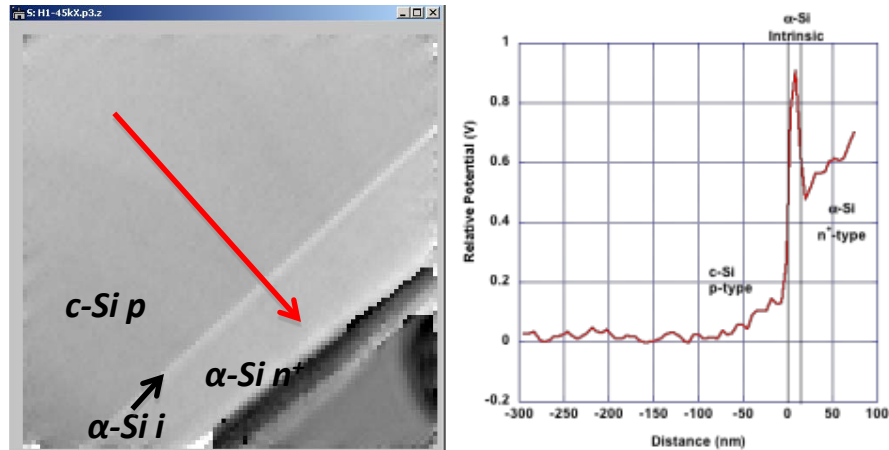


Statistical analysis of single platinum nanoparticle electrocatalysis. **a**), SPR image of an 80 nm platinum nanoparticle microarray. **b**), CV plots of three platinum nanoparticles (locations marked in **a**). **c**), Histogram of the electrocatalytic current at a potential of -0.55V for 30 single platinum nanoparticles, showing the large variability. **d,e**), SPR and AFM images near the edges of an 80nm platinum nanoparticle spot. Scalebars (**a,d,e**), 15mm. **f**), TEM image of 80nm platinum nanoparticles. Scalebar, 100nm.

Advanced Silicon Solar Cells

Multiple approaches are being pursued to improve or develop novel silicon cells that exceed traditional efficiencies utilizing CSSER lithography, cleans, and deposition capabilities combined with the process and analysis capabilities of shared sister laboratories.

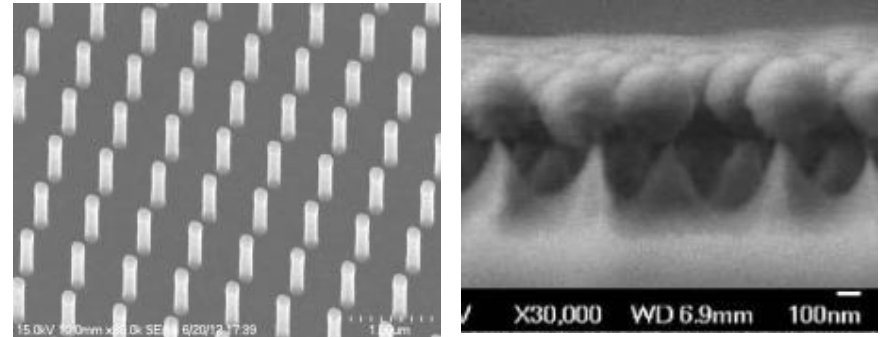
α -Si/c-Si heterojunction studied with e^- holography



Potential derived from reconstructed profile of phase image from electron hologram showing rise at the crystalline/amorphous interface consistent with surface band bending

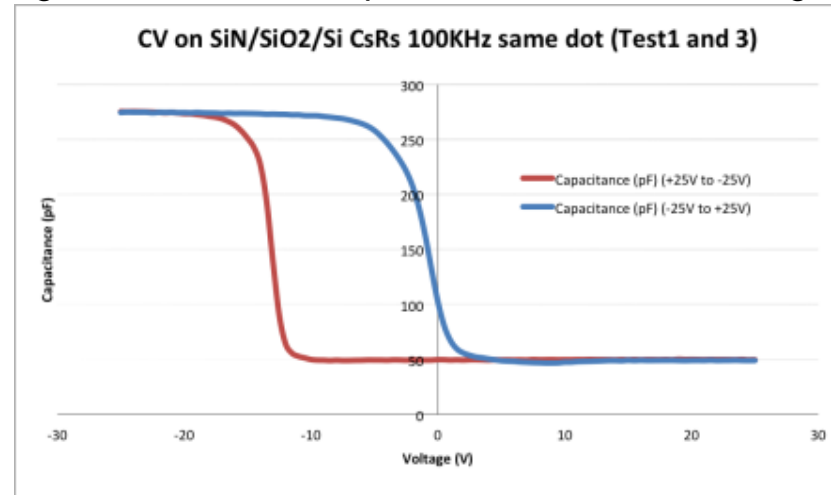
Kunal Ghosh, Jongwon Lee, Vivek Sharma, JeaYoung Choi, Clarence Tracy, Stanislau Herasimenka, and Stuart Bowden, ASU, Solar Power Laboratory.
Work performed at ASU NanoFab

Nanostructures for Multiple Exciton Generation studies



Etched silicon surfaces at sub-optical lithographic dimensions

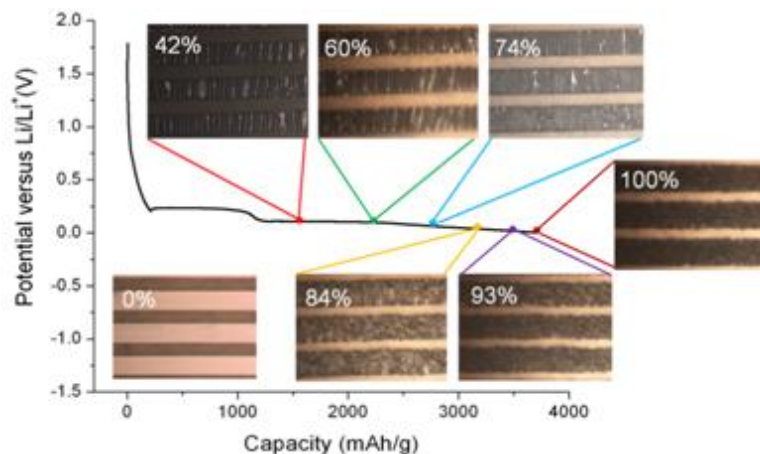
Charge assisted surface passivation in ARC coatings



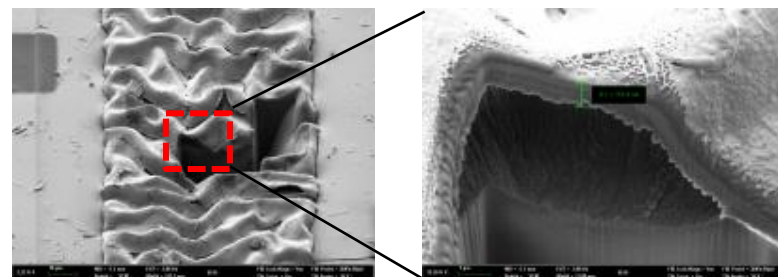
Charge capture by the defects present in bulk SiN_x film / interface

Silicon Anodes on Soft Substrates in Lithium-Ion Batteries

We have developed a silicon thin-film on polydimethylsiloxane (PDMS) substrate as an anode for lithium ion batteries. The mechanically elastomeric PDMS substrate accommodates diffusion-induced strain by buckling silicon thin-film to prevent the anode from cracking and pulverization. Upon charging, the initially flat silicon thin-film becomes highly buckled as a function of Li content, shaping into 1-D ripples, 2-D herringbones and random labyrinths sequentially without cracking. The intactness of the silicon film on soft substrates at fully charging state enables the precise measurement of surface area of buckled silicon film, leading to the capability of measuring volumetric change of lithiated silicon at macro level (several millimeters). The thickness and surface area of buckled Si films are characterized by focused ion beam and confocal microscopy, respectively. The total volume expansion of the fully charged Si film is around 400%. The work is funded by the National Science Foundation.



Morphological changes of Si thin-film as a function of Li content



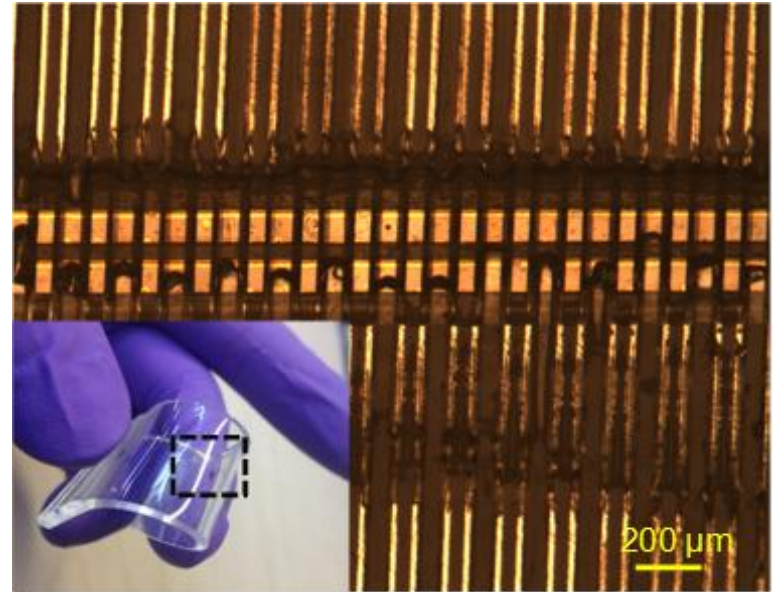
Measuring thickness of buckled Si film on soft substrate by focused ion beam microscopy. The thickness of fully lithiated Si film increases to 754nm from 310nm.

Hanqing Jiang, ASU
School for Engineering of Matter, Transport and Energy
Work performed at the ASU NanoFab

NNIN is supported by NSF ECCS-0335765

3D Flexible Device Fabrication

The goal of this NSF funded project is to fabricate flexible and stretchable 3D micro devices. The process flow uses surface micromachining of polydimethylsiloxane (PDMS) polymer to ensure that the micro devices have full 3D flexibility. A thin film transfer technology has been developed that allows for full stretchability of the electronic components. 3) laser dynamic forming on 3D surface to deform or bond pre-fabricated thin film flexible micro devices on 3D micro surface structure.



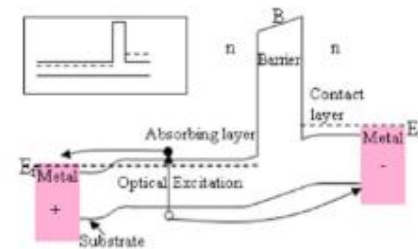
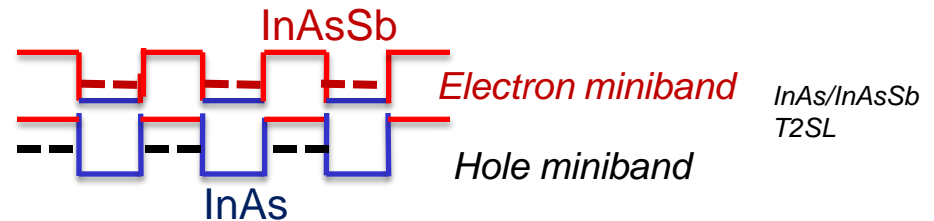
A conformal assembly of a shear stress sensor with a flexible PDMS substrate.

Hongyu Yu
School of Earth and Space Exploration, ASU
Work performed at the ASU NanoFab

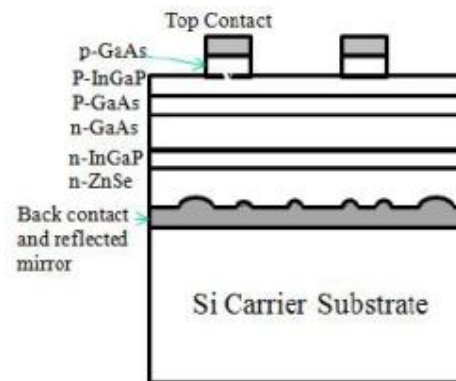
nBn IR Detectors Based on InAs/InAsSb Superlattice & Back Scattering Thin Film Solar Cells

Type-II super-lattice (T2SL) IR photo-detectors have been researched for decades. With their cost-effective fabrication process and competitive device performance, T2SL IR detectors are promising candidates to replace traditional HgCdTe (MCT) IR detectors. Our group is studying Ga-free InAs/InAsSb T2SL. Compared to the well-studied InAs/InGaSb T2SL, it has longer minority carrier lifetime, and hence lower dark current in detectors. We recently demonstrated the world first InAs/InAsSb superlattice nBn photodetectors with excellent performance. The nBn photodetectors consist of three layers, an n-type layer, an electron barrier layer and another n-type layer, as shown in the picture opposite.

Our group is adding a reflective back scattering layer to ultra-thin GaAs single-junction solar cells to improve their efficiency even more. The short-circuit current density is enhanced by periodic-pattern textured interface in our preliminary devices.



A nBn IR detector with the absorbing layer of InAs/InAsSb T2SL

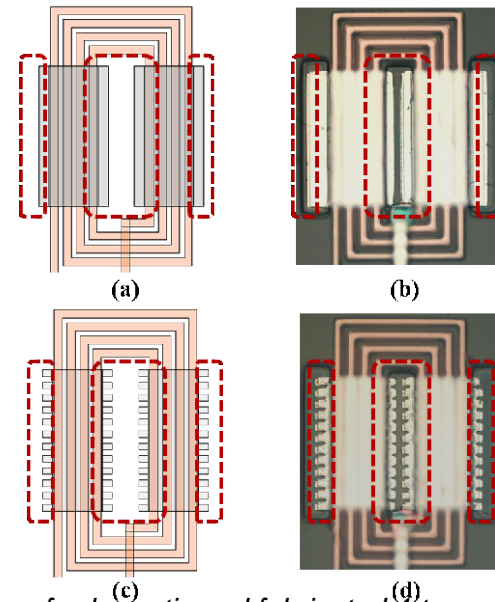


The device structure of the back scattering ultra-thin GaAs single-junction solar cell.

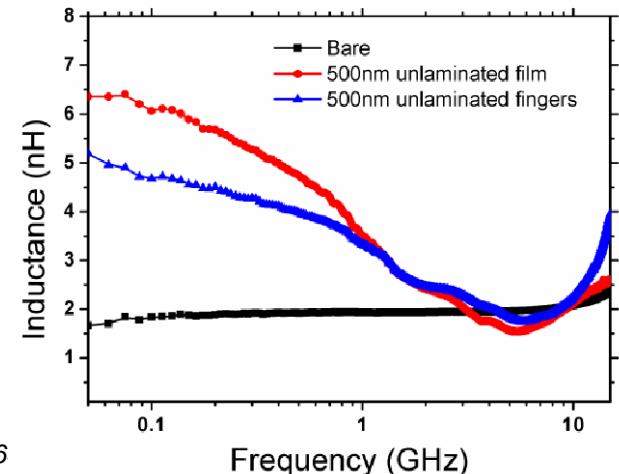
Yong-Hang Zhang,
Center for Photonics Innovation, ASU
Work performed using the ASU NanoFab

Integrated RF On-chip Inductors With Patterned Co-zr-ta-b Films

Integrated on-chip inductors with boron-incorporated amorphous Co-Zr-Ta-B films for reducing the size and increasing the quality factor are presented. A 3.5-fold increase in inductance and a 3.9-fold increase in quality factor over inductors without magnetic films are measured at frequencies as high as 1 GHz. The Co-Zr-Ta-B films are patterned into finger-shaped geometries in magnetic via regions to improve the high frequency response of on-chip inductors. Compared to non-patterned films, finger-shaped magnetic vias result in at least 30% increase in quality factor at GHz range. It is also demonstrated that by using laminations, up to a 9.1X inductance increase with good frequency response up to 2 GHz can be achieved.



Top-view of schematic and fabricated 4-turn spiral inductors with regular (a) (b) and finger-shaped (c) (d) magnetic vias. Cu coils were wrapped around by Co-Zr-Ta-B, and the dashed lines indicated magnetic via regions.



Inductance) measurements from 4-turn rectangular spiral inductors with regular and finger-shaped magnetic vias

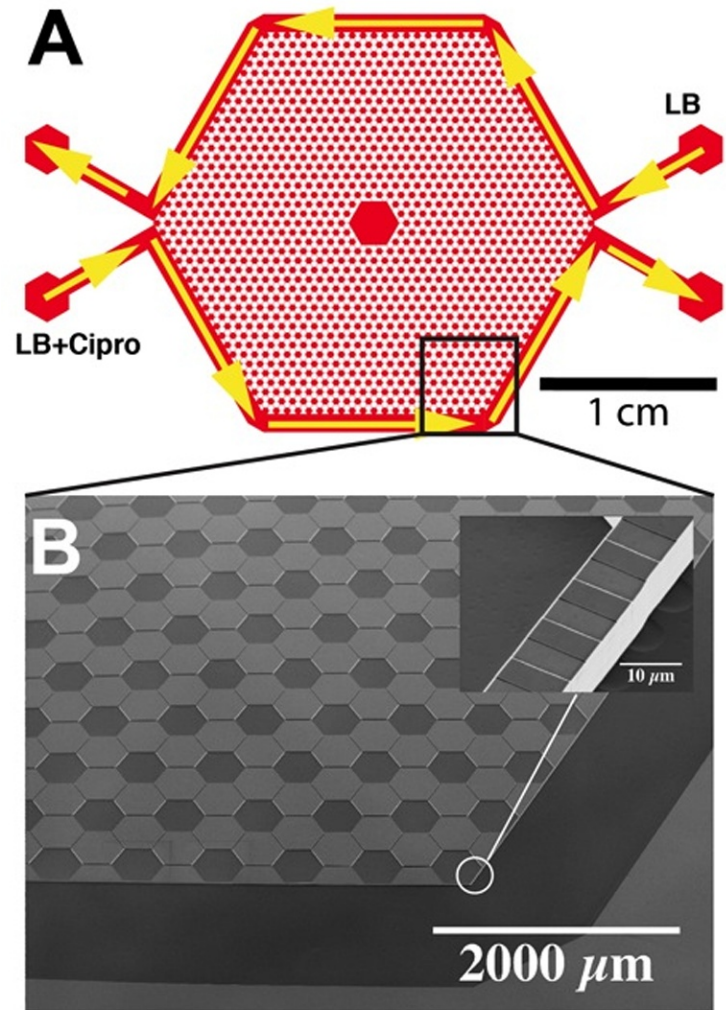
Cornell University

Acceleration of Emergence of Bacterial Antibiotic Resistance in Connected Microenvironments

The emergence of bacterial antibiotic resistance is a growing problem, yet the variables that influence the rate of emergence of resistance are not well understood. In a microfluidic device designed to mimic naturally occurring bacterial niches, resistance of *Escherichia coli* to the antibiotic, ciprofloxacin, developed within 10 hours. The Austin group at Princeton University fabricated a device that consisted of 1200 hexagonal wells etched 10 μm deep into silicon. Each well had sides 200 μm long and was connected to its nearest neighbors via six microchannels that were 200 μm long, 10 μm deep, and 10 μm wide. Nanoslits that were 100 nm deep were etched into the sidewalls of the peripheral wells at the edge of the array to allow nutrients and antibiotic to flow into the interior of the array and create gradients.

G. Lambert and R.H. Austin, Princeton University
Work performed at Cornell NanoScale Facility

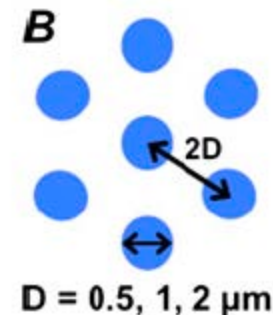
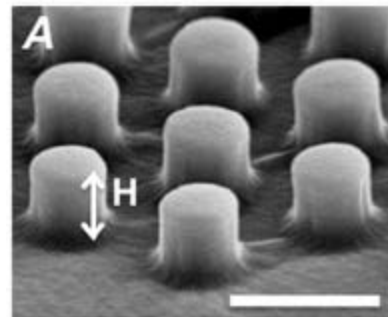
Science **333**, 1746 (2011).



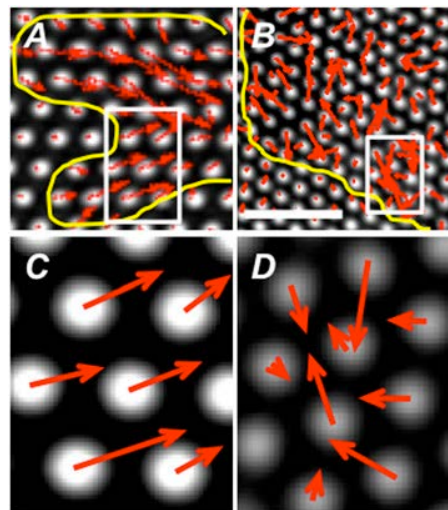
(A) Diagram of the microenvironment chip showing the flow of the nutrient (LB) and nutrient + antibiotic (LB+ Cipro).
(B) SEM of an array of etched hexagons and nanoslits.

Cells Test Substrate Rigidity By Local Contractions On Submicrometer Pillars

Cell growth and differentiation are critically dependent upon matrix rigidity, yet many aspects of the cellular rigidity-sensing mechanism are not understood. The Hone group at Columbia has used devices made at the Cornell NanoScale Facility to analyze matrix forces. The devices consist of a series of elastomeric pillar arrays with 2, 1, and 0.5 μm pillar diameters. The cellular response is fundamentally different on micron-scale and submicron pillars. On 2- μm diameter pillars, a constant maximum force is applied independent of stiffness, while on 0.5- μm diameter pillars, local contractions between neighboring pillars are observed with a maximum displacement of ~ 60 nm, independent of stiffness. Localization of myosin between submicron pillars demonstrates that submicron scale myosin filaments can cause these local contractions. Submicron pillars can capture many details of cellular force generation that are missed on larger pillars and more closely mimic continuous surfaces.



0.5- μm diameter PDMS pillars



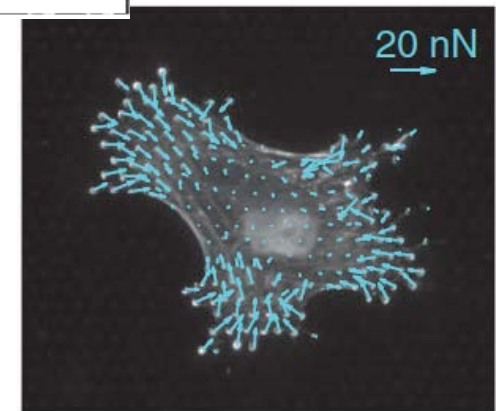
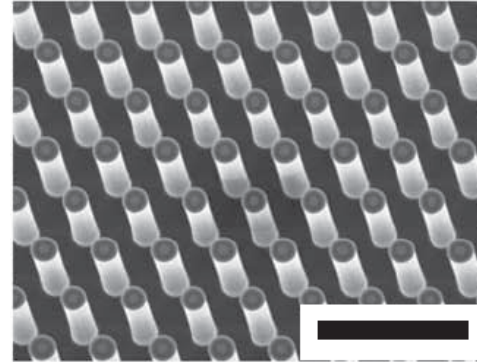
Spatial force distribution (red arrows) near the edge of a single cell (yellow line) on pillars with diameters of 1 μm (A,C) and 0.5 μm (B,D).

Hone group, Columbia University
Work performed at the Cornell NanoScale Facility

S. Ghassemi et al., *Proc. Nat. Acad. Sci.* **109**, 5328 (2012)

Assaying Stem Cell Mechano-biology On Microfabricated Elastomeric Substrates With Geometrically Modulated Rigidity

The C. S. Chen group at the Univ. of Pennsylvania has used the Cornell NanoScale Facility to develop a microfabricated cell culture substrate, consisting of a uniform array of closely spaced, vertical elastomeric microposts, to study the effects of substrate rigidity on cell function. Microposts of different heights are used to yield substrates of different rigidities. The tips of the microposts are functionalized with extracellular matrix through microcontact printing to promote cell adhesion. These substrates, therefore, present identical topographical cues to adherent cells while varying substrate rigidity only through manipulation of the micropost height. Immunofluorescence imaging, traction force analysis, and stem cell differentiation assays are performed on these substrates in order to examine the effect of substrate rigidity on stem cell morphology, traction force generation, focal adhesion organization and differentiation.



Micropost array with 10 μm scale bar. Use of the array to measure traction forces exerted by a cell.

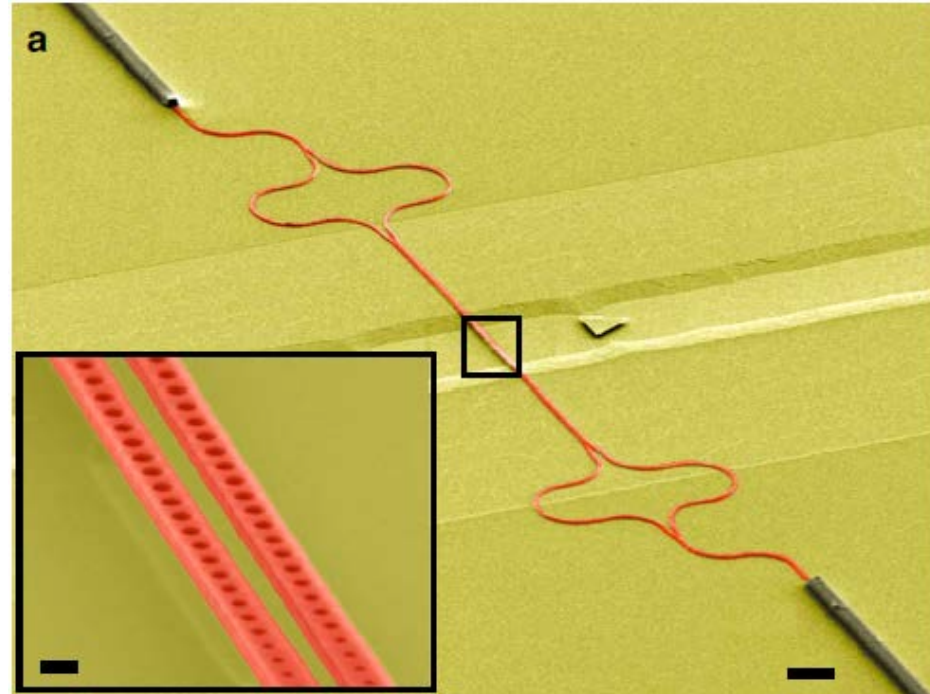
C. S. Chen group, University of Pennsylvania
Work performed at the Cornell NanoScale Facility

M. T. Yang, et al., *Nature Protocols* **6**, 187(2011)

All Optical Reconfiguration Of Optomechanical Filters

Reconfigurable optical filters are of great importance for applications in optical communication and information processing. Of particular interest are tuning techniques that take advantage of mechanical deformation of the devices, as they potentially offer wide tuning ranges. Using devices made at the Cornell NanoScale Facility, the Loncar group at Harvard demonstrated mechanical reconfiguration of coupled photonic crystal nanobeam cavities by using optical gradient force induced mechanical actuation. Propagating waveguide modes that exist over a wide wavelength range were used to actuate the structures and control the resonance of localized cavity modes. Using this all-optical approach, a tuning range of more than 18 linewidths was demonstrated.

Loncar group, Harvard University
Work performed at Cornell NanoScale Facility

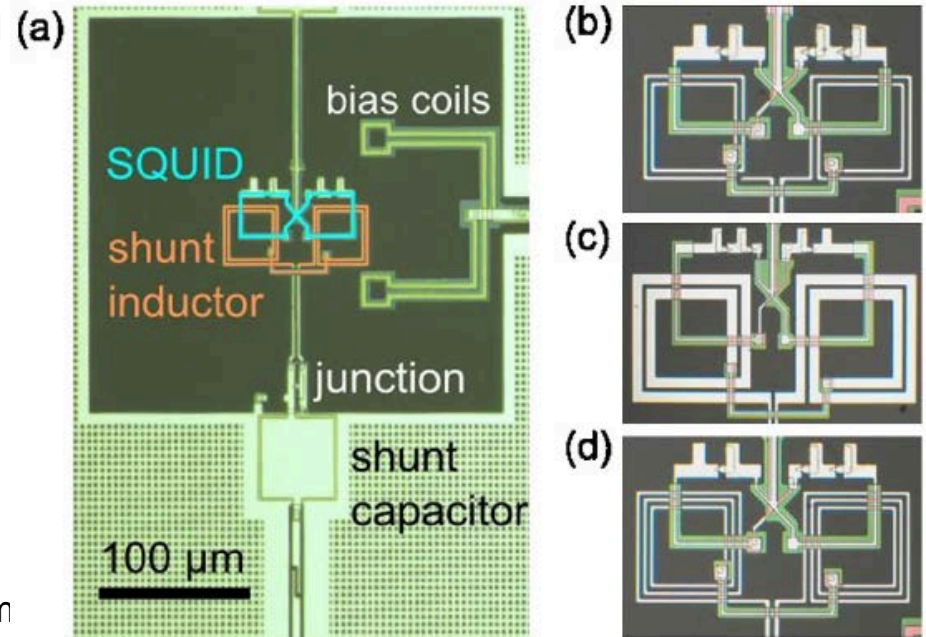


Scanning electron microscope image showing the complete device with the SU-8 coupling pads, balanced Mach-Zehnder interferometer arms, silicon waveguides and the suspended nanobeam cavity region.

P. G. Deotare et al., *Nature Communications* **3**, 846 (2012)

Implementing the Quantum von Neumann Architecture with Superconducting Circuits

The von Neumann architecture for a classical computer comprises a central processing unit and a memory holding instructions and data. The Cleland and Martinis groups at the University of California, Santa Barbara have used NNIN facilities at both Santa Barbara and Cornell to demonstrate a quantum central processing unit that exchanges data with a quantum random-access memory integrated on a chip, with instructions stored on a classical computer. They tested their quantum machine by executing codes that involve seven quantum elements: two superconducting qubits coupled through a quantum bus, two quantum memories, and two zeroing registers. Two vital algorithms for quantum computing were demonstrated, the quantum Fourier transform, with 66% process fidelity, and the three-qubit Toffoli-class OR phase gate, with 98% phase fidelity. These results, in combination especially with longer qubit coherence, illustrate a potentially viable approach to factoring numbers and implementing simple quantum error correction codes.



Superconducting phase qubit devices used in the experiments.

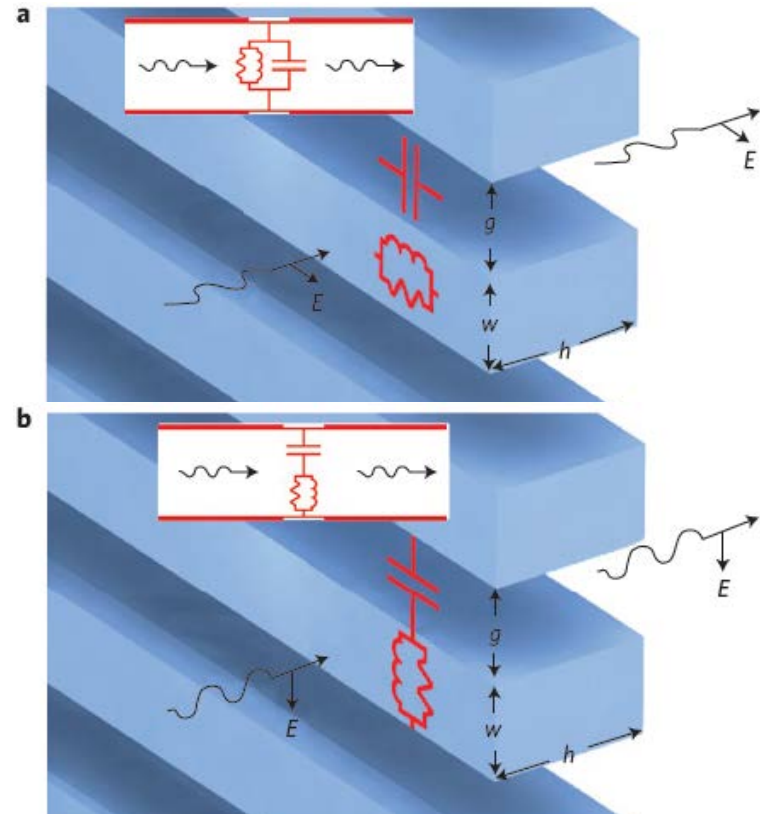
Cleland and Martinis groups, UC Santa Barbara
Work performed at the Santa Barbara and Cornell
NanoScale Facilities

M. Mariantoni et al., *Science* **334**, 61 (2011)

Experimental Realization Of Optical Lumped Nanocircuits At Infrared Wavelengths

In electronics, radiofrequency signals are controlled and manipulated by 'lumped' circuit elements, such as resistors, inductors and capacitors. The Engheta group from the Univ. of Pennsylvania has used the Cornell NanoScale Facility to demonstrate experimentally, for the first time, a two-dimensional *optical* nanocircuit composed of lumped elements operating at mid-infrared wavelengths. With the guidance of circuit theory, they designed and fabricated arrays of Si_3N_4 nanorods with specific subwavelength cross-sections, quantitatively evaluated their equivalent impedance in the mid-infrared, and demonstrated that these nanostructures can indeed function as two-dimensional optical lumped circuit elements. They further showed that the connections among nanocircuit elements, in particular whether they are in series or in parallel combination, can be controlled by the polarization of impinging optical signals.

Engheta group, Univ. of Pennsylvania.
Work performed at the Cornell NanoScale Facility

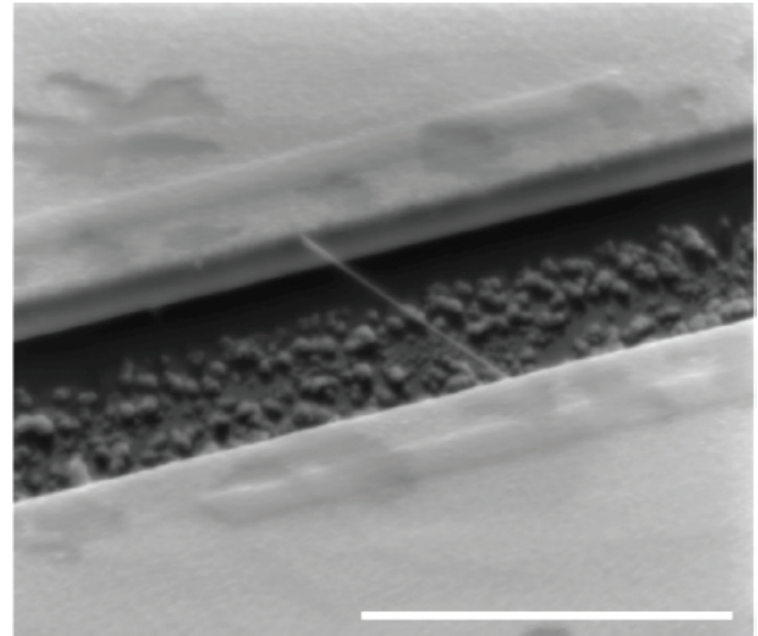


Depending on the polarization of incoming light, dielectric nanorods with air gaps provide effectively different combinations of lumped resistor, capacitor, and inductor characteristics.

Y. Sun et al., *Nature Materials* **11**, 208 (2012)

Fabrication Of Low-noise Carbon Nanotube Field-effect Transistor Biosensors

The resistance of a semiconducting carbon nanotube (CNT) devices is sensitive to the binding of biomolecules onto the CNT surface. Previous work in this field has employed only CNTs lying on substrates. The Minot group at Oregon State University has used the Cornell NanoScale Facility to fabricate suspended CNT biosensor devices, removing the CNTs from the influence of the substrate. They find that the suspended biosensor devices have significantly reduced noise compared to surface-mounted CNTs. The new devices also allow measurements of the interactions between biomolecules and CNTs without interference from the substrate, and they are compatible with microfluidic integration. These properties suggest that the new sensor design is promising for low-noise, high-sensitivity biosensing applications.



Scanning electron microscopy image of a single suspended carbon nanotube bridging between two gold electrodes (scale bar 3 μm).

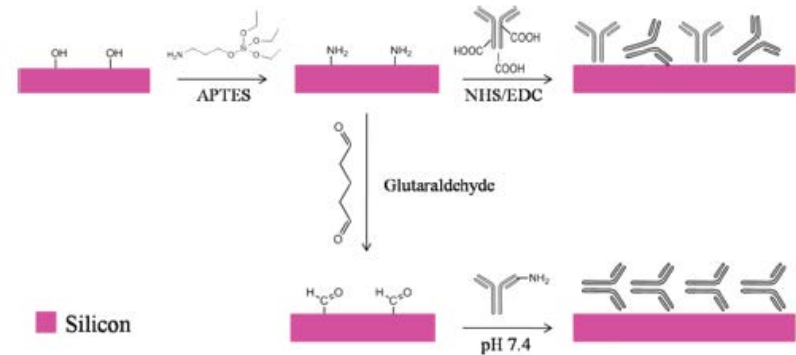
Minot group, Oregon State University
Work performed at the Cornell NanoScale Facility

T. Sharf et al., *Proceedings of the 2011 11th IEEE International Conference on Nanotechnology*

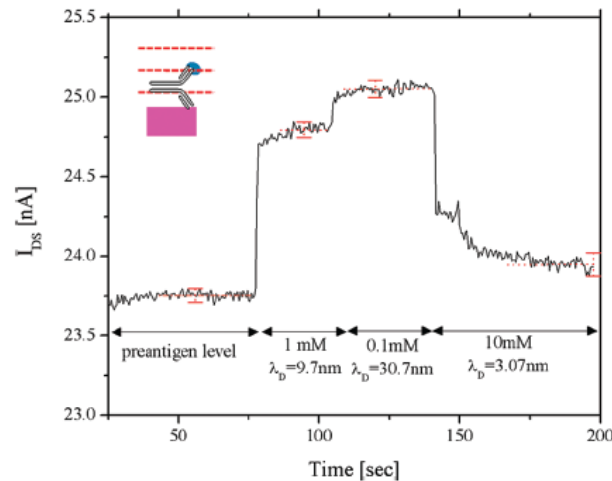
Determination of Molecular Configuration by Debye Length Modulation

Silicon nanowire field effect transistors (FETs) have emerged as ultrasensitive, label-free biodetectors that operate by sensing bound surface charge. However, the ionic strength of the environment (i.e., the Debye length of the solution) dictates the effective magnitude of the surface charge. The Reed group from Yale has used devices fabricated at the Cornell NanoScale Facility to gain a quantitative understanding of this effect. They used two different antibody-antigen systems to bind antigens at different distances from a silicon nanoribbon sensor, and then studied the sensor's signal strength as a function of the Debye length tuned via the ionic strength of the buffer. They showed that control of the Debye length determines the spatial extent of sensed bound surface charge on the sensor.

Reed group, Yale University
Work performed at the Cornell NanoScale Facility



Two schemes of antibody immobilization on the sensor surface resulting in different antibody arrangements.

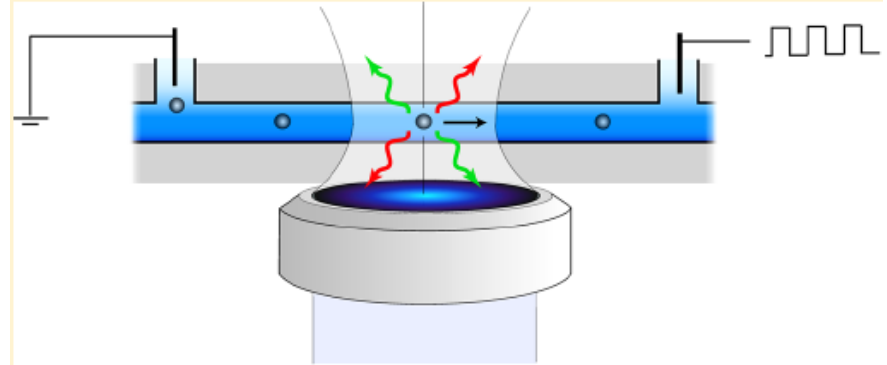


Sensor signal in response to different values of the Debye length.

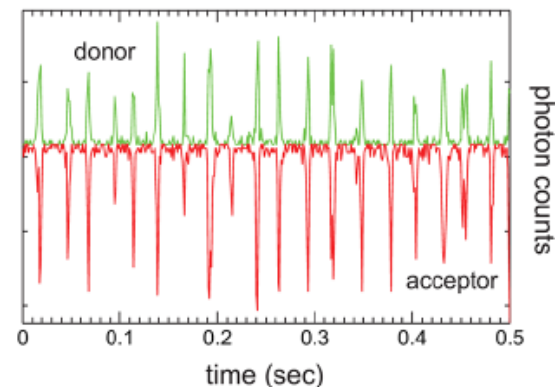
A Vacic et al., *J. Am. Chem. Soc.* **133**, 13386 (2011)

Nanochannel-Based Single Molecule Recycling

The Novotny group at the Univ. of Rochester has used the Cornell NanoScale Facility to develop a method for measuring the fluorescence from a single molecule hundreds of times without surface immobilization. The approach is based on the use of electro-osmosis to repeatedly drive a single target molecule in a fused silica nanochannel through a stationary laser focus. Single molecule fluorescence detected during the transit time through the laser focus is used to repeatedly reverse the electrical potential controlling the flow direction. The group has demonstrated the ability to recycle both proteins and DNA in nanochannels and showed that the procedure can be combined with single-pair Förster energy transfer. Nanochannel-based single molecule recycling holds promise for studying conformational dynamics on the same single molecule in solution and without surface tethering.



Nano-fluidic system constructed to make repeated optical measurements on the same individual molecule in solution.



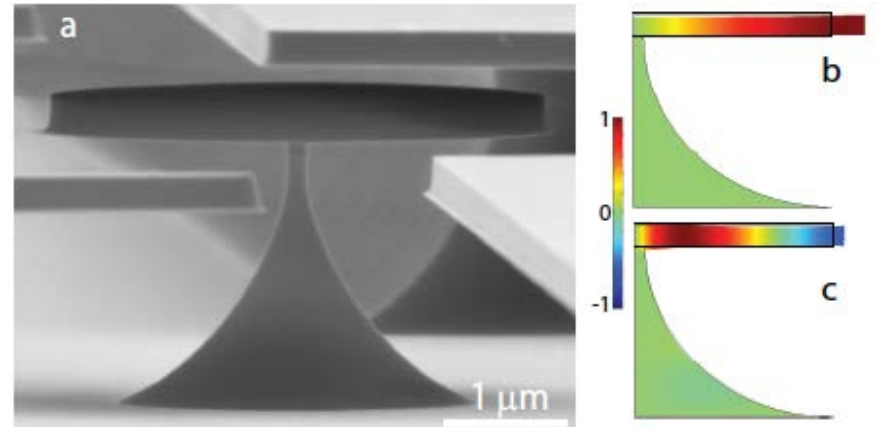
FRET signal measured repeatedly on the same molecule.

Novotny group, Univ. of Rochester.
Work performed at the Cornell NanoScale Facility

J. Lesoine et al., *Nano Letters* **12**, 3273 (2012)

High-frequency Silicon Optomechanical Oscillator With An Ultralow Threshold

Self-sustaining mechanical oscillators have broad application potential in optical/wireless communication, bio-molecule sensing, and frequency metrology. For many practical applications, it is necessary to operate at frequencies above 1 GHz while simultaneously maintaining a high efficiency. The Lin group from the Univ. of Rochester has used the Cornell NanoScale Facility to demonstrate a highly efficient optomechanical oscillator based upon a small silicon microdisk resonator with a 2- μm radius. The device exhibits strong optomechanical coupling and a large mechanical frequency-Q product of 4.32×10^{12} Hz. It is able to operate at 1.294 GHz with an ultralow threshold of $3.56 \mu\text{W}$ while working in air. The high efficiency and high frequency of this device, together with its structural compactness and CMOS compatibility, give it potential for broad applications in photonic-phononic signal processing, sensing, and metrology.



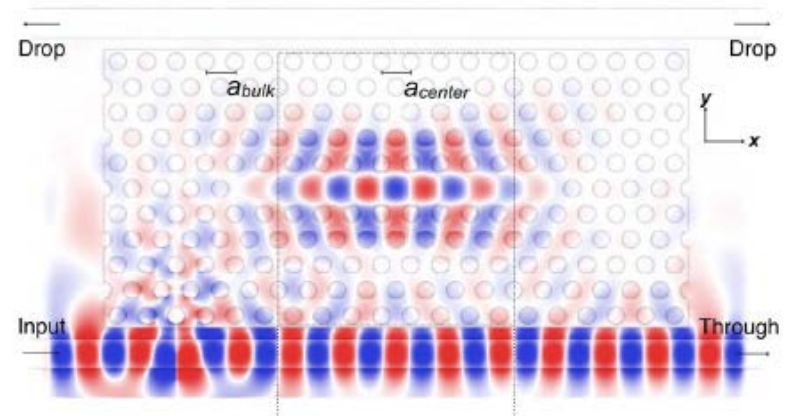
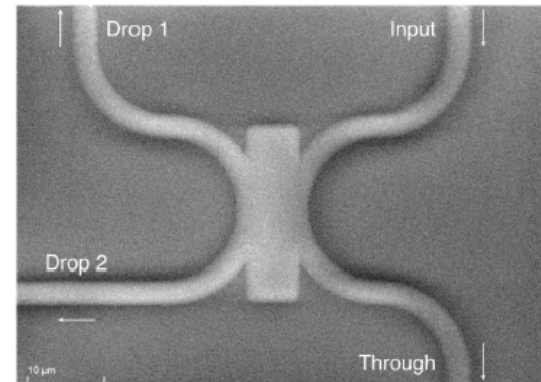
Side-view of the silicon-microdisk resonator, along with simulations of the amplitudes of mechanical displacement in the fundamental and second-order radial-stretching mechanical modes.

Lin group, Univ. of Rochester.
Work performed at the Cornell NanoScale Facility

W. Jiang et al., *Optics Express* **20**, 15991 (2012)

Demonstration of evanescent coupling and photon confinement in oxide-clad silicon microcavities

To use photonic crystals in on-chip and integrated applications, they must be embedded in SiO_2 and integrated with other photonic devices. The Fauchet group from the Univ. of Rochester has used the Cornell NanoScale Facility to make an experimental demonstration of resonance in a SiO_2 -clad two-dimensional photonic crystal microcavity that is coupled to standard silicon strip waveguides. They showed that well over 90% of the resonant field is confined within the cavity's silicon layer (rather than the SiO_2), which is necessary if the microcavity is to be used as a high-efficiency electro-optic modulator.



Silica-clad photonic crystal resonator integrated with silicon optical waveguides, with a simulation of the resonant mode excited by a propagating field in the bus (lower) waveguide.

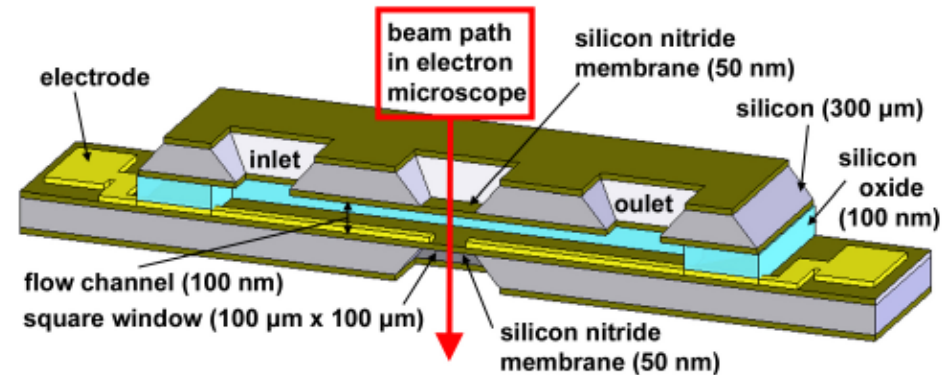
Fauchet group, Univ. of Rochester.
Work performed at the Cornell NanoScale Facility

S. P. Anderson et al., *Optics Lett.* **36**, 2698 (2011)

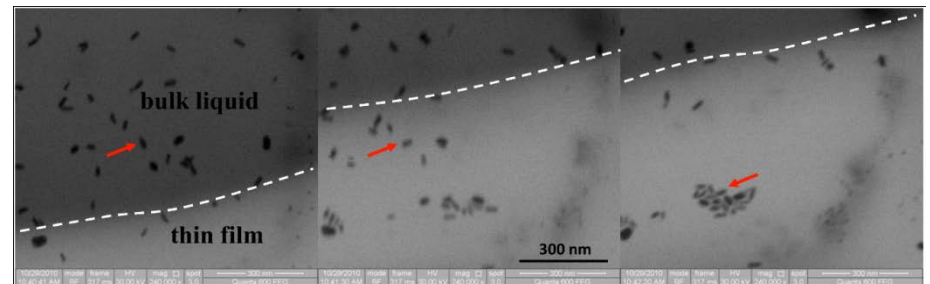
Real Time Electron Microscope Imaging of Nanoparticle Motion Induced by a Moving Contact Line

The Bau group at the University of Pennsylvania has used the Cornell NanoScale Facility to develop the “nano-aquarium” -- a microfabricated nanofluidic device that enables transmission electron microscope (TEM) imaging of dynamical processes taking place in liquid media. It consists of a shallow conduit (~ 100 nm thick) sandwiched between two thin silicon nitride membranes (each 50 nm thick), with the liquid volume in the device hermetically sealed. The conduit height and membrane thickness are among the thinnest of any liquid-cell TEM device, enabling the nanoaquarium to yield high resolution, high contrast images with minimal electron scattering by the suspending medium. As a test of the devices, they were used to obtain real-time videos showing the motion and aggregation of gold nanorods induced by moving contact lines.

Bau group, Univ. of Pennsylvania.
Work performed at the Cornell NanoScale Facility



Schematic depiction of a cross section of the “nano-aquarium”. Not to scale.



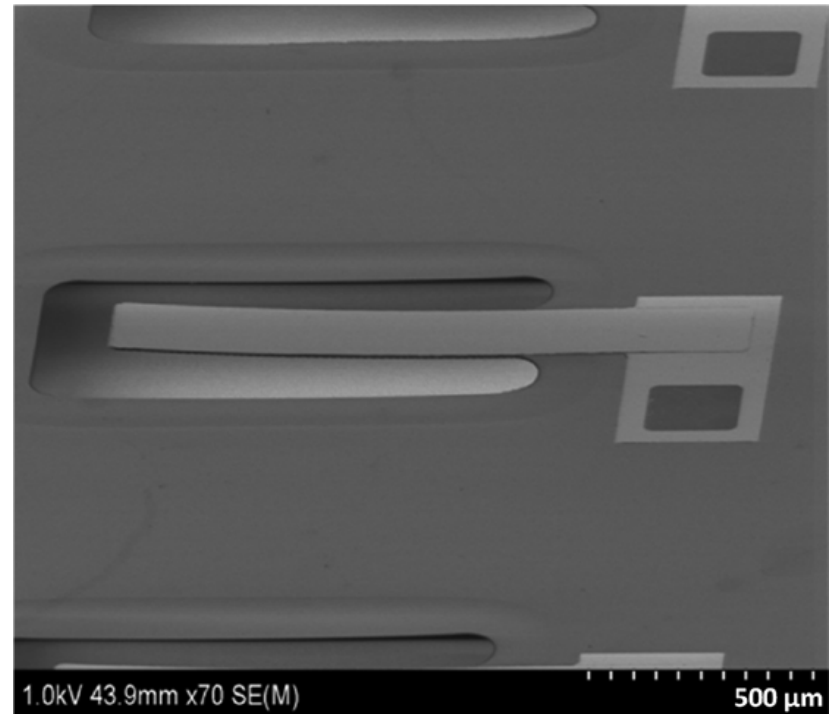
TEM image of gold nanorods aggregating on a surface as they are ejected from a receding liquid contact line. The dark region is the receding liquid and the contact line is indicated by a dashed white line. The same particle is indicated by a red arrow.

J. M. Grogan and H. H. Bau, arXiv:1110.3273 (2011)

Energy Harvesting Properties Of All-thin-film Multiferroic Cantilevers

Self-powered sensor nodes are used in a wide spectrum of wireless applications ranging from in vivo encapsulated implants to industrial process monitoring. There is an acute need for low-cost alternative power sources without batteries, which are undesirable for maintenance-free applications and microsystems. One promising route is to use devices that harvest energy from applied electromagnetic waves. The Takeuchi group from the Univ. of Maryland has used the Cornell NanoScale Facility to fabricate thin-film magnetolectric heterostructures on Si cantilevers for electromagnetic energy harvesting. The devices consist of a magnetostrictive $\text{Fe}_{0.7}\text{Ga}_{0.3}$ thin film coupled to a $\text{Pb}(\text{Zr}_{0.52}\text{Ti}_{0.48})\text{O}_3$ piezoelectric thin film. The harvested peak power at 1 Oe is 0.7 mW/cm^3 (RMS) at the resonant frequency (3.8 kHz) with a load of 12.5 k Ω .

Takeuchi group, Univ. of Maryland.
Work performed at the Cornell NanoScale Facility

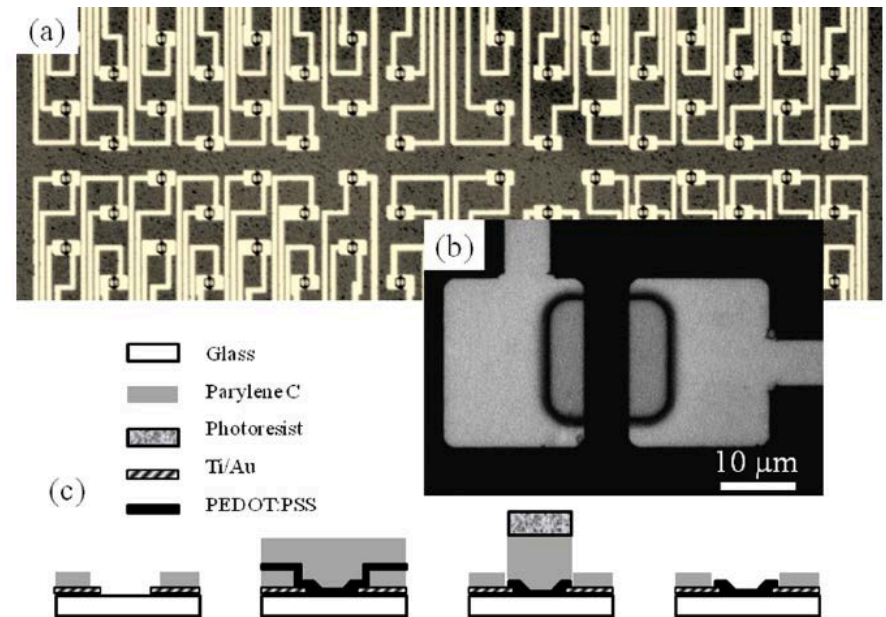


A scanning electron micrograph of a multiferroic energy harvester. The device is a 950- μm long and 200- μm wide released cantilever.

T.-D. Onuta et al., *Appl. Phys. Lett.* **99**, 203506 (2011)

High Speed And High Density Organic Electrochemical Transistor Arrays

Interfacing transistors with aqueous electrolytes is important for the development of biosensors. The Malliaras group has used the Cornell NanoScale Facility to develop a lithographic process that allows the fabrication of high-density organic electrochemical transistor arrays that operate immersed in aqueous electrolytes. The channels of the transistors, which were 6 μm long, were made of a conducting polymer and were in direct contact with phosphate buffered saline. This is the first time that conducting-polymer electrochemical transistors have been made smaller than 10 μm , the scale needed to interact with single electrically active cells. The transistors operated at low voltages and showed a response time of the order of 100 μs .



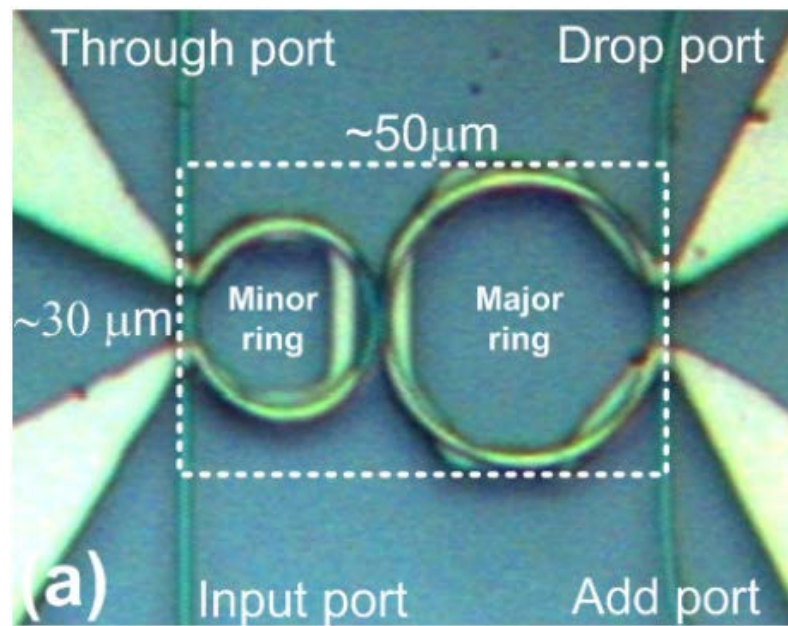
The overall architecture of the organic electrochemical transistor array, with a magnified image of a single transistor.

D. Khodagholy et al., *Appl. Phys. Lett.* **99**, 163304 (2011)

Malliaras group, Ecole Nationale Supérieure des
Mines de Saint Etienne, France.
Work performed at the Cornell NanoScale Facility

Reconfigurable Silicon Thermo-optical Ring Resonator Switch Based on Vernier Effect Control

A collaboration involving research groups from Florida International University, Caltech, and Brazil has used the Cornell NanoScale Facility to demonstrate a new and entirely CMOS compatible reconfigurable optical switch. The device operates by using controlled heating to tune the optical phase difference between two coupled optical ring resonators. Preliminary results show that a single optical device is capable of combining several functionalities, including tunable filtering, non-blocking switching and reconfigurability, with compact footprint ($\sim 50 \mu\text{m} \times 30 \mu\text{m}$).



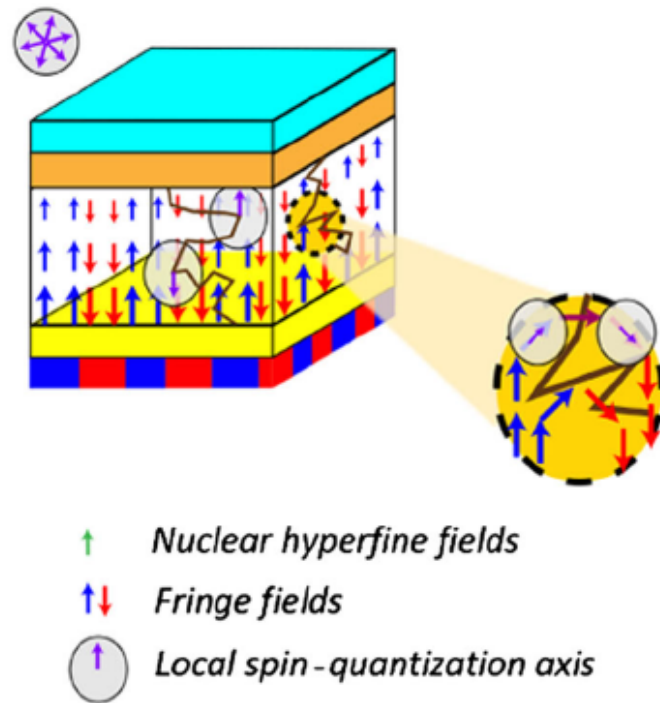
Optical microscope image of the coupled-oscillator optical switch.

Panepucci, Almeida, and Scherer groups, Florida International University, Brazil, and Caltech.
Work performed at the Cornell NanoScale Facility

W. S. Fegadolli et al., *Optics Express* **20**, 14722 (2012)

Magnetic Fringe-Field Control of Electronic Transport in an Organic Film

A collaboration from New York University and the Univ. of Iowa has discovered an entirely unexpected form of magnetoresistance within organic semiconductors in new no-spin-injection magnetoelectronic devices. The devices consist of a ferromagnetic layer adjacent to, but electrically insulated from, a nonmagnetic organic semiconductor (Alq_3) layer. By applying a magnetic field to change the magnetic domain structure in the ferromagnet, the changing magnetic fringe field from the ferromagnet dramatically changes the resistance of the Alq_3 layer, in the absence of any spin injection. The mechanism behind the effect is currently not understood in detail, but this work suggests a new approach for integrating magnetic metals and organic semiconductors to make hybrid spintronic devices.



Magnetic fringe fields influence the flow of electrons in an organic semiconductor layer.

Kent group, NYU;
Wohlgenannt and Flatté groups, Univ. of Iowa.
Work performed at Cornell NanoScale Facility

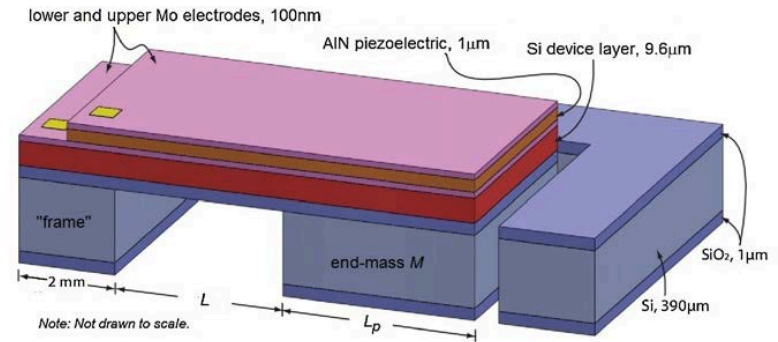
F. Wang et al., *Phys. Rev. X* **2**, 021013 (2012)

MEMS Piezoelectric Vibrational Energy Harvesters With Mass Loading

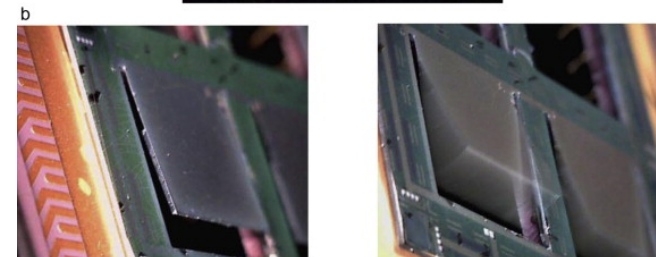
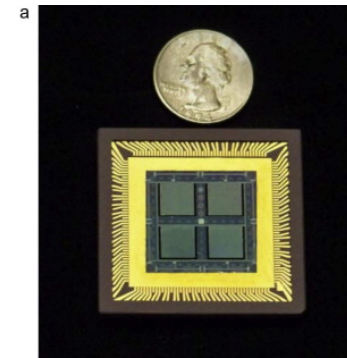
Piezoelectric vibrational energy harvesters (PZEHs) using microelectromechanical systems (MEMS) technology are being developed by MicroGen Systems, Inc. at the Cornell NanoScale Facility. The core body of a PZEH is a “multi-morph” cantilever, where one end is clamped to a base and the other end is free. This “fixed-free” cantilever system includes a proof-mass (also called the end-mass) on the free end that can oscillate with the multi-layer cantilever under continuous sinusoidal excitations of the base motion. A MEMS PZEH prototype resonating at 58 Hz under 0.7g external excitations reached a peak power of 63 μW with an output load impedance Z of 85 k Ω . This PZEH generator has successfully powered a wireless sensor node with the integrated sensor, radio frequency (RF) radio, power management electronics, and an advanced thin-film lithium-ion rechargeable battery for power storage.

R. Andosca, et al., MicroGen Systems, Inc., Univ. Vermont, Infinite Power Solutions, Inc.
Work performed at Cornell NanoScale Facility

Sensors and Actuators A **178**, 76 (2012)



Monomorph (single piezoelectric layer with two electrodes) PZEH cantilever with a proof mass



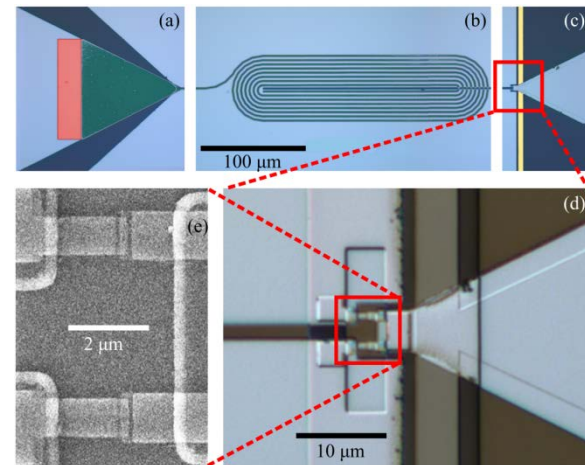
MEMS-based PZEH. (a) static position and (b) vibrating at 58 Hz @ 0.5 g

Superconducting microstrip amplifiers with sub-Kelvin noise temperature near 4 GHz

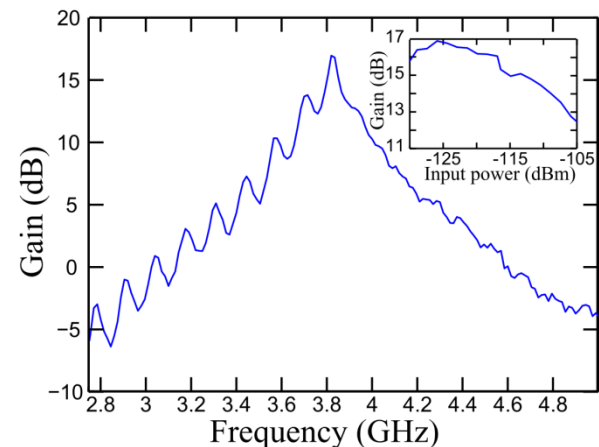
Micro-strip superconducting quantum interference (SQUID) device amplifiers (MSAs) based on resonant microstrip input coils have recently demonstrated their utility in qubit measurement—an MSA was used to perform dispersive readout of a flux qubit. The Plourde group at Syracuse Univ. has used the Cornell NanoScale Facility to develop an alternative design of the MSA input coil and washer. The tunnel junctions are patterned with electron-beam lithography and formed using a double-angle shadow evaporation technique. This design results in an MSA operating at 3.8 GHz with 17 dB of gain and a 150 MHz bandwidth. The researchers also characterized the system noise temperature and demonstrated a substantial reduction compared to a conventional cryogenic HEMT amplifier.

M. DeFeo and B. Plourde, Syracuse Univ.
Work performed at Cornell NanoScale Facility

Appl. Phys. Lett. **101**, 052603 (2012).



(a) False-color optical micrograph of coupling capacitor (red), (b) input coil (green), and (c) Pd shunt resistors (yellow) at scale specified in (b). (d) Closeup optical micrograph of junction and shunt region. (e) Scanning electron micrograph of Josephson junctions.



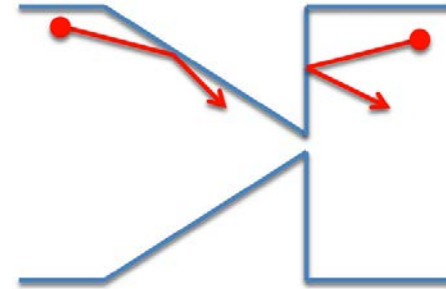
Device gain as a function of frequency biased for maximum gain. (Inset) Maximum device gain as a function of drive power.

Ultrahigh Speed Graphene Diode with Reversible Polarity

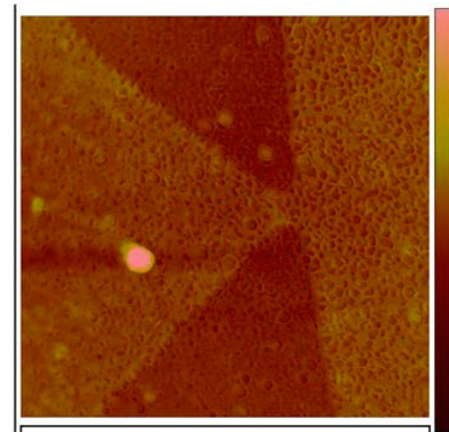
The ability to tune the carrier-type concentration ratio with applied field along with a mean-free path length approaching 1 μm in graphene enabled the Moddel group at the Univ. of Colorado, Boulder to create a new diode in which the diode polarity can be reversed. The diode consists of a thin graphene film with a geometric asymmetry that determines a preferred direction for charge-carrier transport, independent of whether the carriers are electrons or holes. They used the Cornell Nanoscale Facility to fabricate submicron geometric diodes by patterning and etching exfoliated graphene. Applying field-effect voltages to the substrate, they reversed the carrier type and demonstrated reversal of the diode polarity. The graphene geometric diodes exhibited rectification at 28 THz, opening the way to ultrahigh speed applications for these devices.

G. Moddel, et al., Univ. of Colorado, Boulder
Work performed at Cornell NanoScale Facility

Solid State Comm. **152**, 1842 (2012).



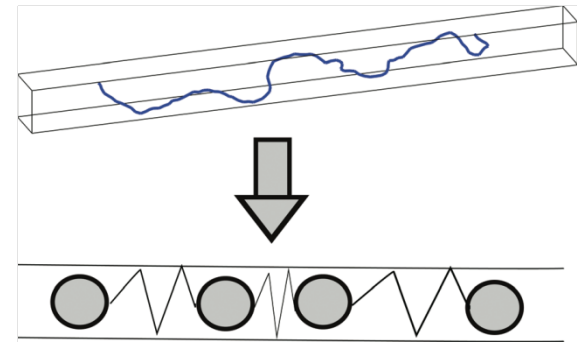
Schematic top view of a geometric diode. In the region to the right of the aperture charges moving leftwards are deflected to the right due to the vertical edge, while charges in the left region moving rightwards collide with the slanting edge, and funnel through the aperture. Inelastic scattering resets the trajectory to a random direction modified by the applied electric field. A charge carrier near the aperture senses the geometric asymmetry on length-scales smaller than the mean-free path length (MFPL), leading to the net flow in the preferred direction.



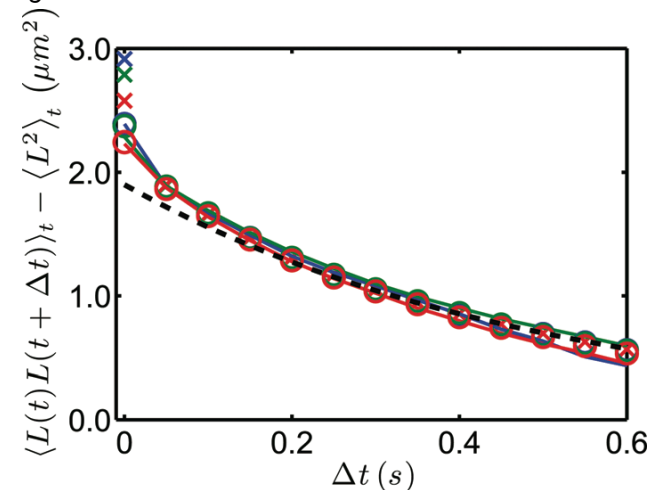
AFM image of a geometric diode made from graphene having a neck width of 75 nm and shoulder width of 400 nm.

Fluctuation Modes of Nanoconfined DNA

The magnitude of length and density fluctuations in DNA that has been stretched in nanofluidic channels were studied by the Riehn group at N.C. State Univ. The experiments used nanofluidic devices fabricated at the Cornell NanoScale Facility. Fluidic channels with a $160 \times 80 \text{ nm}^2$ cross-section and a length of $200 \mu\text{m}$ were placed between microchannels that carried solution from the injection ports of the device to the active zone. DNA was moved through microchannels by application of pressure and injected into nanochannels through application of voltages at the microfluidic ports. The researchers found that the fluctuations of nanoconfined DNA on large length scales can be understood in terms of normal modes of a one-dimensional overdamped oscillator chain with nonzero equilibrium spring length, and that a chain of discrete oscillators yields a better description than a continuous chain. They also showed that the description breaks down beyond a length scale at which finite extensibility and volume interactions become dominant.



Rouse-like model of nanoconfined DNA. Under confinement to a channel much smaller than the radius of gyration, DNA assumes an extended geometry. If the extension is large, the polymer can be modeled as a chain of oscillators with finite equilibrium spring lengths.



Autocorrelation of end-to-end fluctuations of k-DNA at varying duty cycles. Solid lines are the experimental data, circles are simulated data of a 64-bead harmonic oscillator chain, and crosses are analytical predictions. The frame rate was 20 Hz, and the duty cycle was 10% (blue), 30% (green), 90% (red). The black dashed line is a single-exponential fit.

A. Karpusenko, et al., N.C. State Univ.
Fabrication performed at Cornell NanoScale Facility

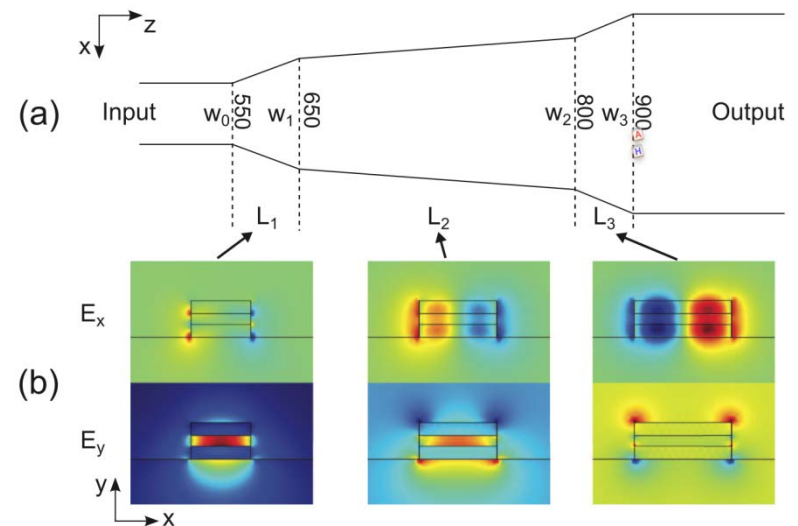
J. Appl. Phys. **111**, 024701 (2012).

Compact, Broadband Slot Waveguide Polarization Rotator

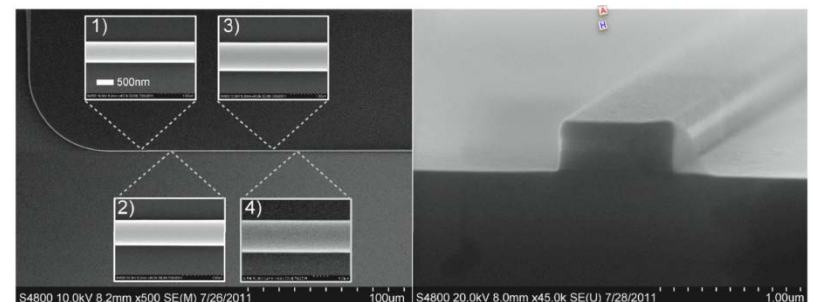
Horizontal slot waveguides can be used to enhance nonlinear effects for optical modulation and detection in photonic integrated circuits. However, the efficiency of coupling to other integrated optical devices is adversely affected by a large polarization mode mismatch. The Zhu group at Clemson Univ. used electron beam lithography at the Cornell NanoScale Facility to fabricate a broadband polarization rotator which can effectively rotate the polarization direction of TM input by 90 degrees while the polarization state of TE input is kept unchanged. The rotator is a horizontal slot waveguide of 100 nm oxide between 120 nm layers of α -Si:H, with tapered sections which cause the adiabatic evolution of the quasi-TM mode to the 2nd quasi-TE mode, resulting in TE dominant polarization at the output port. Measured polarization extinction ratios were about 15 dB and 20 dB for TM and TE input, respectively, over a 35 nm span of input wavelengths.

J. Fan, C. Huang and L. Zhu, Clemson Univ.
Work performed at Cornell NanoScale Facility

AIP Advances 1, 042136 (2011).



(a) Top-view schematic of the three-segment taper structure. (b) Field evolution of the slot waveguide along the device for the input wavelength $\lambda = 1.55\mu\text{m}$. The quasi-TM mode is excited at the input end.



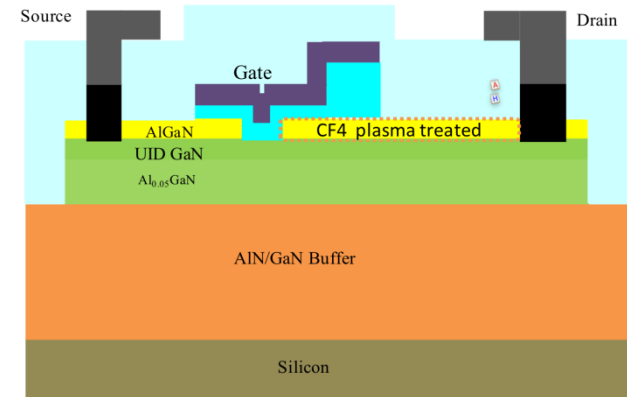
(a) SEM top view (b) cross-section view. The inset figures in (a) show zoomed-in images with the same scale where the waveguide width w is: (1) 550nm (2) 650nm (3) 800nm (4) 900nm.

High Voltage Normally-off GaN MOSC-HEMTs on Silicon Substrates for Power Switching Applications

The Chow group at Rensselaer Polytechnic Inst. has used the Cornell NanoScale Facility to fabricate normally-off GaN Metal-Oxide-Semiconductor Channel high electron mobility transistors (MOSC-HEMT). The GaN MOSC-HEMTs were fabricated using deep submicron MOS channels on two types of custom commercial epitaxial layers grown on silicon substrates. The lowest measured specific on-resistance was $4 \text{ m}\Omega\text{-cm}^2$, and breakdown voltage was up to 840 V. The switching performance of the device was compared to circuit simulations, showing 10% higher system efficiency than commercial GaN HEMTs. They also experimentally demonstrated a bidirectional switch consisting of two GaN MOSC-HEMTs.

Z. Li, et al., Rensselaer Polytechnic Inst.
Work performed at Cornell NanoScale Facility

24th Intl. Symp. on Power Semicond. Dev. and ICs, 45, (2012)



Schematic cross section view of GaN MOSC-HEMTs on silicon substrate with conventional AlGaIn/GaN epi structure and a CF4 plasma treated drift region.

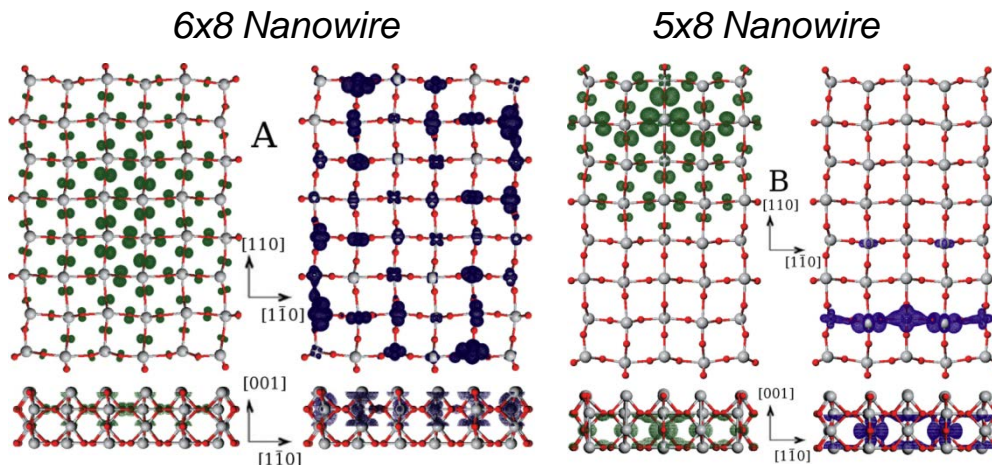


GaN MOSC-HEMT fabricated epitaxial GaN on silicon substrate with circular geometry

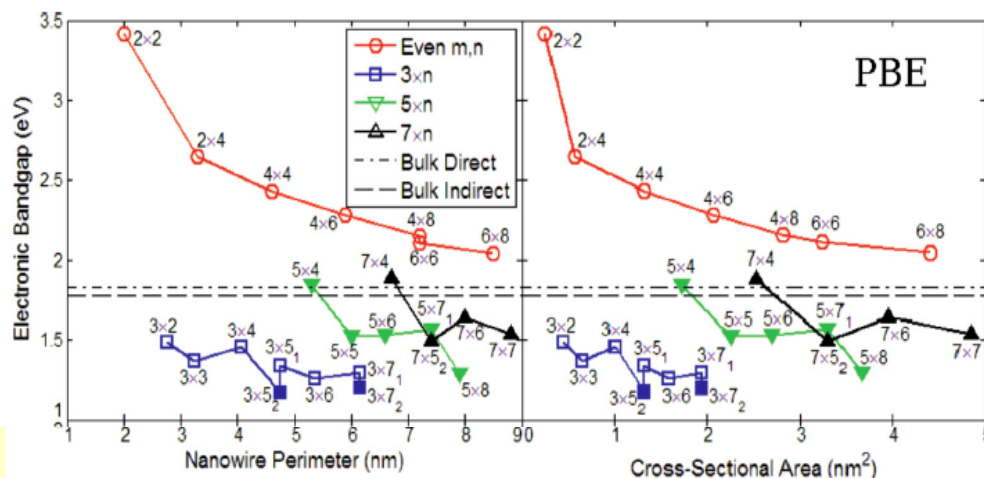
Quantum Confinement and Surface Relaxation Effects in Rutile TiO_2 Nanowires

TiO_2 Nanowires have found applications in solar cells, proton-exchange membrane fuel cells, and gas sensors. Hmiel and Xue from the SUNY Albany have examined how the electronic properties of TiO_2 rectangular nanowires change with size and surface relaxation. For small nanowires, quantum confinement effects can be important. The team has used density functional theory to examine a wide range of nanowire configurations. Their study has found that the presence or absence of a mirror Ti-O plane is a key factor in determining the electronic character of the TiO_2 nanowire. It also indicates that it may be possible to tailor the character (direct vs indirect) and size of the nanowire band gap for specific applications. Work is currently ongoing to understand how functionalization of the surfaces will affect the electronic properties.

A. Hmiel and Y. Xue, SUNY Albany
Simulations performed at Cornell NanoScale Facility



Isosurface plots of the local density of states at the valence band maximum (green) and the conduction band minimum (blue) for a 6x8 (A) and a 5x8 (B) rutile TiO_2 nanowire.



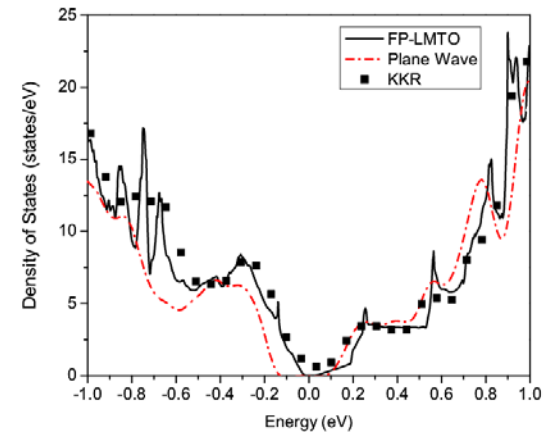
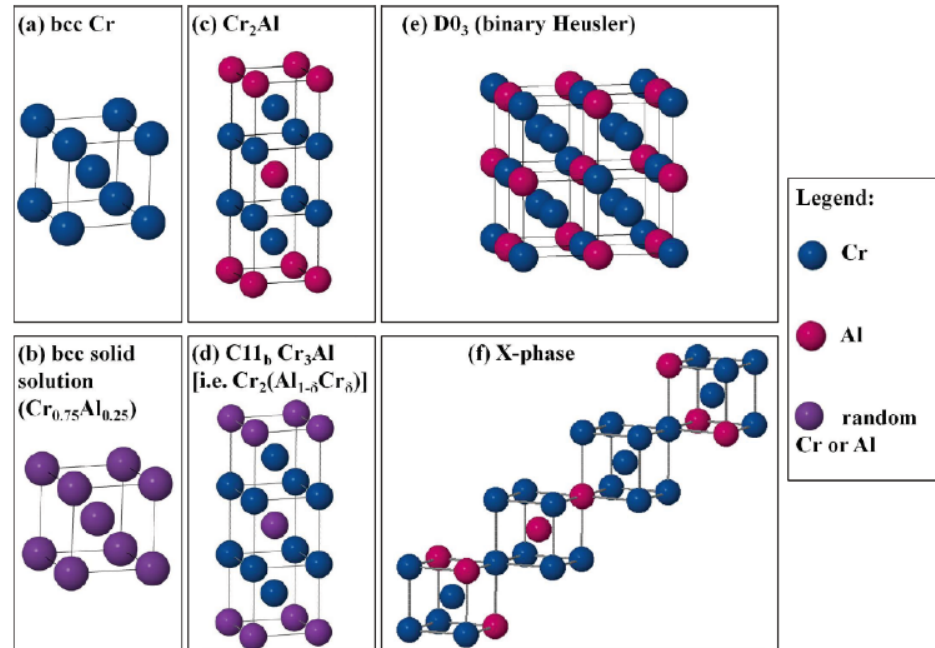
Nanowire Band Gap Energy of TiO_2 nanowires as a function of cross perimeter and cross-sectional area.

Chemical Ordering in Cr_3Al and Semiconducting Behavior

The nature of the band gap in Cr_3Al has recently drawn interest. Experimental results suggest either a semimetal or degenerate semiconductor. A full gap could make Cr_3Al worthy of further study as a possible thermoelectric. Recent theoretical work has also indicated Mn doped Cr_3Al with Heusler ordering (D03) could be a half metal with spintronics applications. However, the Cr-Al phase diagram is not well established.

In this work, Boekelheide and collaborators used a combination of DFT calculations and experimental studies to examine how chemical ordering affect the CrAl electronic structure. Five different crystal structures including disordered ones were examined. The X-phase (f) was found to have a small band gap and be the lowest energy phase. Based on energetics, the D03 phase will not be stable at equilibrium.

Zoe Boekelheide and Frances Hellman, UC Berkeley
Simulations performed at the Cornell Nanoscale Facility

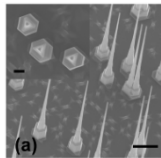


Z. Boekelheide et al., *Phys. Rev. B*, **86**, 085120 (2012).

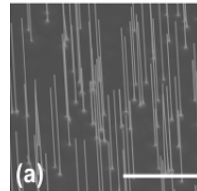
Thermal Transport in InAs Nanowires

How do you predict thermal transport in a material that only exists on the nanoscale?

InAs nanowires switch from a zincblende crystal structure to a wurtzite structure for small diameters. Li Shi's group at the University of Texas Austin found that the thermal conductivity of Wurtzite nanowires was less than the zincblende nanowires. Is this due to the crystal structure or something else?



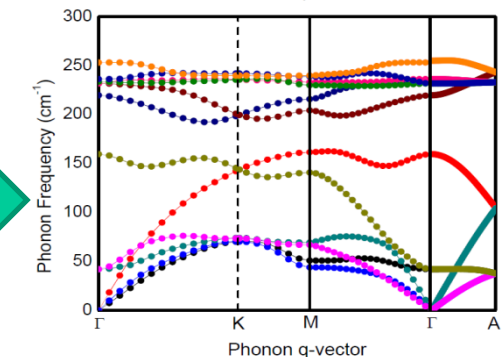
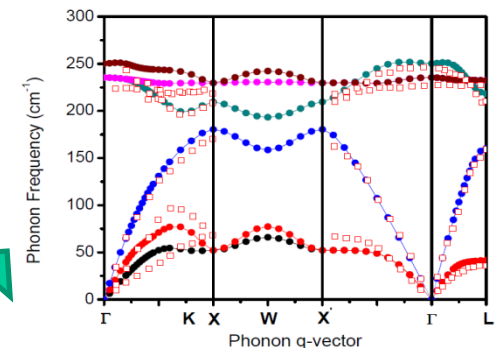
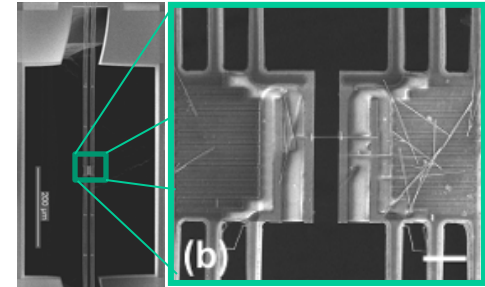
Zincblende
NW



Wurtzite
NW

Since wurtzite InAs doesn't exist in bulk form, nothing is known of its phonon properties.

If we know the sound velocities of the different phonon branches, we can estimate the thermal conductivity. **The phonon dispersion curves were calculated from first principles at the CNF!** Based on this information, it was shown that the change in crystal structure did not affect the thermal conductivity. Rather, differences in cross-section area and surface roughness proved to be the root cause.

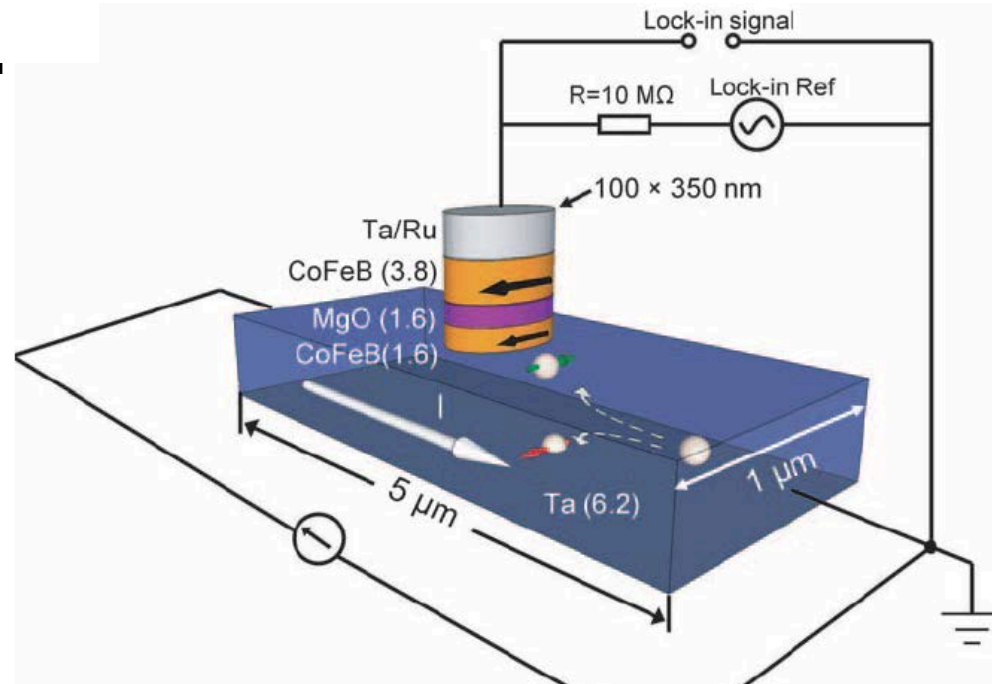


Li Shi et al., Univ. of Texas at Austin
Simulations performed at the Cornell Nanoscale Facility

F. Zhou et al, *Phys. Rev. B*, **83**, 205416 (2011).

Spin-Torque Switching with the Giant Spin Hall Effect of Tantalum

The spin Hall effect is a phenomenon that occurs in metals with large atomic weights, in which electrons with different spins are deflected in different sideways directions, and consequently an applied charge current generates a flow of spin angular momentum transverse to the charge flow. The Buhrman and Ralph groups at Cornell used devices made at the Cornell NanoScale Facility to discover that the spin Hall effect in the high-resistivity form of tantalum is twice as strong as in any other material that has been investigated. They then implemented a new type of nonvolatile magnetic memory device that employs the spin current produced by passing a current through a tantalum layer to switch an adjacent nanomagnet, with a magnetic tunnel junction for read-out. This simple design is more reliable and efficient than competing technologies and eliminates the obstacles that have slowed the development of magnetic memory and nonvolatile spin logic technologies.



A 3-terminal magnetic memory device in which a lateral current flowing in a Ta layer switches the magnetic orientation of the lower magnetic layer in a magnetic tunnel junction by the spin Hall effect.

Buhrman and Ralph groups, Cornell Univ.
Work performed at Cornell NanoScale Facility

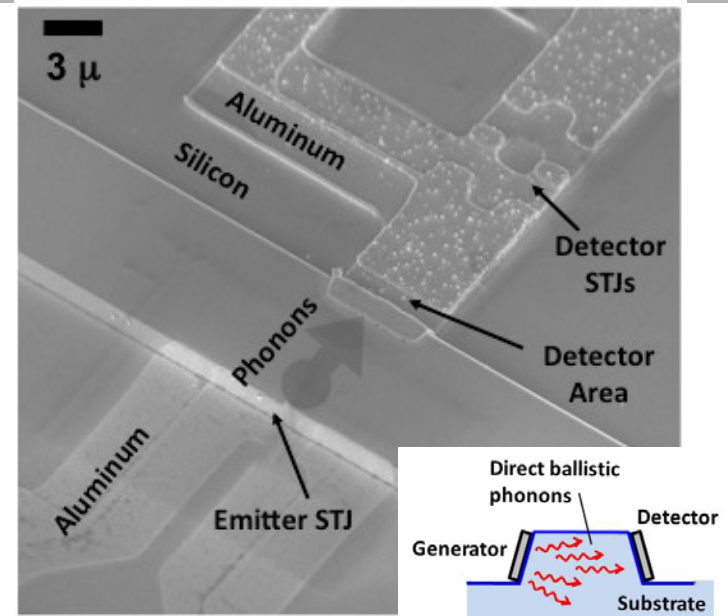
L. Q. Liu et al., *Science* **336**, 555 (2012)

A Microfabricated Spectrometer for Phonons

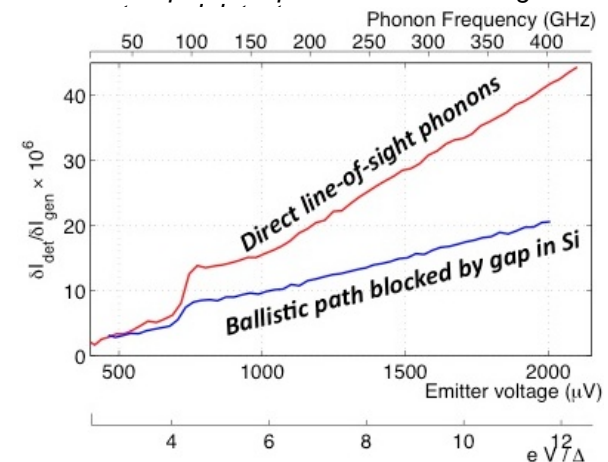
Thermal transport by acoustic phonons in nanoscale dimensions differs markedly from behavior in bulk materials due to phonon interactions with surfaces and interfaces. To help understand this, the Robinson group is developing a microfabricated phonon spectrometer at the Cornell Nanoscale Facility. They recently demonstrated a prototype device that can generate a controllable, non-thermal distribution of acoustic phonons [100-800 GHz]. To generate and detect the non-thermal phonons, the group exploits excitation and decay processes in superconducting tunnel junctions attached to the sides of the silicon microstructure. By measuring phonon transmission through structures with obstructions or surface roughness, they can test current phonon scattering theories in a controlled fashion at specific frequencies. Monte Carlo phonon scattering calculations are also being performed on the CNF computing cluster to aid in interpreting experimental results. This work should provide a better understanding of nanoscale thermal transport which can improve the efficiency of nanostructure thermoelectric materials.

Rev. Sci. Instr. **82**, 104905 (2011).

Richard Robinson, Obafemi Otelaja, Jared Hertzberg, Mahmut Aksit, Cornell University (Project # 1746-09)
Work performed at Cornell NanoScale Facility



Fabricated phonon spectrometer with diagram of

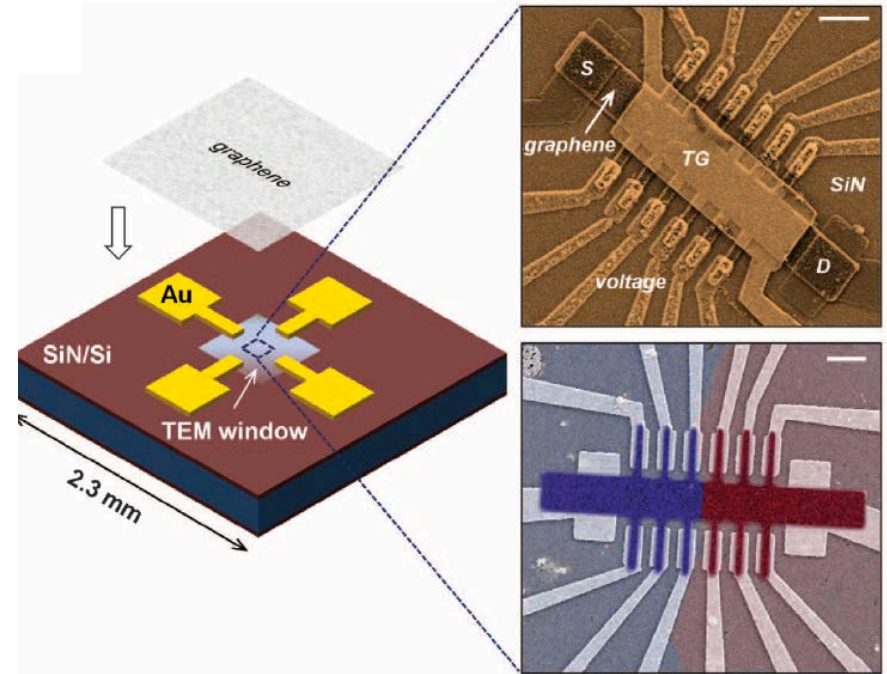


Phonon detected signal for a systems with (blue) and without (red) an etched gap in the silicon bridge.

Tailoring Electrical Transport Across Grain Boundaries in Polycrystalline Graphene

Graphene produced by chemical vapor deposition (CVD) is polycrystalline, and scattering of charge carriers at grain boundaries could degrade its performance relative to exfoliated, single-crystal graphene. To investigate this issue, the groups of Jiwoong Park and David Muller at Cornell have developed a technique to first image and identify the structure of individual grain boundaries in graphene by transmission electron microscopy and then (using the tools of the Cornell NanoScale Facility) to make devices for measuring the electrical properties of these individual grain boundaries. Unexpectedly, the electrical conductance improves by one order of magnitude for grain boundaries with better interdomain connectivity. This study demonstrates that polycrystalline graphene with good stitching can allow for uniformly high electrical performance rivaling that of exfoliated samples.

J. Park and Muller groups, Cornell University
Work performed at the Cornell NanoScale Facility



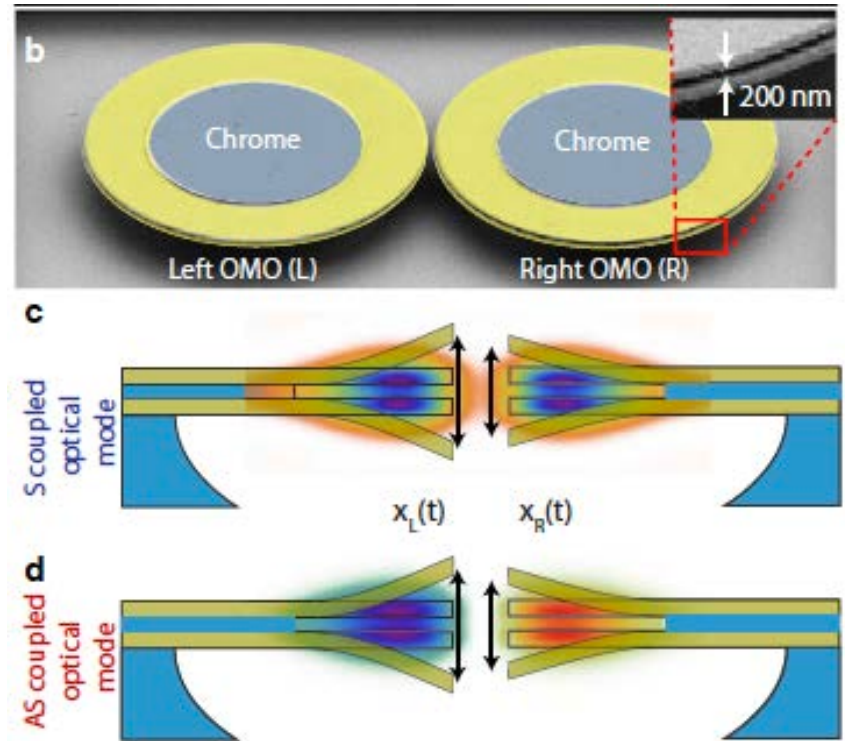
(Left) Schematic of specially fabricated TEM chip compatible with electron beam lithography and electrical measurements. (Top right) SEM image of a top-gated, graphene Hall bar device. (Bottom right) Overlaid SEM and dark field TEM images showing a device crossing a single grain boundary between two domains of graphene.

A. W. Tsen et al., *Science* **336**, 1143 (2012)

Synchronization of Micromechanical Oscillators Using Light

Synchronization, the emergence of spontaneous order in coupled systems, is of fundamental importance in physical and biological systems, and is essential for signal processing and communications technologies. The Lipson and McEuen groups at Cornell, using devices fabricated at the Cornell NanoScale Facility, have demonstrated the synchronization of two dissimilar silicon nitride micromechanical oscillators that are spaced apart by a few hundred nanometers and are coupled only through the optical radiation field, as opposed to coupling through a structural contact or electrostatic interaction. The tunability of the optical coupling between the oscillators enables one to externally control the dynamics and switch between coupled and individual oscillation states. These results pave a path towards realizing synchronized micromechanical oscillator systems connected through optical links.

M. Lipson and McEuen groups, Cornell Univ.
Work performed at the Cornell NanoScale Facility



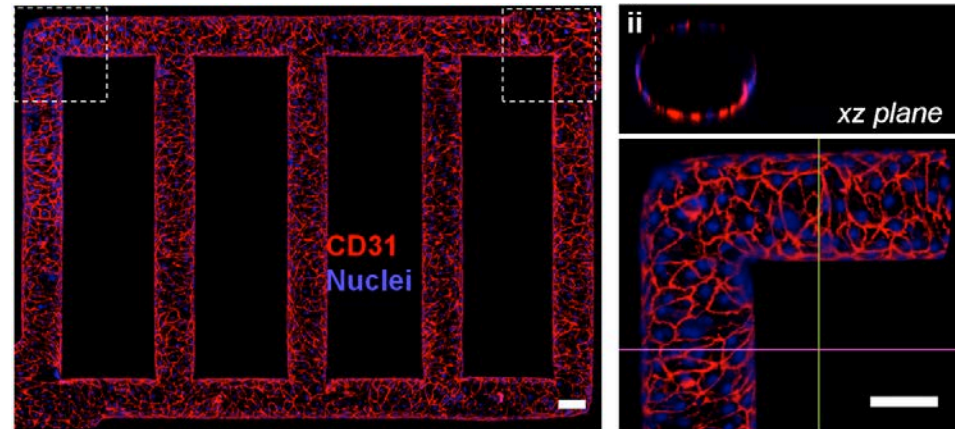
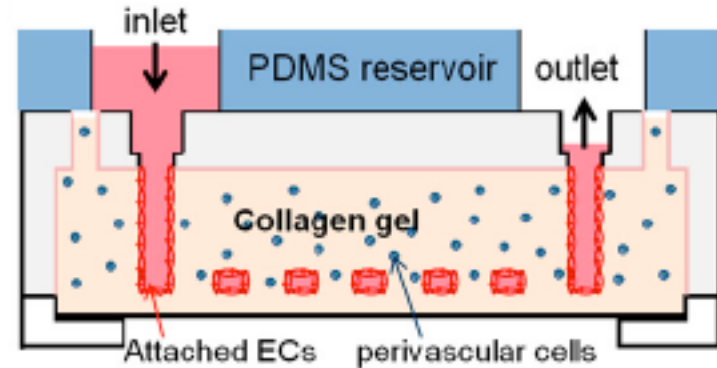
Scanning electron micrograph image of the two optically coupled optomechanical oscillators (OMOs), along with a depiction of the symmetric (S) and anti-symmetric (AS) coupled optical supermodes. The deformation illustrates the mechanical mode that is excited by the optical field.

M. Zhang et al., *arXiv:1112.3636* (2011)

In Vitro Microvessels For The Study Of Angiogenesis And Thrombosis

Microvascular networks support metabolic activity and define microenvironmental conditions within tissues in health and pathology. The Stroock group and collaborators at Cornell have used the Cornell NanoScale Facility to fabricate living microvascular networks in vitro within three-dimensional tissue scaffolds and have demonstrated their biofunctionality. The researchers formed microfluidic vessels coated by endothelial cells within a native collagen matrix; characterized the morphology, mass transfer processes, and long-term stability of the endothelium; elucidated angiogenic activities (formation of new blood vessels); and demonstrated a transition to a thrombotic (blood clotting) state during an inflammatory response. The success of these microvascular networks in recapitulating these phenomena points to the broad potential of this platform for the study of cardiovascular biology and physiology.

Stroock group and collaborators, Cornell Univ.
Work performed at the Cornell NanoScale Facility

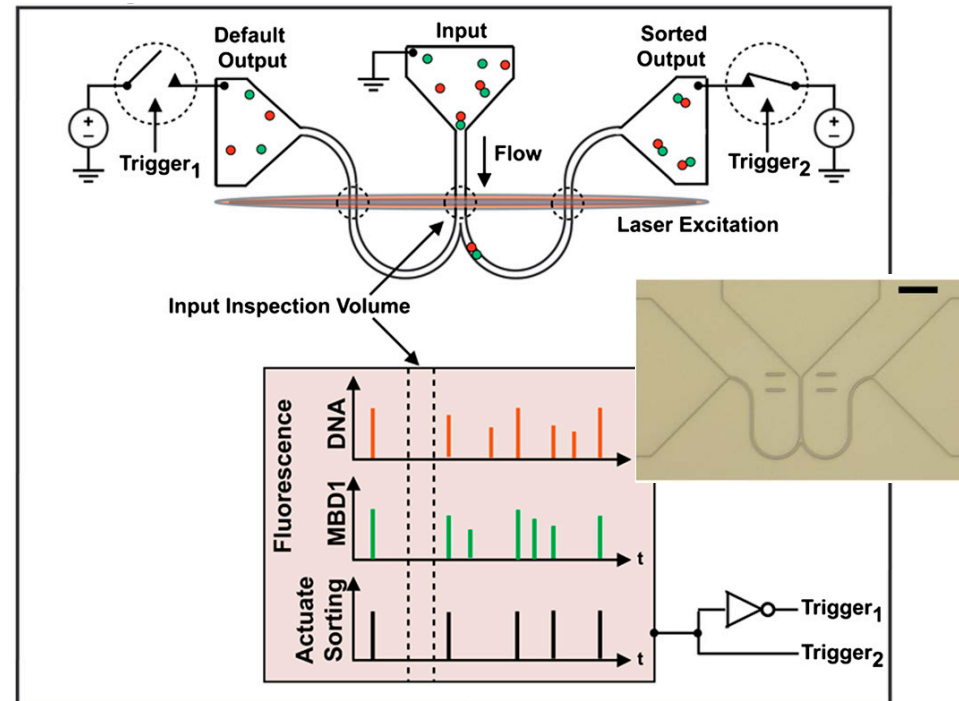


(top) Schematic diagram of microfluidic collagen scaffolds after fabrication. (bottom) Projection of horizontal confocal images of endothelialized microfluidic vessels and views of a corner section.

Y. Zheng et al., *Proc. Nat. Acad. Sci.* **109**, 9342 (2012)

Real-time Analysis Of Methylated DNA By Fluorescence-activated Single Molecule Sorting

Epigenetic modifications, such as DNA and histone methylation, are responsible for regulatory pathways that affect disease. Current epigenetic analyses use bisulfite conversion to identify DNA methylation and chromatin immunoprecipitation to collect molecules bearing a specific histone modification. Craighead group and collaborators, using the Cornell NanoScale Facility, have demonstrated a new method using a nanofluidic device that combines real-time detection and automated sorting of individual molecules based on their epigenetic state. This device evaluates the fluorescence from labeled epigenetic modifications to actuate sorting. This technology has demonstrated up to 98% accuracy in molecule sorting and has achieved postsorting sample recovery on femtogram quantities of genetic material. The functionality enabled by this nanofluidic platform now provides a workflow for color-multiplexed sorting and recovery of single molecules toward subsequent DNA sequencing.



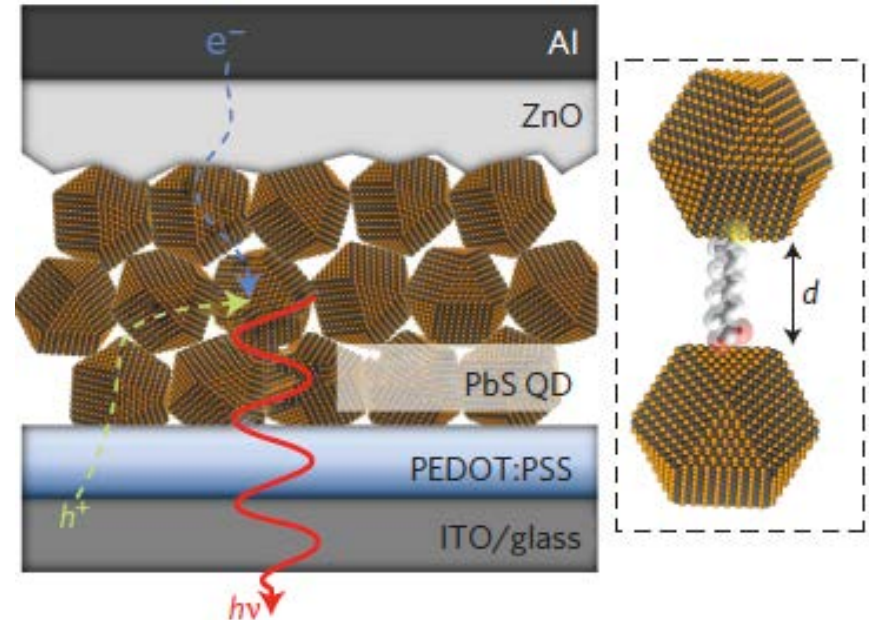
Schematic of the bifurcated nanofluidic device and the experimental scheme used for single molecule sorting. Inset shows a optical micrograph of the fluidic device.

Craighead group and collaborators, Cornell Univ.
Work performed at the Cornell NanoScale Facility

B. R. Cipriany et al., *Proc. Nat. Acad. Sci.* **109**, 8477 (2012)

Bright Infrared Quantum-dot Light-emitting Diodes Through Inter-dot Spacing Control

Infrared light-emitting diodes (LEDs) are currently fabricated from direct-gap semiconductors using epitaxy, which makes them expensive and difficult to integrate with other materials. LEDs based on colloidal semiconductor quantum dots, on the other hand, can be solution-processed at low cost, and can be directly integrated with silicon. However, so far, exciton dissociation and recombination have not been well controlled in these devices, and this has limited their performance. Wise group and collaborators at Cornell have fabricated quantum dot LEDs at the Cornell NanoScale Facility in which they tune the distance between adjacent PbS quantum dots using well-selected linker molecules. By thus optimizing the balance between charge injection and radiative exciton recombination they achieve radiances eight times higher and external quantum efficiencies two times higher than the highest values previously reported for quantum-dot LEDs. The electroluminescent powers of the best devices are comparable to those produced by commercial InGaAsP LEDs.



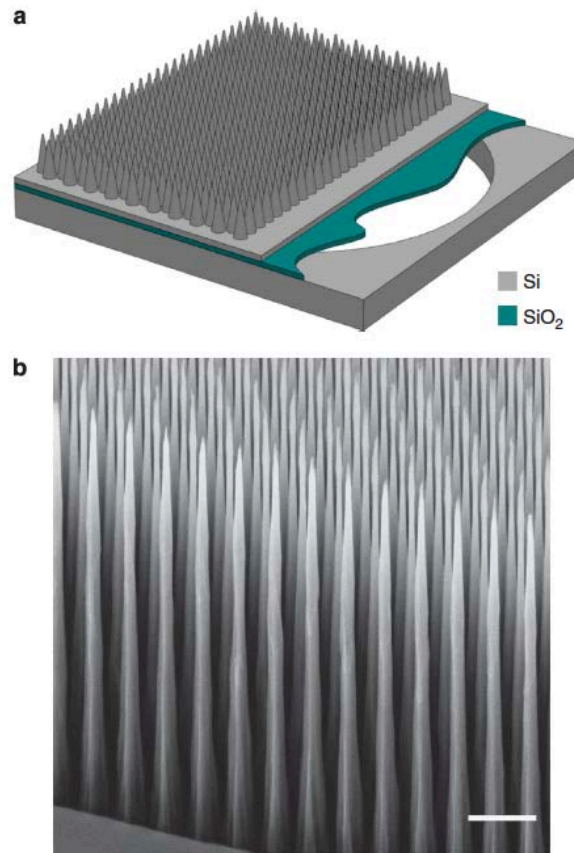
Schematic device structure of the new quantum dot LEDs, in which the distance between PbS quantum dots is controlled by well-selected linker molecules.

Wise, Hanrath, and Malliaras groups, Cornell Univ.
Work performed at the Cornell NanoScale Facility

L. Sun et al., *Nature Nanotechnology* **7**, 369 (2012)

Low-concentration mechanical biosensor based on a photonic crystal nanowire array

The main challenge for new biosensors is to achieve detection of biomolecules at low concentrations, e.g., for early-stage disease detection. The Lal group at Cornell has used the Cornell NanoScale Facility to develop a novel nanomechanical biosensor that achieves low-concentration (500 aM sensitivity) detection of DNA. This high sensitivity is achieved by covering the surface of the resonator with an ordered vertical nanowire array to enhance the surface-to-volume ratio and by designing the resonator to provide state-of-the-art mass-per-unit-area resolution. Furthermore, the nanowire array forms a photonic crystal that provides strong light trapping and absorption, enabling high-efficiency optical actuation and measurement of the resonator motion via optothermomechanical coupling. This method therefore represents a high-performance mass-detection platform technology for sensing molecules at low concentrations.



Design of the nanomechanical biosensor, consisting of an ordered array of vertical Si nanowires on top of a Si/SiO₂ membrane. Scale bar = 200 nm.

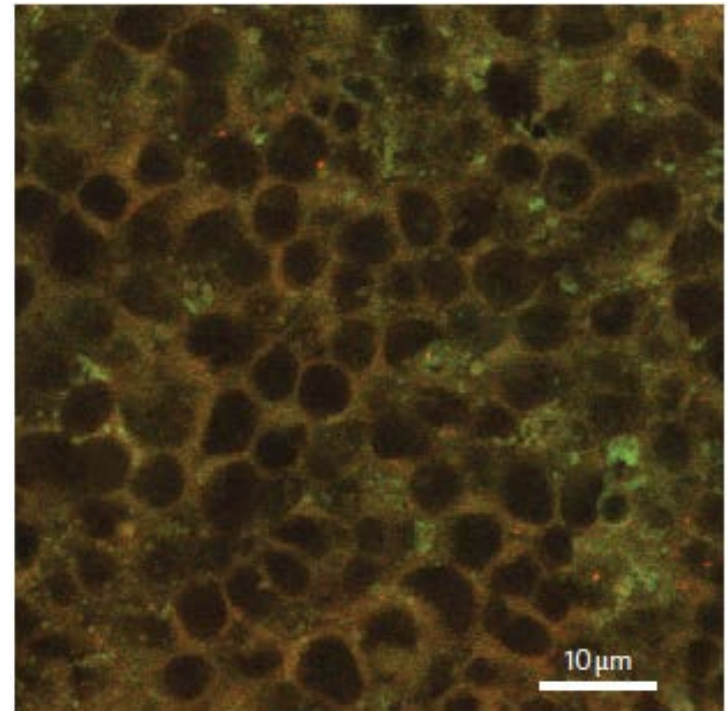
Lal group, Cornell University.
Work performed at the Cornell NanoScale Facility

Y. Lu et al., *Nature Communications* **2**, 578 (2011)

Oral Exposure to Polystyrene Nanoparticles Affects Iron Absorption

The use of engineered nanoparticles in food and pharmaceuticals is expected to increase, but the impact of chronic oral exposure to nanoparticles on human health remains unknown. The Shuler group at Cornell has used the capabilities of the Cornell NanoScale Facility to show that chronic and acute oral exposure to polystyrene nanoparticles can influence iron uptake and iron transport in an in vitro model of the intestinal epithelium. Intestinal cells that are exposed to high doses of nanoparticles showed increased iron transport due to nanoparticle disruption of the cell membrane. They confirmed these results in an in vivo chicken intestinal loop model -- chickens acutely exposed to carboxylated particles (50 nm in diameter) had a lower iron absorption than unexposed or chronically exposed birds. The agreement between the in vitro and in vivo results suggests that the in vitro intestinal epithelium model is potentially useful for toxicology studies.

Shuler group, Cornell University.
Work performed at the Cornell NanoScale Facility

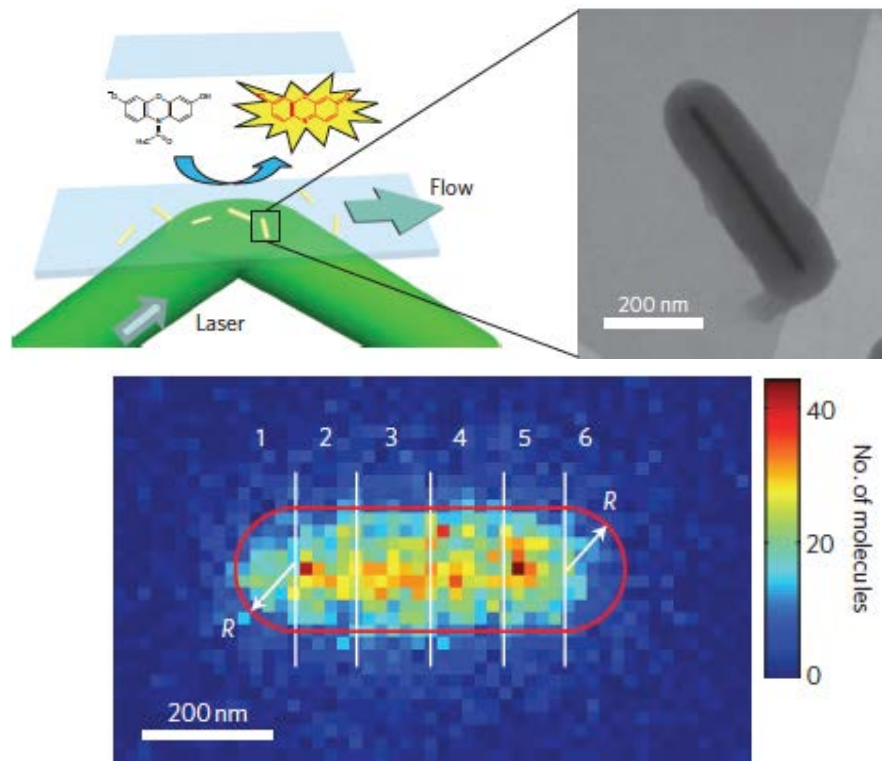


+M cell monolayer stained with CellTracker CM-Dil cell membrane stain (red) after 4 h exposure to 50 nm carboxylated polystyrene nanoparticles (green). The green particles and red cell membranes overlap, showing that the hydrophobic polystyrene particles diffuse through hydrophobic cell membranes.

G. J. Mahler et al., *Nature Nanotechnology* **7**, 264 (2012)

Quantitative Super-resolution Imaging Uncovers Reactivity Patterns on Single Nanocatalysts

Metal nanoparticles are used as catalysts in a variety of important chemical reactions and can have a range of different shapes, with facets and sites that differ in catalytic reactivity. To develop better catalysts it is necessary to determine where catalysis occurs on such nanoparticles and what sites are most reactive. The Peng Chen group at Cornell has used the capabilities of the Cornell NanoScale Facility to help quantify the catalysis of individual gold nanorods at a spatial resolution of ~ 40 nm using super-resolution fluorescence microscopy. They find that within the same surface facets on the sides of a single nanorod, the reactivity exhibits a gradient from the centre of the nanorod towards its two ends. Furthermore, the ratio of the reactivity at the ends of the nanorod to the reactivity at the sides varies significantly between nanorods. This work shows that defects on the surface of the nanorod provide the most reactive catalytic sites.



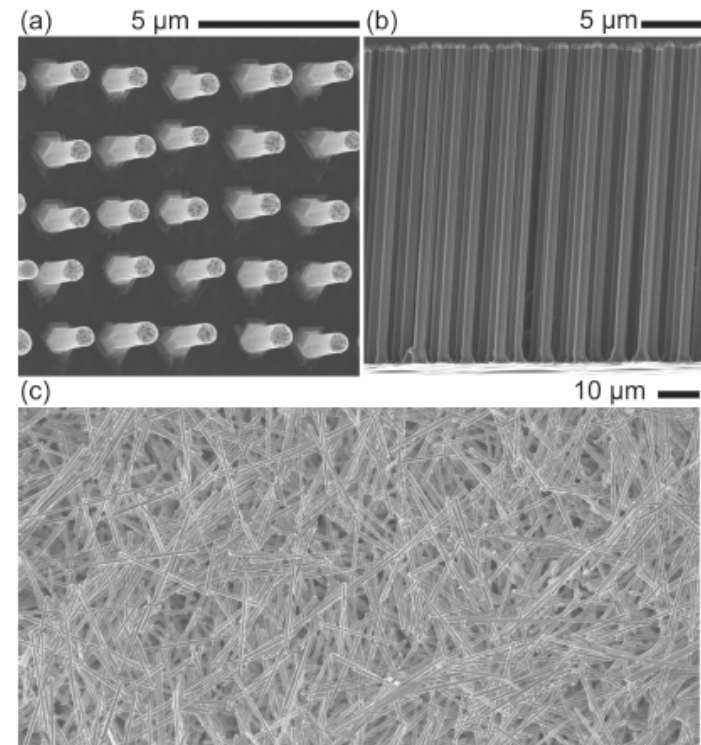
(top) Schematic of the super-resolution fluorescence microscopy technique to measure catalytic activity.
(bottom) Map of catalytic activity for a single gold nanorod.

Peng Chen group, Cornell University.
Work performed at the Cornell NanoScale Facility

X. Zhou et al., *Nature Nanotechnology* **7**, 237 (2012)

Contactless Measurement of Surface Dominated Recombination in Silicon Nanowires

The carrier lifetime is a critical parameter for the performance of many types of semiconductor devices. Semiconductor nanowires have attracted recent interest for device use due to their intrinsic nanoscale size and tunable properties, yet there has been no convenient way to measure their carrier lifetimes. The Tiwari group at Cornell has used the Cornell NanoScale Facility to measure carrier lifetimes in silicon nanowires using an extension of the classic contactless photoconductivity decay method. The samples measured consist of a thin aggregated film of oxide passivated wires that are grown using gold or aluminum catalysts. The researchers found that recombination in these wires is controlled by the surface or near surface effects, not bulk impurities. The surface controlled nature of the recombination implies larger diameter wires will offer better performance in devices that rely on minority carrier transport.



Silicon nanowires as grown (top), and after transfer to a fused silica wafer for contactless measurement of the carrier lifetime (bottom).

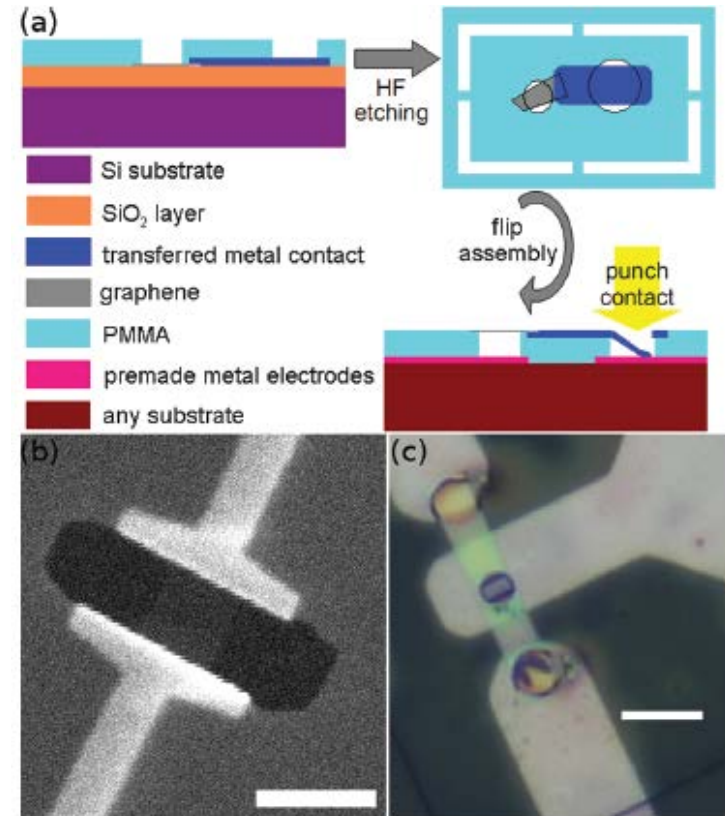
Tiwari group, Cornell University.
Work performed at the Cornell NanoScale Facility

B. A. Bryce et al., *Nano Letters* **11**, 4282 (2011)

Stamp Transferred Suspended Graphene Mechanical Resonators for Radio Frequency Electrical Readout

Graphene is a perfect two-dimensional crystal with high Young's modulus and extremely low mass, which makes it a promising material to make high-frequency, high-Q resonators for use as extremely low-mass sensors and for studies of mechanical resonance at the quantum limit. However, to scale graphene resonators to the 1 micron scale and below using electrical readout requires a fabrication technique capable of integrating graphene with low-capacitance electrodes. The Craighead and Parpia groups at Cornell have used the Cornell NanoScale Facility to develop a simple micromanipulation technique to transfer suspended graphene flakes onto any substrate and to assemble them with small localized gates into mechanical resonators, thereby achieving electrical readout with resonance frequencies up to 178 MHz.

Craighead and Parpia groups, Cornell University.
Work performed at the Cornell NanoScale Facility

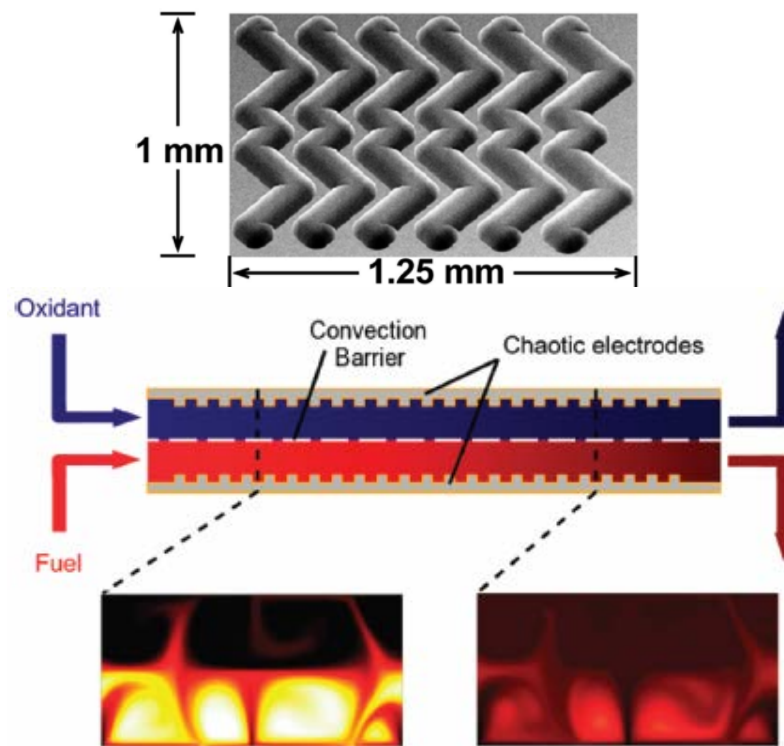


Process for making suspended graphene structures on any substrate using a PMMA stamp, with examples of completed devices. Scale bar is 1 μm in (b) and 5 μm in (c).

X. Song et al., *Nano Letters* **12**, 198 (2012)

Membraneless, Room-Temperature, Direct Borohydride/Cerium Fuel Cell with Power Density Over 0.25 W/cm²

The widespread adoption and deployment of fuel cells as an alternative energy technology have been hampered by a number of formidable technical challenges, including the cost and long-term stability of electrocatalyst and membrane materials. The Abruña and Stroock groups at Cornell have used the Cornell NanoScale Facility to develop a microfluidic fuel cell that overcomes many of these obstacles while achieving power densities in excess of 250 mW/cm². The poisoning and sluggish reaction rate associated with CO-contaminated H₂ and methanol are averted by employing the promising, high-energy density fuel borohydride. Expensive, ineffective membrane materials are replaced with laminar flow and a nonselective, porous convection barrier to separate the fuel and oxidant streams. The result is a room-temperature fuel cell that has the highest power density per unit mass of Pt catalyst employed for a non-H₂ fuel cell, and exceeds the power density of a typical H₂ fuel cell by 50%.



The new fuel cell design incorporates grooved electrodes, which induce chaotic flow to separately mix the fuel and oxidant solutions. The flow creates separate convection cells in the fuel and oxidant streams that are stirred symmetrically.

Abruña and Stroock groups, Cornell University.
Work performed at the Cornell NanoScale Facility

N. Da Mota et al., *J. Am. Chem. Soc.* **134**, 6076 (2012)

Controlled Photonic Manipulation of Proteins and Other Nanomaterials

A new approach to near-field optical trapping that produces a near neutral thermal background was demonstrated by the Erickson group at Cornell Univ. using specially designed silicon nitride photonic crystal (PhC) resonators fabricated at the Cornell NanoScale Facility. The researchers controlled the trapping and release of 22 nm polymer particles, quantum dots (QDs), and proteins with a temperature increase of less than 0.3 K, small enough prevent damage to trapped biomolecules. To reduce the temperature rise and heating-induced fluid mechanical effects that can prevent trapping, silicon nitride was used to fabricate the devices instead of silicon to enable operating the PhC resonators with 1064 nm light. At this wavelength the optical absorption of water is 2 orders of magnitude lower than that at 1550 nm, the wavelength commonly used in silicon-based nanophotonic devices.

Erickson group, Cornell Univ.
Work performed at Cornell NanoScale Facility

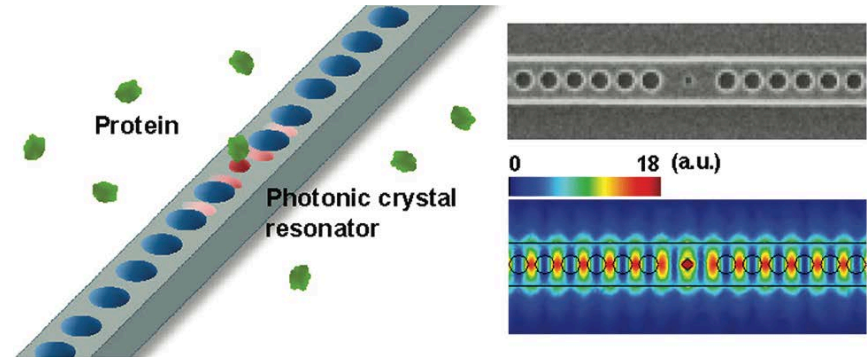
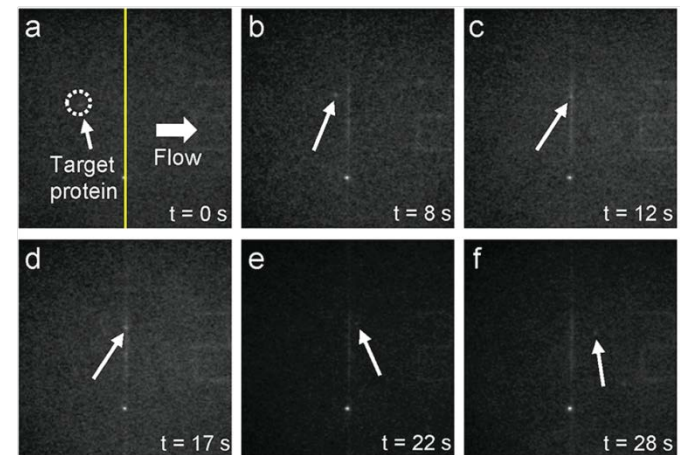


Diagram and scanning electron microscope image of a silicon nitride PhC resonator.



(a-d) Cy5-labeled Wilson disease proteins (indicated by arrows) are trapped when they arrive at the vicinity of an optically excited resonator. (e,f) The proteins are released from the resonator when the laser is switched off.

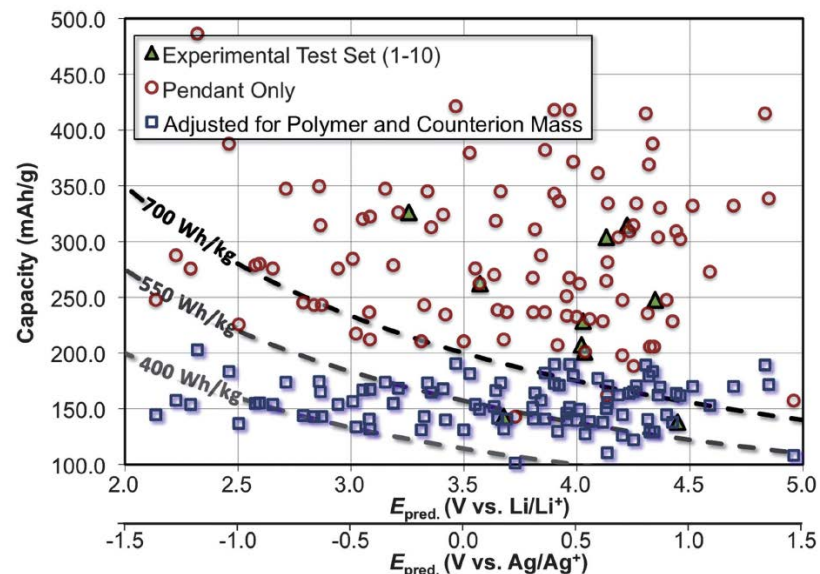
Y-F. Chen, et al., *Nano Lett.* **12**, 1633 (2012).

Tailored Redox Functionality Of Small Organics For Pseudocapacitive Electrodes

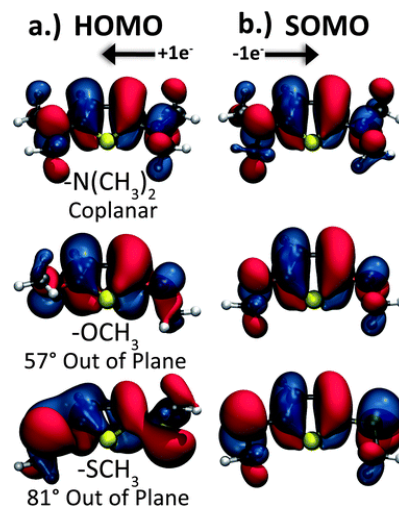
In order for intermittent alternative energy sources like solar and wind to be successful, we need to develop new energy storage systems that have high energy and power densities and that are also inexpensive. Organic materials like conducting polymers for have received a great deal of interest due to the fact that (1) the material properties can be tuned through chemistry and (2) the source materials are light weight and cheap.

In this work, researchers at Cornell have undertaken a systematic theoretical exploration of ~100 compounds to screen for possible high energy density organics. By combining knowledge from these simulations with experimental electrochemical data, the researchers have been able to establish structure-property relationships which should guide in the development of new organic energy storage systems.

Stephen Burkhardt, Michael Lowe et al., Cornell
Simulations performed at Cornell NanoScale Facility



Screening results for experimental and theoretical energy storage pendants.



Isodensity surfaces of (a) the HOMO for each substituted thiophene and (b) the SOMO for each substituted thiophene. Greater coplanarity of the donor group is consistent with greater electron donating strength of the substitution.

Energy Environ. Sci. **5**, 7176 (2012).

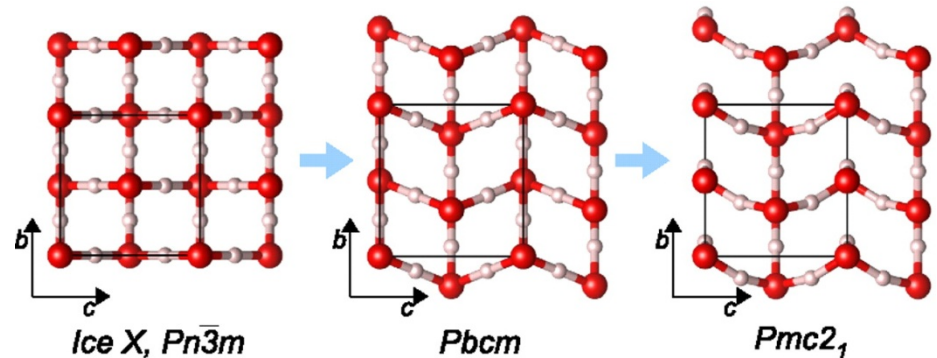
High Pressure Ices

The crystalline or ice forms of H₂O has drawn the interest of scientist for decades. The phase diagram of H₂O exhibits a wide range of stable and meta-stable ices. Previous studies have also predicted that high pressure ices could be metallic, which could have important implications for planetary models for Neptune or Uranus.

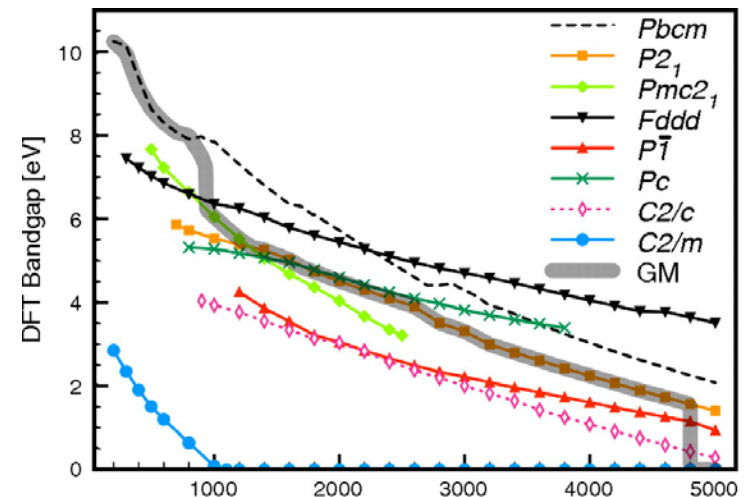
A typical challenge of material science is the large number of crystalline phases that need to be explored to find the minimum energy structures. In this work, the Hoffmann group at Cornell University used a genetic search algorithm, XtalOpt coupled with density functional calculations to explore this vast parameter space. This study found new stable high pressure ice phases. They also found that ice does not become metallic until much higher pressures that previously predicted by other groups.

Hoffmann group at Cornell
Simulations performed at Cornell NanoScale Facility

A. Hermann, N. W. Ashcroft, R. Hoffmann
Proc. Natl Acad. Sci. PNAS **109**, 745 (2012).



Different ice crystal phases predicted at 700 GPa. The $Pmc2_1$ becomes stable in the regime from 1-1.3TPa. As pressure increases, water ice transform from a 3D interpenetrating network to two-dimensional corrugated sheets.



Band gap energy for various ice phases as a function of pressure. The metallic phase ($C2/m$) does not become stable until 4.8 TPa.

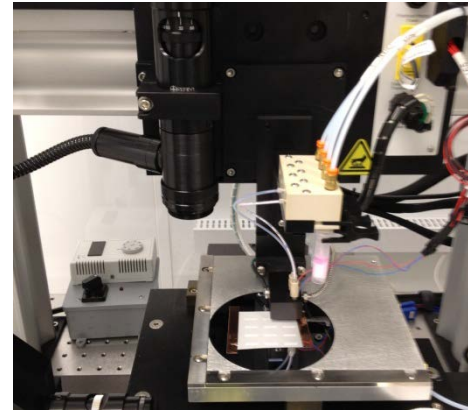
Georgia Tech

Biomolecule Inkjet Printing: Tissue Engineering of a Ligament

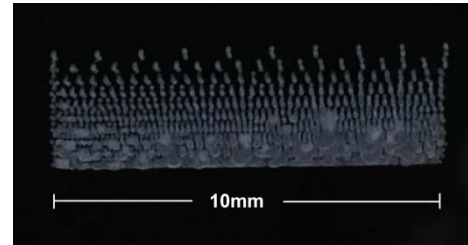
This investigation incorporates the fabrication of a tissue scaffold designed to support unique, hierarchical cellular development for use in studies of a bioengineered ligament and bone-ligament interface. Biomolecule deposition via the JetLab II inkjet printing system is utilized to immobilize various bioinks on an aligned fibrous polymer matrix, creating hierarchical, spatially organized structures that are capable of inducing zone-specific cellular responses.

To date, nanoscale particles of hydroxyapatite have been printed over a spatial distribution gradient on an aligned, electrospun poly(lactic) acid fiber tissue scaffold. This morphology is mimetic of the gradual increase in cellular mineralization as the ligament transitions into bone. Future studies will include the addition of bioinks comprised of various growth factors and additional biological response modifiers to further promote hierarchical cellular development.

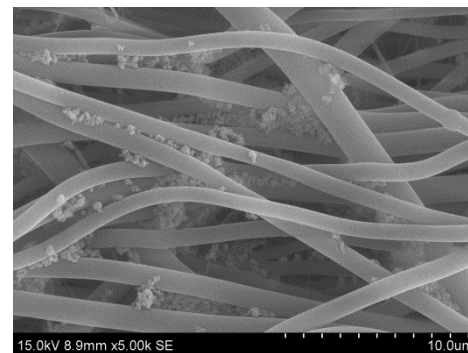
Andrew Uehlin and Derrick Dean, University of Alabama at Birmingham
Work performed at Georgia Tech Institute for Electronics and Nanotechnology



JetLab II inkjet printer deposition of a nano-hydroxyapatite bioink on an electrospun poly(lactic acid) tissue scaffold



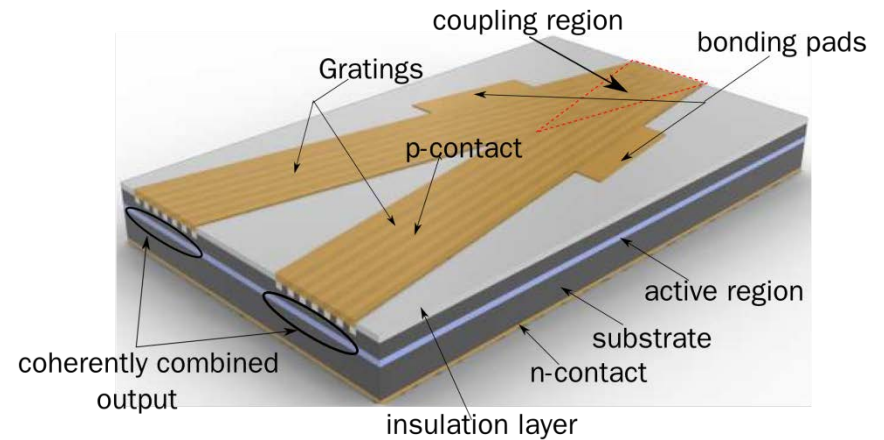
Spatial distribution gradient of nano-hydroxyapatite printed by the JetLab II on a silicon substrate



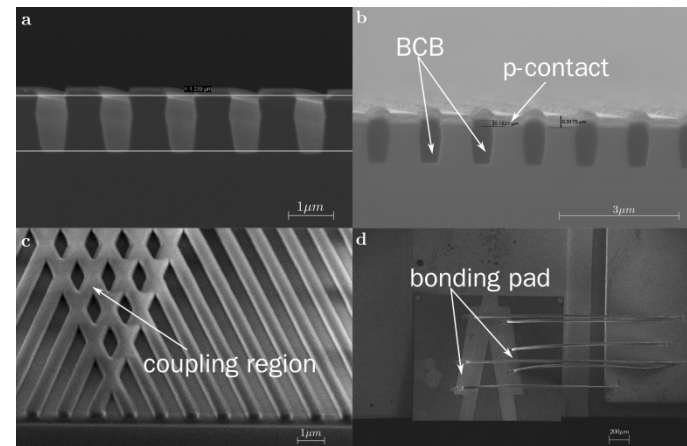
SEM image of deposited nano-hydroxyapatite particles on electrospun poly(lactic acid) fibers (5000X magnification)

On-chip coherently combined angled grating broad-area laser

The on-chip coherently combined angled grating broad-area laser is aimed to provide high power and high brightness light output. The laser structure is built on angled grating broad-area lasers which are coherently combined monolithically by a 2D coupling region. The observed interference patterns of two output ports confirm the coherent combination in our laser design. The whole laser chip is fabricated in GT IEN Centers. The gratings are defined by an advanced JEOL 9300 EBL system and then transferred to an InP-based MQW wafer by dry etching.



Schematic plot of the laser chip



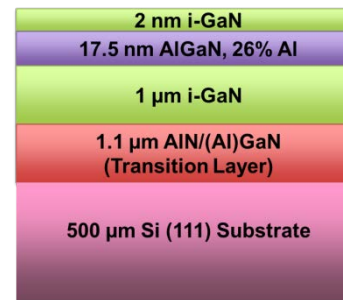
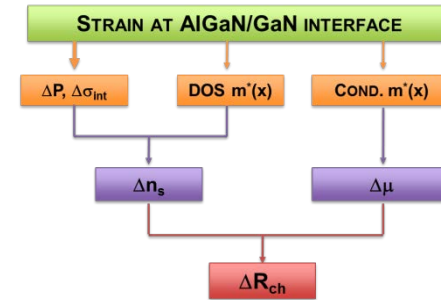
SEM images at different fabrication phases. Last figure shows a completed laser device after die bonding and wire bonding.

Yunsong Zhao and Lin Zhu, Clemson University
Work performed at Georgia Tech Institute for
Electronics and Nanotechnology

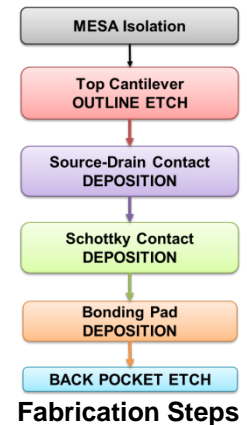
Ultrasensitive III-V Nitride Piezoresistive Microcantilevers for Sensing Applications

The goal of this project is to develop III-V Nitride microcantilever based sensors for chemical and bio-molecule detection. The technical advantages of this include utilization of piezoelectric properties of AlGaIn/GaN heterostructure, non-contact potentiometric sensing using microcantilever enclosed in vacuum, and standoff/non-invasive detection of analytes based on photoacoustic principles. Accomplishments include successful development of III-V Nitride microcantilevers with extremely high gauge factor of >3500 and demonstration of highly sensitive ultrasonic sensor with sub nm detection capability. We have also developed a surface work function based molecular detection using cantilever resonant amplitude and demonstrated a unique 2-dimensional signature extraction for analytes resulting in analyte detection using non-contact potentiometry or photoacoustic spectroscopy .

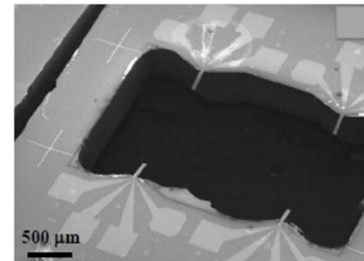
Abdul Talukdar , Muhammad Qazi, and Goutam Koley,
University of South Carolina
Work performed at Georgia Tech Institute for
Electronics and Nanotechnology



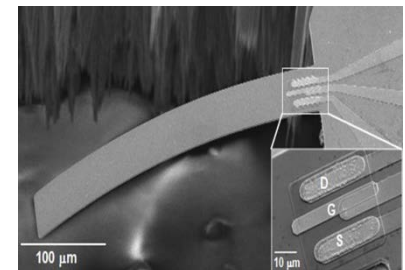
Layers on Wafer



Fabrication Steps



SEM Image of Sensor Array with 4 Microcantilevers

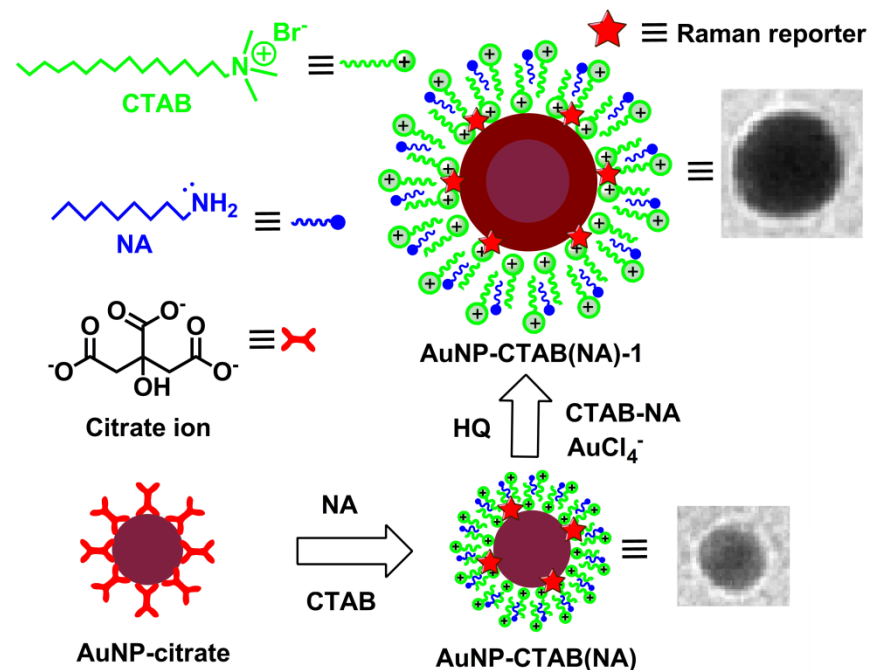
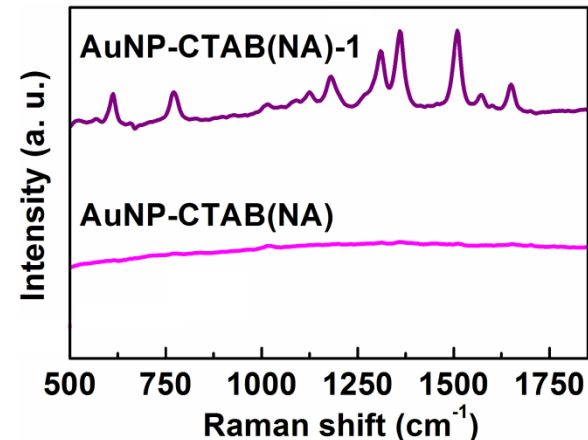


SEM Image of the fabricated GaN Microcantilever (350 × 50 × 2 μm³) Sensor with AlGaIn/GaN HFET at the base

Nanoparticles Surface Modification, Seed Growth and SERS Activity

We surface modified the classical citrate capped gold nanoparticles (AuNPs) with a surfactant bilayer along with a partially hydrophobic amine. These AuNPs were further grown to an optimum size by seed growth method. The larger AuNPs serve as SERS substrates to identify hydrophobic dye molecules in solution. Particles were characterized by FTIR, UV-Vis, DLS, and TEM.

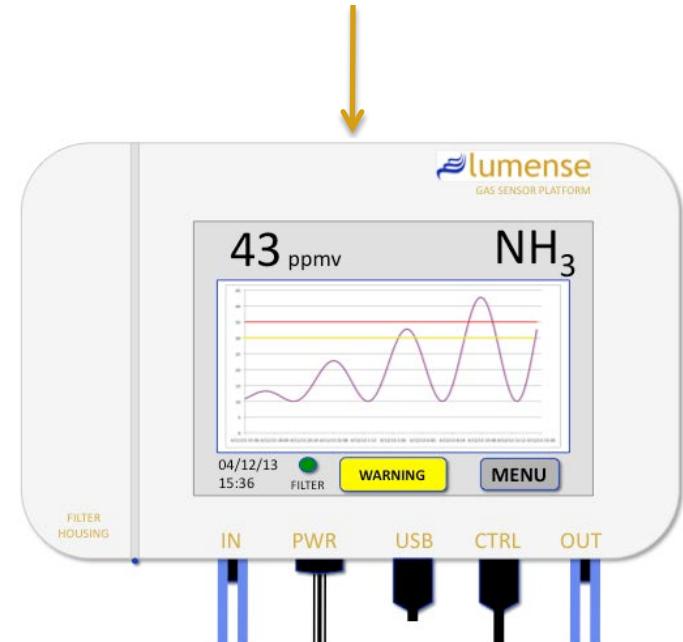
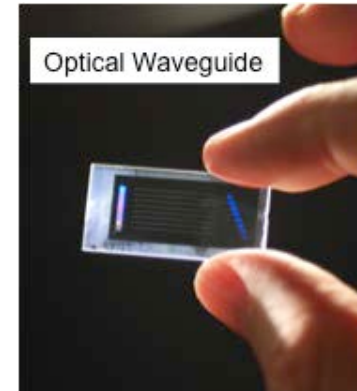
Bharat Baruah, Carl Craighead, and Caleb Abolarin,
Kennesaw State Univ. and Cornell
Work performed at Georgia Tech Institute for
Electronics and Nanotechnology.



Lumense Interferometric Sensor

Lumense offers chemical and biological sensors based on technology derived from \$20 million in research spending over 20 years at the Georgia Tech Research Institute. The core of the technology is an optical waveguide which has coatings that modify the speed of light in the waveguide. The platform technology works for a wide range of targets, is highly specific, and has important attributes which include: Continuous, real-time, accurate, gas and liquid phase (air, water, CO₂, oil, blood,...), in-situ, point-of-use solution, in-line, on-line, automated, scalable, and low cost.

Janet Cobb-Sullivan and Ken Johnson, Lumense
Work performed at Georgia Tech Institute for
Electronics and Nanotechnology



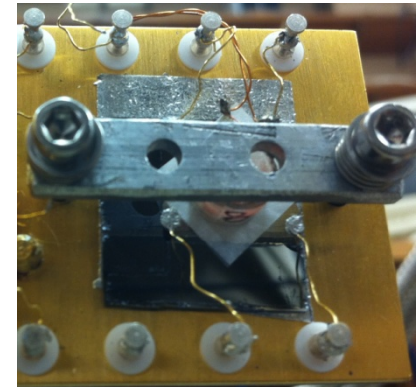
Nb/Ni Bilayers: Superconductivity

The purpose of this research is to study the upper critical field of S/F (superconductor/ferromagnet) bilayers and see how it varies in comparison to how the transition temperature varies. Films were grown by magnetron sputtering, with film thicknesses measured at the IEN at Georgia Tech.

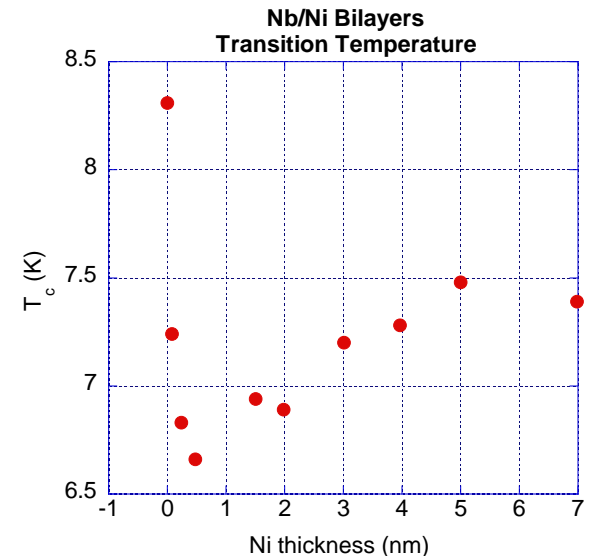
Films were measured both resistively and inductively as a function of both temperature and magnetic field. Niobium thickness was held at 33 nm, and Nickel thickness was varied from 0 to 8 nm.

Tim Ahrenholz, Emily Davis and Phillip Broussard,
Covenant College
Work performed at Georgia Tech Institute for
Electronics and Nanotechnology

At right we show the film with leads and coil in place to measure film properties at low temperature.



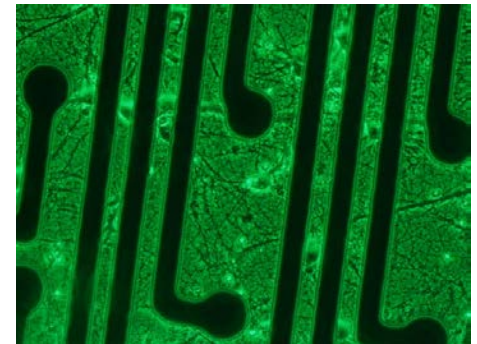
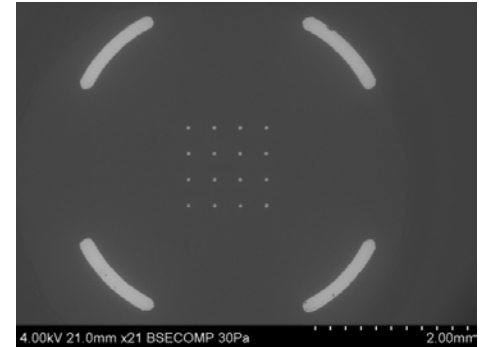
Critical temperature follows the nonmonotonic behavior of Usadel theory.



In-vitro High-Throughput Microelectrode Arrays

Axion BioSystems is a start-up company based on Georgia Tech campus that develops and manufactures *in-vitro* Microelectrode Arrays (MEAs) – single well and high-throughput for screening of compounds, drugs, toxins, environmentally-harmful materials, nanoparticles etc.

Axion is currently focused on advanced prototyping and low volume manufacturing of 12-well MEAs (based on glass-MEMS technologies) and 48-well MEAs (based on polymer-MEMS technologies). Both platforms provide 768 microelectrodes distributed in an ANSI-compliant plate area for recording and stimulation (from electrically active cells) with nano-porous surface coatings for low-impedance performance. These MEAs have also been characterized with various cell lines – rat cortical neurons, human iPS stem cells and cardiomyocytes for electrical performance.



Polymer-MEMS fabrication and packaging technologies are utilized to build 48-well MEAs (top); Glass-MEMS fabrication and packaging technologies are utilized to develop 12-well MEAs (bottom); Rat cortical neuronal cell cultures on 12-well MEAs (bottom right)

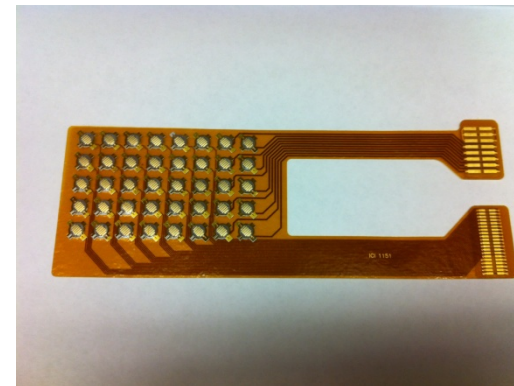
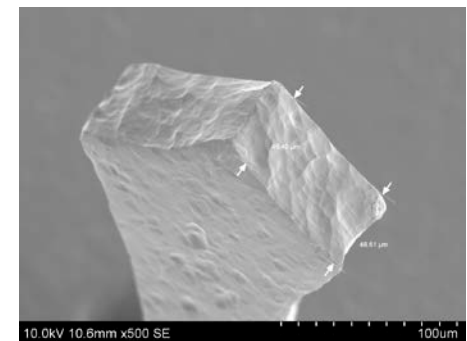
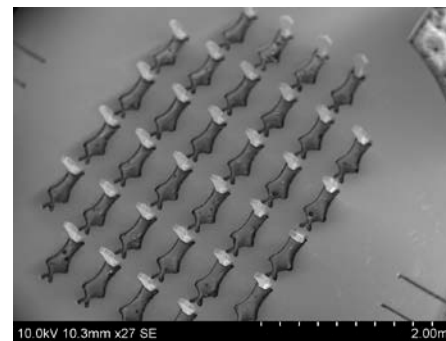
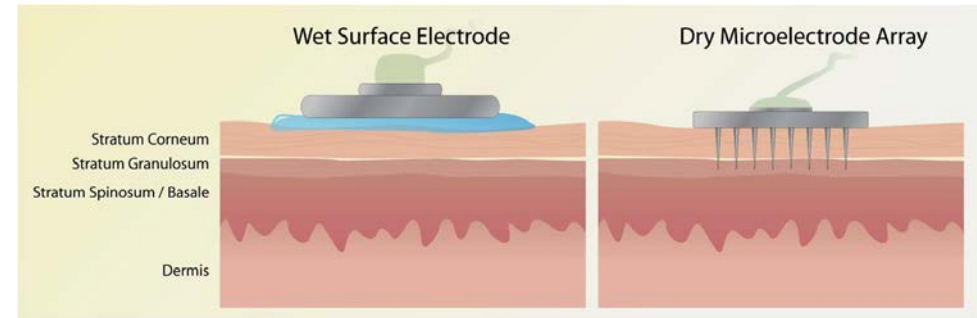
Chandana Karnati, Ricardo Aguilar, Colin Arrowood, Robert Grier and Swaminathan Rajaraman, Axion BioSystems Inc.
Work performed at Georgia Tech Institute for Electronics and Nanotechnology

NNIN is supported by NSF ECCS-0335765

“On-the-body” Microelectrode Arrays

In addition to developing and manufacturing *in-vitro* MEAs, Axion is developing “on the body” MEAs and implantable MEAs. Both of these projects are in early stage R&D.

The “On the body” MEAs are targeted specifically at detection and tracking of neuropathies like Carpal Tunnel Syndrome, ALS, Guillian Barre etc. Traditional electrodes for such a diagnostic application are large “skin-surface” electrodes that ineffectually overcome the skin impedance problem posed by the high impedance *stratum corneum* (SC) layer. Axion has developed proprietary technologies for 3-D microneedle-type electrodes that can penetrate the SC-layer in a minimally invasive fashion providing a low impedance pathway for electrical signals. Additionally we have developed packaging technologies through which these 3-D microneedle electrodes are arrayed on a flexible Kapton patch.



Concept of a microneedle-type 3-D electrode (top); SEMs of MEAs (middle); flexible Kapton patch with 3-D microelectrodes (bottom).

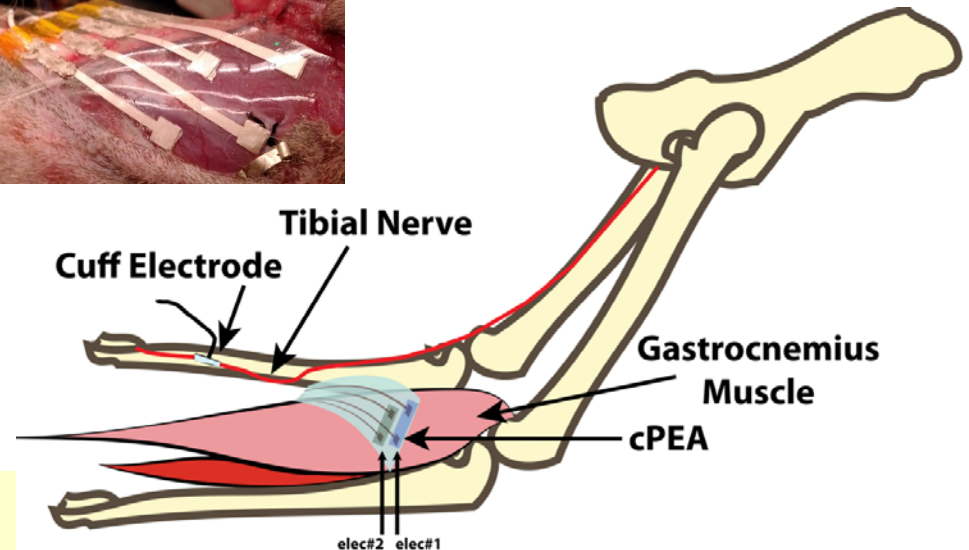
Chandana Karnati, Ricardo Aguilar, Robert Grier and Swaminathan Rajaraman, Axion BioSystems Inc.
Work performed at Georgia Tech Institute for Electronics and Nanotechnology

Implantable Microelectrode Arrays

A third area where Axion is developing new MEA technologies is in implantable microelectrodes.

In order to enable activation of *soft* muscle tissue over a large area with high spatial resolution, new microelectrode arrays are required. These MEAs need to be built on non-standard, soft materials which can match the Young's modulus of the muscles. Most common microfabrication substrates (silicon, glass etc.) are several orders of magnitude stiffer than muscles. Most softer materials (e.g. PDMS) are difficult to work with in high-vacuum, high temperature environments. So we are developing novel materials (e.g. conductive PDMS) and unique topographies that can enable such implantable MEAs. These MEAs, unlike their stiffer counterparts can provide activation capabilities without damaging muscle tissue.

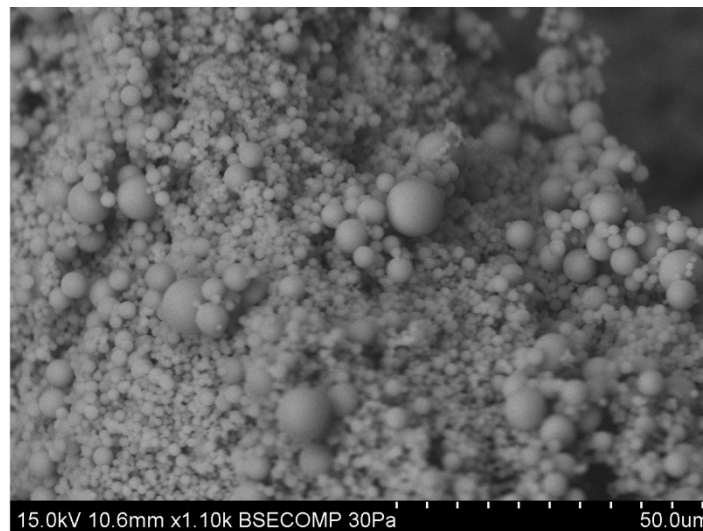
Gareth Guvanasen*, Stephen DeWeerth*, Richard Nichols* and Swaminathan Rajaraman, Axion BioSystems Inc. and *Georgia Tech
Work performed at Georgia Tech Institute for Electronics and Nanotechnology



Optical images of a conductive PDMS implantable MEA (top); Schematic and optical image of an implanted cPDMS array in the gastrocnemius muscle of a cat.

Analysis and Characterization of Albumin and Dextran Microparticles Carrying Encapsulated Membranes

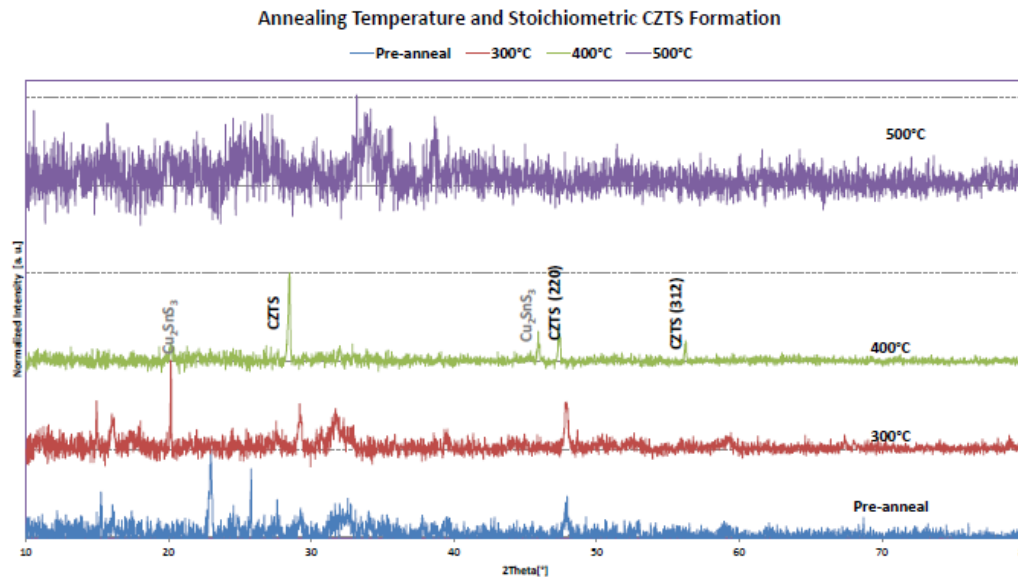
Cancer's central feature of immune escape presents a problem yet to be solved. In an attempt to create a novel cancer vaccine system, a murine T-cell lymphoma cell line was grown in mass and lysed to yield tumor membranes. These tumor membranes were then encapsulated in cyclodextrane or cross-linked albumin microspheres. To ensure that the encapsulation of tumor membranes did not interfere the geometry or size of the microspheres vpSEM was conducted. The micrographs show that the encapsulating tumor membranes does not affect the geometry nor does it affect the size drastically.



Periyasami Selvaraj and Sanjay Srivatsan, Emory University
Work performed at Georgia Tech Institute for Electronics and Nanotechnology

Development of Low Cost, Efficient CZTS Thin Films and Solar Cells

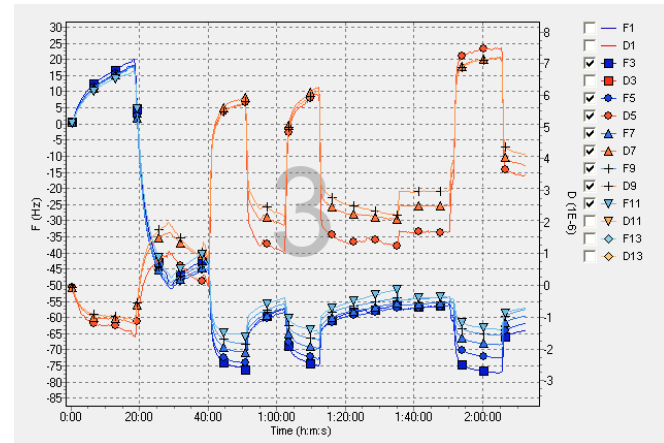
Copper zinc tin sulfur ($\text{Cu}_2\text{ZnSnS}_4$) CZTS polycrystalline thin films were prepared by a non-vacuum liquid-based coating method enabling the fabrication of high efficiency, low cost and toxicity solar cell devices. A particle solution (slurry) was developed using the CZTS constituents, varying the range of composition ratios to achieve a stable stoichiometric kesterite CZTS crystal lattice structure.



C. Burke, J. Waters, R. Williams, T. Mosely, A. Love, G. Setgum, E. Jones, B. Jones, and Deidra R. Hodges, Southern Polytechnic State University
Work performed at Georgia Tech Institute for Electronics and Nanotechnology

Development of Stroke Sensors

This work reports on a complementary use of surface of quartz crystal microbalance with frequency & dissipation monitoring (QCM) technologies to study interactions between a peptide antigen and polyclonal antibodies, in an experimental format suitable for diagnostic assays. In the chosen model, a synthetic antigen-peptide or their antibody (Ab) were immobilized to QCM sensors. The optimization of antigen and Ab amounts yielded in surface saturation within 3-5 min at 2-10 nm self-assembled monolayers respectively. Bound to golden surface antigen/Ab were stable beyond 1 month (stored at +4°C). The antigen-antibody binding were specific for both sensor types and demonstrated corresponding binding ratios.

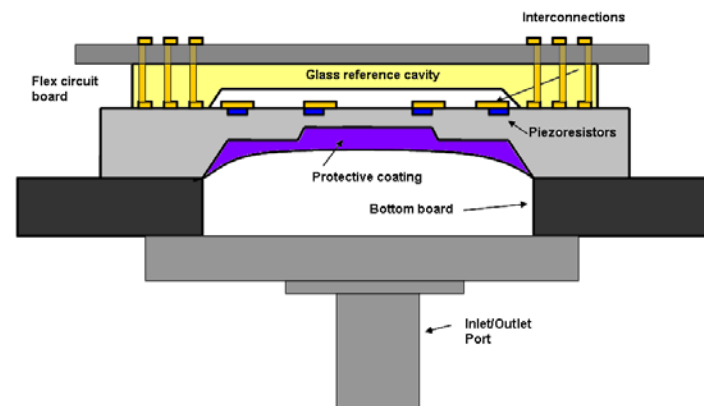


Svetlana A. Dambinova, Galina A. Izykenova, and Arthur Bagumyan, Kennesaw State University and CIS Biotech, Inc.
Work performed at Georgia Tech Institute for Electronics and Nanotechnology

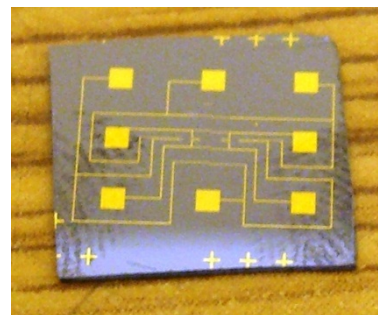
Harsh Environment Packages for N/MEMS Ocean Sensors

The major goal of this project is to develop systems that allow measurement of significant and complementary ocean parameters throughout large volumes and over large time spans. The approach is to design and fabricate temperature-compensated reinforced depth sensor array (up to 500 m of water with better than 0.01% resolution). And further evaluate protective materials/coatings to withstand harsh environment. Our ultimate aim is to develop an application-specific system-in-package. Currently, our goal is to investigate the design and development of a harsh environmental packaging scheme for micro-sensors and systems deployed in the ocean.

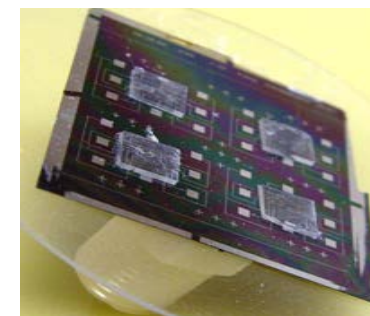
Shyam Aravamudhan and Paul Joseph, North Carolina A & T State University and Georgia Tech
Work performed at Georgia Tech Institute for Electronics and Nanotechnology



System-level packaging of reinforced depth sensors



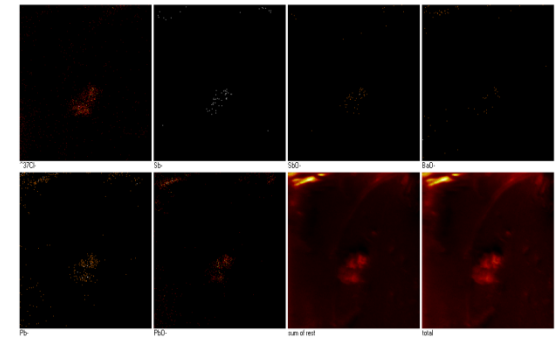
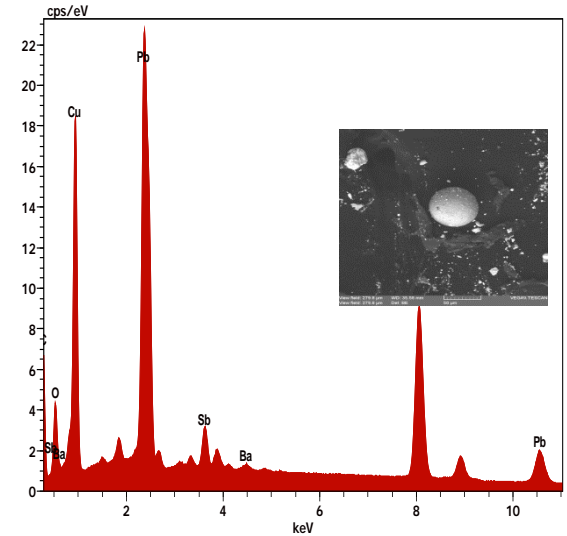
Zeroth-level package



Array of depth sensors with protective package

Surface Chemistry of Gunshot Residue Particles

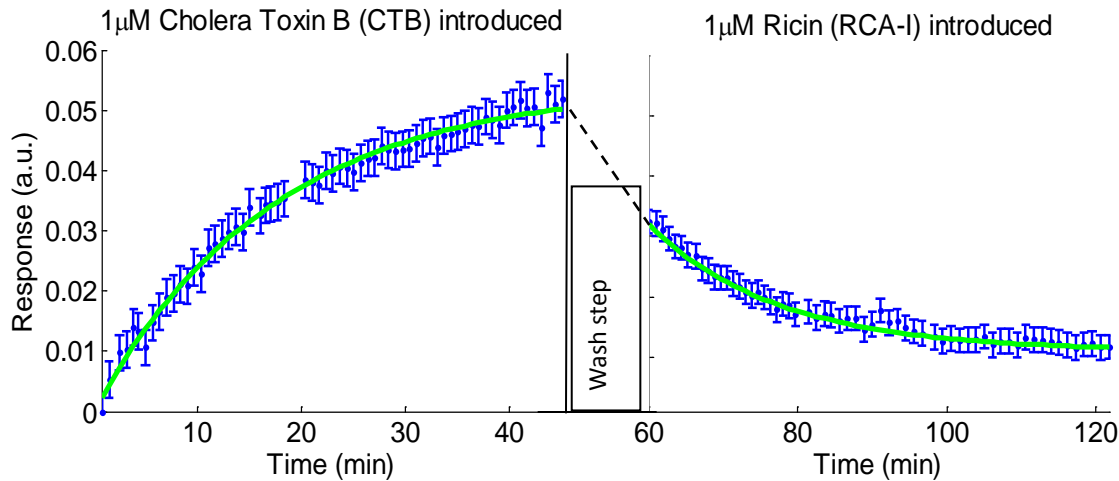
The research presented here is a study of gunshot residue (GSR) discharged by 0.22 Remington Gold ammunition. SEM-EDX is used to detect the morphology and chemical composition of the discharged particles. Spherical and non-spherical particles in the size range of 3-50 μm are observed and their compositions are examined using EDX. Composition varies with the size and shape of the particles. Combination of Lead (Pb), Barium (Ba) Antimony (Sb) or Pb, and Ba are found and characterized as GSR particles. The same specimens are further subjected ToF SIMS analysis with a view to identify the respective surface chemistry, molecular nature and molecular mass of the GSR particles. Secondary ion mass spectrum and the image analysis are carried out for selected particles. The mass peaks of oxides of lead, barium and antimony apart from the elemental masses are found. The combination of Pb/Ba/Sb and their oxides in a particular particle specifically establish the characteristics of a typical GSR particle.



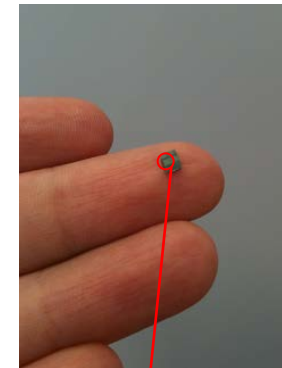
Zachariah Oommen and Paul Joseph, Albany State University (GA) and Georgia Tech
Work performed at Georgia Tech Institute for Electronics and Nanotechnology

Multiplexed Toxin Detection Using Glycans

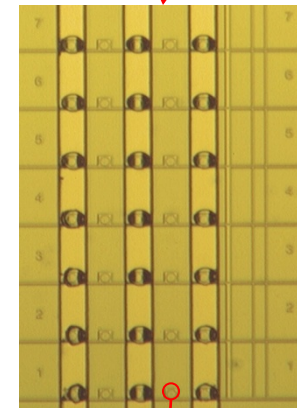
On-chip multiplexed photonic sensors benefit from sensitive monitoring, high multiplexing capability, miniature size, and low-cost mass manufacture. Si wafer serves as the support for a silicon nitride thin film (240nm) sitting on silicon dioxide substrate. The fabrication and immobilization of surface receptors are performed at IEN. The fluidics delivery system will be subsequently bonded on top. Glycans (provided by R. Cummings at Emory) serve as surface receptor to enable multiplexed toxin detection.



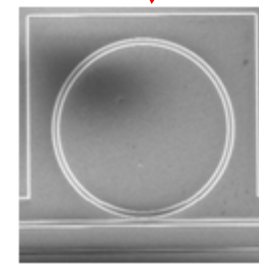
Farshid Ghasemi, Ali Adibi and Richard D. Cummings, Georgia Tech, Emory
Work performed at Georgia Tech Institute for Electronics and Nanotechnology



A Silicon Nitride on-chip sensor, fabricated at IEN.



Microscope micrograph of the sensor array.



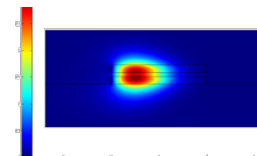
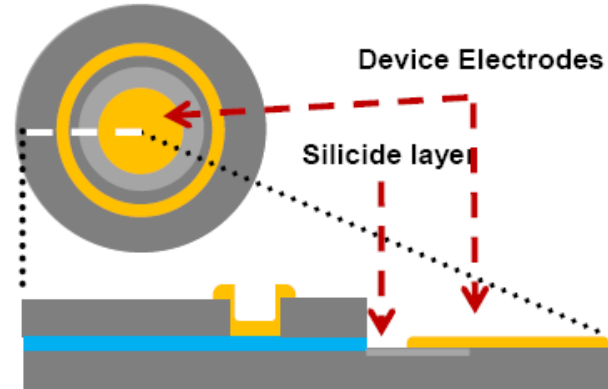
SEM of the silicon nitride microring sensor.

5µm

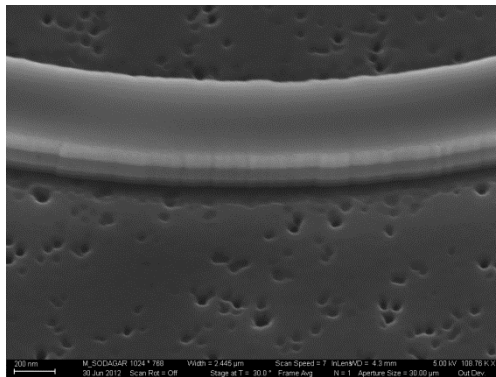
Accumulation Based Modulator

The purpose of the Accumulation Mode modulator is to achieve a high-speed low-power optical modulator for telecommunication wavelengths.

The outcome of this research will have a great impact to both on-chip data communication and high speed communication network.

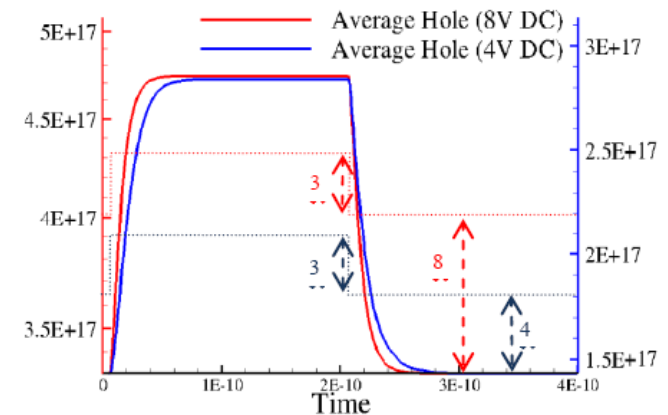


Top image and cross-section of the modulator device along with the optical field. The isolator layer in this case is SiO₂ film



Resonator etched on an SOI-SOI bonded sample

Majid Sodagar, Ali A. Eftekhari, and Ali Adibi, Georgia Tech Work performed at Georgia Tech Institute for Electronics and Nanotechnology

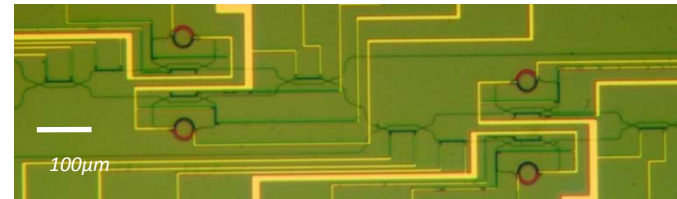


The variation in the average concentration of the electrons and holes in the modulator by applying a pulse voltage with an amplitude of 3V for two different bias voltages (4 V and 8 V).

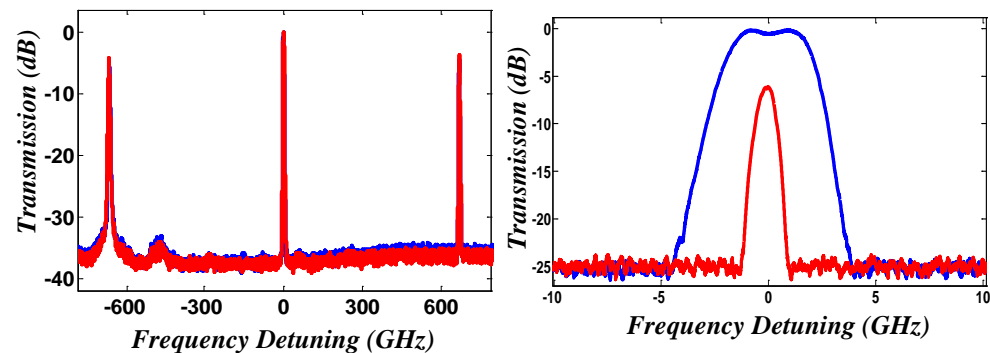
Reconfigurable RF-Photonic Filters for Silicon-On-Insulator (SOI) Platform

The purpose of this project is to utilize high-quality-factor (Q) microdisk resonators as optical delay lines in order to implement integrated photonic filters on SOI, which are both compact (total area < 0.25 mm²) and low-loss. Sub-micro-second reconfiguration is achieved through the thermo-optic effect by means of metallic micro-heaters, and the filter architecture is designed to allow for full control over the placement of poles and zeroes, thereby resulting in the full reconfigurability of the filter response. The wide bandwidth and high tunability of integrated photonic chips make them suitable as a part of RF signal processing systems through an E-O-E arrangement.

P. Alipour, A. A. Eftekhar, A. H. Atabaki, Q. Li, S. Yegnanarayanan, C. K. Madsen, and A. Adibi, Georgia Tech and Texas A&M University
Work performed at Georgia Tech Institute for Electronics and Nanotechnology

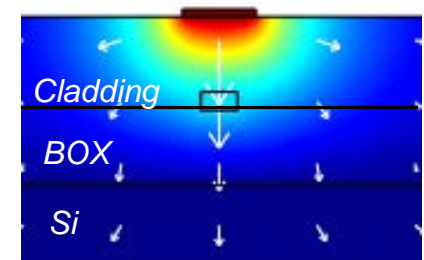


A 4th-order cascaded reconfigurable photonic filter



Spectral transmission response of a 4th-order cascaded band-pass filter, showing greater than 38 dB out-of-band rejection and a tunable bandwidth of 900MHz-4GHz

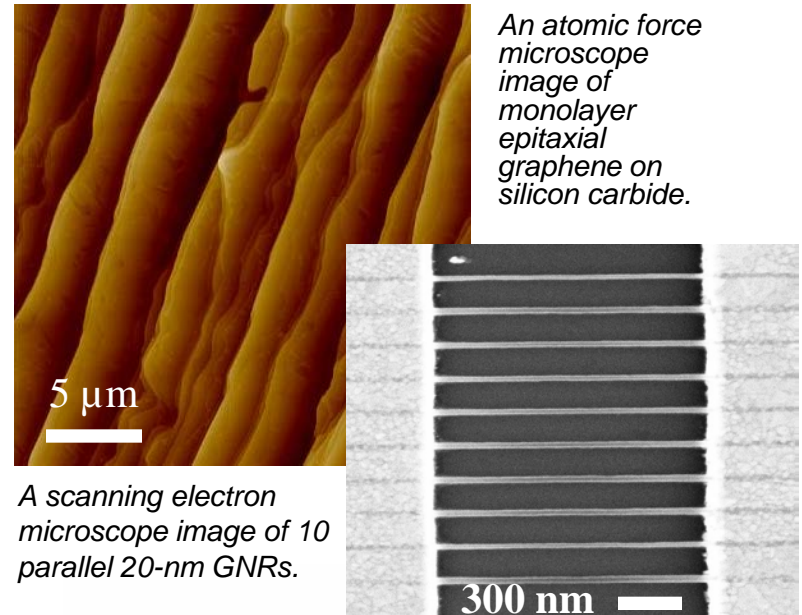
Heat distribution plot for a metallic micro-heater on top of an SOI ridge waveguide



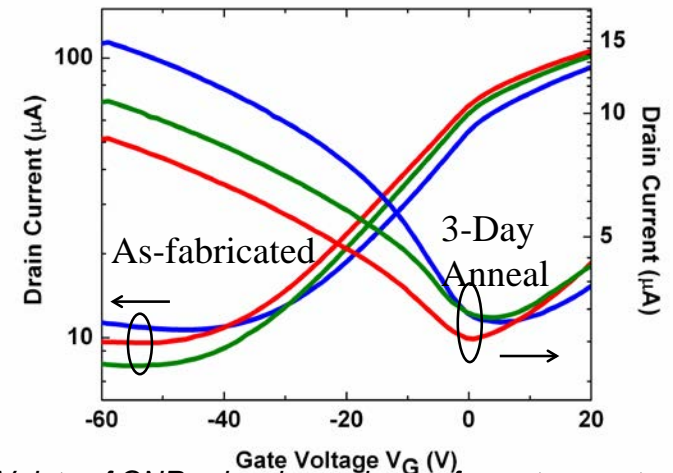
Epitaxial Graphene Nanoribbon Transistors

Graphene, an atomically thin sheet of carbon atoms, holds great promise as a future replacement material for silicon-based devices. The goal of this research is to investigate how epitaxial graphene, produced on silicon carbide substrates, behaves at the nanoscale, as such small feature sizes are necessary for future device scaling. We have investigated the mobility degradation in graphene nanoribbons (GNRs) as a function of line width, and found that improvements in both lithographically patterned line edge roughness and the substrate morphology are necessary to maintain high levels of conduction. In addition, we have demonstrated the first electrical measurements of p-type epitaxial GNRs, obtained by the simple thermal annealing of the electron-beam resist HSQ.

Sarah E. Bryan, Yinxiao Yang, Kevin Brenner, Raghu Murali, and James D. Meindl, Georgia Tech
Work performed at Georgia Tech Institute for Electronics and Nanotechnology



A scanning electron microscope image of 10 parallel 20-nm GNRs.

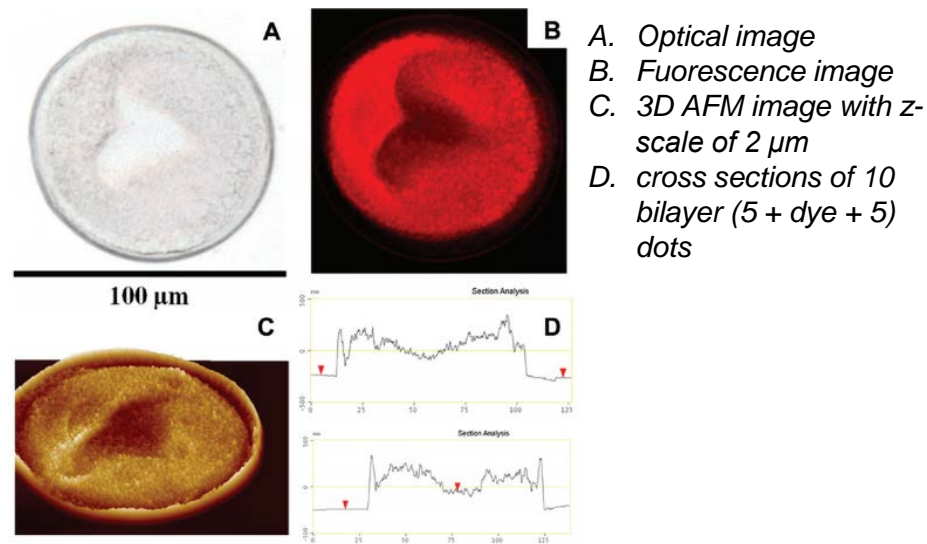


I-V data of GNRs showing a change from strong n-type doping to p-type doping via thermal annealing.

Inkjet-Assisted Layer-by-Layer Printing of Encapsulated Arrays

We demonstrate patterned encapsulation of Rhodamine dye as a model compound within poly(vinylpyrrolidone)/poly(methacrylic acid) (PVPON/PMAA) LbL dots constructed without an intermediate washing step. The inkjet printing technique improves encapsulation efficiency, reduces processing time, facilitates complex patterning, and controls lateral and vertical dimensions with diameters ranging from 130 to 35 μm . This facile, fast, and sophisticated inkjet encapsulation method can be applied to other systems for fast fabrication of large-scale, high-resolution complex arrays of dye-encapsulated LbL dots

Rattanon Suntivich, Olga Shchepelina, Ikjun Choi, and Vladimir V. Tsukruk, Georgia Tech School of Materials Science and Engineering
Work performed at Georgia Tech Institute for Electronics and Nanotechnology

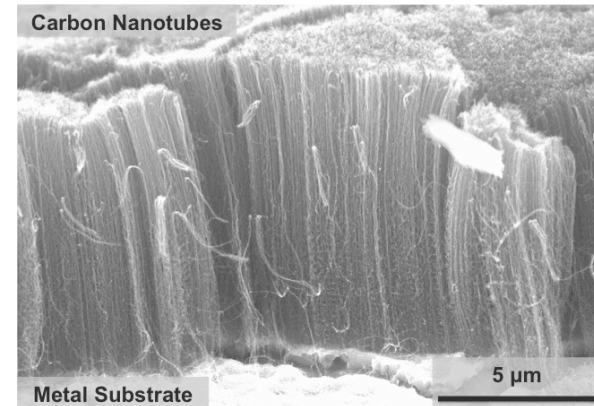


Optical (A, B) and fluorescent (C) image of inkjet-assisted LbL patterns: (A) GT logo and (B, C) inverted GT logo

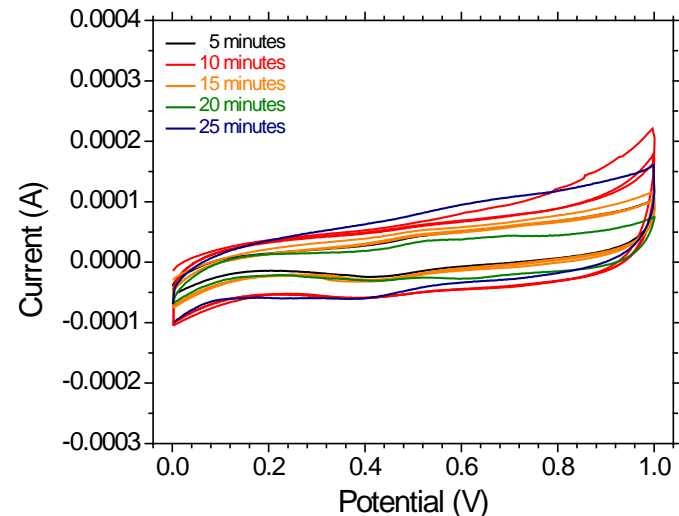
Carbon Nanotubes for Supercapacitors

Supercapacitors are unique energy-storage devices that exhibit large power densities, fast charge cycles, and high cyclability.

Significant improvements in capacitance can be achieved by fine-tuning the electrodes of these devices. This study fabricates vertically aligned carbon nanotubes (VACNTs) on metal substrates to create electrodes that have large active surface area, high electrical conductivity, high porosity, and mechanical flexibility.



SEM image of VACNTs grown directly onto metal substrate

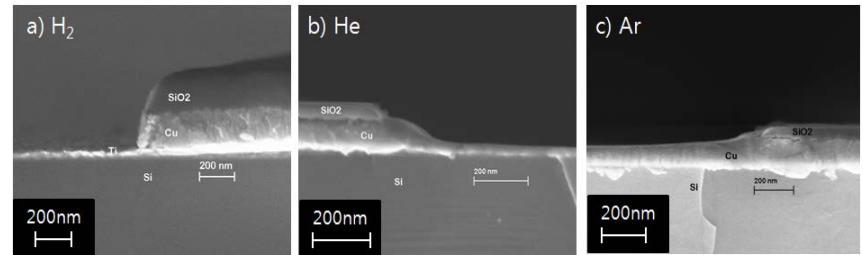


Cyclic voltammetry graphs showing curves for VACNTs grown directly on Al with varying growth times.

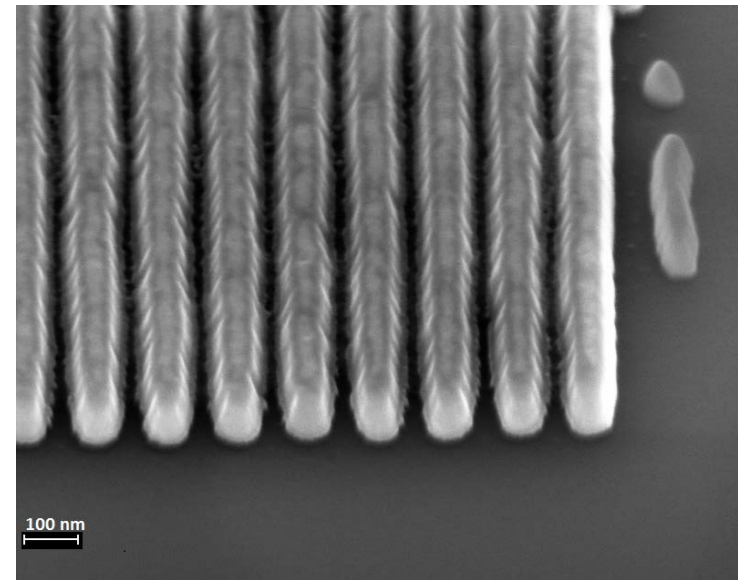
Justin Nguyen, Radu Reit, and W. Jud Ready, Georgia Tech Research Institute
Work performed at Georgia Tech Institute for Electronics and Nanotechnology

Increasing Electronic Device Speed by Patterning Copper Films in Plasmas

The extensive use of microelectronic devices or integrated circuits (ICs) has arisen from device speed increases due to continuous device miniaturization. A critical limitation to further increases in device speed is the inability to pattern copper using plasmas or glow discharges. Copper films have been patterned at low temperature while controlling the shape of 50-60 nm patterns using hydrogen plasmas. This process will allow the IC industry to improve throughput, increase device speed, minimize processing cost and establish a more environmentally benign process than the current copper patterning method.



Cross-sectional SEMs of SiO₂ masked 100 nm Cu films. (a) H₂ etch gas, (b) He etch gas, (c) Ar etch gas .



60 nm features patterned in hydrogen plasma

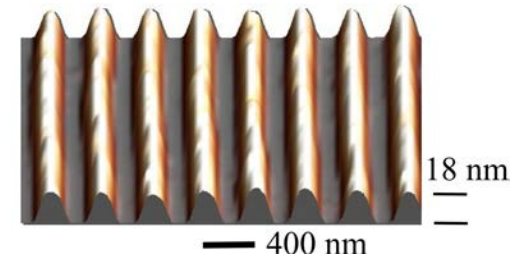
Fangyu Wu, Galit Levitin, Tae-Seop Choi and Dennis Hess,
Georgia Tech
Work performed at Georgia Tech Institute for Electronics
and Nanotechnology

Bottom-up Creation of Graphene Wire Arrays

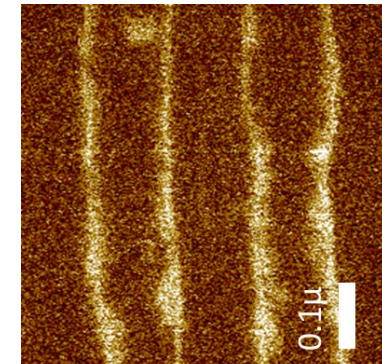
The purpose of this project was to demonstrate an alternative **bottom-up** method to creating graphene wires capable of creating smaller features with better electronic conduction than is currently possible with top-down shaping of the graphene through a lithographically-defined etch mask. Electron beam lithography is used to define a series of rectangular apertures in silicon carbide (SiC) that are then etched into trenches using a plasma. In the lab, these features are heated to about 1500C, where the silicon preferentially evaporates from the sides of the trenches, with the remaining carbon-rich layer spontaneously forming graphene. We have so far used this technique to demonstrate 10nm-wide graphene strips spaced 100nm apart over a 1.5mm x 1.5mm area.

Jeremy Hicks and Edward H. Conrad in collaboration with the Epitaxial Graphene group, Georgia Tech Work performed at Georgia Tech Institute for Electronics and Nanotechnology

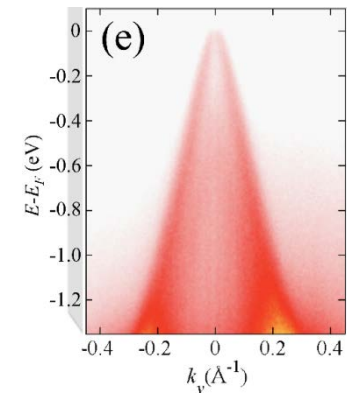
3D rendering of trenches etched into SiC as seen by atomic force microscopy (AFM)



Zoomed-in electrostatic force microscopy (EFM) image, with bright areas denoting graphene confined to the trench sidewalls. Dark areas are either the trenches or the plateaus between trenches

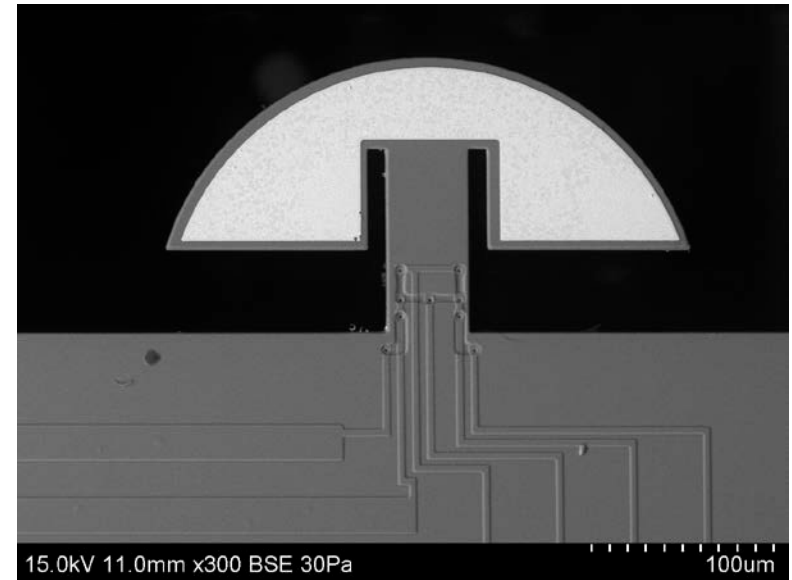


Band structure of the trench sidewalls measured using angle-resolved photoemission spectroscopy (ARPES) showing typical cone-like graphene band structure



Detection of Anti-IgG Using Cantilever-Type Resonant Microstructures

This work targets a cantilever-based mass-sensitive microsensor platform for the detection of biomolecules in the liquid phase. The resonant microstructures feature integrated thermal excitation and piezoresistive detection elements to excite and sense the structure's fundamental in-plane flexural mode. A gold film on the cantilevers allows for the local immobilization of biomolecules using gold-thiol chemistry. Using the in-plane flexural mode, quality factors of the order of 30-50 are obtained in water at resonance frequencies around 500 kHz. The reduced liquid damping enables closed-loop operation of the resonators with frequency stabilities in the ppm-range. Using a microfabricated flow cell, anti-IgG is detected in PBS with limits of detection on the order of 50 ng/ml.

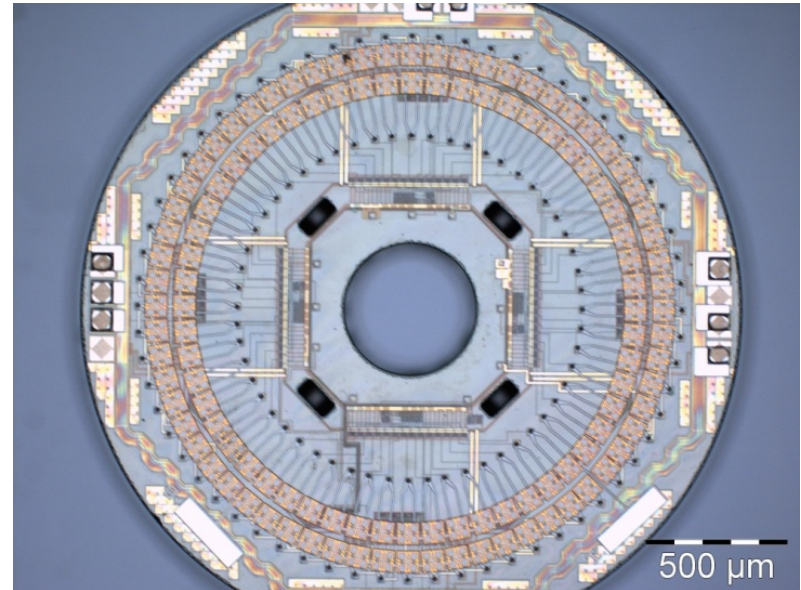


SEM micrograph of resonant microstructure with integrated resistors for thermal excitation and piezoresistive detection of in-plane oscillations.

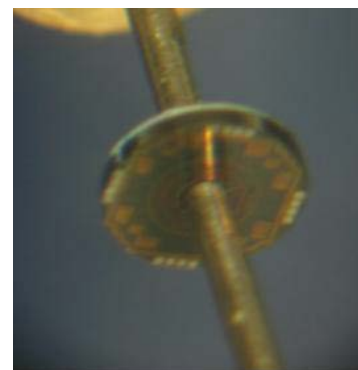
Luke A. Beardslee, Paul Joseph and Oliver Brand,
Georgia Institute of Technology
Work performed at Georgia Tech Institute for Electronics
and Nanotechnology

Capacitive Micro-machined Ultrasonic Transducers (CMUTs)

CMUTs have been fabricated in the IEN cleanrooms in order to perform intravascular and intra-cardiac real time ultrasound imaging. These devices are operated in the 10-20 MHz frequency range. The surface micro-machined membranes are monolithically integrated with CMOS ICs on a single chip.



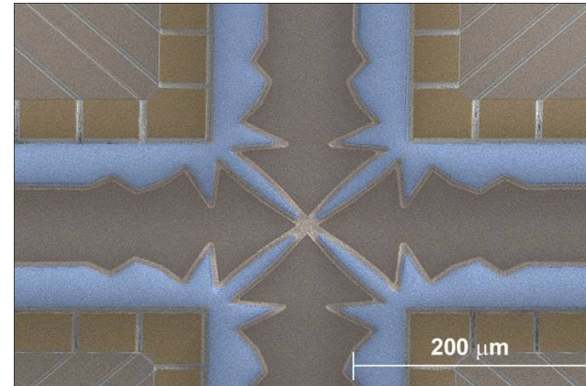
Toby Xu and Levent Degertekin, Georgia Institute of Technology
Work performed at Georgia Tech Institute for Electronics and Nanotechnology



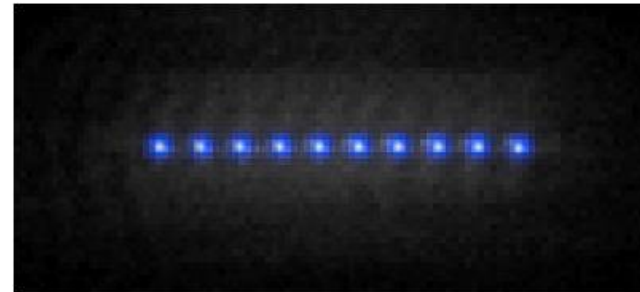
Ion Trap Fabrication for Quantum Computing

The Quantum Information Systems Group (QIS), a part of the Georgia Tech Research Institute's Advanced Concepts Lab, develops systems used to advance fundamental research in quantum information science and novel devices based on quantum technologies. This work includes designing, fabricating, and testing microfabricated ion traps for use in quantum computing. To date, eight ion trap designs have been fabricated in the NRC and successfully tested at GTRI, advancing the state of the art of ion traps. These include an X-junction ion trap capable of transporting and reordering ions, and the first microfabricated ion trap with integrated microwave electrodes that enable global qubit rotations.

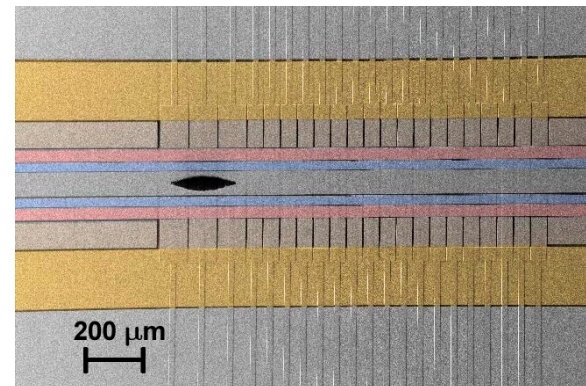
Harley Hayden, Quantum Information Systems Group,
GTRI Advanced Concepts Lab
Work performed at Georgia Tech Institute for
Electronics and Nanotechnology



A cross junction ion trap used for transport and controlled reordering of ions .



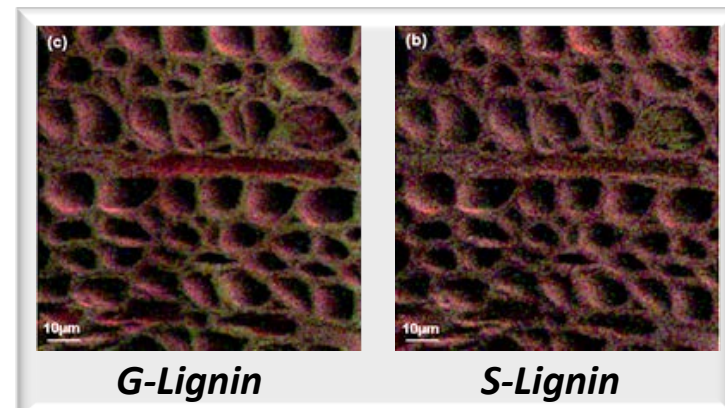
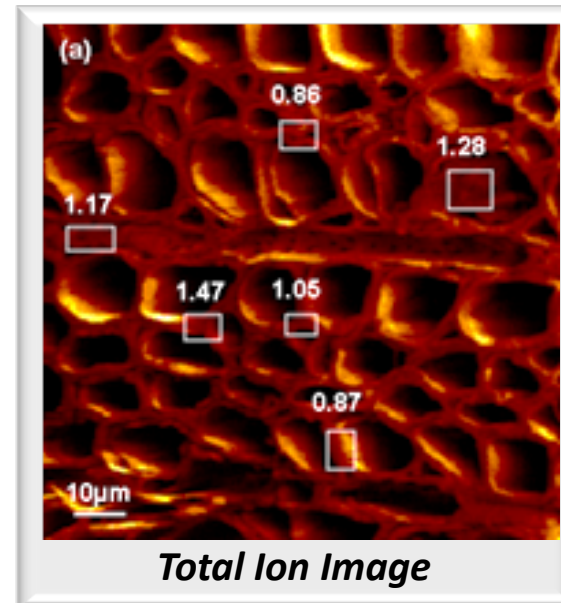
A chain of ten ions in an ion trap fabricated at the NRC.



An ion trap with integrated microwave electrodes designed to enable global qubit rotations.

Investigation of Site-Specific Lignin Distribution by ToF-SIMS

TOF-SIMS has been recently been applied to estimate the S-lignin/G-lignin ratio in synthetic lignin model compounds. Thin sections of extractive-free Transgenic Poplar cores were analyzed using the Time-of-Flight SIMS (ToF-SIMS) system available at the GT-IEN. From the spectral data, mass peak intensities of G- and S-unit fragments were calculated. Aryl ether 8-O-4' linked polymer model compounds were detected at relative peak intensities very similar to the actual S/G molar ratio. In the SIMS image at top left, S/G ratios are shown calculated at selected regions of interest (ROIs). The lower images show ToF-SIMS images displaying the spatial distribution of lignin compounds.



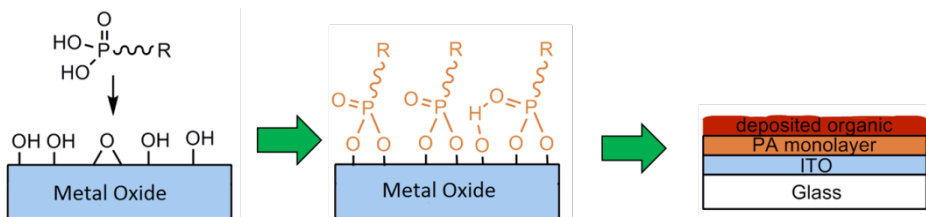
Lignin ions (Green) are overlaid on total ion (red) image

Tao Ma and Arthur Ragauskas, Georgia Tech and IPST
Work performed at Georgia Tech Institute for
Electronics and Nanotechnology

XPS/UPS studies of organic monolayers on metal oxides in Kratos Ultra^{DLD} system

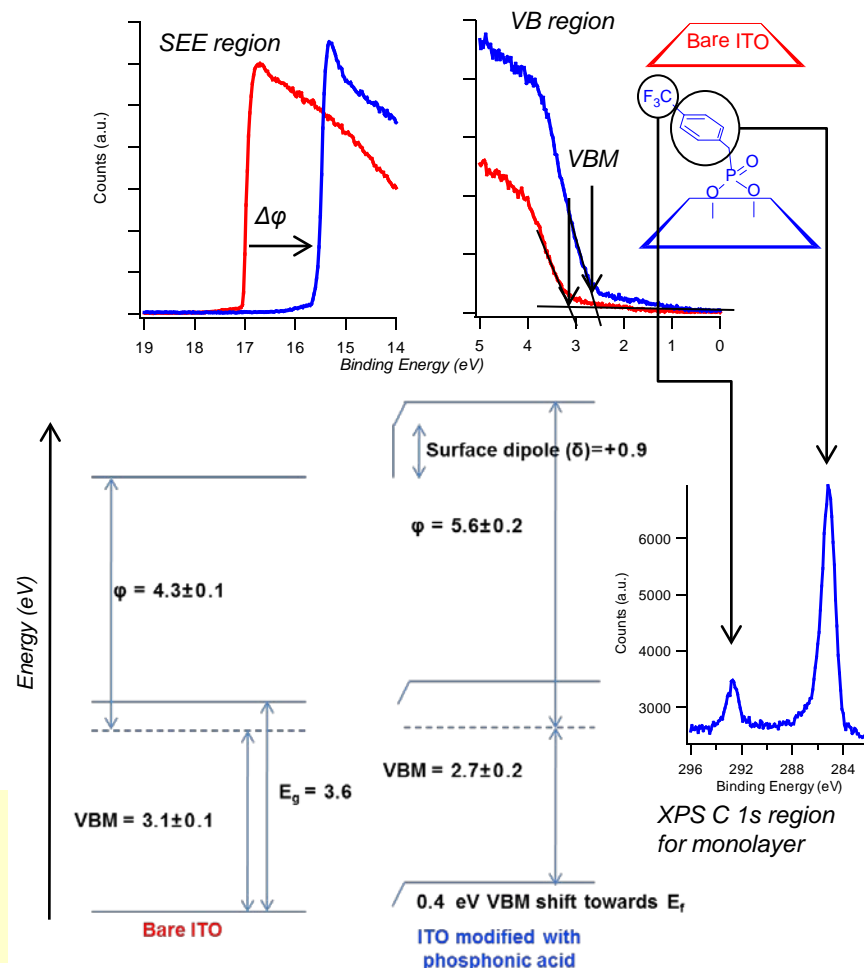
Phosphonic acid monolayers are currently being used as surface modifiers of metals oxides (such as indium-tin oxide) to change its work function and surface energies, among other properties for a wide range of applications including organic light emitting diodes and excitonic solar cells. The XPS/UPS Kratos system has helped to characterize the quality of the organic overlayers as well as the coverage and thickness by X-ray Photoelectron Spectroscopy and probe the energy levels at the surface by Ultraviolet Photoelectron Spectroscopy. Studies on a representative system are shown on the right.

Organic monolayer is covalently attached to substrate, changing its interfacial properties to tailor it for specific applications such as organic electronic devices (i.e. OLEDs, OFETs, etc).



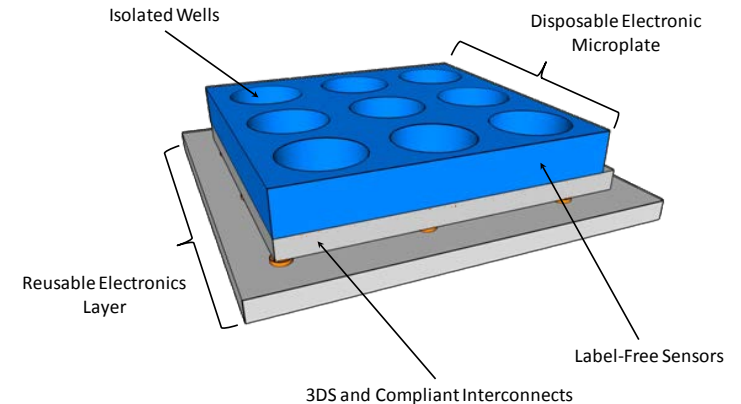
S. A. Paniagua, A.J. Giordano, O. Smith, S. R. Marder, Georgia Tech
Work performed at Georgia Tech Institute for Electronics and Nanotechnology

The absolute work function ϕ and its change can be determined from the secondary electron edge (SEE) in the UP spectra of both the modified and unmodified ITO; the valence band maximum is directly measured relative to the Fermi level.

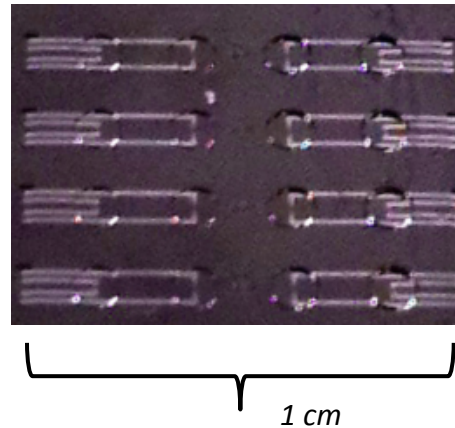


An Ultra-High Density Electronic Biosensing Platform

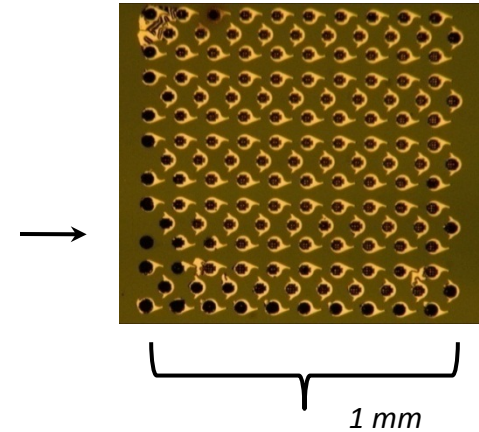
The objective of this research is to develop a highly scalable and label-free electronic biosensing platform. Current immunoassays are becoming increasingly incapable of taking advantage of the latest advances in disease biomarker identification, hindering their utility in the potential early-stage diagnosis and treatment of many diseases. The platform presented here – termed the electronic microplate – embodies a number of qualities necessary for clinical and laboratory relevance as a next-generation immunoassay tool.



2010 (16 isolated sensors/cm²)



2011 w/3DS (10,000 isolated sensors/cm²)

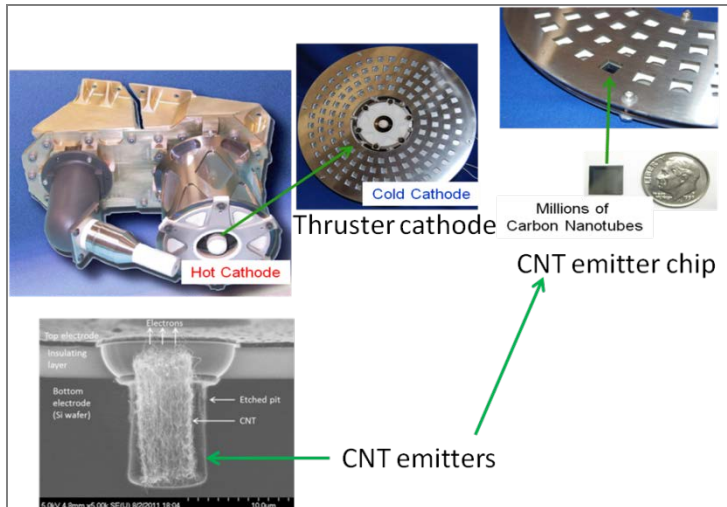


R. Ravindran, P. Modarres, K. Scarberry, M. Bakir, J. McDonald, and J. Meindl, Georgia Institute of Technology

Work performed at Georgia Tech Institute for Electronics and Nanotechnology

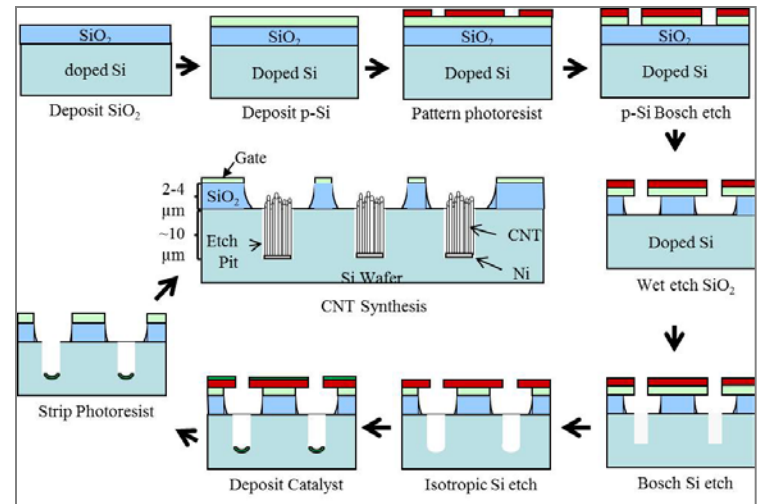
Carbon Nanotube-based Field Emitters for Hall Effect Thrusters

The purpose of the work is to provide a more efficient electron source for Spacecraft propelled with Hall Effect Thrusters. Carbon Nanotube (CNT) Field Emission devices model a Spindt-cathode type electron emitter are fabricated using a number of conventional lithographic, etch and deposition techniques.

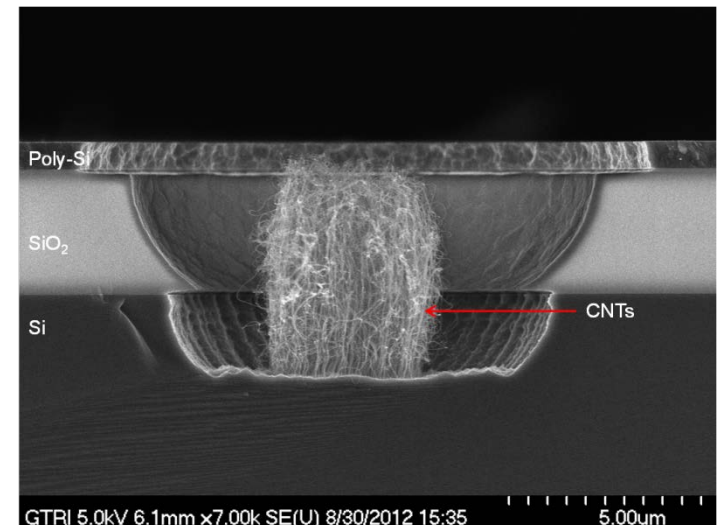


Schematic of Hall Effect Thruster incorporating CNT Field Emitter Devices

Jud Ready, Stephan Turano and Graham Sanborn, GTRI
Work performed at Georgia Tech Institute for Electronics and Nanotechnology



Process flow for CNT Field Emitter fabrication

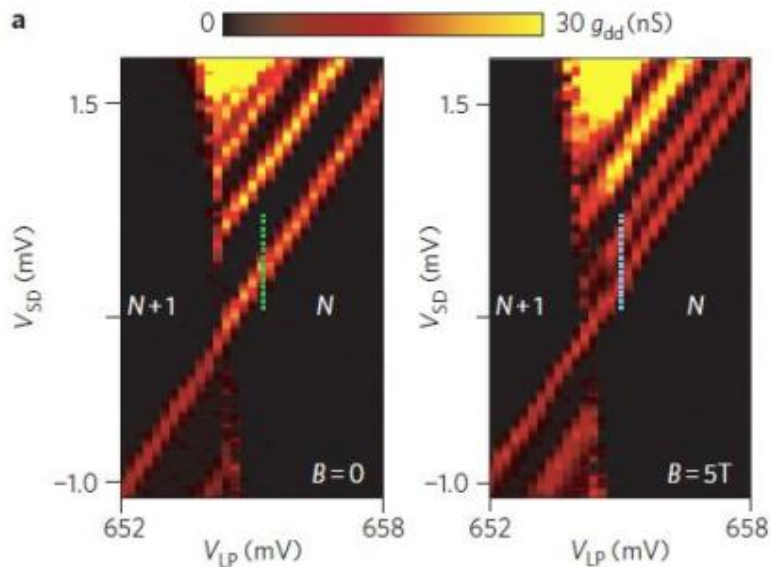


SEM micrograph depicting a single CNT field emitter

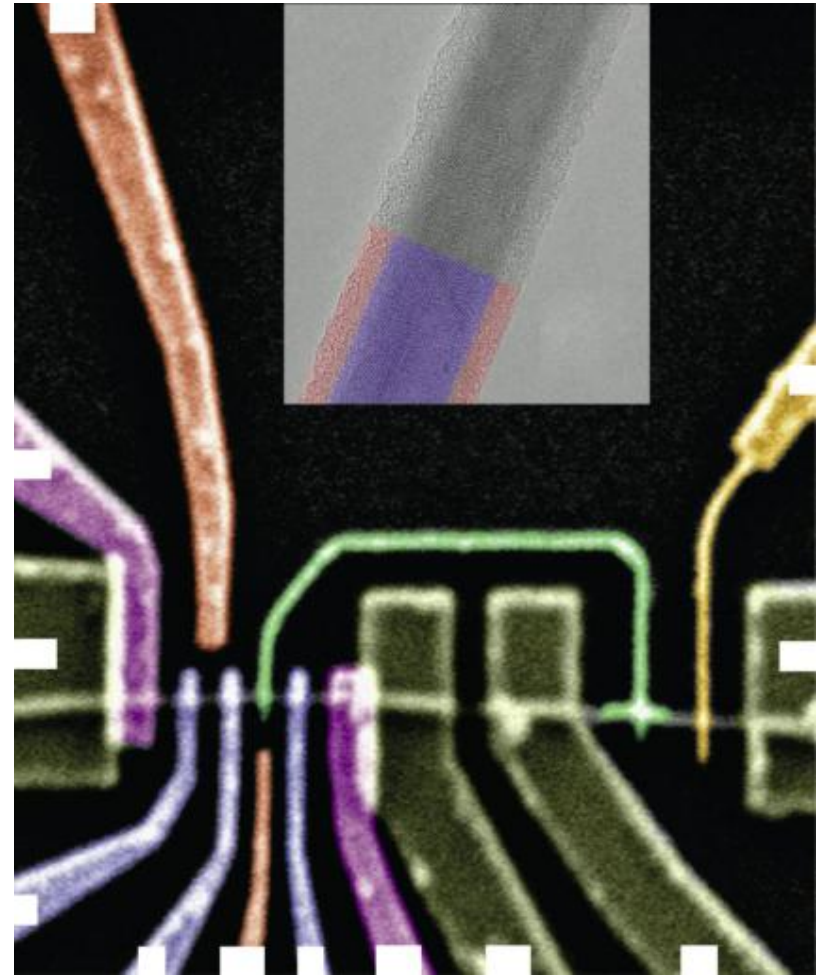
Harvard University

Hole Spin Relaxation In Ge–Si Core–shell Nanowire Qubits

- Developed Group IV materials for coherent spintronics
- Synthesis of Ge/Si core/shell heterostructures from bottom-up
- Successfully Implemented pulsed-gate and integrated charge sensor
- Demonstrated spin state preparation, control and readout
- Achieved long spin lifetimes



Yongjie Hu and Prof. Gang Chen, MIT
Work performed at Harvard Center for
Nanoscale Systems



Nature Nanotechnology 7, 47, 2012.

Surface Plasmonic Resonance Enhanced Photodetection

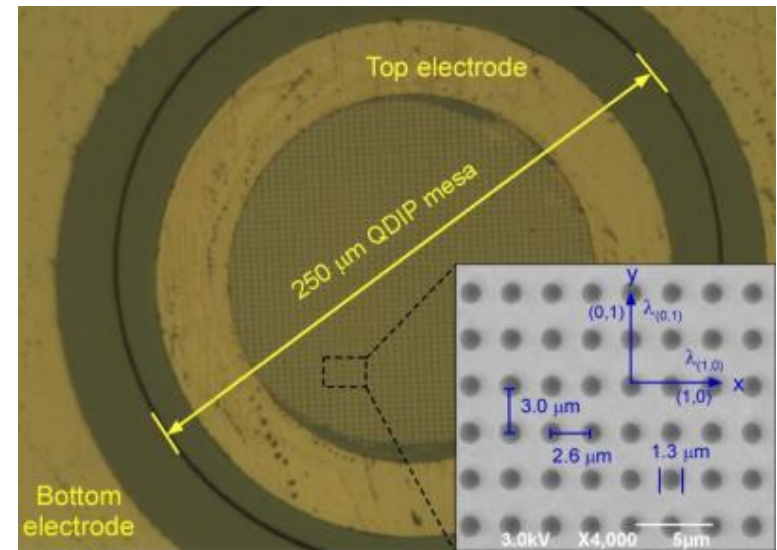
The primary goal of the proposal is to develop a surface plasmonic resonance (SPR) enhanced middlewave and longwave infrared (MWIR/LWIR) quantum dot (QD) photodetector with polarimetric sensing capability and high photodetectivity.

SPR offers an effective surface light trapping and enhancement technique that enables high efficient light absorption using considerably thinner active light absorption regions. Such SPR surface light trapping and enhancement technique provides a promising solution to improve the absorption efficiency using thin active QD regions.

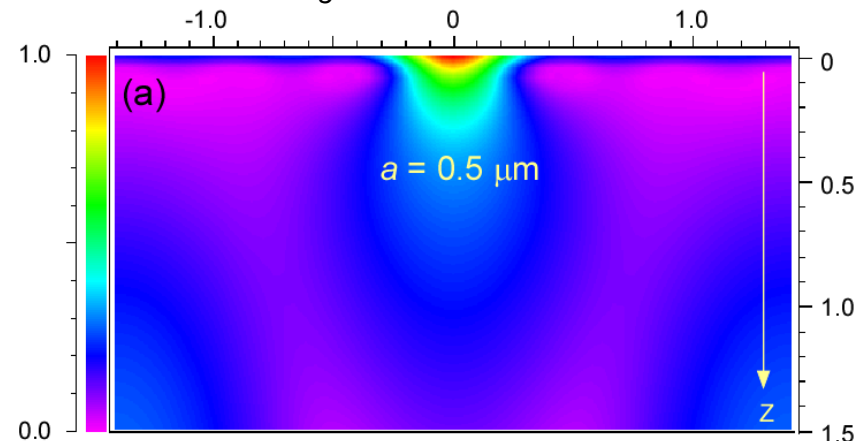
In addition, by properly designing the SPR structure, polarimetric sensing with band-pass spectral filtering has been achieved.

*Puminun Vasinajindakaw, Guiru, Gu, and Xuejun Lu,
U. Massachusetts Lowell*

Device fabrication performed at Harvard Center for Nanoscale Systems



Picture of the QDIP with the SPR structure. The inset shows an SEM image of the SPR structure.



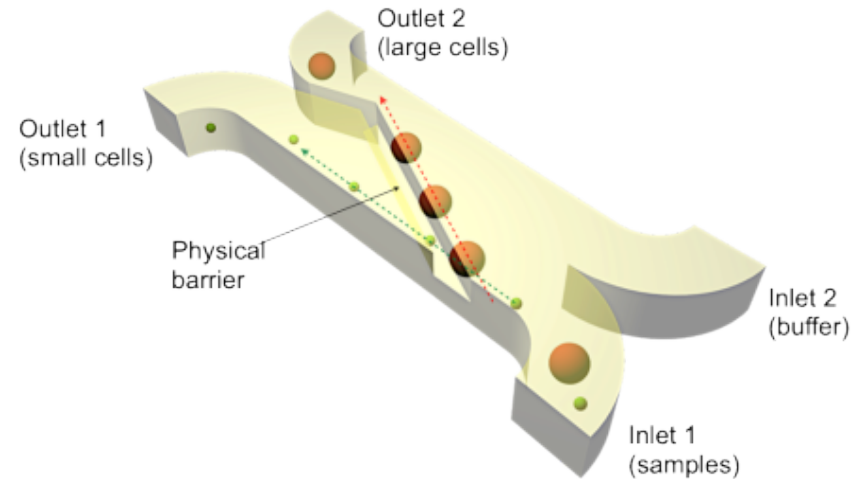
Simulated near field profiles of the SPR structure. The E-field is confined near the surface.

Microfluidic Cell Sorter

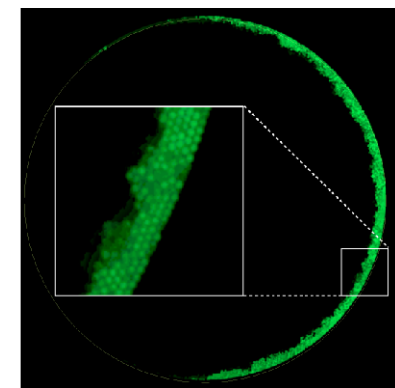
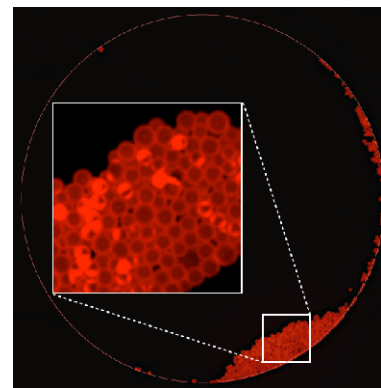
A new type of CTC processing system, a microfluidic cell sorter (μ FCS), was developed for the isolation and comprehensive analyses of CTCs. The μ FCS employs a modified weir-style physical barrier to separate and capture tumor cells based on their size, and subsequently allows on-chip tumor identification through molecular characterization. The operation is performed in a continuous-flow manner, processing large volumes of samples at high flow rates without clogging or pressure buildup. The captured cells can be analyzed *in situ* for comprehensive and multifaceted evaluation. They can also be cultured on-chip or retrieved for subsequent off-chip assays.

Jaehoon Chung*, Huilin Shao*, Thomas Reiner, David Issadore, Ralph Weissleder, Hakho Lee, Massachusetts General Hospital

Device fabricated at Harvard Center for Nanoscale Systems



Working principle of the microfluidic cell sorter. Cells are separated in-flow, based on their size.

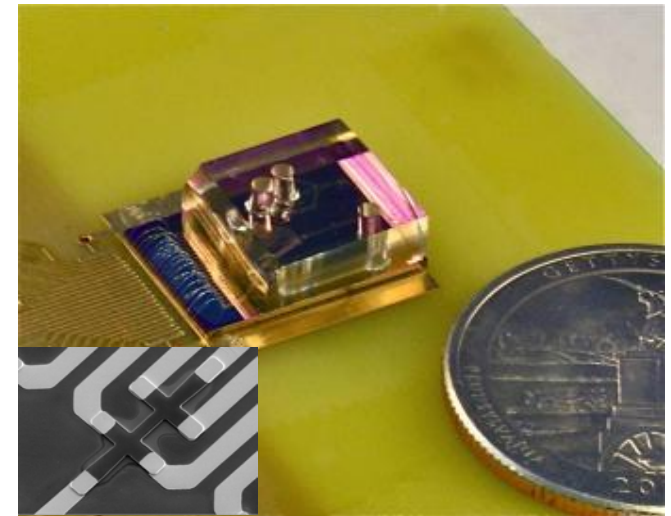


Cells collected in the outlet regions. Cancer cells (left), leukocytes (right).

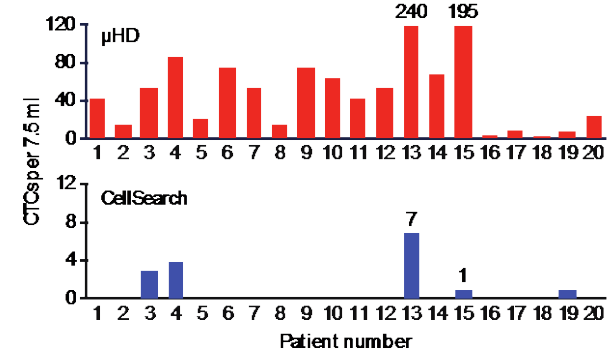
Adv. Healthcare Mater. 1, 432-436 (2012).

Miniaturized Hall Sensor for Cellular Profiling

A microfluidic chip-based micro-Hall detector (μ HD) was developed, which can directly measure single, immunomagnetically tagged cells in whole blood. The μ HD can detect single cells even in the presence of vast numbers of blood cells and unbound reactants, and does not require any washing or purification steps. The clinical utility of the μ HD chip was demonstrated by detecting circulating tumor cells in whole blood of ovarian cancer patients. Furthermore, the use of a panel of magnetic nanoparticles, distinguished with unique magnetization properties and bio-orthogonal chemistry, allowed simultaneous detection of the multiple biomarkers.



MicroHall detector (μ HD) for single cell detection. Inset shows the Hall elements.



The μ HD demonstrated superior detection sensitivity in CTC detection compared to the current gold standard (CellSearch).

David Issadore, Jaehoon Chung, Huilin Shao, Monty Liong, Arezou A. Ghazani, Cesar M. Castro, Ralph Weissleder, Hakho Lee, Massachusetts General Hospital

Device fabricated at Harvard Center for Nanoscale Systems

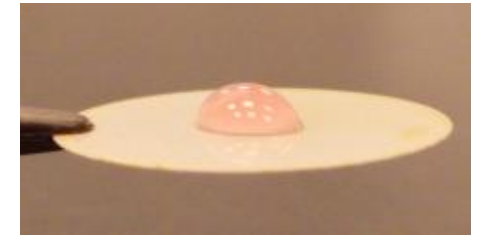
Sci. Transl. Med. **4**, 141ra92 (2012).

Novel RO Membrane for Desalination via Short Hydrophobic Nanopores

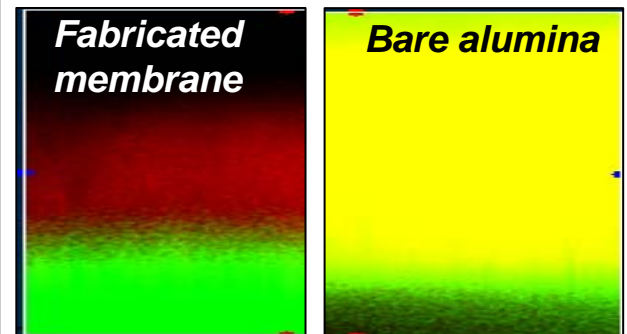
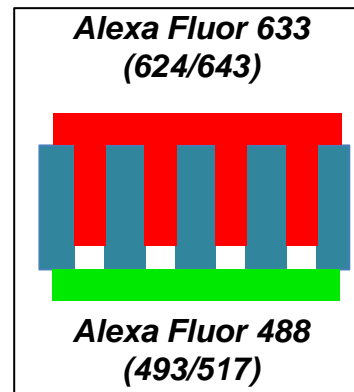
Efficient desalination would provide a perfect solution for global water shortage issues. Feed salt water is pressurized against short hydrophobic nanopores, through which evaporated water is transported to fresh water chamber on the other side. Due to the low transport resistance of short nanopores, the facilitated vapor transport could result in about 3 – 5 times faster fresh water generation than widely used conventional Reverse Osmosis (RO) membrane. We fabricated such a membrane based on porous alumina template.



Water droplet on top surface (hydrophobic)



Water droplet on bottom surface (hydrophilic)



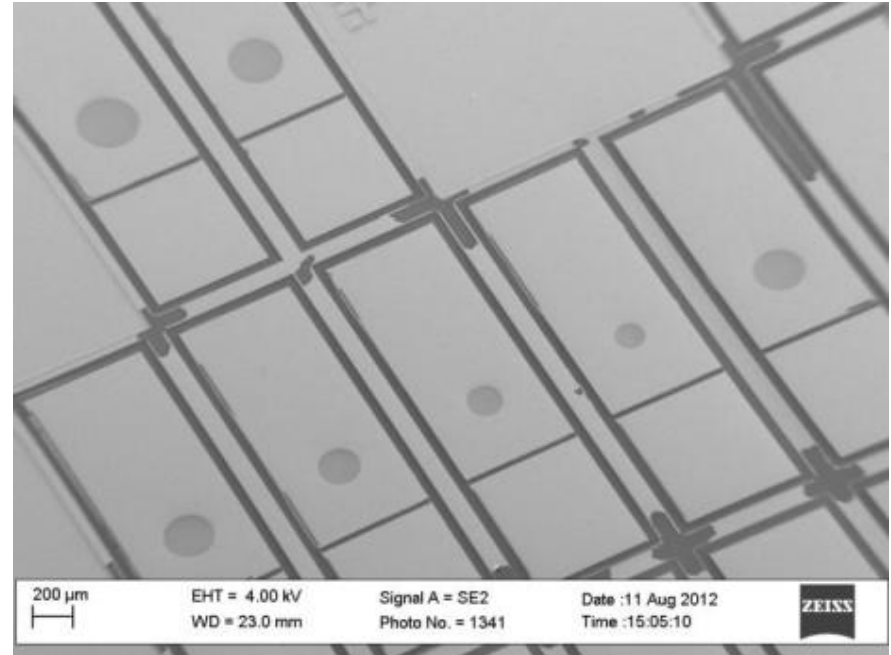
Confocal microscope images through membranes

Jongho Lee, Prof. Rohit Karnik, MechE MIT
Work performed at Harvard Center for Nanoscale Systems

Strain-compensated Thermophotovoltaics

The purpose of the strain compensation TPV project is to grow TPV cells on lattice mismatched substrates. CNS is used for most of the processing steps, which include lithography, etching, chemical processing, cleaning, thin film deposition, metrology, and imaging.

The goal of this project is to be able to compare the performance of GaSb TPV cells grown on GaSb substrates to GaSb TPV cells grown on GaAs substrates (which are 5 to 10 times cheaper) using an interfacial misfit array strain compensation technique.



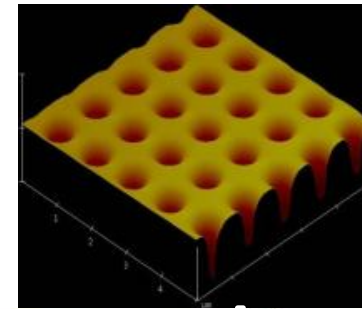
SEM image of TPV cells after liftoff

Dante DeMeo, Corey Shemelya, Thomas Vandervelde, Tufts University
Work performed at Harvard Center for Nanoscale Systems

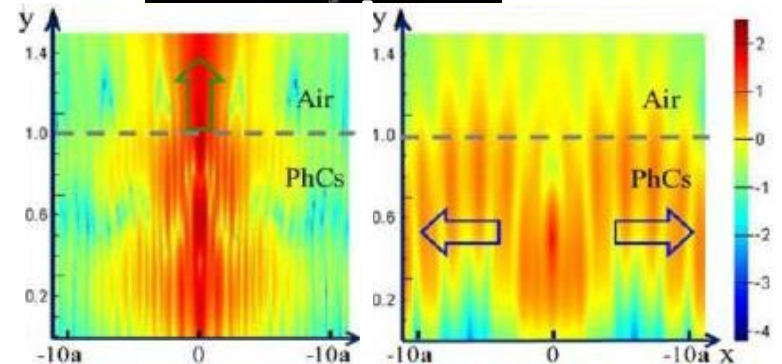
Anisotropic On-Chip Light Source

Anisotropic light emission from rare-earth doped tellurite thin films is demonstrated using $\text{Er}^{3+}\text{-TeO}_2$ photonic crystals (PhCs). Rare earth doped thin films have extended emission spectral range and compatibility with monolithic integration. Particularly tellurite glass is known for its high erbium solubility, which significantly increases the concentration of PL emission centers. The TeO_2 thin films are compatible with monolithic Si-CMOS processes because they can be deposited at room temperature and require no post-annealing. For these reasons, erbium doped tellurite thin films are a promising light source for chem-bio-photonic platforms and optical communication systems..

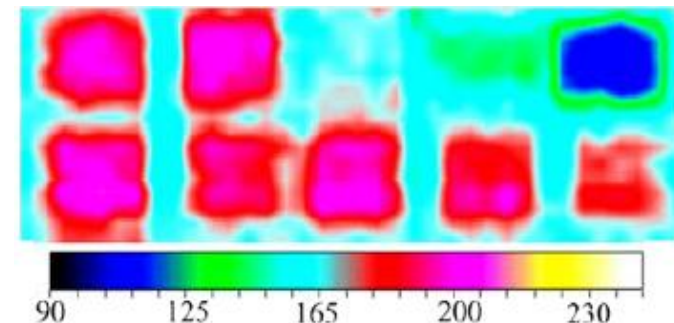
Pao Lin, L. Kimerling, A. Agarwal, MIT, Work performed at Harvard Center for Nanoscale Systems



Erbium doped tellurite ($\text{Er}\text{-TeO}_2$) thin film photonic crystals (PhCs). No roughness is introduced during the nano-scale ion beam milling.



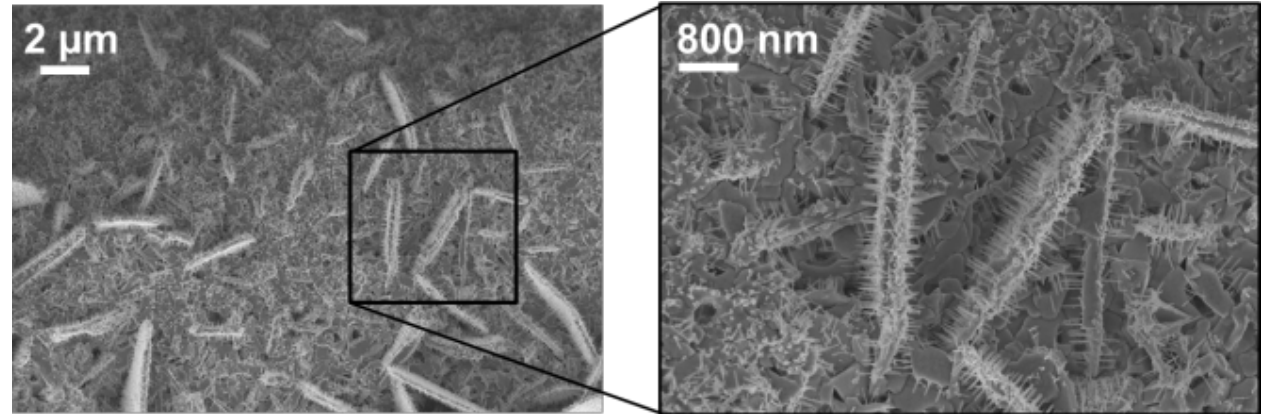
Anisotropic light emission from the $\text{Er}\text{-TeO}_2$ PhCs – direction of emission is tunable using the PhC lattice spacing.



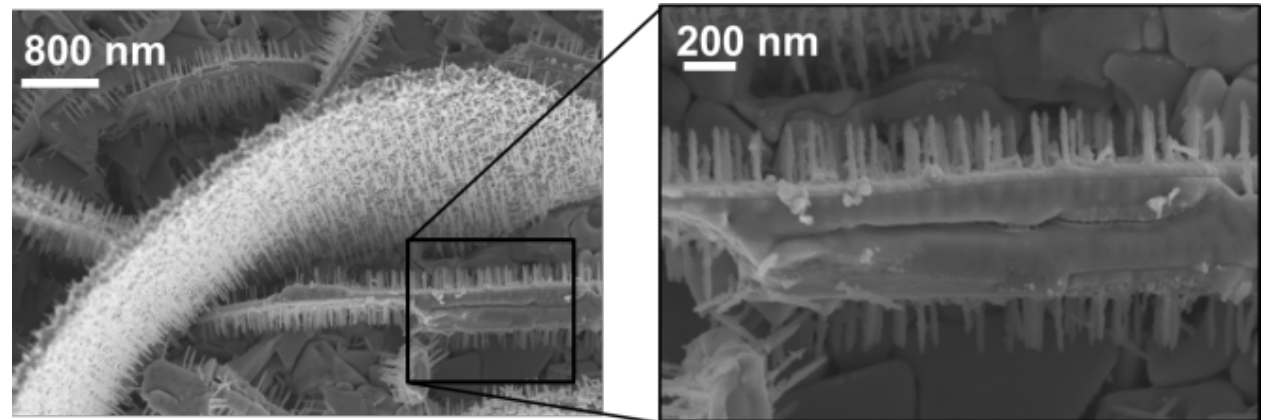
Light extraction efficiency is enhanced by utilizing the photonic band gap structures.

Single Step Formation of Hierarchical Copper Oxide Nanostructures for Phase Change Applications

A novel copper oxide nanostructure has recently been discovered that forms during a CVD silane deposition step of the process. The structure is unique in that it has a dual scale roughness (micro and nanoscale) and hence forms a hierarchical structured surface in one single step of CVD processing. Such surfaces could potentially be used for high-efficiency heat transfer applications such as enhancement of critical heat flux in boiling.



Copper oxide nanostructure having microscale walls and nanowires



FESEM high resolution image of copper oxide nanostructure

Top down view of the structure showing horizontal nanowires

Nenad Miljkovic and Evelyn N Wang, MIT
Work performed at Harvard Center for Nanoscale Systems

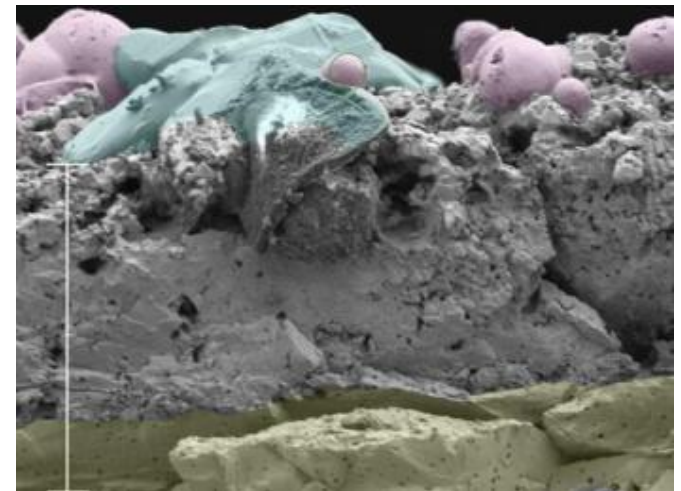
Acumentrics SOFC Degradation Study

Acumentrics SOFC Corporation is a private company commercially producing tubular solid oxide fuel cells (SOFC) for power generation in remote applications. The SOFC is a supported thin film ceramic construct based on an oxygen conducting electrolyte. It exploits an oxygen partial pressure gradient to efficiently produce electricity from hydrocarbon fuels. Because they have few moving parts SOFCs can operate maintenance free while continuously outputting high quality electricity. Lifetimes in excess of a year have been proven even in remote, rugged terrain. However, since the SOFC operates at temperatures of 700-850°C, a host of adverse solid state and deposition reactions can occur over the long term.

Our study aims to identify material degradation that has occurred in cells operating in real life applications in order to aid commercialization. The advanced instruments at Harvard CNS have allowed the unambiguous identification of unexpected reaction products in cells.



1kW SOFC units deployed in remote terrain

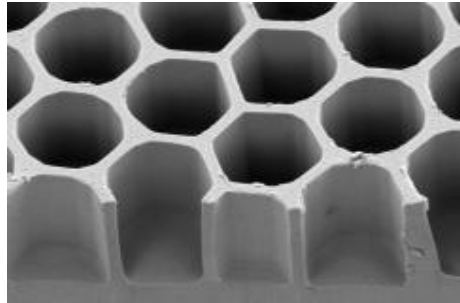
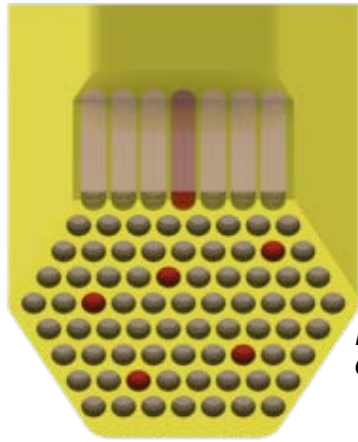


Chemical identification of phases using SEM and EDS.

Acumentrics

Work performed at Harvard Center for Nanoscale Systems

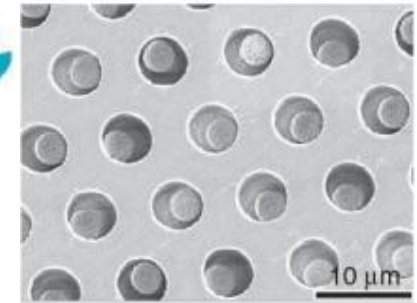
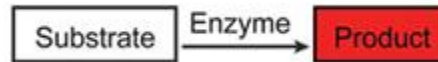
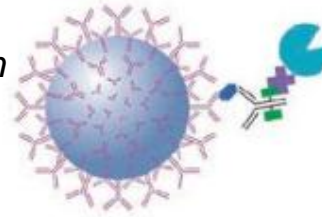
Microwell Array For Single Molecule Analysis



Femto-liter microwell array etched on tip of a fiberoptic bundle.

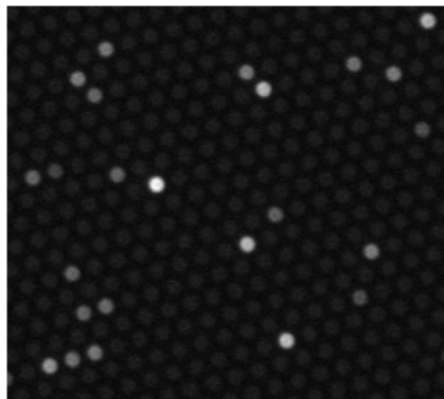
Analytes:

- Protein
- DNA
- RNA

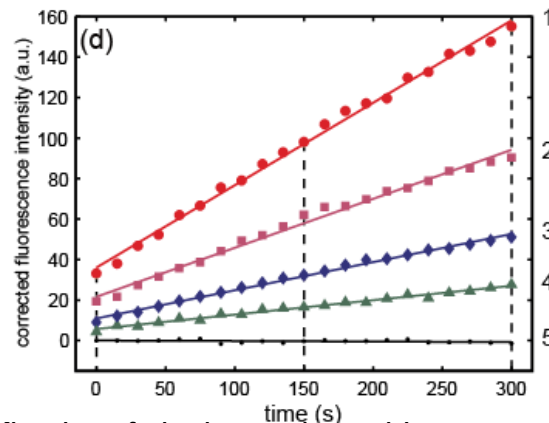


Single molecules of an analyte are captured by functionalized beads, labeled with enzymes, and sealed in microwells with non-fluorescent substrates. Fluorescent products accumulate only in microwells containing both an analyte and enzyme label.

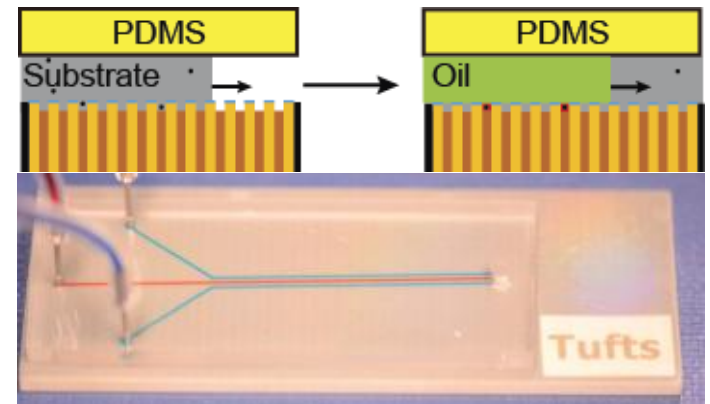
Example---High-density arrays of femto-liter microwells were used to perform single molecule analysis. This technique has been used in early detection of cancers, pathogen detection, and single molecule enzymology. CNS facilities were used to characterize physical and chemical properties of microwells, and fabricate microfluidic channels.



"Counting" molecules



Kinetics of single β -galactosidase enzymes



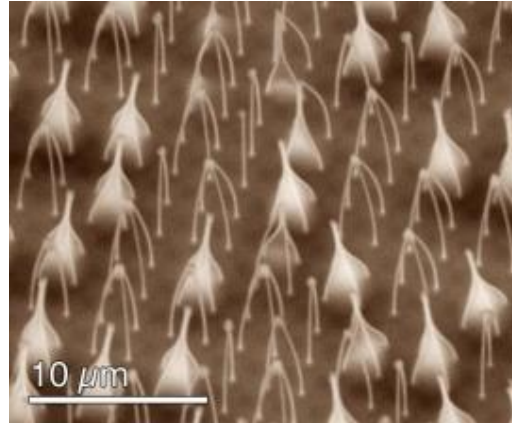
Microwell array integrated into microfluidics

David R. Walt group at Tufts University Work performed at Harvard Center for Nanoscale Systems

NNIN is supported by NSF ECCS-0335765

Liquid Evaporation on Superhydrophobic and Superhydrophilic Nanostructured Surfaces

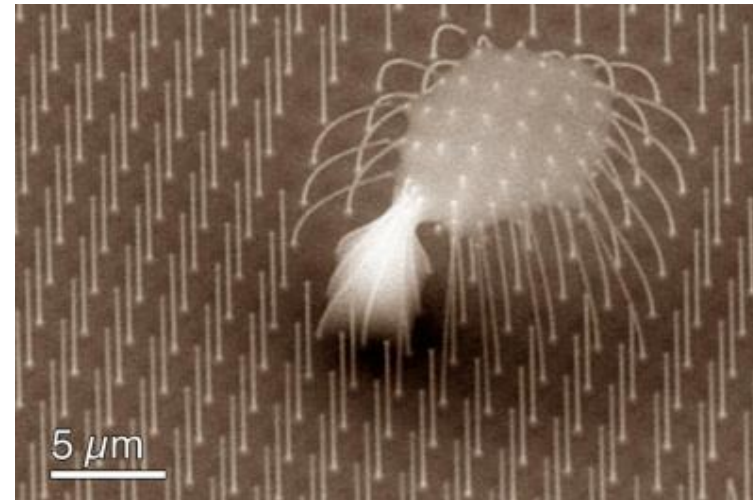
The three images capture the late stages of evaporation on the nanostructured surfaces. Capillary forces generated by the receding meniscus on the hydrophilic surface result in liquid entrapment and 'kissing' pillars as shown in the top left image. These 'kissing' pillars allow for the formation of a rare metastable pinned droplet with a highly irregular contact line as shown in the top right image. The bottom image depicts the remains of a mixed wetting mode droplet, in the Cassie and Wenzel states, on hydrophobic nanostructures comprised of silane-coated silicon. The droplets cause the pillars to bend due to surface tension forces. The visualizations provide insight into these complex interactions, which is important for integration of nanostructured surfaces in thermal management devices..



Entrapped droplets on a superhydrophilic surface



Pinned droplet on a superhydrophilic surface



Remains of a mixed mode wetting droplet, Cassie and Wenzel states, on a superhydrophobic surface

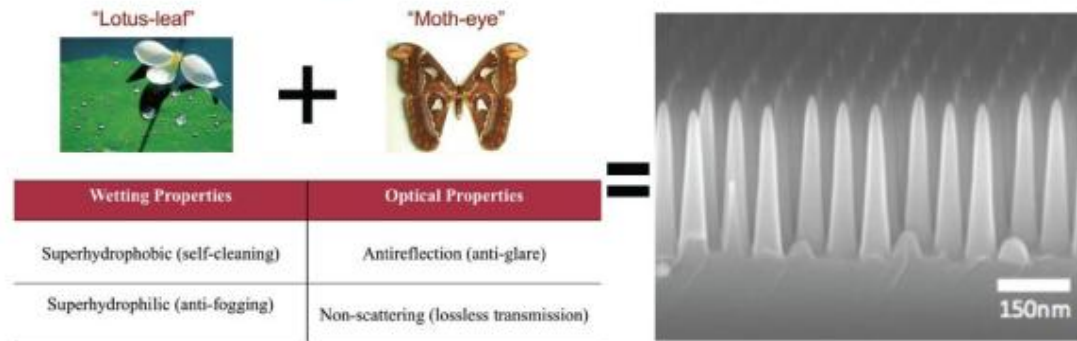
Nenad Miljkovic and Evelyn N Wang, MIT,
Work performed at Harvard Center for Nanoscale
Systems

Bio-inspired Multifunctional Surfaces

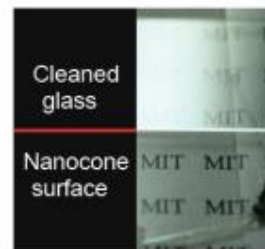
We designed and fabricated a high aspect-ratio nanocone structure possessing highly robust superhydrophobicity or enhanced structural superhydrophilicity, (depending on chemical treatment) as well as broadband omnidirectional anti-reflectance and near-lossless transparency that are superior to structures found in nature.

To fabricate high aspect ratio nanocone structures we employed a multiple-step plasma etching technique using shrinking masks to get more flexible choices of materials and thicknesses for a better control of the height and profile of nanocone structures

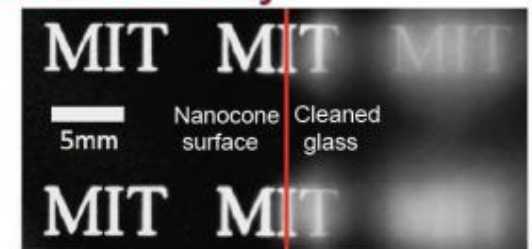
Bio-inspired Multifunctional Surface



Multi-functionality



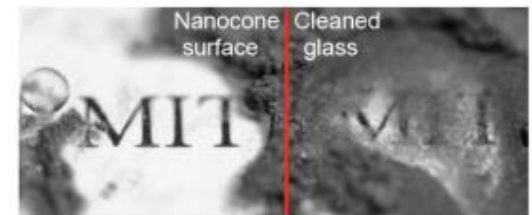
Anti-reflectivity



Anti-fogging property



Superhydrophobicity

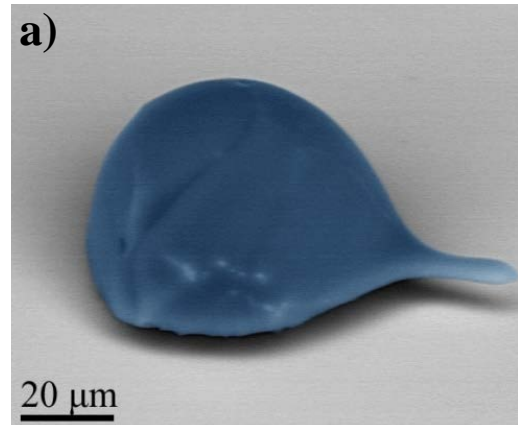


Self-cleaning effect

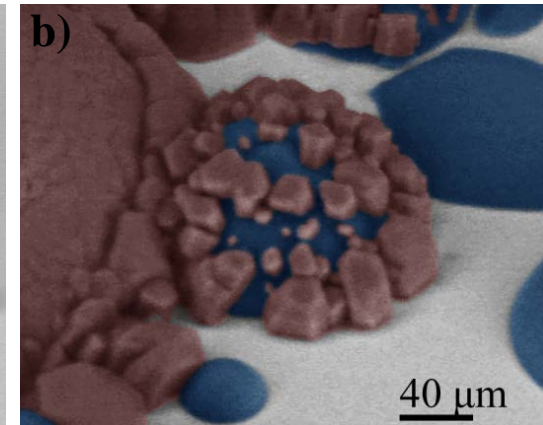
Cohen, McKinley, and Barbastathis groups, MIT
Work performed at Harvard CNS Facility

Liquid Freezing Dynamics on Hydrophobic and Superhydrophobic Surfaces

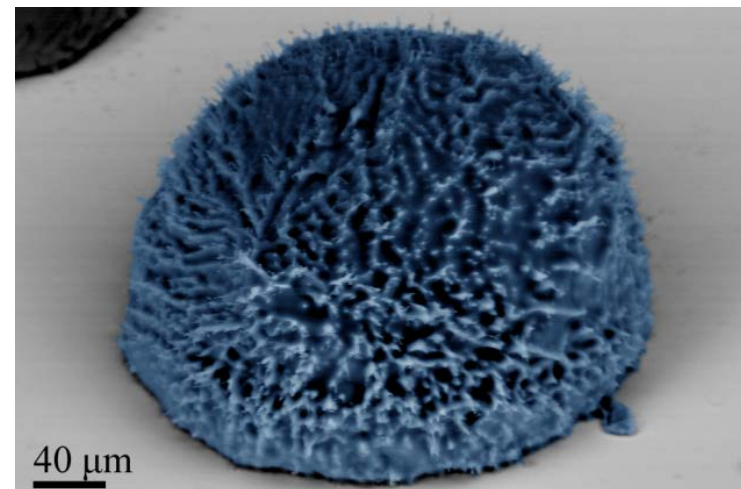
The three images capture the freezing dynamics on hydrophobic and superhydrophobic surfaces. Top left (a) shows a snapshot of droplet coalescence between a large droplet (left) and a smaller droplet (right) on a nanostructured surface. Due to rapid freezing (top right (b)), ice droplets maintained an 'amorphous' spherical structure (blue). Subsequent deposition of ice preferentially initiated on the droplet interface and formed crystallographic ice (red). Bottom (c) shows a larger scale droplet ($R \sim 100 \mu\text{m}$) undergoing rapid freezing with notable protrusions. These distinct freezing droplet behaviors can significantly alter dynamics of phase-change phenomena on these surfaces. The visualizations provide insight into these complex droplet-surface interactions, which are important for the development of de-icing surfaces.



Frozen coalescing droplets



Frozen amorphous droplets (blue) nucleating ice crystals (red)



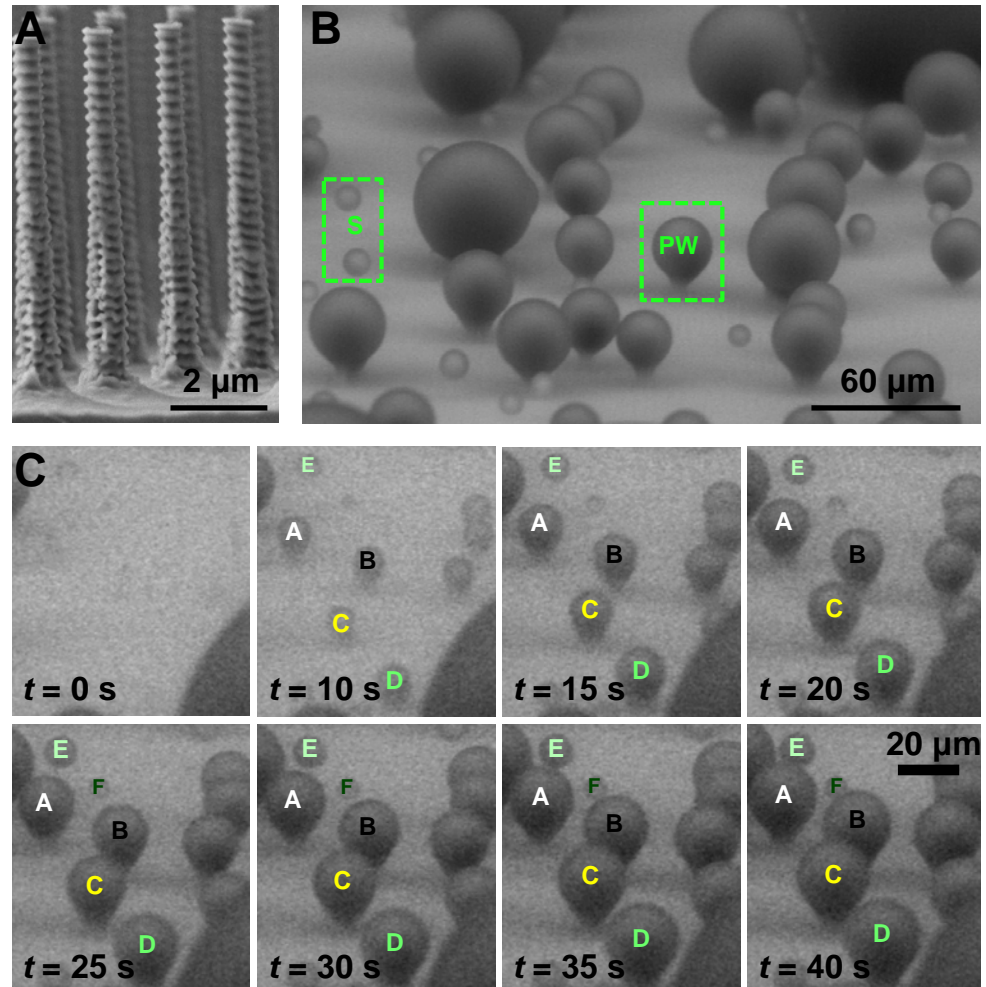
Frozen droplet with disrupted solid-vapor interface created by rapid freezing

Nenad Miljkovic and Evelyn N Wang, MIT,
Work performed at Harvard Center for Nanoscale
Systems

Effect of Droplet Morphology on Growth Dynamics and Heat Transfer during Condensation on Superhydrophobic Nanostructured Surfaces

Condensation on superhydrophobic nanostructured surfaces offers new opportunities for enhanced energy conversion. These surfaces are designed to be Cassie stable and favor the formation of suspended droplets on top of the nanostructures as compared to partially wetting droplets which locally wet the base of the nanostructures. These suspended droplets promise minimal contact line pinning and promote passive droplet shedding at sizes smaller than the characteristic capillary length. However, the gas films underneath such droplets may significantly hinder the overall heat and mass transfer performance, which has not been considered previously. In this work, we investigated droplet growth dynamics on superhydrophobic nanostructured surfaces to elucidate the importance of droplet morphology on heat and mass transfer.

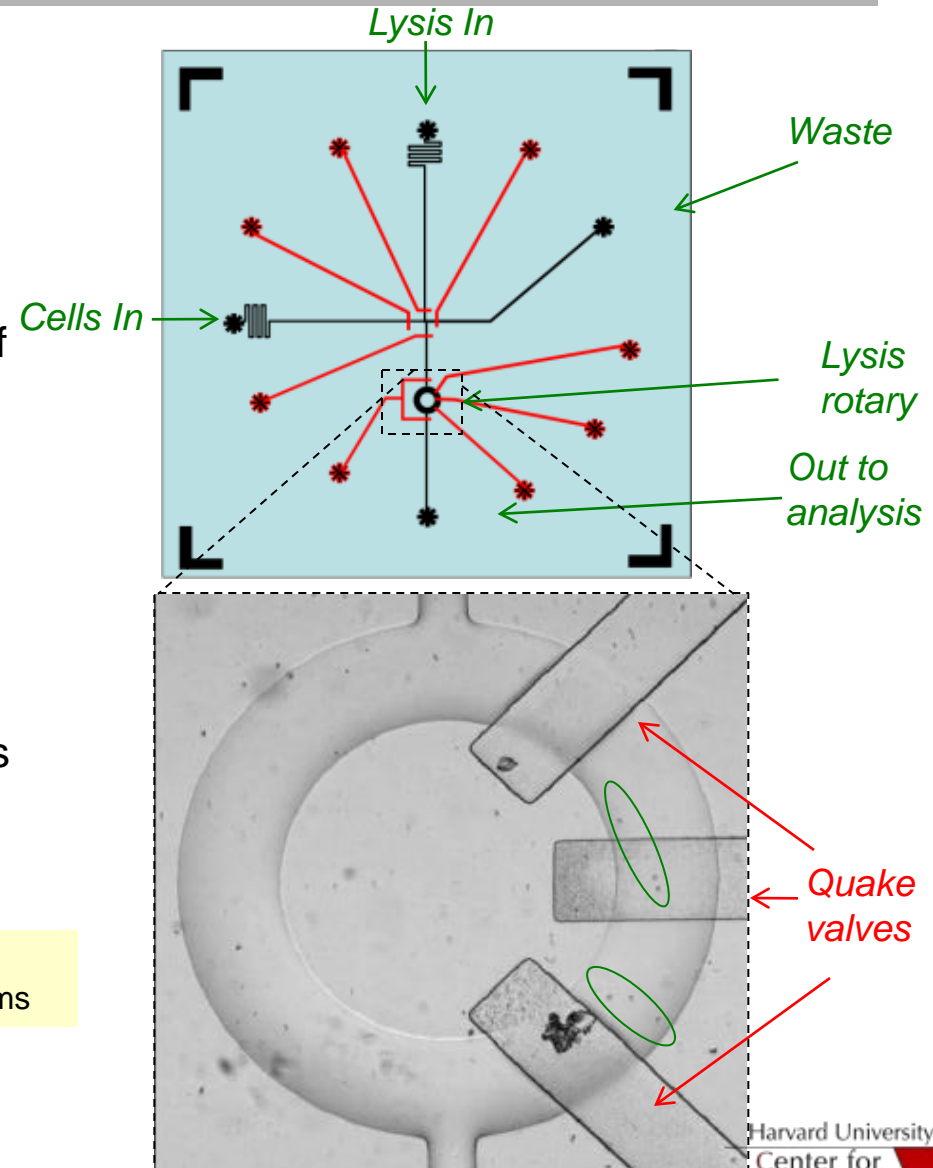
Nenad Miljkovic and Evelyn N Wang, MIT,
Work performed at Harvard Center for
Nanoscale Systems



(A) Scanning electron micrograph (SEM) of an array of the sample. (B) Environmental scanning electron micrograph (ESEM) of water condensation on (A). (C) Time lapse images of condensation captured via ESEM showing the difference in growth behavior between PW and S droplets.

On-Chip Biochemical Analysis of Single Cells

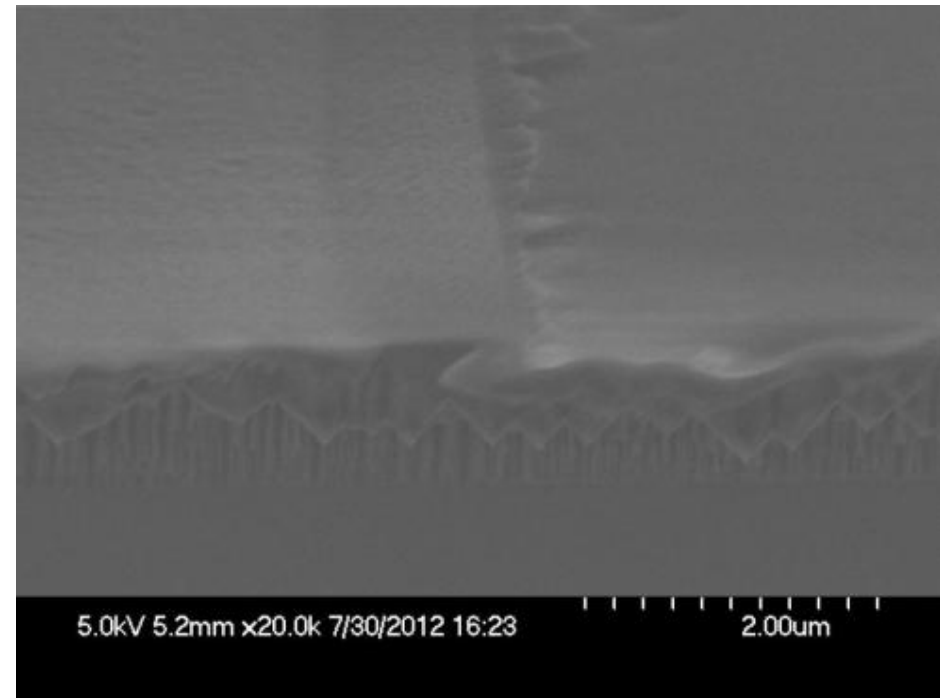
We are fabricating simple microfluidic devices to isolate, lyse, and measure the content of single cells. The device shown here is capable of separating individual cells from a sample and lysing them. The cellular content can then be exported off of the chip to another module for analysis using fluorescence microscopy. The red lines in the schematic are Quake valves and are used to stop the flow and introduce reagents. In the micrograph shown, six cells are contained (green ovals) by the Quake valves and lysis buffer is being introduced. After the valves are opened only those six cells are lysed and their content is sent off of the chip.



Christopher N. LaFratta, David R. Walt, Tufts University
Work performed at Harvard Center for Nanoscale Systems

LED Wafer Etch for Display Applications

This project focuses on the use of a chlorine based plasma etch to etch compound semiconductor wafers. In particular, InGaN LED wafers are obtained from a commercial foundry and by using the Harvard Unaxis RIE tool, LED pixels are segmented on a single sample for display applications. Right is an SEM cross sectional image of an initial result of this etch process. Work is on-going to characterize this etch process and make large array of LEDs.

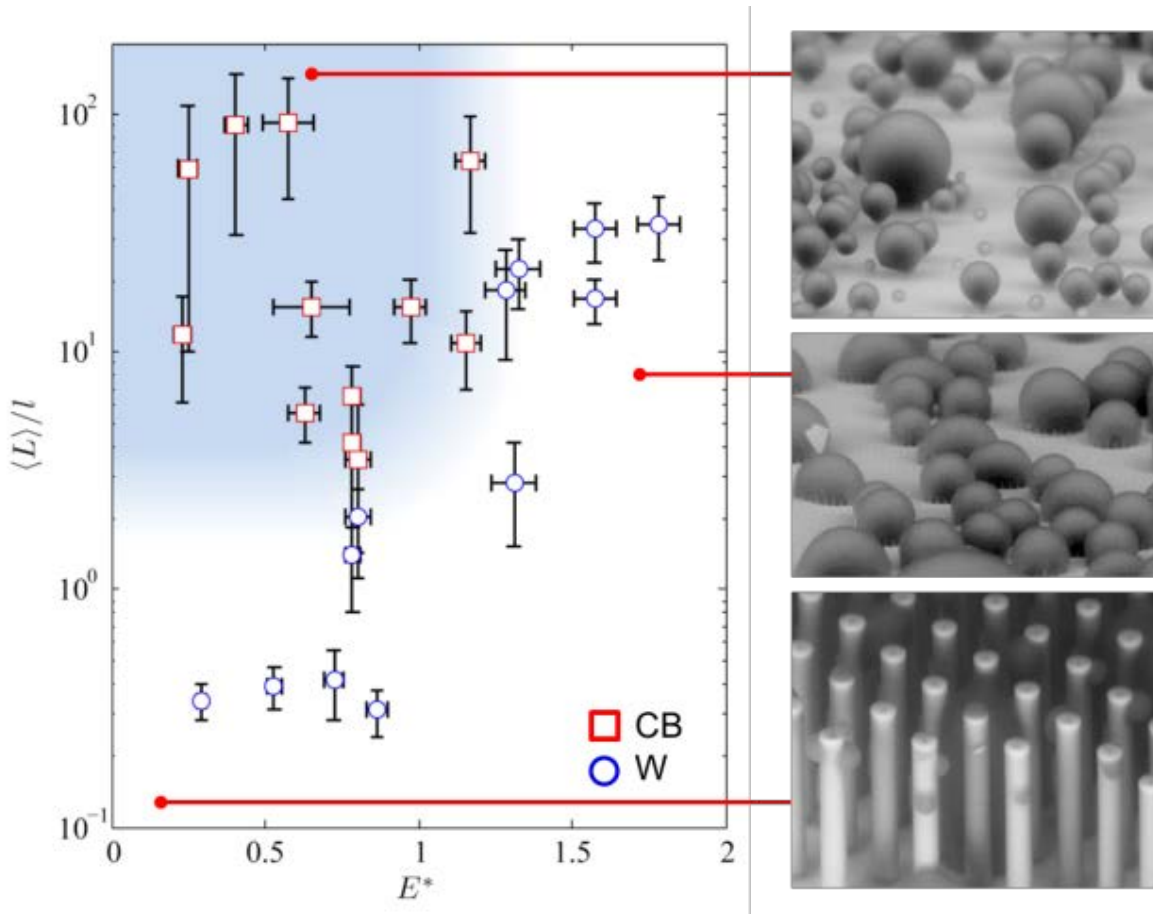


Micrograph of LED etch Profile

Vincent W. Lee (User), Ioannis Kymissis (PI),
Columbia University
Work performed at Harvard Center for Nanoscale
Systems

Condensation on Superhydrophobic Surfaces: The Role of Local Energy Barriers and Structure Length-Scale

Water condensation on surfaces is a ubiquitous phase-change process that plays a crucial role in nature and across a range of industrial applications. Nanotechnology has created opportunities to manipulate this process through the precise control of surface structure and chemistry. In this work, we elucidate, through imaging experiments on surfaces with structure length scales ranging from 100 nm to 10 μm and wetting physics, how local energy barriers are essential to understanding non-equilibrium condensed droplet morphologies and demonstrate that overcoming these barriers via nucleation-mediated droplet-droplet interactions leads to the emergence of wetting states not predicted by scale-invariant global thermodynamic analysis.



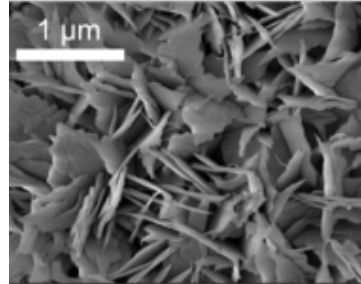
Regime map characterizing the dominant wetting behavior observed during condensation with coordinates of $\langle L \rangle / l$ and E^* . Cassie morphologies emerge at large $\langle L \rangle / l$ and $E^* \lesssim 1$ (shaded region). Wenzel morphologies emerge at low $\langle L \rangle / l$ and/or $E^* \gtrsim 1$.

Ryan Enright, Nenad Miljkovic and Evelyn N Wang, MIT,
Work performed at Harvard Center for Nanoscale Systems

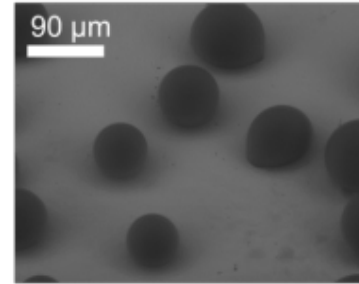
NNIN is supported by NSF ECCS-0335765

Increased Nucleation Density on Liquid-Solid Composite Surfaces for Enhanced Dropwise Condensation Heat Transfer

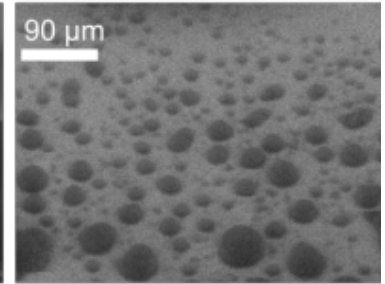
Condensation heat transfer has broad applications in various systems such as heat exchangers, heat pipes, and power plants. Recently, a composite surface has been demonstrated by infusing superhydrophobic microstructured surfaces with low surface tension oil. In this work, we show that by infusing heterogeneous surfaces (copper oxide) with oil (Krytox), we could achieve high nucleation density and easy droplet removal at the same time, making such surfaces ideal for condensation. Such surfaces could potentially be used for high-efficiency heat transfer and water-harvesting applications.



Copper Oxide Surface



Nucleation on silanated copper oxide surface



Nucleation on oil-infused silanated copper oxide surface



Photographs of water condensation on hydrophobic dropwise surface



Photographs of water condensation on oil-infused composite surface

Rong Xiao, Nenad Miljkovic and Evelyn N Wang, MIT,
Work performed at Harvard Center for Nanoscale Systems

Multi-State Quantum Dot Channel (QDC) and Spatial Wavefunction Switched (SWS) FETs

Quantum dot superlattice (QDSL) channel exhibits multiple states in QDC-FETs, allowing simultaneous multi-bit processing enables reduced device count, power dissipation, and extend Moore's law. The QDSL also enables high mobility channels on nano Si thin films. Device applications include compact efficient DRAMs storing 20bits.

Multi-bit SWS-FETs:

- (1) Over An order of magnitude reduction in power, and # FETs.
- (2) Significant increase in speed due to reduction in propagation delay and input capacitance.

2-bit Full Adder 25nm Process	Si FETs	SWS Si	SWS InGaAs
FET Count	64	6	6
Power ($p=1/2CV^2$)	16p-64p	2.5p	2.5p
Delay (ps)	10.4	1.38	0.138

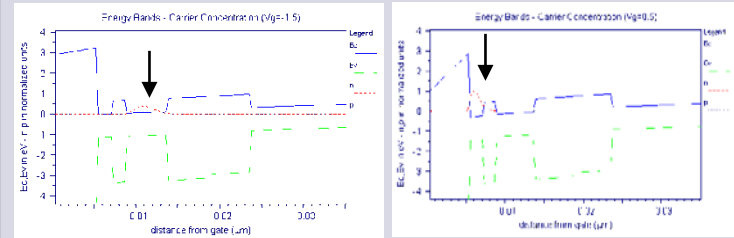
Unipolar SWS-FET Logic:

Multiple channels/thresholds enables CMOS like logic with only fast n-channel SWS-FETs.

F. Jain, ECE, University of Connecticut
Work performed at Harvard Center for Nanoscale Systems

1. Spatial Wavefunction Switching (SWS) in 2- & 3-quantum well FETs.

Gate voltage shifts electron wavefunctions between upper and lower coupled quantum wells that comprise the transport channel, creating a FET with two threshold voltages.

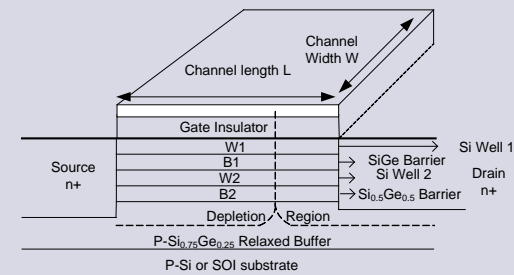


Wavefunction in Well #2

Wavefunction in Well #1

2. Experimental demonstration of vertical charge transfer in a 2-well MOS device.

3. Process multiple bits at once in one SWSFET.



Cell parameters	CMOS	SWS-FETs
Device count per bits	4	1
R/W bits on 8 wide data bus	8 bits	16 bits
Data Interconnect density	2X	1X

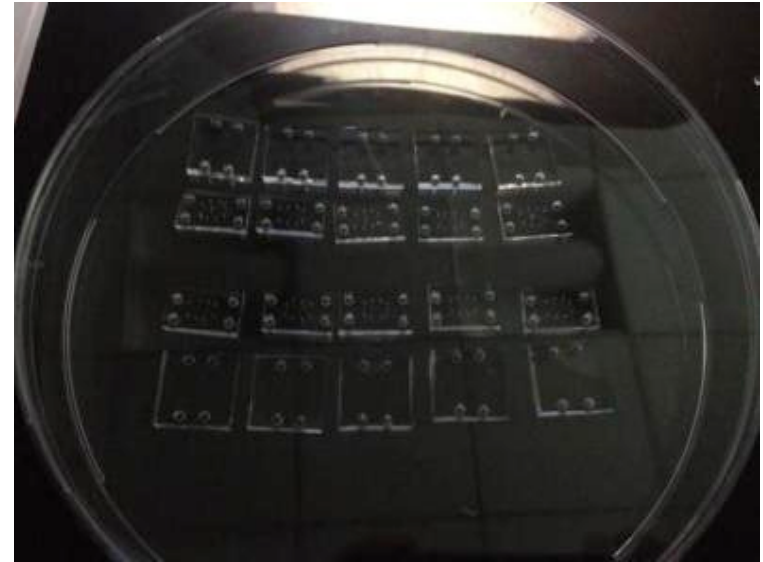
Microfluidics Integrated Nanopore Devices

Nanopore devices have shown significant potential for label-free, direct electronic measurement of biomolecules. However, as passage of molecules through solid state nanopores is often quite rapid ($< 100 \mu\text{s}$) while generating small currents ($\sim 200 \text{ pA}$), signal to noise considerations are vital to accurate biomolecular characterization. The purpose of this project is to significantly reduce capacitive noise in nanopore devices by integrating solid state nanopore membranes into PMDS microfluidic devices. The CNS-fabricated components of this system consist of photolithography for defining SU-8 molds for PDMS soft lithography, and atomic layer deposition on silicon nitride membranes for decreasing nanopore size.

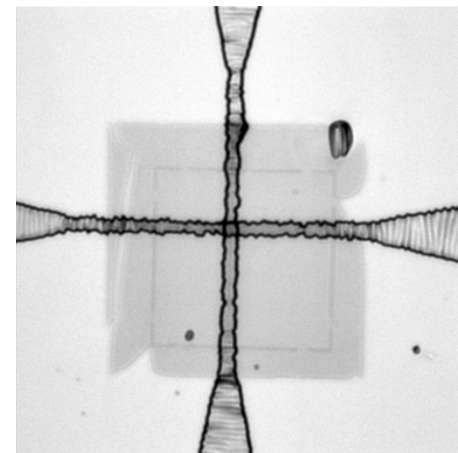
Tarun Jain¹, Carlos Aguilar², and Rohit Karnik¹

1. Massachusetts Institute of Technology
2. Lincoln Laboratory, Massachusetts Institute of Technology

Work performed at Harvard Center for Nanoscale Systems



Set of PDMS fabricated from SU-8 molds

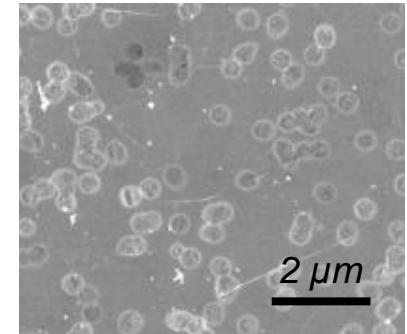
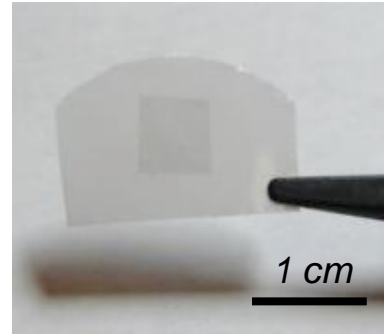


Close-up of nanopore membrane integrated into microfluidic device

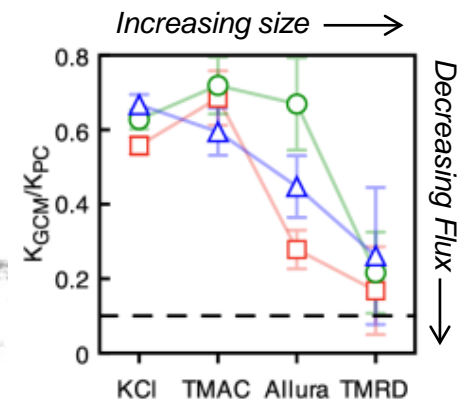
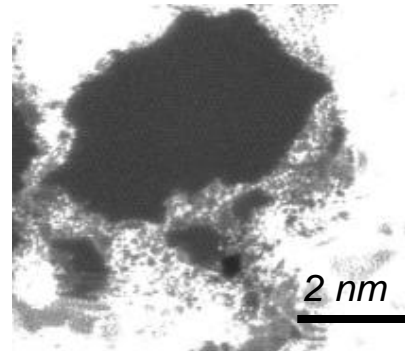
Selective molecular transport through graphene membranes

Graphene, being both atomically thin and incredibly strong, has the potential to be a highly selective, highly efficient filtration membrane through the creation of controlled nanometer-scale holes in the lattice. We have fabricated a large-area graphene membrane consisting of CVD-grown graphene adhered to a porous polymer support and have found holes of 1-10 nm in diameter intrinsic to the graphene. Through diffusive transport experiments, we have found these holes reject the transport of organic molecules larger than 10 nm in diameter, yet permit the transport of smaller molecules such as potassium chloride. Our fabrication and characterization represent the first step in the development of graphene membranes for future applications. Raman characterization of graphene and transmission electron microscopy performed at the CNS.

Sean O'Hern, Cameron A. Stewart, and Rohit Karnik at MIT and Juan-Carlos Idrobo at Oak Ridge National Laboratory
Work performed at Harvard Center for Nanoscale Systems



Graphene membrane consists of CVD graphene adhered to polycarbonate track etch membrane with 200 nm pores.

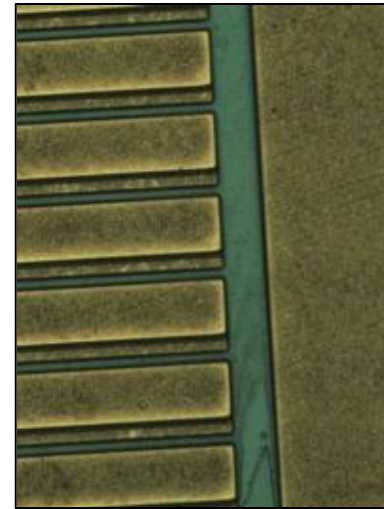


1-10 nm holes in graphene result in size selective transport through graphene. Chart represents the transport through the graphene normalized by the transport through the bare polycarbonate track etch membrane for three different membranes.

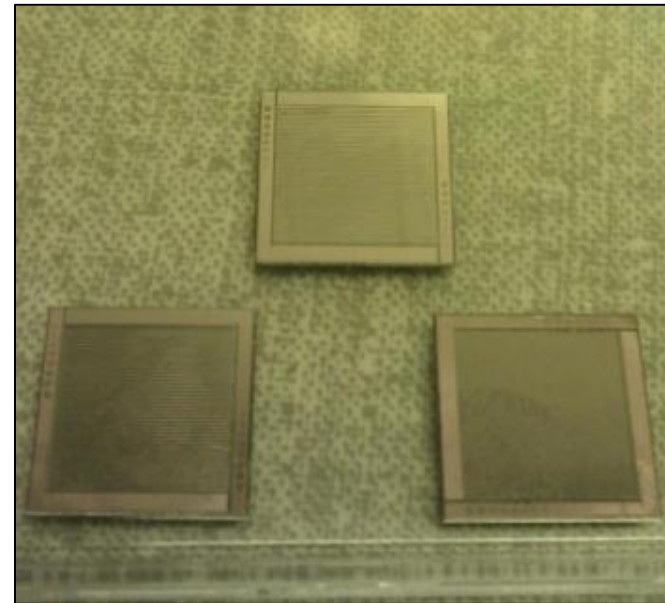
Low Temperature Thermophotovoltaics

The purpose of the Low Temp. TPV project is to extend the operational range of this thermal harvesting technology so it can convert lower temperature heat directly into electricity. CNS is absolutely necessary for this research to etch through the III-V materials, to deposit CVD passivation layers, and to deposit the required contact metals. Many other CNS tools are used as well because they are either better than what we have here at Tufts, or for convenience of processing while at the CNS facilities. The cells are grown via MBE through our research partners and then processed at CNS, where we do lithography, etching, chemical processing, cleaning, thin film deposition, metrology, and imaging.

Dante DeMeo, Corey Shemelya, Thomas Vandervelde,
Tufts University
Work performed at Harvard Center for Nanoscale
Systems



TPV cell after two etch steps and silicon nitride deposition and patterning

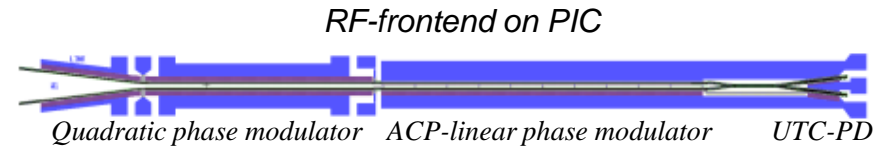


Completed cells, after processing and dicing.

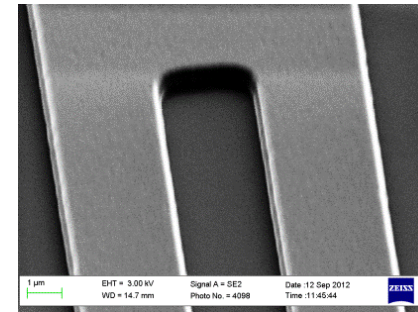
RF Frontend On Photonic Integrated Circuits

The goal of the *RF Frontend on Photonic Integrated Circuits* project is to realize a phase modulated coherent optical link on a Photonic Integrated Circuit (PIC) chip. The PIC chip monolithically integrates linear/quadratic quantum well phase modulators, a compact 3dB optical coupler and a balanced Uni-Traveling Carrier (UTC) waveguide photodetector pair on an InP base wafer. The PIC chips, which are being fabricated using CNS facilities, aim to achieve high Spurious Free Dynamic Range (SFDR), sufficient power efficiency, and cost efficiency, so that they surpass the performance of state-of-the-art electronic amplifiers or mixers, and ultimately enables replacement.

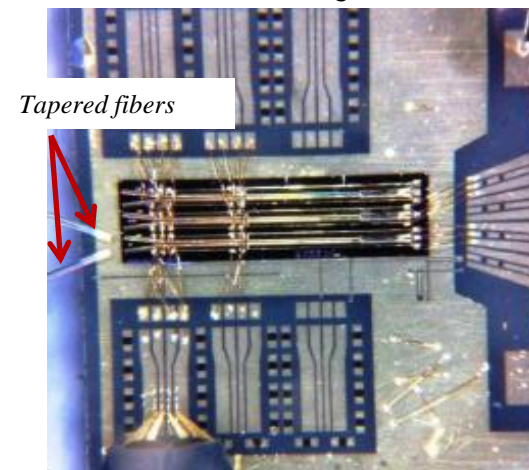
Yifei Li, the University of Massachusetts, Dartmouth
Work performed at Harvard Center for Nanoscale Systems



Deep ridge optical waveguide (of a MMI coupler section)



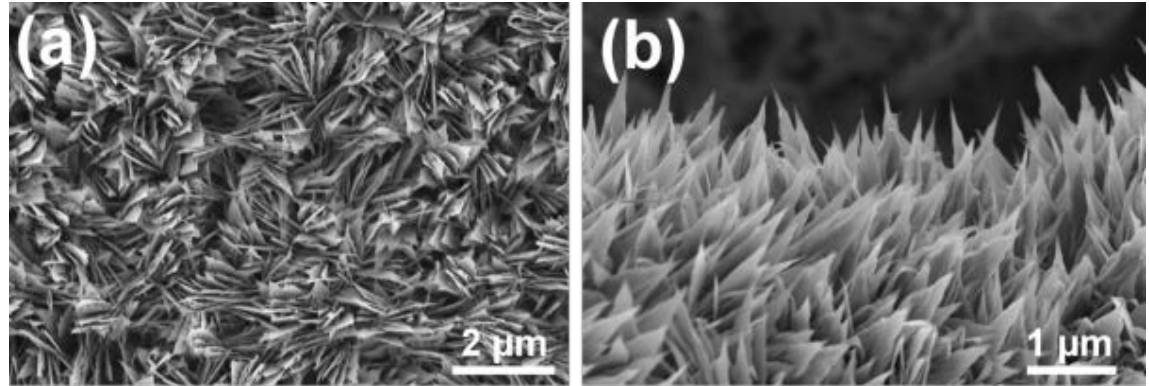
RF Frontend on PIC sitting on an AlN carrier



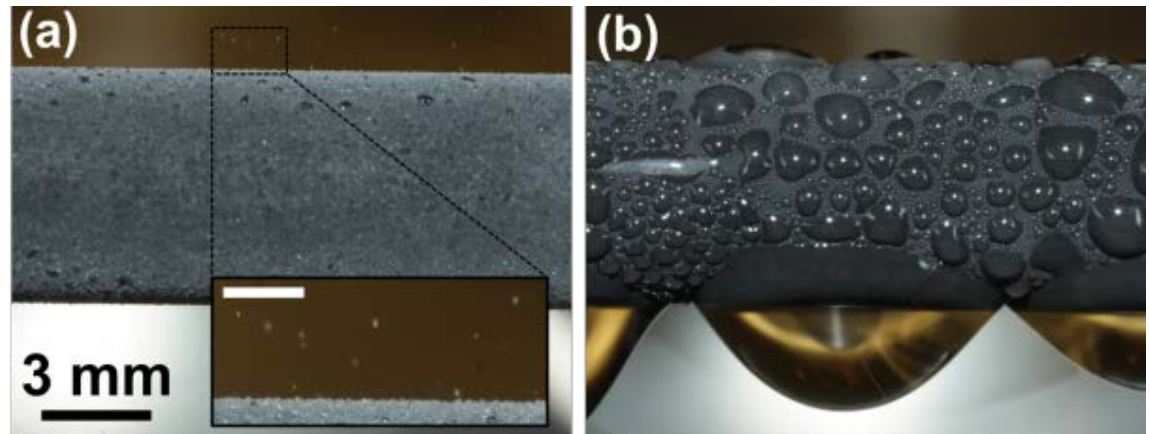
GSSG Probe

Scalable Superhydrophobic Nanostructured Copper Surfaces for Enhanced Condensation Heat Transfer

Superhydrophobic nanostructured surfaces offer a direct path to achieving highly efficient droplet removal and, accordingly, have the potential to enhance condensation heat transfer. The present experimental study demonstrates a simple and scalable method of nanostructuring copper, one of the most widely used heat transfer materials, for highly efficient condensation heat transfer. Coalescence induced droplet jumping is observed and experimentally shown to have ~25% higher overall condensation heat flux and ~30% higher transfer coefficients than state-of-the-art hydrophobic condensing surfaces.



FESEM images of a CuO surface with (a) top view, (b) side view.



Photographs of water condensation on (a) nanostructured CuO tube undergoing jumping condensation (Inset: magnified view of the jumping phenomena, scale bar is 500 μm), and (b) nanostructured CuO tube undergoing flooded superhydrophobic (SHC) condensation.

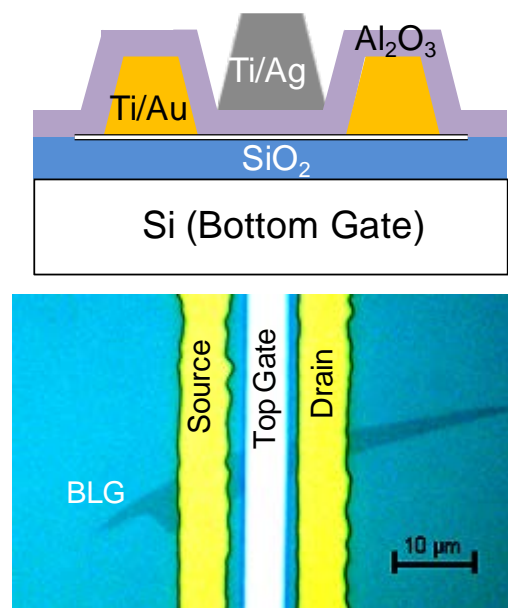
Nenad Miljkovic and Evelyn N Wang, MIT,
Work performed at Harvard Center for Nanoscale Systems

NNIN is supported by NSF ECCS-0335765

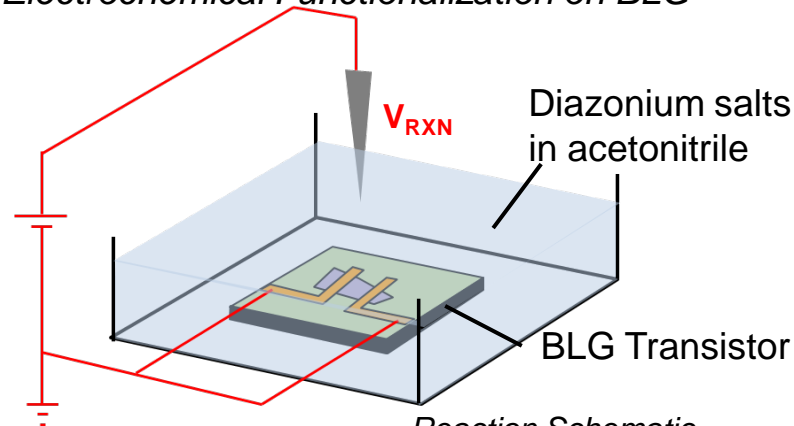
Electronic Transport in Covalently Functionalized Bilayer Graphene (BLG)

Bilayer graphene is emerging as one of the most promising candidates for post-silicon nanoelectronics. Here we present high-throughput functionalization and demonstrate enhanced transport in a FET device structure.

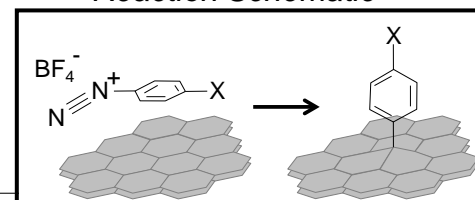
BLG Device Schematic



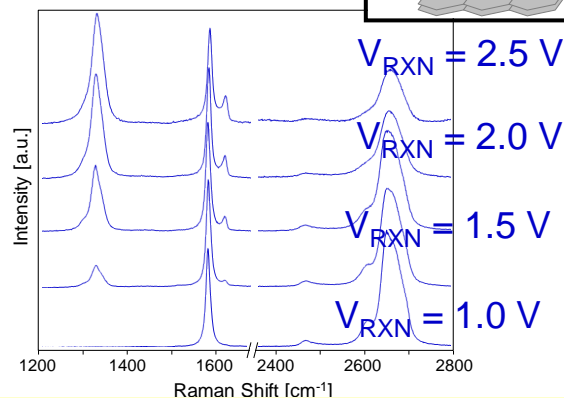
Electrochemical Functionalization on BLG



Reaction Schematic



Raman Spectra of Functionalized BLG



Strano group, MIT

Work performed at Harvard Center for Nanoscale Systems

NNIN is supported by NSF ECCS-0335765

Nitride HEMT Gate Dielectrics by ALD

AlGaN-GaN HEMTs are good candidates for high power amplifiers and switching devices.

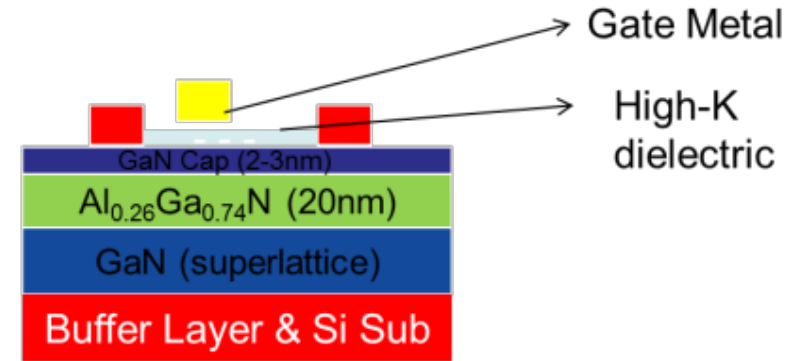
High-K gate dielectrics play a crucial part in this material system by reducing gate leakage current in devices, and providing good passivation.

Over the years, ALD has been reported to be a very potent technique for depositing high-k dielectrics because of:

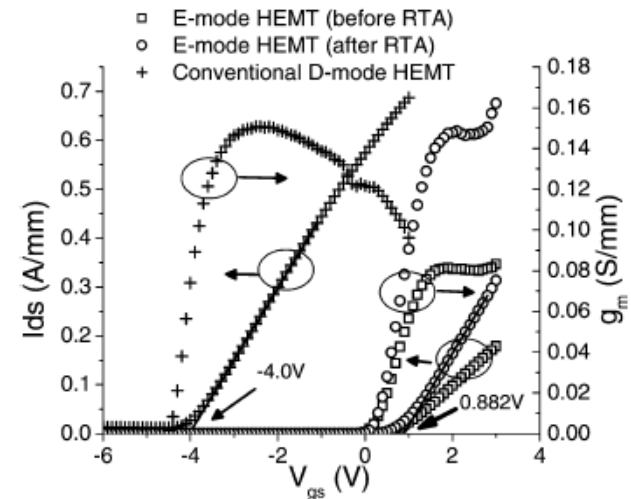
- Extremely conformal deposition
- Less interface scattering due to amorphous nature of oxides
- Ease of use compared to CVD growth reactors

Currently, we are exploring new materials for gate dielectrics with the goals of:

- Obtaining Normally off (i.e positive threshold voltage) devices in AlGaN/GaN system
- Studying Mechanical stress due to dielectrics and passivation and its impact on device performance
- Studying dielectric- channel interface properties using XPS



Typical HEMT structure

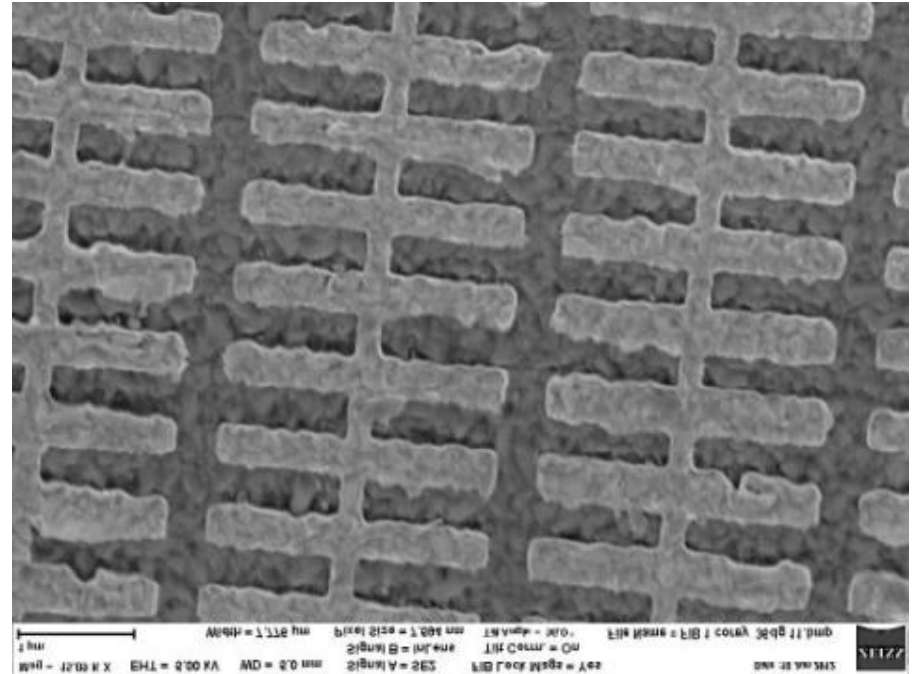


T. Palacios group, MIT
Work performed at Harvard Center for Nanoscale Systems

Metamaterial Polarizers

The purpose of the metamaterial polarizer project is to create a polarizer whose properties can be changed by applying a voltage bias. CNS is used for most of the processing steps, which include electron-beam lithography, chemical processing, cleaning, thin film deposition, metrology, and imaging.

The metamaterial polarizer will have a different polarization with no bias compared to an applied bias. Eventual uses include integration with infrared cameras for detecting manmade objects.



SEM image of metamaterial

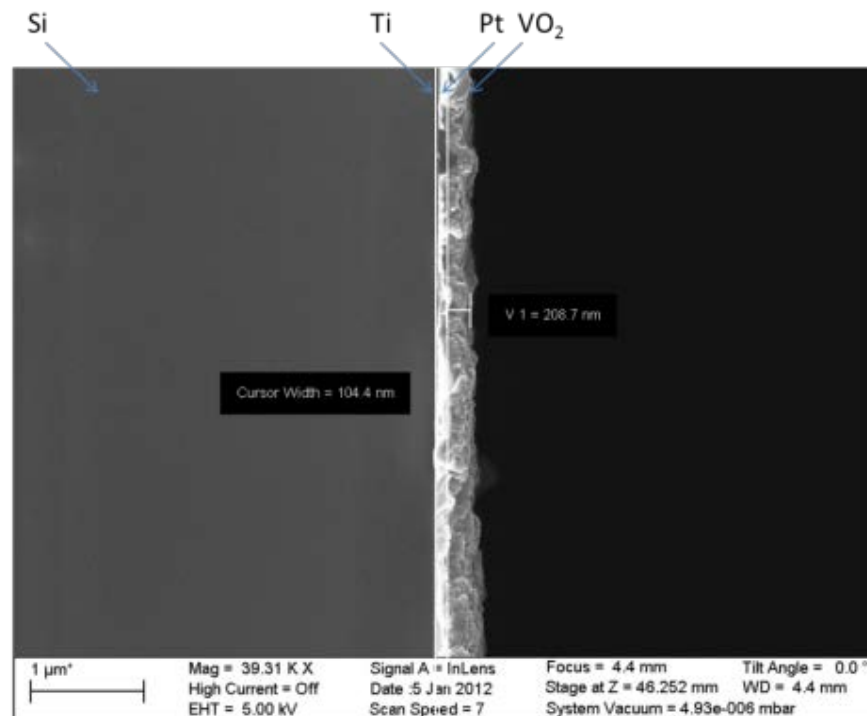
Dante DeMeo, Corey Shemelya, Thomas Vandervelde,
Tufts University
Work performed at Harvard Center for Nanoscale
Systems

VO₂ and SiN Enabled 8-10 um Focal Plane Array

The Harvard CNS facilities were harnessed in a project to build a long wave (8-10 um) polarization detecting focal plane array.

Instrumental in the project was the use of the PECVD tool for deposition of low stress SiN layers allowing precise downstream photolithographic steps and accurate wafer bonding alignment steps.

High temperature D.C. reactive sputtering method allowed temperature dependent phase change VO₂ thin layers for optical applications.



Layered structure on the top of Si substrate: Titanium adhesive layer (not seen on the picture, thickness ~5nm) Platinum, and VO₂.

Andrii Golovin, Center for Metamaterials, City University of New York
Work performed at Harvard Center for Nanoscale Systems

CVD of Thin Film Materials for Microelectronics

The packing density of microelectronic devices has increased exponentially over the past four decades. Continuous enhancements in device performance and functionality have been achieved by the introduction of new materials and fabrication techniques. Professor Gordon's research group at Harvard University has recently developed a few thin film materials and metallization processes by chemical vapor deposition (CVD). These materials and processes have the potential to build future generations of microelectronic devices with higher speeds and longer lifetimes.

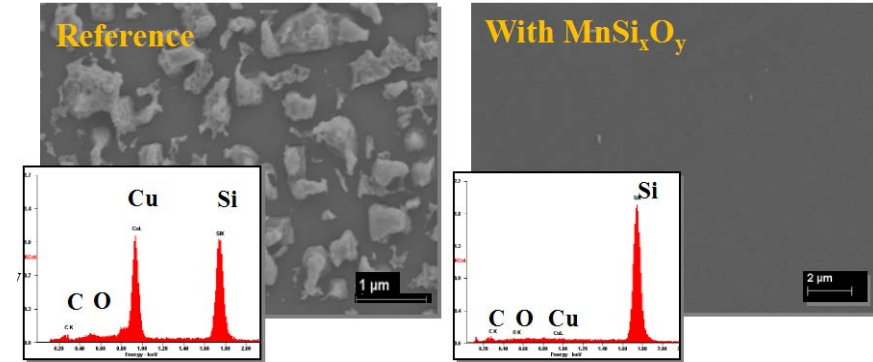


Fig. 1 Highly conformal, amorphous and insulating manganese silicate ($MnSi_xO_y$) layers as excellent barriers to diffusion of copper, oxygen and water

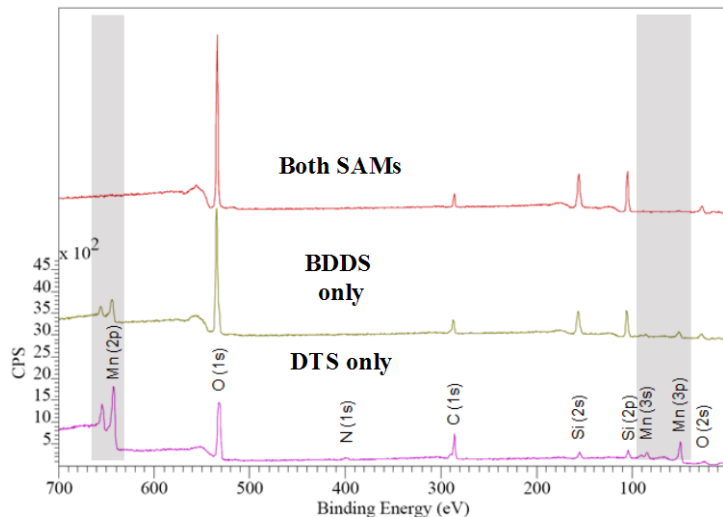


Fig 2. Selective CVD manganese capping process that strengthens the interface between copper and dielectric insulators to improve the electromigration reliability

Fig 3. Surfactant-catalyzed CVD process that fills sub-20 nm trenches or forms continuous Cu seed layers in high aspect ratio Through-silicon vias (TSVs)

Yeung Au and Roy Gordon, Harvard University
Work performed at Harvard Center for Nanoscale Systems (CNS)

NNIN is supported by NSF ECCS-0335765

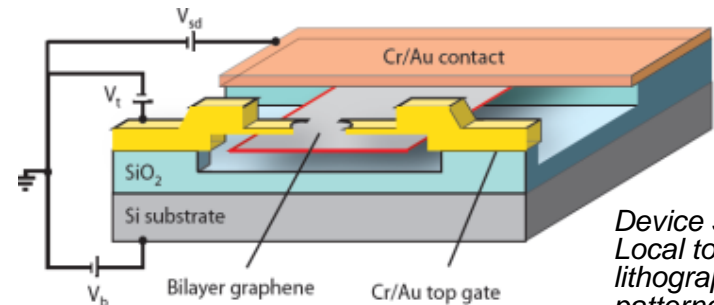


Gate-defined Quantum Confinement in Suspended Bilayer Graphene

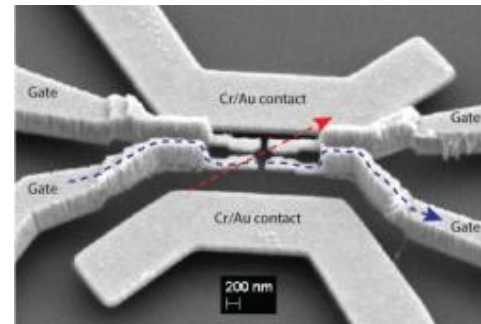
Quantum confined devices in carbon-based materials offer unique possibilities for applications ranging from quantum bits to electrochemical sensing. Allen *et al.* present a novel approach to quantum confinement utilizing tunnel barriers defined by local electric fields that break sublattice symmetry in suspended bilayer graphene. This technique electrostatically confines charges via band structure control, thereby eliminating the edge and substrate disorder that hinders on-chip etched nanostructures to date. The observed Coulomb blockade periodicity concurs with electrostatic simulations based on local top-gate geometry, a direct demonstration of local control over the band structure of graphene. The ability to externally tailor the graphene bandgap over nanometer scales opens a new unexplored avenue for creating quantum devices.

Reference: Allen, M. T. et al. Nature Communications. 3:934 doi: 10.1038/ncomms1945 (2012)

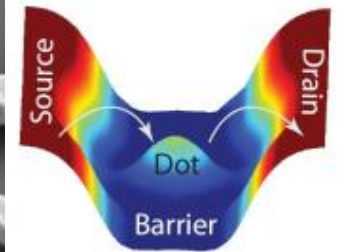
Monica Allen, Jens Martin, and Prof. Amir Yacoby,
Dept. of Physics, Harvard University
Nanofabrication performed at Harvard CNS



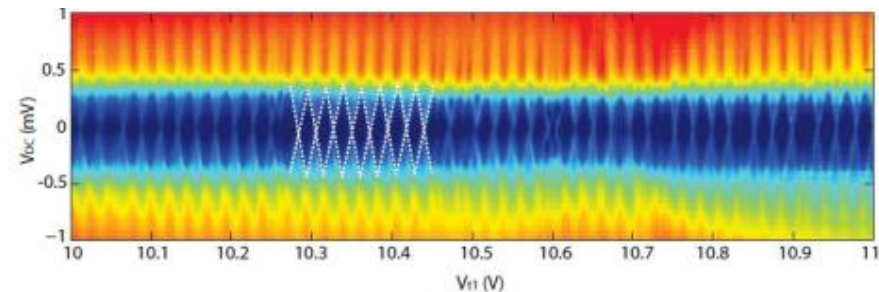
Device schematic. Local top gates are lithographically patterned



SEM image of a suspended gate-defined quantum dot



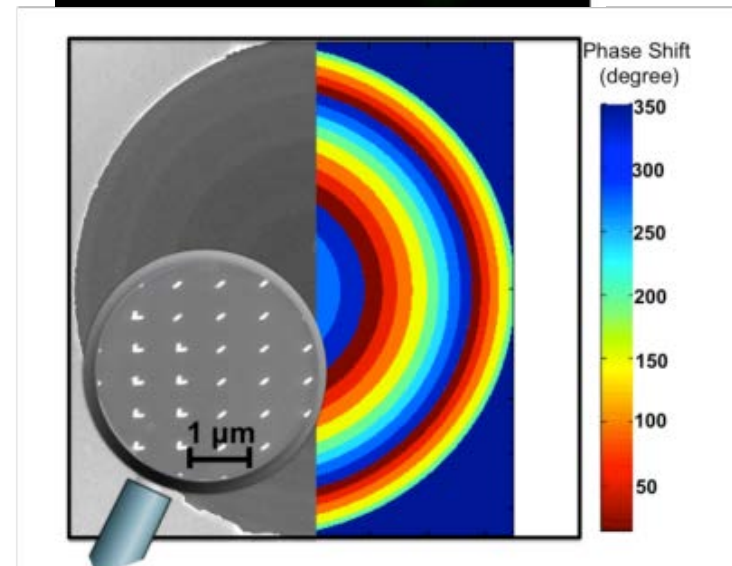
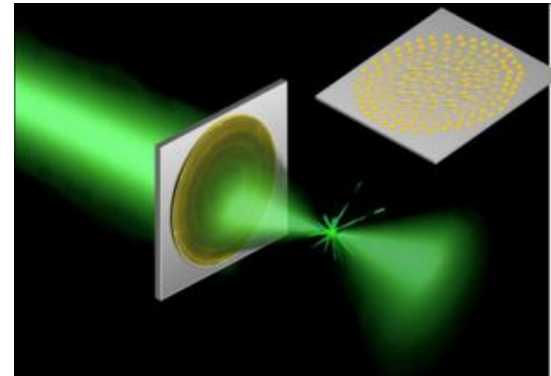
Simulated carrier density profile illustrates confinement



Single electron tunneling in the quantum Hall regime: Coulomb blockade oscillations using the Landau level gap for confinement.

Aberration-Free Ultrathin Flat Lenses based on Plasmonic Metasurfaces

We applied the concept of optical phase discontinuities to the design and demonstration of aberration-free planar lenses. At a 60 nanometers thick, the flat lens is essentially two-dimensional, yet its focusing power approaches the physical diffraction limit. The flat lens eliminates optical aberrations such as spherical, astigmatism and coma aberrations, so the resulting image does not require any corrective technique.

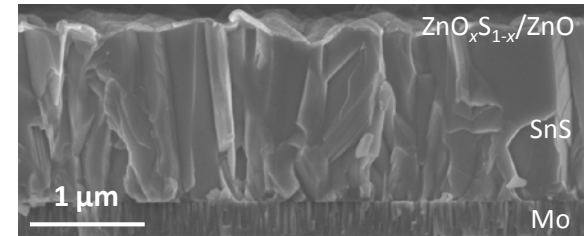


A new ultrathin, flat lens focuses light without imparting distortions. Right: A micrograph of the flat lens (diameter approximately 1 mm). The surface is coated with concentric rings of gold optical nanoantennas (inset). The colored rings show the magnitude of the phase delay corresponding to each ring.

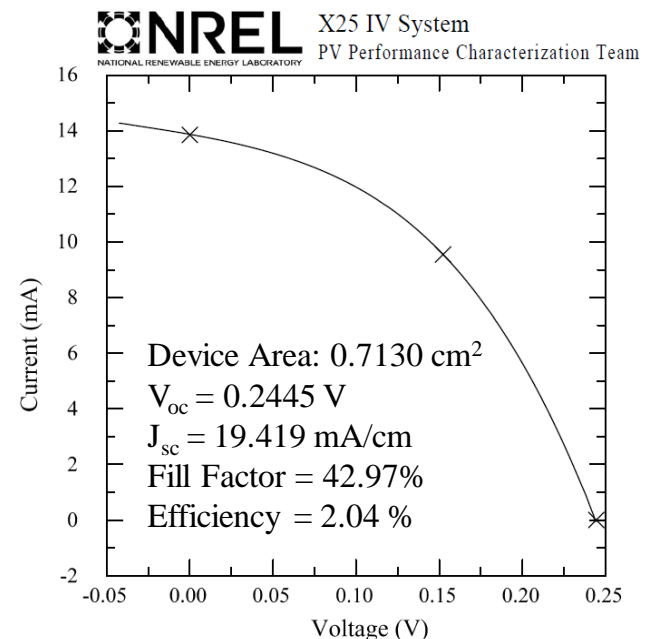
Federico Capasso group, Harvard University
Work performed at Harvard Center for Nanoscale Systems (CNS)

Earth-Abundant SnS Thin Film Solar Cells

The purpose of this project is to find an alternative earth-abundant absorber material to replace the current thin-film PV technologies (CdTe and Cu(In,Ga)Se₂) whose widespread use is limited by their use of scarce, costly, and toxic elements. The device structure is glass/Mo/SnS/ZnO_{1-x}S_x/ZnO/ITO/Al. SnS film serves as a *p*-type absorber layer to generate photocurrent. SnS was deposited from pulsed chemical vapor deposition (pulsed-CVD) using an organometallic Sn precursor (Sn(MeC(N-*i*Pr)₂)₂) and hydrogen sulfide (H₂S). ZnO_{1-x}S_x is made by atomic layer deposition (ALD) and used as an *n*-type partner to SnS. By adjusting the composition of ZnO_{1-x}S_x, a record efficiency for SnS solar cells, 2.04%, was achieved. Material defect engineering and device optimization are under investigation to improve the performance of SnS-based solar cell up to a potential commercial level (>10%).



Cross-sectional SEM image of the device before top contact deposition.



A current world-record SnS-based solar cell, certified by NREL.

Prasert Sinsermakul¹, Tonio Bounassisi², and Roy Gordon¹. ¹Harvard and ²MIT.

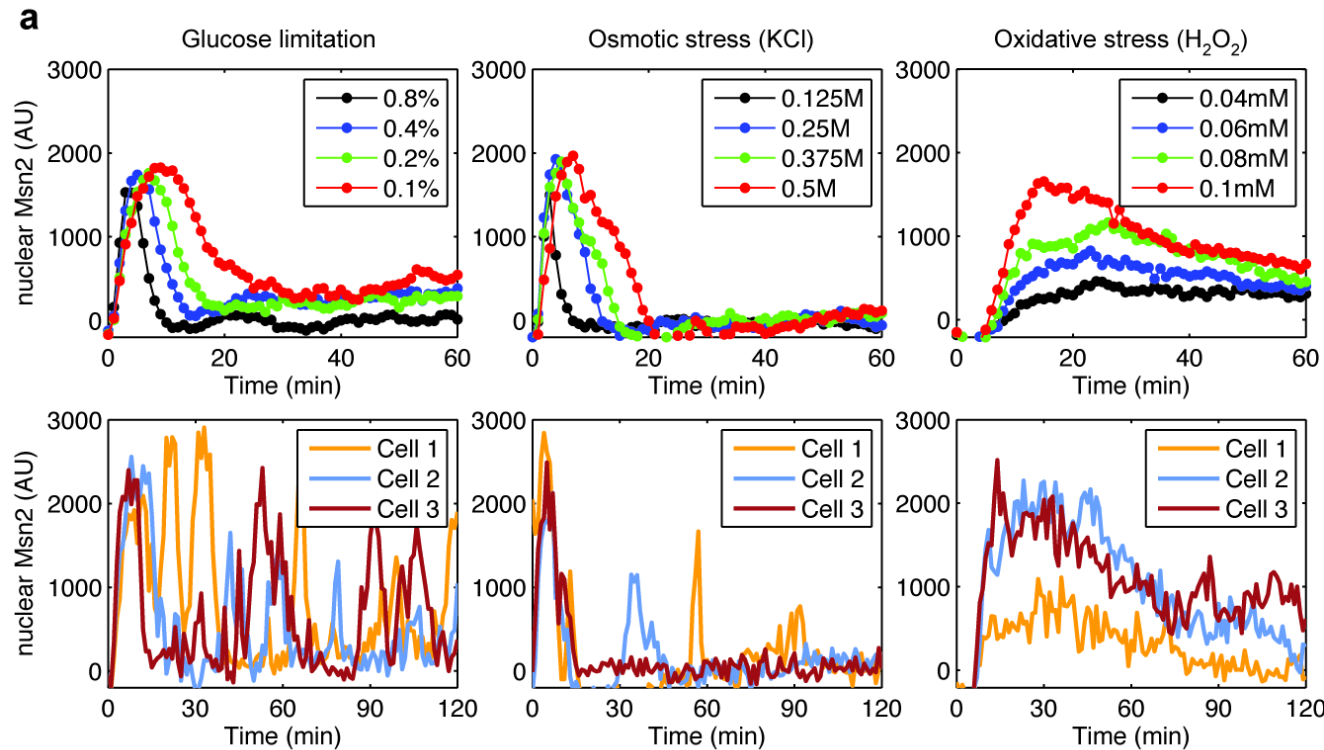
Work performed at Harvard Center for Nanoscale Systems

Microfluidic System For Evaluating Signaling Information In Transcription Factor Dynamics

Using microfluidic systems fabricated at CNS, we observed that transcription factor Msn2 exhibits qualitatively different translocation dynamics in response to different natural stresses

➤ Nuclear translocation of Msn2-YFP was monitored in single cells cultured within a microfluidic platform (made in the CNS facility) using time-lapse fluorescence microscopy.

➤ We used the microfluidic device to control the amplitude, duration and frequency of TF Msn2 nuclear translocation and studied the gene expression outputs.



Nan Hao and Erin K. O'Shea Harvard University
Work performed at Harvard Center for Nanoscale Systems

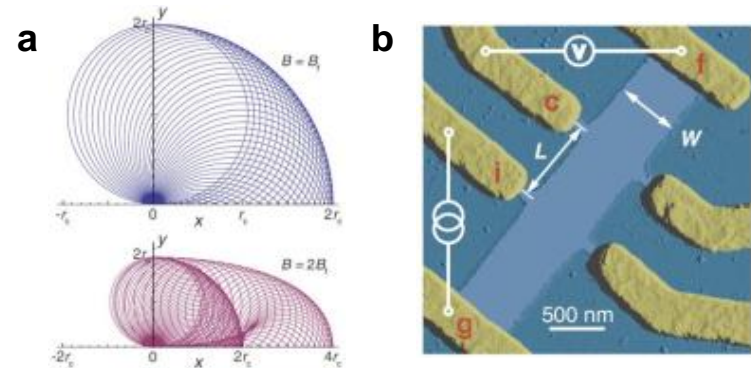
Electron Focusing in Graphene

Electrons in a periodic lattice can propagate without scattering for macroscopic distances despite the presence of the non-uniform Coulomb potential due to the nuclei. Such ballistic motion of electrons allows the use of a magnetic field to focus electrons. This phenomenon is known as magnetic electron focusing (MEF).

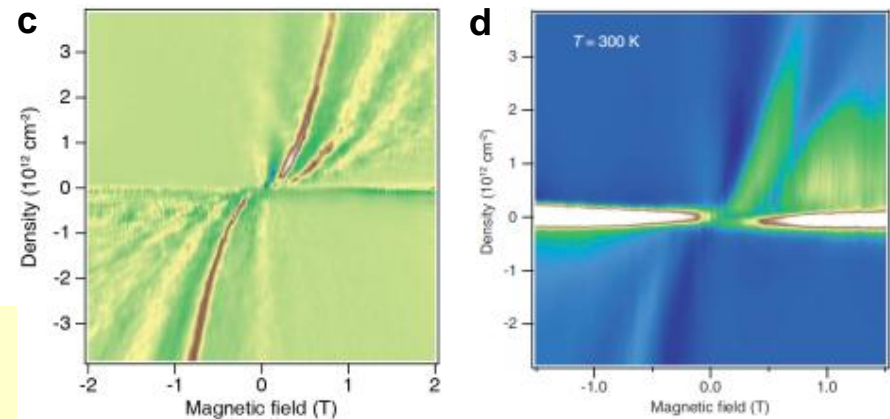
Here we observe MEF in ultra-high quality graphene devices. The ability to tune the graphene carrier density enables us for the first time to investigate MEF continuously from the hole to the electron regime and analyze the resulting "focusing fan". Finally, we demonstrate that MEF survives in graphene up to 300K, by far the highest temperature reported for any system, opening the door to room temperature applications based on electron-optics, such as Veselago lensing.

Thiti Taychatanapat, Kenji Watanabe, Takashi Taniguchi, and Pablo Jarillo-Herrero
Harvard, NIMS, and MIT

Work performed at Harvard Center for Nanoscale Systems



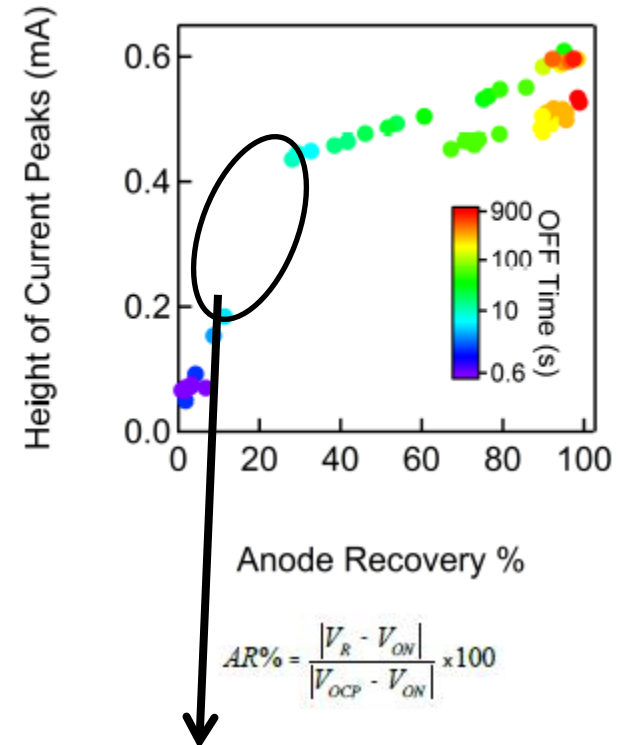
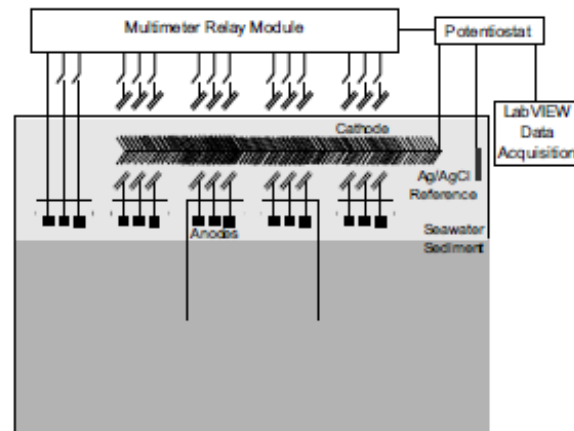
a) Classical trajectories of electrons injected isotropically from the origin at $B = B_f$ (top) and $B = 2B_f$ (bottom, including one bounce off the edge). Electrons are focused at an integer multiple of $2r_c$ along the x -axis. **b)** False color atomic force microscopy (AFM) image of a MEF device.



c-d) The MEF spectra as a function of density and magnetic field in graphene at 5 K and 300 K respectively.

Duty Cycling Influences Current Generation in a Multi-Anode Environmental Microbial Fuel Cell

We have demonstrated microbial fuel cells which do not require research-grade materials. The fuel cells operate because of a particular trait of anaerobic bacteria. As these bacteria live and metabolize food in their oxygen-free environments, they produce extra electrons, which are normally released into the material around them. By introducing an electrode, those electrons can be harvested to create a small electrical current.



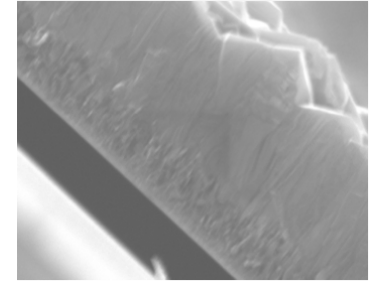
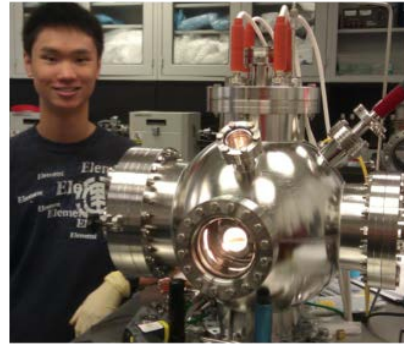
Emily J. Gardel, Mark E. Nielsen, Philip T. Grisdela Jr., Peter R. Girguis, Harvard University.
Work performed at Harvard Center for Nanoscale Systems

This cross-over in current corresponds to the amount of time it takes for substrate (organics used for microbial metabolism) to pass through both the diffusion layer and biofilm.

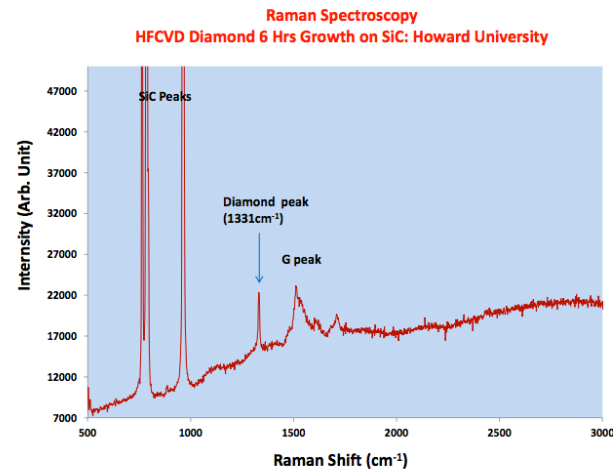
Howard University

CVD Growth of Diamond

- Large area of Hot-Filament CVD growth of diamond from CH_4 and H_2
- Substrates include SiC (6H,3C,4H) and Si
- Diamond seeding and un methods
- up to 8 hour growths at $0.25\mu\text{m/hr}$
- filament temperature $>2000^\circ\text{C}$ at 30 torr



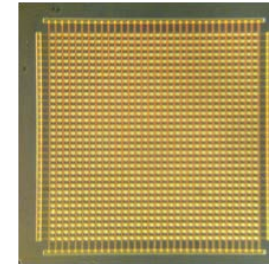
diamond on SiC $3\mu\text{m}$ thick



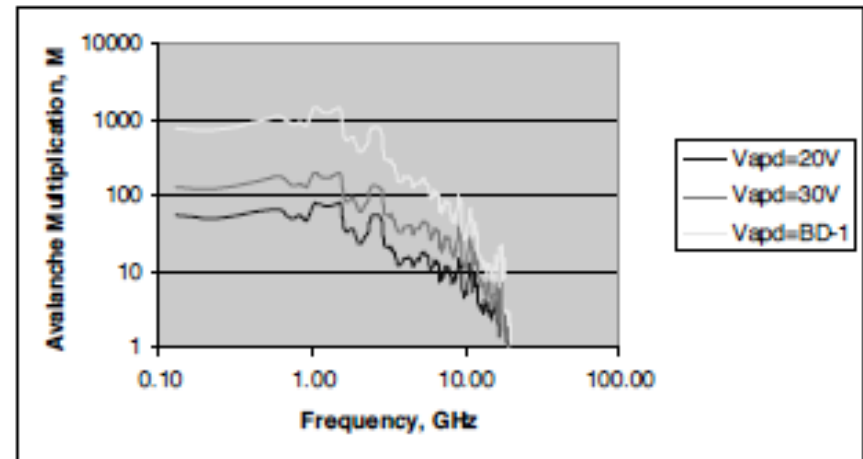
*R. Westervelt (Harvard U.), A. Tam (Rice),
G.L.Harris (Howard), RD Vipute (Blue Wave
Semiconductor)
Growth performed at Howard University*

Avalanche Photodiode Fabrication & Growth

- Epitaxial Technologies have hired two researchers that work at HNF
- Researchers trained users on HNF
- Wafers growth at HNF
- 8 by 8 and 32 by 32 arrays
- APD arrays being used to produce :single photon receivers, laser warning receivers



32 by 32 APDs

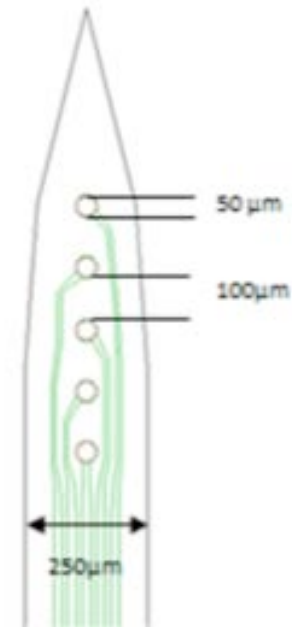
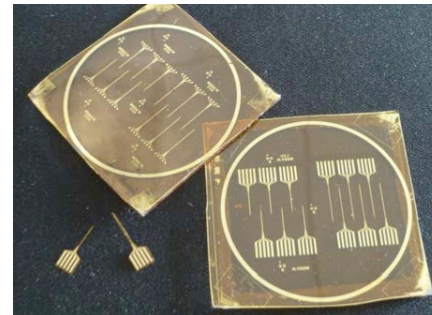


RF gain characteristics

*L. Aina and A. Jackson (Epitaxial Technologies Inc.)
Work performed at Howard University*

Development And Investigation Of Flexible Polymer Neural Probe For Chronic Neural Recording

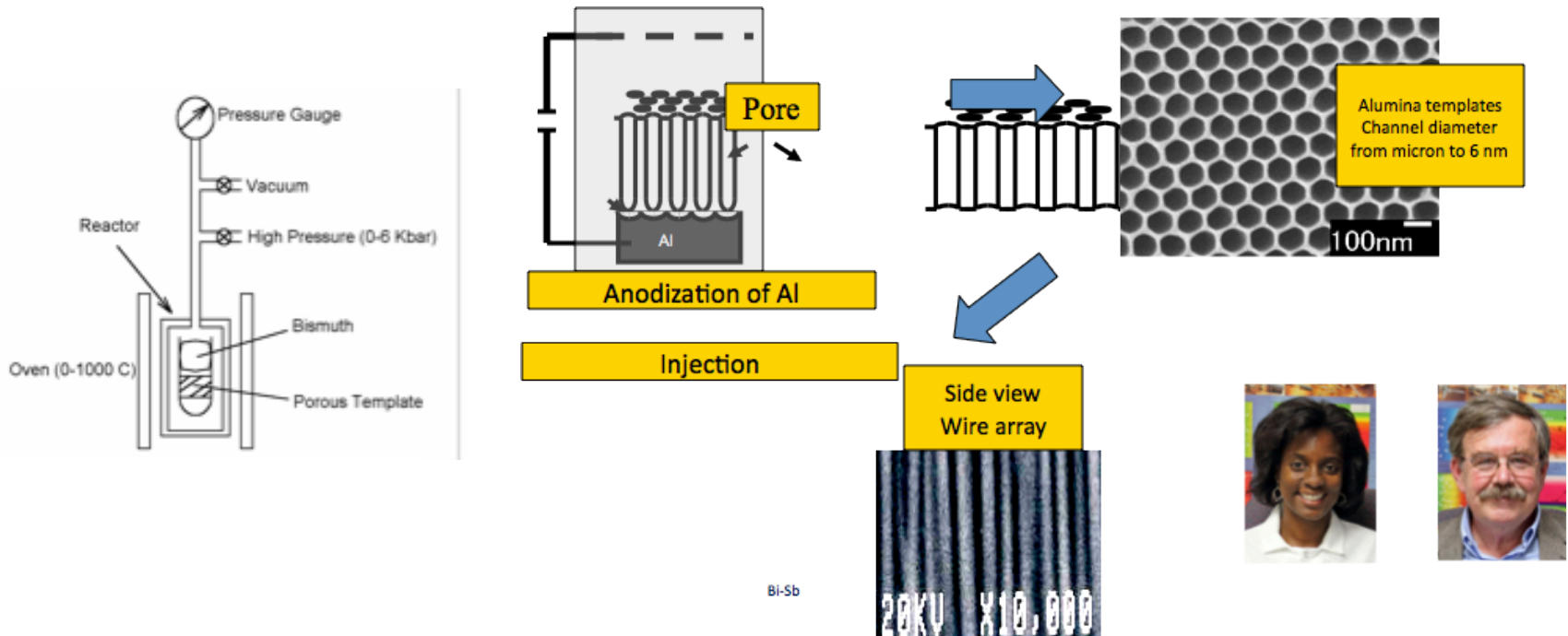
- To aid the pathologic study of virus infection and evaluation of therapeutic treatment in the brain, a chronic and in-vivo sensing method is developed.
- The efficacy of the 3-dimensional nanoelectrode is investigated using an electrochemical analysis



needle structures and recording sites

H. Yoon and C S. Smith, Electronics Engineering, Norfolk State University, W. Kim, T. Zeng, and L.D. Sanford Eastern VA Medical School, Work performed at Howard University

Fabrication of Bi Sb Nanowires for Thermoelectric Applications



T.E. Huber *et al.*, Phys. Rev. B 83, 235414 (2011) and J. App. Phys 111,043709(2012).

T. Brower-Thomas, T. Huber (Howard), S Johnson & S. Sinex (Prince George's Community College)
Work performed at Howard University

Growth and Characterization of GaAs/InAs Quantum Dots by Molecular Beam Epitaxy

- Stranski-Krastonov (SK) growth of GaAs/InAs
- Calibrate both InAs and GaAs growth rate and doping of GaAs
- Fabrication and characterization of GaAs/InAs quantum dot structure
- Ideality 1.134, R_s 61 Ω

Quantum Dots Sample

<i>Au Schottky contact</i>
<i>MBE n-GaAs cap layer</i>
<i>MBE n-GAs confining Layer</i>
<i>InAs QD (3 monolayer)</i>
<i>MBE n-GaAs buffer</i>
<i>n= -GaAs substrate</i>
<i>AuGeNi ohmic contact</i>

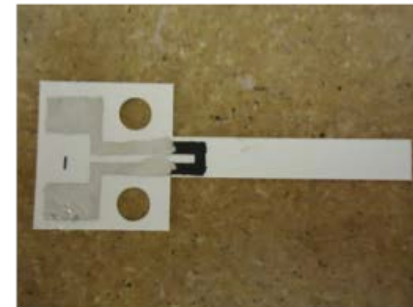
*D. McArthur (Norfolk State U.), J. Griffin (Howard),
Work performed at Howard University*

Fabrication of MEMS Using Inexpensive Substrates

- Cheap substrates like paper for MEMS devices
- Fabrication of several MEMS devices like cantilevers using paper
- Goals is to maximize the cost - to - performance ratio
- Minimize and explore new paper types



*paper microphone use piezoresisitivity
carbon*



MEMs cantilever on paper resolution 100 μ N

*W. Rose (Howard U.), R. Gaudreau (Stony Brook University),
G.L.Harris (Howard)
Work performed at Howard University*

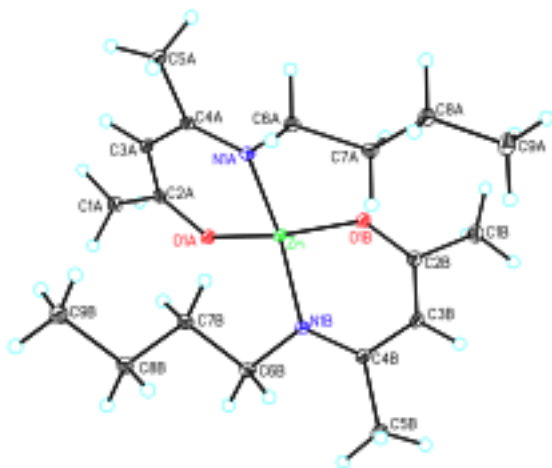
CVD Large Area Graphene

- Cu or Ni evaporation + annealing on SiO_2 deposited on Si
- Methane CVD of graphene
- Transfer on graphene layer using PMMA/photoresist
- graphene release with $\text{HCl} + \text{H}_2\text{O}$
- Also growth of graphene by Hot filament CVD and SiC surface conversion



*M.G. Spencer(Cornell U.), J Halpern(Howard), G.L.Harris (Howard)
Work performed at Howard University*

Synthesis and Evaluation of Novel ZnO MOCVD Precursors



bis(4-N-n-butylamino-2-pentanonato) zinc

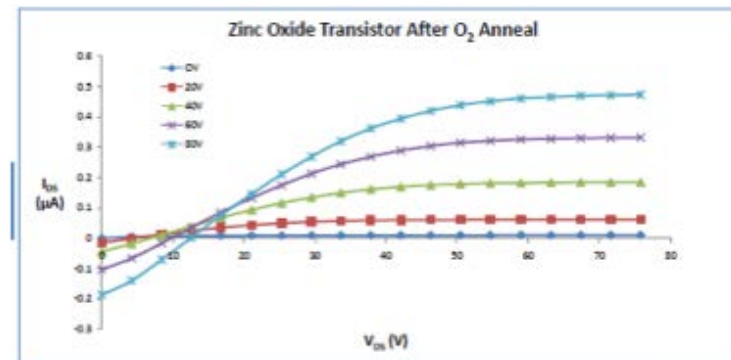


Fig. 4-5: The Voltage (V_{DS}) - Current (I_{DS}) under different Gate Voltage (V_G)

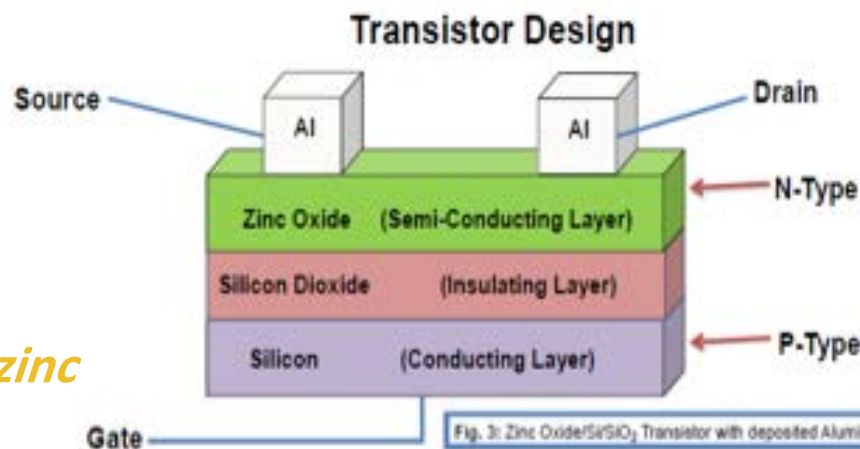


Fig. 3: Zinc Oxide/SrSiO₃ Transistor with deposited Aluminum electrodes

Chemistry: Matthews Research Group: K. O. Johnson (PhD Candidate), Jason S. Matthews, PhD
Work performed at Howard University

Summer Camp for Teachers in Materials Science Nanotechnology

- 29 High School teachers from the Washington Area
- One Week on Training in Materials Science and Nanotechnology
- Laboratory base:HNF lab and general chemistry
- Taught by senior teachers and HNF staff



*Sponsored by: US Air force STEM office, HNF and ADM Materials Foundation
Work performed at Howard University*

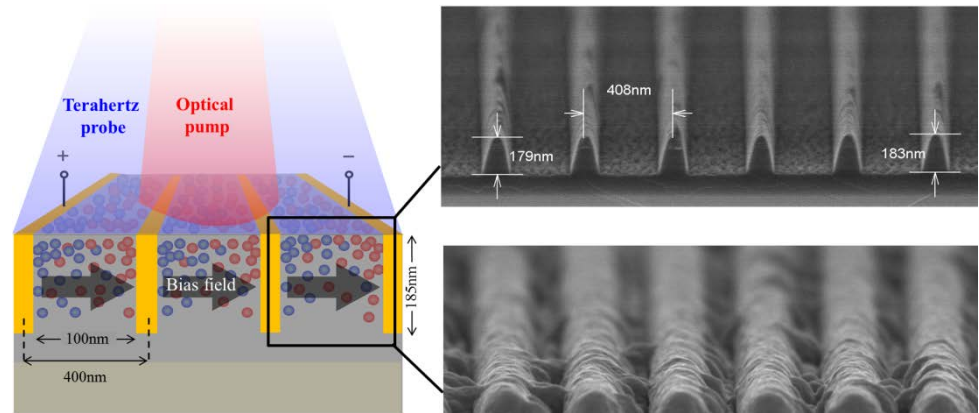
Stanford University

Plasmonic Terahertz Optoelectronics Project

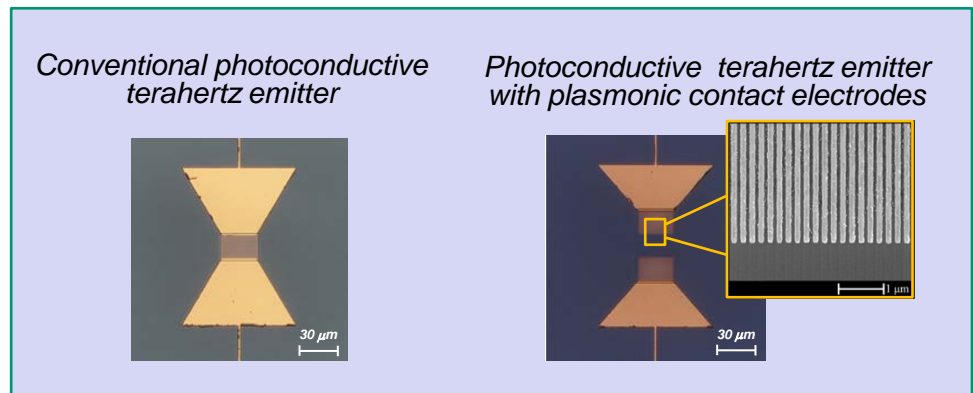
The purpose of the Plasmonic Terahertz Optoelectronics Project is to investigate unique properties of plasmonic antennas to mitigate efficiency degradation of conventional antennas interacting with nano-electronics at terahertz and optical frequencies. The SNF-fabricated prototypes of this study have been meta-surfaces used for efficient interaction of terahertz and optical waves at the nano-scale.

Following this study, our group has demonstrated multi-spectral plasmonic antennas enabling single-photon terahertz spectrometry at room-temperature. We have also demonstrated two orders of magnitude terahertz power enhancement by using plasmonic photoconductive terahertz sources compared with conventional designs.

Mona Jarrahi, University of Michigan, Ann Arbor
Work performed at Stanford Nanofabrication Facility



Multi-spectral plasmonic gratings enabling efficient interaction of optical and terahertz waves at the nanoscale



Plasmonic terahertz emitters enabling two orders of magnitude higher optical-to-terahertz conversion efficiencies compared to conventional photoconductive emitters

Shrinking Atomic Force Microscope (AFM) Probes

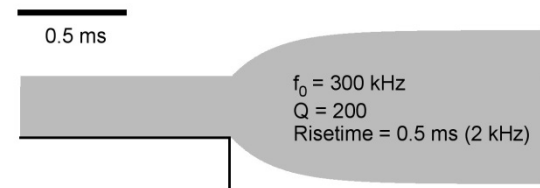
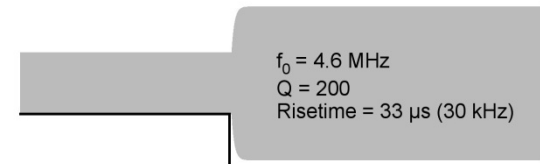
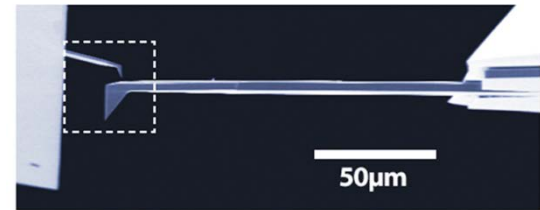
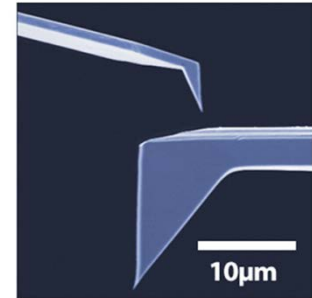
The purpose of the project is to improve AFM performance by increasing the detection bandwidth and lowering the detection noise to allow higher imaging speeds and fidelity. Scaling down the size of the probe increases their mechanical resonance while reducing their thermal noise.

We have fabricated probes 10x smaller than the state-of-the-art. Like their predecessors, these novel probes have been fabricated on silicon wafers. However, entirely different processes are required because the novel probe geometries are smaller than the variations inherent with the previous probe fabrication techniques. Preliminary results indicate that the process is commercially viable.

The novel small probes consist entirely of silicon for a high and repeatable mechanical quality. Their spring constants are tunable for a variety of imaging modes and the tips are atomically sharp. They can be coated or doped with materials to accommodate most AFM applications.

*Hector Cavazos, Asylum Research Corporation
Work performed at Stanford University and UC Santa Barbara
Nanofabrication Facilities*

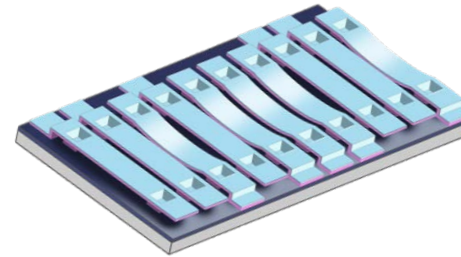
Novel small probe landing on a commercially available probe.



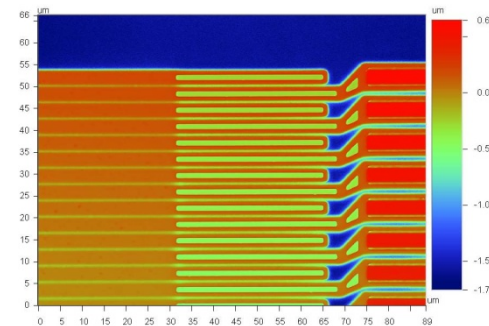
A faster reaction time of a novel short probe (top) VS standard probe (bottom) while scanning over a step in AC mode.

MEMS Light Modulator & Microdisplay

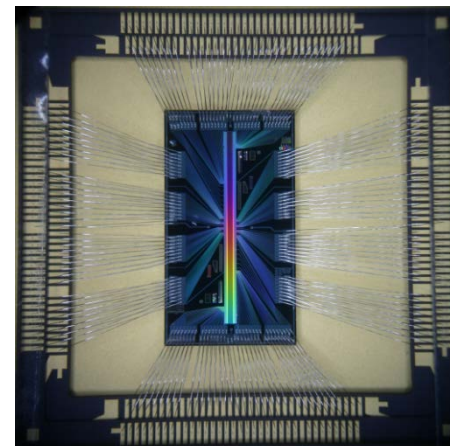
Alces' MEMS light modulator is the cornerstone of next-generation laser-based display and sensor systems. When coupled with Alces' unique optical architectures, this MEMS light modulator opens up many new possibilities for high-performance projection displays, 3D depth sensors, and optical storage applications. Using CMOS-compatible fabrication processes, MEMS arrays are fabricated at SNF's facilities for use in Alces' custom metrology and display systems. The MEMS "pixels" are engineered from a bilayer of silicon nitride and aluminum suspended across a sacrificial layer of amorphous silicon over a conductive silicon substrate. After releasing in XeF_2 , the MEMS ribbons can be electrostatically controlled in an analog fashion with response times of roughly 250ns.



Alces' MEMS light modulator is composed of a linear-array of electrostatically addressable and reflective "ribbons"



The MEMS ribbon flatness is a critical feature for enabling high-performance light modulation



Recently Alces has begun fabricating devices with a much larger number of MEMS elements. Shown here is an 8mm array with roughly 2000 light modulating MEMS ribbons

Dave Bloom, Matt Leone
Alces Technology, Inc. Jackson, WY
Work performed at Stanford Nanofabrication Facility

ALD-Metal Bolometer and Capacitive Pressure Sensors



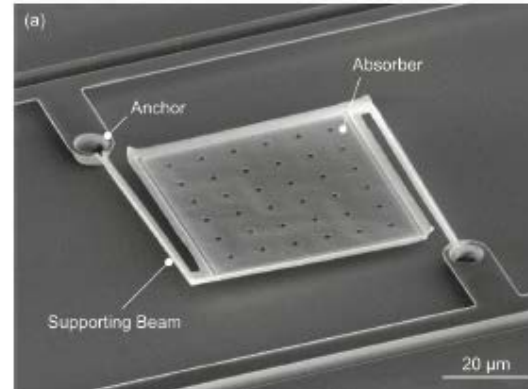
BOSCH

Invented for life

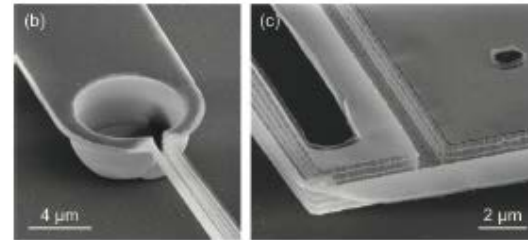
A bolometer is a thermal detector that makes use of a temperature-dependent resistor. The purpose of this work is to create an uncooled bolometer with improved performance via the use of a freestanding, several nanometer thick platinum layer deposited using atomic layer deposition (ALD). The structures were fabricated using a combination of the Stanford Nanofabrication Facility and other labs.

In addition to completely new devices, the SNF is also being used to perform research on well established MEMS devices. To leverage their relatively low temperature sensitivity, a new type of capacitive pressure sensor is being investigated that makes use of an electrically isolated electrode embedded in the membrane layer. Such a device allows an increased fractional capacitance change and reduced sensitivity to package stress.

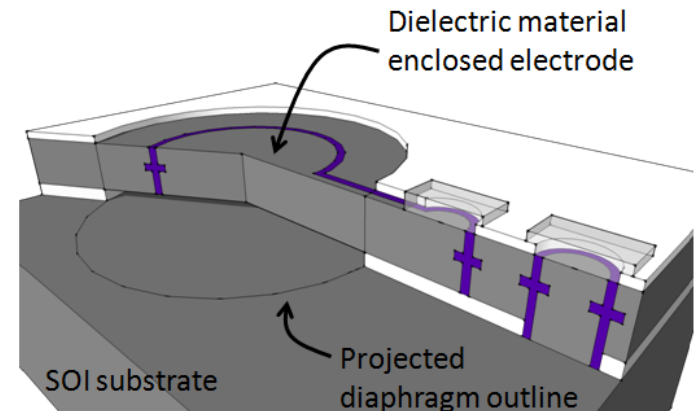
Various researchers at Robert Bosch LLC Research and Technology Center, Palo Alto, CA in collaboration with students, faculty, and staff at Stanford University
Work performed at the Stanford Nanofabrication Facility



An uncooled ALD-metal bolometer



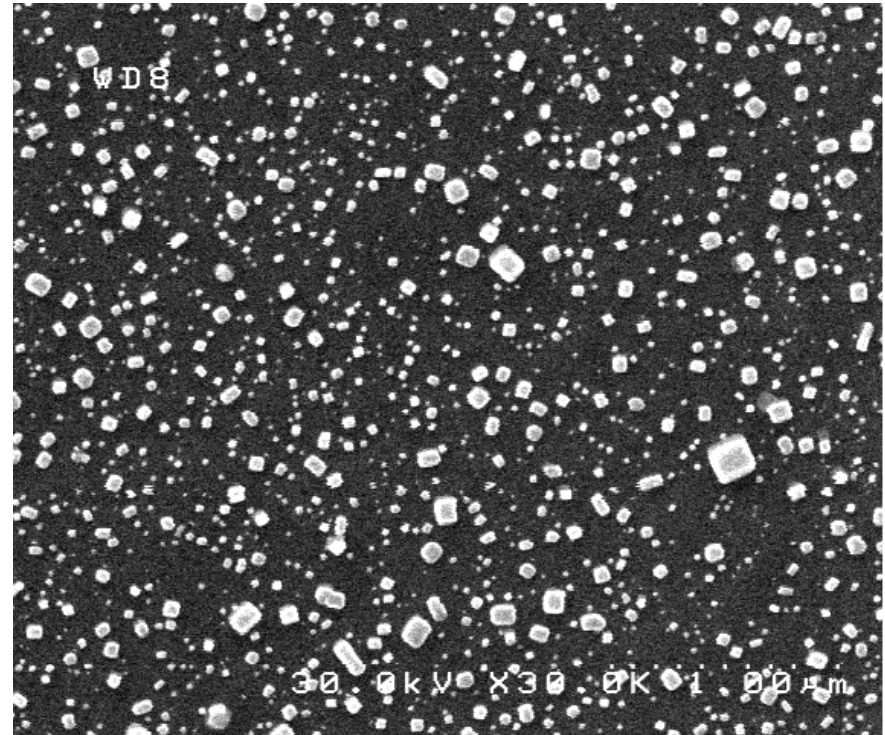
The bolometer anchor and stiffening trench



A capacitive pressure sensor with an electrically isolated electrode incorporated into the released membrane.

Measurement Of Salt Particles For Use In A Geoengineering Scheme

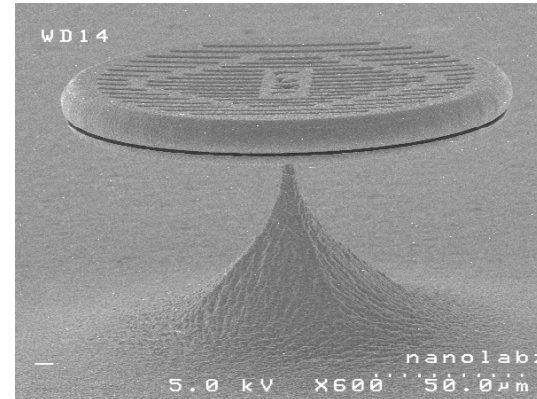
Working with Prof. David Keith (now at Harvard University) the Silver Lining research group prepared submicron-sized sodium chloride distributions for potential use as cloud condensation nuclei (CCN) in a geoengineering scheme (Latham-Salter marine cloud brightening (MCB)). The crystals were collected electrostatically on a silicon wafer and images, like the one shown above, were created using the Hitachi 4160 SEM at the Stanford Nanofabrication Facility. Later image analysis gives the dimensions of the lognormal distribution—in this case a mean distribution diameter of 33.7 nm with a GSD of 1.83.



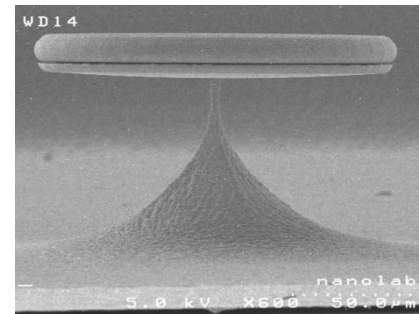
Gary Cooper, University of Calgary
Work performed at Stanford Nanofabrication Facility

Micro-Structured Targets For High Energy Laser Physics

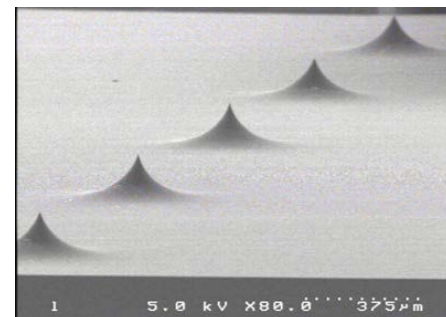
Micro structured targets have been fabricated at the Stanford Nanofabrication Facility that have been used in the area of high-energy laser physics. In 2009 Nanolabz was credited with helping achieve a world-record for accelerating protons at velocities never before seen with a laser. This work was done on the Trident Laser at Los Alamos National Lab. Laser accelerated protons have potential applications in the medical field for proton therapy cancer treatment and the complex micro-structure targets that are fabricated at SNF are being used as helpful diagnostic tools for a promising new technology.



Example of a micro-structured target: a circular flat top region connected to the tip of a hollow pointed structure



Profile of the same target from above: The circular portion at top is connected to the hollow pointed structure and the laser pulse enters from the back-side of the large opening of the pointed structure

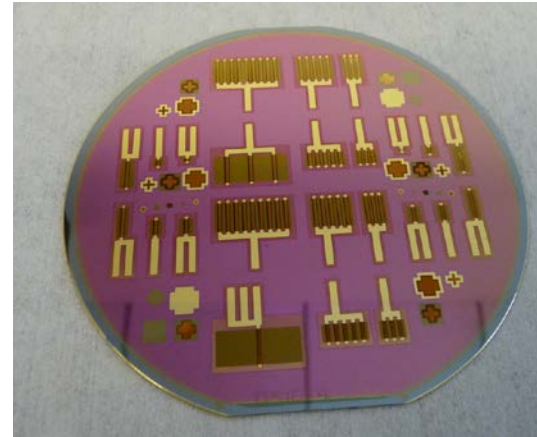


Example of pointed structures without a flat top

Steven Malekos, Grant Korgan, Jesse Adams –
Nanolabz
Work was performed at Stanford Nanofabrication Facility

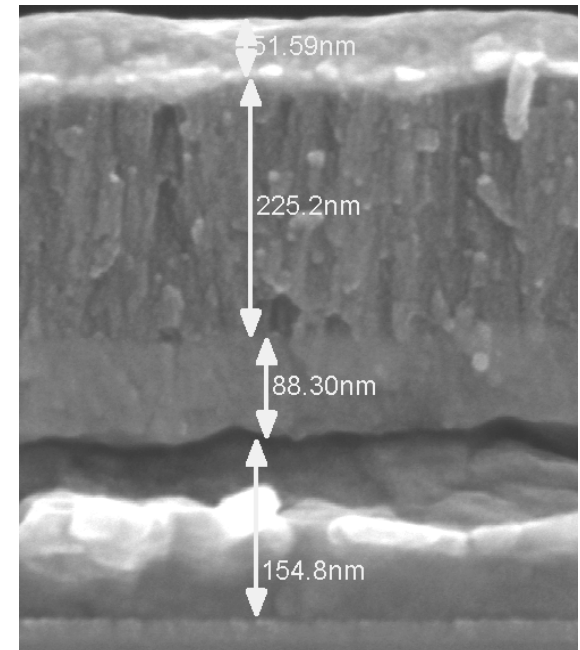
Nano-Dimensioned Clean Energy Conversion Technologies

The purpose of nano-dimensioned clean energy conversion technologies is to convert chemical energy to an electrical potential. It is not a battery, energy storage system or a fuel-cell. SNFs thin film deposition tools (evaporator, sputterer and ALD) were used in device fabrication. Characterizations were done using ellipsometry, SEM, TEM, XPS and XRD tools.



Device Wafer

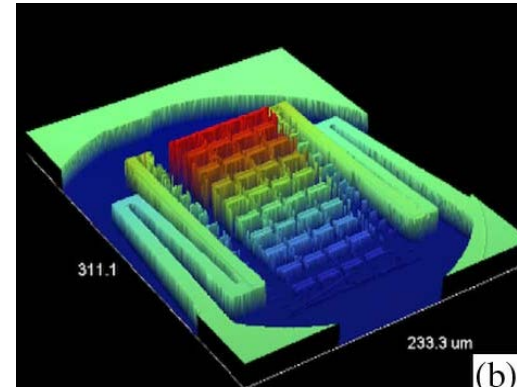
SEM of a typical Nano-Dimensioned Device



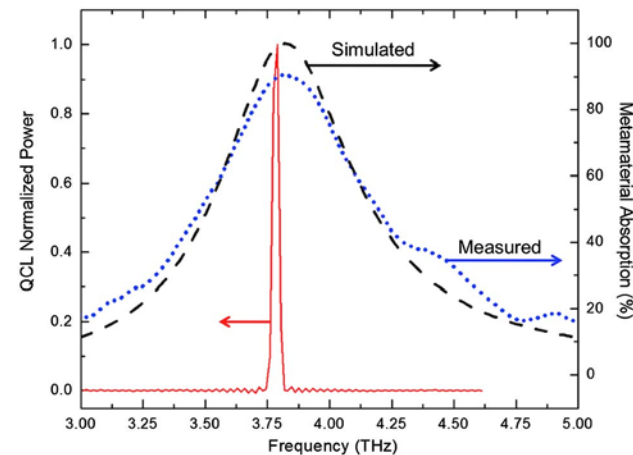
QuSwami, Inc.
Work performed at Stanford Nano-Fabrication Facility

THz Imaging Arrays

The purpose of the microfabrication of MEMS-based, bimaterial, THz focal plane arrays is to enable, low-cost robust imaging system for THz imaging. THz imaging has experienced large growth in the last several years due to its potential for medical and security applications. Being non-ionizing, THz radiation poses no risk to damaging human tissue and could present a safer alternative to X-ray based full body scanners as it penetrates through many non-metallic materials such as textiles, styrofoam or cardboard. However, at the moment, THz imaging is only possible using external illumination for which we use quantum cascaded lasers (QCL). This project aims to design focal plane arrays with integrated metamaterials, optimized for 100% absorption at frequencies of illuminating QCL.



Optical profilometer profile of one of actual detectors.



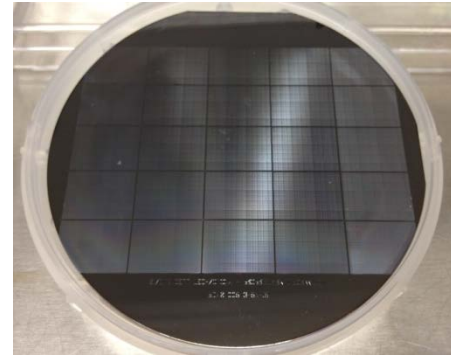
Measured (dotted curve) and simulated (dashed curve) absorption spectra of the metamaterial structure. Note that the peak absorption matches well with the measured QCL emission frequency (solid curve).

Dragoslav Grbovic, Fabio Alves and Gamani Karunasiri, Naval Postgraduate School
Work performed at Stanford Nanofabrication Facility

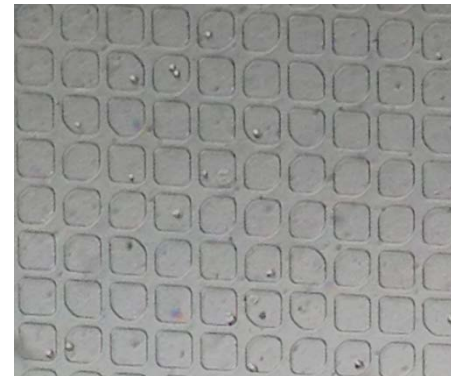
Single Cell Analysis

The purpose of the project is to enable paralleled single-cell analysis. At SNF, we fabricated wafers (top right) to be used as master molds for manufacturing microfluidic devices (middle right). A device contains thousands of wells that can harbor single cells, enabling us to capture and characterize various biomolecules, especially mRNA using a custom design multifunctional DNA microarray (lower right). The microarray contains oligo-nucleotide features which in turn contain a unique tag sequence. Captured mRNA is converted into cDNA on the DNA microarray; the conversion process incorporates the tag. The tagged cDNA molecules are analyzed by next generation sequencing technology. The tag allows identification of mRNA from the originating single cells.

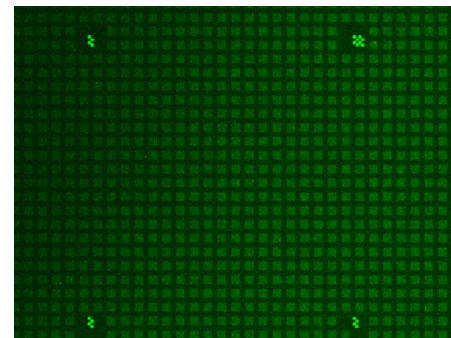
Jim Bowlby and Chun-Nan Chen, Single Cell Technology, Inc.
Wafers (top right) were fabricated at the Stanford Nanofabrication Facility (SNF)



A picture of a patterned wafer manufactured at SNF by Single Cell Technology personnel.



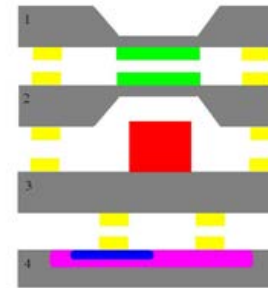
A close-up microscope image of our microfluidic device with cells deposited in wells.



A representative image of a custom design oligo-nucleotide array. Each feature was visualized by hybridizing with a fluorescently labeled oligo. The four unusual features are fiducials placed by the supplier.

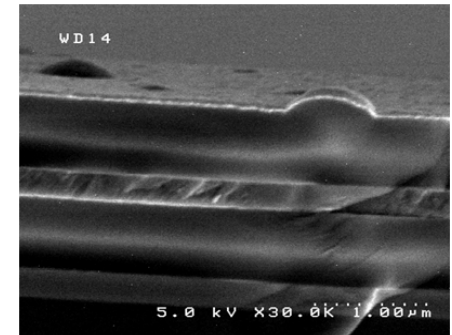
MWIR MEMS Optical Filter Project

The purpose of the MWIR MEMS-based Fabry-Perot interferometer Project is to develop an optical filter that works in the mid-wave infrared (MWIR) spectrum. The SNF-fabricated components of this system have been the dielectric Bragg stacks that act as mirrors, and complete MEMS devices. The Bragg reflectors are fabricated by PECVD and e-beam sputtering. The mechanical components have been fabricated on SOI wafers by optical lithography and deep reactive ion etching.

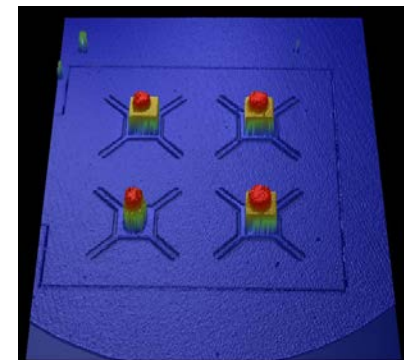


Goal of the project: Wafer-scale integration of optical filters, HgCdTe detectors and electronics

Germanium and silicon oxide Bragg stacks used as mirrors in optical filter



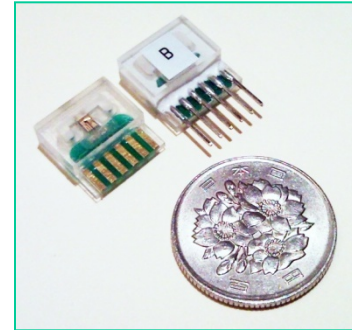
Dmitry Kozak and Joel Kubby, UCSC
Work performed at Stanford Nanofabrication Facility



First-ever arrays of independently controllable pixel filters

Sensing chip for infusion pumps

The market demands for homecare infusion pumps are about 40M per year with a value over \$5B. In the past 5 years there were over 56,000 MDRs (medical device report) for the current infusion pump usage. Development of a better controlled pump system shall bring in huge benefit in all aspects. A MEMS sensing device in the new system shall not only provide the best dynamic measurement capability, a controllable injection, but capability to prevent harmful incidents such as bubble invasions. The cost advantages also make the MEMS technology the best choice.



Disposable sensing chip for control of infusion pumps.

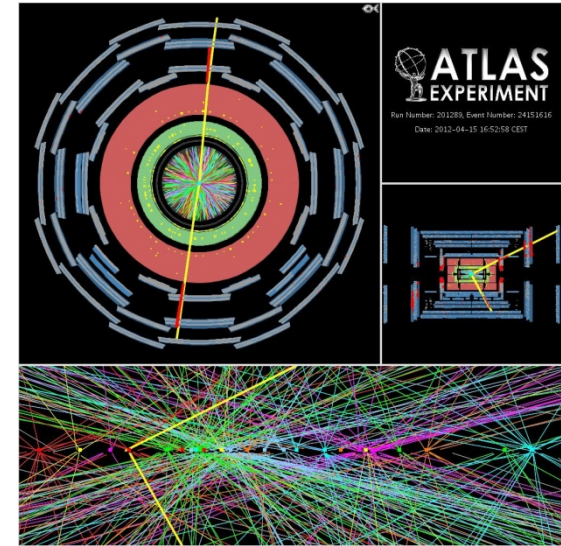


An example of the infusion pump

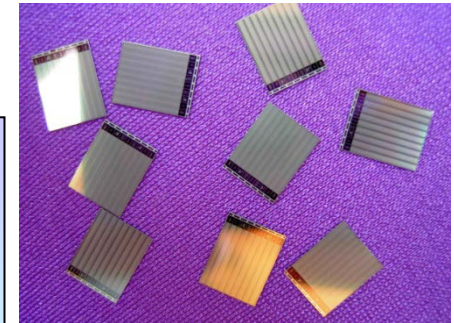
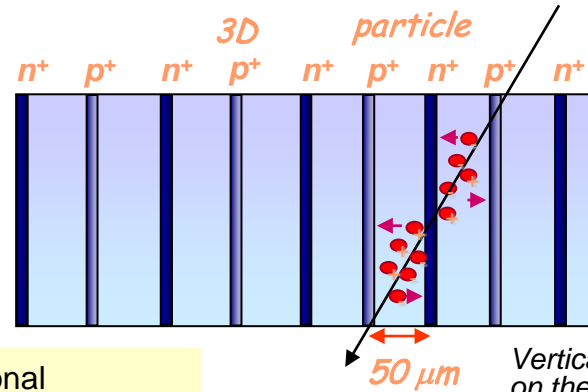
ChihChang Chen and Liji Huang
Siargo, Inc.
Work performed at Stanford Nanofabrication Facility

Vertex Detector for the Large Hadron Collider

A resonance, which has many characteristics of the Higgs boson, has recently been observed at the Large Hadron Collider. The pixelated vertex detectors positioned near the interaction point were crucial in this discovery. However, these sensors are easily damaged in this intense radiation environment. A new sub-detector will be inserted very close to the Higgs Boson creation point in 2014. A technology which has through-wafer diode arrays and hence is highly radiation tolerant has been developed at the Stanford Nano-fabrication Facility. Sensors based on this technology have been selected for use in the innermost detector system in ATLAS.



One beam crossing within ATLAS detector at the LHC



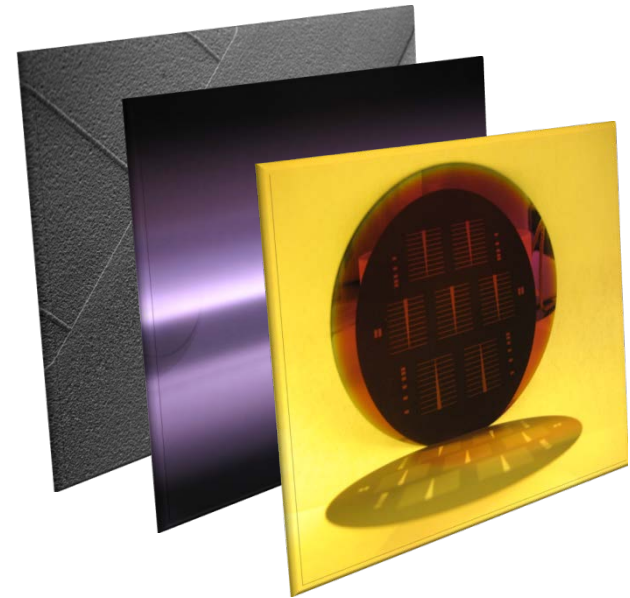
Vertical diode array concept illustrated on the left, and set of 3D-architecture sensors on the right.

J. Hasi, C. Keneny, P. Grenier SLAC National Accelerator Lab., S. Parker University of Hawaii, C. Da Via Manchester University
Work performed at Stanford Nanofabrication Facility

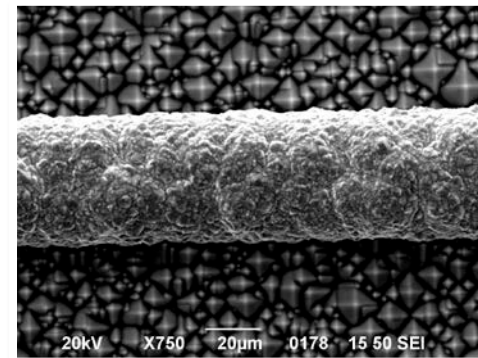
High-Efficiency Crystalline Silicon Solar Cells

In order to reduce the cost of energy delivered from photovoltaics, the efficiency of the conversion of incident photons into electron-hole pairs is the key metric. The optical properties of a solar cell are mostly dominated by the shading of incident light by metal contacts and by the ability to trap photons inside the silicon wafer to enhance the collection of infrared light. Work performed at SNF included the deposition and characterization of the complex refractive indices of dielectric layers which act as antireflection coatings. The optimization takes the solar spectrum in between 300-1200 nm into account to maximize the achievable photogeneration. Applied on the rear side of a solar cell, they act as internal reflectors and are optimized for infrared light. Using optimized optical layer systems in combination with a fine line metallization grid led to solar cell efficiencies of 21%.

Oliver Schultz-Wittmann, TetraSun Inc
Work performed at Stanford Nanofabrication Facility



Optimized optical layers on the front and the rear side of a solar cell improve photon collection.

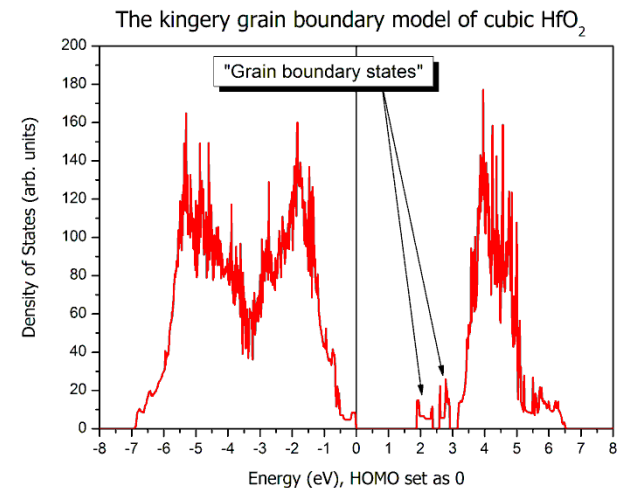
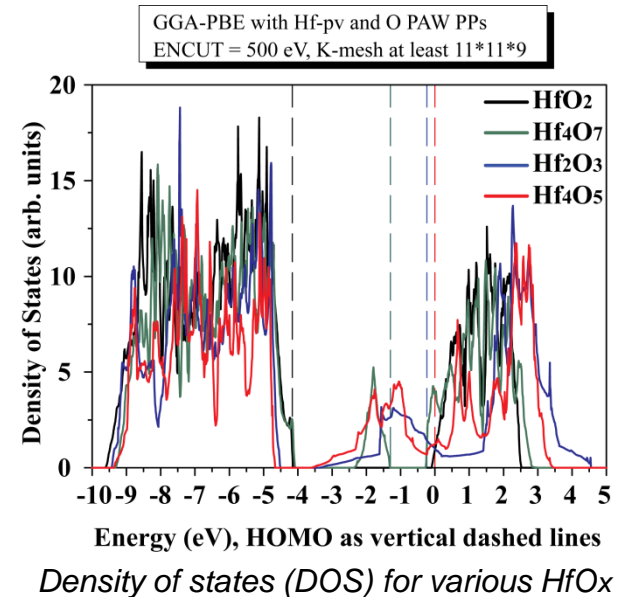


A fine line finger metallization reduces the effective shading losses in high-efficiency crystalline silicon solar cells.

Metallic HfO_x in resistive RAM

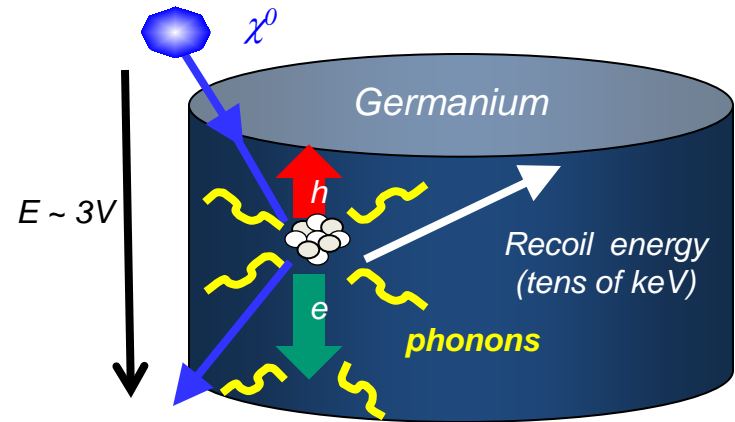
This work is intended to reveal the working mechanism of HfO_2 resistive memory (RRAM). An unexplained metallic state emerges in this device after an electroforming process. Several possible origins of this metallic state can be: aligned oxygen vacancies, strong off-stoichiometry and grain boundary effects. Using first-principles calculations, we show that aligned oxygen vacancy chains are not sufficient to result in a metallic state like that is discovered in the device, but a strong off-stoichiometric HfO_x is required. The transition from insulator to metal in HfO_x occurs somewhere between $x=1.5$ and $x=1.75$, close to $x=1.5$. The grain boundary itself does not cause metallic conduction, but may promote the formation of a conductive state in the grains through defect segregation.

Kan-Hao Xue, Yoshio Nishi, Philippe Blaise, Gabriel Molas, and Gerald Ghibaudo, *IMEP-LAHC, Stanford University* and *CEA-LETI*
Work performed at Stanford Nanofabrication Facility

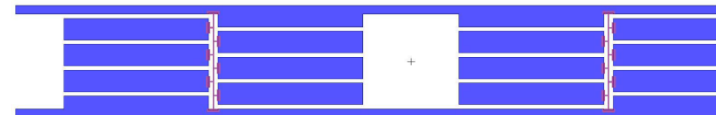
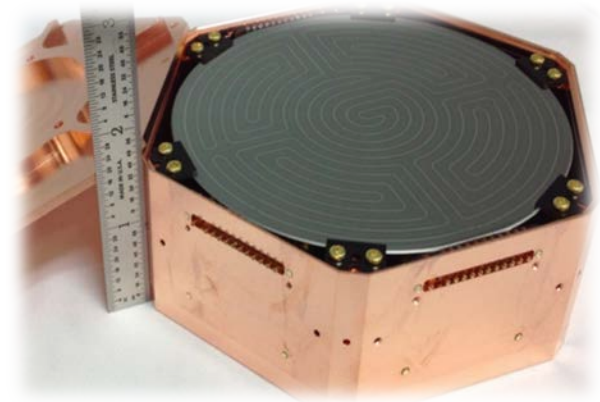


CDMS Dark Matter Detector

The CDMS collaboration has pioneered the development of semiconductor dark matter detectors that utilize both ionization and phonon measurements of the deposited energy. The semiconductor crystals act as both target and detector, with 76 mm diameter, 25 mm thick Ge crystals used in SuperCDMS Soudan and 100 mm diameter, 33.3 mm thick crystals planned for SuperCDMS SNOLAB. The ionization measurement is made by drifting electrons and holes to electrodes on opposite face of the crystal in a weak electric field ($\approx 1\text{V/cm}$). The phonon measurement utilizes the advanced athermal phonon sensor technology (ZIP) developed for CDMS II. Athermal phonons propagating in the crystal scatter off superconducting Al electrodes at the crystal surfaces, breaking Cooper pairs to form unpaired quasi-particles in the Al electrode. Diffusion of these quasi-particles to a nearby tungsten "Transition Edge Sensor" (TES) increases the temperature and resistance of the TES, which is biased to lie in the transition region between its normal and superconducting states through electro-thermal feedback. The change in TES resistance is detected as a change in current through the TES, producing a phonon signal that is proportional to the energy deposited in the detector.



iZIP 100mm Diameter 33.3mm thick



One of the >1000 Al-W TESs on a CDMS detector. Al films (blue) are $50\ \mu\text{m} \times 300\ \mu\text{m}$; W TES (red) are $220\ \mu\text{m} \times 2\ \mu\text{m}$.

SuperCDMS Collaboration
Professor Blas Cabrera, Stanford University
Detector fabrication performed at Stanford Nanofabrication Facility

Screen Printed Piezo-ceramics on Organic Substrates

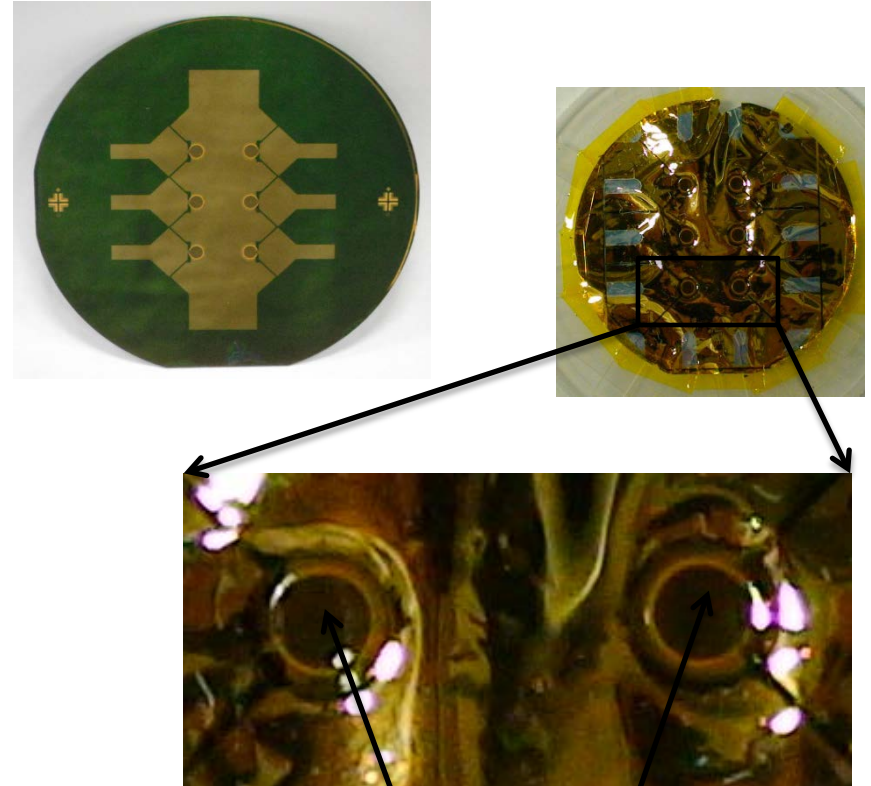
The goal of this research is to enable integration of mezzo scale piezo-ceramic elements with micro and nano fabricated networks. The relatively large size of the piezo-ceramic will enable greater actuation and strain signal propagation over longer distances than traditional thin film piezoelectric materials.

This is particularly applicable Structural Health Monitoring, wherein ultrasonic strain signals are propagated through a structure, and changes in the signal over time can be interpreted as damage. This field is seeking smaller scale transducers to minimize the parasitic effects on host structures.

Development of non-standard processing based on traditional C-Mos processes has enabled considerable development. Processing includes spin coating, photolithography, metallization, chemical etching and screen printing.

Nathan Salowitz and Fu-Kuo Chang Stanford University work performed at The Stanford Nanofabrication Facility

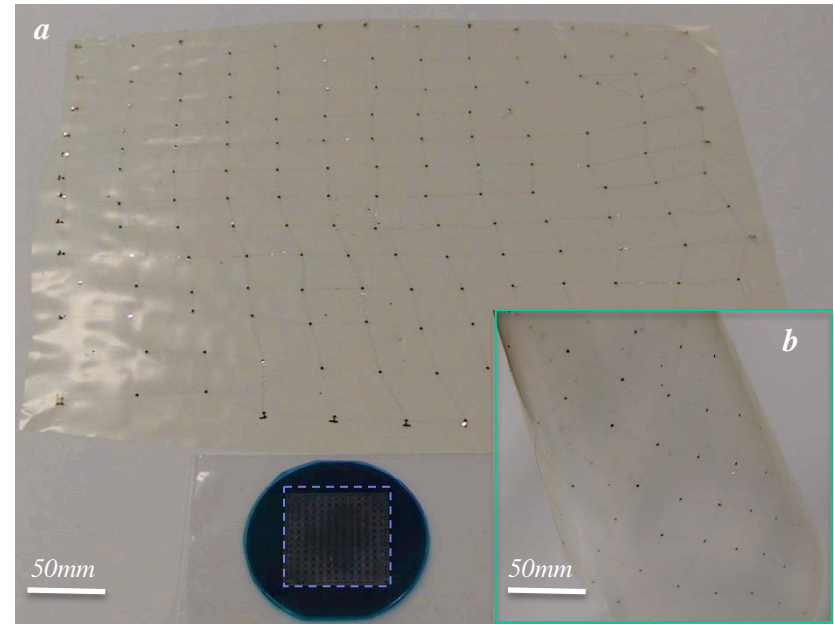
Screen Printed Piezo-ceramics released onto a polyimide film



Piezos

Bio-inspired Smart Skin Based on Stretchable Network

The purpose of the Smart Skin Project is to enable large area sensing by stretching a micro-fabricated sensory network. The SNF-fabricated components of this system have been the highly stretchable network with sensors, switches and electrodes. The network is based on polyimide substrate with an unique stretchable pattern defined by lithography. Si wafers serve as carriers for these polyimide substrate during processing.



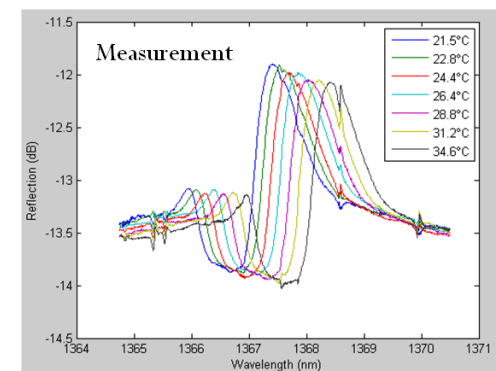
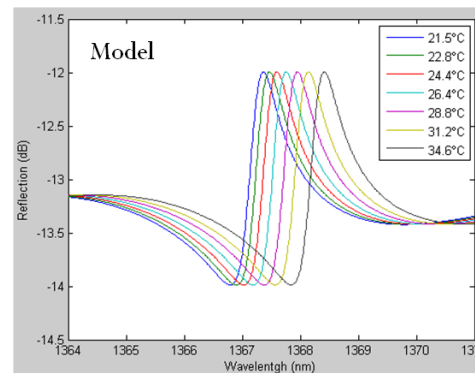
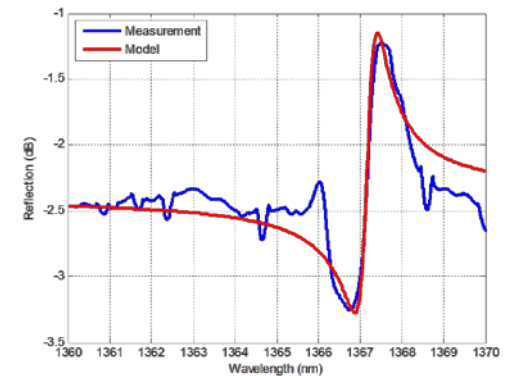
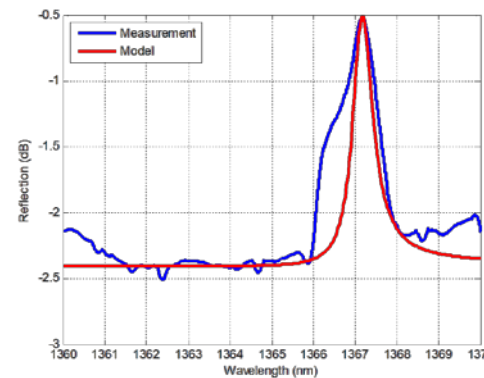
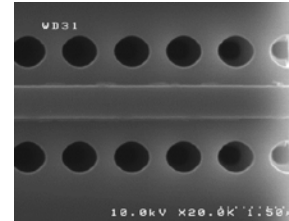
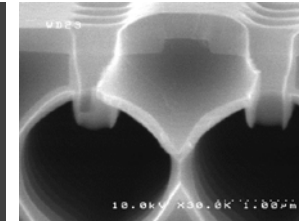
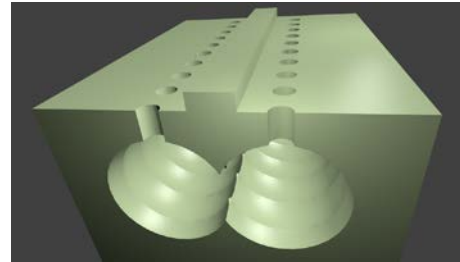
(a) Electronic skin after expansion (the square with dashed lines indicates the size of the electronic skin before expansion). (b) Electronic skin deforms with plastic film.

Zhiqiang Guo and Fu-Kuo Chang Stanford University
Work performed at at The Stanford Nanofabrication Facility

Silicon photonics for optical sensing

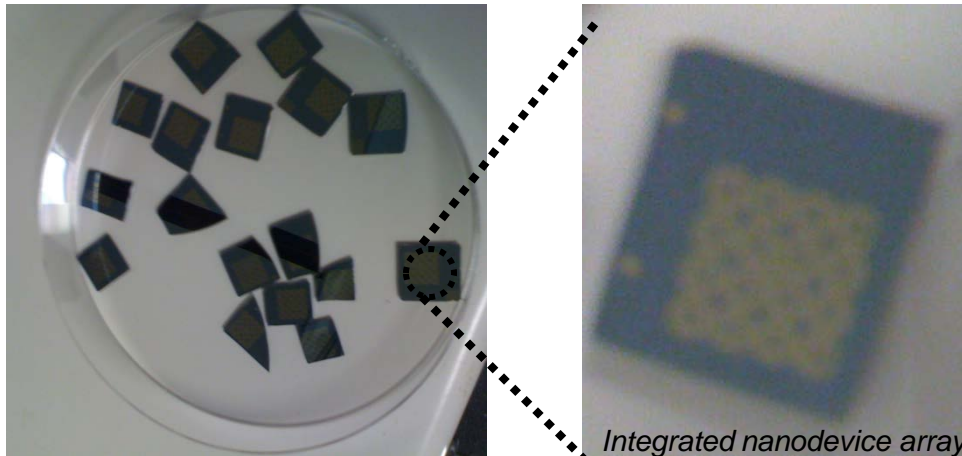
monolithic silicon Bragg reflectors

We characterize asymmetric Fano resonances in silicon Bragg reflectors. By properly changing the relative phase of the reflected light, we generate different Fano lineshapes optimized for different sensing applications. We then demonstrate temperature sensors based on asymmetric Fano resonances in integrated silicon Bragg reflectors.

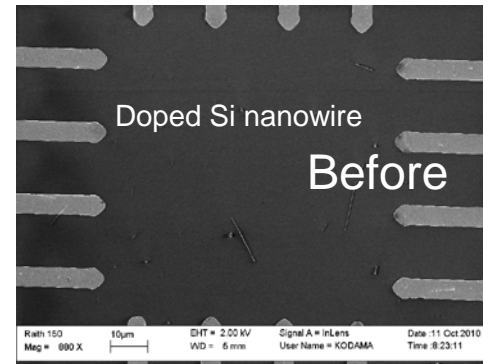
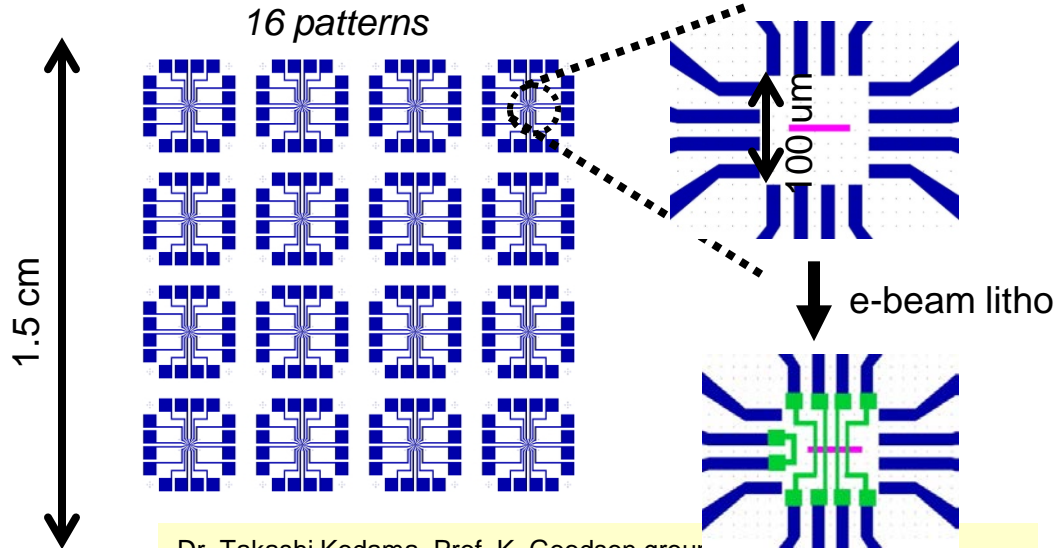


C. -M. Chang and O. Solgaard, Stanford University
Work performed at Stanford Nanofabrication Facility

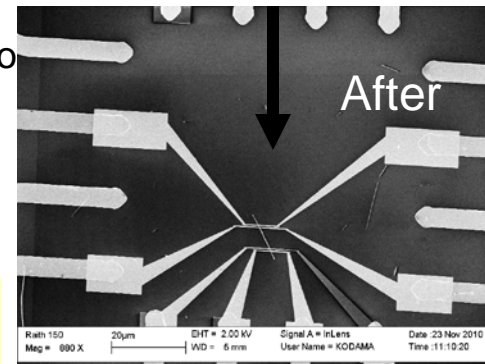
Multipurpose nanodevice fabrication



Combination process of photolithography and electron beam lithography was developed. Flexible design was performed for multipurpose nanodevice fabrication. Multistep e-beam lithography for complicated nanodevice fabrication led to high spatial resolution (<30 nm) and alignment accuracy (<100 nm).



Representative SEM images of nanowire devices fabrication.



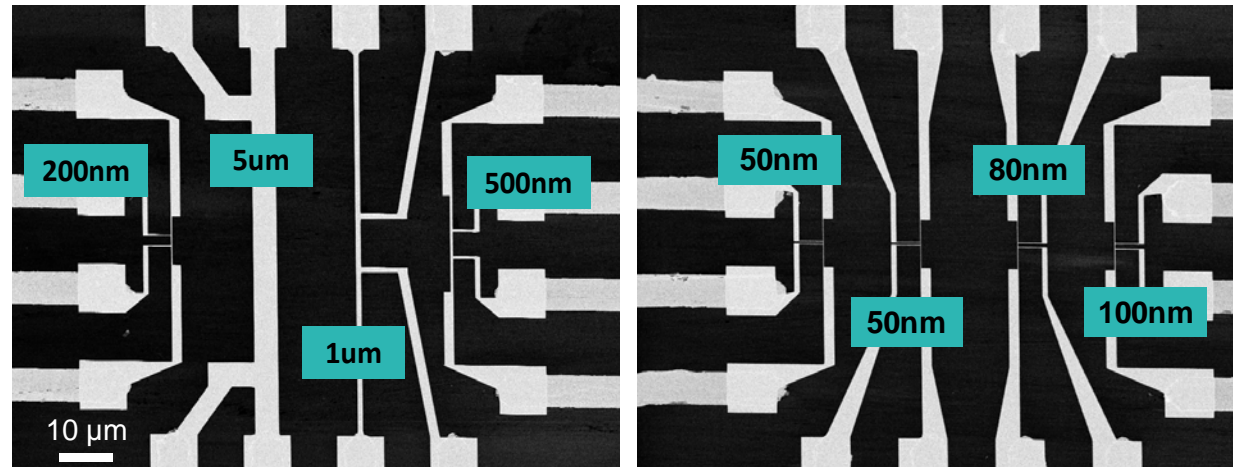
Selected publication:
S. Leblanc, T. Kodama,
K. Goodson et al, ASME
Journal of Heat Transfer,
134 (2012) 080910-1.

S. Leblanc, T. Kodama,
K. Goodson et al, Appl.
Phys. Lett., 100 (2012)
163105.

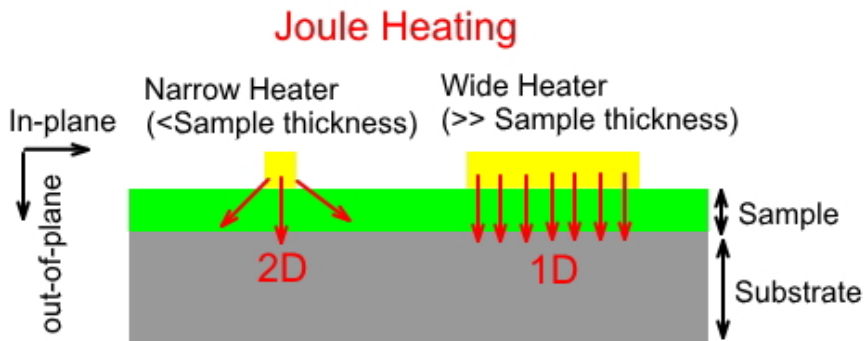
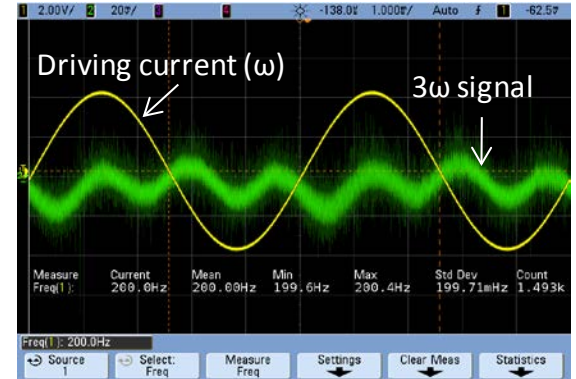
Dr. Takashi Kodama, Prof. K. Goodson group,
Mechanical Engineering Department, Stanford University;
Work performed at Stanford Nanofabrication Facility

Nanoscale Thermal Conductivity Measurement

Experimental structure for thermal conductivity measurement on Mo/Si multilayers, Z. Li, T.Kodama, K. Goodson et al, Nano Letters., 12 (2012) 3121.



3 omega signals in thermal conductivity measurements.



Schematic of the side view.

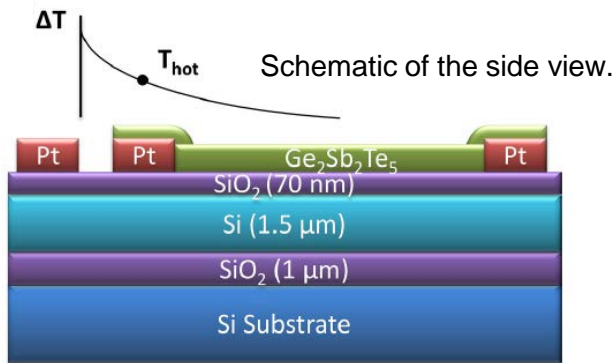
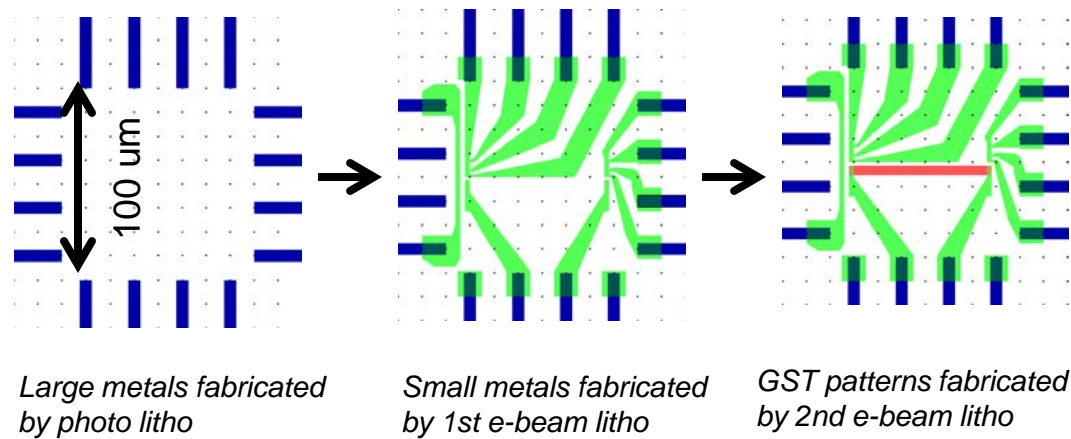
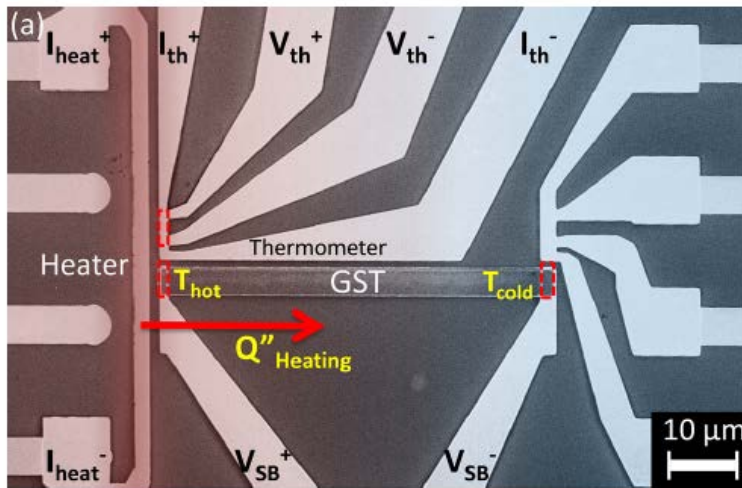
Dr. Takashi Kodama, Prof. K. Goodson group,
Mechanical Engineering Department, Stanford University;

Work performed at Stanford Nanofabrication Facility

Nanoscale heaters down to 50 nm were fabricated by the combination of photolithography and e-beam lithography. Multiscale heaters for separating in-plane and out-of-plane component of the thermal conductivity were produced. Much improved lateral resolution compared was achieved with conventional 3ω measurements.

Nanoscale Thermoelectric Measurement

Experimental structure for Seebeck coefficient measurement on $\text{Ge}_2\text{Sb}_2\text{Te}_5$ films, J. Lee, T. Kodama, K. Goodson et al, J. Appl. Phys., in press.



Substrates for heating length control were designed, including nanoscale metal patterns (heater/thermometer/electrodes) for high measurement accuracy. 2 step e-beam lithography for positioning GST nanostructures on nanoelectrodes were achieved with high alignment accuracy (< 100 nm).

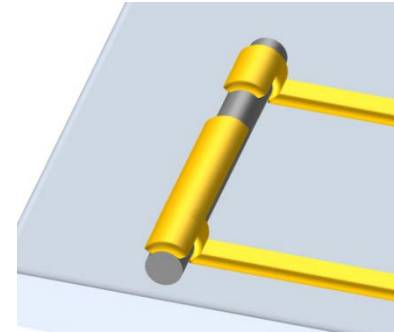
Dr. Takashi Kodama, Prof. K. Goodson group, Mechanical Engineering Department, Stanford University;

Work performed at Stanford Nanofabrication Facility

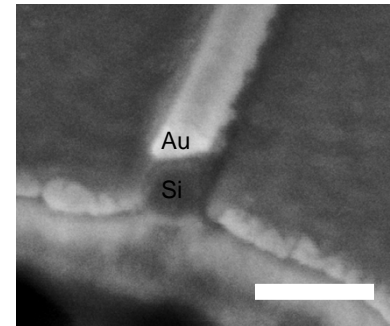
Invisible Photodetector Project

The project is aimed to explore the potential of engineering optical responses from optoelectronic devices by rationally designing hybrid metal-semiconductor nanostructures. A promising demonstration of an “invisible” photodetector was made possible by a Si nanowire detector overcoated with thin gold layer, which act as an optical cloak that renders the structure “invisible” due to cancelling scattering from the nanowire via a phenomenon known as plasmonic cloaking. State-of-the-art electron beam lithography techniques allow for accurate fabrication of such hybrid metal-semiconductor nanostructures and devices.

Pengyu Fan and Mark Brongersma, Stanford University
Work performed at Stanford Nanofabrication Facility
Collaborated with Uday Chettiar and Nader Engheta, UPenn

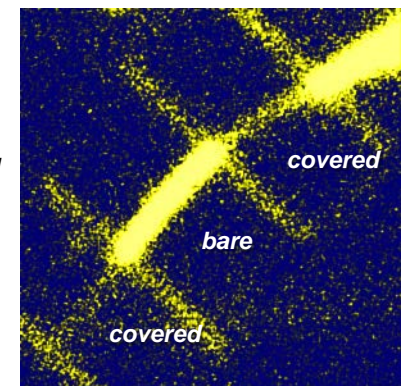


Sketch of an invisible photodetector consists of a Si nanowire device overcoated by a thin gold layer as a plasmonic cloak.



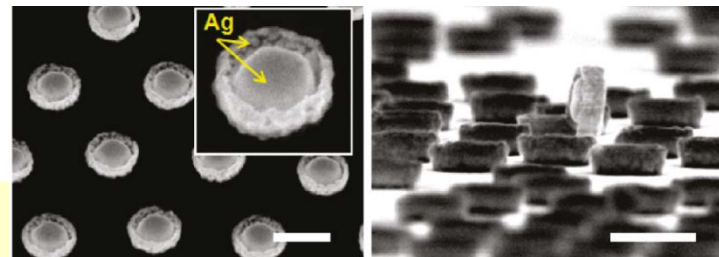
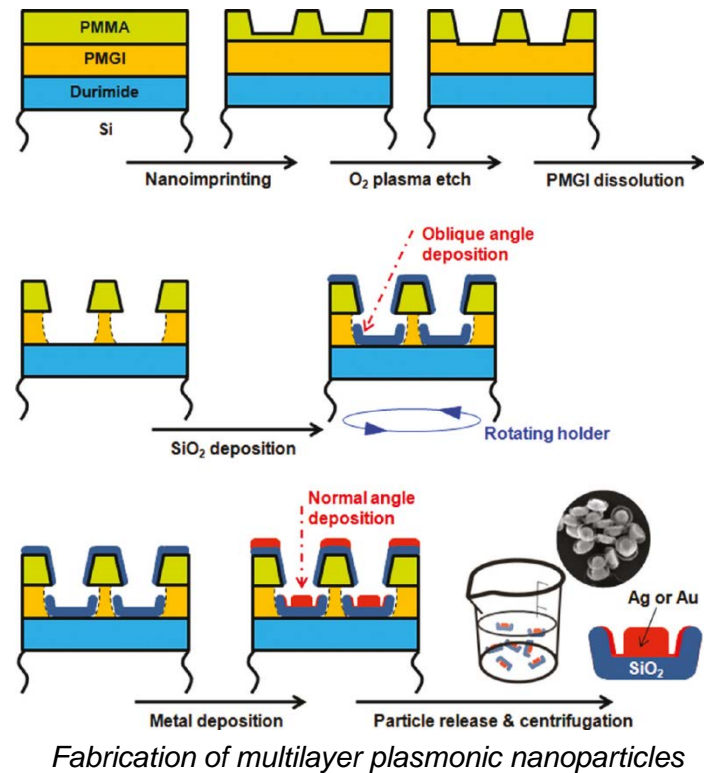
SEM image of device cross section of a 50-nm-diameter Si nanowire with 20-nm-thick Au coating. Scale bar is 100 nm

Microscope image shows that the nanowire being covered by gold shows minimal scattering comparing to bare Si nanowire due to scattering cancellation.



Plasmonic Nanoparticles

Top-down synthesis of monodisperse plasmonic nanoparticles designed to contain internal Raman hot spots. Raman-active nanoparticles are fabricated using nanoimprint lithography and thin-film deposition and are composed of novel internal structures with sublithographic dimensions. Raman hot spots appear at the inside perimeter of individual nanoparticles and serve as the source of a 1000-fold improvement of minimum molecular detection level that enables detection of signals from a few molecules near hot spots. These results illustrate the potential of direct fabrication for creating exotic monodisperse nanoparticles, which combine engineered internal nanostructures and multilayer composite materials, for use in nanoparticle-based molecular imaging and detection.



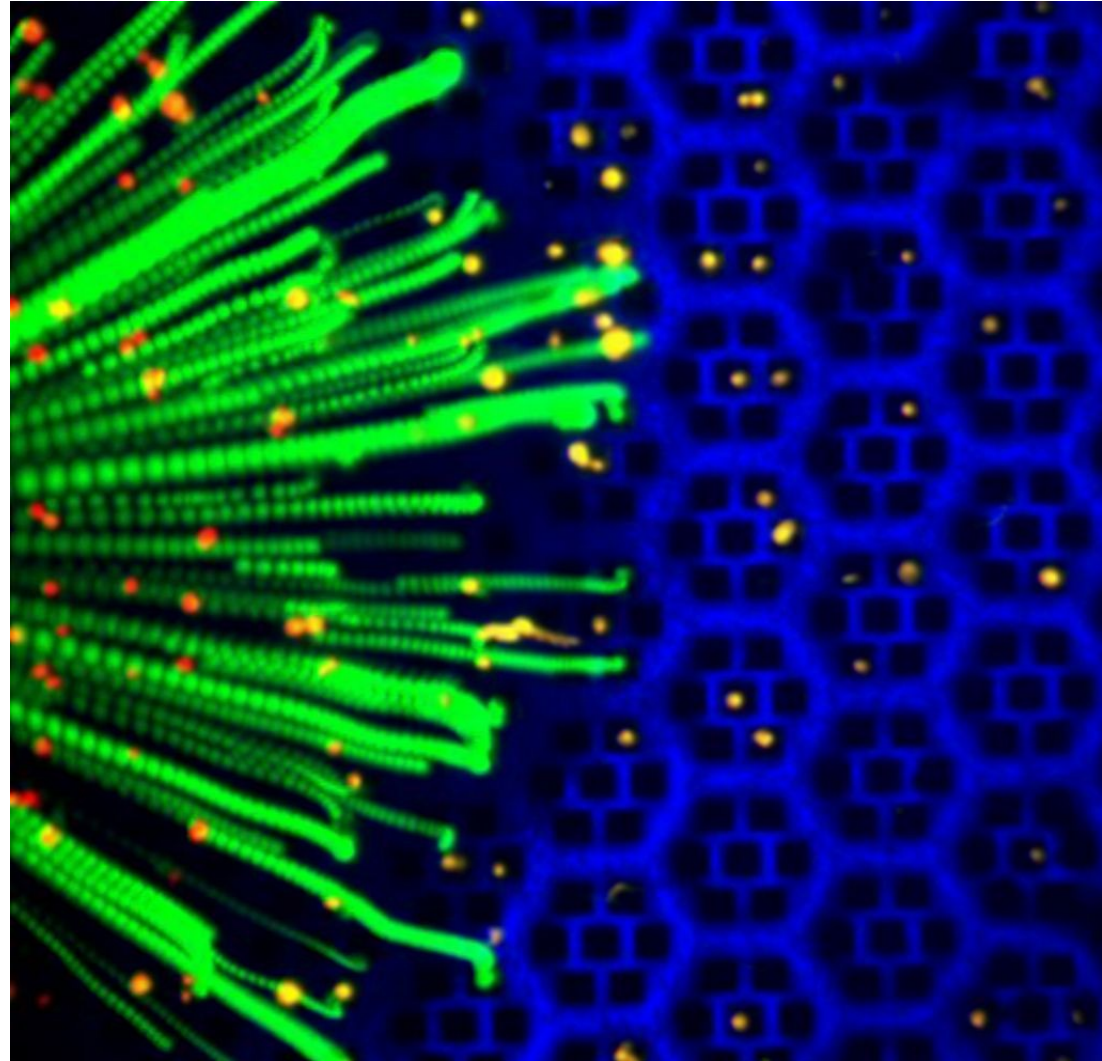
SEM images of Ag/SiO₂ SERS nanoparticle arrays. Scale bars are 200 nm.

Jung-Sub Wi, Edward S. Barnard, Robert J. Wilson, Mingliang Zhang, Mary Tang, Mark L. Brongersma, and Shan X. Wang Stanford University
Work performed at Stanford Nanofabrication Facility

Magnetic Sifter

Researchers at the Stanford University Center of Cancer Nanotechnology Excellence have developed novel devices in SNF to isolate cancer cells. This time-lapse image shows the trajectories of NIH H1650 tumor cells (green) moving through a blood sample. After being stained with fluorescent dyes and magnetic nanoparticles, the tumor cells were captured by a 3D magnetic sifter device that was micromachined from a silicon wafer.

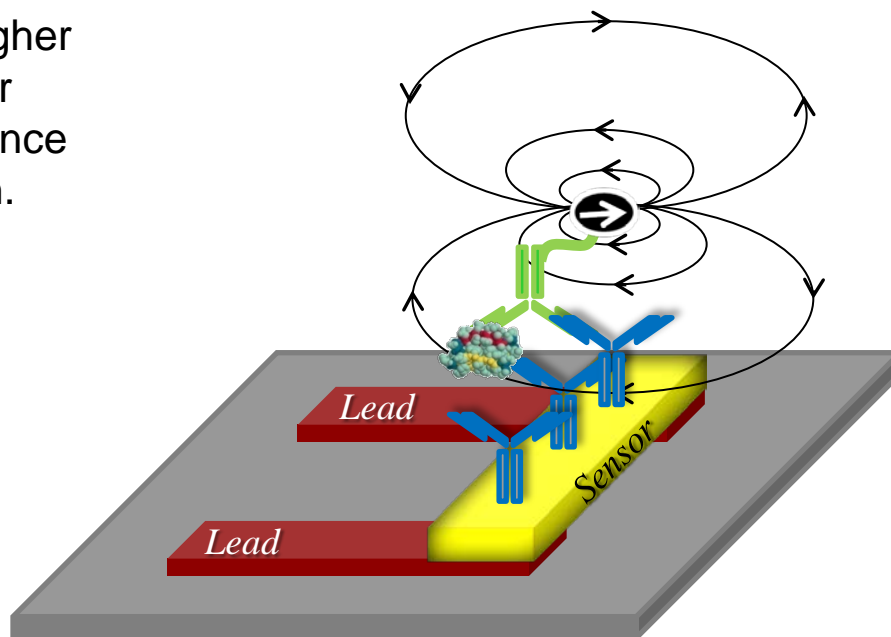
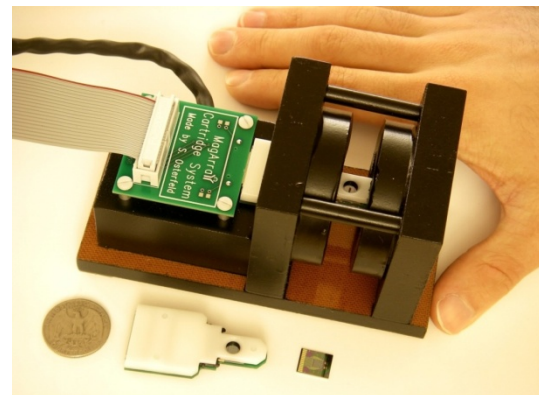
R. J. Wilson, C. M. Earhart, S. X. Wang
Stanford University work performed at
Stanford Nanofabrication Facility



Magneto-Nano Sensors for Cancer Detection

Using the same principles employed in the magnetic storage industry, Prof. Shan Wang's group has developed a nanomagnetic sensor chip for detecting cancer. By using magnetic nanoparticles to 'tag' proteins indicative of cancer and reading them out using magnetic sensors Wang Group has demonstrated much higher sensitivity (1 picogram/mL or femto-molar level) than conventional optical fluorescence assays, enabling earlier cancer detection.

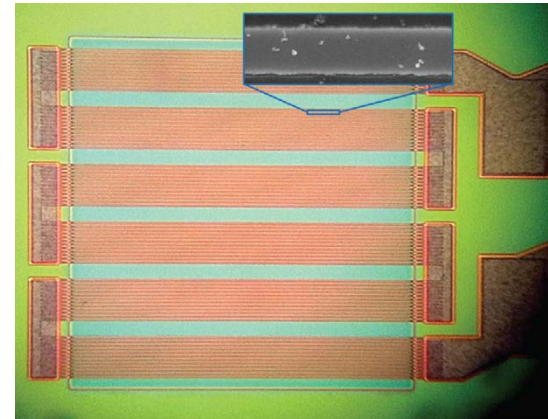
S. Osterfeld et al., Stanford University
work performed at Stanford
Nanofabrication Facility



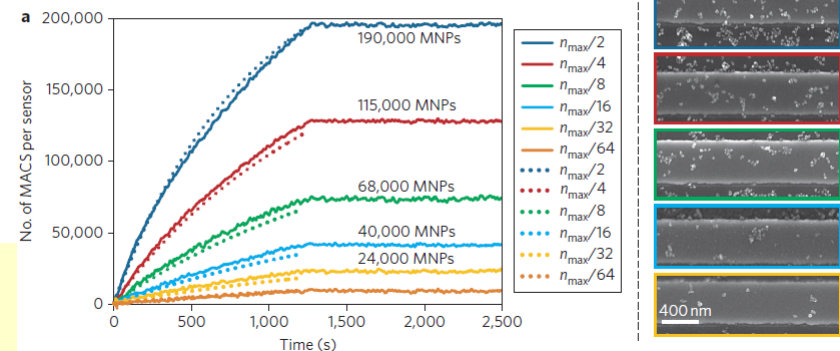
High-density GMR Sensor Arrays

Monitoring the kinetics of protein interactions on a high-density sensor array is vital to drug development and proteomic analysis. We have shown that magnetically responsive nanosensors that have been scaled to over 100,000 sensors per cm^2 can be used to measure the binding kinetics of various proteins with high spatial and temporal resolution. The GMR sensor used in our experiment has a bottom spin valve structure of the type Si /Ta(5) /seed layer /IrMn(8) /CoFe(2) /Ru/ (0.8) /CoFe(2) /Cu(2.3) /CoFe(1.5) /Ta(3), where all numbers in parentheses are in nanometres. Each GMR sensor in the array covers a total area of $100 \text{ mm} \times 100 \text{ mm}$ and comprises 12 parallel GMR sensor stripes that are connected in series six times, producing a total of 72 stripes per sensor.

Richard S. Gaster, Liang Xu, Shu-Jen Han, Robert J. Wilson, Drew A. Hall, Sebastian J. Osterfeld, Heng Yu and Shan X. Wang. Stanford University
Sensor prototypes developed at Stanford Nanofabrication Facility



Optical micrograph showing the GMR sensor architecture comprising 72 stripes connected in parallel and in series. Inset: SEM image of one stripe of the GMR sensor with several bound magnetic nanoparticle tags.

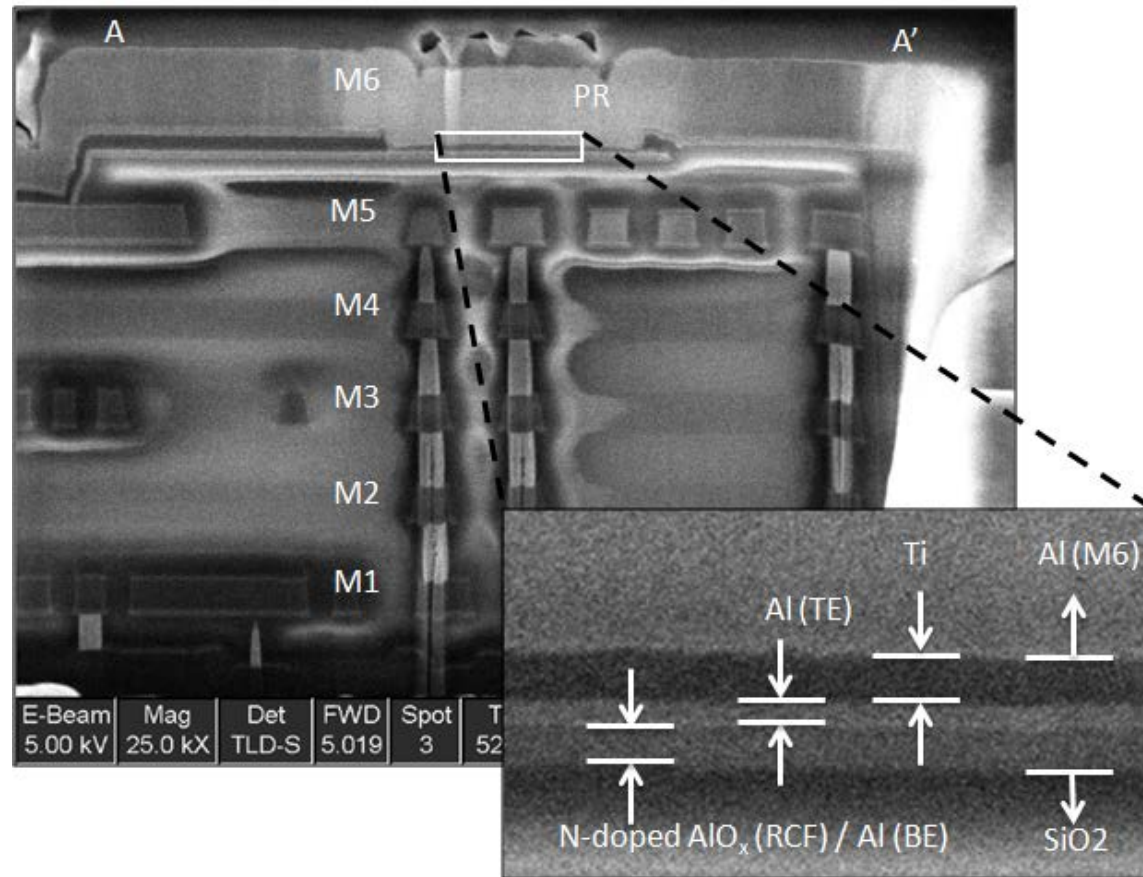


Real-time binding curves of magnetic tags to GMR sensor (a), and corresponding SEM images showing coverage of magnetic nanotags on GMR sensor surface (b).

3D Field Programmable Gate Array

Cross-sectional SEM View of 3D-FPGA

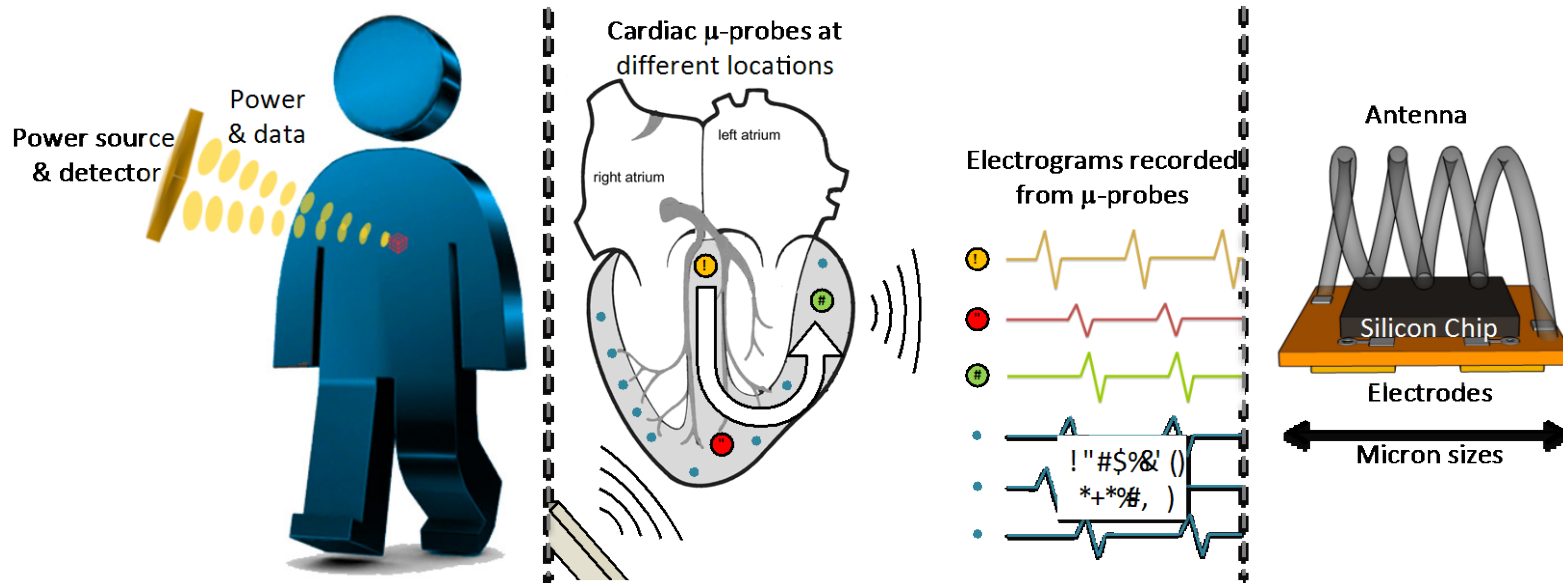
The purpose of this project is to demonstrate the advantages of 3D integration in reducing chip area, signal delay and operational power of integrated circuits. The substrate CMOS wafer with 5 metal layers was fabricated at a commercial wafer foundry. The resistive random access memory (RRAM) layer and 6th layer of metal were then fabricated at SNF. When compared with conventional 2D-FPGA, the 3D-FPGA achieves 1.6X improvement in logic density, 1.2X in speed and 0.85X in dynamic power.



Expanded view of RRAM integrated on CMOS

Young Yang-Liau, Zhiping Zhang, Wanki Kim,
S. Simon Wong, Stanford University
Work performed at Stanford Nanofabrication Facility

3D Electrocardiography With Wireless Micro-electrodes



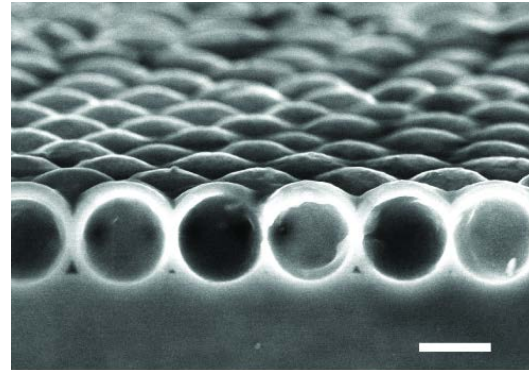
Electrodes and stents have been implanted in human hearts for several decades. They have been deployed in the cardiac chambers as well as cardiac venous and arterial structures. Electrodes are currently millimeters in size and usually require a direct wired connection for operation. Stents measuring 50–100 microns in thickness are deployed routinely in the coronary arteries but lack of the ability to report back information from the local environment. The goal of this project is to replace these large “dumb” and tethered electrodes by hundreds to thousands of injectable “smart” untethered wireless-powered integrated circuit (IC) chips where each IC chip is attached a charge sensor to detect the electrogram, a wireless interface to transmit the electrogram to an external detector, and a unique identification to locate it. The miniaturized electrodes are fabricated in the SNF.

Ada Poon, Stanford University work performed at Stanford Nanofabrication Facility

Low-Q Resonator for Solar Cells

The purpose of this project to design a low-Q resonator in order to increase the light absorption in a thin absorber layer. Thin nano-crystalline Si (50 nm-thick) deposited over nanoparticles by LPCVD formed a monolayer of Si nanoshell. The Si nanoshells achieved 20-fold enhancement of light absorption. The incident light was confined and guided along the shell, which resulted in the increase of the optical path length and the increase of light absorption.

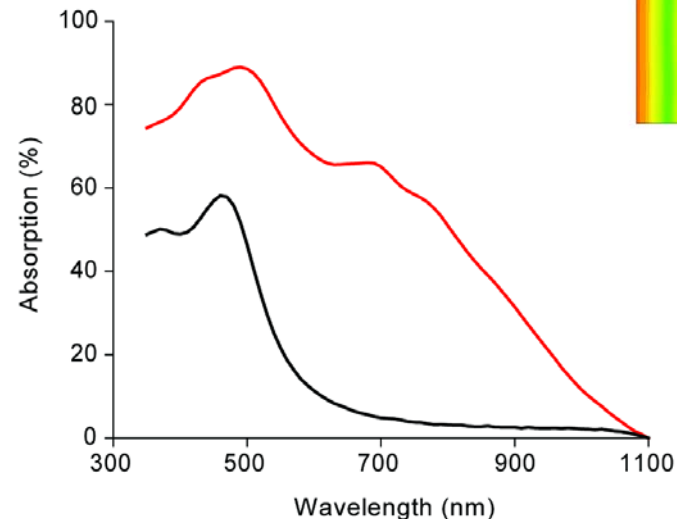
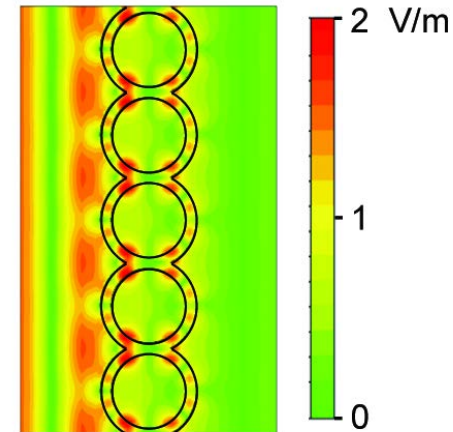
Y. Yao*, J. Yao*, et al., Stanford University work performed at Stanford Nanofabrication Facility



Cross-sectional image of Si nanoshell.

Scale bar equals 300 nm.

Electric field distribution around nanoshell Si.

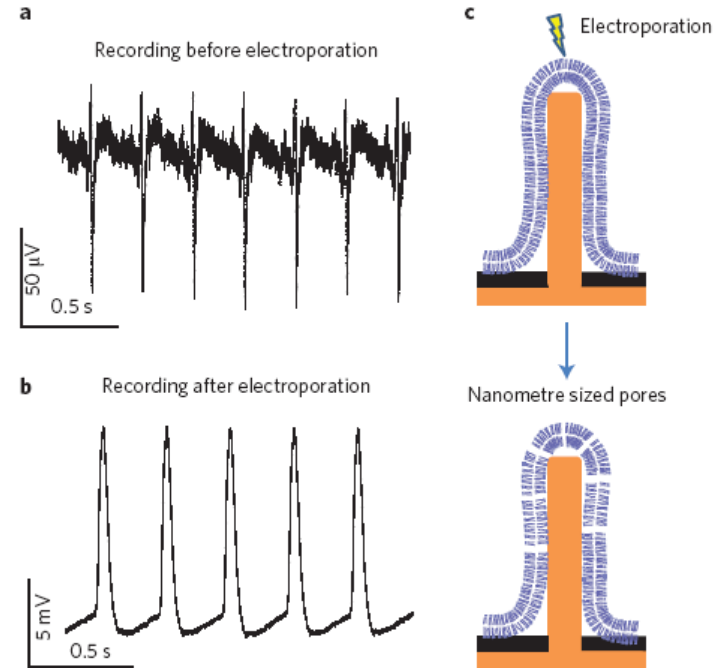


Light absorption spectrum of flat Si sample (black) and nanoshell Si sample (red).

NNIN is supported by NSF ECCS-0335765

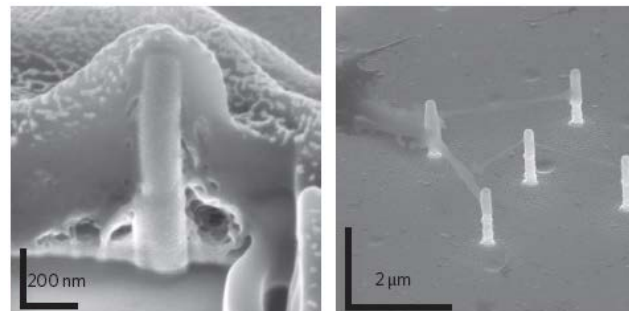
Recording of Action Potentials with Nanopillar

The purpose of this project is to design a high throughput intracellular recording system. Vertical nanopillar electrodes can record both the extracellular and intracellular action potentials of cultured cells over a long period of time with excellent signal strength. In the system, metal electrode (Ti/Pt) pads were exposed through an insulation layer for having interfaces locally with cells. The system was fabricated using standard photolithography and plasma-enhanced chemical vapor deposition (PECVD).



Recording action potentials before and after electroporation.

C. Xie*, Z. Lin*, et al., Stanford University work performed at Stanford Nanofabrication Facility



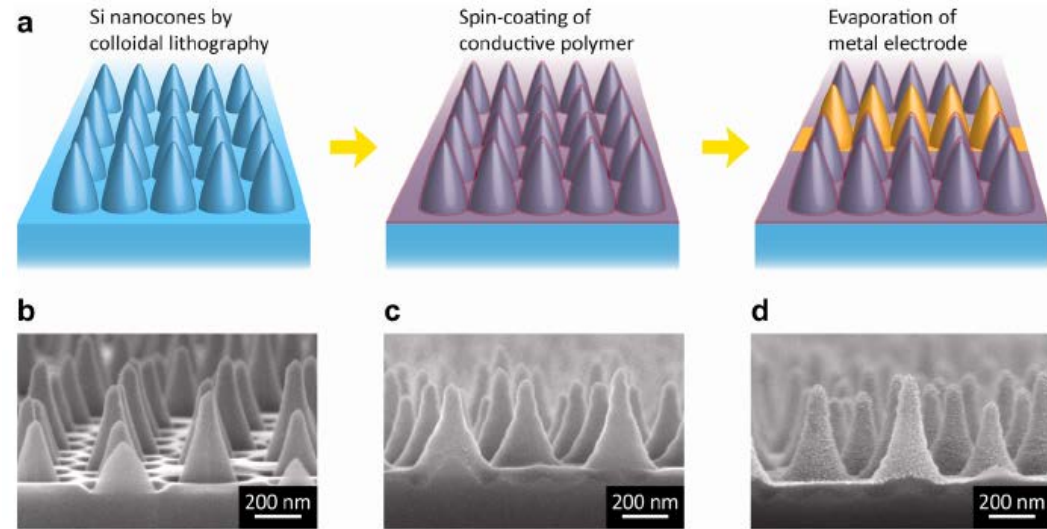
SEM images showing the cell-nanopillar electrode interface.

Hybrid Si Nanocones/Polymer Solar Cell

The purpose of this project is to design a hybrid solar cell with low-cost processing. Si nanocones fabricated by colloidal lithography were covered with a conductive polymer, which formed a Schottky junction between the Si and polymer. All the processes were conducted at temperatures below 120 ° C.

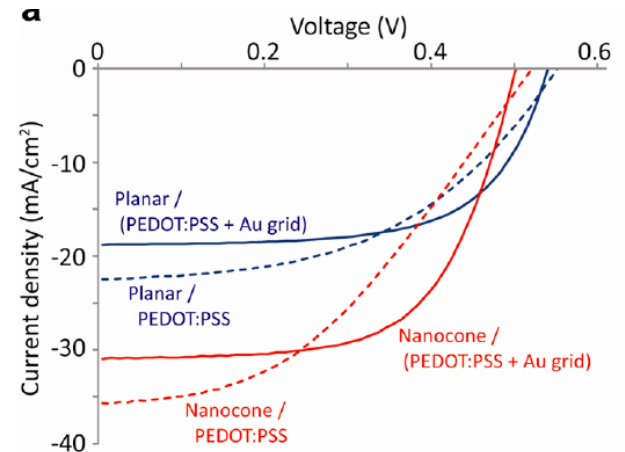
The power conversion efficiency of the hybrid Si/polymer device was more than 11 %, which is the world-record among the hybrid devices.

S. Jeong, et al., Stanford University
work performed at Stanford
Nanofabrication Facility



Fabrication processes of a Si nanocones/polymer hybrid solar cell.

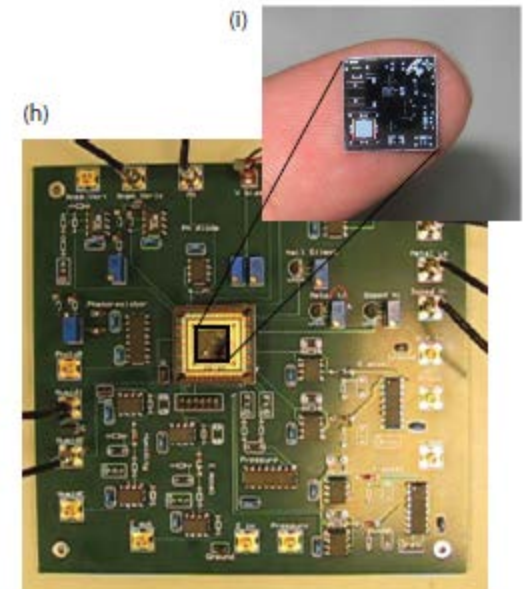
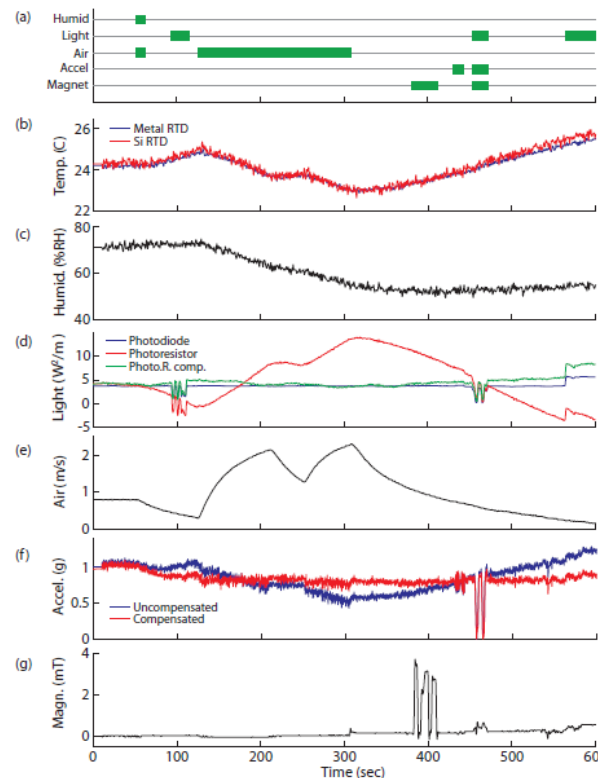
Characteristics of hybrid
Si/polymer solar cells.



Multi-Functional Integrated Sensors (MFISes)

The goal of MFISes is to demonstrate a low cost, low power, multi-functional sensor to push the boundaries of “sensor fusion”. The future of sensing is using the power of many sensing modalities, combined through networking and computation, to deliver information which is otherwise unavailable. This requires microfabrication process integration and device design for a variety of sensors which have never been demonstrated together, as well as computation, radio, and energy harvesting capabilities.

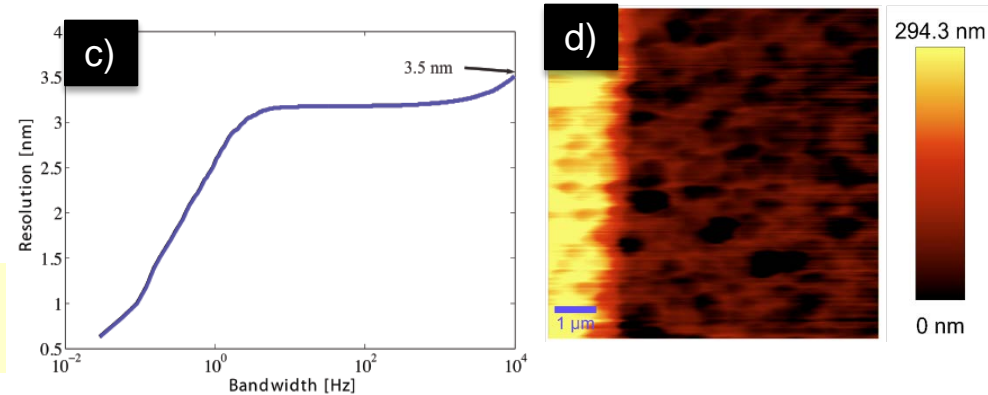
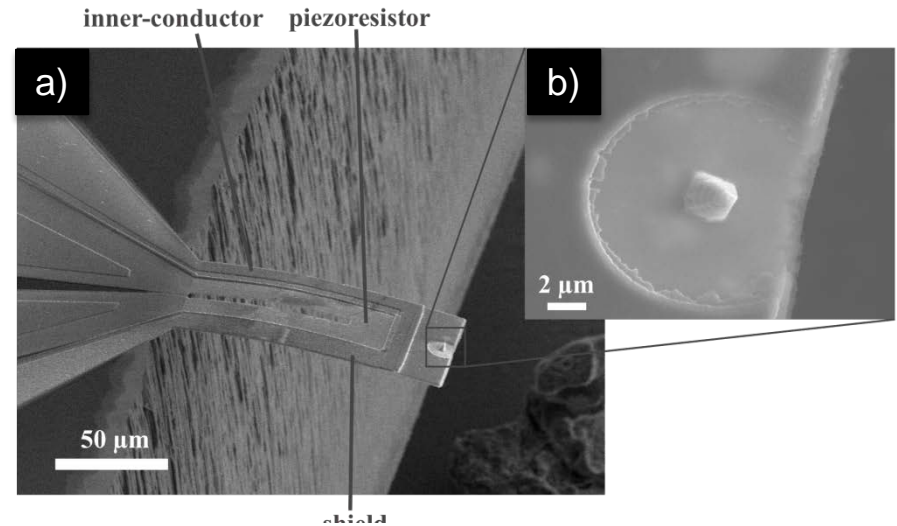
Demonstration of MFISes multi-functional sensing capabilities. (a) Time points when humidity, light intensity, air speed, acceleration, and magnetic field parameters were varied, (b) measurements of temperature using metal and doped silicon RTDs, (c) relative humidity, (d) light intensity using the photodiode and photoresistor and the photoresistor output after temperature compensation using the RTD data, (e) anemometer measurement of air speed, (f) acceleration measurement using piezoresistive z-axis accelerometer with and without temperature compensation, and (g) magnetic field strength, (h) sensor and analog electronics used in multi-functional demonstration and (i) close up of MFISes device.



C. Roozeboom et al. Stanford University work performed at Stanford Nanofabrication Facility

Low-Impedance Shielded Tip Piezoresistive Probe

Piezoresistive probes were fabricated for displacement self-sensing with integrated conductive shielded tip. (Figure a, b) We achieved nm displacement resolution in air (figure c) and carried out atomic force microscopy scan on Al electrodes on SiO₂ (figure d). We measured low tip-shield impedance (30Ω, 9.5pF) enabling portable scanning microwave microscopy.



A.J. Haemmerli et. al. Stanford University work performed at Stanford Nanofabrication Facility

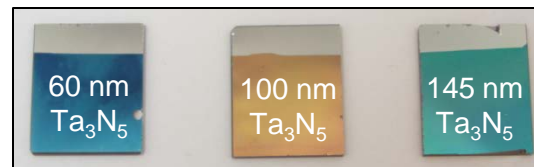
Deconstructing Charge Transport in Ta_3N_5 & TaON Photoanodes for Water Splitting

The goal of this project is to identify and overcome fundamental charge transport limitations in Ta_3N_5 and TaON which could arise from poor (i) bulk transport of photogenerated electrons (e^-) and holes (h^+), (ii) charge transport across grain boundaries, and (iii) charge transfer across the interface at the back contact. Electron beam evaporation is used to deposit a Pt contact on quartz followed by a thin film of Ta metal which is subsequently oxidized and nitrided. Major benefits of this approach are tight control of film thickness and a much more uniform morphology compared to films synthesized from Ta foils; both are key to the study of charge transport in these materials.

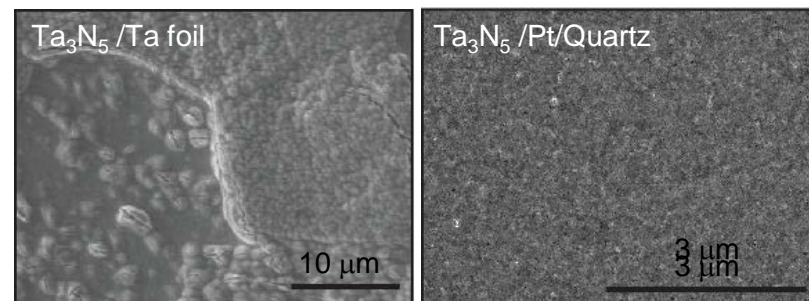
Blaise A. Pinaud (P.I. Thomas F. Jaramillo)
Stanford University
Work performed at Stanford Nanofabrication Facility



Photoelectrochemical testing of a Ta_3N_5 photoanode.



Different colors caused by optical interference are evidence of the excellent film uniformity.

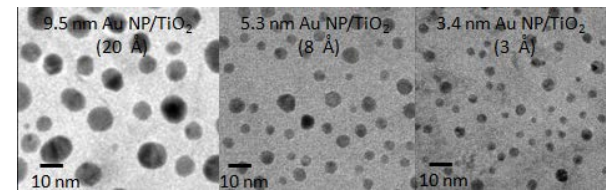


Scanning electron micrographs show that films grown on Ta foils (left) are much rougher and cracked compared to films grown from electron beam evaporated Ta (right).

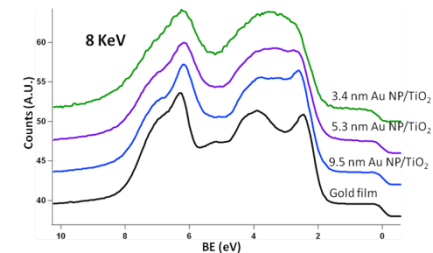
The Origins of the Catalytic Activity of Supported Gold Nanoparticles

The purpose of this project is to determine the main factors controlling the high catalytic activity of supported gold nanoparticles. To carry out this purpose, we synthesize gold nanoparticles on a Titania support using the Innotec electron beam evaporator in the Stanford Nanofabrication Facility. Various methods are used subsequently to determine the electronic properties, the morphology and the catalytic activity of the synthesized nanoparticles.

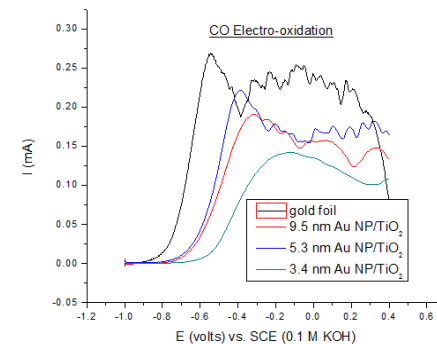
Benjamin N. Reinecke (P.I. Thomas F. Jaramillo),
Stanford University
Work performed at Stanford Nanofabrication Facility



This figure shows the TEM plan view of the gold nanoparticles on TiO_2 . The average sizes of the 3, 8 and 20 Å gold nanoparticles on TiO_2 are 3.4, 5.3, and 9.5 nm.



This figure shows the valence band electronic structure of TiO_2 supported gold nanoparticles after the TiO_2 background subtraction



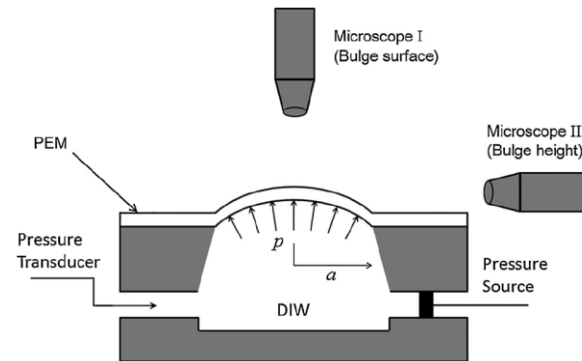
The electrocatalytic CO oxidation activity of TiO_2 supported gold nanoparticles.

Engineering of Graphene Bandgap

The semiconductor industry is interested in graphene as a high mobility, patternable semiconductor to potentially extend CMOS; however, it doesn't have a bandgap. Our study looks into correlation of strain with bandgap formation, and bandgap generation via substrate induced strain.

We developed a process to transfer and clamp a CVD graphene grown on copper, to a flexible PDMS substrate that allows application of strain to the graphene and measurement of Raman spectra and the resistance. Strain application device was fabricated that enables strain up to 25% to be applied to the graphene films. In addition, to characterize the valence band structure as a function of strain and measure transitions from the valence band to the conduction band, SRPES and NEXAFS are used.

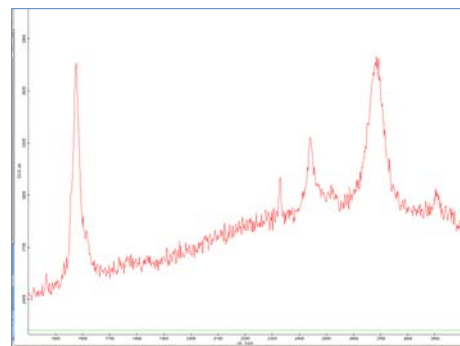
Yoshio Nishi, C. Michael Garner, and Marjan Aslani
Stanford University work performed at Stanford
Nanofabrication Facility



Schematic of strain application device



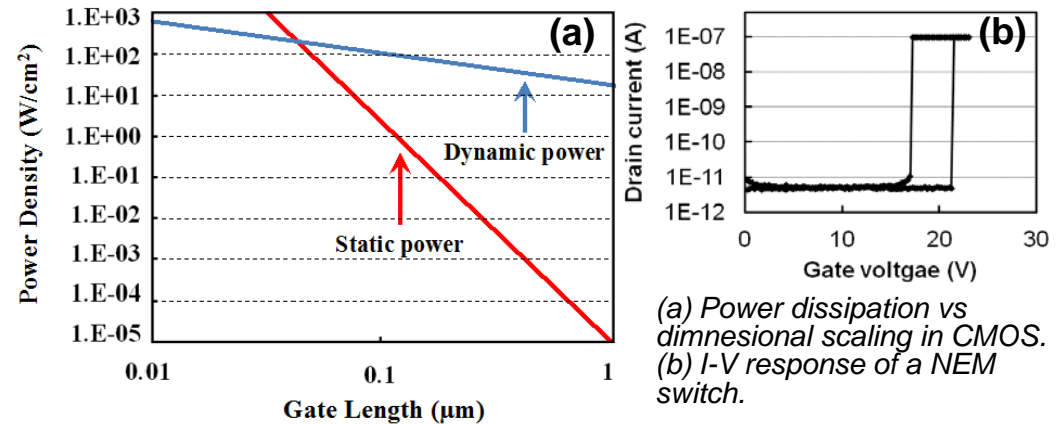
Optical image of strained graphene on flexible substrate



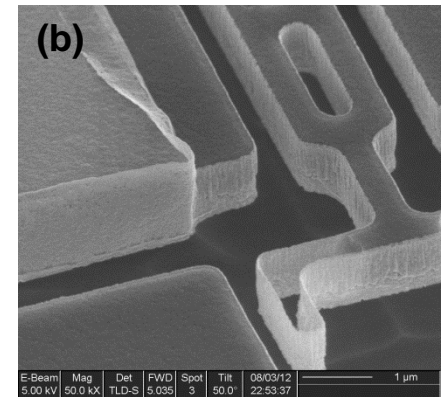
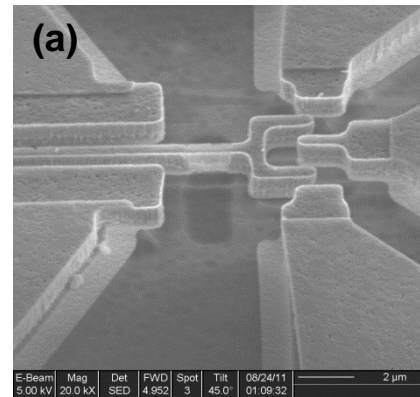
Raman spectra of strained graphene on flexible substrate

Nanoelectromechanical Low Power Electronics

Nanoelectromechanical (NEM) relays can drastically reduce the static power dissipation in hybrid NEM/CMOS electronics and are ideal candidates for a number of applications SRAMs and FPGAs. The SNF fabricated NEM relays target two objectives: improving energy efficiency by reducing the switching voltage and contact resistance and increasing the robustness by solving the reliability issues such as yield, repeatability and life time. Availability of different recipes for atomic layer deposition (ALD) of a number of conductive coating on the side wall of the relays such as platinum (Pt) and titanium nitride (TiN) allows to reduce the reliability issues and drastically reduce the contact resistance.



(a) Power dissipation vs dimensional scaling in CMOS. (b) I-V response of a NEM switch.

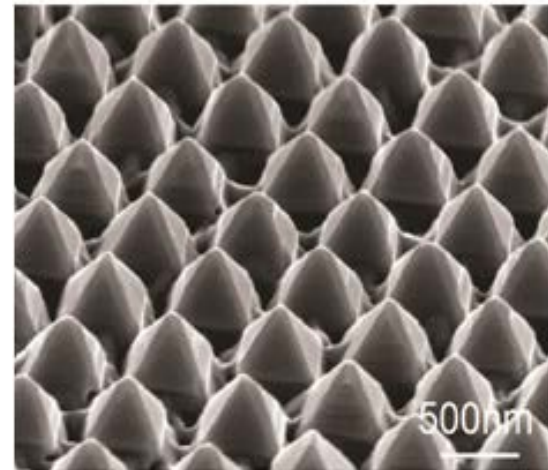
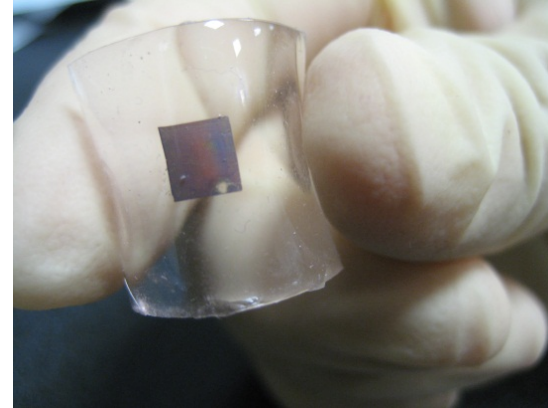


(a) A 6-terminal logic gate with ALD TiN side wall coating and electrical isolation. (b) A 5-terminal relay with ALD Pt thin-wall and hollow source-drain contact.

W. Scott Lee and R. T. Howe, Electrical Engineering, Stanford University
Work performed at Stanford Nanofabrication Facility (SNF).

Ultra Thin Film Nanostructure Solar Cell

The purpose of the Ultra Thin Film Nanostructure Solar Cell is to make an optimal structure to achieve high solar cell efficiency with low material cost, excellent angle acceptance and potential to be flexible. Nanostructure has been designed to enhance light absorption through antireflection and light trapping and also improve internal quantum efficiency by decoupling of light path and minority carrier transport path. Silica nanospheres have been used as an etch mask to fabricate Ge nanopiramids on top of silicon wafer. Then, GaAs layer is grown to form GaAs-Ge core-shell nanopiramids. After nanopiramid structure attaches to the PDMS layer, Si substrate and Ge grown layer is etched using XeF_2 to form GaAs hollow nanopiramids.

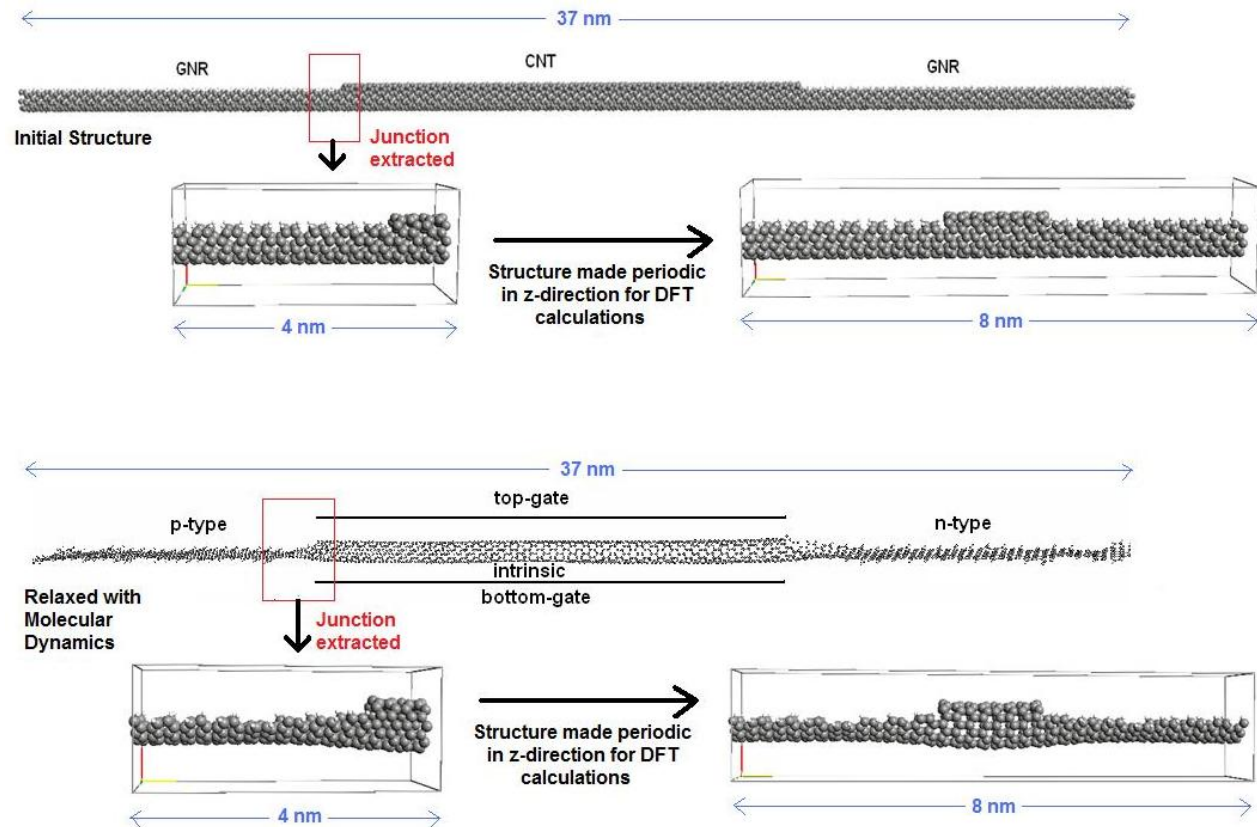


45-degree view of GaAs-Ge core-shell nanopiramids.

Dong Liang, Yijie Huo, Yangsen Kang and James S. Harris Stanford University work performed at Stanford Nanofabrication Facility

Strain Induced Carrier-Mobility Changes in the Heterojunction Region of the Unzipped-CNT based TFET

In case of the TFETs, the carrier-mobility in the channel region is predominantly controlled by the transport rather than the various scattering mechanisms. But in the case unzipped CNTs, the actual channel definition is a question of ambiguity. This calls for a need to understand in what direction the strain in the hetero-junction region is influencing the carrier mobility. The previous simulations we did assumed the abrupt junction between the CNT/GNR, which will not be the case in practically fabricated device. To understand the functionality of the unzipped CNT based devices it is therefore important to understand the mobility changes due to strain in the hetero-junction region. This study will make conclusions on the same.

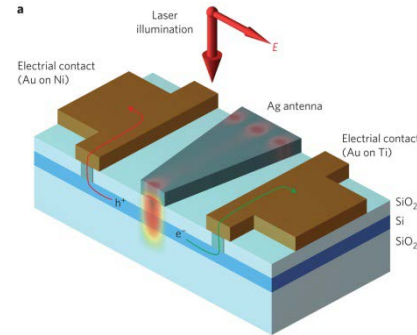


Ashutosh Srivastava, Larkhoon Leem, Blanka Magyari-Kope, Stanford University.
Work performed at Exiton Cluster at Stanford Nanofabrication Facility.

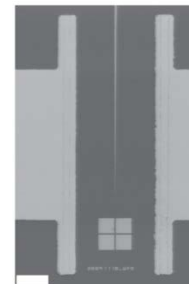
Optical Antenna Photocurrent Project

The project is aimed to use photocurrent mapping technique to image near field of an optical antenna resonance. Electron beam lithography defined wedge shaped silver plasmonic antenna was placed on a thin film silicon-on-insulator photodetector. Photocurrent measured from the detector will contain both spectroscopic and spatial information related to the antenna resonance. Such platform allows a new approach, complementary to traditional near field scanning optical microscopy, to provide insight of specific optical antenna structure of interest.

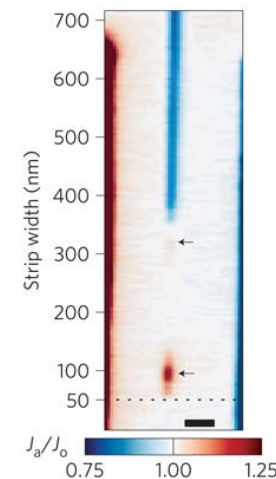
Edward Barnard and Mark Brongersma, Stanford University
Work performed at Stanford Nanofabrication Facility



Sketch of detector structure shows a Ag wedge antenna placed upon a thin film Si detector. And incident light can excite resonances at different locations of the Ag wedge.



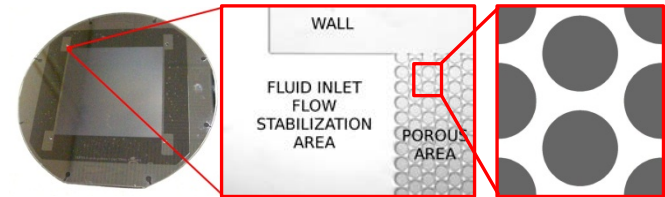
SEM image of a real device, showing the Ag wedge placed between two contact electrodes of the detector. Scale bar is 10um.



Photocurrent mapping near a Ag wedge at 700nm incident wavelength. The two arrows indicate two photocurrent "hotspots" which is attributed to excitation of plasmonic resonances of Ag antenna.

Fluid Flow in Porous Media: Instabilities

The aim of the Flow Instabilities in Porous Media Project is to provide a better understanding of why and how a less viscous fluid displacing a more viscous fluid generally leads to an instable flow (“fingers” of one fluid entering the domain mostly occupied by the other fluid). The implications go from more efficient chemical catalyzers to aquifer pollution control, but our principal interest is in CO₂ geological sequestration. As main part of our experimental setup, we need 2-D porous media (“micromodels”) made at SNF by etching a Si wafer, drilling injection ports through it, and anodically bonding a glass wafer on top of it. We have conducted most of the experiments for a highly homogeneous porous medium, and are planning to introduce heterogeneities in our systems.



The highly homogenous 2-D porous medium “micromodel” and its pattern (cylinders are 40 μ m in diameter, 25 μ m in height and separated by gaps of 10 μ m)

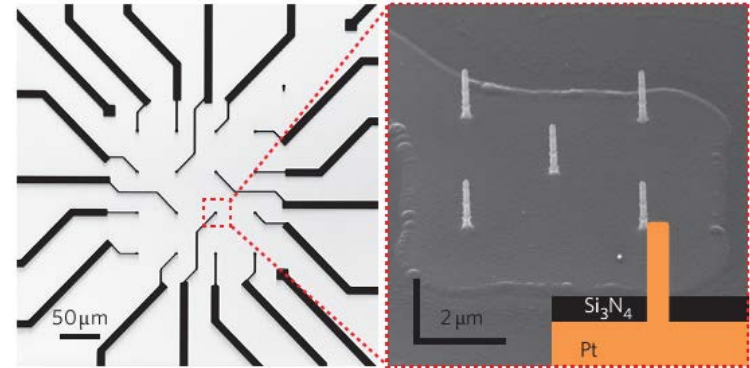


Example of unstable flow in the highly homogenous micromodel: CO₂ (grey) displacing UV-died water (green)

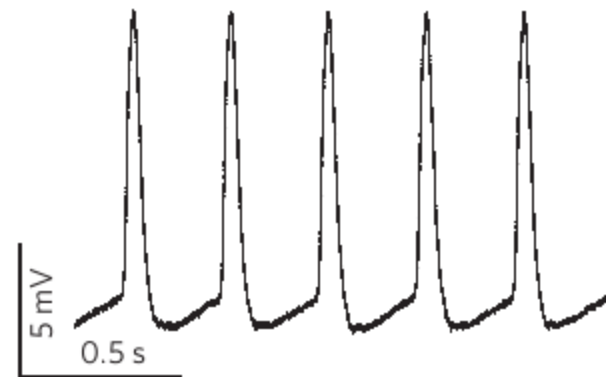
Christophe Duchateau and Anthony Kavscek, Stanford University, Energy Resources Engineering Dpt.
Work performed at Stanford Nanofabrication Facility

Intracellular Recording by Nanopillars

The purpose of the Nanopillar Project is to use vertical nanoscale metallic electrodes to perform intracellular recording of action potentials. The image on right shows an array of 5 nanopillar electrodes residing on the metallic leads that connects the recorder. We then culture rat cardiac cells on top of the nanopillars and record intracellular action potentials. The device is fabricated in SNF and SNL. This work is published in *Nat. Nanotechnology*, 7, 185 (2012).



Nanopillar electrode array fabricated in SNF and SNL

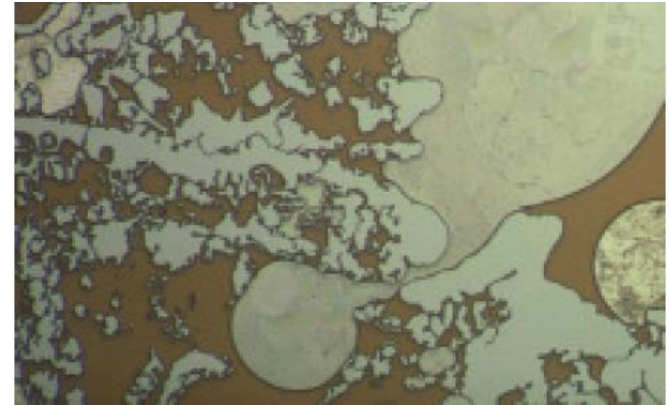


Intracellular recording of cardiac cell action potentials by nanopillar electrodes

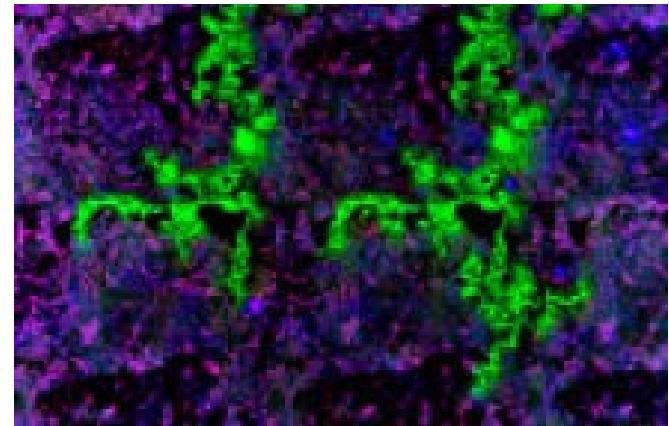
Ziliang Carter Lin, Chong Xie, Yi Cui, Bianxiao Cui
Stanford University work performed at Stanford
Nanofabrication Facility and Stanford
Nanocharacterization Facility

Fluid Flow in Porous Media: Rock Replicas

The Fluid Flow in Porous Media: Rock Replicas Project aims at improving our understanding of fluid flows under realistic geological conditions. The main purpose is to provide better parameters for oil production models and for testing chemicals used to enhance oil recovery, but this work can be re-used for other geologic systems and conditions. Starting from a rock thin section, we acquire an SEM image. We use image analysis to distinguish pores on one hand and rock on the other hand, and then we create an artificial 2-D porous medium similar to the original picture. Different carbonate and sandstone samples have been mimicked, are used, and have already lead to significant progress.



Water injection (beige) in a carbonate-replica micromodel (light grey) presaturated with oil (brown)



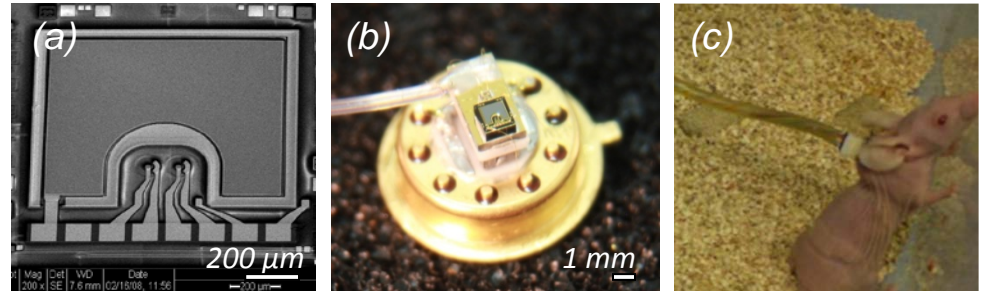
Fluorescence of a UV-died water injection (green) in a water-saturated double porosity carbonate micromodel. The water follows the path of higher porosity areas

Markus Buchgraber, Salem Al Dousary and Anthony Kavscek, Stanford University
Work performed at Stanford Nanofabrication Facility

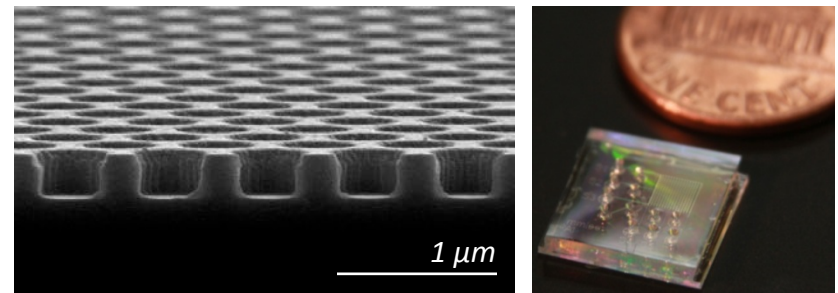
Integrated Optical Biosensors Project

This project focuses on the development of semiconductor-based integrated optical sensors that are cost-effective for point-of-care biomedical analysis. The components fabricated with the use of SNF equipment have included 1 cm x 1 cm SiNx/fused silica photonic crystal slabs and arrays of monolithically integrated Vertical Cavity Surface Emitting Lasers (VCSELs) /photodetectors. These have been utilized to demonstrate label-free sensing in a *lab-on-a-chip* platform and fluorescence sensing in freely moving mice, both at 670 nm in the VIS-NIR biological transparency window.

James S. Harris, Shanhui Fan, Sanjiv S. Gambhir,
Stanford Electrical Engineering and Radiology
Departments Stanford University
Work performed at Stanford Nanofabrication
Facility



(a) Monolithically integrated VCSEL/ photodetector used for
(b) tunable-wavelength label-free sensing and
(c) in vivo fluorescence sensing in a freely moving mouse



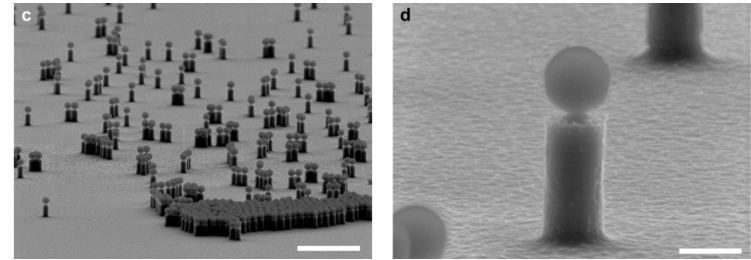
Photonic crystal slab integrated with PDMS microfluidics

Images: T. O'Sullivan et al., *Opt. Ex.* 18, 2010
and M.M. Lee et al., *SPIE DSS*, 2011

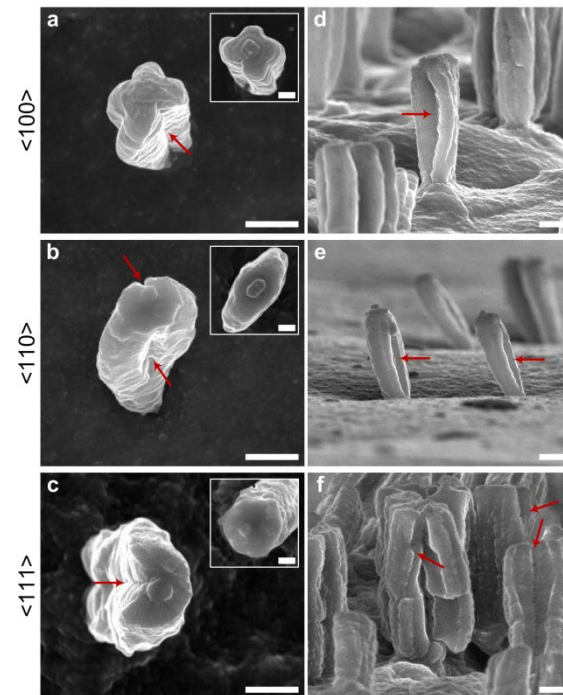
Fracture of Crystalline Silicon nanopillar during lithiation

We show that fracture locations are highly anisotropic for lithiation of crystalline Si nanopillars and that fracture is strongly correlated with previously discovered anisotropic expansion. The pillars were fabricated by Deep Reactive Ion Etching process on Si wafers. Contrary to earlier theoretical models based on diffusion-induced stresses where fracture is predicted to occur in the core of the pillars during lithiation, the observed cracks are present only in the amorphous lithiated shell. We also show that the critical fracture size is between about 240 and 360 nm and that it depends on the electrochemical reaction rate.

S. W. Lee, M. T. McDowell, L. A. Berla, W. D. Nix, Y. Cui, Stanford University work performed at Stanford Nanofabrication Facility



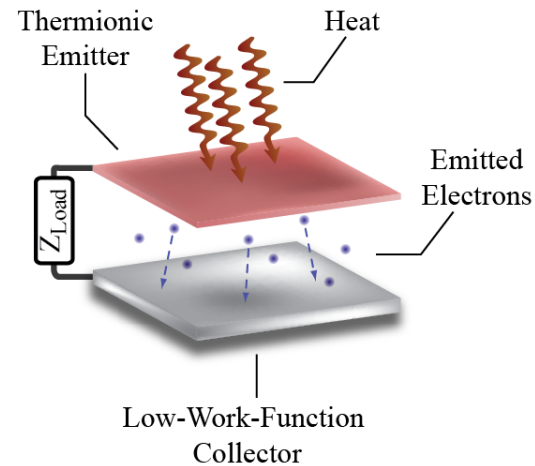
Fabricated Si nanopillars on Si wafer by DeepRIE process.



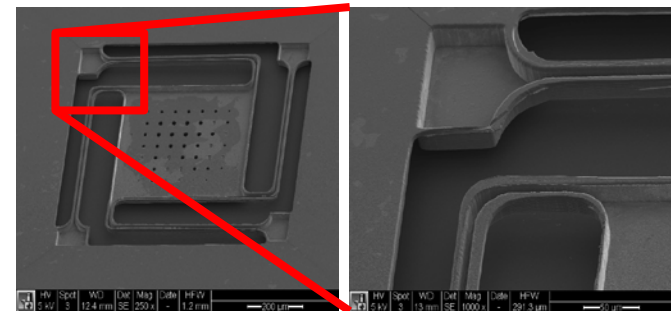
Fracture of Si nanopillars of various axial crystalline orientation after lithiation.

Microfabricated Thermionic Energy Converters

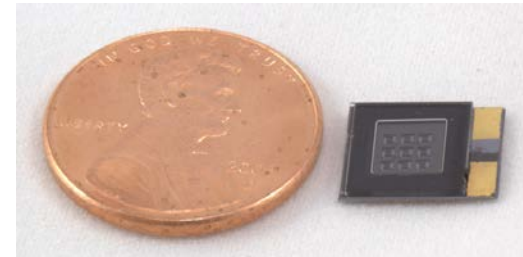
Microfabricated thermionic energy converters (μ -TECs) can convert very high-temperature heat (>1000 C) directly to electricity using evaporation of electrons from solid surfaces (thermionic effect). Microfabrication is the optimal manufacturing approach for thermionic energy converters because the optimal cathode–anode gap for TECs is in the range of 1–10 μm , which is highly suitable for MEMS-based fabrication processes. The devices are fabricated out of silicon carbide and include barium-oxide coatings to reduce the work function. Small arrays of converters were encapsulated under a glass lid using wafer-scale anodic bonding.



Schematic of a μ -TEC. Electrons are emitted from the hot emitter, cross the vacuum gap, are absorbed in the collector, and finally return via electric load, doing useful work.



Microfabricated silicon carbide emitters. The U-shaped leg give the structure out-of-plane rigidity.

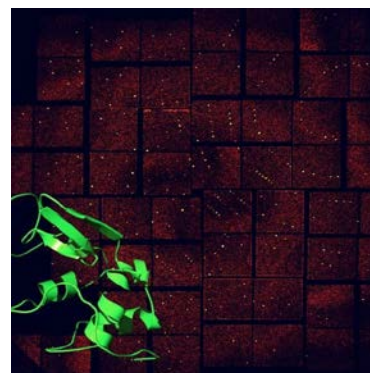


An encapsulated 3 × 3 array of μ -TEC emitters.

J.-H. Lee, I. Bargatin, and R. T. Howe, Stanford University
Work performed at Stanford Nanofabrication Facility

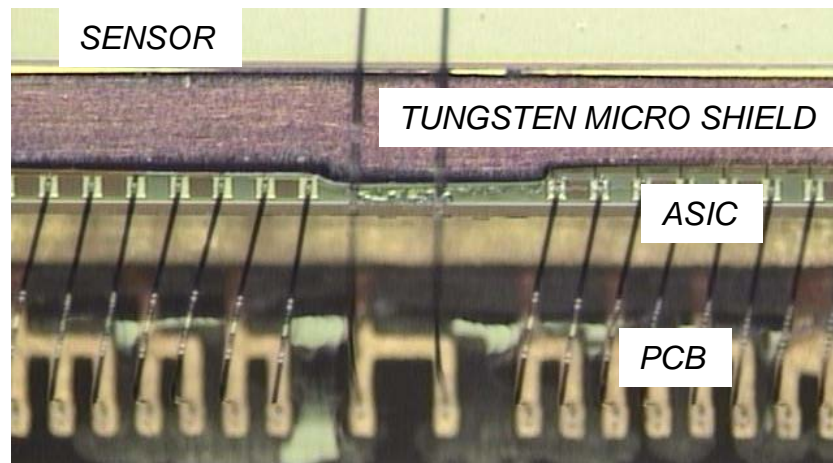
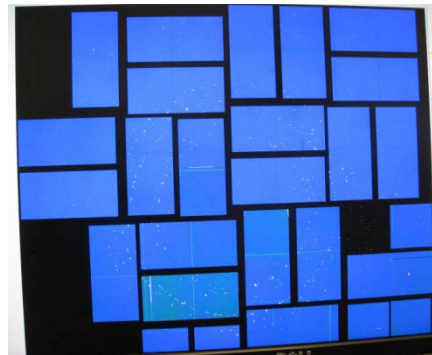
Micro-Radiation Shields for Free-Electron X-ray Laser Detectors

Special x-ray detectors are critical to performing a variety of science, such as femto-second nano-crystallography and pump-probe techniques, at the LCLS. These involve the use of ultra-brilliant x-ray beams. Such beams can radiation damage a circuit chip essentially instantaneously. Given the cost of making these detectors the use of micro-patterned, dielectric-coated tungsten foils has allowed a set of detectors to operate without the lose of a circuit chip for the last year.



Advanced, high frame rate, x-ray detectors are used for Femto-second Nano-crystallography at the LCLS

Extreme radiation environment can destroy a circuit chip in 50 femtoseconds

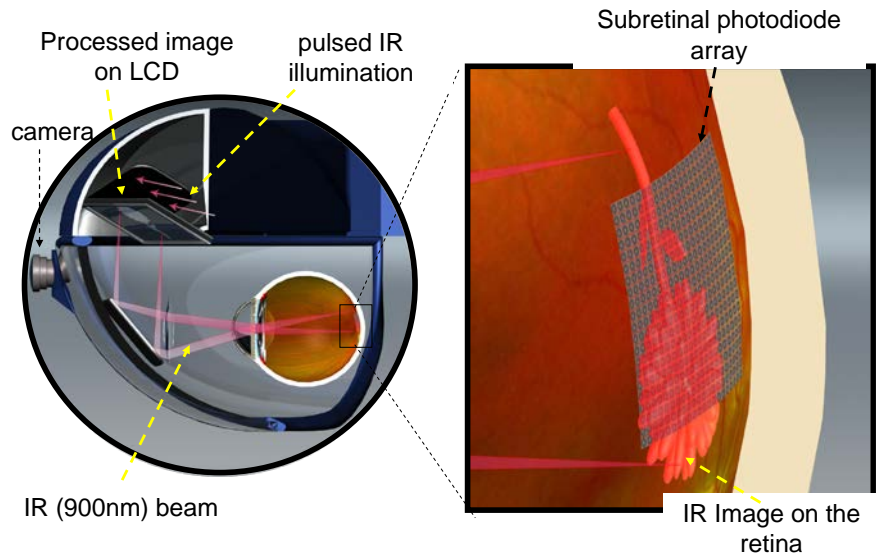


Close up of an installed x-ray shield

A. Tomada, L. Manger, J. Tice, C. Kenney, G. Williams, S. Boutet, M. Messerschmidt SLAC National Accelerator Lab, Stanford University
Work performed at Stanford Nano-fabrication Facility

Photovoltaic Retinal Prosthesis for Restoring Sight to the Blind

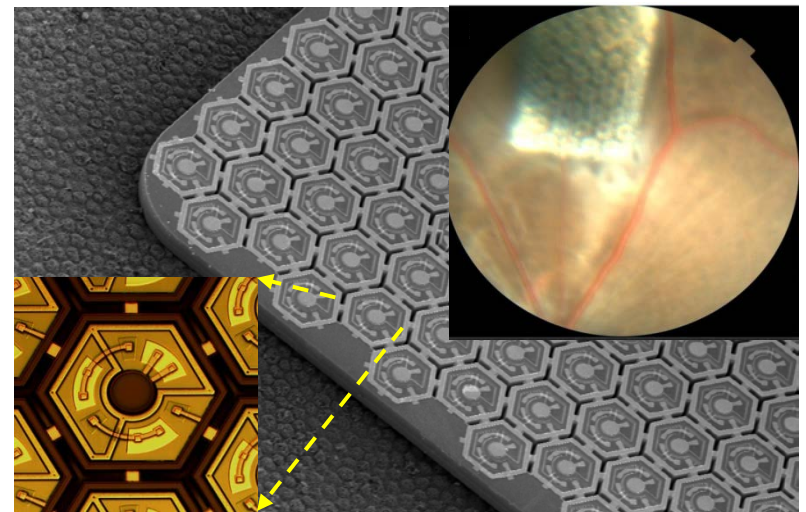
Retinal degeneration leads to blindness due to loss of photoreceptors. Sight can be restored by patterned electrical stimulation of the surviving inner retinal neurons. Photovoltaic subretinal prosthesis directly converts pulsed light into pulsed electric current in each pixel, stimulating nearby neurons. Visual information is projected onto retina by video goggles using pulsed NIR (~900 nm) light. Photovoltaic arrays including 3 diodes in each pixels were fabricated in SNF. Retinal response was elicited in-vitro and in-vivo with pixel sizes down to 70 μm .



Video goggles projecting captured image onto subretinal photovoltaic array using pulsed near-IR light (~900nm).

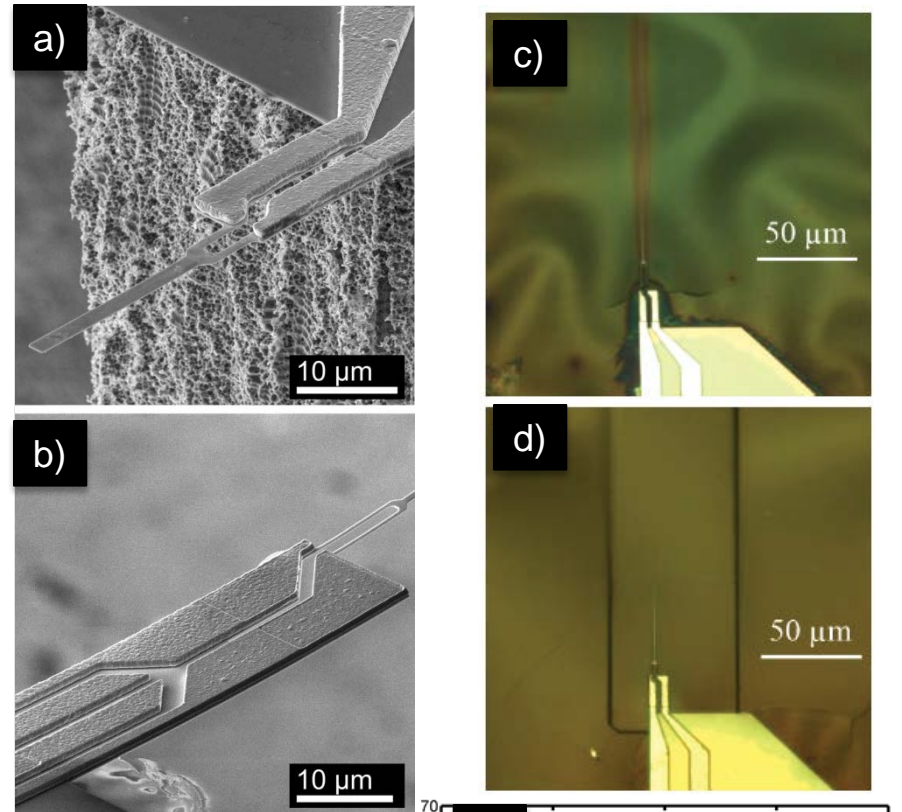
Photovoltaic array implanted under the retina in a blind rat. Higher magnification view shows the array itself, and a single pixel of the implant.

Daniel Palanker's group (Ophthalmology and HEPL) and James Harris's group (EE) at Stanford U., Alexander Sher's group at UCSC. Fabrication performed at Stanford Nanofabrication Facility



High Speed Force Probes for Hair Cell Biology

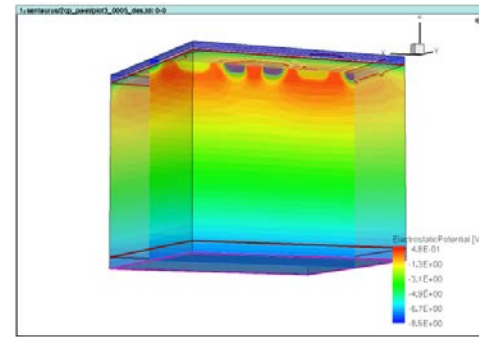
In this work we fabricated piezoresistive cantilever with integrated piezoelectric actuator for high-speed self-sensing and self-actuating (figures a and b). Integrated cracks patterning in buried oxide for fabrication yield improvement (figures c and d). 60pN force resolution at 200 kHz in water was achieved (figure e).



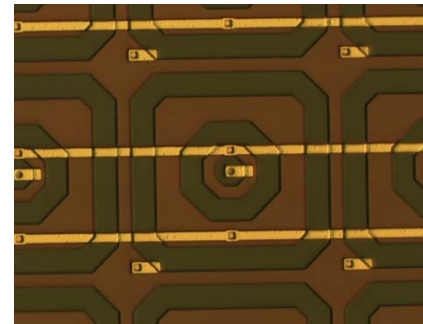
a), b), J.C. Doll et. al. Stanford University
Work performed at Stanford Nanofabrication
Facility

X-ray Photon Correlation Spectroscopy Sensor

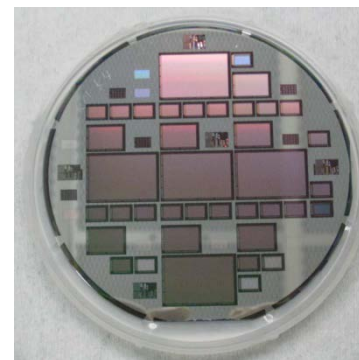
One method used to study the dynamics of molecular and nanometer scale systems is X-ray Photon Correlation Spectroscopy. In this technique correlations within the recorded x-ray image provides information on structure and motion in the sample. The beam coherence of the LCLS allows the understanding of dynamics with femto-second durations. A unique sensor that is similar to a one-stage CCD has is being fabricated at Stanford with small pixels and low electronics noise.



Electric fields within a pixel modelled using Synopsys TCAD



Close up of a single pixel showing concentric electrodes for storing and transferring the electronic signal.

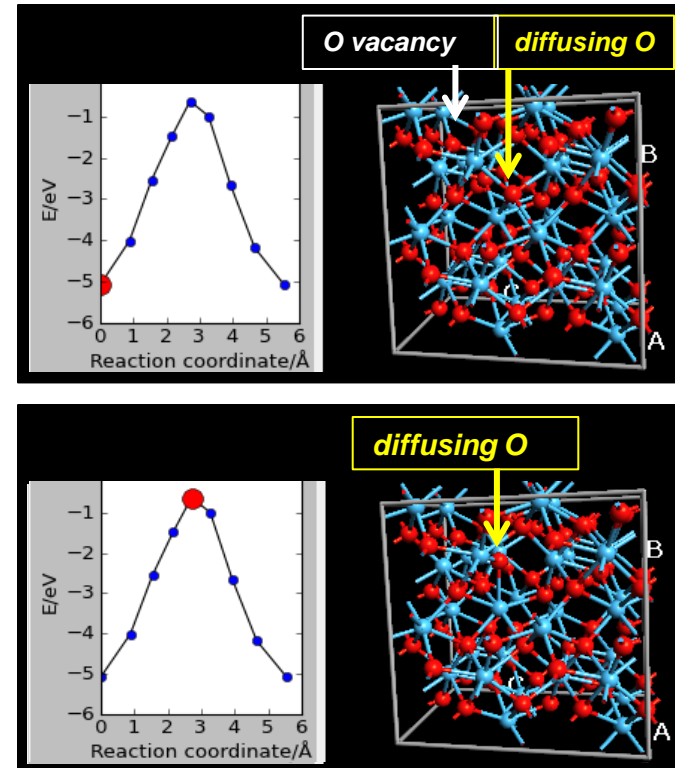


Finished wafer with novel x-ray sensors optimized for XPCS science at the LCLS.

J. Segal, C. Kenney, G. Carini. A. Robert SLAC National Accelerator Lab, Stanford University; P. Rehak, P Siddons Brookhaven Nat. Lab.
Work performed at Stanford Nanofabrication Facility

Kinetics of RRAM Switching Mechanism

In resistive random-access memory (RRAM) devices, information is stored by switching the material between high- and low-resistivity states of a “conductive filament” formed in the device. Development of RRAM materials with superior characteristics requires detailed understanding of switching mechanism and quantitative description of switching kinetics, as well as the description of the initial conductive filament forming process. We use first-principles simulations to study how the energy profiles for the diffusion of oxygen vacancies and Frenkel pair formation in RRAM materials change under different conditions, including changes in atomic configuration and applied electric field.



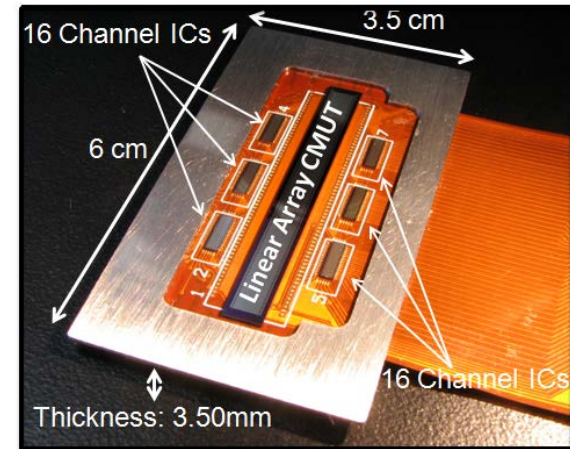
O ion diffusion barriers in HfO₂ vary from <0.5 eV to >4eV, depending on the diffusion path, charge state and applied electric field, according to the ab initio nudged-elastic-band simulation results. One of the disfavored paths is shown. Minimizing the variability in switching is one of the goals in RRAM studies.

Sergey V. Barabash, Blanka Magyari-Kope,
Intermolecular Inc. and Cornell
Work performed at NNIN Exiton Computing Cluster

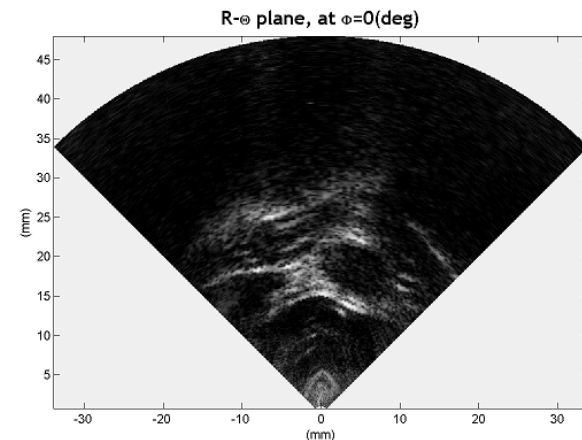
Miniaturized, Wearable Ultrasound Probe

The purpose of the Miniaturized, Wearable Ultrasound Project is to develop a low-profile ultrasound probe, which can be taped on a patient for constant monitoring of organ functions. The SNF-fabricated ultrasonic transducer is integrated with application-specific ICs on a flexible PCB and the assembly is fully compatible with commercial ultrasound imaging systems.

For ultrasound imaging applications, the transducer consists of a 64-elements linear array. Each element is made of thin silicon plates, which are fusion bonded on a pre-patterned silicon substrate. The plates are actuated by electrostatic force through sub-micron vacuum gap to transmit and receive ultrasound.



Integration of IC & transducer array on a flexible PCB



Cross-section image taken from

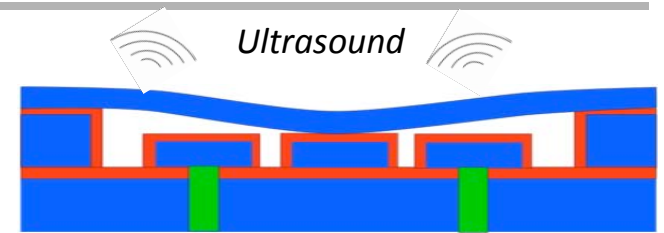
Anshuman Bhuyan, Jung Woo Choe, and Butrus T. Khuri-Yakub, Stanford University work performed at Stanford Nanofabrication Facility

Capacitive Micromachined Ultrasonic Transducers in High Ambient Pressure

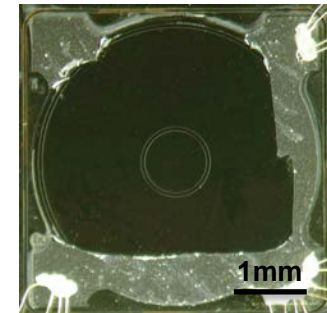
The purpose of the Capacitive Micromachined Ultrasonic Transducers (CMUTs) in High Ambient Pressure Project is to develop versatile air transducers, which operate under a wide and varying pressure range (1–20 atm) for various applications, such as ultrasonic flow metering (UFM).

The air transducer is fabricated in SNF; Thick silicon plate (10–20 μm) is fusion boned on the pre-defined cavity in a vacuum condition. A pressure difference between the cavity and the ambient deflects the plate inward and the center of the plate contacts with the bottom of the cavity. This contact mode inherently increases the electromechanical coupling coefficient and makes the device robust to the high ambient pressure. A successful demonstration of ultrasound pitch-catch is performed at elevated ambient pressure up to 7 atm.

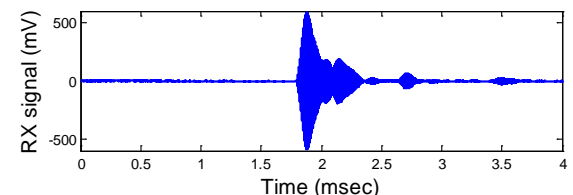
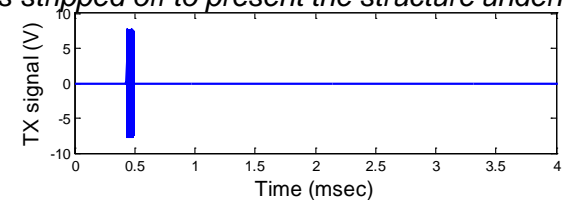
Min-Chieh Ho, Mario Kupnik, Kwan Kyu Park, and Butrus T. Khuri-Yakub, Stanford University work performed at Stanford Nanofabrication Facility



Cross-section schematic of the ultrasound transducer. (Blue: Single Crystal Silicon, Red: Thermal oxide)



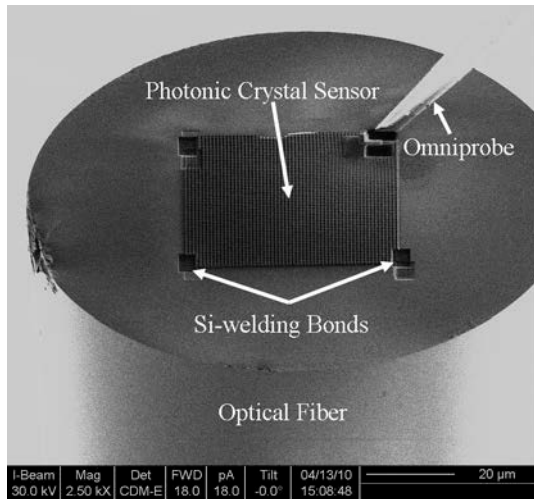
Optical picture (top view) of a fabricated device. A silicon plate is stripped off to present the structure underneath.



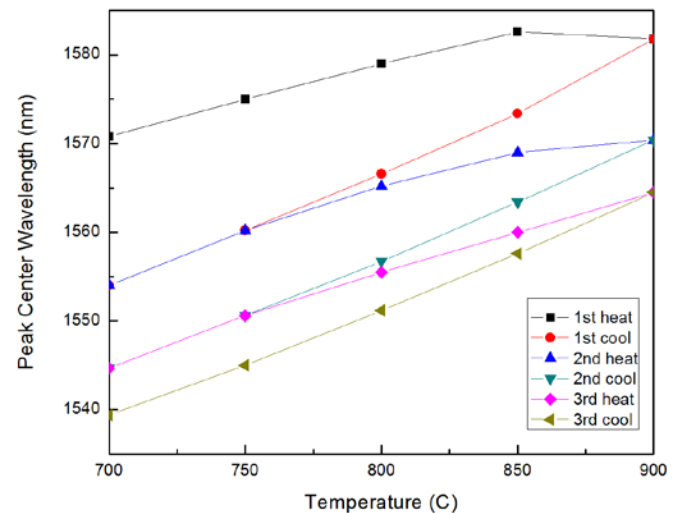
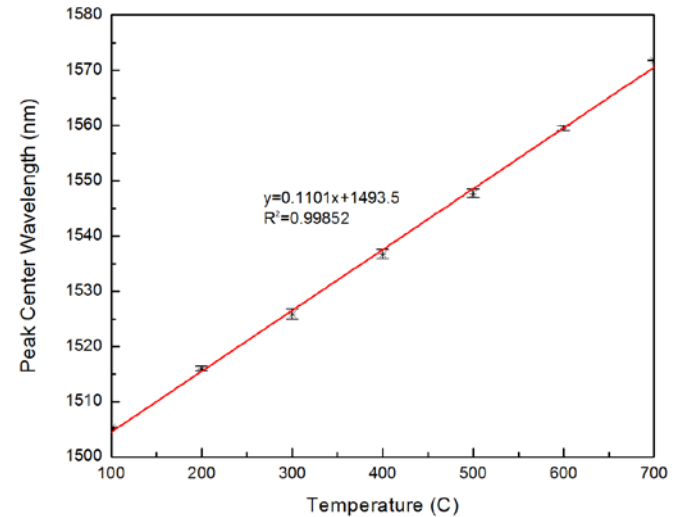
Pitch-catch signal of the transducer at a high ambient pressure, 7 atm.

Photonic Crystal Fiber Sensor for High Temperature Measurement

Photonic crystals were assembled on optical fiber using Focused Ion Beam (FIB). Stable operation occurred up to 700C with high sensitivity of 0.11nm/C (an order higher sensitivity than Fiber Bragg Grating sensors). Performance degradation above 700C was mainly due to thermal oxidation of Si photonic crystal.

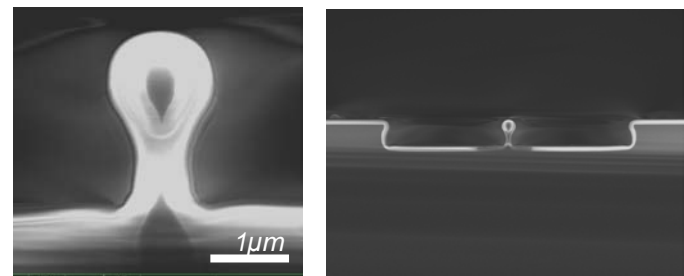
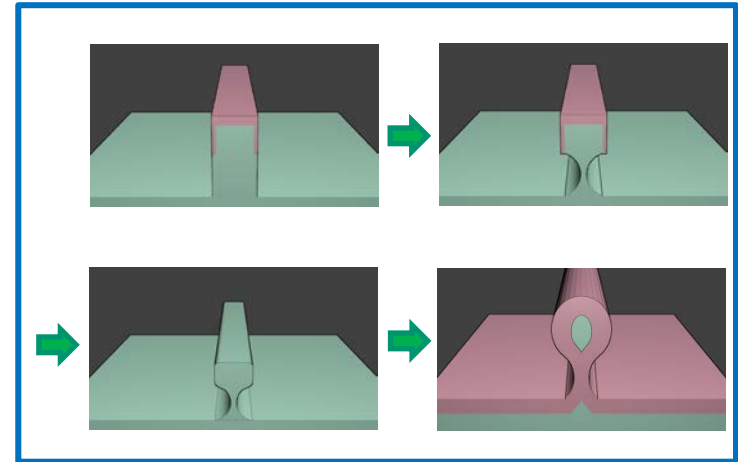


Bryan Park and Olav Solgaard Stanford University
Work performed at Stanford Nanofabrication Facility

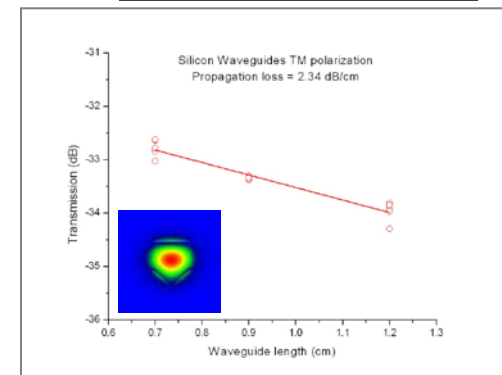


Silicon photonics for optical interconnects monolithic silicon waveguides in silicon wafers

We demonstrate silicon waveguides fabricated in standard silicon wafers using CMOS compatible processes. By properly designing and fabricating the devices, we accomplish high-performance and compact channel waveguides, with TM: 2.34 dB/cm and oval shape: 360 nm x 630 nm. Our fabrication method simplifies integration of electronics and photonics and is therefore promising for implementation of silicon-photonics applications.



C.-M. Chang and O. Solgaard, Stanford University
Work performed at Stanford Nanofabrication Facility



UCSB

Gecko-inspired Adhesives Project

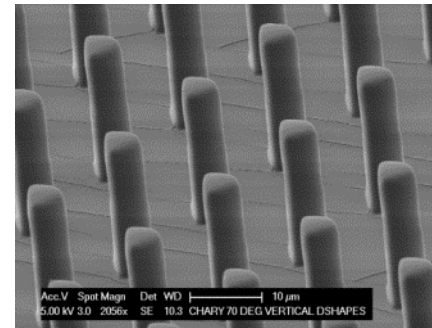
Geckos are able to adhere strongly and release easily from surfaces because the structurally anisotropic fibers on their toes naturally exhibit force anisotropy based on the direction of articulation. Hence, 10 μm diameter semicircular PDMS fibers, with varying amounts of contact area on the two faces, were investigated to ascertain whether fiber shape can be used to gain anisotropy in shear and shear adhesion forces. Testing of fiber arrays against a flat glass puck showed that shear and shear adhesion forces were two to five times greater when in-plane movement caused the flat face, rather than the curved face, of the fiber to come in contact with the glass puck, clearly demonstrating how fiber shape may be used to influence the properties of the adhesive. This result has broad applicability, and by combining the results shown here with other current vertical and angled designs, synthetic adhesives can be further improved to behave more like their natural counterparts.

*John Tamelier, Sathya Chary, and Kimberly L. Turner,
Dept. of Mechanical Engineering, UC Santa Barbara.
Work performed at UCSB Nanofabrication Facility.*

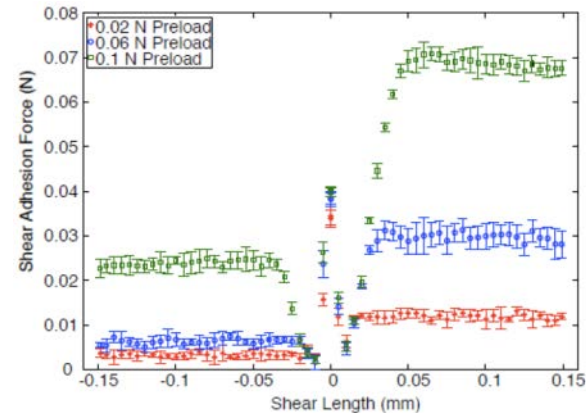
Langmuir, 28, 8746–8752 (2012).

Funded by: Institute for Collaborative Biotechnologies, through ARO

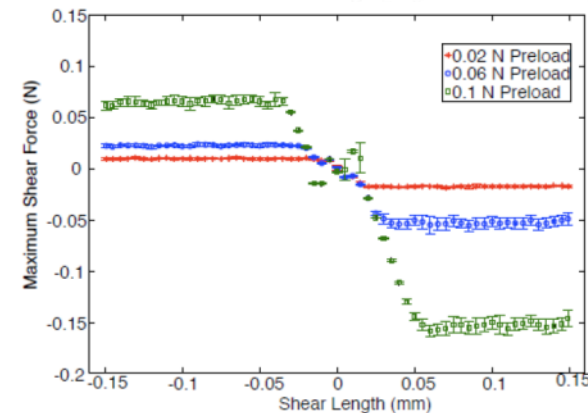
NNIN is supported by NSF ECCS-0335765



SEM image of vertical half-cylinder PDMS microfibers of 19.0 μm height and 10.0 μm diameter



Anisotropic shear adhesion forces generated as functions of the preload and shear length

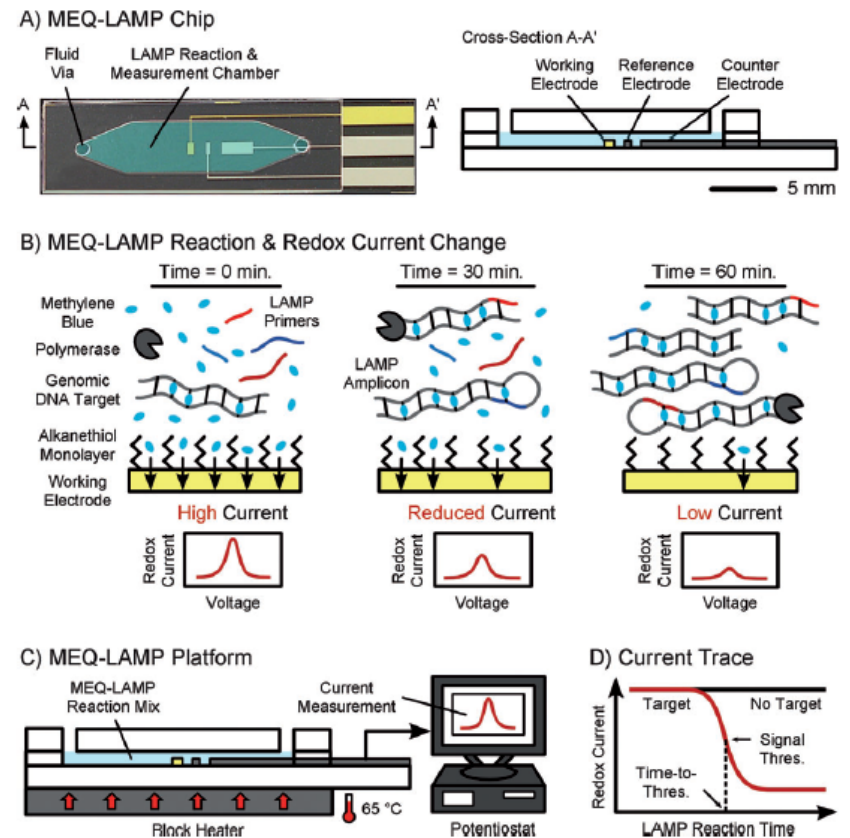


Anisotropic shear (friction) forces generated as functions of the preload and shear length

Rapid, Sensitive, and Quantitative Detection of Pathogenic DNA through Microfluidic Electrochemical Quantitative Loop-Mediated Isothermal Amplification

Genetic detection of pathogens at the point of care (POC) has become increasingly important in applications ranging from molecular diagnostics and food safety testing to environmental monitoring and homeland security. To this end, we have developed the microfluidic electrochemical quantitative loop-mediated isothermal amplification (MEQ-LAMP) system—an integrated microfluidic platform for the rapid, sensitive, and quantitative detection of pathogenic DNA, offering a powerful alternative to PCR in terms of sensitivity, reaction speed, and amplicon yield, and can be applied to non-denatured genomic DNA samples under isothermal reaction conditions. This amplification technique also employs six different primers, conferring exquisite specificity and enabling MEQ-LAMP to readily distinguish pathogens of interest from non-target genomic DNA. As a demonstration of the platform effectiveness, we report the direct and quantitative detection of as few as 16 copies of genomic DNA of *Salmonella enterica enterica* Typhimurium—a pathogen that causes food poisoning—in less than an hour.

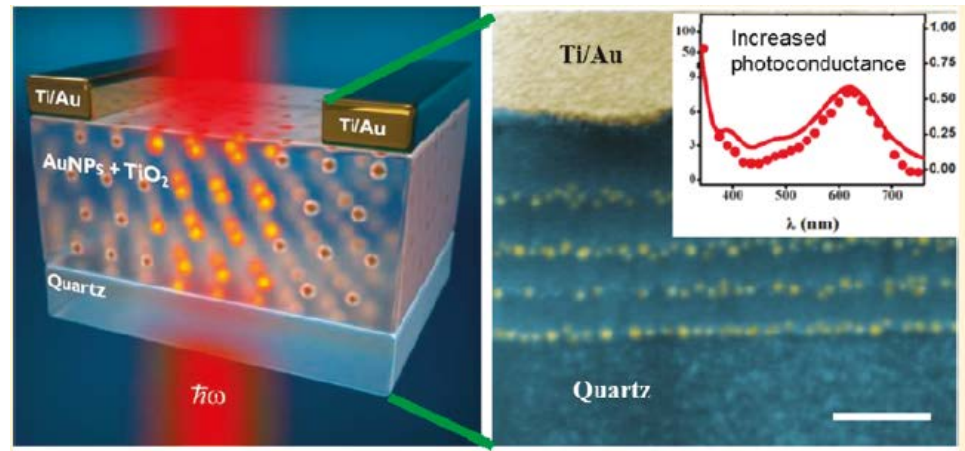
K. Hsieh, et. al., Plaxco and Soh groups, UCSB.
Work partially performed at UCSB Nanofabrication Facility.



Overview of the MEQ-LAMP. A) Reaction performed within a single-chamber microfluidic chip, which functions as both the LAMP reaction well and the electrochemical measurement cell. B) The MEQ-LAMP reaction solution contains an electrochemically active DNA-binding compound methylene blue. Prior to amplification, MB is free in solution and thus generates a redox current (left). As the LAMP reaction progresses, MB intercalates into the newly formed, double-stranded product (middle), decreasing the observed redox current (right). C) In the complete MEQ-LAMP system, the microfluidic chip is connected to a potentiostat for current measurement. D) Real-time redox current measurements produce a current trace as a function of the reaction time.

Gold nanoparticles convert TiO_2 into a panchromatic photoconductor

Devices fabricated by embedding Au nanoparticles in TiO_2 show significant additional photoconductances ($\sim 30\%$) when illuminated by light with photon energies well below the band gap. The photoconductance is found to track the plasmonic absorption/extinction spectrum of the AuNPs faithfully. This impressive change in photoconductance is ascribed both to quantum tunneling of hot electrons from the metal directly into the conduction band of the TiO_2 for those electrons with energies lower than the 0.9 eV needed to overcome the barrier and to energetic electrons going over the barrier transport. All of these electrons originate as electron-hole pairs in the gold NPs produced by plasmonic excitation and decay. Device impedance measurements carried out in the dark and under illumination with UV and red wavelengths reinforce this mechanism.



Left: Schematic of a solid TiO_2 film containing several layers of non-percolating Au nanoparticles. **Right:** When illuminated with visible light, the conductance of the AuNP/ TiO_2 film faithfully tracks the surface plasmon resonance spectrum of AuNPs.

Syed Mubeen, Gerardo Hernandez-Sosa, Daniel Moses, Joun Lee, and Martin Moskovits, UC Santa Barbara

Work performed at The UC Santa Barbara Nanofabrication Facility

Nano Lett., **11**, 5548–5552, (2011)

Frequency dispersion in III-V metal-oxide-semiconductor capacitors

Extensive research activities have focused on developing dielectrics, such as Al_2O_3 and on $\text{In}_{0.53}\text{Ga}_{0.47}\text{As}$ for metal-oxide-semiconductor field effect transistors (MOSFETs). One of the most important unresolved issues remains the lack of understanding of the large frequency dispersion that is observed in accumulation, for dielectrics on n- $\text{In}_{0.53}\text{Ga}_{0.47}\text{As}$. This dispersion is particularly severe for more highly scaled, high-capacitance-density metal-oxide-semiconductor capacitor (MOSCAP) structures, such as the one shown in Fig. 1.

In this work, we propose a recombination-controlled tunneling model to explain the strong frequency dispersion (Fig. 2). In this model, the parallel conductance is large when, at positive gate biases, the metal Fermi level lines up with a large density of interface states in the semiconductor band gap. We show that the model explains in a semi-quantitative manner the experimentally observed capacitor characteristics.

Susanne Stemmer (UCSB), Varistha Chobpattana (UCSB), and Siddharth Rajan (OSU)
Work performed at UCSB Nanofabrication Facility

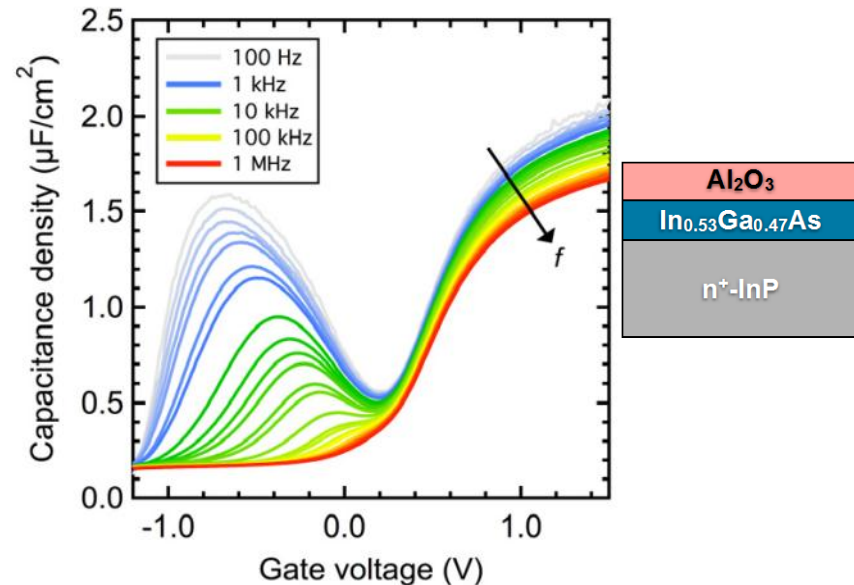


Fig. 1: Capacitance voltage characteristics of a MOSCAP with a 3 nm Al_2O_3 dielectric fabricated in UCSB's NanoFab. The Al_2O_3 was deposited with a new ALD tool.

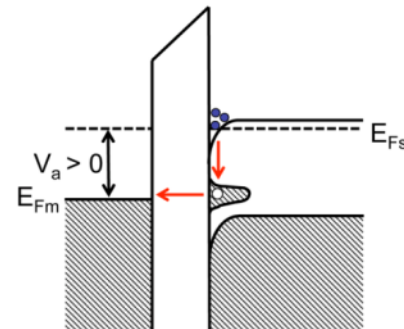


Fig. 2: Recombination controlled tunneling mechanism for communication between the gate metal and the interface states.

Spin Wave Modes In Ferromagnetic Tubes

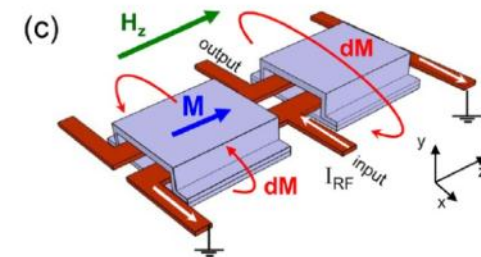
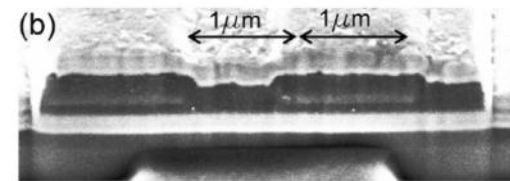
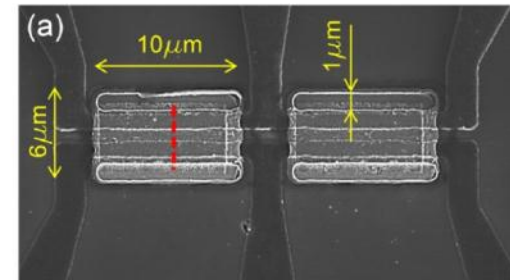
Coplanar waveguides coupled by microstructured, ferromagnetic, $\text{Co}_{90}\text{Ta}_5\text{Zr}_5$ tubes that support resonant magnetostatic waves have been fabricated and tested. These structures are potentially important for on-chip tunable filters.

Periodic boundary conditions dictated by the tube perimeter and applied to magnetostatic surface waves quantitatively account for the experimentally observed frequencies of excited modes, despite the contorted tubular shape. The tubular topology appears to be more important than the shape details.

Kozhanov, M. Popov, Zavislyak, D. Ouellette, W. Lee, S. X. Wang, M. Rodwell, and S. J. Allen – UCSB

Taras Shevchenko - National University of Kyiv, Ukraine, Stanford University

Work performed at UCSB



The shorted ends of two coplanar waveguides are coupled by a ferromagnetic “tube.” Top view SEM (a) and SEM micrograph of structure cross section (b). Schematic of fabricated structure (c).

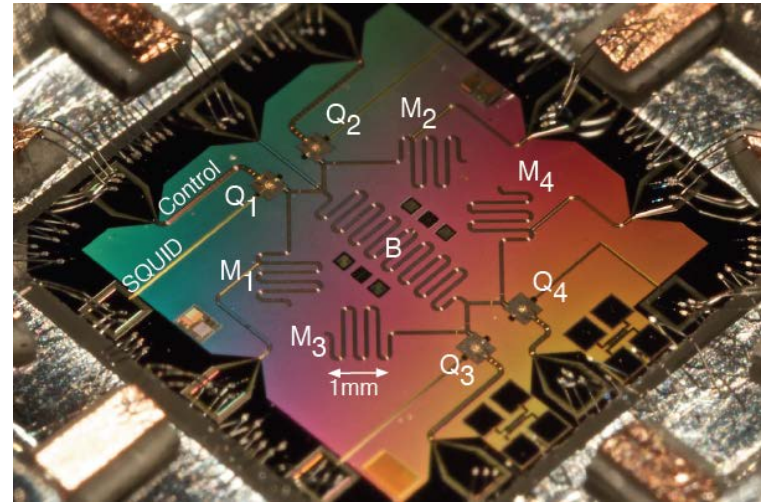
Computing Prime Factors With A Josephson Phase Qubit Quantum Processor

A quantum processor (QuP) can be used to exploit quantum mechanics to find the prime factors of composite numbers. Two advantages of superconducting qubit architectures are the use of conventional microfabrication techniques, which allow straightforward scaling to large numbers of qubits, and a toolkit of circuit elements that can be used to engineer a variety of qubit types and interactions. Here we demonstrate a nine-quantum-element solid-state QuP. To demonstrate this we run a three-qubit compiled version of Shor's algorithm to factor the number 15, and successfully find the prime factors 48% of the time. Improvements in the superconducting qubit coherence times and more complex circuits should provide the resources necessary to factor larger composite numbers and run more intricate quantum algorithms.

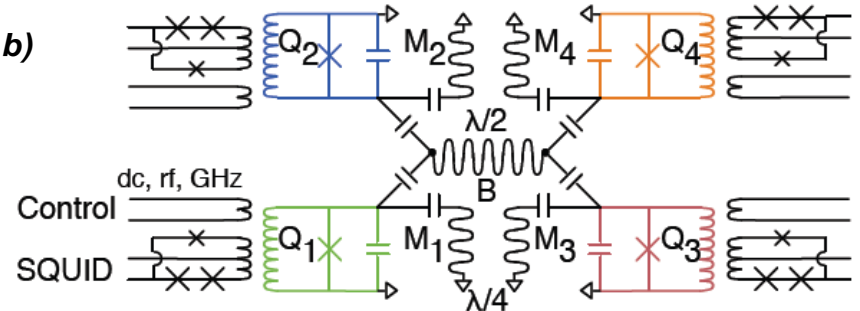
Erik Lucero et. al. Martinis, Cleland Groups, UCSB
Physics Department
Work performed at UCSB Nanofabrication Facility

Funded by IARPA through ARO

a)



b)

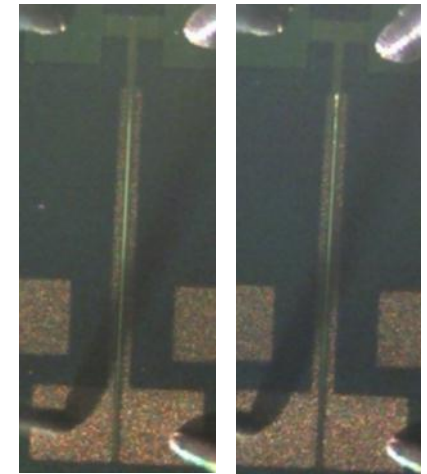
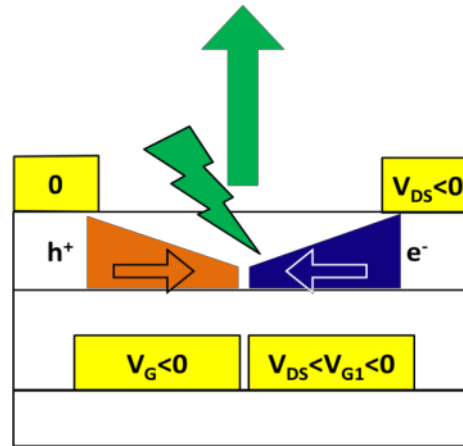


a, Photomicrograph of the sample, fabricated with aluminum (colored) on sapphire substrate (dark). **b**, Schematic of the QuP. Each phase qubit Q_i is capacitively coupled to the central half-wavelength bus resonator B and a quarter-wavelength memory resonator M_i . The control lines carry GHz microwave pulses to produce single qubit operations. Each Q_i is coupled to a superconducting quantum interference device (SQUID) for single-shot readout.

Split-gate Light Emitting Field Effect Transistors

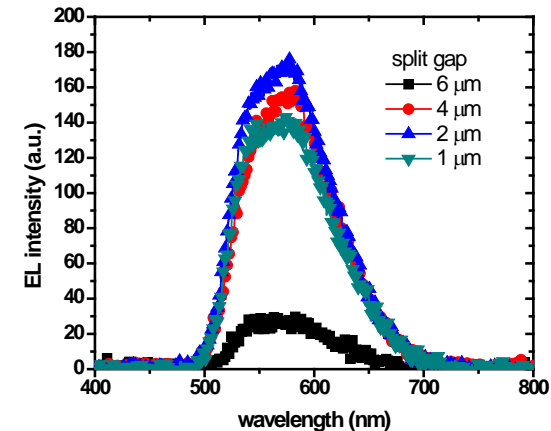
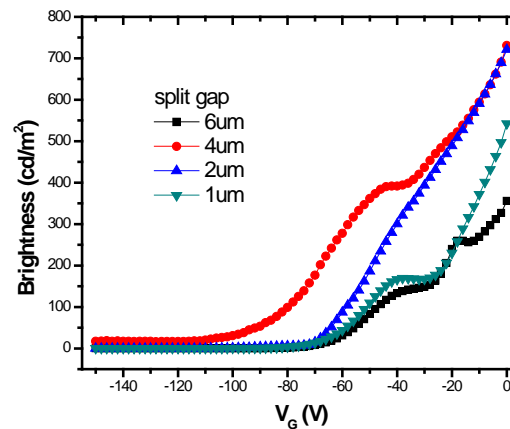
SG-LEFETs provide a powerful pathway to actively control charge injection to enable high efficiency electroluminescence. The split gate architecture can overcome the passive response of an ambipolar material to a continuous distribution of the gate voltage. Thus, transport can be independently chosen as either n type, p type, or both. By breaking the continuous channel, the brightest luminescent area was positioned far from the metal source-drain contacts. With the SG, field-induced carriers over the first gate can efficiently capture oppositely charged field-induced carriers over the second gate. The most important aspect of the SG architecture is that geometric design dramatically shifts the highest efficiency from the lowest current regime with very low brightness to the regime with maximum injection current, hence largest brightness

Ben, Bang-Yu Hsu and Alan, J. Heeger, UCSB
 Work partially performed at UCSB
 Nanofabrication Facility



2 um gap 4 um gap

Device schematic and picture



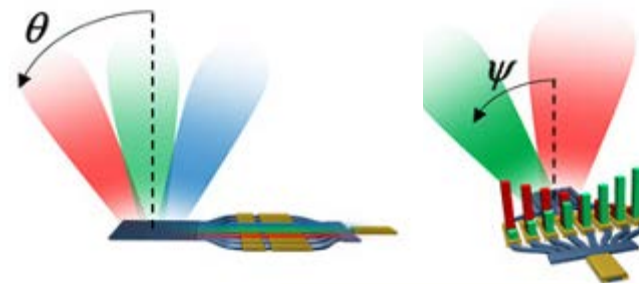
Brightness and electroluminescence spectra of the split-gate LEFETs

SWEEPER – 2D Free-space Beam Steering Chip

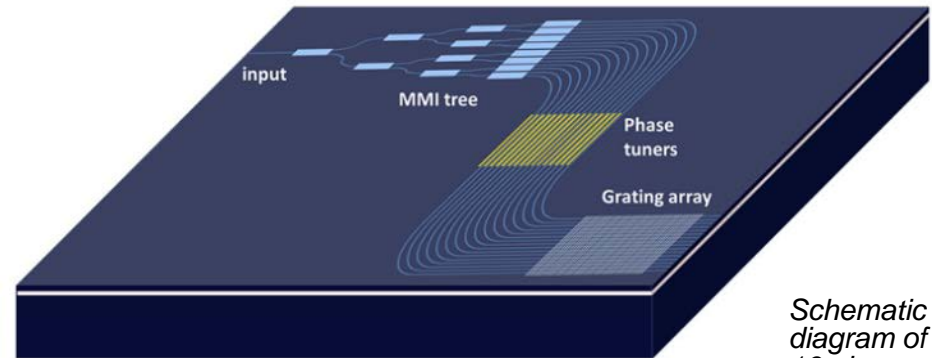
In the SWEEPER project we have realized 2-dimensional free space beam steering by means of an integrated silicon-on-insulator (SOI) chip. Beam steering in the longitudinal direction is achieved by vertical grating couplers: changing the wavelength of the light will change the output angle. In the lateral direction beam steering is achieved by controlling the phase of the output of an array of these grating couplers: an optical phased array.

We have demonstrated a 16-channel SOI device with thermo-optic phase tuners. The beam has a width of $0.6^\circ \times 1.6^\circ$ and can be steered over $20^\circ \times 14^\circ$. We also realized an 8-channel hybrid silicon 1D beam steering device with integrated single-wavelength source and on-chip optical amplification.

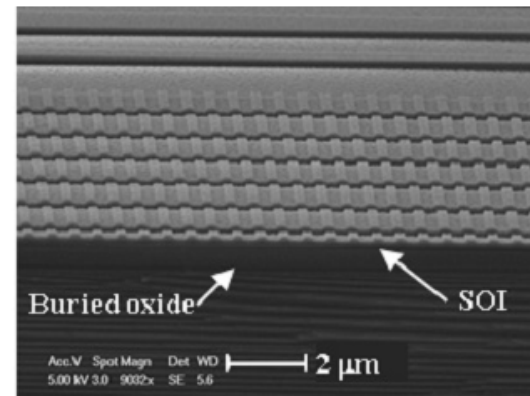
J.K. Doylend, et. al. Coldren and Bowers groups, UCSB
Work partially performed at UCSB Nanofabrication Facility



Longitudinal beam steering θ by wavelength tuning;
Lateral beam steering ψ by tuning of array of phase modulators.



Schematic diagram of the 16-channel grating array



Scanning electron microscope image of the grating array cross-section

Optics Express , **19** (22), 21595 (2011)

DARPA Sweeper program

NNIN is supported by NSF ECCS-0335765

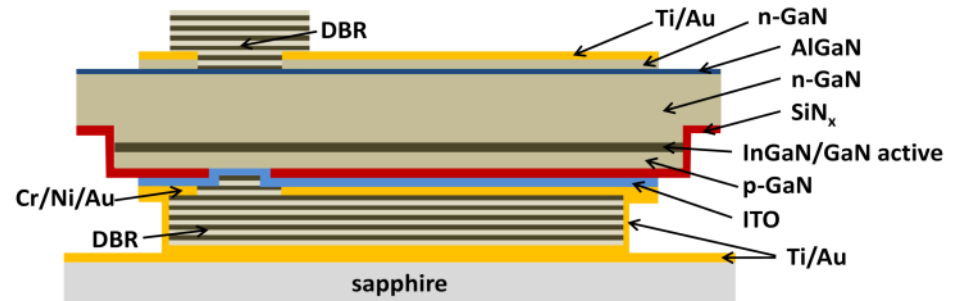
Nonpolar GaN VCSEL: First Demonstration

We have demonstrated the first-known nonpolar m-plane GaN-based VCSEL, achieving room-temperature electrically-injected lasing at $\sim 412\text{nm}$. Nonpolar GaN has the potential to significantly increase GaN VCSEL performance over polar devices, including higher gain leading to lower threshold currents and higher efficiency devices.

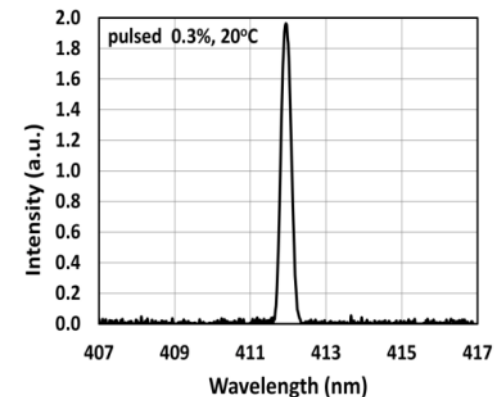
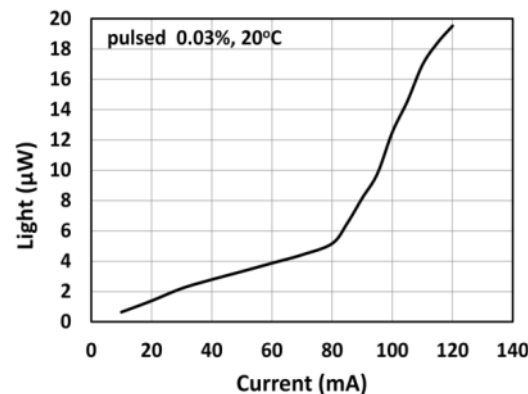
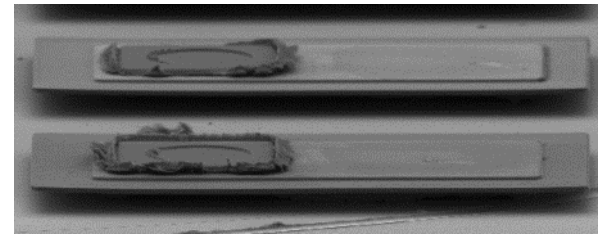
Additionally, nonpolar GaN VCSELs exhibit the unique feature of polarization locking, whereby all the devices are polarized in the same direction, with the electric field aligned along the a-direction of the GaN wurtzite crystal structure.

We also demonstrate a novel method for VCSEL fabrication, where the bulk GaN substrate is removed and the cavity length is defined by photoelectrochemical (PEC) etching, giving precise control of cavity length.

Casey Holder, Daniel Feezell, James S. Speck, Steven P. DenBaars, Shuji Nakamura, UCSB
Work partially performed at UCSB Nanofabrication Facility



Device schematic and SEM pictures

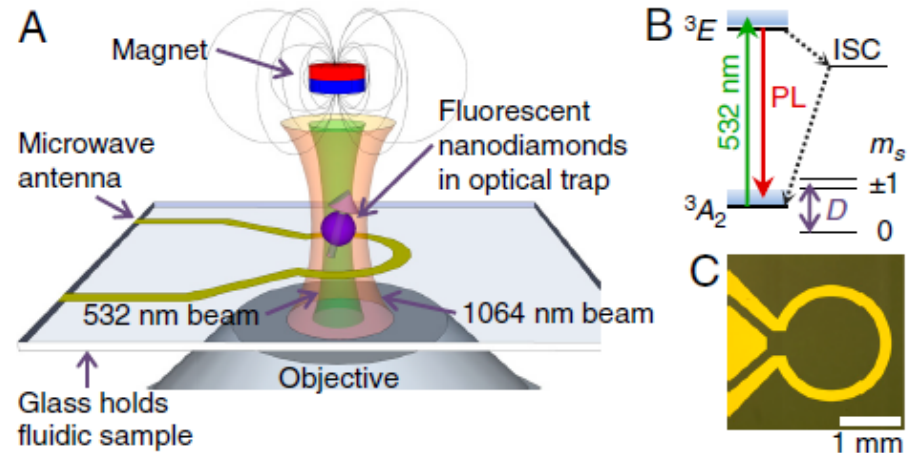


Light-Current curve and lasing spectra at room temperature pulsed operation.

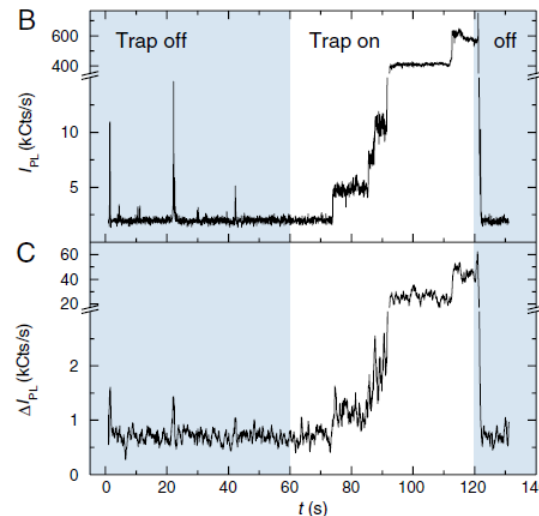
Electron Spin Resonance Of Nitrogen-vacancy Centers In Optically Trapped Nanodiamonds

Using an optical tweezers apparatus, we demonstrate three-dimensional control of nanodiamonds in solution with simultaneous readout of ground-state electron-spin resonance (ESR) transitions in an ensemble of diamond nitrogen vacancy color centers. Despite the motion and random orientation of nitrogen-vacancy centers suspended in the optical trap, we observe distinct peaks in the measured ESR spectra qualitatively similar to the same measurement in bulk. Accounting for the random dynamics, we model the ESR spectra observed in an externally applied magnetic field to enable dc magnetometry in solution. We estimate the dc magnetic field sensitivity based on variations in ESR line shapes to be approximately $50 \mu\text{T}/(\text{Hz})^{1/2}$. This technique may provide a pathway for spin-based magnetic, electric, and thermal sensing in fluidic environments and biophysical systems inaccessible to existing scanning probe techniques.

V. Horowitz, et.al. Awschalom Group, UCSB
 Work partially performed at UCSB Nanofabrication Facility



(A) Schematic of experimental setup. (B) Energy level diagram of the diamond NV center. (C) Micrograph of the 50- Ω -impedance-matched antenna that drives coherent transitions between spin states.



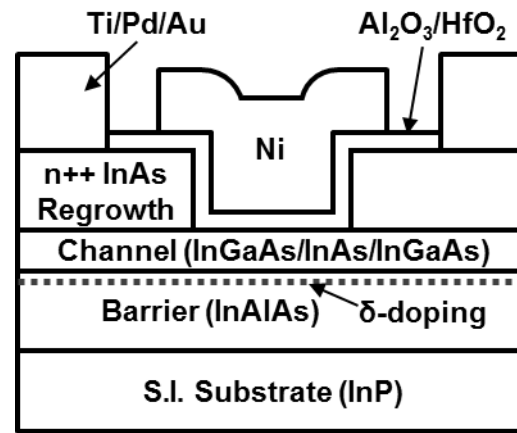
Measured IPL and contrast ΔIPL before and after turning on the trapping beam. As the trapping beam remains on, fluorescent nanodiamonds stochastically enter the trap and cause IPL to increase in discrete steps, with coincident rises in ΔIPL indicating the presence of NV centers.

III-V MOS Transistors

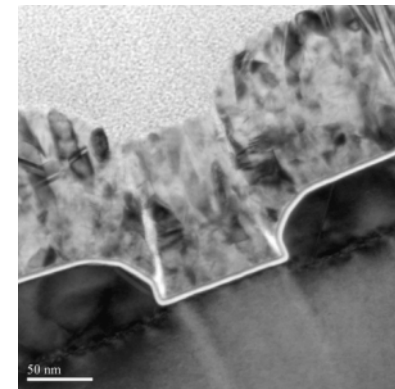
III-V compound semiconductor channel materials are being investigated for use in VLSI ICs at scaling generations at and beyond 9 nm. III-V channel materials offer the potential for significantly increased drive currents due to lower transport effective mass. The main goal of this project is to demonstrate that highly scaled III-V MOSFETs can provide greater drive current than comparable Si devices. Efforts in this project have focused on demonstration of a 22 nm device using process modules which could, with appropriate industrial development, be scaled to 9 nm.

Recently, we have demonstrated a high performance III-V MOSFET using substitutional-gate and MBE source drain regrowth, which shows 1.0 mS/ μm peak transconductance at $V_{ds} = 0.5$ V and 0.8 mA/ μm on-current at $V_{gs} - V_{th} = 0.8$ V and $V_{ds} = 0.5$ V

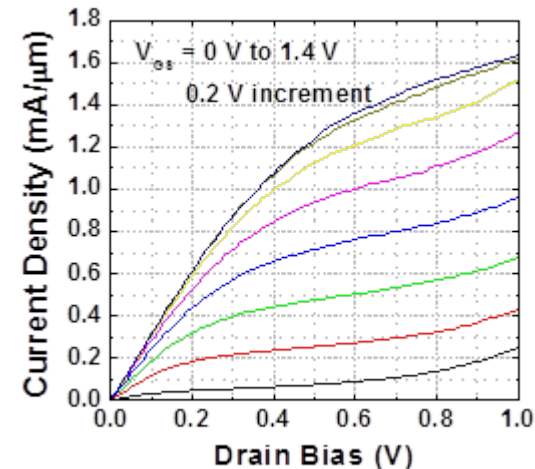
S. Lee, A. Carter, J. Law, et. al. Rodwell Group, UCSB
Work performed at UCSB Nanofabrication Facility



Schematic cross-section of III-V MOSFETs using substitutional gate and source-drain regrowth techniques.



Cross-sectional TEM image for a substitutional gate III-V MOSFET

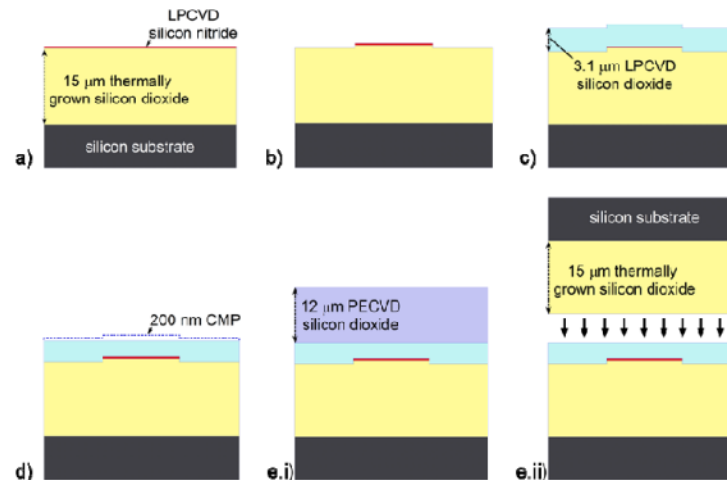


Output characteristic ($I_{ds} - V_{ds}$) for a device with 50 nm gate length

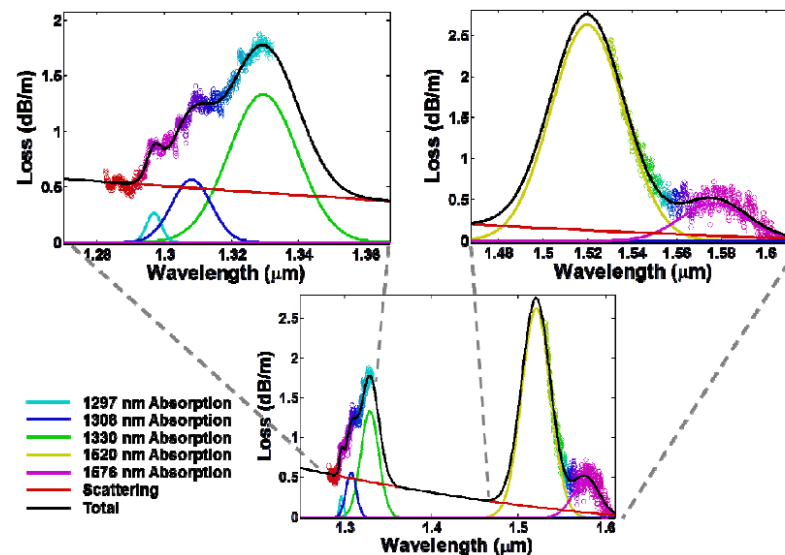
Planar Waveguides With Less Than 0.1 Db/M Propagation Loss Fabricated With Wafer Bonding

Planar waveguides with ultra-low propagation loss are necessary for the long propagation distances and high quality factor resonators used in photonic rotational velocity sensors, true-time-delay networks, optical buffers, and narrowband photonic filters. The history of optical fiber loss reduction suggests that a large modal overlap with undoped silica is a path to ultra-low propagation loss. In this work, we demonstrate a wafer-bonded silica-on-silicon planar waveguide platform with record low total propagation loss of 0.045 ± 0.04 dB/m near the free space wavelength of 1580 nm. Using coherent optical frequency domain reflectometry, we characterize the group index, fiber-to chip coupling loss, critical bend radius, and propagation loss of these waveguides.

J. Bauters, et.al. Bowers/Blumenthal, UCSB
 Work partially performed at UCSB
 Nanofabrication Facility



A schematic overview of the processes used to fabricate the waveguides discussed in this paper. e.i and e.ii illustrate the two upper cladding approaches

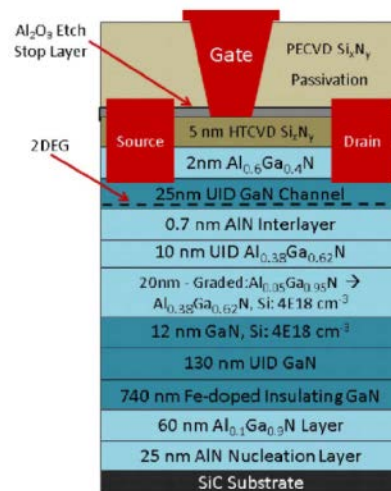


Total propagation loss (circles) vs. wavelength for a 50-nm-thick by 6.5-μm-wide waveguide with PECVD oxide upper cladding. The solid lines are fits of Gaussians (absorption loss) and a polynomial (scattering loss) to the data. The color key gives the loss type colors and the center wavelengths of the various Gaussian fits.

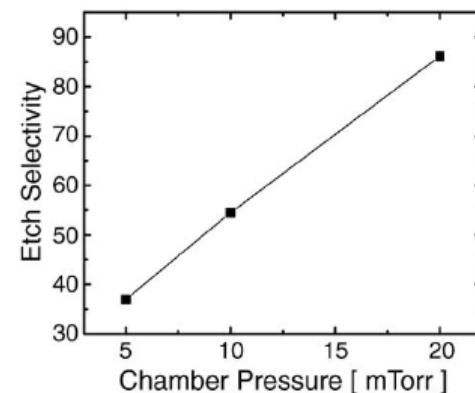
Record Microwave Power Performance for N-Polar GaN MISHEMTs Grown by MOCVD on SiC

In this work, we demonstrate record RF power performance of N-polar AlGaN/GaN metal–insulator–semiconductor high-electron-mobility transistors (MISHEMTs) grown by metal–organic chemical vapor deposition (MOCVD) on semi-insulating SiC substrates at 10 and 4 GHz. Additionally, an Al₂O₃-based etch-stop technology was demonstrated for improving the manufacturability of N-polar GaN HEMTs with Si₃N₄ passivation. The reported output power densities of 16.7 W/mm at 10 GHz and 20.7 W/mm at 4 GHz represent the highest reported values so far for an N-polar device, at both of these frequencies. The improvements achieved in the RF output power density when compared with previously reported N-polar MISHEMTs can be attributed to high breakdown voltage of N-polar devices grown by MOCVD and high thermal conductivity of the SiC substrate.

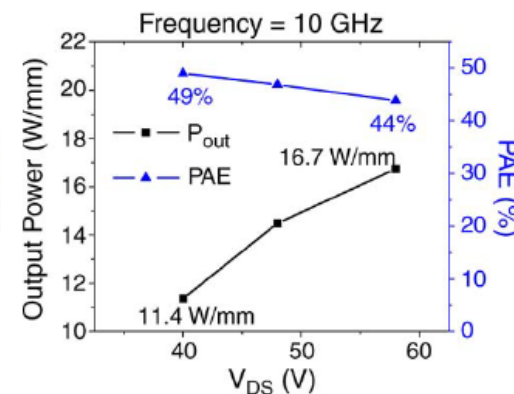
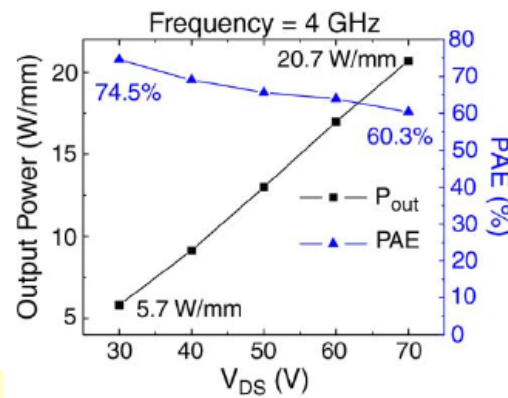
S. Kolluri, et. al. Mishra Group, UCSB
Work performed at UCSB Nanofabrication Facility



Schematic cross-section of N-polar GaN MISHEMT with Al₂O₃ stop etch layer.



Etch selectivity of Si_xN_y to Al₂O₃ using CF₄/O₂ RIE.



Output power and Power Added Efficiency (PAE) at 4GHz and 10GHz.

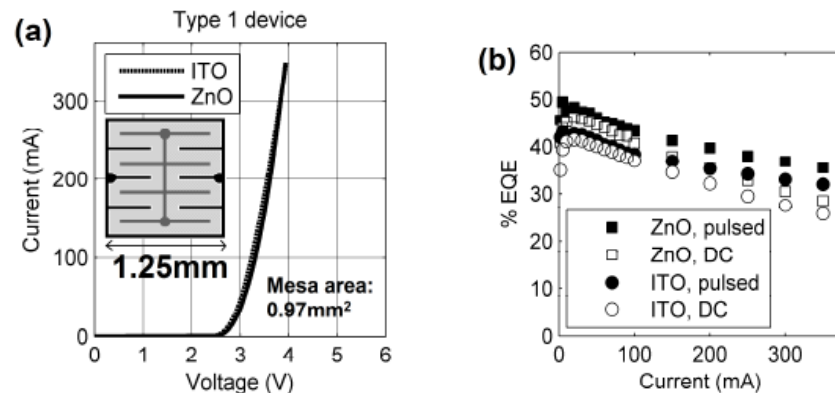
High Efficiency White Leds With 90 C Deposited Single-crystal ZnO Current Spreading Layers

Highly efficient white light-emitting diodes (LEDs) can reduce energy use in interior, automobile, and display lighting. A common approach to efficiently generate white light is to couple a yellow-emitting phosphor with a high-brightness blue gallium nitride (GaN) based LED. The ultimate performance depends on converting electrical energy to photons, and on extracting those photons to the phosphor, and out of the LED package. To efficiently accomplish this, current should be injected uniformly into the active layer of the GaN LED substrate while maintaining optical transparency. Heteroepitaxial ZnO transparent current spreading layers were deposited on GaN-based light emitting diodes using aqueous solution phase epitaxy at temperatures below 90 C. White LEDs with ZnO layers provided high luminous efficacy—157 lm/W at 0.5A/cm², and 84.8 lm/W at 35A/cm², 24% and 50% higher, respectively, than devices with ITO layers. The improvement appears to be due to the enhanced current spreading and low optical absorption provided by the ZnO.

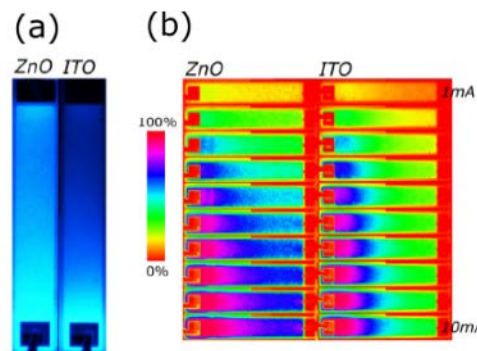
A. Reading, et. al.

DenBaars/Nakamura Groups, UCSB

Work performed at UCSB Nanofabrication Facility



IV and External Quantum Efficiency for Blue LEDs fabricated with ZnO and ITO transparent current spreading layers



(a) Illuminated LED strips operating under 100mA current injection. (b) Color contrast intensity images (rotated) showing current spreading in 1mA increments.

Current Density	ZnO CSL			ITO CSL		
	Luminous Efficacy (lm/W)	Color temperature (K)	CRI	Luminous Efficacy (lm/W)	Color temperature (K)	CRI
0.5 A/cm ²	157	4496	65.4	126	4458	67.1
2 A/cm ²	142	4479	65.2	115	4466	66.0
10 A/cm ²	124	4466	65.4	93.0	4443	64.9
35 A/cm ²	84.8	4442	65.2	56.2	4437	65.2

Packaged white LED performance.

Opt. Express **20**, A13 (2012)

Yield Improvement Of Memristive Devices

L. Gao, F. Alibart, G. Adam, B. Hoskins, and D. B. Strukov

Resistive (“memristive”) switching, the reversible modulation of electronic conductivity in thin films under electrical stress, has been observed in a wide range of material systems. Research activity in this area has been traditionally fueled by the search for a perfect electronic memory candidate, but recently it opens doors to new applications in reconfigurable and neuromorphic computing. In our most recent works we designed a simple algorithm to tune the device resistance (Fig.1) and we also improved device yield by creating nanoscale electrode protrusions with e-beam lithography (Fig.2).

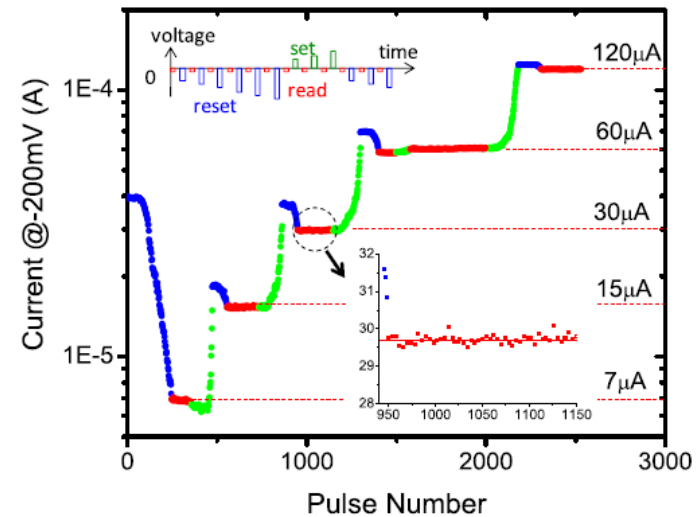


Fig. 1. Demonstration of the algorithm to tune the resistive state of the device to 7, 15, 30, 60 or 120 μA within an accuracy of 1% using the algorithm shown in the top inset.

L. Gao, F. Alibart, et. al. Strukov Group, UCSB
Work performed at UCSB Nanofabrication
Facility

[1] Strukov, D. et. al. H. MRS Bulletin, 2012, 37, 108.
[2] Alibart, F.; Gao, L.; Hoskins, B.; Strukov, D.B.
Nanotechnology 2012, 23, 075201.

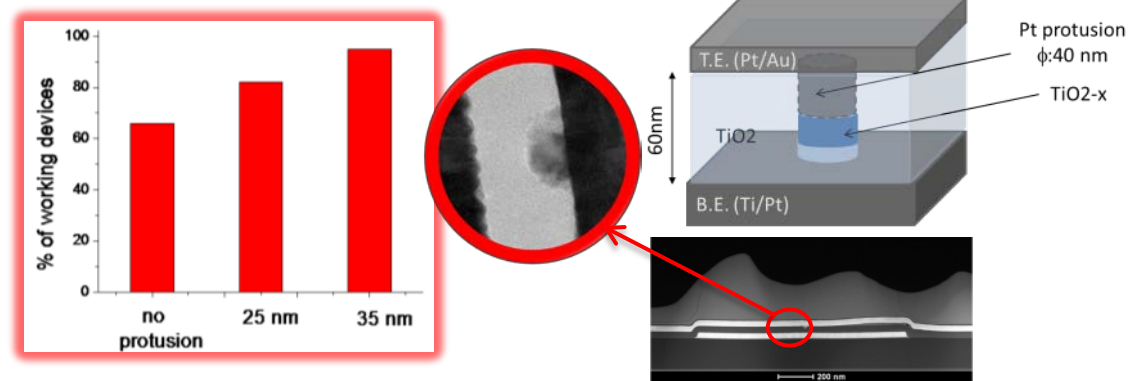


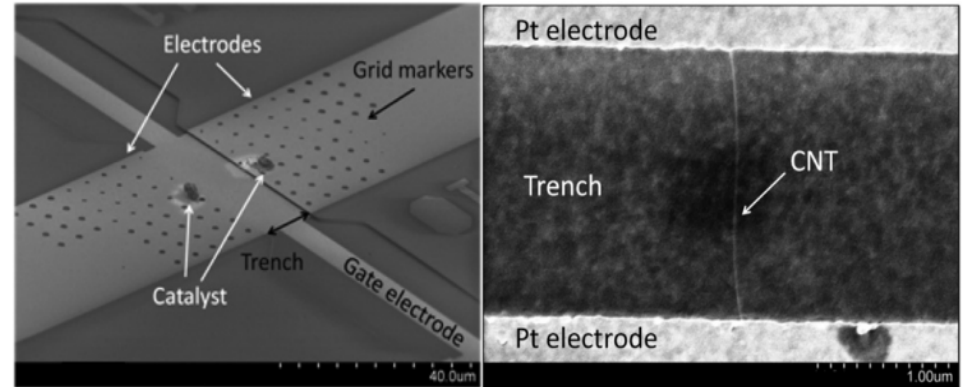
Fig. 2. (Left) Yield improvements from ~60% for the blanket film devices to about 95% for the devices with protrusion. (Right) Cross-view of protrusion device

NNIN is supported by NSF ECCS-0335765

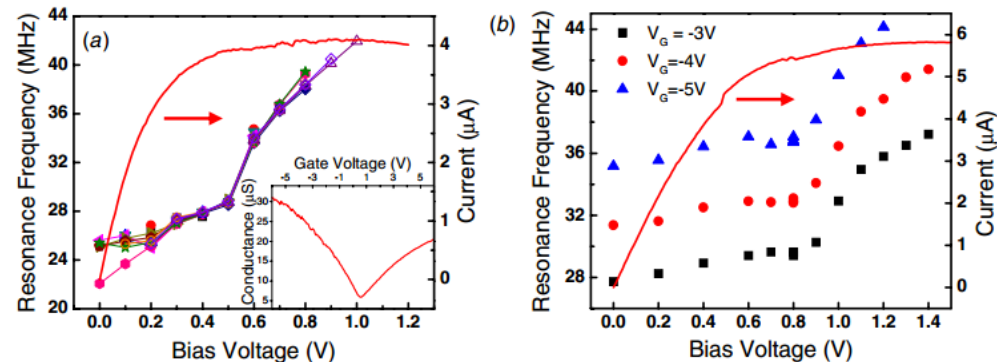
Electromechanical Resonance Behavior Of Suspended Single Walled Carbon Nanotubes Under High Bias Voltages

The fundamental electrical and electro-mechanical properties of carbon nanotubes (CNTs) continue to expose interesting underlying physics. In this work, we characterize the nanoelectromechanical response of suspended individual CNTs under high voltage biases. An abrupt upshift in the mechanical resonance frequency of approximately 3 MHz is observed at high bias. While several possible mechanisms are discussed, this upshift is attributed to the onset of optical phonon emission, which results in a sudden contraction of the nanotube due to its negative thermal expansion coefficient. This, in turn, causes an increase in the tension in the suspended CNT, which upshifts its mechanical resonance frequency. This upshift is consistent with Raman spectral measurements, which show a sudden downshift of the optical phonon modes at high bias voltages. Using a simple model for oscillations on a string, we estimate the effective change in the length of the nanotube to be $\Delta L/L \approx -2 \times 10^{-5}$ at a bias voltage of 1 V

M. Aykol, et. al. Cronin Group,
University of Southern California
Partial work performed at UCSB Nano Facility



SEM images of a suspended CNT sample device. The right panel shows a high resolution SEM image of an individual CNT

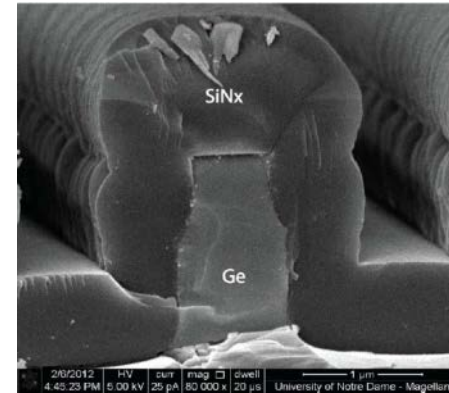


Bias voltage dependence of the mechanical resonance frequency of two different suspended CNTs. (a) Data taken on different days at a constant gate voltage of $V_G = -3$ V, demonstrating the repeatability of the observed effect. The inset in (a) shows the $I-V$ characteristics of this device, which exhibit metallic behavior. The red solid lines represent the $I-V$ bias and conductance- V gate characteristics of the device.

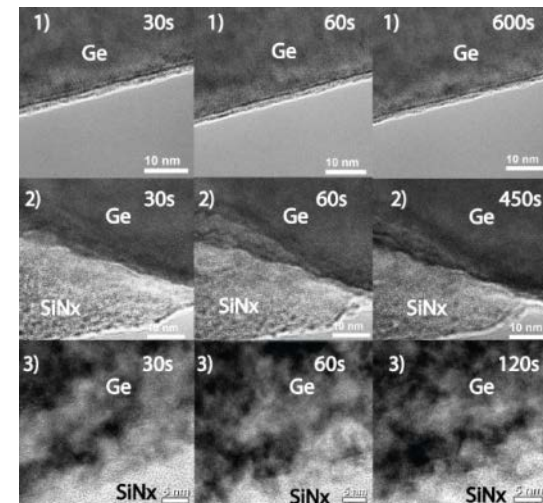
This research was supported in part by (ONR) Award No. N000141010511, (DOE) Award No. DE-FG02-07ER46376, and (NSF) Award No. CBET-0854118.

Stability of Tensile-strained Ge Studied by Transmission Electron Microscopy

Tensile-strained germanium has been studied recently as a possible laser material due to its nearly-direct bandgap and the compatibility with CMOS technology. Theoretically, 1.4% biaxial tensile strain could produce a direct bandgap in Ge. In this work, three-dimensional strain in Ge waveguides was introduced by SiNx stress liners, which are widely used for CMOS. Ge waveguides, with widths from 0.5 micron to 80 micron, were patterned and coated with thick strained SiNx with stress of 1 GPa or 2 GPa. By Raman spectroscopy we observed a Ge peak shift of up to 11 cm⁻¹. From this shift we expected direct bandgap emission. However, photoluminescence (PL) showed weak signals in highly strained waveguides and little wavelength shift in weakly strained waveguides. To study the strained Ge interface, we performed a time-dependent damage study under TEM irradiation on two 0.5 μm-width waveguides. We found that highly strained Ge interfaces were susceptible to damage under ebeam irradiation, and that dislocations propagated deep into the waveguide, suggesting possible limits to achievable strain and laser performance.



Ge waveguide buried in 2GPa compressive SiNx



Time dependent damage study of Ge/SiNx interface by HRTEM. 1) Relaxed strain. No obvious damage. 2) Weakly strained waveguide. Damage found within 2-3 nm from interface. 3) Highly strained waveguide, severe damage can be found propagating into deep area along with exposure time.

Meng Qi, et. al. Wistey Group, Notre Dame, EE Dept.
Work partially performed at UCSB Nanofab Facility

Silicon-Germanium Technology and Device Meeting
(ISTDM), 4-6 June 2012

NNIN is supported by NSF ECCS-0335765

Ultrafast Thermal Dynamics in ErAs:GaAs Photoconductive Switches

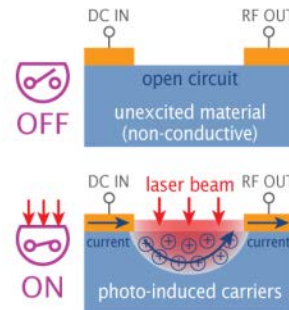
The goal of this work is to use photoconductive switches with an ErAs:GaAs active medium for the study of ultrafast heating dynamics. The dynamics are measured through thermal monitoring of the central electrode during transmission of RF electrical pulses with laser thermoreflectance.

Key results include observations of picosecond Joule heating [bottom left figure], tracking pulse propagation and attenuation of electrical pulses by probing different positions on the electrode [bottom right figure], and ultrafast thermal diffusion in the gold [not shown]

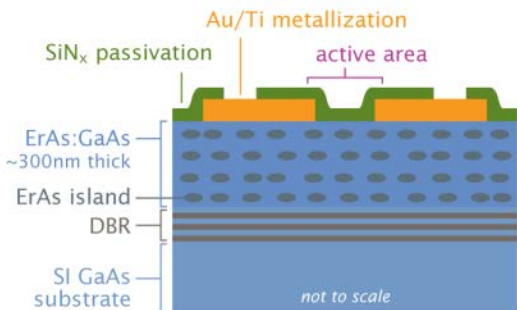
*B. Vermeersch, et. al. UC Santa Cruz
Work partially performed at UCSB
Nanofabrication Facility*

*XIV International Conference on Phonon Scattering
in Condensed Matter (PHONONS 2012), Ann Arbor,
Michigan USA, July 2012*

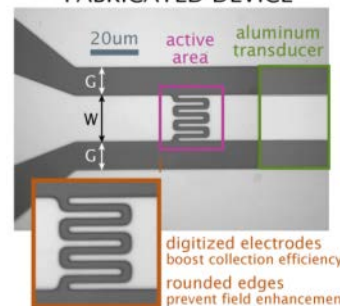
SCHMATIC PRINCIPLE



SAMPLE CROSS-SECTION STRUCTURE



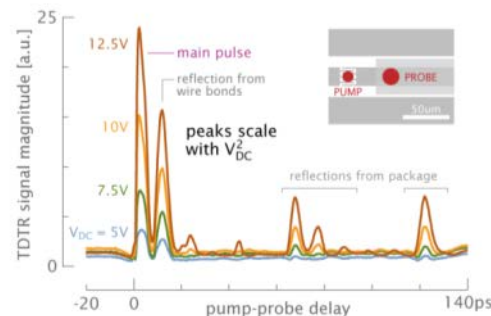
FABRICATED DEVICE



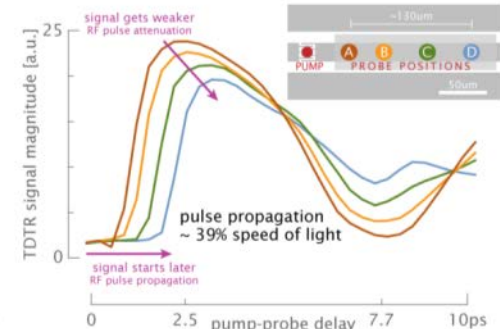
*Principle of operation and
device schematic for
photoconductive switches.
Measurements shown
below*

FEMTOSECOND LASER THERMOPREFLECTANCE MEASUREMENTS

Picosecond Joule heating in signal electrode

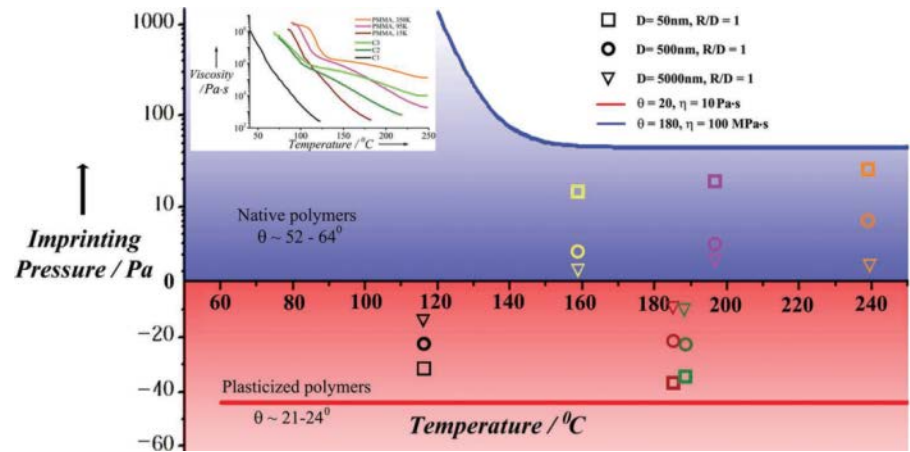


Propagation and attenuation of electric RF pulses

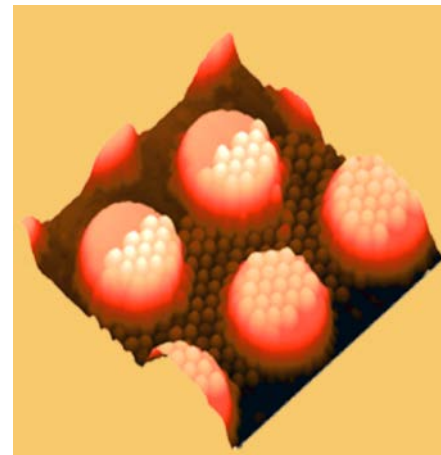


Nanoimprint by Melt Processing

A new technique called nanoimprinting by melt processing (NIMP) has been developed to print large area nanopatterns with varied feature sizes over underlying topographies with a high degree of fidelity. This will be highly beneficial to scientists working in a diverse field of science and technology for developing versatile nanostructures. The key development in this technique involves using plasticizer (diphenyl isophthalate) mixed with low molecular weight polymer (15,000 Mw PMMA) to enable improved polymer wettability for lower pressure imprinting at the melting temperature of the plasticized polymer.



Imprinting pressures and temperatures for Native polymers versus plasticized polymers. Temperature and pressure needed for complete filling is reduced at all Molecular weights



Simultaneous imprinting of micron-sized (large) features and nano-scale features using the NIMP technique.

J. Thomas, et. al. University of Central Florida
Work partially performed at UCSB Nanofabrication Facility

Adv. Mater. **23**, 4782 (2011)

Shrinking Atomic Force Microscope (AFM) Probes

The purpose of the project is to improve AFM performance by increasing the detection bandwidth and lowering the detection noise to allow higher imaging speeds and fidelity. Scaling down the size of the probe increases their mechanical resonance while reducing their thermal noise.

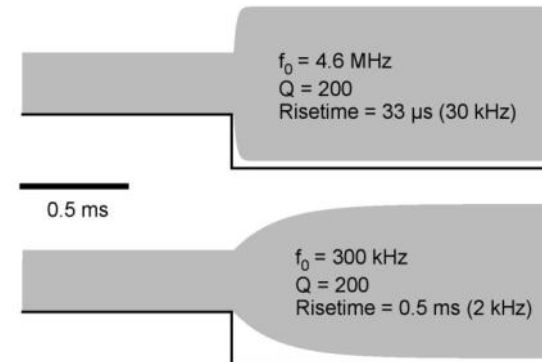
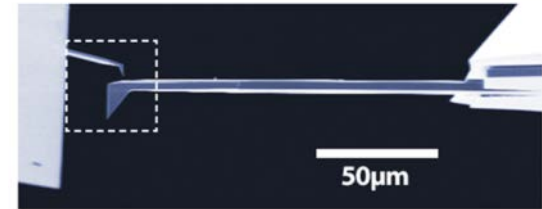
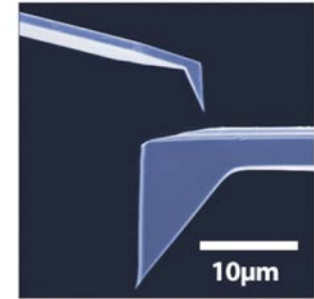
We have fabricated probes 10x smaller than the state-of-the-art. Like their predecessors, these novel probes have been fabricated on silicon wafers. However, entirely different processes are required because the novel probe geometries are smaller than the variations inherent with the previous probe fabrication techniques. Preliminary results indicate that the process is commercially viable.

The novel small probes consist entirely of silicon for a high and repeatable mechanical quality. Their spring constants are tunable for a variety of imaging modes and the tips are atomically sharp. They can be coated or doped with materials to accommodate most AFM applications.

Hector Cavazos, Asylum Research Corporation

Work performed at Stanford University and UC Santa Barbara Nanofabrication Facilities

Novel small probe landing on a commercially available probe.



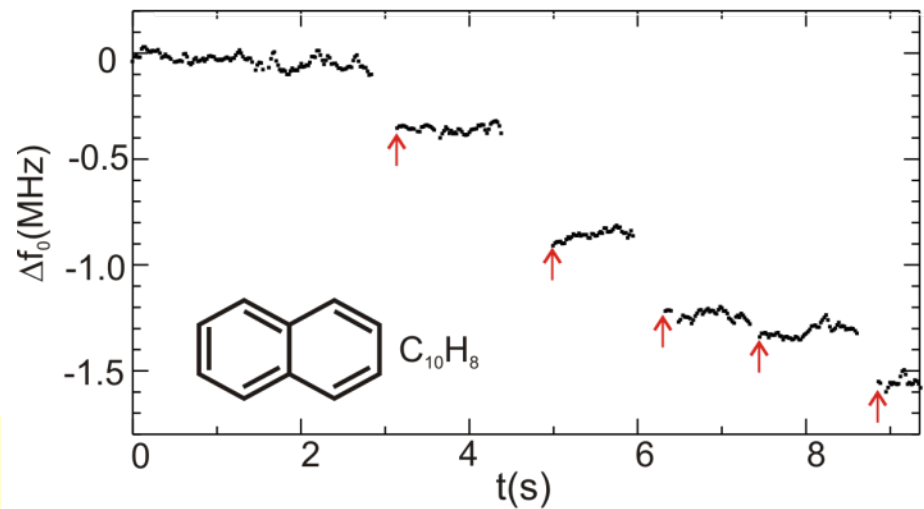
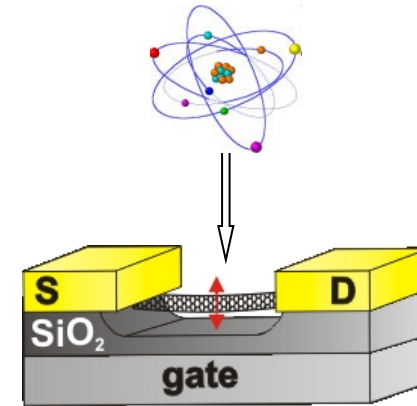
A faster reaction time of a novel short probe (top) VS standard probe (bottom) while scanning over a step in AC mode.

Mass sensing with a mechanical resonator

Nanomechanical resonators have been used to weigh cells, biomolecules and gas molecules, and to study basic phenomena in surface science, such as phase transitions and diffusion. These experiments all rely on the ability of nanomechanical mass sensors to resolve small masses. Here, we report mass sensing experiments with a resolution of 1.7 yg (1 yg = 10^{-24} g), which corresponds to the mass of one proton. The resonator is a carbon nanotube of length ~ 150 nm that vibrates at a frequency of almost 2 GHz. This unprecedented level of sensitivity allows us to detect adsorption events of naphthalene molecules ($C_{10}H_8$), and to measure the binding energy of a xenon atom on the nanotube surface. These ultrasensitive nanotube resonators could have applications in mass spectrometry, magnetometry and surface science.

Chaste, et. al. *Catalan Institute of Nanotechnology, CIN2(ICN-CSIC), Campus de la UAB, 08193 Bellaterra, Barcelona, Spain*

Work partially performed at UCSB nanofabrication facility



Δf_0 versus time at 4.3 K when naphthalene molecules are being dosed. Red arrows point to the shifts of the resonance frequency consistent with the adsorption of $C_{10}H_8$ molecules.

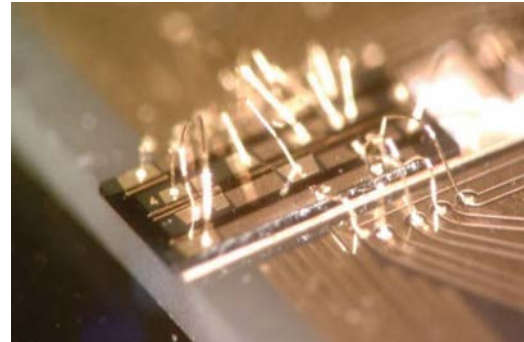
Widely Tunable Compact Monolithically Integrated Photonic Coherent Receiver

Coherent optical systems are of great interest for future fiber optic deployment, due to their high spectral efficiencies and the ability to mitigate signal degradation through available access to both optical phase and amplitude information. One of the main challenges in creating a compact monolithically integrated receiver is implementing a widely tunable, low noise, and high power local oscillator (LO).

In this work, a monolithically integrated, photonic, dual polarization capable coherent receiver, with an on-chip widely tunable local oscillator laser has been fabricated and tested. A 20-Gb/s operation with nonreturn-to-zero-quadrature phase-shift-keyed signal, and local oscillator tuning over 40 nm of input wavelength span has been demonstrated.

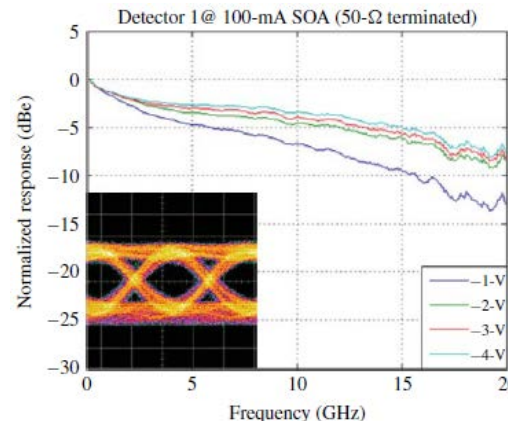
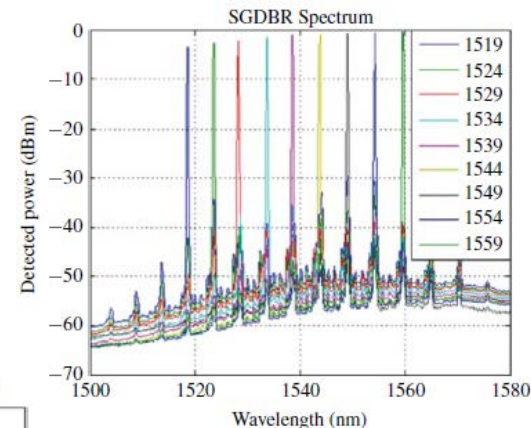
Steven B. Estrella, et. al. *Freedom Photonics*
Work partially performed at UC Santa Barbara
Nanofabrication Facility

IEEE Photonics Technology Letters, 24(5), 365 (2012)



Photograph of the widely tunable optical receiver integrated circuit mounted on an Aluminum-Nitride ceramic carrier.

Typical output wavelength spectra over the tuning range of the widely tunable laser obtained from test device



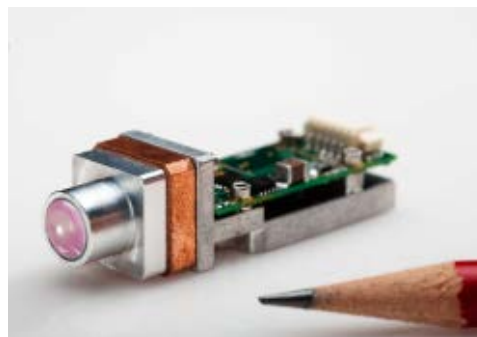
Measured frequency response of a single 50- μ m long detector, terminated into 50-. A detected eye diagram at 10-Gb/s NRZ is inset

Wide Area SWIR Arrays and Active Illuminators

SWIR imaging provides information that cannot be obtained in the visible or thermal IR regions. Due to its longer wavelength, compared to visible light, it can be used to see through haze. In addition, it provides additional contrast not available in the visible wavelengths. Furthermore, in contrast to other infrared bands (mid-wavelength infrared and longwavelength infrared), the SWIR band utilizes reflected light instead of emitted light and therefore looks more like imaging in the visible waveband.

For NIR/SWIR illumination at wavelengths in the 800 nm to 1100 nm range, FLIR has developed a 2W illuminator system. This illuminator is composed of a 1 mm 2x2 array mounted on a submount and soldered onto a copper heatsink and is designed to operate up to 70 C using passive cooling.

*Michael MacDougal, et. al. , FLIR EOC, LLC
Work partially performed at UCSB
Nanofabrication Facility*



2 W packaged SWIR Illuminator. (975 nm or 1064 nm).

SWIR night-time image without the use of illuminators. 30mS acquisition time

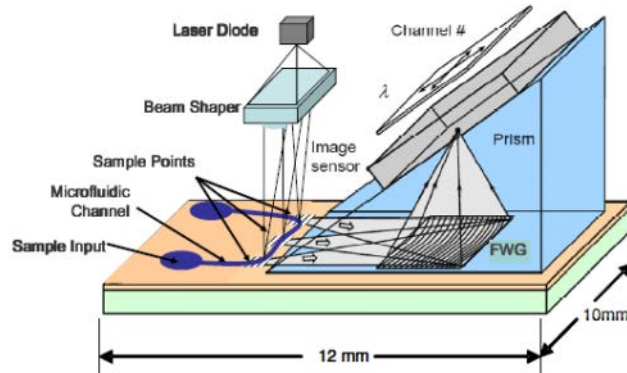


SWIR night-time image with the use of the 2W illuminators. 30mS acquisition time. Image clarity dramatically improved.

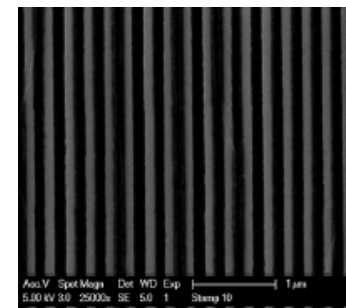
Compact, Low Cost Waveguide Based Optical Spectrometer for Detection of Chemical/Biological Agents

Conventional optical spectrometers that are based on bulk optical components tend to be relatively large and expensive compared to the other components used in systems designed for detecting chemical/biological agents. Microspectrometers based on focusing waveguide gratings incorporate both spectral dispersion and focusing functions into a single component that can be fabricated hundreds at a time at the wafer level using nano-imprint lithography techniques. These types of spectrometers are ideal for integration into micro-fluidic systems because the signals can be directly coupled into the planar waveguide. The ultimate goal of this project is to develop a waveguide grating based instrument platform capable of high resolution spectroscopic interrogation of multiple sample channels. We demonstrate preliminary data from a prototype system and compare resolving power and system size with commercial spectrometers.

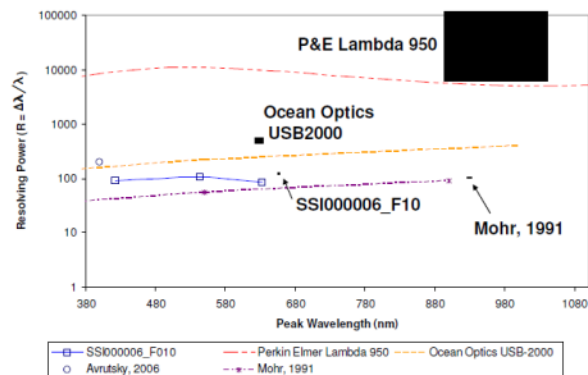
Compact Instrument platform based on a planar waveguide spectrometer. Light is focused onto the sample grid of a disposable chip. Optical signals from multiple samples are collected, dispersed, and focused onto an image sensor using a focusing waveguide grating.



FWGs nanoimprinted and etched into the waveguide material from e-beam lithography masters. One master to produce many copies for low cost production.



Brent Bergner, Ivan Avrutsky, et. al. , Spectrum Scientific Inc. and Wayne State University
Work partially performed at UCSB Nanofabrication Facility



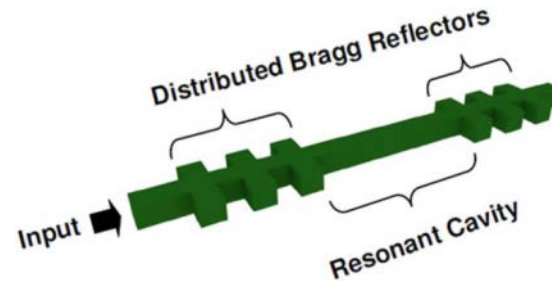
Comparison of resolving power and range of various spectrometers. The results of our devices are labeled as SSI000006_F10. The boxes represent the relative size of the instrument footprints.

Optical Bistability in a Silicon Waveguide Distributed Bragg Reflector Fabry–Pérot Resonator

Bistability occurs in devices that are composed of a material with nonlinear optical response. In the bistable regime, the output power of the device ceases to be uniquely determined by the input power because multiple powers within the cavity satisfy the resonance condition. Bistable devices are a versatile foundation for optical signal processing because they display both nonlinearity and hysteresis. This allows for the realization of photonic circuitry with functions including switching, memory, combinatorial and sequential logic, and modulation.

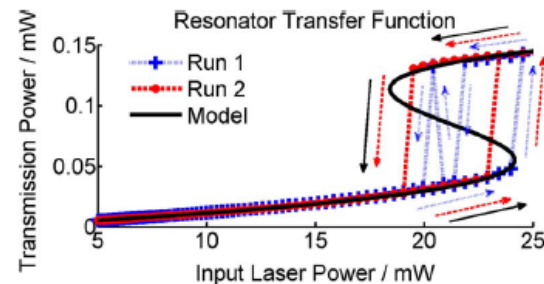
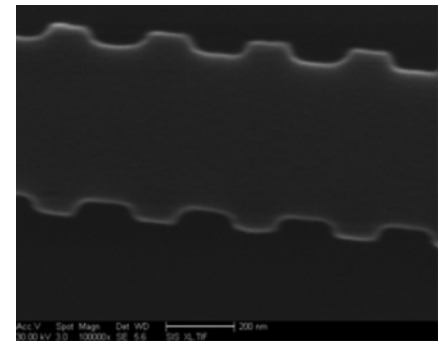
In this work we demonstrate optical bistability in a waveguide Fabry–Pérot resonator created from a pair of distributed Bragg reflectors within a strip waveguide. This design has the advantage of maintaining the small footprint and high packing density of a periodically structured dielectric waveguide, while taking advantage of the reduced power consumption featured in devices based on resonant cavities.

A. Grieco et al., *Fainman Group, UCSD*
Work partially performed at UCSB
Nanofabrication Facility



Top-down diagram of a Fabry–Pérot resonator created from a pair of distributed Bragg reflectors in a strip waveguide. Note that the diagram is for conceptual purposes and is not drawn to scale.

Scanning electron micrograph of an uncladded section of the SOI strip waveguide distributed Bragg reflector employed in this experiment. Note that the scale bar label is 200 nm.

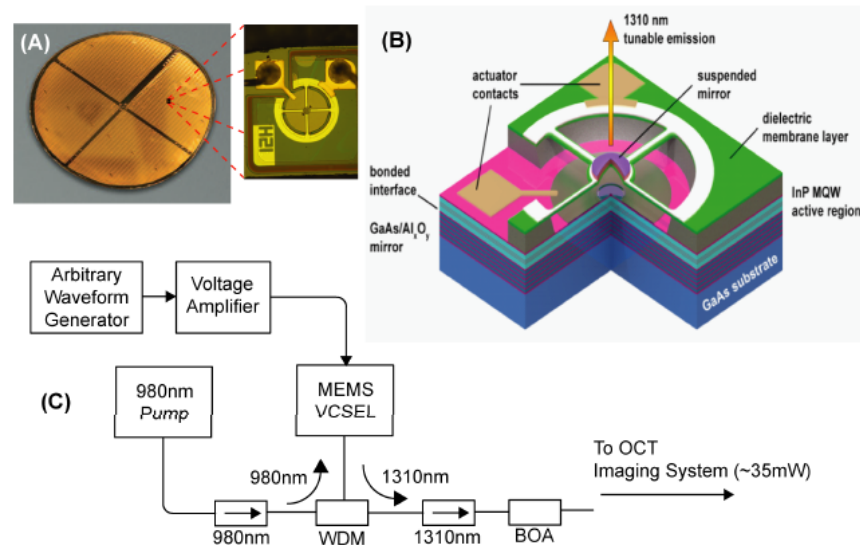


Measurements and theoretical response of the transfer function of the quasi-TE mode of the distributed Bragg reflector Fabry–Pérot resonator. Run 1 and Run 2 were made 8 min apart.

MEMS Tunable VCSEL Light Source For Ultrahigh Speed And Long Range Centimeter Class OCT Imaging

We demonstrate a new wavelength swept light source technology, MEMS tunable VCSELs, for OCT imaging. The VCSEL achieves a combination of ultrahigh sweep speeds, wide spectral tuning range, flexibility in sweep trajectory, and extremely long coherence length, which cannot be simultaneously achieved with other technologies. A prototype VCSEL is optically pumped at 980nm and a low mass electrostatically tunable mirror enables high speed wavelength tuning centered at ~1310nm with ~110nm of tunable bandwidth. Record coherence length >100mm enables extremely long imaging range. By changing the drive waveform, a single 1310nm VCSEL was driven to sweep at speeds from 100kHz to 1.2MHz axial scan rate with unidirectional and bidirectional high duty cycle sweeps. We demonstrate long range and high resolution 1310nm OCT imaging of the human anterior eye at 100kHz axial scan rate and imaging of biological samples at speeds of 60kHz – 1MHz.

Benjamin Potsaid, Vijaysekhar Jayaraman,
Praevium and Thor Labs
Work partially performed at UCSB
Nanofabrication Facility



(A) Wafer Scale Processing of VCSELs. (B) MEMS tunable VCSEL schematic. (C) OCT system diagram.

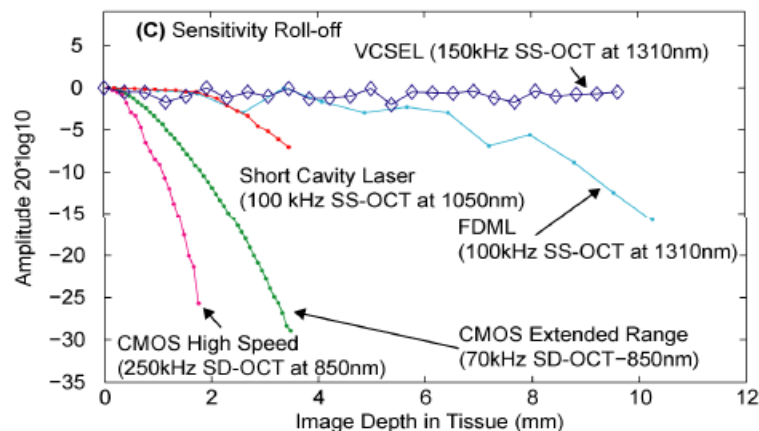
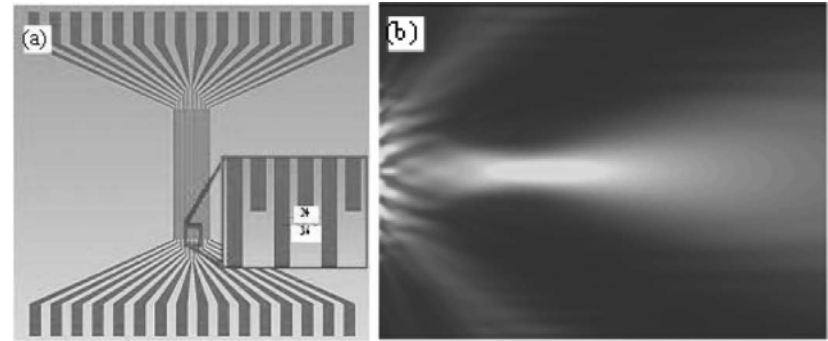


Image depth comparison of VCSEL based OCT versus other competing options.

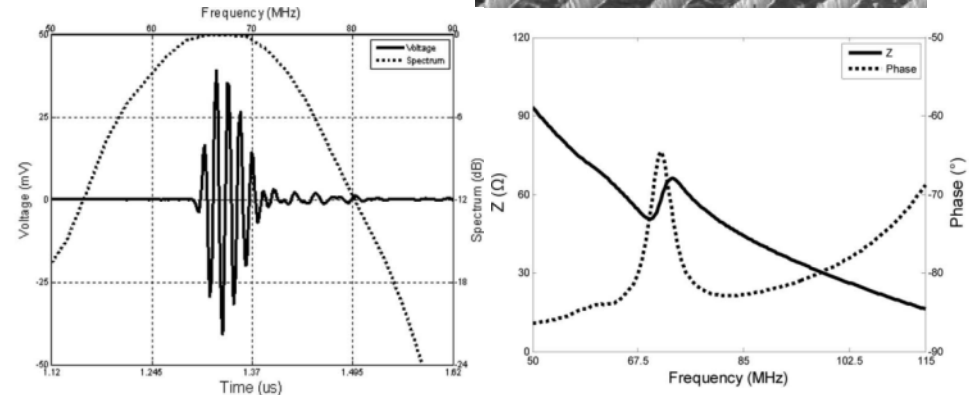
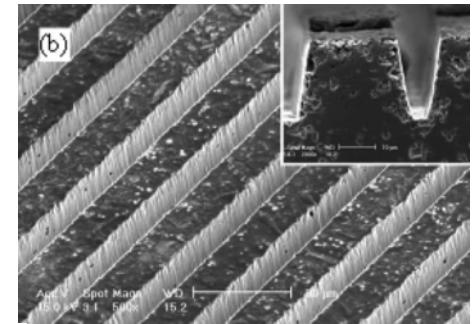
High-Frequency (>50 MHz) Medical Ultrasound Linear Arrays Fabricated From Micromachined Bulk PZT Materials

High-frequency, wideband ultrasound transducer arrays can provide the necessary spatial resolution for applications in dermatology, ophthalmology, and other medical disciplines for which high-quality subsurface imaging is required. Unlike high-frequency single-element transducers, one of the major challenges in developing high-frequency ultrasound transducer arrays is the patterning of small-scale features within the array. For example, linear arrays designed for 50-MHz operation should have array elements with a pitch of 36 μm and a kerf width of 12 μm . Linear arrays made from micromachining bulk PZT at frequencies over 50 MHz have been developed using a DRIE dry-etching technique. The arrays consist of 32 elements with an element width of 24 μm and a kerf width of 12 μm . The element length is 4 mm, and the thickness is approximately 32 μm . Values for the -6 dB bandwidth and two-way insertion loss are about 40% and 26 dB, respectively.



(a) Layout of one transducer array for 50 MHz and (b) simulated pressure pattern using PZFlex.

SEM image of deeply etched PZT that forms the linear array transducer. PZT was etched using Cl2 ICP-RIE.



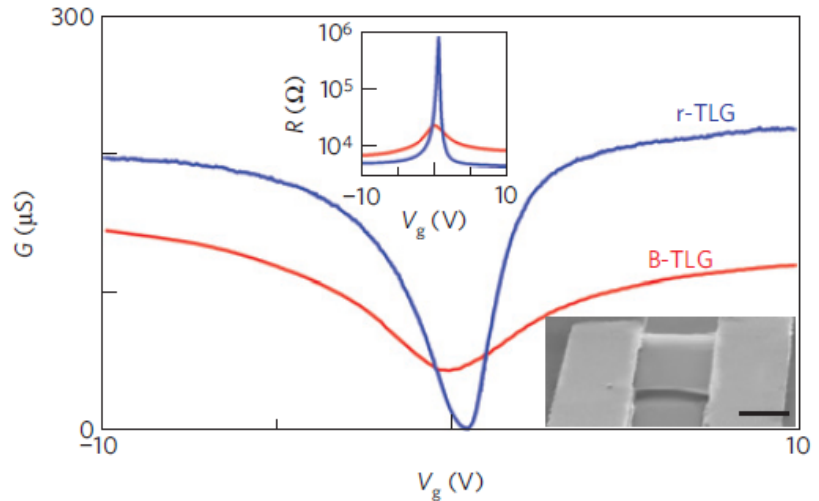
Pulse echo response of a typical array element and electrical impedance

C. Liu, et. al., Shung Group, USC
Work partially performed at UCSB
Nanofabrication Facility

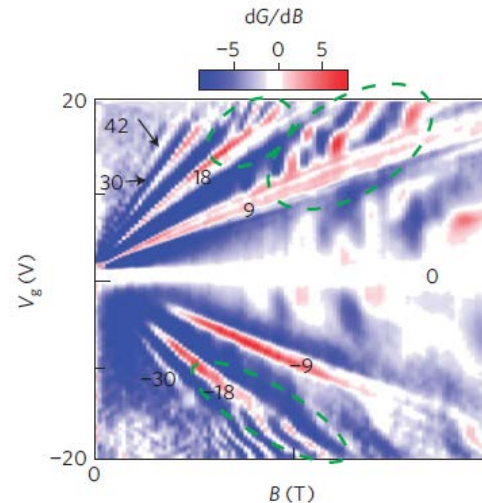
Stacking-dependent band gap and quantum transport in trilayer graphene

Graphene is an extraordinary two-dimensional (2D) system with chiral charge carriers and fascinating electronic, mechanical and thermal properties. In multilayer graphene, stacking order provides an important yet rarely explored degree of freedom for tuning its electronic properties. These multilayer graphenes are also expected to exhibit rich novel phenomena at low charge densities owing to enhanced electronic interactions and competing symmetries. Here we demonstrate the dramatically different transport and electronic structure properties in TLG with different stacking orders. At the Dirac point, B-TLG remains metallic, whereas r-TLG becomes insulating. In magnetic fields, well developed quantum Hall (QH) plateaus in r-TLG split into three branches at higher fields. Such splitting is a signature of the Lifshitz transition, a topological change in the Fermi surface, that is found only in r-TLG. Our results underscore the rich interaction induced phenomena in trilayer graphene with different stacking orders.

W. Bao, et. al. C.N. Lau group UC Riverside
Work partially performed at UCSB
Nanofabrication Facility



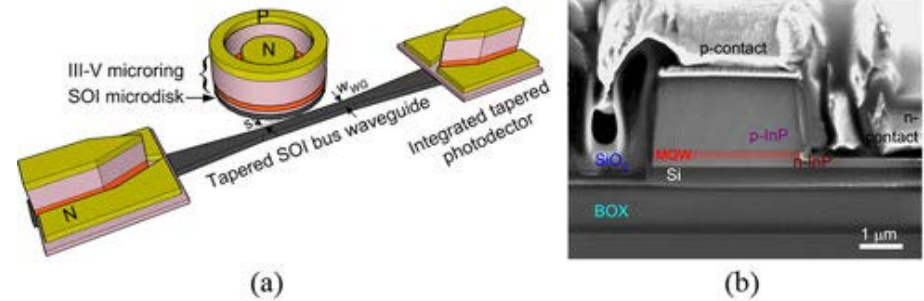
$G(V_g)$ for two different suspended TLG devices at TD1:5 K. Upper inset: $R(V_g)$ in log-linear scales for the same devices. Lower inset: SEM image of a suspended graphene device. Scale bar, 2 μm .



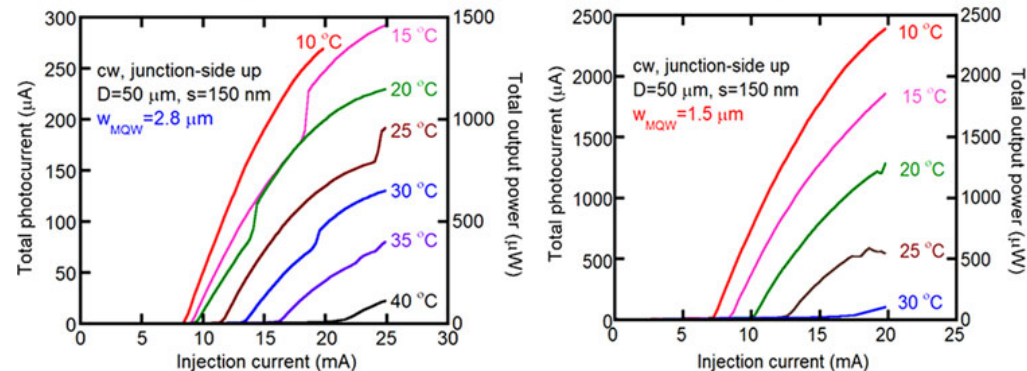
$dG/dB(V_g, B)$. The numbers indicate the filling factors of the features. The splittings at 9 and ± 18 are indicated by the dotted circles. Such splittings are signatures of the Lifshitz transition, a topological change in the Fermi surface.

Low Threshold Electrically-Pumped Hybrid Silicon Microring Lasers

Microring and microdisk-based photonic devices with small-cavity design recently have been used to realize a variety of functionalities in photonic integrated circuits. Microring-based modulators, optical buffers, memories, add-drop filters, etc. have been demonstrated. Microrings are also an attractive structure for the design of on-chip lasers. Ring cavities with their travelling wave resonance modes do not require feedback mirrors, and multiple ring lasers can be coupled to a single bus waveguide for wavelength division multiplexing applications. We have significantly improved performance of a compact hybrid silicon microring lasers obtained by selectively reducing the volume of active region through undercutting of the multiple quantum well (MQW) region to force carriers to flow toward the outer edge of the microring for better gain/optical mode overlap. We observe a reduction of the threshold of over 20% and up to 80% output power enhancement.



(a) Schematic of silicon microring resonator laser with integrated, tapered photodetectors. (b) SEM cross-sectional images of microring resonator showing contacts, and III-V-on-SOI structure.



Di Liang, et. al, HP Laboratories
Work partially performed at UC Santa Barbara
Nanofabrication Facility

Measured photocurrent (laser power) for early devices with 2.8μm wide active regions and for improved devices where active region undercutting reduced the active width to 1.5μm. A dramatic improvement in power and efficiency is seen

University of Colorado

Solid State Ionic Field Effect Transistor

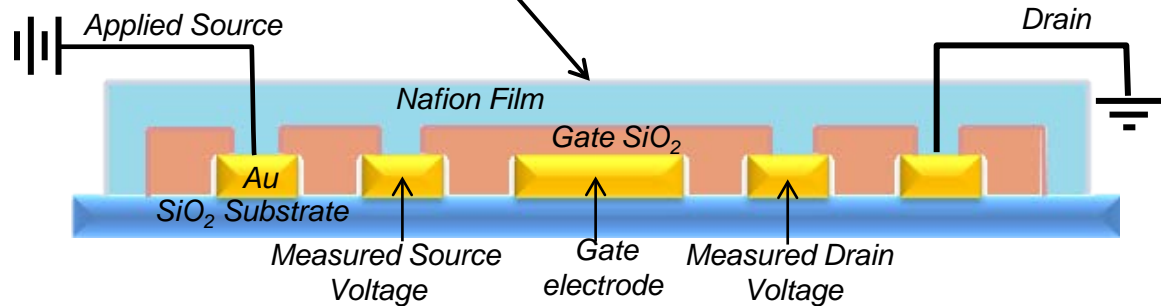
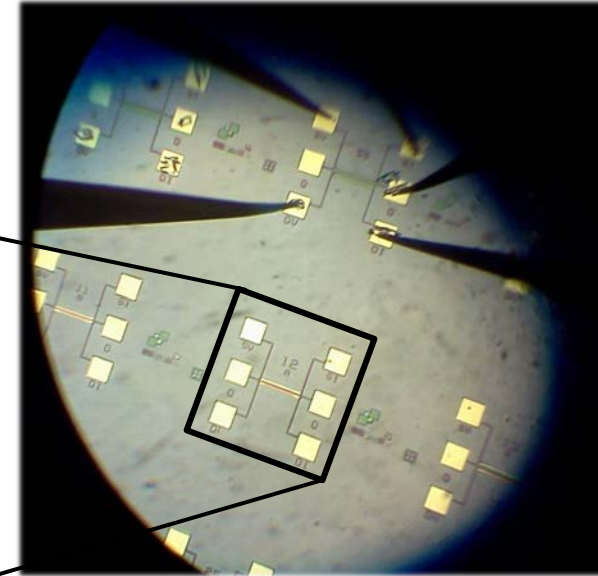
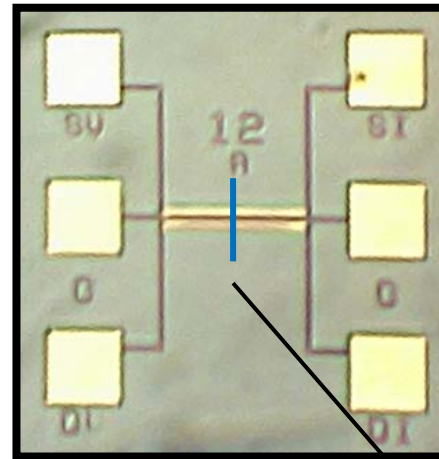
First demonstration of an CMOS-compatible solid-state ionic field effect transistor .

Protons rather than electrons provide conduction in the FET channel and can be used for sensing and logic operations just like a silicon CMOS transistor.

Nafion[®] , a common material, is used as a channel. Other materials as well as the fabrication techniques are compatible with CMOS.

Application include characterization of organic/inorganic thin films and operation in aqueous environments

Top view of the Ionic FET



Cross section of the Ionic FET

K. Risky, P.C. Taylor , and R. O'Hayre,
Colorado School of Mines, REMRSEC
Work performed at the Colorado Nanofabrication Lab

Non-contact And All-electrical Method For Monitoring The Motion Of Semiconducting Nanowires

An all-electric, non-contact method has been developed to monitor the motion of semiconducting nanowires.

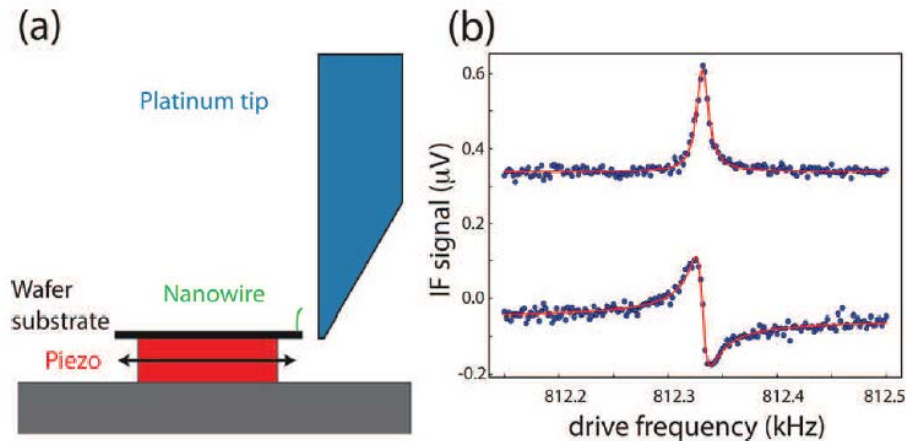
This technique uses a microwave resonant circuit whose resonance is modulated by the varying capacitance between the GaN nanowires and a platinum tip.

This method is predicted to be capable of detecting motion with a sensitivity of $1\text{pm}/\sqrt{\text{Hz}}$.

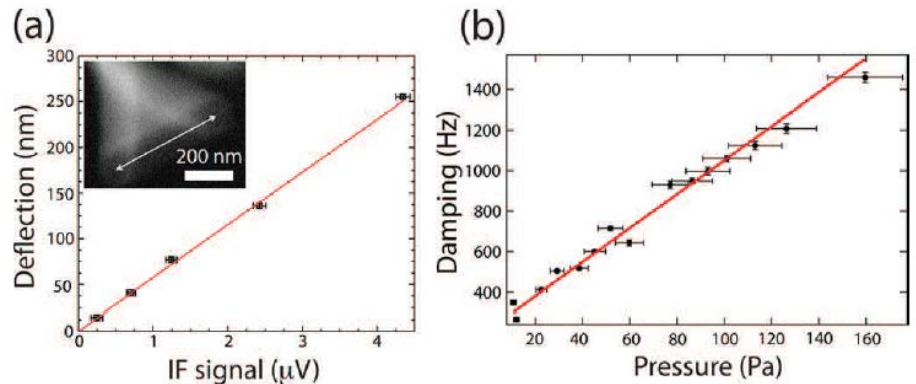
It also provides a way to measure the pressure dependence of a nanowire's mechanical damping resulting in a value of $8.37\text{Hz}/\text{Pa}$.

S. W. Hoch, J. R. Montague, V. M. Bright, C. T. Rogers, K. A. Bertness, J. D. Teufel, and K. W. Lehnert, Univ. of Colorado, JILA and NIST

Work performed at the Colorado Nanofabrication Lab



a) Experimental set-up and b) a typical measured signal



a) Deflection vs. voltage and b) damping vs. pressure as measured with this technique.

Ultra High Speed Graphene Diode With Reversible Polarity

Geometric diodes have the potential to provide rectification at ultra high frequencies.

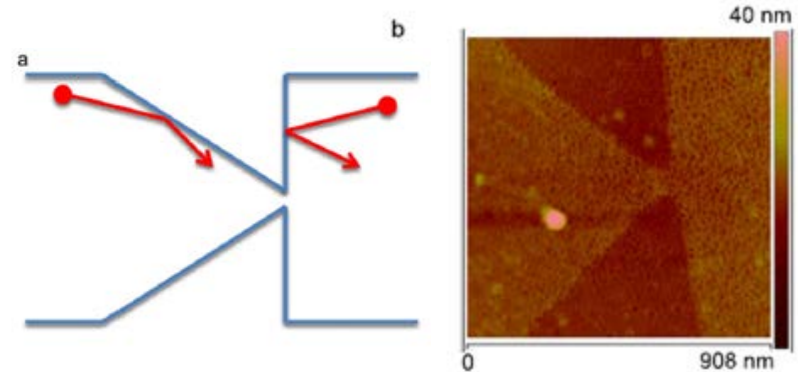
Geometric diodes made out of graphene utilize the large mean-free path length ($\sim 1 \mu\text{m}$) of graphene. In addition, the carrier type can be modulated resulting in a reversal of the diode polarity as the main carrier type changes from electron to holes.

Submicron geometric diodes were fabricated by patterning and etching exfoliated graphene on silicon dioxide on a silicon wafer.

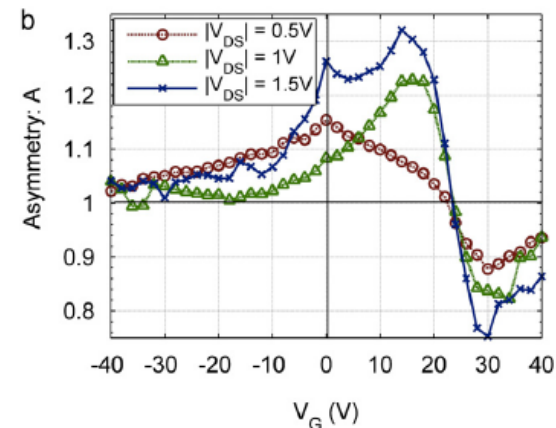
Reversal of the carrier type was obtained when sweeping the substrate voltage, thereby demonstrating the reversal of the diode polarity.

The graphene geometric diodes exhibited rectification at 28 THz, opening the way to ultrahigh speed applications.

Garret Model, Zixu Zhu, Sachit Grover, and Saumil Joshi
University of Colorado
Work performed at the Colorado Nanofabrication Lab



a) Schematic diagram of the geometric diode and b) AFM image of a fabricated graphene geometric diode



Change in asymmetry as a function of the gate voltage

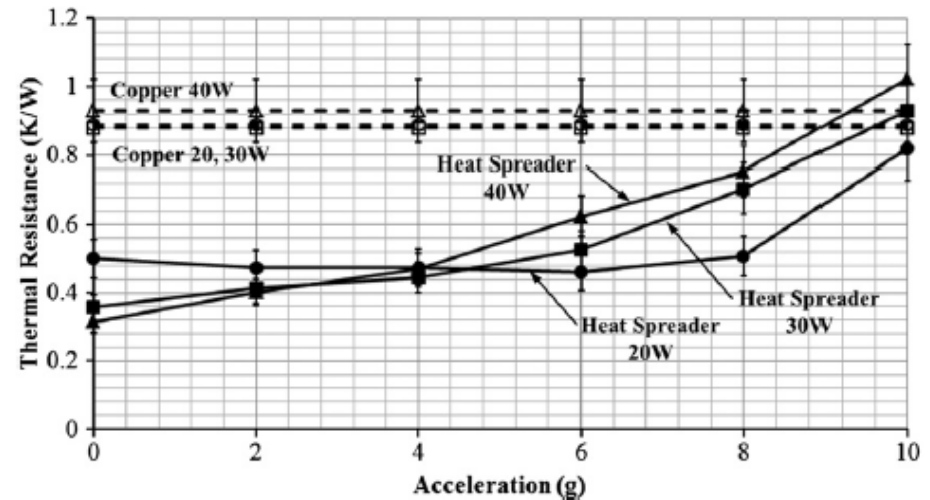
Polymer Heat Pipe Heat Spreader Under High Acceleration

This work entails the fabrication and application of a micro-scale hybrid wicking structure in a flat polymer-based heat pipe heat spreader, improving the heat transfer performance under high adverse acceleration.

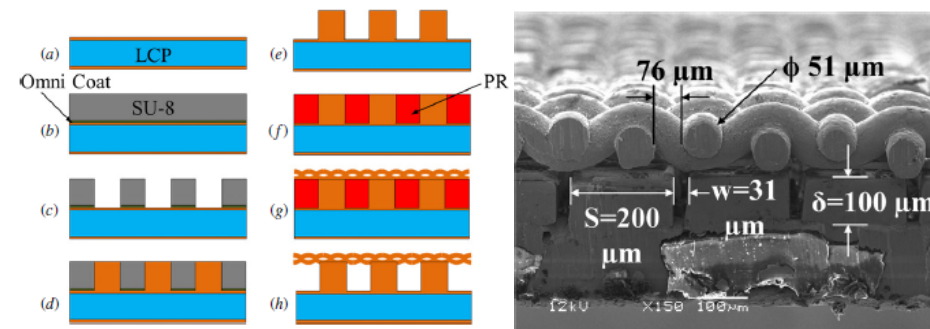
The hybrid wicking structure enhances evaporation and condensation heat transfer under adverse acceleration. It consists of an array of square electroplated copper micro-pillars separated by narrow grooves for liquid flow and covered with a woven copper mesh.

This novel device structure was shown to be superior to a copper heat spreader with the same dimensions up to 10 g acceleration, leading the way to flexible, polymer-based heat pipe heat spreaders compatible with standardized printed circuit board technologies that are capable of efficiently extracting heat at high acceleration levels.

C. Oshman, Q. Li, L. Liew, R. Yang, Y C Lee, V. M Bright, D. J. Sharar, N. R Jankowski and B. C. Morgan,
University of Colorado
Work performed at the Colorado Nanofabrication Lab



Thermal resistance of the heat spreaders vs. acceleration.



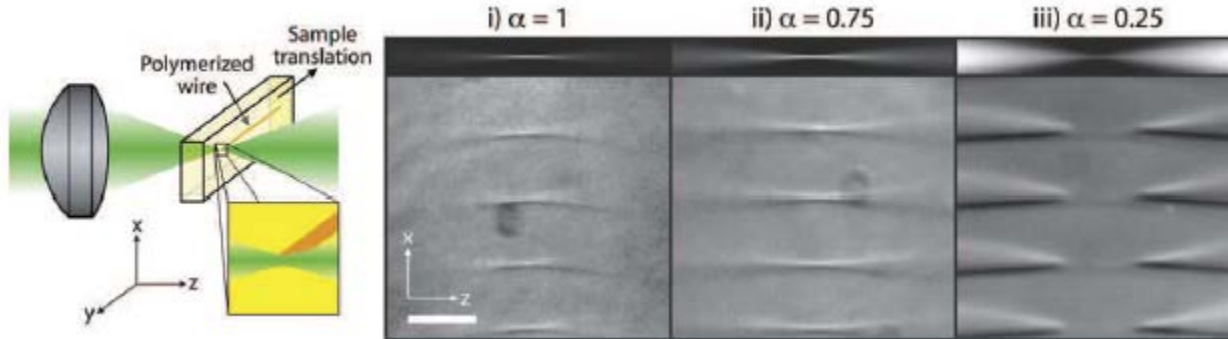
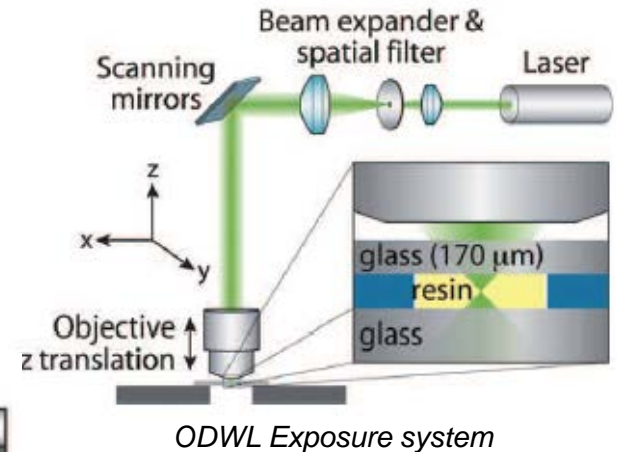
Process sequence

Cross section of the heat spreader indicating the width, S , height, δ , and spacing, w , of the micro-pillars

Principles Of Voxel Refinement In Optical Direct Write Lithography

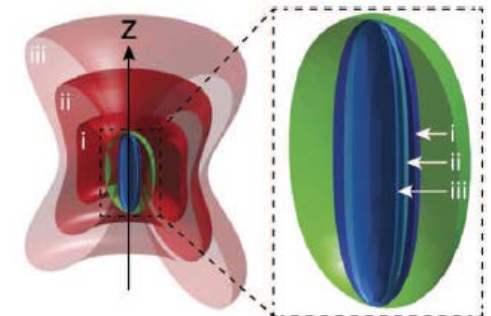
Two-photon optical direct write lithography can provide extreme sub-wavelength resolution 3-D voxel exposure.

Voxel shapes with a transverse resolution of 155 nm were achieved using irradiation at 810 nm as the photoinitiator whereas depletion of the photo-initiator excited state, prior to singlet to triplet intersystem crossing and radical generation, was accomplished by concurrent, continuous irradiation at 532 nm.



Differential interference contrast micrographs of wires fabricated via single-photon ODWL. The polymerization mechanisms include i) cationic, ii) radical, and iii) high irradiation intensity radical polymerizations. A decrease in the scaling exponent (α) effects a progressive loss of axial polymerization confinement. Scale bar, 35 nm.

T. F. Scott, C. J. Kloxin, D. L. Forman, R. R. McLeod and C. N. Bowman,
University of Colorado
Work performed at the Colorado Nanofabrication Lab



Voxel shape as a function of beam intensity using two-photon irradiation with 810 nm as the photoinitiator and 532 nm as the continuous irradiation.

J. Mater. Chem., 2011, 21, 14150 ; DOI: 10.1039/c1jm11915j

NNIN is supported by NSF ECCS-0335765

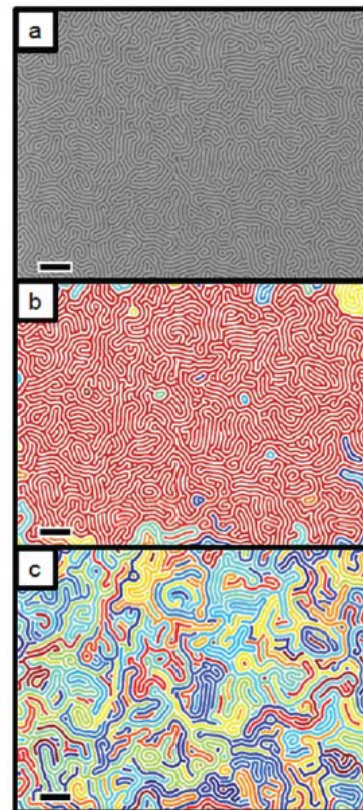
Network Connectivity and Long-Range Continuity of Lamellar Morphologies in Block Copolymer Thin Films

The connectivity in a lamellar polystyrene-block-poly(methyl methacrylate) copolymer in thin films depends on the volume fraction and can be shifted by homopolymer addition of either polystyrene (PS) or poly(methyl methacrylate) (PMMA) domains.

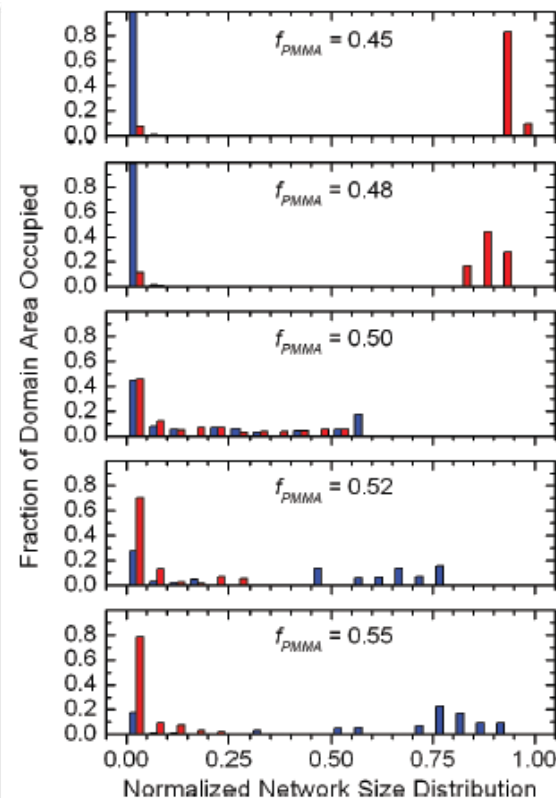
The transition in network continuity from the PS to PMMA domain as a function of copolymer volumetric composition (from $f_{\text{PMMA}} = 0.45$ to 0.55) was correlated with a 5-fold increase in the PMMA branch point density and a concomitant 3-fold reduction in the PMMA end point density.

These results indicate that the copolymer's composition drastically impacts the self-assembled lamellar morphology in thin films and is an important design consideration when using such materials for lithographic applications, including for directed assembly to generate long-range, defect-free order.

I. P. Campbell, G. J. Lau, J. L. Feaver, and M. P. Stoykovich, University of Colorado
Work performed at the Colorado Nanofabrication Lab



SEM images of an assembled PS-*b*-PMMA copolymers shown in (a) with colorized networks for the (b) PS and (c) PMMA domains. Images are $3.56 \mu\text{m} \times 4.8 \mu\text{m}$, and the scale bar corresponds to 400 nm.



Normalized size distribution of connected networks of PS (red) and PMMA (blue).

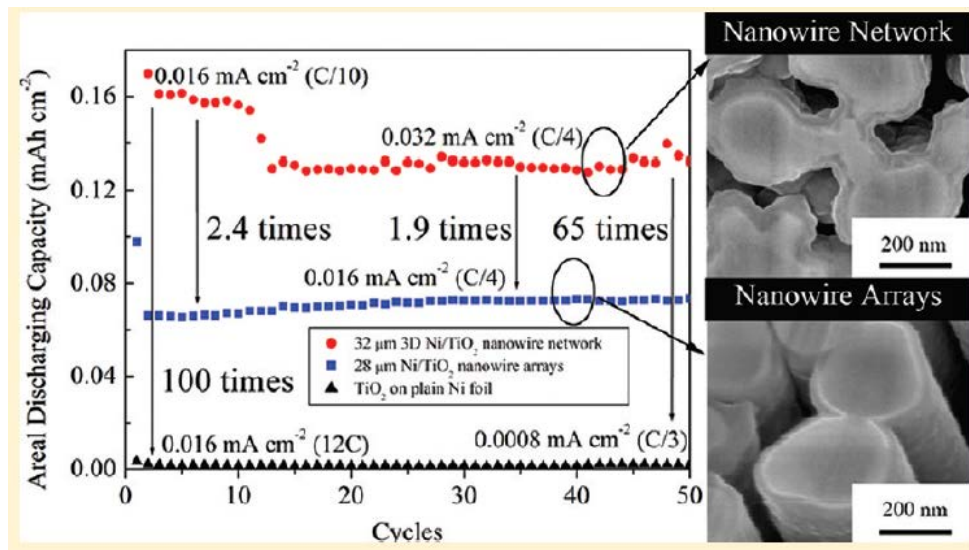
Three-Dimensional Ni/TiO₂ Nanowire Network for High Areal Capacity Lithium Ion Microbattery Applications

The areal capacity of nanowire-based microbatteries can be increased by increasing the length of nanowires, while the high aspect ratio of such wire is known to degrade their performance for lithium ion battery applications.

As an alternate, a three-dimensional Ni/TiO₂ nanowire network was fabricated using a 3-D porous anodic alumina template-assisted electrodeposition of Ni followed by TiO₂ coating using atomic layer deposition.

Compared to the straight Ni/TiO₂ nanowire arrays the 3-D Ni/TiO₂ nanowire network shows higher areal discharging capacity, increasing proportionally with the length of nanowires.

This work paves the way to build reliable 3-D nanostructured electrodes for high areal capacity microbatteries.



Comparison of the areal discharge capacitance of a nanowire network versus nanowire arrays and a planar TiO₂ layer on nickel foil

W. Wang, M. Tian, A. Abdulagatov, S. M. George, Y. C. Lee, and R. Yang, University of Colorado
Work performed at the Colorado Nanofabrication Lab

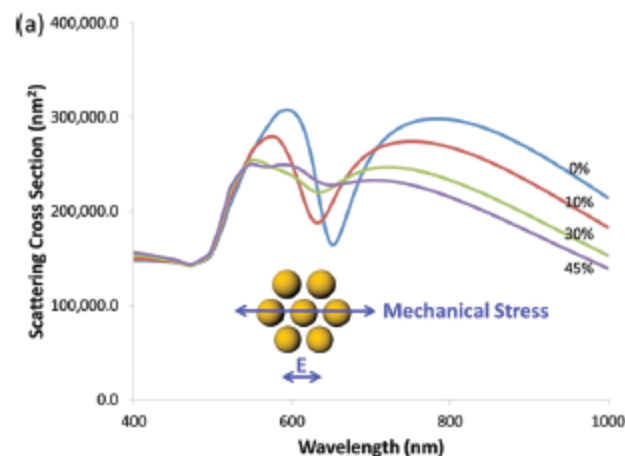
Dynamic Tuning and Symmetry Lowering of Fano Resonances in Plasmonic Nanostructure

Dynamic tuning and symmetry lowering of Fano resonances in gold heptamers were explored by applying uniaxial mechanical stress. A flexible heptamer structure was fabricated by embedding the seven-gold-nanocylinder complex in a polydimethylsiloxane membrane.

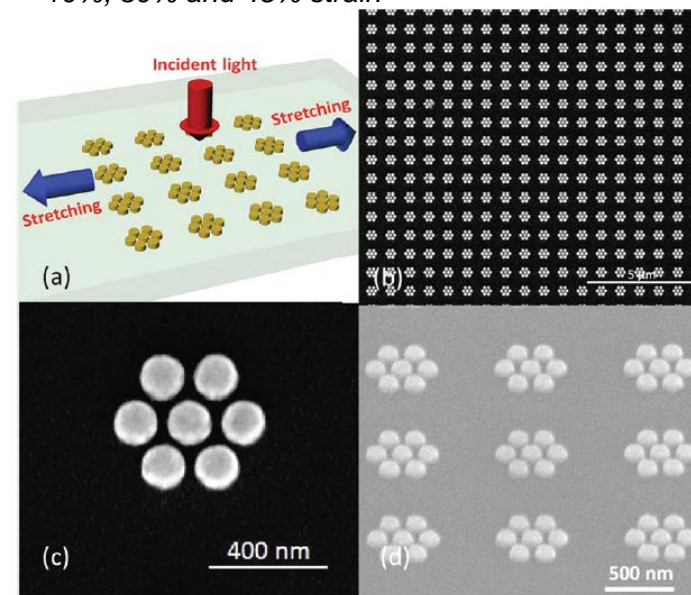
Under uniaxial stress, the Fano resonance exhibited opposite spectral shifts for the two orthogonal polarizations parallel and perpendicular to the mechanical stress. Furthermore, a new resonance was observed for polarization parallel to the mechanical stress but not for the perpendicular polarization.

The symmetry tuning enabled by applying mechanical stress is a simple and efficient way to engineer the nature of coupled plasmon resonances in complex nanostructures. The mechanically tunable plasmonic nanostructures also provide an excellent platform for dynamically tunable nanophotonic devices such as tunable filters and sensors.

Y. Cui, J. Zhou, V. A. Tamma, and W. Park, University of Colorado
Work performed at the Colorado Nanofabrication Lab



Scattering cross section vs. wavelength for 0%, 10%, 30% and 45% strain



Gold heptamers fabricated on a stretchable polydimethylsiloxane (PDMS) membrane

Ultrafast Thermoreflectance Techniques For Measuring Thermal Conductivity Of Thin Films

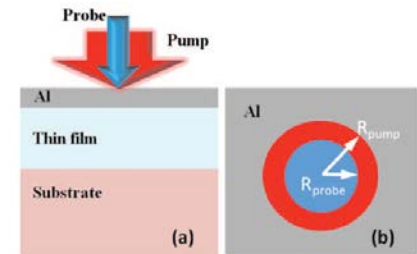
Ultrafast laser-based thermoreflectance techniques, including the time-domain thermoreflectance (TDTR) and the frequency-domain thermoreflectance (FDTR) techniques are excellent approaches for the challenging measurements of interface thermal conductance of dissimilar materials.

A patterned trilayer microfabricated structure was fabricated and characterized. TDTR and FDTR signals were obtained and compared with a thermal conduction model.

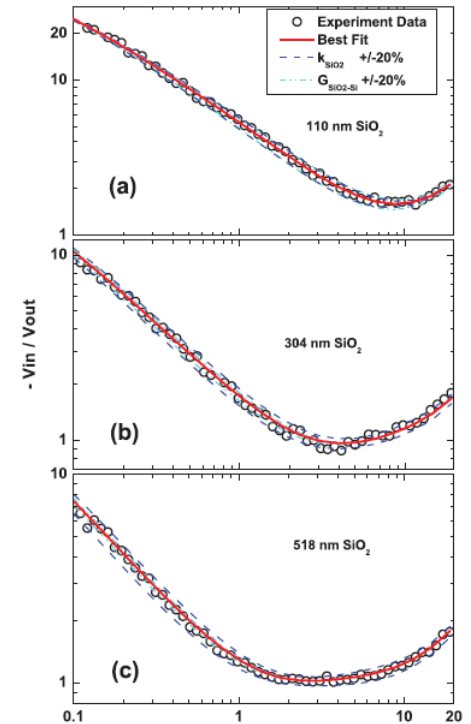
It was concluded that in FDTR method, the heat transport in a trilayer structure could be divided into three regimes, and the thermal conductivity of thin films and interface thermal conductance can be obtained subsequently by fitting the data in different frequency range of one FDTR measurement.

Both TDTR and FDTR measurements were obtained. FDTR measurement results agree well with the TDTR measurements, while they are found to be easier to obtain compared to TDTR measurements..

J. Zhu, D. Tang, W. Wang, J. Liu, K. W. Holub, and R. Yang, University of Colorado.
Work performed at the Colorado Nanofabrication Lab



Experimental setup

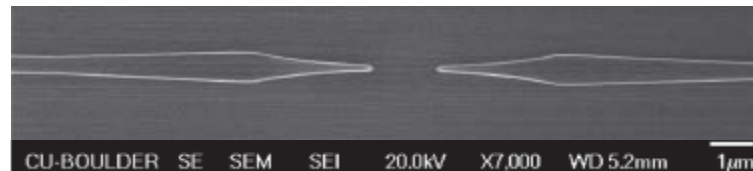


Nanoscale Optical Dielectric Rod Antenna for On-Chip Interconnecting Networks

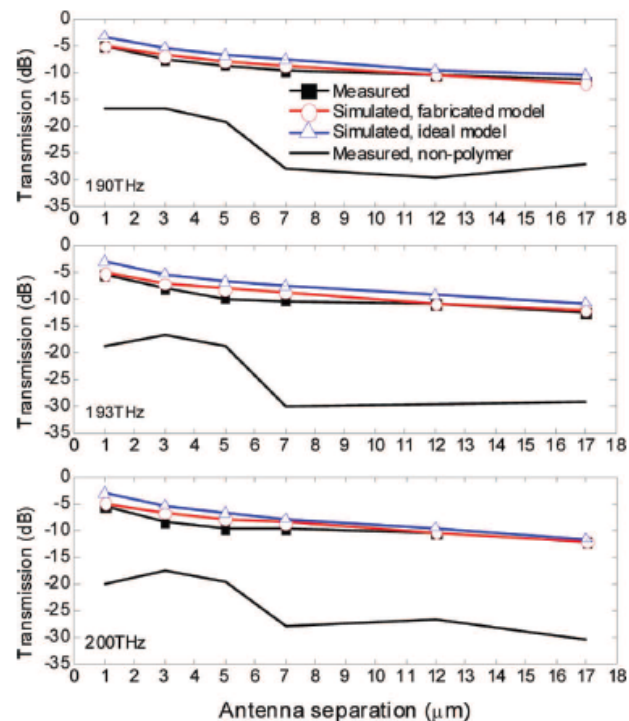
A nanoscale on-chip optical dielectric rod antenna was demonstrated. The antenna is designed and fabricated on a 200-mm silicon-on-insulator platform, using 193-nm-deep UV lithography. A 500-nm-thick polymer layer is designed and deposited to act as an asymmetric slab waveguide, confining the radiated wave within the layer.

Six antenna pairs with 1, 3, 5, 7, 12, and 17 μm separations were fabricated.

Transmission between antenna pairs was measured from 190 to 200 THz providing good agreement with simulation and superior performance vs. non-polymer antennas.



Fabricated antennas with 1 μm separation



Measured transmission versus antenna separation measured at 190 THz, 193 THz and 200 THz

H. Zhou, X. Chen, D. S. Espinoza, A. Mickelson, and D. S. Filipovic, University of Colorado
Work performed at the Colorado Nanofabrication Lab

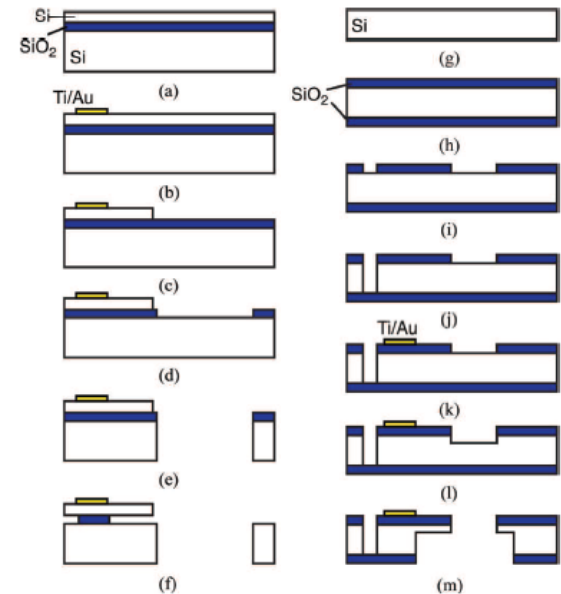
A Universal Microscale Mechanical Tester

This work is aimed at creating a microfabricated mechanical test platform. This system consists of a reusable chip capable of large-displacement actuation, while interfacing to a test coupon chip compatible with synthesis conditions for several nanomaterials.

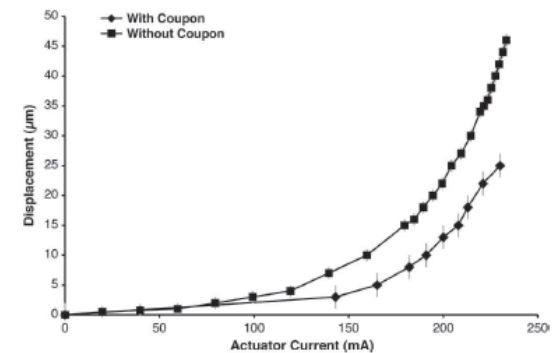
The actuated test platform chip contains a thermal actuator driving a compliant displacement amplification transmission, and a bulk-micromachined well in which the test coupon chips may be placed and removed.

The displacement amplification structure provides 40 μm of output displacement, extending a probe over the well and into contact with the test coupon. The test coupon contains compliant structures that are actuated by the probe from the test platform.

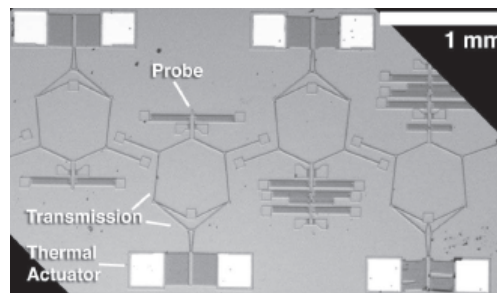
J. J. Brown, D. A. Dikin, R. S. Ruoff, and V. M. Bright,
 University of Colorado
 Work performed at the Colorado Nanofabrication Lab



Fabrication process sequence



Displacement versus actuator input current measured for a UTC chip with and without a test coupon



Micrograph of one of the universal test structures including a thermal actuator, a transmission structure and probe.

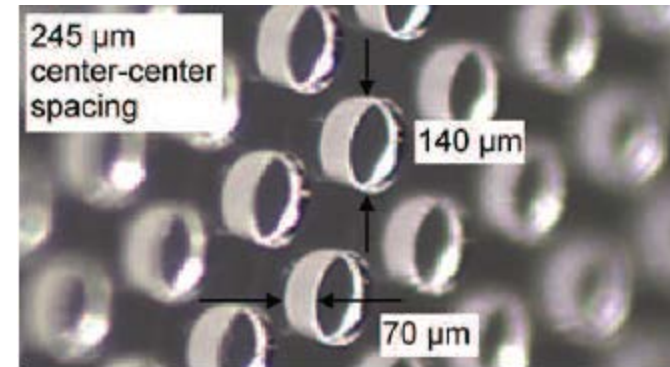
A Testing Platform for Quantitative Evaluation of Tread Performance on Multiple Biological Substrates

An experimental platform is developed to quantitatively measure the performance of robotic wheel treads in a dynamic environment.

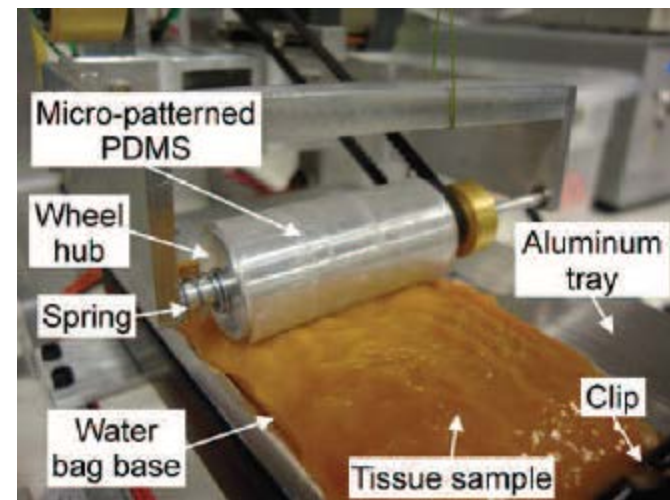
The testing platform is characterized by testing a micropatterned polydimethylsiloxane (PDMS) tread on three substrates (dry synthetic tissue, hydrated synthetic tissue, and excised porcine small bowel tissue), at three normal forces, 13 slip ratios, and three translational speeds .

The variance between trials was found to be minimal when compared to the normal force, translational speed, slip ratio, tread, and substrate variances .

Future use of the platform will lead to an optimized micropattern-based mobility system, under given operating conditions, for implementation on a robotic capsule endoscope.



Isometric view of the micropatterned PDMS wheel tread.



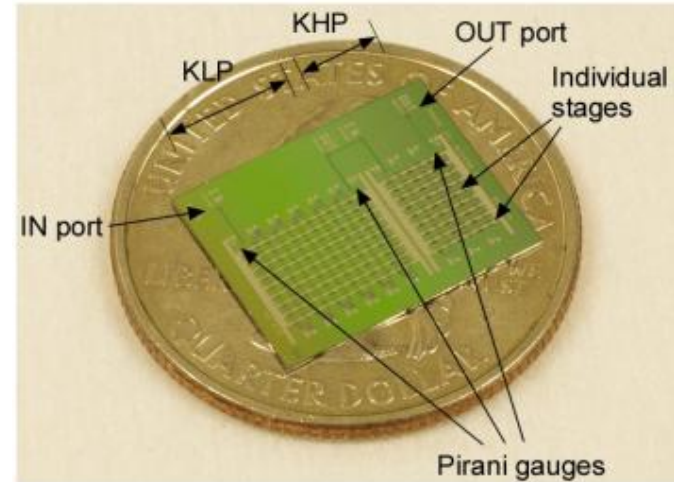
Experimental setup for the dynamic benchtop testing platform characterization (excised porcine intestine pictured).

L. J. Sliker and M. E. Rentschler, University of Colorado
Work performed at the Colorado Nanofabrication Lab

University of Michigan

High Vacuum Knudsen Pumps

Knudsen pumps utilize a motionless gas pumping mechanism based on the phenomenon of thermal transpiration. Recent advances in micro-manufacturing technologies have fueled efforts toward high vacuum Knudsen pumps for atmospheric pressure operation. Our research has resulted in several microscale Knudsen pumps appropriate for a wide range of applications. In 2011, a Si-micromachined, 48-stage, monolithic Knudsen pump, pumped down from 760 to <50 Torr or from 250 to ≈ 5 Torr, using input power of 1.3 W. These compression ratios of 15 and 50 offer $10\times$ improvement over those reported in the past. In 2012, a 162-stage monolithic Knudsen pump (footprint = $12 \times 15 \text{ mm}^2$) is reported, with a two-part stage design of Knudsen high-pressure part (KHP) and Knudsen low-pressure part (KLP). The compression ratio of 109 (760 to 7 Torr) exceeds our previous best by $2\times$, using $3\times$ reduced power ($\approx 0.44 \text{ W}$).

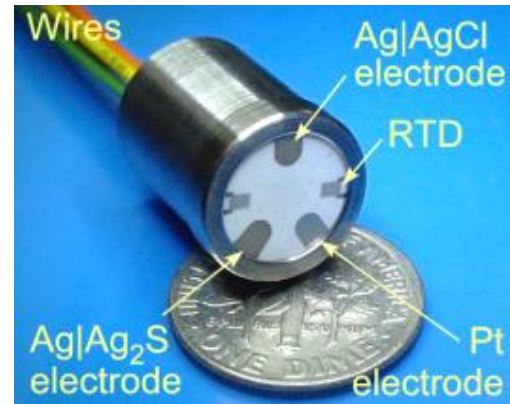


High vacuum pump using a monolithic 162-stage two-part (KHP and KLP) multistage Knudsen pump.

*Yogesh Gianchandani and Seungdo An, University of Michigan
Work performed at the Lurie Nanofabrication Facility*

Chemical Sensors in Extreme Environments

The lack of performing and reliable chemical sensors limits the quantitative studies of hydrothermal system at mid-ocean ridge. We propose here to improve the measurement of chemical components associated with hydrothermal vent fluids using high performance miniaturized sensor assembly and by ultimately developing on-board signal processing. The sensor has been designed and fabricated. Initial test results of the preliminary devices indicate validity of the sensor design and the integrity of the YSZ|HgO|Hg electrode, which is the core component of the device. Further sensor characterization and device testing under harsh environments are in progress.

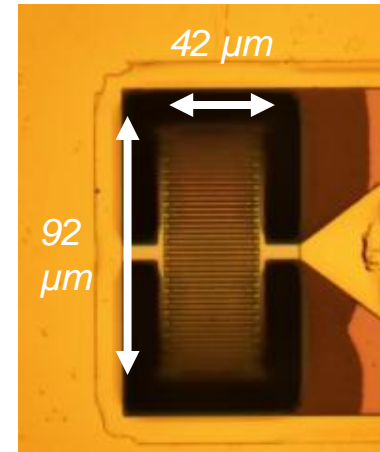


Integrated device in Ti alloy housing on a US dime. The YSZ diaphragm is shown, along with three thin-film metal electrodes and RTDs on the diaphragm. The length of the Ti housing is for demonstration only.

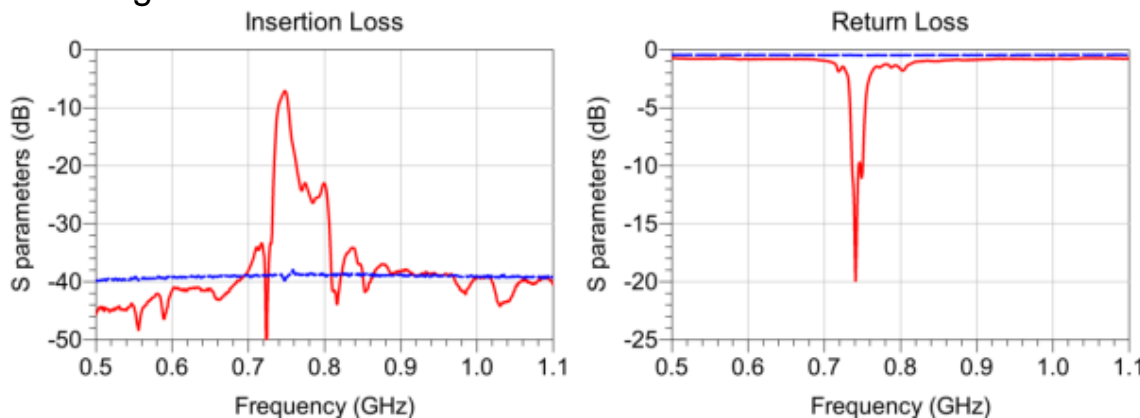
Yogesh Gianchandani and Tao Li, University of Michigan
And William Seyfried and Kang Ding, University of Minnesota
Work performed at the Lurie Nanofabrication Facility

Intrinsically Switchable Ferroelectric Resonators and Filters Project

The goal is to develop reconfigurable radios such as software-defined radios and cognitive radios using ferroelectric thin film technology. Some unique properties of ferroelectrics are utilized to develop microwave resonators and filters which can be switched on and off by applying and removing a dc bias voltage. Many of these devices can be placed in parallel to form resonator and filter banks which can select the operating band of a frequency agile radio. These devices are fabricated on high resistivity Si wafers with the ferroelectric thin film sandwiched between two layer of platinum forming a membrane.

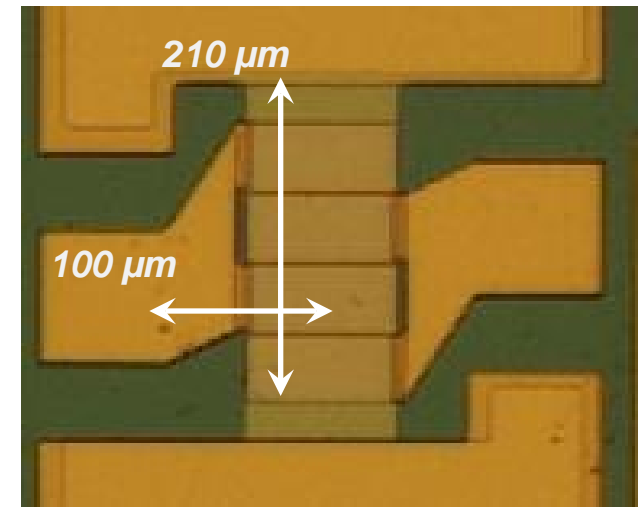


An intrinsically switchable 1.67 GHz resonator which can be turned on and off by controlling the applied dc bias voltage.



The on and off response of a ferroelectric acoustically coupled RF band pass filter.

Amir Mortazawi, Victor Lee, and Seyit Ahmet Sis, University of Michigan
Work performed at the Lurie Nanofabrication Facility



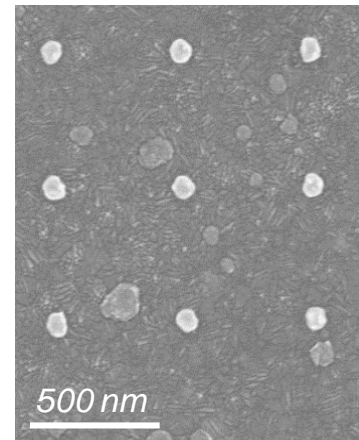
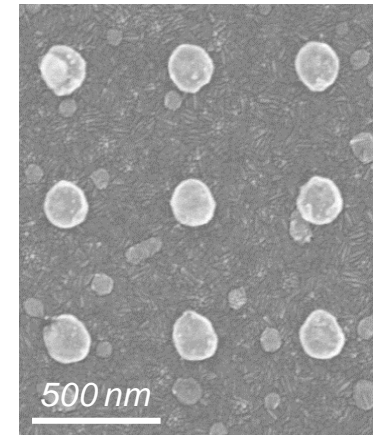
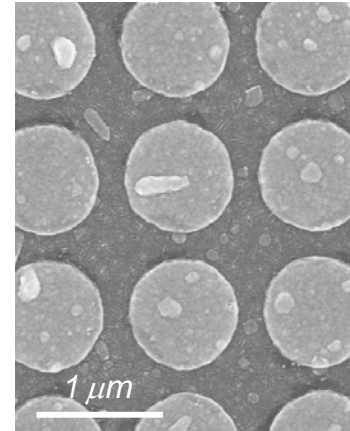
An intrinsically switchable acoustically coupled RF band pass filter with a center frequency of 750 MHz.

Plasmon-enhanced single-molecule fluorescence imaging

The goal of this project is to use of single molecule super-resolution imaging techniques to optically probe and study the local field around metal nanoparticles on a nanometer scale.

The Lurie Nanofabrication facility tools were used to fabricate and characterize these metal nanoparticles of various sizes that are then studied optically.

ITO is deposited on glass coverslips to form an optically transparent conductive layer, and e-beam lithography is used to form various configurations of nano-particle arrays then a thin film of gold is evaporated unto the patterns to form the structures.

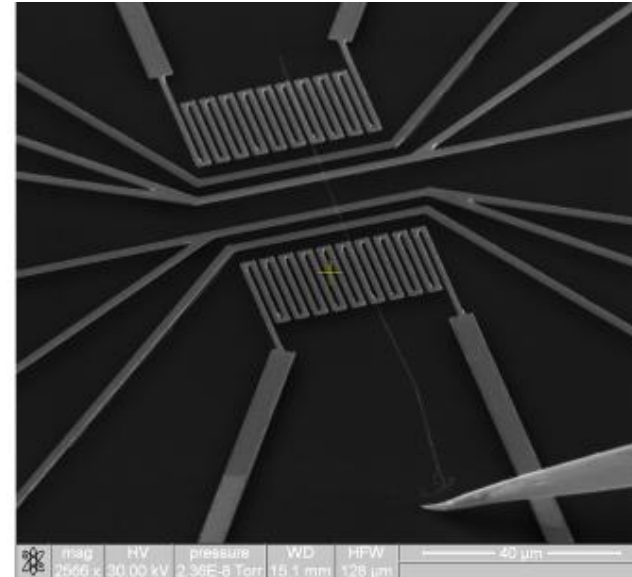


SEM images of different size gold nano-islands

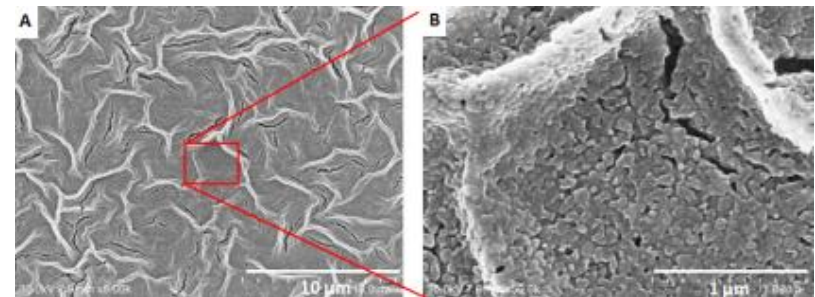
Esther Wertz and Julie S. Biteen, University of Michigan
Work performed at the Lurie Nanofabrication Facility

Nanostructured Inorganic Oxide Thermoelectric Devices

While thermoelectric devices will likely play a key role in enhancing the capabilities of future portable power generation systems, most thermoelectric materials in current use are based on exotic, inorganic materials and suffer from low efficiency and high cost. The efficiency of a thermoelectric system is parameterized by its figure of merit ZT . The purpose of this project is to enhance the figure of merit of inorganic oxides by providing independent control over the electrical and thermal conductivities.



A polycrystalline oxide nanofiber placed across the electrodes of the measuring device

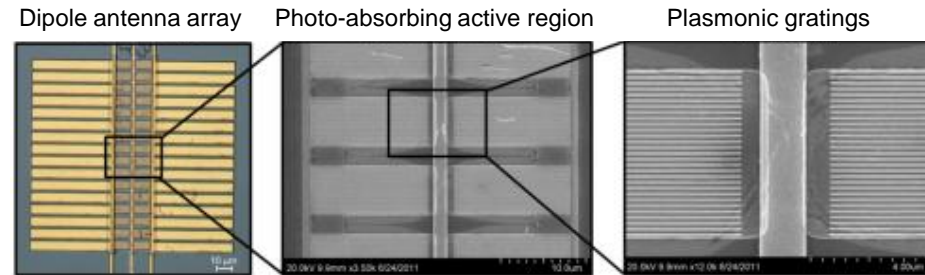


Nanostructured bulk oxide

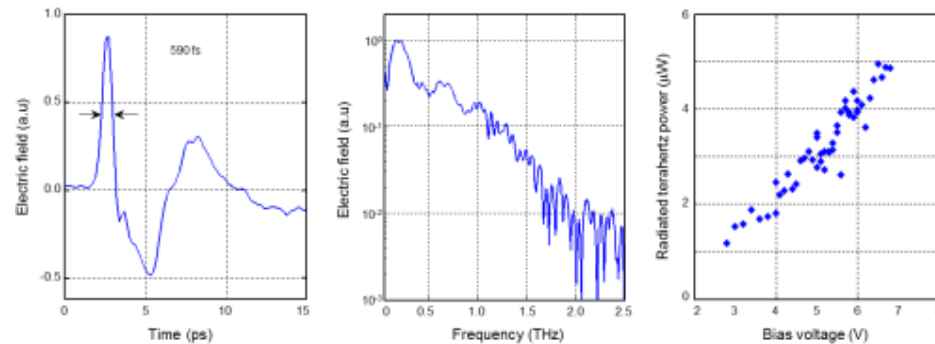
Eleanor Coyle and Anish Tuteja, University of Michigan
Work performed in part at the Lurie Nanofabrication Facility

Plasmonic Photoconductive Terahertz Sources

One of the most commonly used methods for generating terahertz radiation is based on photoconductive terahertz sources. Conventional source design limits the maximum output power and quantum efficiency. Through the use of nano-scale, plasmonic gratings, we introduce a new type of photoconductive terahertz source. The plasmonic gratings greatly increases the optical-to-electrical conversion efficiency in the device. As such, this new design allows for up to 2 orders of magnitude higher terahertz output power.



Plasmonic photoconductive terahertz source design.



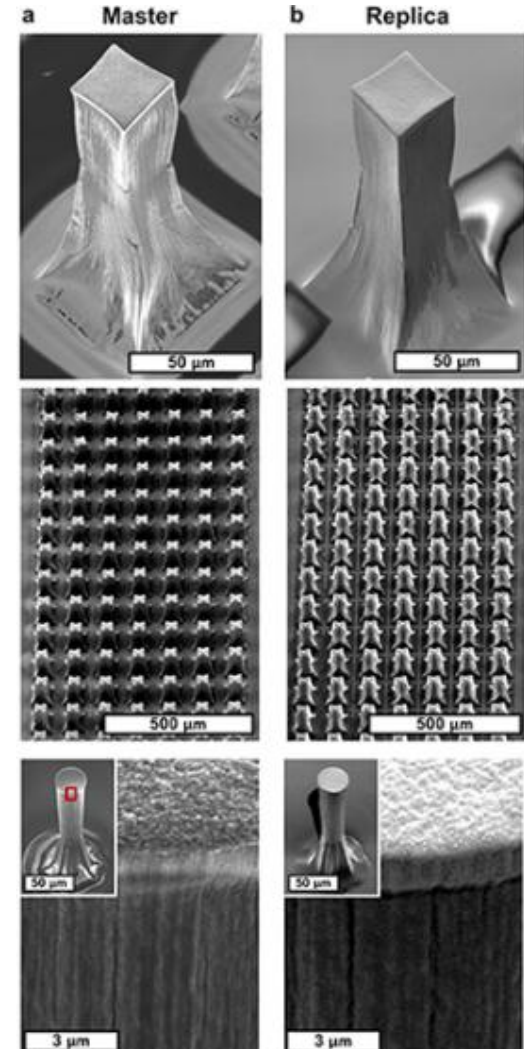
Measured terahertz radiation from an InGaAs-based plasmonic photoconductive terahertz source.

Christopher Berry and Mona Jarrahi, University of Michigan
Work performed at the Lurie Nanofabrication Facility

Fabrication, Densification, and Replica Molding Carbon Nanotube Microstructures

Scalable and cost effective patterning of polymer structures and their surface textures is essential to engineer material properties such as liquid wetting and dry adhesion, and to design artificial biological interfaces. Further, fabrication of high-aspect-ratio microstructures often requires controlled deep-etching methods or high-intensity exposure. We demonstrate that carbon nanotube (CNT) composites can be used as master molds for fabrication of polymer microstructures having anisotropic nanoscale textures. The master molds are made by growth of vertically aligned CNT patterns, capillary densification of the CNTs using organic solvents, and capillary-driven infiltration of the CNT structures with SU-8. The composite master structures are then replicated in SU-8 using standard PDMS transfer molding methods. This process enables batch manufacturing of polymer features that capture complex nanoscale shapes and textures, while requiring only optical lithography and conventional thermal processing.

Davor Copic, Sei Jin Park, Sameh Tawfick, Michael De Volder, and A. John Hart,
University of Michigan
Work performed at *the Lurie Nanofabrication Facility*

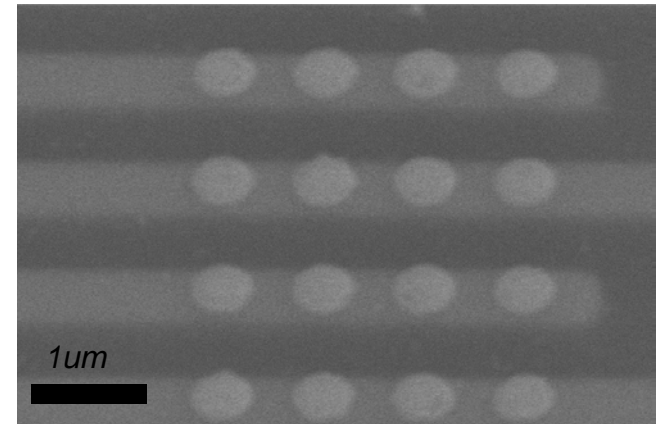


CNT-polymer composite master and high fidelity replica at various scales.

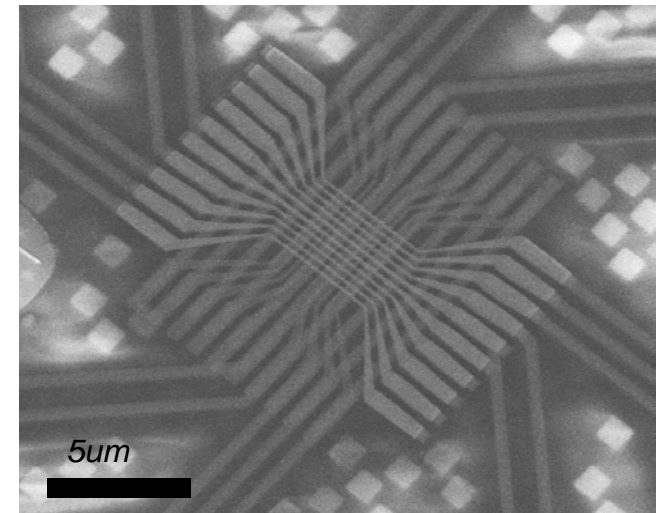
The SyNAPSE Project

The final goal for the SyNAPSE project is to develop solid state memristive devices (or “memristors”) which mimic neurons/synapses in biological systems for neuromorphic applications. Intensive fabrication effort is dedicated to integrating small memristor arrays (e.g. 10x10) with existing CMOS technology so that memristors and CMOS circuits can function as synapses and neurons, respectively. W plugs are made to access the buried Cu interconnects for better process stability. The planarization process relies on reactive ion etching. Both photo- and e-beam lithography are utilized. Sputtered W films are used for W plugs and bottom electrodes. Top electrodes and contact pads are evaporated.

*T. Chang, S. H. Jo, P. Sheridan, and W. Lu, University of Michigan
Work performed at the Lurie Nanofabrication Facility*



SEM image of planarized W plugs

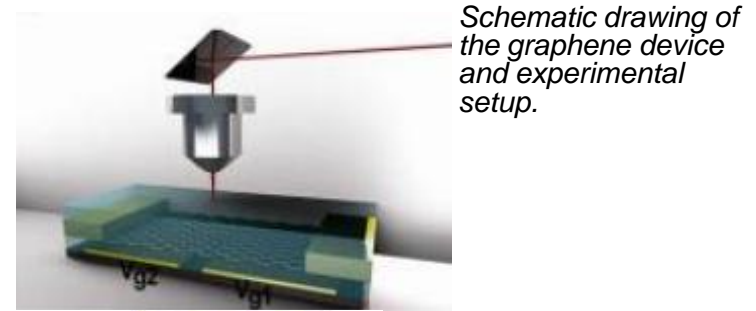


SEM image of integrated crossbar devices on top of CMOS circuit

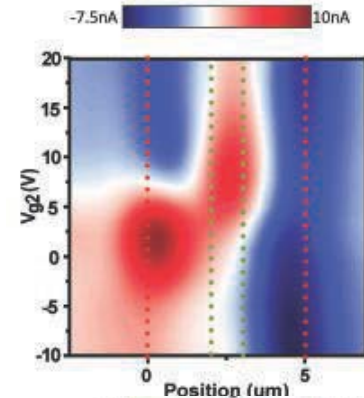
Investigation of graphene photocurrent generation project

The purpose of this project is to study graphene photocurrent generation mechanisms at graphene-metal junction and graphene pn junction. The studied graphene device includes a pair of split bottom gates, which can electrostatically tune the graphene-metal junction, and form the p-n junction in between. By scanning the focused laser spot on the graphene device, we could spatially investigate the gate dependence of photoresponse. It was observed that the photoresponse of graphene device excited by femtosecond pulse laser showed unusual gate dependence compared with continuous wave laser excitation. This unusual photoresponse is due to none equilibrium hot carrier generation, which can be confirmed by our laser power dependence studies. In addition, hot carrier extraction is found to be most efficient when operating the graphene device near the Dirac point, which also agrees with the theoretical predictions. These fundamental observations would open the door for developing graphene based hot carrier optoelectronics.

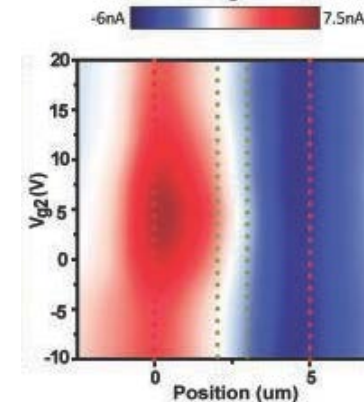
Chang-Hua Liu, Nanditha M. Dissanayake, Seunghyun Lee, Kyunghoon Lee, and Zhaohui Zhong, University of Michigan
Work performed at the Lurie Nanofabrication Facility



Schematic drawing of the graphene device and experimental setup.



Gate-dependent photocurrent map under CW laser excitation



Gate-dependent photocurrent map under Pulse laser excitation

“Evidence for Extraction of Photoexcited Hot Carriers from Graphene”, Accepted by *ACS Nano* (2012)

STigma Free Diagnostics, LLC

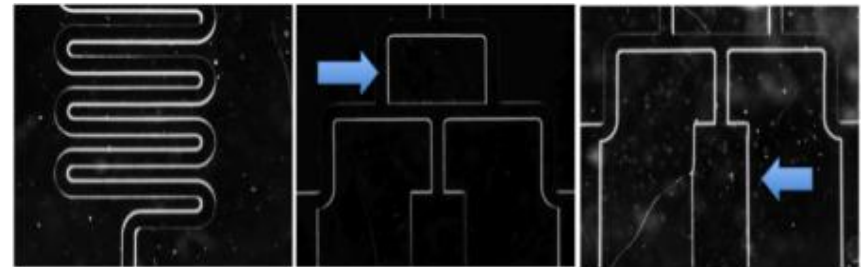
STigma Free Diagnostics, LLC develops point-of-care (POC) diagnostic devices for small clinical use utilizing novel microfluidic and BioMEMS technology to ensure quick, efficient, and accurate results. Our diagnostic device, will enable greater access to testing for the most common curable sexually transmitted infections (STIs) - Chlamydia, gonorrhea, and Trichomoniasis.

Devices integrate microfluidics and micro-fabricated cantilevers into a receptacle cup for gravity-driven, user-friendly operation. Urine samples from patients are collected in the receptacle and drive the flow into microfluidic channels for homogenization, multiplexing and detection. High sensitivity testing is achieved through real-time protein and cell-fragment sensing using in-channel cantilevers.

Jeremy Holzwarth, Patrick Ingram, Sasha Cai, Leshar-Perez, Ramashwar Rao, and Josh White, University of Michigan
Work performed at the Lurie Nanofabrication Facility



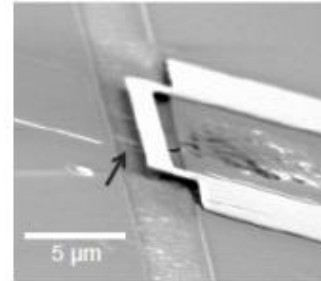
Microfabricated PDMS prototype for sample processing and handling



Microfluidic subcomponents for homogenization, multiplexing, and detection.

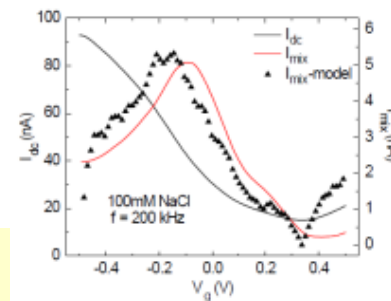
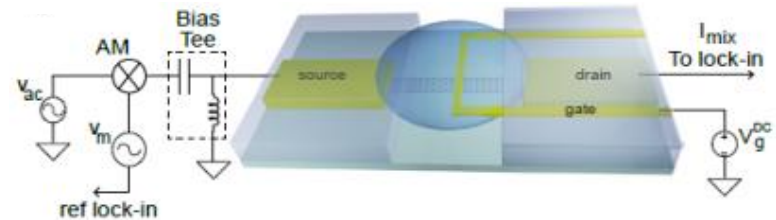
Detection beyond Debye screening length in high frequency nanoelectronic biosensor

The motivation for this work is to overcome the fundamental ionic screening effect in high background ionic solutions where the mobile ions screen off the biomolecules, thereby reducing the biosensor sensitivity. We fabricate carbon nanotube (CNT) transistors as our biosensor. The CNTs are grown on a LPCVD nitride-on-oxide silicon wafer in a CVD furnace. Ti/Au is deposited for source-drain contacts. Cr/Au is deposited for top gate structure. To suspend the top gate as shown in figure, a 1:20 BHF wet etch is carried out. We operate this CNT transistor as a frequency mixer. The nonlinear mixing between alternation current excitation filed and molecular dipole field can generate mixing current sensitive to surface bound biomolecules.



An SEM image of suspended top gate CNT FET

Device measurement schematic for frequency mixing

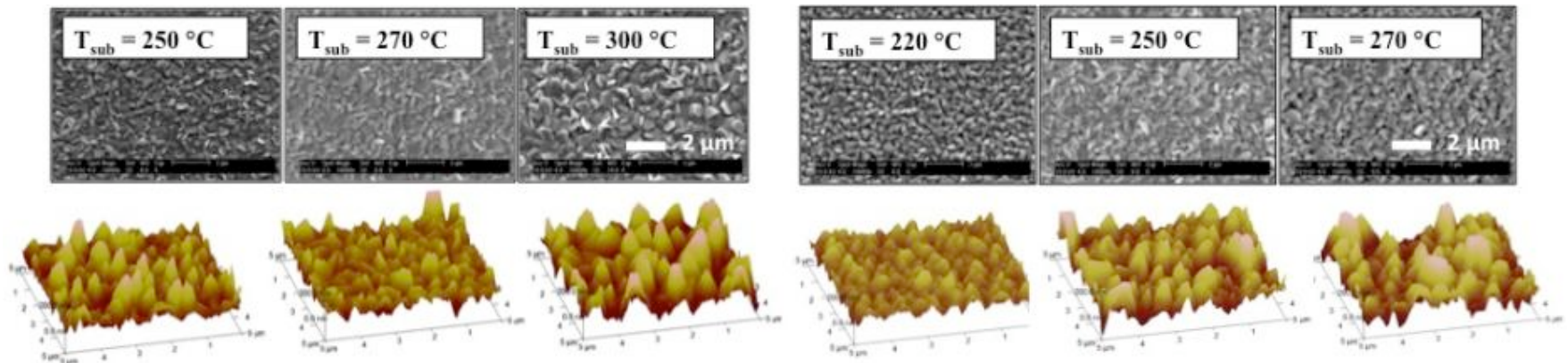


Typical frequency mixing I-V response

Girish S Kulkarni and Zhaohui Zhong, University of Michigan
Work performed at the Lurie Nanofabrication Facility

Bismuth Telluride and Antimony Telluride Based Co-Evaporated Thermoelectric Thin Films

Solid-state thermoelectric generators are useful for energy harvesting in many microsystems such as implantable devices and sensor network applications. Thermoelectric (TE) materials are capable of directly converting a temperature difference to electrical energy and vice versa. Bismuth/antimony telluride compounds are the best room-temperature TE materials that can be fabricated as *n/p*-type thin films. High-quality TE thin films with good adhesion and uniformity are needed on a variety of substrates in order to provide design flexibility for thermoelectric microsystems. However, for each substrate optimization is needed of film adhesion, stress, and co-evaporation conditions for high-TE figure of merits, namely the substrate temperature (T_{sub}) and flux ratio. Here we study the effect of substrate on TE thin film electrical and thermal properties, morphology, crystal structure, grain size, surface roughness and composition.



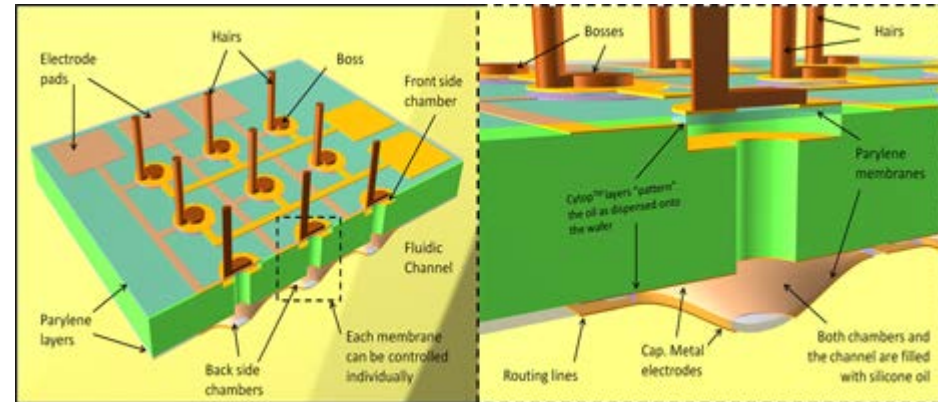
SEM and AFM images showing top surface of bismuth telluride (left) and antimony telluride (right) thermoelectric thin films co-evaporated at different substrate temperatures on oxide.

Niloufar Ghafouri, Rebecca L. Peterson, Ctirad Uher and Khalil Najafi, University of Michigan
Work performed in part at the Lurie Nanofabrication Facility

Micro-Hydraulic Structure for High Performance Bio-Mimetic Hair-like Air Flow Sensor Arrays

Biological hair is characterized by arrays of high aspect ratio, three-dimensional structures, with mechanical amplification of movement. In this project we develop a novel bio-mimetic micro-hydraulic structure consisting of two chambers on the front and back side of a silicon wafer which are connected through a channel and filled with an incompressible liquid. Utilizing the area ratio between the chambers, we can achieve amplification of either force or displacement. A pair of electrodes on the back side can be used for electrostatic actuation (i.e. to provide internal pressure) or capacitive sensing.

We build an air flow sensor by attaching a tall hair-like cilia to the top membrane, which converts the drag force from surrounding fluid/air flow into an applied pressure on the hydraulic membrane. The micro-hydraulic architecture allows for sensors with record dynamic range. Electrostatic sensing enables low-power operation. The resulting air flow sensor detects flow speeds ranging from < 0.1 to > 10 m.s⁻¹.



Array of bio-mimetic MEMS hair-like structures for air-flow sensing (left). Schematic of micro-hydraulic chambers and channel, with attached cilia (right).

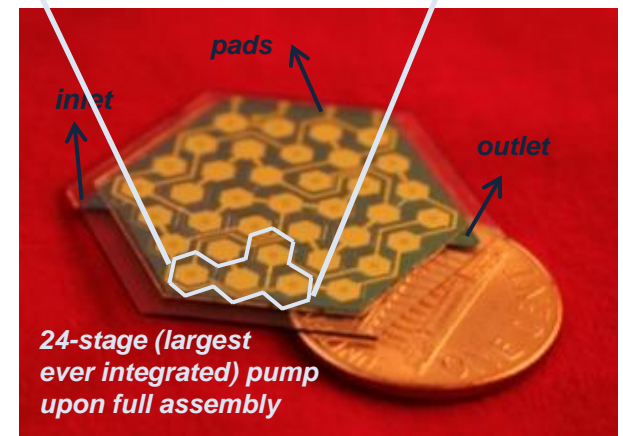
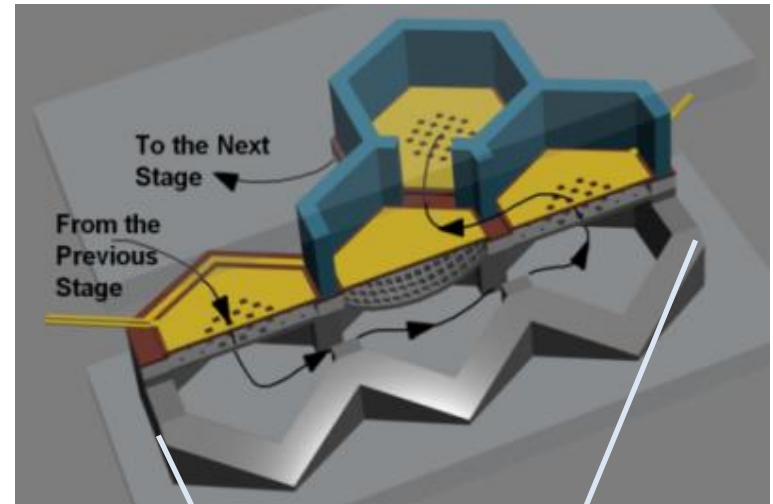


Assembled air flow sensor, including attached cilia

Mahdi Sadeghi, Rebecca L. Peterson and Khalil Najafi, University of Michigan
Work performed in part at the Lurie Nanofabrication Facility.

A Scalable Modular Multi-Stage Peristaltic Electrostatic Gas Micropump

Gas micropumps are needed in many emerging applications, including gas chromatography and mass spectrometers. Previous gas micropumps exhibit limited capabilities due to use of bulky actuators, often were slow or power/size inefficient, and lacked scaling/integration capabilities. This project seeks to develop a MEMS pump that can be used as the roughing pump in a three-part micro-scale vacuum system. The pump utilizes the electrostatic peristaltic architecture previously reported by our group, but with modified device architecture, new fabrication technology and modular assembly/packaging. The modular fabrication technology has a final process yield of 90% with a high throughput and high control over critical design parameters (<5% error). Moreover, the device total size is 60% smaller than the old design, due to the use of a novel honeycomb planar architecture. Under preliminary testing, the microfabricated 24-stage pump successfully produced a flow rate of 0.36 sccm and a pressure accumulation of ~500 Pa at 22 kHz.

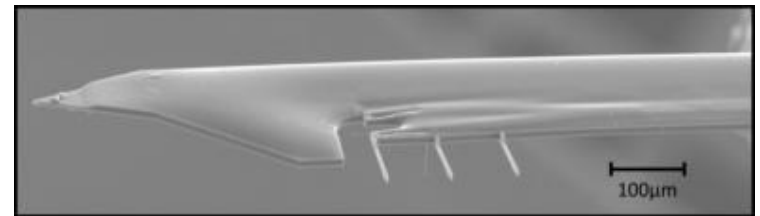
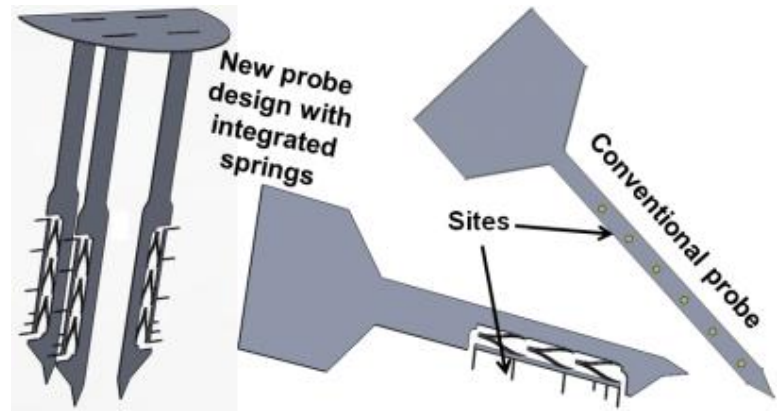


Ali Besharatian, Karthik Kumar, Rebecca L. Peterson, Luis P. Bernal, and Khalil Najafi, University of Michigan
Work performed in part at the Lurie Nanofabrication Facility

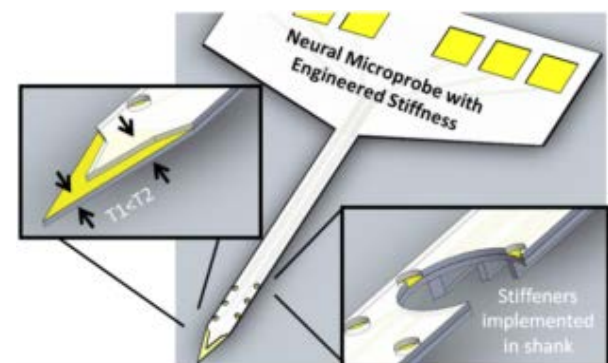
Illustration of the smallest pumping unit, consisting of two stages, showing the detailed layout of each chamber and fluidic paths (top), and photo of a fabricated and packaged 24-stage device on a U.S. penny (bottom).

Silicon and Parylene Intracortical Neural Probes for Chronically-Stable Recording

Next-generation neuroprostheses assist functional motor control, aid the visually impaired or those suffering loss of hearing. We have developed two neural probe technologies to allow mitigation of the immune response to implantation to enable long-term probe use. The probes consist of silicon or parylene millimeter-long needle-like shanks hosting multiple microelectrodes. The silicon technology (at right) supports individual electrodes that are placed at the end of very fine and flexible needle extensions to the shank that are deployed after implantation. The sites then act like satellites, floating almost freely inside the brain tissue. *The parylene approach (at left) addresses a tradeoff between designing a shank large enough such that it can be reliably implanted, and the increase in tissue damage with size of the shank. The developed process technologies allow forming sharp tips, and strategic design of the shank increases its mechanical robustness without significantly increasing its size.*



Silicon neural probes with integrated springs that displace sites off the shank after implantation using a bio-dissolvable coating.

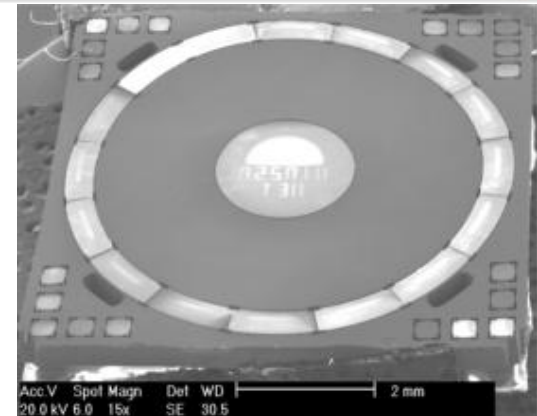
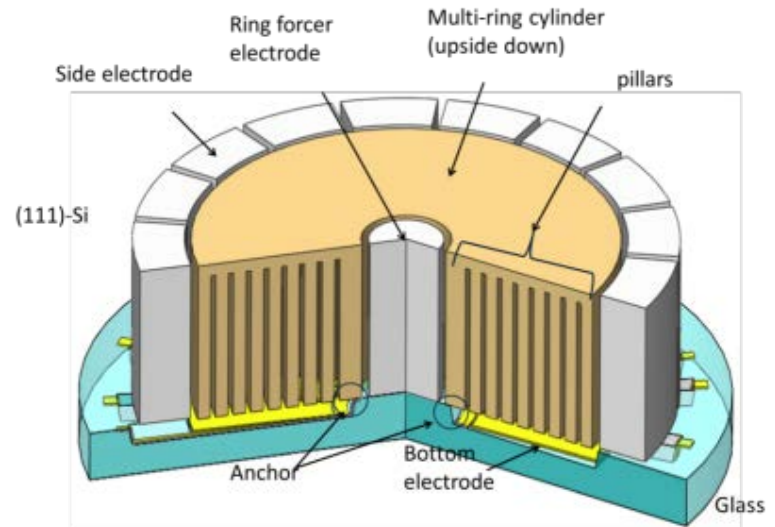


Parylene neural probes with integrated stiffeners and sharp tips for improved insertion.

Daniel Egert, Rebecca L. Peterson and Khalil Najafi,
University of Michigan
Work performed in part at the Lurie Nanofabrication Facility

High Performance Micromachined Rate-Integrating Gyroscope

A novel axisymmetric single-crystal-silicon rate-integrating gyroscope (RIG), called the Cylindrical Rate-Integrating Gyro (CING), is developed. The RIG offers advantages of absolute angular readout and larger bandwidth full-scale range than the conventional MEMS rate gyroscope. The CING offers advantages of self-alignment of anchor resonator, and electrodes, and a large wineglass-to-parasitic mode frequency ratio ($f_{\text{parasitic}}/f_{\text{WG}} > 1.7$). The gyro is made of (111) Si using the Si-on-glass (SOG) process. Two versions of the CING operate at 18kHz and 3kHz. The 3kHz CING has a Q of $\sim 100,000$ at $< 5\text{mTorr}$, an original frequency mismatch (Δf) of 7Hz, and a damping mismatch ($\Delta 1/\tau$, $\tau = 2Q/\omega$) of 10mHz. Using digital interface circuitry under exact mode matching ($\Delta f < 20\text{mHz}$), the CING measures an angle random walk of $0.09^\circ / \sqrt{\text{Hr}}$, a bias stability of $129^\circ / \text{Hr}$, and an offset drift of $1^\circ / \text{s/Hr}$ in the rate sensing mode. In the rate-integrating mode, the CING measures a constant angular gain (A_g) (~ 0.01) over mode mismatch of 20~80mHz for several days without accurate temperature control.



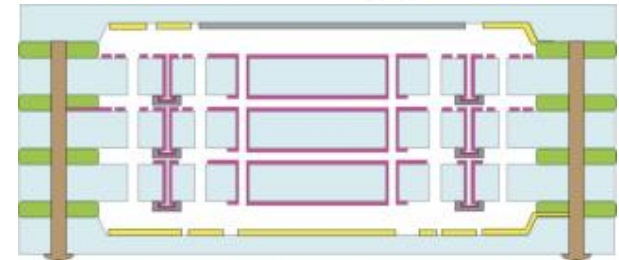
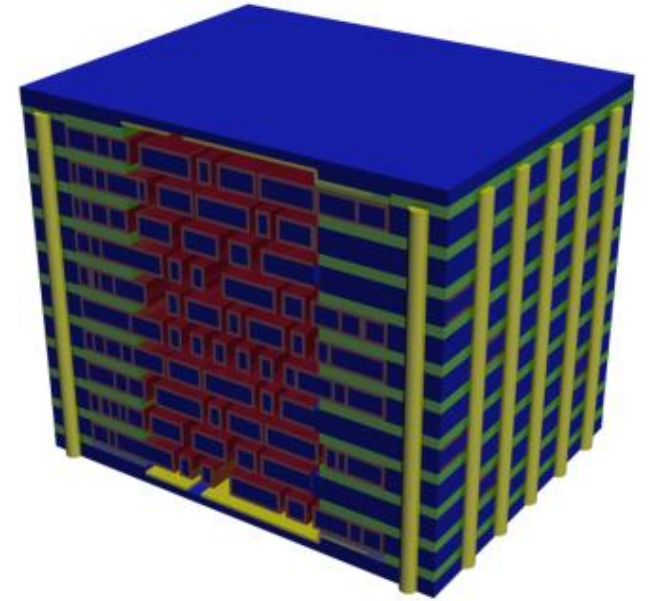
Jae Yoong Cho, Jeffrey A. Gregory, and Khalil Najafi, University of Michigan Work performed in part at the Lurie Nanofabrication Facility

Top: architecture of the Cylindrical Rate-Integrating Gyroscope (CING), Bottom: SEM picture of the fabricated CING using Si-on-glass (SOG) process

Package of Silica for Timing & Inertial Measurement

Timing and inertial measurement units (TIMU) consist of a package of accelerometers and gyroscopes along with a clock. They are used to detect the change in position of an object relative to a previously known position through dead reckoning. In this project, we build an extremely compact, integrated TIMU using a multi-layer stack of fused silica for the devices and the packaging. By vertically stacking multiple device layers, we greatly reduce the total footprint of our finished device. This design also allows for integration of vertical sensors.

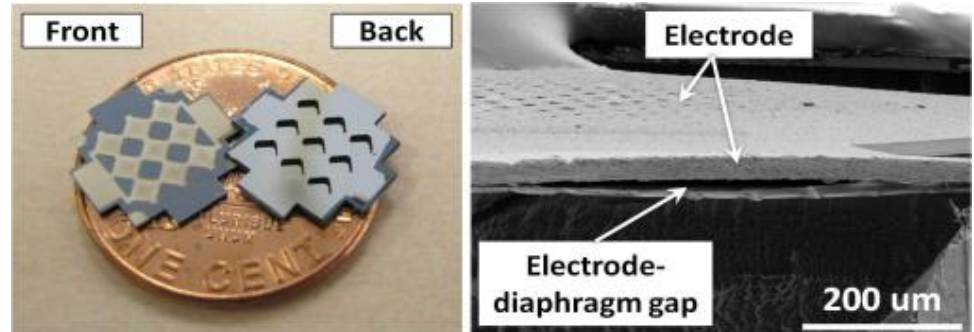
Zongliang Cao, Jialiang Yan, Yi Yuan, Jae Yoong Cho, Guohong He, Rebecca L. Peterson, and Khalil Najafi, University of Michigan
Work performed in part at the Lurie Nanofabrication Facility



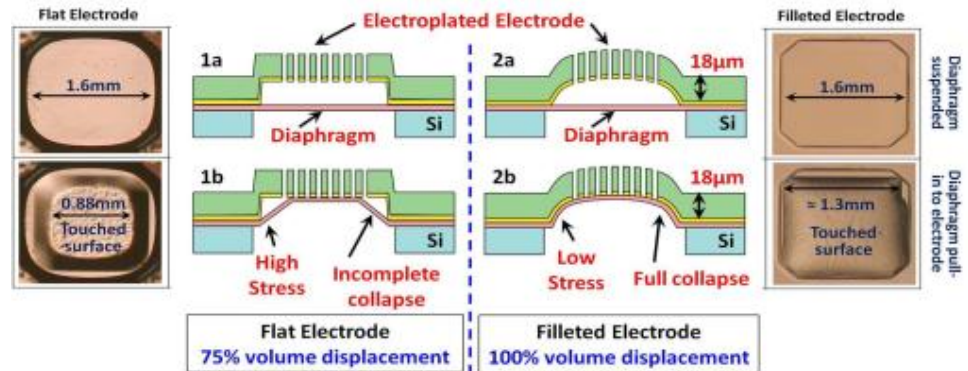
Schematic diagram and cross-sectional view of TIMU package

High-Frequency Large-Deflection Electrostatic Diaphragm Actuators with Maximized Volume Displacement

Many MEMS applications such as micro propulsion, micro gas pumping, microchip cooling and micro speaker require actuators with large volume displacement at high frequency. For high frequency actuation, highly-stressed thin diaphragms ($\sim 74\text{MPa}$) with a large gap ($>8\mu\text{m}$) between the diaphragm and perforated electrode are fabricated with a simple 3-mask process. The fabrication process allows easy manipulation of the size and shape of the electrode; filleted electrodes are made through a reflow process. The filleted electrode diaphragm hugs the electrode profile, displacing 100% of the air gap volume compared to the flat electrode diaphragm which displaces only 75% of the air gap volume. The filleted electrode also can actuate at a lower pull-in voltage than the flat electrode, and actuates more reliably.



Fabricated device with an array of nine electrostatic actuators and SEM of flat electrode cross section.

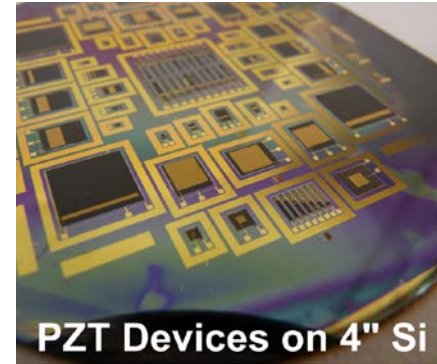


Filleted electrode shape maximizes volume displacement by “hugging” of electrode to membrane.

Seow Yuen Yee, Rebecca L. Peterson, Luis P. Bernal, and Khalil Najafi, University of Michigan
Work performed in part at the Lurie Nanofabrication Facility

Integration of Bulk Piezoelectrics with MEMS

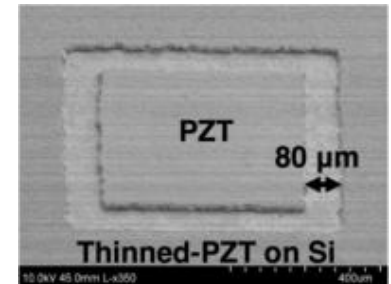
Bulk piezoelectric ceramics provide greater electro-mechanical coupling than deposited piezoelectric thin films, which is highly desirable in many MEMS applications including high-force actuators and micro-power scavengers. We have developed a new CMOS-compatible wafer-level process to obtain thin films of bulk piezoelectric materials on silicon. The process involves low-temperature aligned solder bonding of bulk piezoelectric substrates on silicon, mechanical thinning to obtain the desired PZT (lead zirconate titanate) thickness, micro-machining of PZT films via dicing saw, laser ablation, and wet-etching.



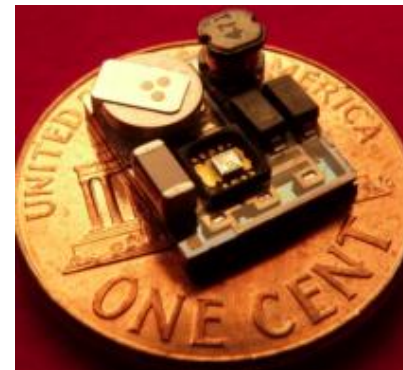
Fabricated PZT cantilever beam and diaphragm actuators, and vibration energy harvesters on a 4" silicon wafer.

PZT Devices on 4" Si

SEM image of solder bonded, thinned, and wet-etch patterned PZT film on a 4-inch silicon substrate.



Thinned-PZT on Si

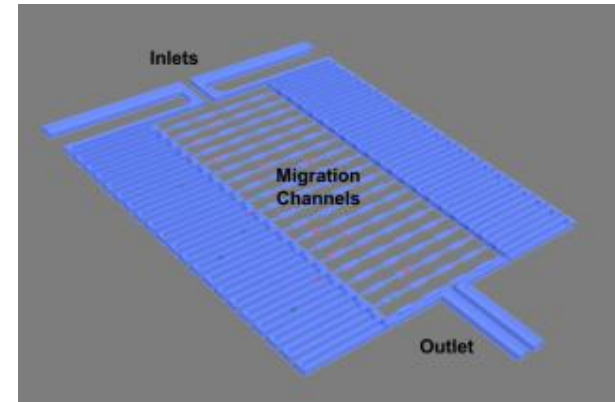


A packaged thinned-PZT vibration energy harvester integrated with its power management IC and surface mount circuit components.

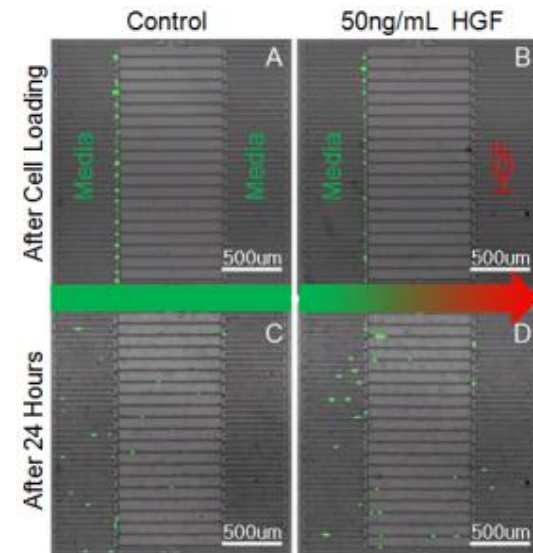
Ethem Erkan Aktakka, Rebecca L. Peterson, and Khalil Najafi
University of Michigan
Work performed in part at the Lurie Nanofabrication Facility

Single Cell Migration Project

The purpose of the Retinal Implant Project is to monitor chemotaxis at single cell resolution. The single cell migration chip uses a cell capturing scheme based on the difference in hydrodynamic resistance between flow paths and cellular valving. A high capture rate over 94% is achieved by optimizing the geometry of capture sites and the length of serpentine structures. After capturing, cell migration experiments induced by chemotaxis were carried out using the fabricated platform, and the behavior of each single cell was successfully traced.



Schematics of single cell migration project

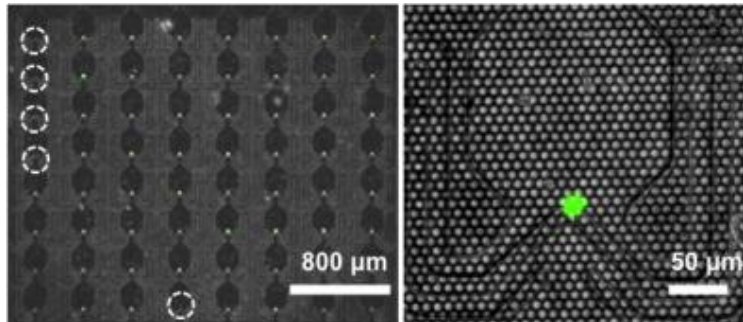


Cell migration behavior with the attraction of HGF

Yu-Chih Chen and Euisik Yoon, University of Michigan
Work performed at the Lurie Nanofabrication Facility

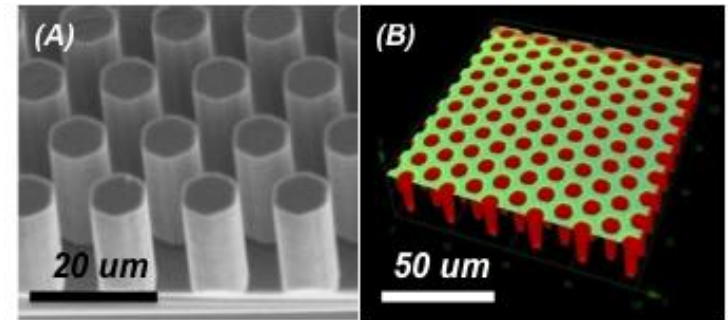
Topographically Patterned PDMS for Microfluidic Sphere Culture

In this project we have focused on non-adherent single cell derived sphere growth on hydrophobic surfaces, formed in polydimethylsiloxane (PDMS). Growing cancer spheroids from single cells allows identification of tumor initiating subsets, and high throughput assays of these kind are beneficial for oncologists studying these phenomena. The surfaces have been fabricated and the hydrophobicity characterized. Various cell types have been grown on the surfaces to characterize adhesion. Cancer spheroids have been grown in suspension starting from single cancer stem cells both in macro-scale wells and in integrated microfluidic microwells.

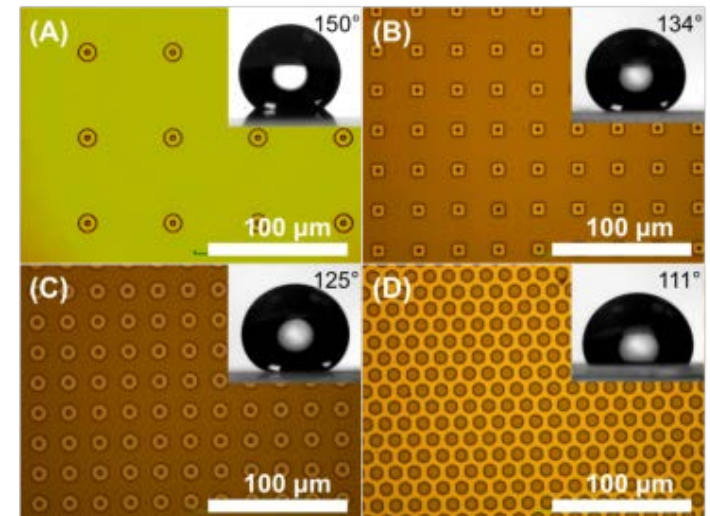


Single cell capture microfluidic channels were integrated onto patterned PDMS surfaces for high throughput single cell derived sphere growth. SUM159 cells were captured and grown for 14 days. White circles indicate where no cell was captured

Patrick Ingram, Maesoon Im, Sean McDermott, Max Wicha, and Euisik Yoon, University of Michigan
Work performed at the Lurie Nanofabrication Facility



(A) SEM image of DRIE etched honeycomb pattern silicon. (B) Confocal laser microscopy images of the fabricated PDMS honeycombs



Optical images of 10 μ L droplets on hydrophobic surfaces with droplet contact angles and the corresponding patterns of masks used in fabrication.

Evaluating Nanoparticulate Photosensitizer Efficacy Utilizing Microfluidic Chips

In this project we are utilizing microfluidic chips for evaluating the new nanoparticulate photosensitizer's efficacy in photodynamic therapy (PDT). Developing new generation of nanoparticulate photosensitizers has become a major research focus in PDT. Microfluidic technologies have demonstrated powerful screening capability for general PDTs, but more customized features are required for nanodrugs such as size changes, incubation time and selective targeting capability. To meet these requirements, we developed microfluidic chips specifically fit for evaluating tumor-targeted nanoparticulate (NP) photosensitizers' efficacy in PDT treatment. Major features of our approach include: (1) automatic NP concentration gradient generation with modified microfluidic gradient generator, (2) temporal control of drug feeding for evaluating NP drug delivery to cancer cells; and (3) simultaneous screening of multiple cell types for targeted delivery of functionalized NPs.

X. Lou, G. Kim, Y.-E. L. Koo, R. Kopelman, E. Yoon,
University of Michigan
Work performed at the Lurie Nanofabrication Facility

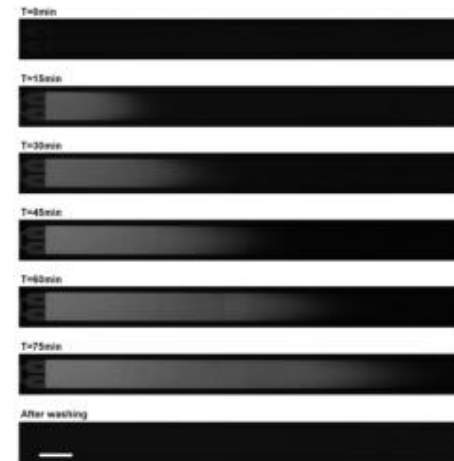


Figure 1. Microfluidic incubation time gradient generation via controlled NP solution feeding.

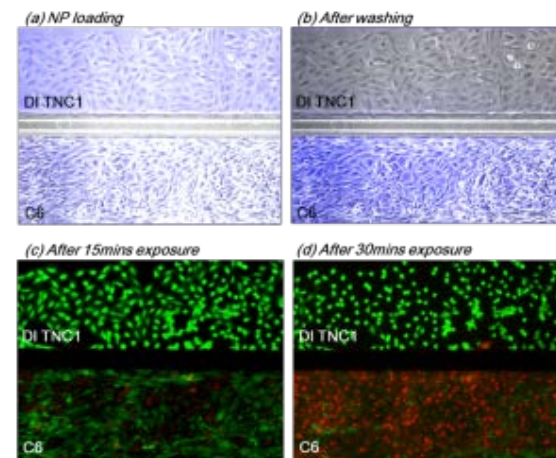


Figure 2. Nanoparticle's selective targeting on cancer cells in PDT treatment.

BioBolt: A Minimally-Invasive Neural Interface for Wireless Epidural Recording by Intra-Skin Communication

Recent technology progresses in CMOS and MEMS technologies have enhanced monitoring capability of neural activities for diagnosis of neural disorders, brain-machine interface and prosthetic applications. Recently, epidural recording gains its attention as an optimal solution for balanced signal fidelity and safety. In this project, we report a bolt-shape Minimally-Invasive Neural Interface, BioBolt, which have (1) Low-Power Analog Front-Ends, (2) Epidural Record Capability in order to minimize any infection and tissue reaction, and (3) Intra-Skin Communication for low-power data transmission. The proposed bolt-shape structure (Fig. 1.) allows simple operation procedures during implantation and removal. The 16-channel analog front-end has been implemented in $0.25\mu\text{m}$ and consumes $365\mu\text{W}$ with $3.2\times 0.9\text{mm}^2$. With the proposed pseudo-floating body transistor, we could achieve the measured input-referred noise of $5.62\mu\text{Vrms}$ ($\text{NEF}=1.69$). The proposed ADC with time-delayed control unit consumes 87.41nW (20.1fJ/c-s) at 31.25kS/s . As shown in Fig. 2 (a), we also propose a low-power wireless ISCOM with charge balanced current driver using skin as a signal pathway

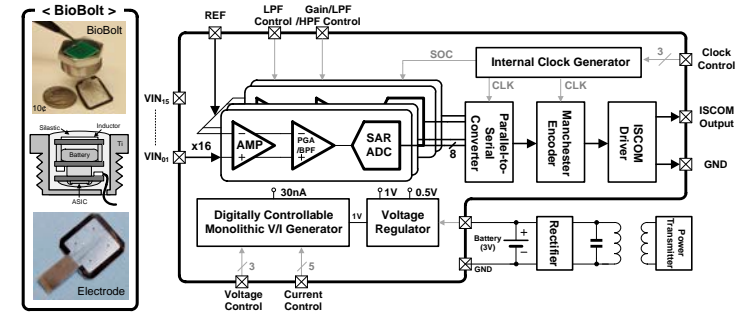


Figure 1: Overall architecture of BioBolt and block diagram

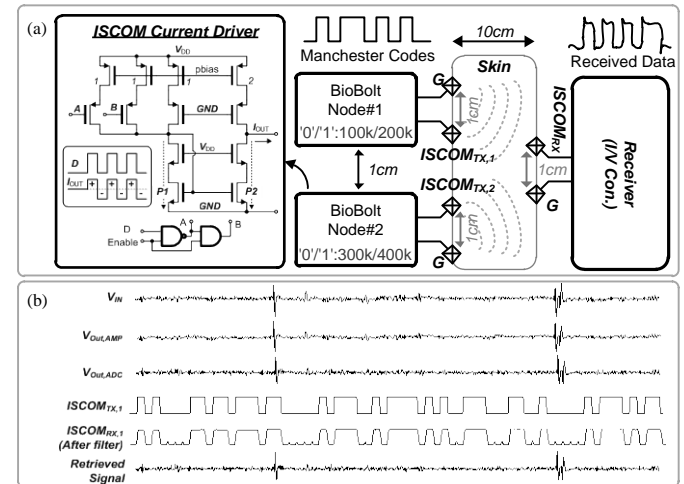
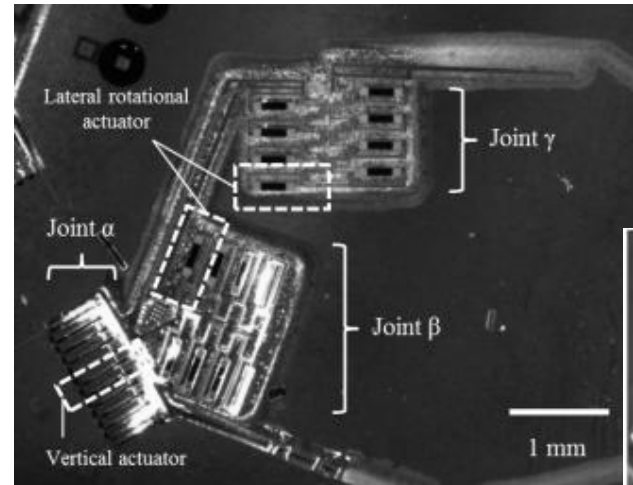


Fig. 2: (a) Conceptual diagram of ISCOM with its current driver and (b) the measured neural signal chain through preamplifier, ADC, ISCOM (skin) and retrieved signal

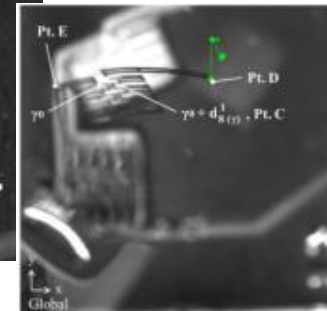
Sun-II Chang, Khaled Al-Ashmouny, and E. Yoon, University of Michigan
Work performed at the Lurie Nanofabrication Facility

Thin-film Piezoelectric Micro-robots

The purpose of this micro-robotics project is to demonstrate highly-mobile millimeter-scale terrestrial robots. Thin-film lead-zirconate-titanate (PZT) is used as the active material in prototype robots, due to high work density at relatively low voltages. In collaboration with the U.S. Army Research Laboratory, novel techniques for integrating complex silicon micro-structures with the PZT films have been developed. Prototype robots are being integrated with ultra-low-power control strategies to move towards autonomous, high-speed walking gaits.

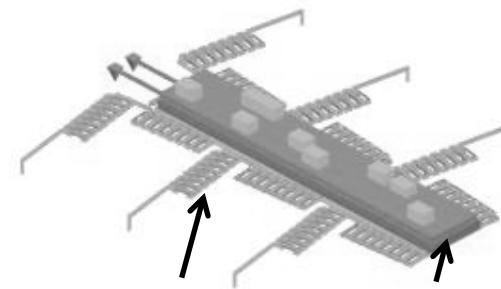


Prototype multi-degree-of-freedom robot leg.



Released robot leg during static displacement testing.

Concept drawing of 10mm long micro-robot based on mDoF legs



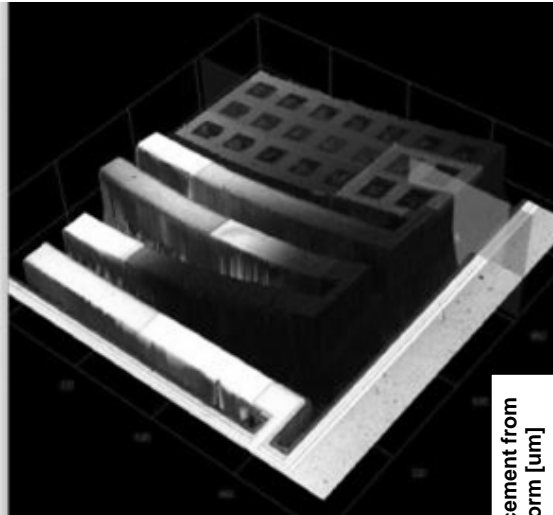
Thin-film piezoelectric actuator array

Power and control circuitry

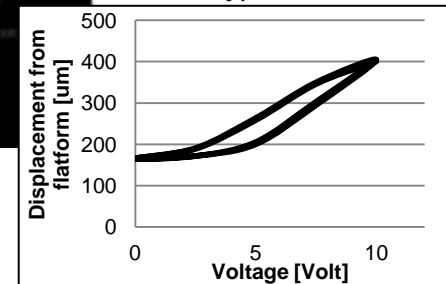
Kenn Oldham, University of Michigan
Work performed in part at the Lurie Nanofabrication

Endoscopic Dual-Axes Confocal Microscopy

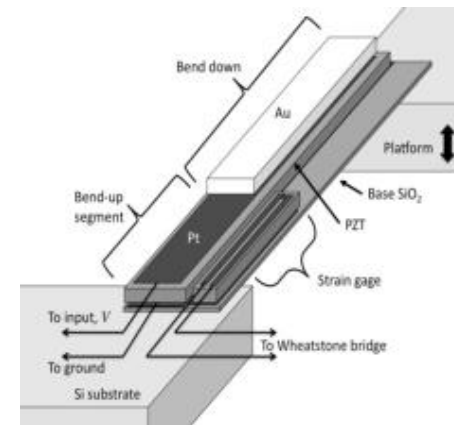
Microactuators are being developed for the purpose of dual-axes confocal microscopy from an endoscope-compatible instrument. The primary micro-actuators under development are thin-film lead-zirconate-titanate (PZT) vertical translational actuators, with stroke length > 400 microns at 15 V and bandwidth > 50 Hz (unloaded). These actuators will enable cross-sectional, dual-axes confocal imaging of in-vivo tissue from an instrument < 5 mm in diameter, with imaging depths potentially as large as 500 microns. Actuators integrating x- and y-axis scanning capabilities with into-tissue motion have also recently been demonstrated.



Characterization of into-tissue scanning actuator performance by optical profilometry (left) and associated displacement versus voltage (below); 250 μm @ 10 V, 400 μm @ 15 V typical.



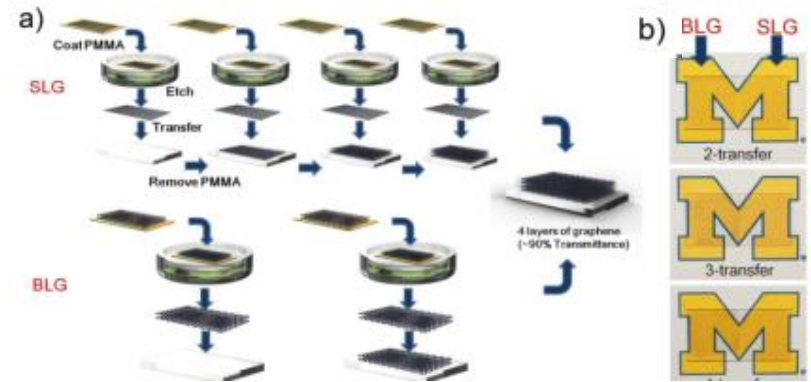
Kenn Oldham, Katsuo Kurabayashi, and Thomas D. Wang,
University of Michigan
Work performed in part at the Lurie Nanofabrication Facility



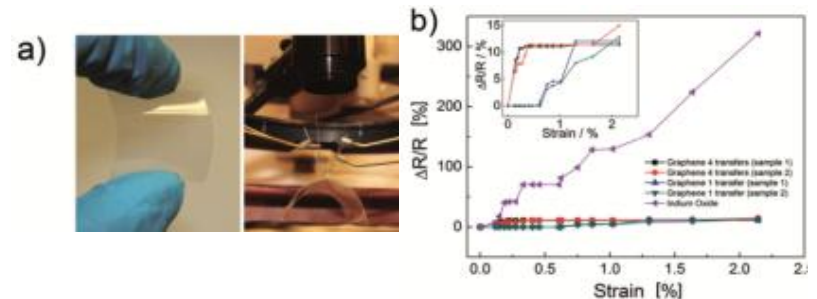
Schematic view of thin-film piezoelectric actuator structure.

Homogeneous Bilayer Graphene Film Based Flexible Transparent Conductor

Graphene is considered a promising candidate to replace conventional transparent conductors due to its low opacity, high carrier mobility and flexible structure. Multi-layer graphene or stacked single layer graphenes have been investigated in the past but both have their drawbacks. The uniformity of multi-layer graphene is still questionable, and single layer graphene stacks require many transfer processes to achieve sufficiently low sheet resistance. In this work, bilayer graphene film grown with low pressure chemical vapor deposition was used as a transparent conductor for the first time. The technique was demonstrated to be highly efficient in fabricating a conductive and uniform transparent conductor compared to multi-layer or single layer graphene. Four transfers of bilayer graphene yielded a transparent conducting film with a sheet resistance of $180 \Omega/\square$ at a transmittance of 83%. In addition, bilayer graphene films transferred onto plastic substrate showed remarkable robustness against bending, with sheet resistance change less than 15% at 2.14% strain, a 20-fold improvement over commercial indium oxide films.



(a) Schematic comparison of SLG method and BLG method to synthesize 4 layers of graphene stack to achieve lower sheet resistance. (b) optical comparison of SLG and BLG graphene stacks on glass substrate for 1,2,3,4 transfers.

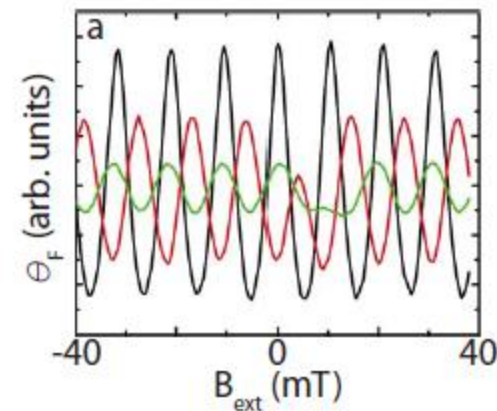
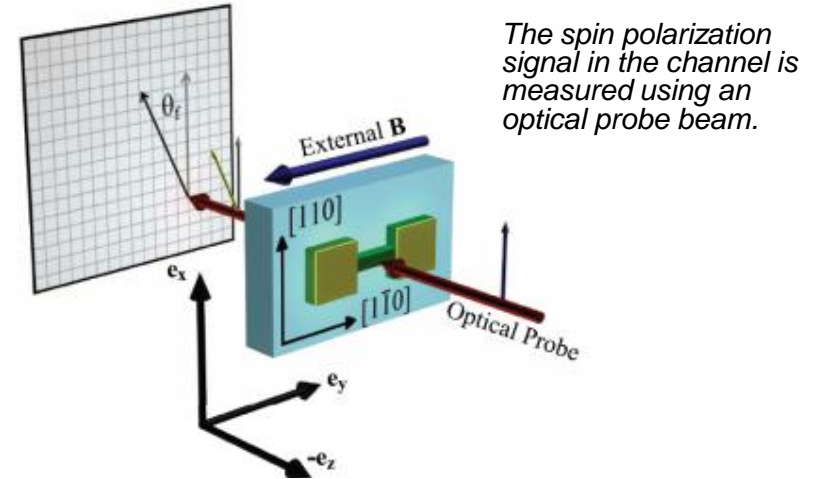


(a) Photographs of graphene film on flexed PET substrate(left) and measurement setup of strained substrates (right). (b) Variation in resistance of stacked BLG films and indium oxide films on 200µm thick PET substrate as a function of strain values.

Seunghyun Lee, Kyunghoon Lee, Chang-Hua Liu and Zhaohui Zhong,
University of Michigan
Work performed at the Lurie Nanofabrication Facility

Electrically-generated Spin-orbit Effects In Semiconductors

The purpose of investigating electrically-generated spin-orbit effects in semiconductors is to demonstrate the manipulation of spin polarization using local, electric fields. At LNF, we have fabricated electrically-contacted channels that enable us to apply voltages to change the net drift momentum of carriers in order to study spin-orbit effects and electrically-generated spin polarization. The samples consist of an indium gallium arsenide epilayer grown on a gallium arsenide substrate. A mesa is etched in order to define the channel and then AuGe ohmic contacts are deposited using electron-beam evaporation.



As the voltage applied to the channel is increased from 0 V (black) to 1 V (red) to 2 V (green), increasing spin-orbit effects alter the cosinusoidal signal.

Vanessa Sih, University of Michigan
Work performed at the Lurie Nanofabrication Facility

Interactions of AlGaN/GaN High Electron Mobility Transistors with Surface Acoustic Waves

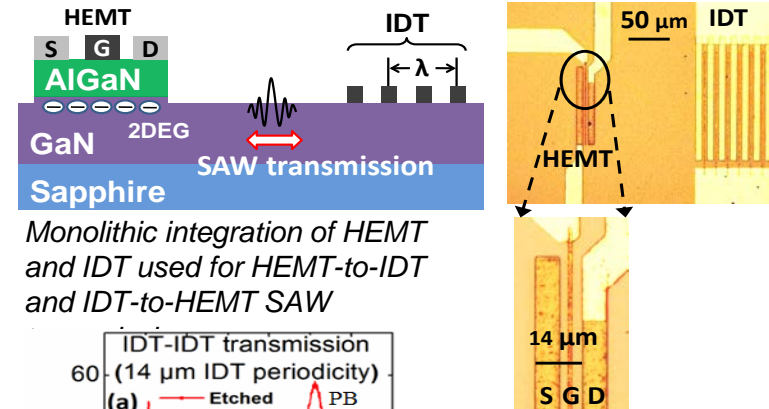
DESCRIPTION AND MOTIVATION

- We have studied the direct interaction of SAWs and HEMTs, i.e., the emission and detection of SAWs by a HEMT that is modulated in the various regimes of transistor operation.
- SAWs emitted by a HEMT could provide a means to nondestructively sample the degradation of its epitaxy and 2DEG in real time
- SAWs incident on a HEMT could dynamically strain modulate the HEMT over short times, potentially without the degradation effects that often occur when such strain is incorporated through lattice mismatch.
- HEMT-based SAW detectors could provide a means for direct electrical amplification of SAW signals.

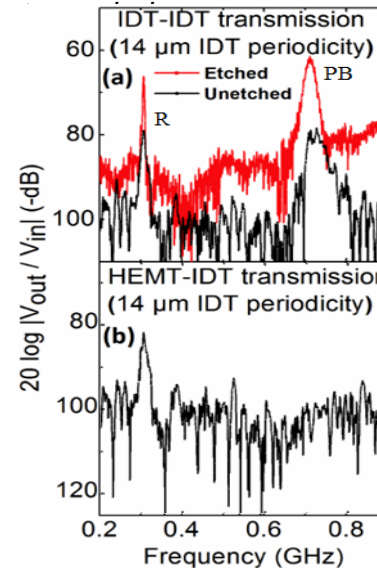
RESULTS

- We have detected SAWs emitted by HEMTs using integrated IDTs and measured their bias dependences.
- We have demonstrated the detection of SAWs by HEMTs and shown how SAWs emitted by an integrated IDT can be used to provide dynamic strain modulation of a HEMT.
- Using an optical reflectance method, we showed that various resonant modes with different polarization and penetration depths are emitted by a HEMT under normal RF operation.
- We demonstrated that different DC bias points can be used to selectively emit certain SAW modes.

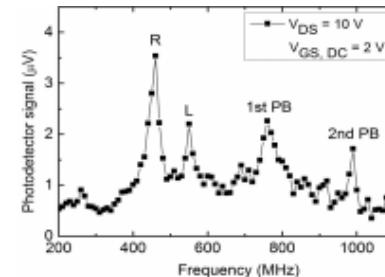
L. Shao, M. Zhang, A. Banerjee, P. Bhattacharya and K. P. Pipe,
University of Michigan
Work performed at the Lurie Nanofabrication Facility



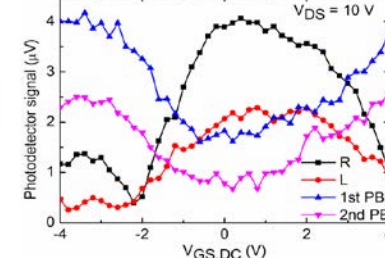
Monolithic integration of HEMT and IDT used for HEMT-to-IDT and IDT-to-HEMT SAW



Rayleigh SAW peak seen in IDT-IDT pairs is measured in HEMT-IDT pairs, confirming SAW emission by HEMT



HEMT SAW spectrum

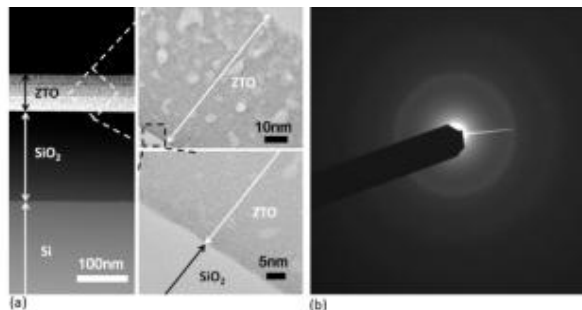


Electrical control of emitted SAW modes

Solution-Processed Inorganic Thin Film Transistors

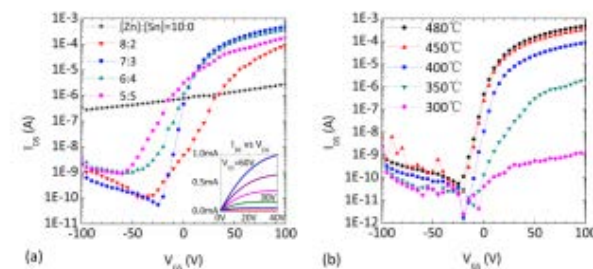
Solution-processed zinc tin oxide (ZTO) thin film transistors are ideal for display backplanes and flexible electronics, owing to their relatively high mobility, transparency, stability and scalability. ZTO layers are fabricated by spin-coating a precursor ink onto SiO₂/Si substrate, followed by annealing. The annealing temperature and the stoichiometric ratio of Zn to Sn precursors in the ink are found to affect transistor performance.

Cryogenic current-voltage (I-V) measurements from 77K to 300K indicate percolation-like conduction with a pinned Fermi level and thermal activation of carriers into mobile states. The position and concentration of the donor-like states and sub-gap density of states also depend on process conditions. The best solution-processed devices are equivalent to those made by sputter deposition.

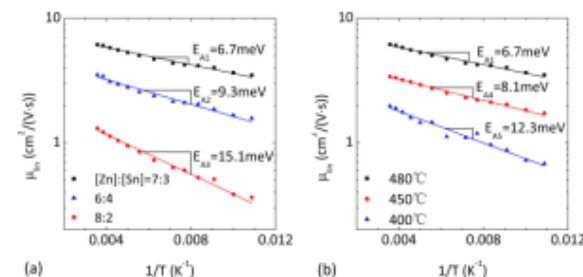


Amorphous ZTO layer, as shown by transmission electron microscopy and selected area electron diffraction taken at the University of Michigan Electron Microbeam Analysis Laboratory (EMAL)

ZTO transistor transfer I-V curves for (a) different Zn to Sn ink ratio & (b) different annealing temperature



Solution-processed ZTO mobility vs. 1/T, with Arrhenius energy fits lines for (a) different Zn to Sn ink ratio & (b) different annealing temperature

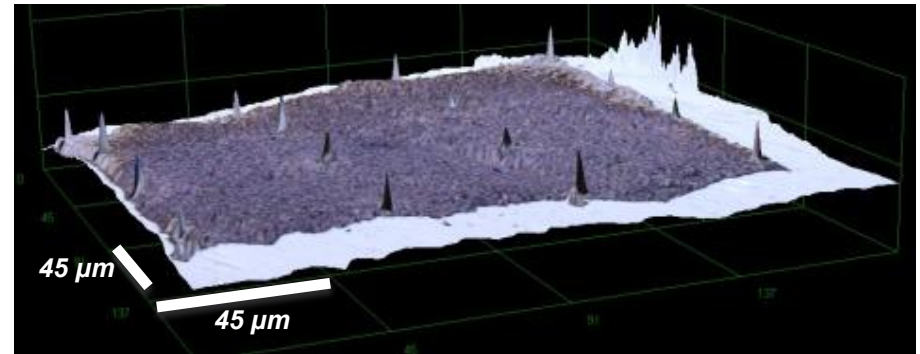


Figures from Hu and Peterson, JMR vol 27, 2012.

Wenbing Hu and Dr. Becky Peterson, University of Michigan
Work performed in part at the Lurie Nanofabrication Facility

Tensile Sample Surface Topography Mapping

Scanning Electron Microscopy combined with Digital Image Correlation (SEM-DIC) is a powerful tool for investigating deformation at the scale of a material's microstructure. However it can only measure in-plane deformation. The Olympus LEXT Interferometer in the Lurie Nanofabrication Facility allows us to measure the out of plane displacements that occurs during tensile tests. The data obtained from the microscope allows for identification of active slip systems and quantification of dilatatory strains and displacements that appear in the DIC data due to out of plane motion.



A surface topography image of a pure Al tensile sample obtained from the Olympus LEXT Interferometer. The regular peaks in the field of view are Pt markers that have been applied to the surface. Investigation of the surface profile near shear bands will allow for determination of the active slip systems.

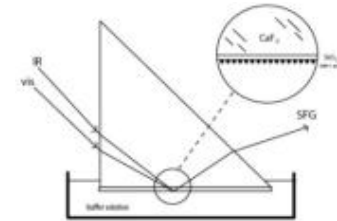
Adam Kammers and Samantha Daly, The University of Michigan
Work performed at the Lurie Nanofabrication Facility

SFG Investigation Of Peptides And Proteins At Chemically Immobilized Surfaces

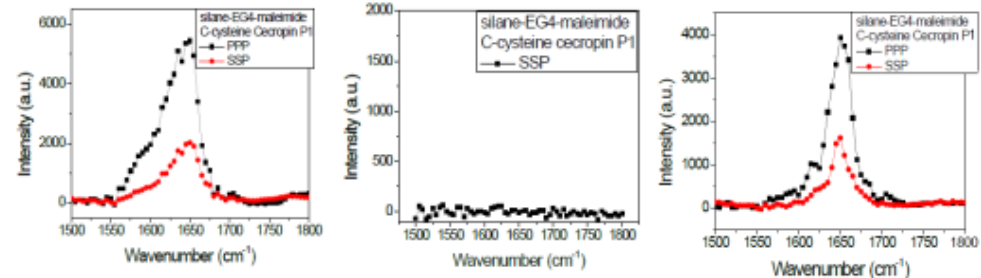
Our work focuses on using sum frequency generation (SFG) to calculate orientations of proteins at interfaces. By using polarization-dependent measurements and near total reflection geometry, we are able to accurately describe how proteins orient themselves at interfaces.

Project 1: Once orientations have been determined, it is our goal to use different methods to help maintain protein structure and function in the absence of water. Our SFG results have shown structure is present in aqueous environments and orientation can be calculated.

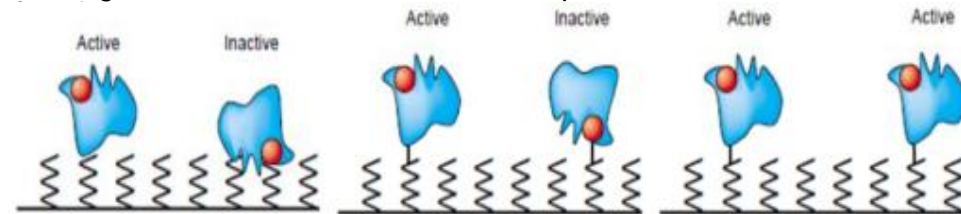
Project 2: It is important for maximize enzyme efficiency for reliable enzyme-based sensors. Our goal is to determine orientation of enzymes bound at different positions to a solid surface. There we can determine how orientation dictates efficiency.



Experimental design. Protein is chemically bonded to the silica surface in distinct orientations and placed in different humid environments



Above are spectral signatures of peptides bound to the silica surface in different environments. (Left) – PBS, (Middle) – Air, and (Right) – Glycerol. Our goal is to retrieve the same signal in buffer as in air, creating a “water-free” environment where proteins can still maintain



Yuwei Liu, Xiaofeng Han, Lei Shen, Fugen Wu, Joshua Jasensky, and Zhan Chen, University of Michigan
Work performed at the Lurie Nanofabrication Facility

Electrohydrodynamic Jet Printing Project

The objective of this project is to utilize a micro/nano scale additive manufacturing process, electrohydrodynamic jet (E-Jet) printing, to realize high-resolution components and assemblies. E-jet uses voltage potential to extract material from a glass micropipette (Fig. 1). The micropipette and substrate are sputtered with gold in order to create conductive surfaces. An advantage of this process is that it enables high-resolution printing ($<200\text{ nm}$) with a diversity of inks (metals, polymers, biological materials) and on a variety of substrates. It has the potential to be used in a wide range of high-value applications including flexible electronics and biosensors (Figs. 2 and 3).

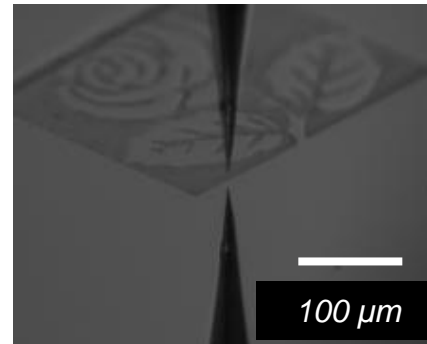


Fig. 1 High resolution additive manufacturing: 0.5×10^6 drops printed in <15 min. Area coverage of 6.5 cm^2 .

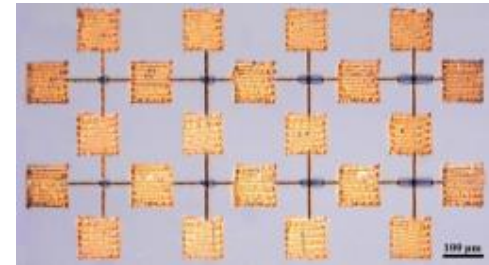


Fig. 2 - Application: Crossover structure for gold interconnect lines linking an array of gold pads

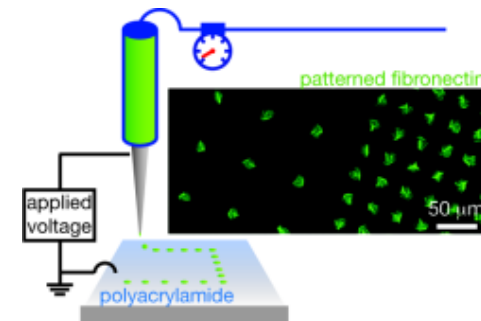


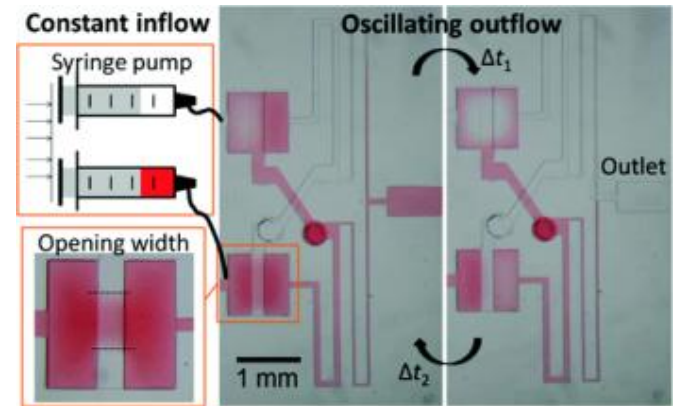
Fig 3. - Application: Patterned hydrogel substrates for cell culture for biosensors

Leo Tse and Kira Barton, University of Michigan
Work performed in part at the Lurie Nanofabrication Facility

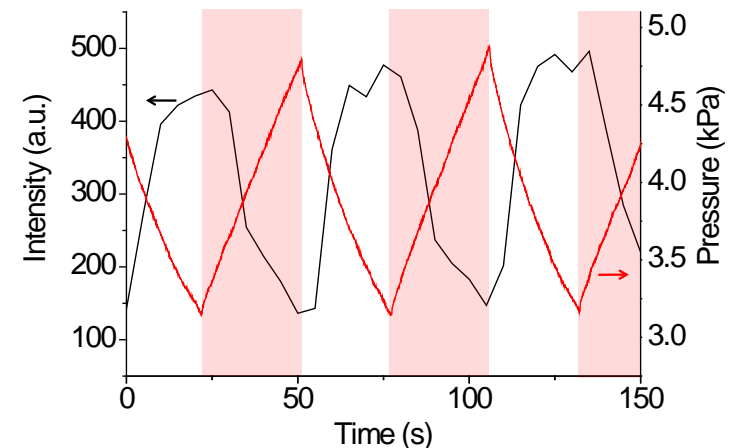
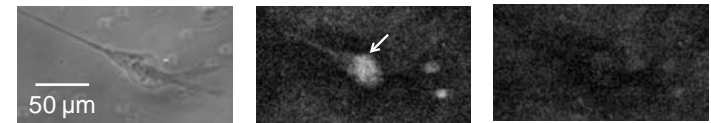
Microfluidic Oscillator Project

The purpose of the Microfluidic Oscillator Project is to recreate dynamic environments for cells, with minimal reliance on external controllers. Also, we capture cells' behaviors under such environments that have periodic biochemical and physical stimulations. Although a wide range of microfluidic devices have been proposed to recreate these dynamic environments to accurately capture cell behaviors, these systems largely rely on external equipment, which prevents widespread use of microfluidic devices. To minimize this reliance, we work on constant input-driven microfluidic oscillator. The system transforms constant input flows into oscillating output flows, one that is analogous to electrical DC to AC converter.

Sung-Jin Kim, Ryuji Yokokawa, Sasha Cai Leshner-Perez, and Shuichi Takayama, University of Michigan
Work performed in part at the Lurie Nanofabrication Facility



Constant flow-driven microfluidic oscillator.



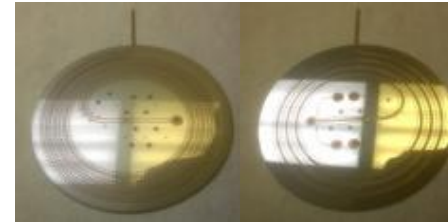
Periodic staining of cell nucleus. Nuclei of cells are periodically stained with a fluorescent dye. Red region in the graph is valve-off state for the fluorescent solution, and clear solution flows during this time.

A Chip-based Continuous-wave Atom Laser

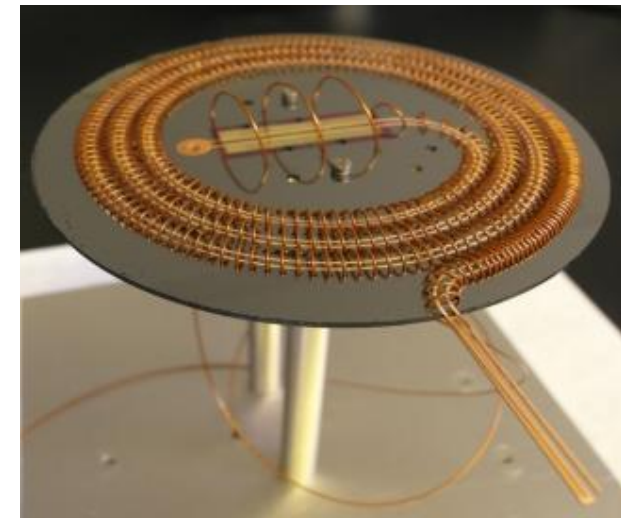
Coherent matter waves are highly desirable for a large number of sensing applications, e.g. gravitational sensing, accelerations and rotation, and probing weak electric or magnetic fields. A continuous-wave (CW) atom laser, created by extracting atoms from a continuously refilled Bose-Einstein condensate (BEC) is realized by combining surface adsorption evaporative cooling with magnetic atom guiding. Atoms loaded onto the chip are guided over 70cm, moving from an initial height 0.5mm above the chip to 0.025mm above the surface. Hot atoms are skimmed from the outside of the atom cloud as it descends, and the remaining cold atoms re-thermalize to form a BEC. A far off-resonant laser acts as a barrier to the atomic flow; the barrier height is tuned to allow some BEC atoms to tunnel through and create a CW atom laser beam.



1.25mm thick Si wafers are etched in a DRIE tool



Copper wires are epoxied into the etched channels. Excess epoxy is polished away.



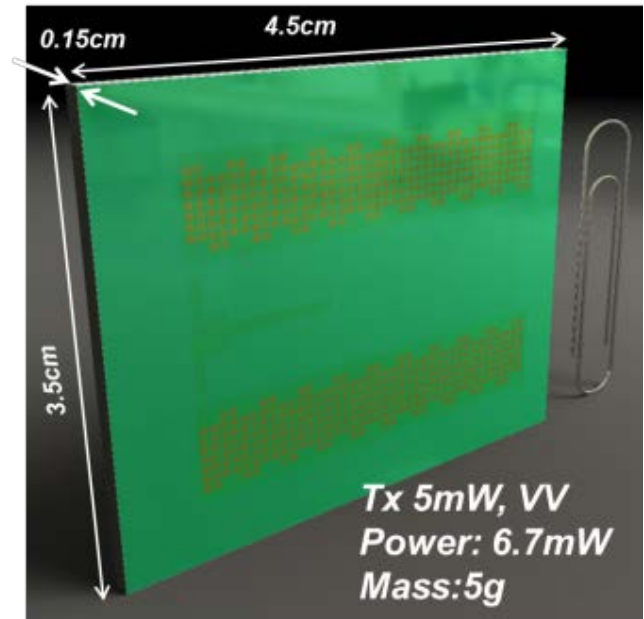
A solenoid is sewn through the chip—this is required to obtain a BEC

Erik Power and Georg Raithel, University of Michigan
Work performed at *the* Lurie Nanofabrication Facility

MMW Radar System for Navigation of Micro-Autonomous Robotic Systems

Our research group is engaged in developing an ultra lightweight short range MMW radar system operating at Y-band frequencies for collision avoidance and navigation of micro autonomous robotic platforms.

- Tx 5mW, VV
- Power: 6.7mW
- Weight: 5g



Mehrnoosh Vahidpour, Meysam Moallem, Armin Jam, Dr. Jack East, Prof. Kamal Sarabandi, University of Michigan
Work performed at Radiation Laboratory and Lurie Nanofabrication Facility, University of Michigan

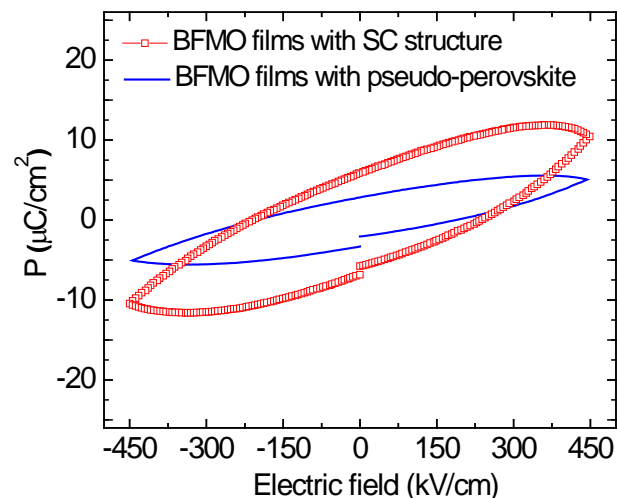
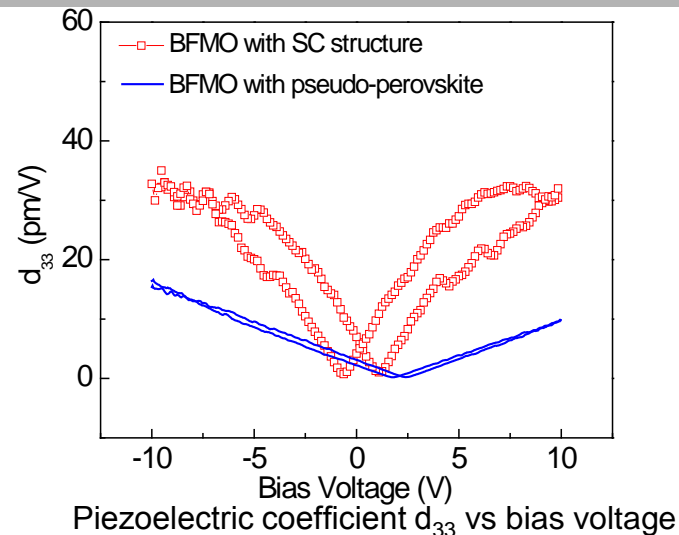


The first prototype 2011

A new class of room temperature multiferroic $\text{Bi}_3\text{Fe}_2\text{Mn}_2\text{O}_{10+\delta}$ thin films

A new class of room temperature multiferroic phase $\text{Bi}_3\text{Fe}_2\text{Mn}_2\text{O}_{10+\delta}$ has been fabricated by the intergrowth of two partially miscible phases of BiFeO_3 and BiMnO_3 . The new phase presents a unique Super-Cell (SC) structure with the bismuth bilayer sublattice structure in commensurate with the Fe-O-Mn sublattice. The SC heterostructures exhibit a room temperature ferrimagnetism of ~ 100 emu/cc and a remnant polarization P_r of $\sim 6 \mu\text{C}/\text{cm}^2$, simultaneously. These results open a new avenue for exploring room temperature single-phase multiferroic thin films by controlling the phase mixing of two perovskite BiRO_3 ($R=\text{Cr, Mn, Fe, Co, Ni}$) materials.

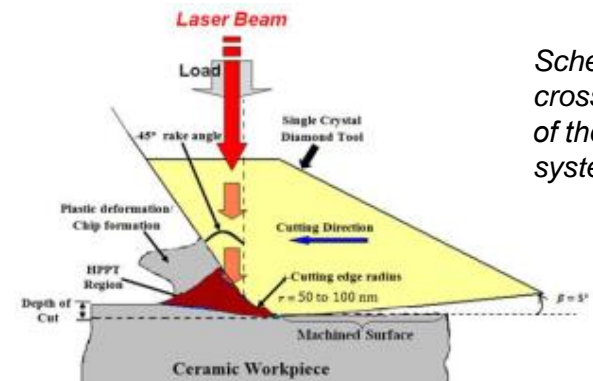
Chen, H. Zhou, Z. Bi, Y. Zhu, Z. Luo, A. Bayraktaroglu, J. Phillips, E.-M. Choi, J. L. MacManus-Driscoll, S. J. Pennycook, J. Narayan, Q. X. Jia, X. Zhang, and H. Wang, University of Michigan
Work performed in part at the Lurie Nanofabrication Facility



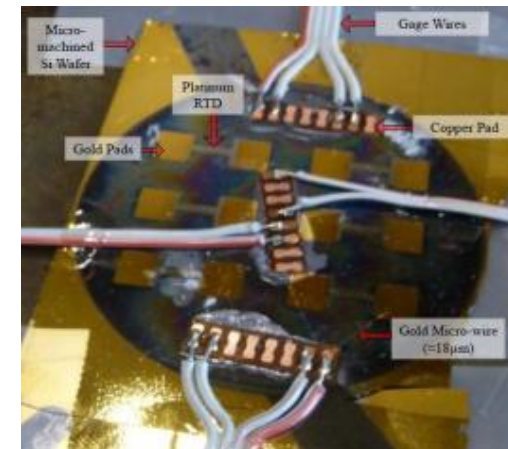
The polarization-electric field (P-E) hysteresis loops

Temperature Measurement and Study of the Thermal Effects during the Micro-Laser Assisted Machining Process

Micro-Laser Assisted Machining (μ LAM) is a process used to achieve atomic level surface smoothness of semiconductor materials while increasing the material removal rate and reducing tool wear. This is achieved by scratching the surface of the work piece (the semiconductor) with a diamond tool while a laser is passed through the tool to thermally soften the High Pressure Phase Transformation (HPPT) Region created beneath the diamond tool during the μ LAM process. Ductile-region machining is ensured throughout the process by controlling the machining parameters, e.g., cutting speed, load applied, and power and wavelength of the laser. In order to optimize the μ LAM process, a temperature measurement of the HPPT is desired. An in-situ temperature measurement of the HPPT region was performed by reducing the thickness of the work piece (Silicon) through lithography and depositing a thin film Platinum Resistance Temperature Detector (RTD) on the backside of the machined wafer. The temperature of the HPPT was measured from the backside of the Si wafer using a voltage divider circuit connected to the RTD while the wafer was being machined on the opposite side. The temperature obtained with the RTD was correlated to the temperature of the HPPT region using the corresponding heat transfer equations.



Schematic cross-section of the μ -LAM system



The 104 μ m-thick wafer and RTD with leads bonded

Dionisio V. Del Orbe, Jared D. McKinley, Muralidhar K. Ghantasala, John Patten, and Deepak Ravindra, Western Michigan University
Work performed at the Lurie Nanofabrication Facility

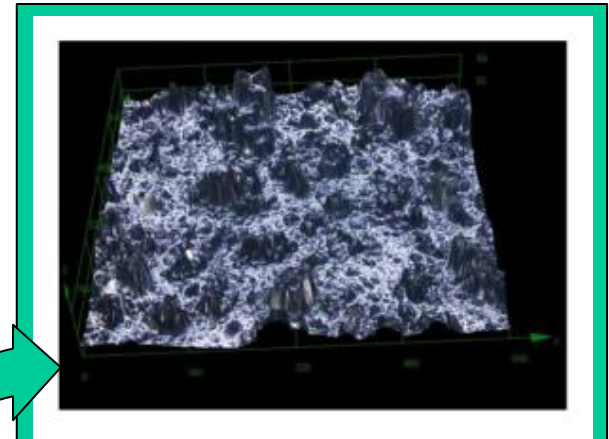
Surface Roughness Extraction from Images

Our goal is to extract roughness information from a single image. The challenge is to obtain height information from the image dimension. There are several algorithms proposed in the vision community for extracting depth from shading and we plan to utilize these as well as develop our own model. We compare our results with roughness measurements performed at LNF.

Our aim is to obtain roughness information from materials that cannot be directly measured in a laboratory setting.

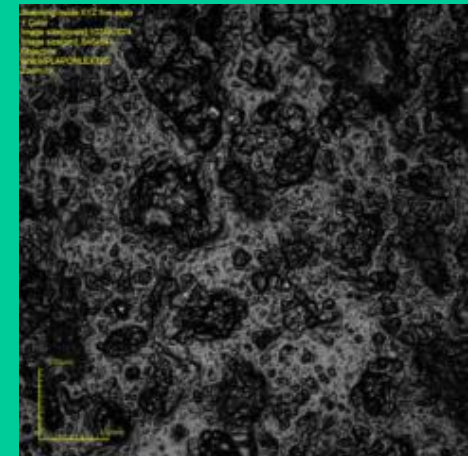
Cynthia Aku-Leh, ISciences LLC
Work performed at the Lurie Nanofabrication Facility

To here



3D surface data

From here

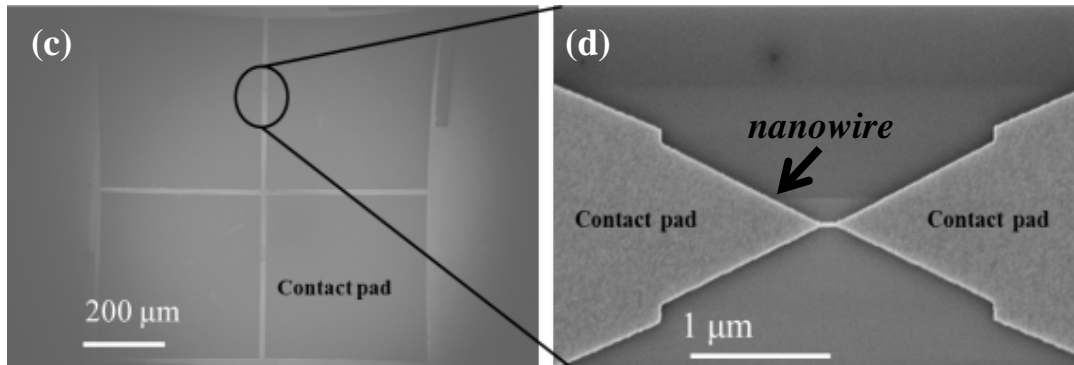


2D Image

Nanoelectronics: Scalable Junctions for Molecular Electronics & Chemical Sensors

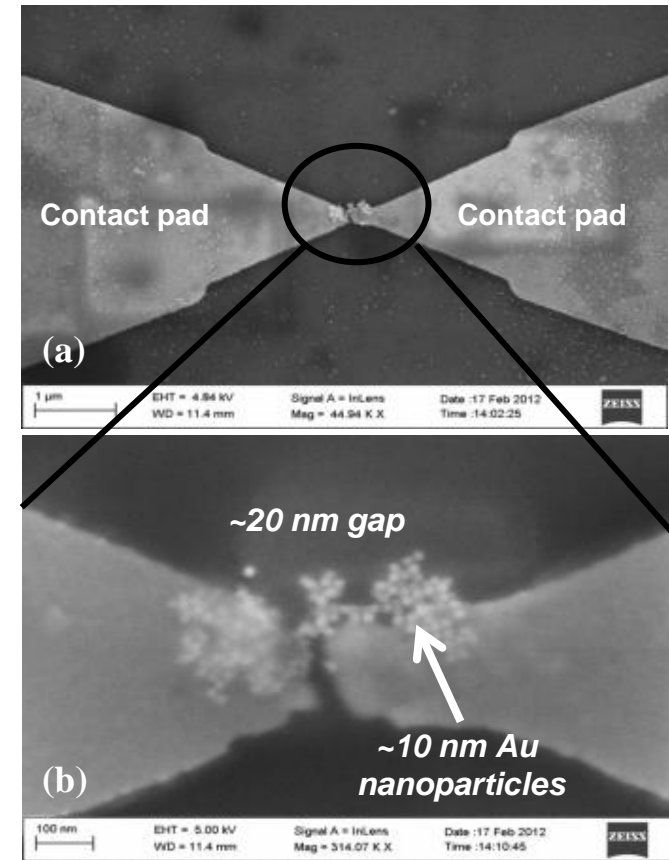
Our goal is to use nanometer-sized junctions to build molecular circuits, which can function as switches & diodes. We are investigating devices that can move current in only one direction through individual molecules or control electrical switching in a single molecule; and we are building a multifunctional detection platform using chemiresistor sensors.

Devices consist of nanowires with dimensions of 30 nm x 200 nm. These wires are used to create scalable nanogaps between 2–40 nm using a progressive electromigration technique. To build molecular circuits and chemical sensors, molecules or gold nanoparticles are trapped in the nanogap via a self-assembly or an electrostatic trapping technique.



- c) SEM image of 40 μm contact pads fabricated by photolithography. The area circled is the location of a nanowire.
- d) Magnified image of the nanowire formed by electron beam lithography on silicon oxide substrates.

Swatilekha Saha and K. M. Lewis, Rensselaer Polytechnic Institute
Work performed at the Lurie Nanofabrication Facility



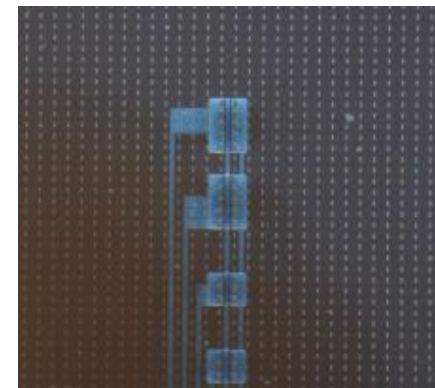
- (a) SEM image of gold particles displaced near a nanogap. (b) The particles (i.e. the sensing element) bridge the nanogap to form a chemical sensor.

A SOI-CMOS compatible flexible electronics technology

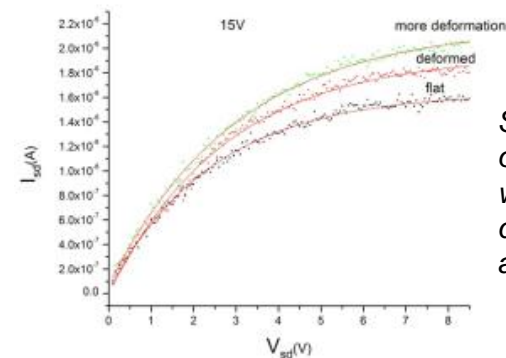
We successfully demonstrated a simple SOI-CMOS compatible technology to make flexible electronics. Compared with existing technologies such as direct fabrication on flexible substrate and transfer printing, the biggest advantage of this new technology is its SOI-CMOS compatibility. Consequently, high performance and high density CMOS circuits can be first fabricated on SOI wafers, and then be integrated into flexible substrates. The yield is also improved by eliminating the transfer printing step. Furthermore, the new technology allows the integration of various sensors and microfluidic devices into the flexible substrate. To demonstrate the concept of this technology, flexible MOSFETs have been successfully fabricated.



A bent flexible device held by a pair of tweezers.



Optical micrograph of four MOSFETs with different channel widths

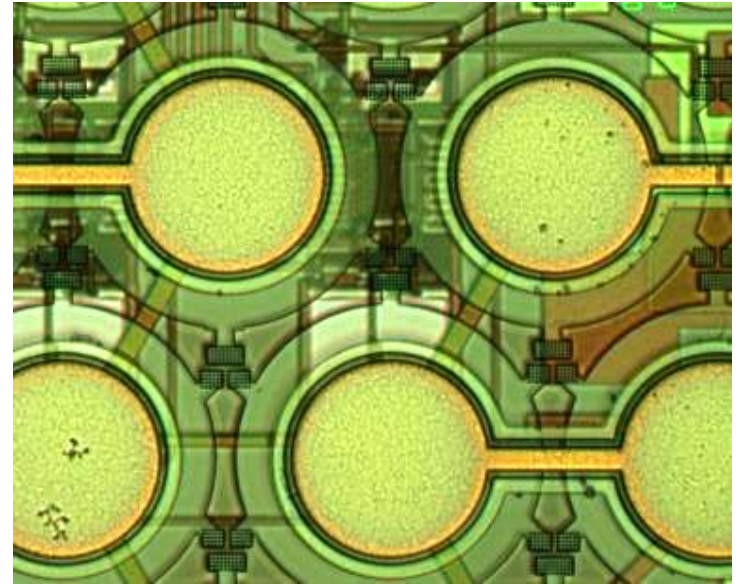


Shift of I_{sd} - V_{sd} curves of one PMOS device when the device was deformed (V_{sg} is fixed at 15 V)

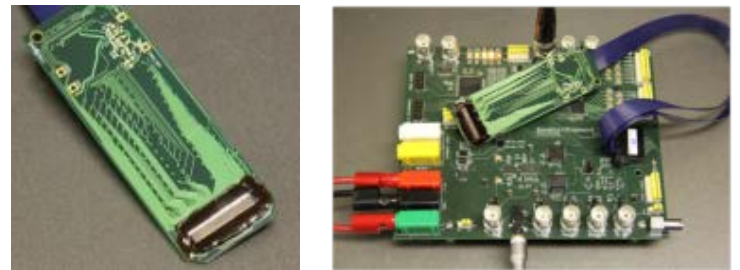
Hongen Tu and Yong Xu, Wayne State University
Work performed at the Lurie Nanofabrication Facility

Micromachined Transducer Arrays for 3D Imaging

Sonetics Ultrasound, Inc. is developing large-scale MEMS transducer arrays intended for real-time 3D ultrasound imaging and niche applications such as blood flow monitoring. Sonetics' patent-pending technology uses standard integrated circuit fabrication steps to build thousands of micromachined electrostatic membrane transducers on a chip. These transducers produce short pulses of acoustic energy and detect echoes returning from features in tissue. When combined with low-noise front-end circuits and sophisticated signal processing hardware, high-quality 3D medical images can be acquired. Because the arrays are batch fabricated on silicon wafers, they promise to provide significant cost-savings and performance improvements over traditional manually-assembled piezoelectric transducer technology. The transducer array fabrication sequence relies on standard CMOS processes plus specialized metal etching and deposition of thin films such as PECVD dielectrics and parylene.



MEMS ultrasound transducer elements with CMOS circuits integrated beneath.



(Left) MEMS array chip mounted on a small board for Doppler blood flow measurements. (Right) Electronics module used to interface to MEMS array.

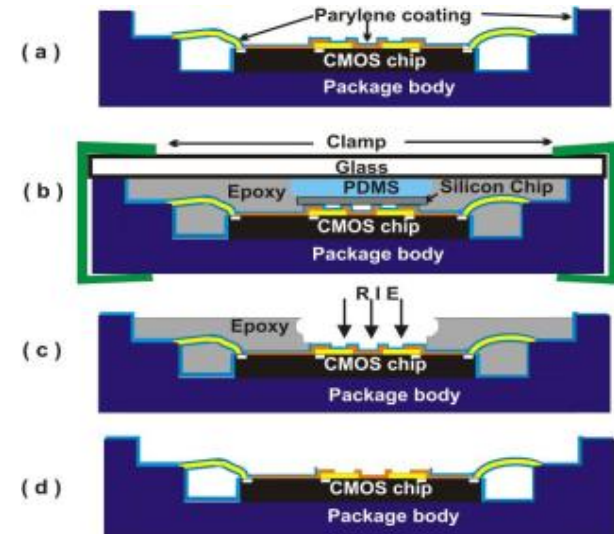
David Lemmerhirt , Sushma Srinivas, and Collin Rich
Sonetics Ultrasound, Inc.

Work performed at the Lurie Nanofabrication Facility

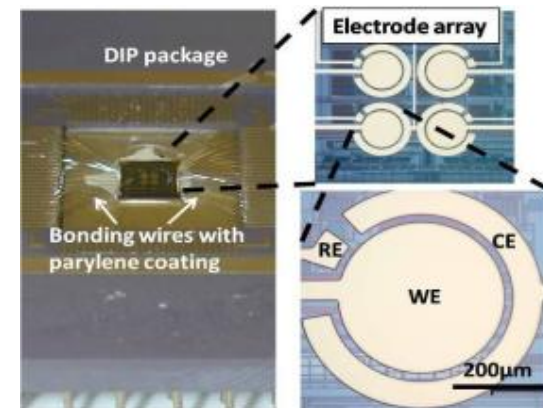
Post-CMOS Parylene Packaging for On-chip Biosensor Arrays

The opportunity to integrate microfluidic devices with CMOS instrumentation is attractive to many biological and biomedical sensor applications. However, the packaging of CMOS circuitry for use within a liquid environment remains as an open challenge. The goal of this project was to develop a unique packaging scheme that enabled a CMOS circuit chip with on-chip biosensor elements to operate in liquid environment under microfluidic control. Parylene was used as the packaging material because of its excellent biocompatibility and chemical inertness. Electrochemical electrode arrays were fabricated on CMOS chips that were wire bonded to a ceramic package and then coated with parylene. This structure permitted electrochemical measurements on the surface of the CMOS chip. This project is supported by the National Science Foundation under award number DBI-0649847.

Lin Li and Andrew Mason, Michigan State University
Work performed in part at the Lurie Nanofabrication Facility



Process flow of chip-in-package sealing for liquid environment.



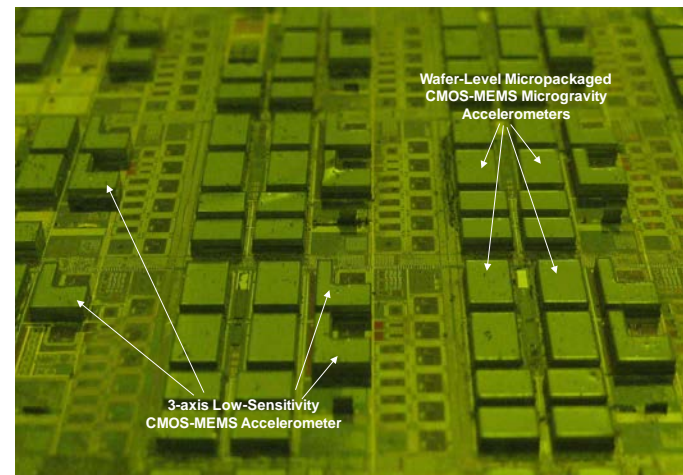
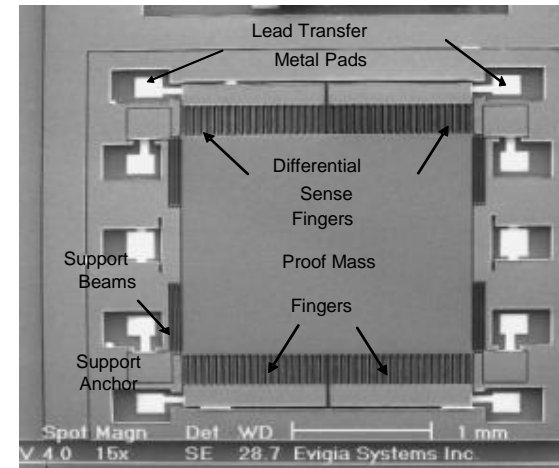
Photograph of a CMOS biosensor array chip-in-package and close up views of the post-CMOS surface electrode array.

Evigia Systems Sensors

Evigia is currently developing a variety of energy-efficient sensors and sensing systems for integration with radio-frequency identification tags (RFID). Evigia's core technology is on post-CMOS proprietary integration of MEMS/NEMS sensors and circuits and packaging at wafer-level, and ultra low-power circuits and ultra low-power sensors. The LNF is essential for Evigia to produce prototypes and to perform R&D activities prior to technology transfer to standard commercial MEMS manufacturing facilities for production ramp.

One of the sensors fabricated at LNF is a microgravity accelerometer for precision acceleration measurements at micro-g levels. The sensor is fabricated atop of CMOS wafers providing high-sensitivity, low-noise and high-stability, and sealed at wafer-level with silicon-cap lowering drift and shielding EMI. It has a sensitivity of 1.8V/g and noise floor of 1.2 μ g/rt-Hz.

Robert Nidetz, Weibin Zhu, Yafan Zhang, Evigia Systems, Inc.
Work performed at the Lurie Nanofabrication Facility

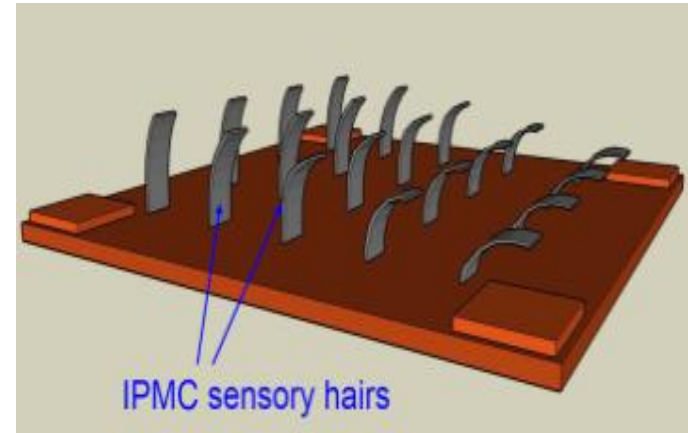


Single-Chip CMOS-MEMS
Microgravity Accelerometer

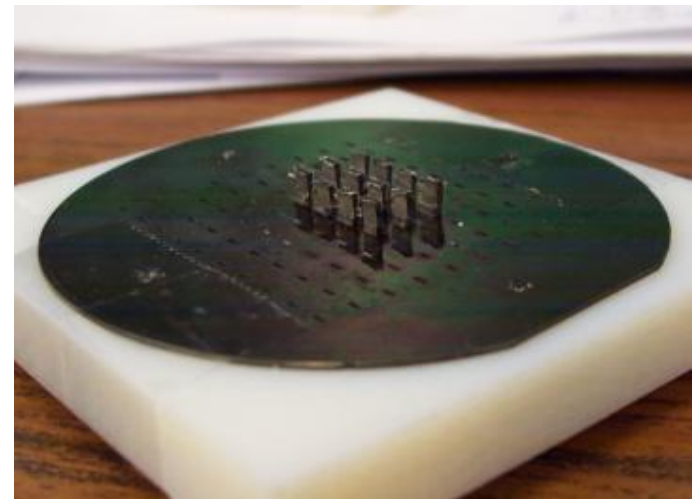
IPMC-based Artificial Lateral Line System

This ONR project aims to develop an artificial lateral line system consisting of arrays of IPMC (Ionic Polymer-Metal Composite) cilia, which are micro flow sensors created by micro-fabrication processes. Si wafers are etched through by DRIE (Pegasus 6 in LNF), serving as substrate for these freestanding IPMC hairs. The typical IPMC fabrication process is modified to fit this micro-scale device. Liquid Nafion solution is casted and then solidified on top of the substrate to form the standing hair structure. Parylene deposition (PDS 2035 in LNF) and anisotropic plasma etching (Plasmatherm 790 in LNF) are used to solve the problem of selectively forming the electrodes on two surfaces of the standing Nafion hairs. This interdisciplinary project has extended to another ONR project of “Bio-inspired Flow Sensing and Control for Autonomous Underwater Vehicles” in collaboration with Profs. Derek Paley, Sean Humbert from Univ. of Maryland and Sheryl Coombs from Bowling Green State Univ.

Hong Lei and Xiaobo Tan, Michigan State University
Work performed in part at the Lurie Nanofabrication Facility



Envision of artificial lateral line system based on micro IPMC flow sensors



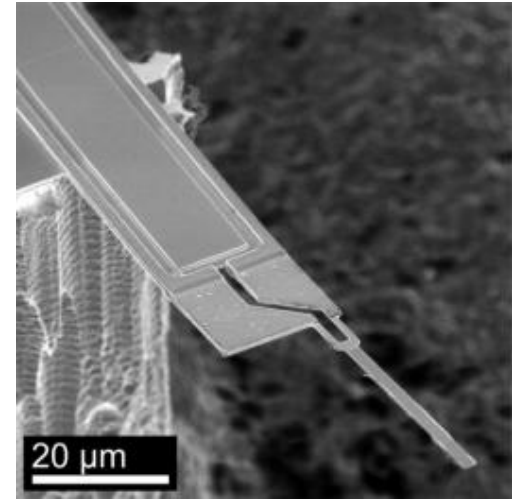
First prototype of batch-fabricated IPMC flow sensor

Nanomechanical force probes for hearing research

We have developed scientific instruments with an unprecedented combination of force and time resolution to study the sense of hearing. The devices integrate a piezoresistive sensor and piezoelectric actuator onto a cantilever beam, allowing the measurement and application of atomic-scale forces with microsecond-scale time resolution. The study of mammalian hearing has been limited by instrument speed to date, and the force probes were developed to address this technological gap.

Numerous fabrication steps are performed at the SNF before the backside DRIE step, which releases the cantilevers from the wafer, is performed at the LNF. The DRIE step is critical to the overall performance of the device.

Joseph Doll and Beth Pruitt, Stanford University
Work performed in part at the Lurie Nanofabrication Facility



Scanning electron micrograph of a completed force probe, which consists of a stiff piezoelectric at the base of a flexible piezoresistive sensor.



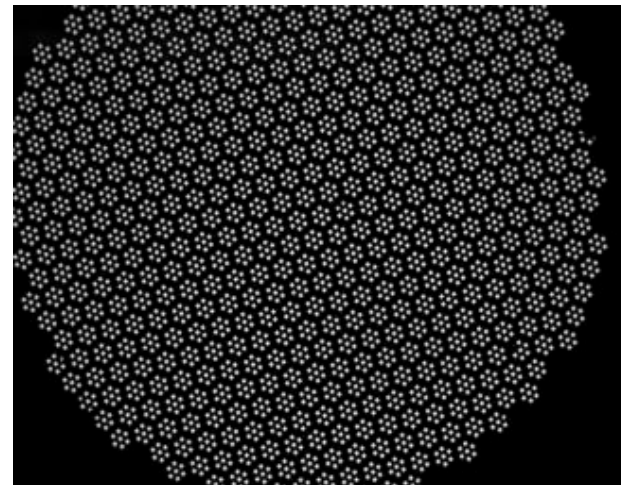
Parylene coated force probe in the vicinity an inner hair cell. Mechanical stimuli are delivered to the hair cells along the indicated axis.

Mag Sifter Project

The purpose of the MagSifter Project is to fabricate a microdevice consisting of pores in a membrane structure that we can subsequently sputter magnetic films on. This allows us to use the device as a separation device to remove various magnetic particles in flow. The LNF-fabricated component of this system is the actual pore structure, consisting of an etched nitride membrane on a silicon backbone.



A Microfabricated Magnetic Sifter



Pores in the structure

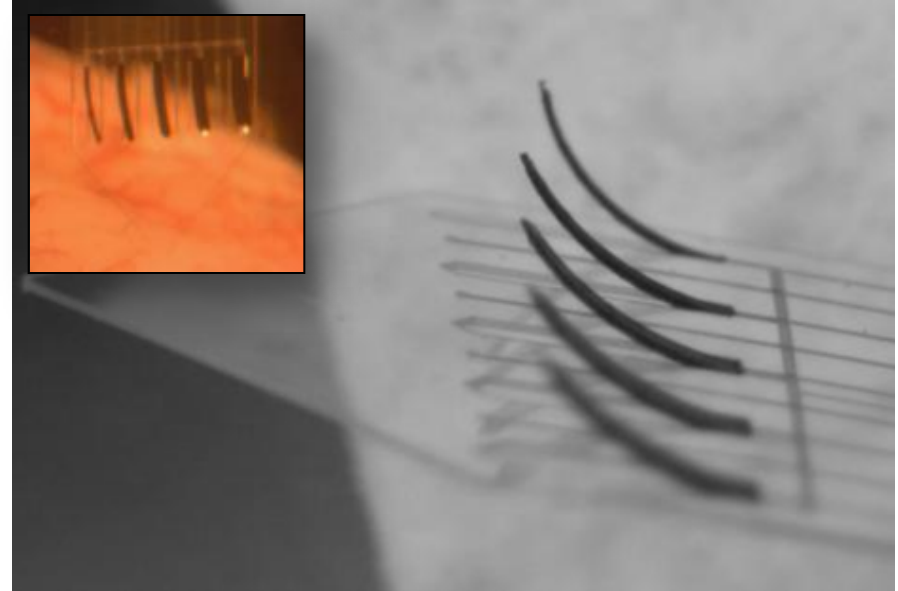
Chin Chun Ooi, Christopher M. Earhart, Robert J. Wilson, Shan X. Wang, Stanford University
Work performed at the Lurie Nanofabrication Facility

Articulating Neural Electrodes

The goal of this project is to improve the proximity of a neural interface to its target for a variety of biomedical applications. We investigate implantable neural interface devices that have controllable articulated elements using conjugated polymer actuators.

By applying less than 1 Volt, conjugated polymer actuators may be oxidized or reduced causing influx and/or efflux of ions and their hydration shells into the porous polymer matrix, thereby swelling or shrinking the actuators.

Modulating the proximity of electrode sites to the neural tissue may have benefits of increased signal-to-noise ratios and lower thresholds for stimulation therapy. In addition, using these actuators as insertion guides may provide a mechanism for non-linear trajectories and active steering.



Articulating neural electrode projections of varying widths deflected out of plane with no voltage applied. Inset: image of an array of electrode projections with electrode sites actuated out of plane while cycling in artificial cerebral spinal fluid. Light can be seen reflecting off of the last two electrode sites from the right.

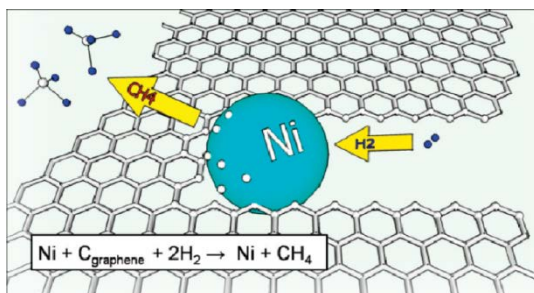
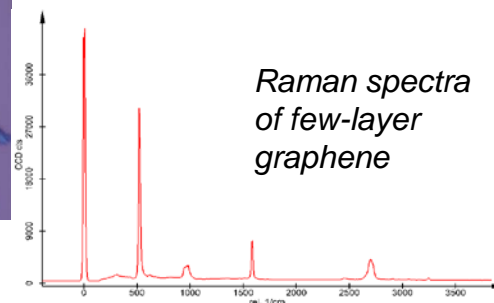
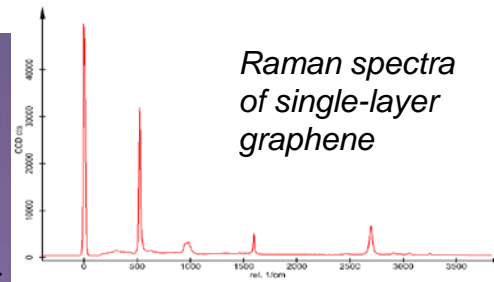
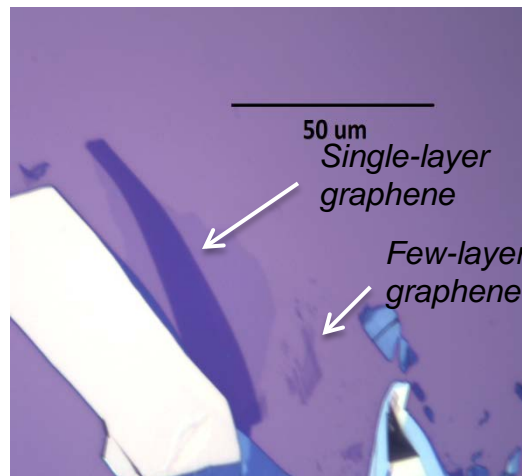
Eugene D. Daneshvar, and Daryl Kipke, University of Michigan and Elisabeth Smela, University of Maryland
Work performed in part at the Lurie Nanofabrication Facility

University of Minnesota

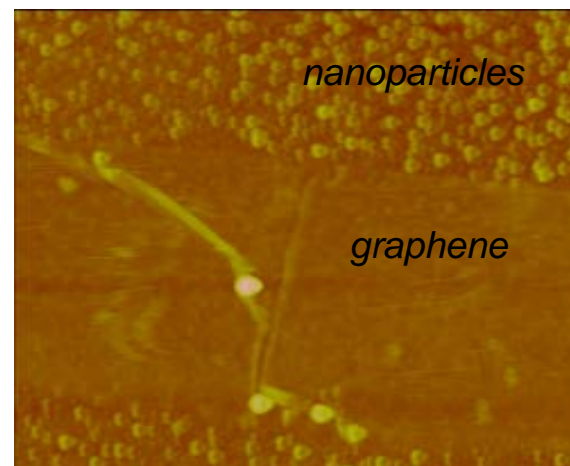
Graphene Nanoribbon Fabrication using Templated Nanoparticle Etching

The Graphene Nanoribbon Fabrication Project involves graphene exfoliation from graphite, characterization of graphene using Raman spectroscopy and atomic force microscopy.

Nanoparticles have been successfully deposited on graphene. However, the inadequate capability of the existing furnace to run hydrogen gas at high temperature (~1000° C) has caused the nanoparticles to be immobile.



Campos et al. (2009)



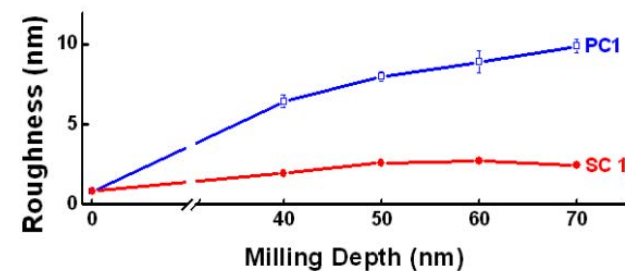
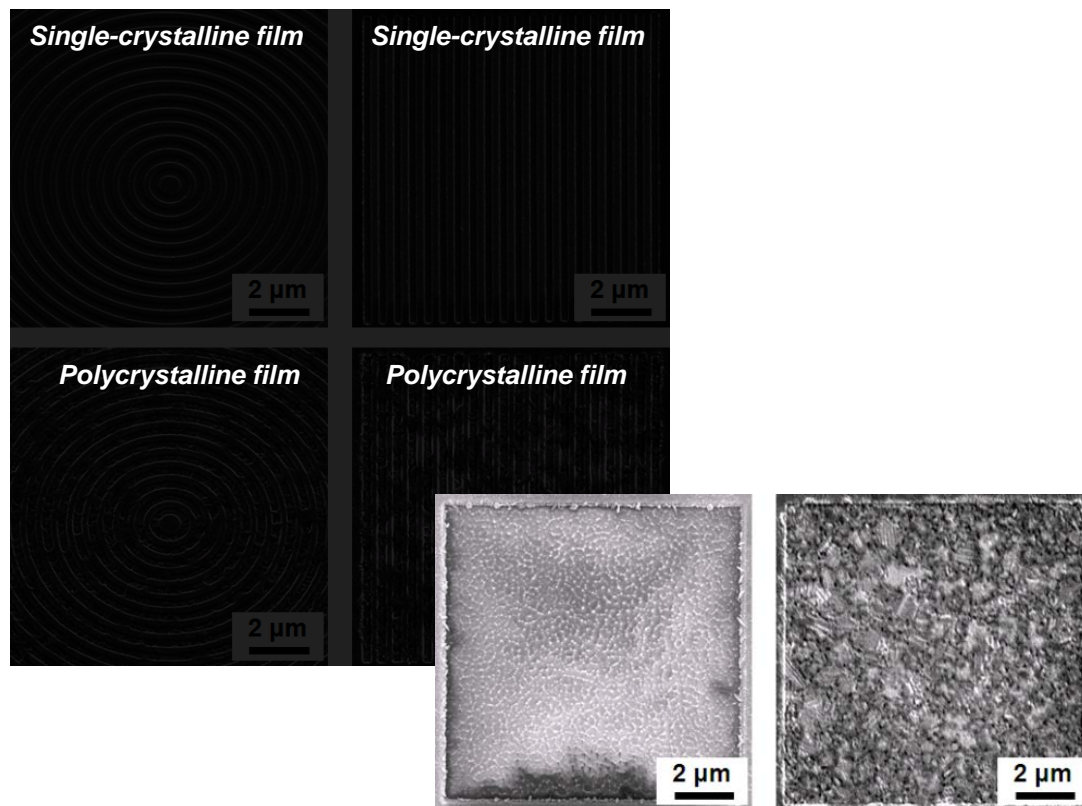
AFM image of graphene and deposited nanoparticles

Steven Koester and Yoska Anugrah, University of Minnesota, Electrical and Computer Engineering
Work performed at University of Minnesota
Nanofabrication Center

Precise Nanopatterning on Single-Crystalline Metal Films

Precisely patterned nanostructures have been highly demanded for plasmonic applications. Ultraflat single-crystalline metal films are prepared by epitaxial growth and then patterned via focused ion beam milling.

A uniform milling rate on single-crystalline films allows precise patterning of nanostructures while the structures on polycrystalline films show very rough morphology.



David Norris and Jong Hyuk Park, University of Minnesota,
Chemical Engineering and Materials Science
Work performed at University of Minnesota Nanofabrication
Center

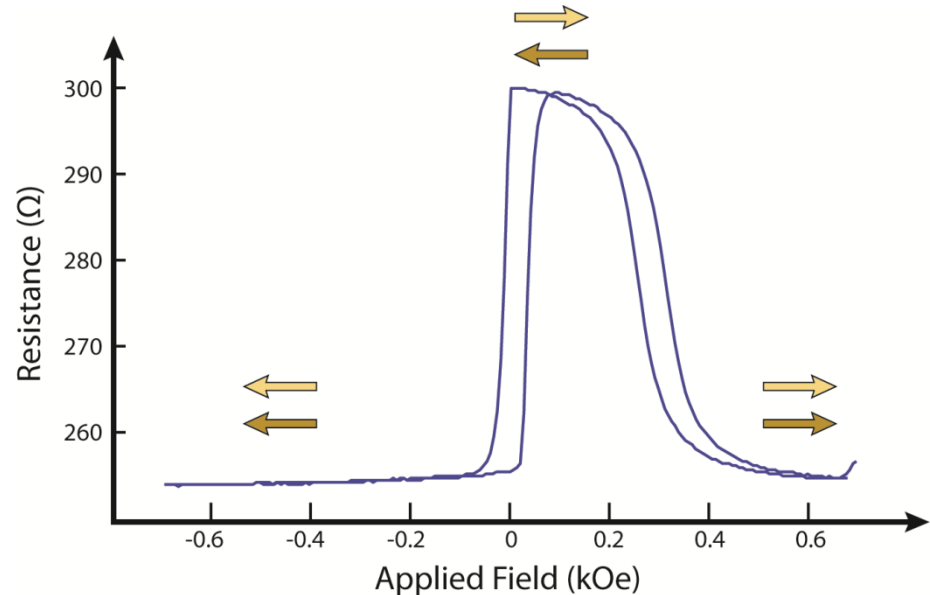
Probing the Tunnel Density of States with Magnetic Junctions

Deposition and subtractive processing are used to make both contact pads for magnetic tunnel junctions and the MTJs themselves.

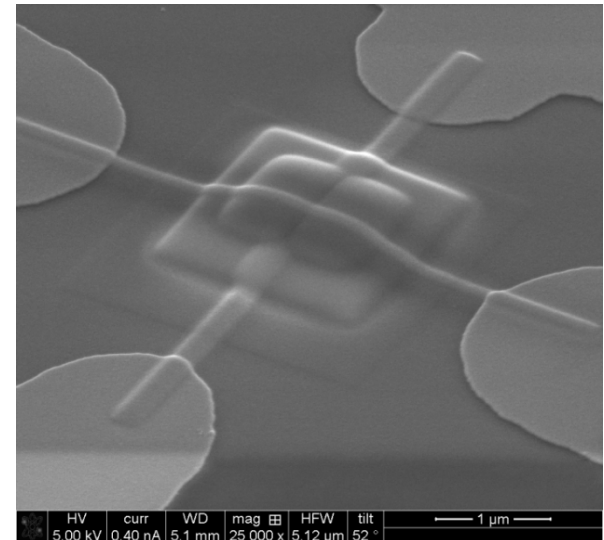
The goals of the MTJ studies are to measure DOS effects on tunneling using differential conductance measurements in single MTJs and spin injection in double MTJs.

The differential conductance feature observed in Ni-backed tunnel junctions potentially could be used as a reference marker for more involved studies into the nature of quantum tunneling.

A new process is currently underway for the fabrication of DMTJs through additive EBID processing to facilitate the manipulation of the center electrode of a DMTJ.



*E. Dan Dahlberg, Barry Costanzi, and Bern Youngblood,
University of Minnesota, Chemical Engineering and
Materials Science
Work performed at University of Minnesota Nanofabrication
Center*

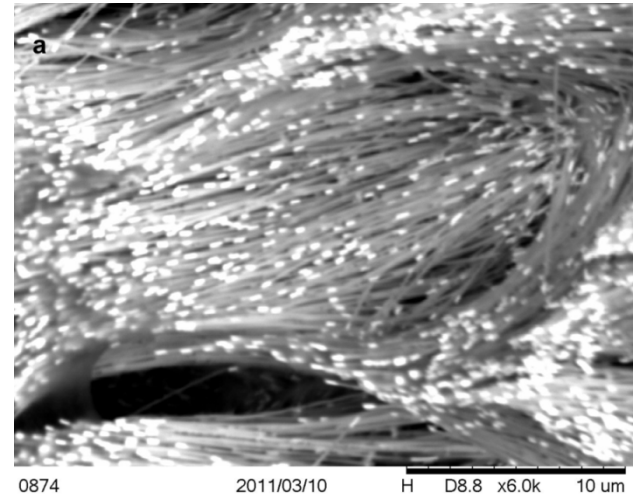


Cell Manipulation and Separation using Magnetic Barcode Nanowires

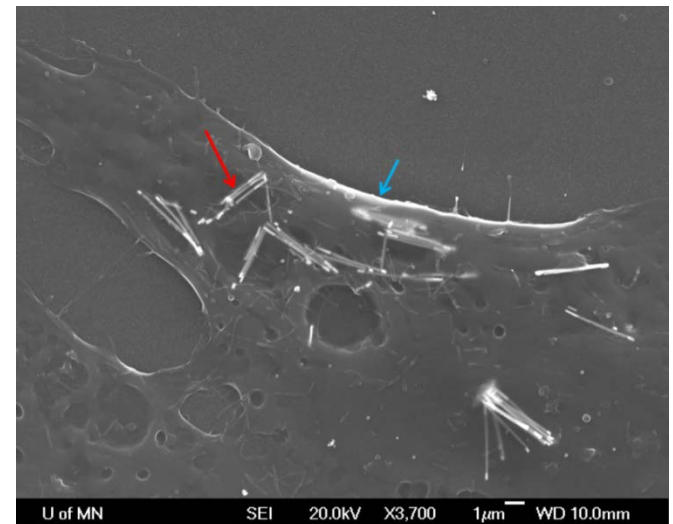
The Magnetic Barcode Nanowires Project focuses on three goals: fabrication of gold/nickel multi-segmented magnetic “barcode” nanowires, non-specific uptake of barcode nanowires by Osteosarcoma cells (OSCA), and specific uptake of nanowires and cell separation from a mixture of analytes.

Scanning electron microscopy images indicate non-specific uptake of nanowires by OSCA cells. The nanowires appear to be non-cytotoxic from initial viability studies.

*Bethanie J.H. Stadler and Allison Hubel,
University of Minnesota,
Work performed at University of Minnesota
Nanofabrication Center*



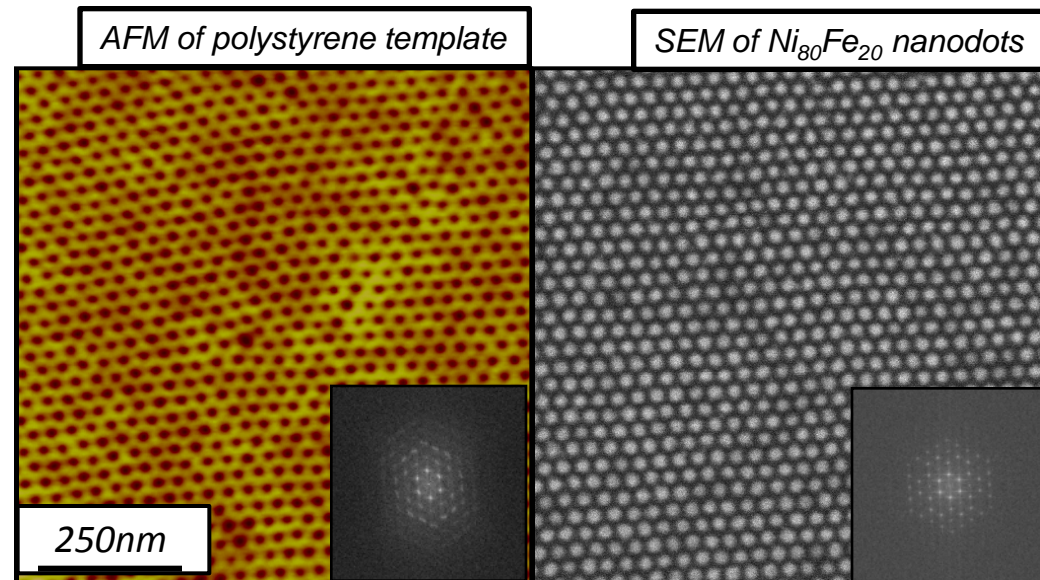
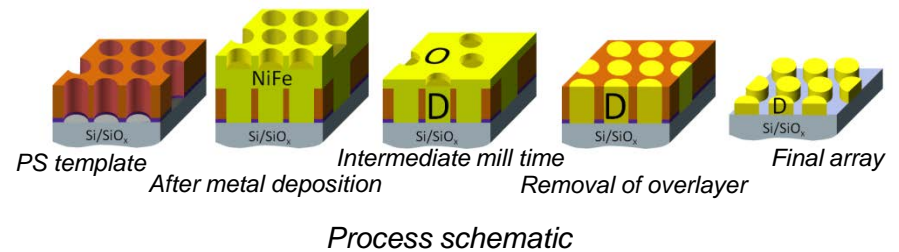
SEM micrographs of (above) as-fabricated barcode nanowires and (below) nanowires (red arrow) uptaken by cancer cell (cell membrane-blue arrow)



Block Copolymer Patterning of Magnetic Nanostructures

The patterning process involves spin casting poly(styrene-*b*-lactide) onto a Si wafer. The incorporating solvent annealing leads to self assembled, perpendicularly oriented cylinders. Aqueous degradation of the cylinders leaves a polystyrene template behind. Evaporation of NiFe, in excess, on top of the template fills the dimples. Normal incidence Ar ion beam milling planarizes the surface, eventually removing the overlayer. The disparity in milling times for polystyrene (10nm/min) and NiFe (2nm/min) leads to pattern reversal and the formation of NiFe nanodots.

This new and optimized process scheme leads to high fidelity pattern transfer from a self-assembled polymer template to magnetic metal. The magnetic metal retains about 70% of its bulk magnetization (reduced etch damage).



Chris Leighton, Marc Hillmyer, and Andrew Baruth,
University of Minnesota,
Work performed at University of Minnesota
Nanofabrication Center

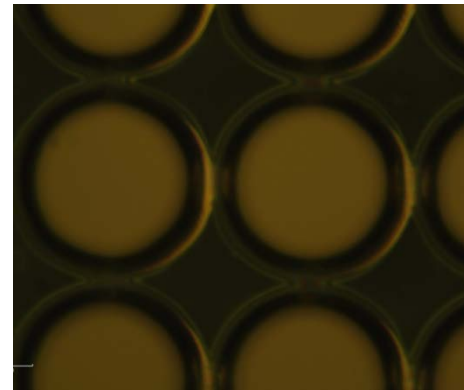
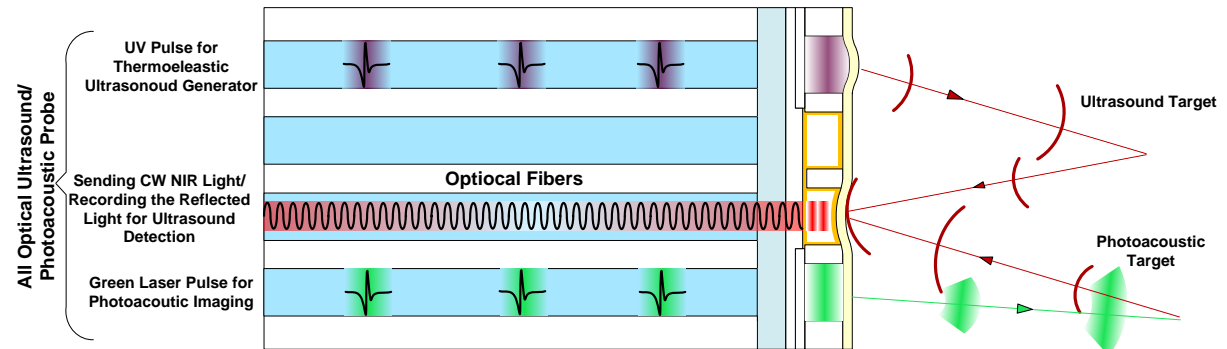
NNIN is supported by NSF ECCS-0335765

All Optical Probe for Ultrasound and Photoacoustic Imaging

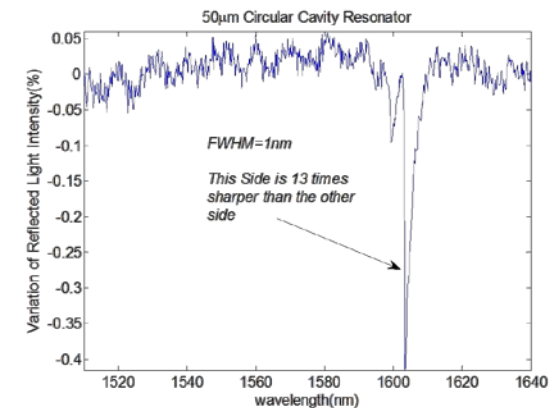
The All Optical Probe for Ultrasound and Photoacoustic Imaging Project uses an optical cavity as an ultrasound detector, a UV absorber/green light transparent polymer as an ultrasound transmitter, and a window for photoacoustic imaging.

This imaging scheme provides improved optical properties and sensitivity of the ultrasound detector, compared to the other competitive device for this purpose.

The group is also making a tiny array for dual modality intravascular imaging.



Fabricated cavities



Characteristic Curve (Optical Sensitivity) Improvement

Shai Ashkenazi and Mohammad Amin Tadayon,
University of Minnesota, Biomedical Engineering
Work performed at University of Minnesota
Nanofabrication Center

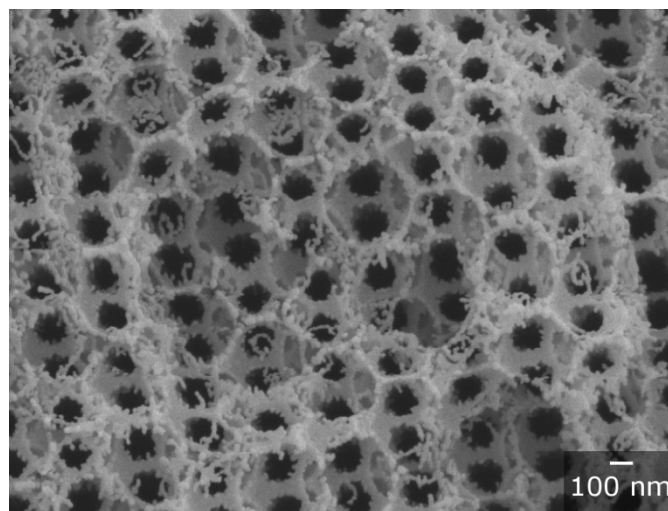
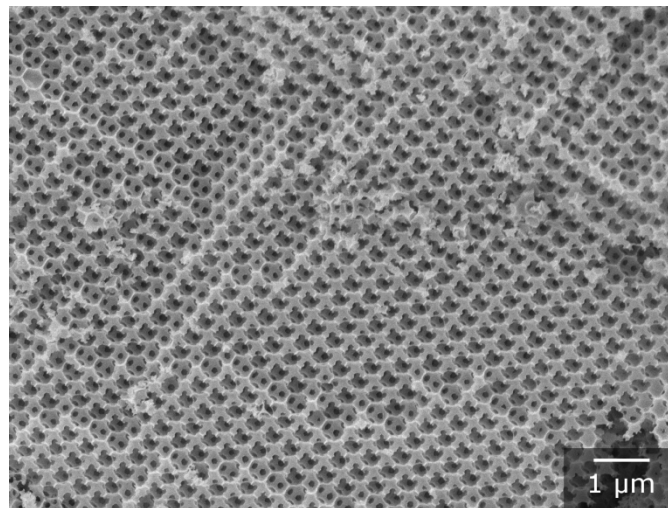
Cerium-based Oxides for Solar Fuel Production

This project's work on solar fuel production involves the study of CeO_2 and $\text{Ce}_{1-x}\text{Zr}_x\text{O}_2$ as materials for the solar thermochemical splitting of water.

The group increases surface area via the use of colloidal crystal templating. Changes caused by high temperature redox cycling are analyzed.

3DOM CeO_2 and $\text{Ce}_{1-x}\text{Zr}_x\text{O}_2$ are produced via colloid crystal templating. It has been observed that redox cycling causes sintering and crystallite growth. Sintering can be mitigated via the addition of Zr cations.

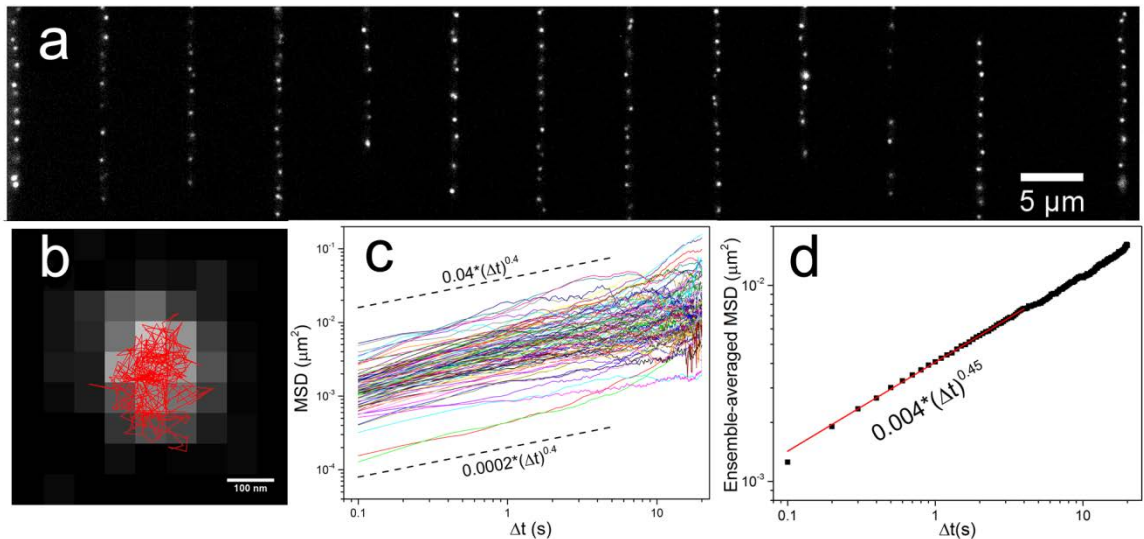
*Andreas Stein and Nicholas Petkovich,
University of Minnesota, Chemistry
Work performed at University of Minnesota
Nanofabrication Center*



Microfluidic Chemostat for Bacteria

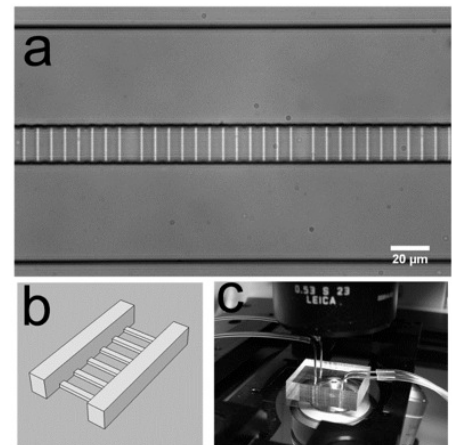
A microfluidic chemostat has been developed that allows trapping of *E. coli* cells and forces them to grow in lines for days.

Growth dynamics and gene expressing at the single cell level can be measured for many generations. The group has tracked the movements of fluorescently tagged loci in more than one thousand cells on a single microdevice.



High throughput loci tracking. a) Fluorescently tagged loci; b) The trajectory (in red) of the centroid of a locus; c) Mean square displacements (MSD) of all loci; d) Ensemble-averaged MSD

The microfluidic chemostat



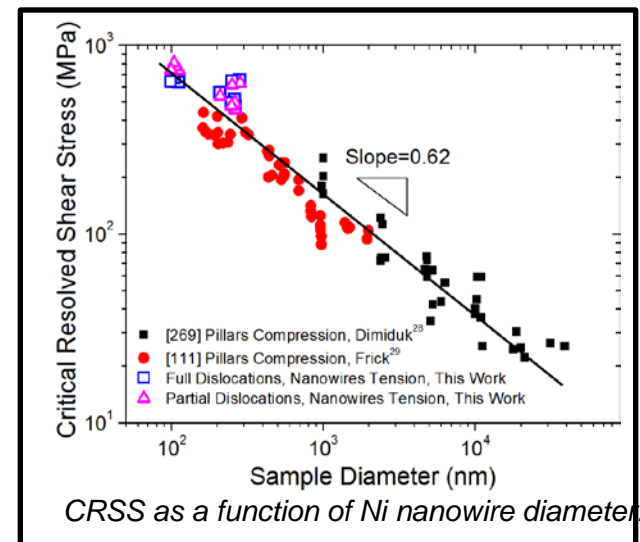
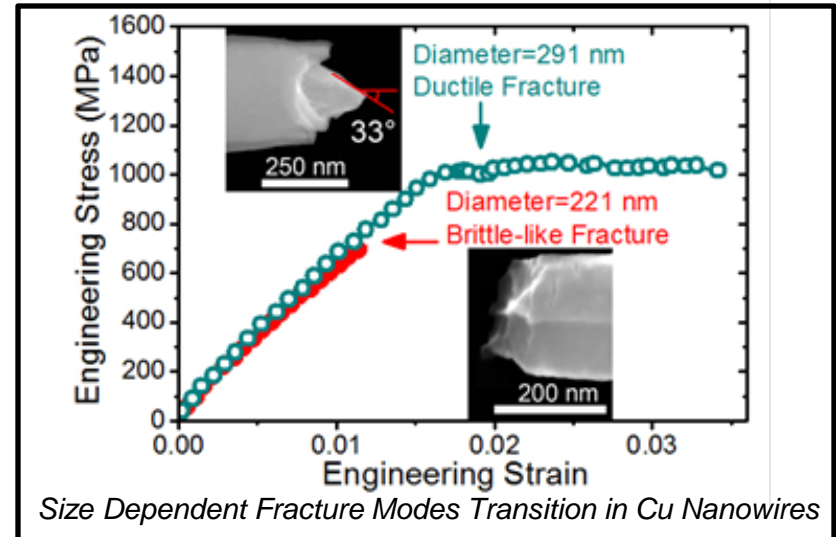
Kevin Dorfman and Zhicheng Long
University of Minnesota
Chemical Engineering and Materials Science
Work performed at University of Minnesota Nanofabrication Center

Electro-mechanical Characterization of Nanowires by MEMS

The research goal of this project is to probe one of the most important problems on the mechanical behavior of metals at the nanoscale, namely experimental verification of the existence of a mechanism of plasticity involving the transition from a dislocation interaction controlled regime to a surface dislocation nucleation dominated regime.

In the course of this work, considerably high strengths and yield stresses were found in both Ni and Cu nanowires. Two different fracture modes, ductile and brittle-like fractures, were found within the same batch of Cu nanowires. And the critical resolved shear stress (CRSS) was found to increase as the Ni nanowire diameters decreased, showing strong size dependence.

*Jun Lou and Cheng Peng, Rice University, Mechanical Engineering and Materials Science
Work performed at University of Minnesota Nanofabrication Center*



Single Molecule Tunneling with Sub-molecular Resolution for DNA Sequence and Fragment Sizing Applications

Our work deals with the fabrication of devices for single molecule electrical detection. We are working on the development of a nanopore-tunneling junction combined platform and the study of DNA for future biomedical applications.

Nanometer-scale pores (nanopores) are versatile single molecule sensors for the label-free detection and structural analysis of biological polymers such as DNA, RNA, polypeptides, and DNA-protein complexes in solution.

We have observed the alignment of a nanopore and a nanoelectrode couple using the Focused Ion Beam technique. We see different dynamics of DNA translocation through the device.

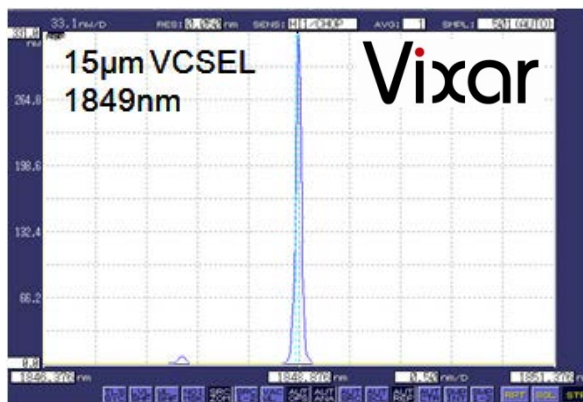
We developed a simple method to fabricate tunneling junctions aligned to a nanopore and proof-of-principle experiments demonstrating simultaneous detection of DNA translocations using both tunneling and ionic currents in a nanopore platform.

*Joshua Edel, Tim Albrecht, Emanuele Instuli, Alexandar Ivanov, Imperial College London, Department of Chemistry
Work performed at University of Minnesota Nanofabrication Center*

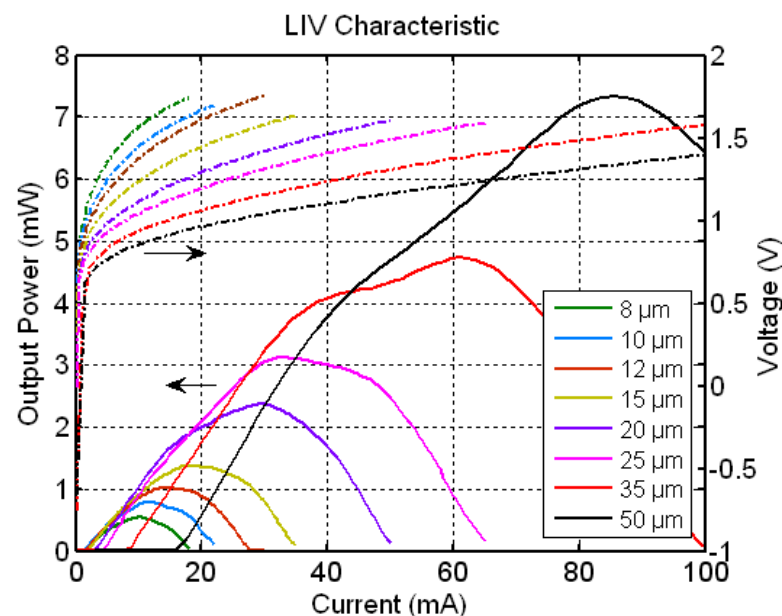
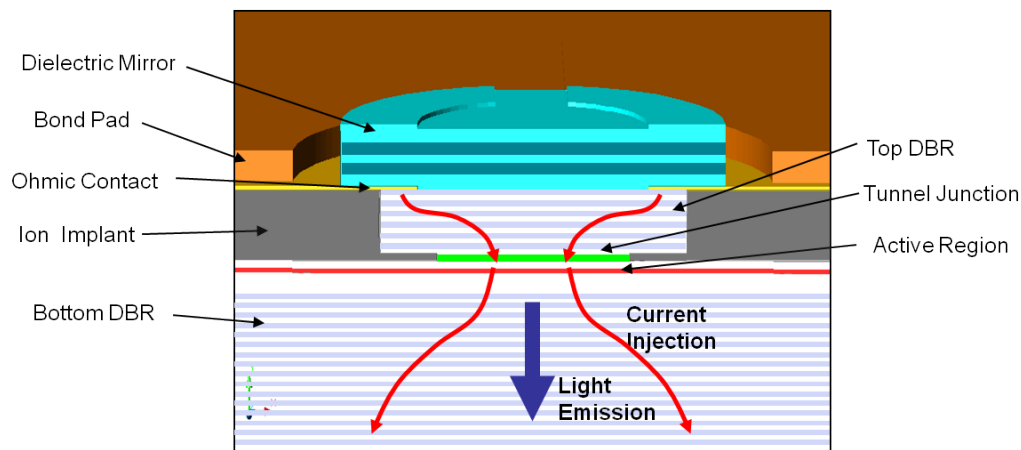
Long Wavelength VCSELs

This work centers around vertical cavity surface emitting lasers (VCSELs) for biomedical sensing and stimulation. They have a 1850nm wavelength and In-P based material platform.

1850nm laser performance allows power up to 7mW, a single mode spectrum less than 0.1nm FWHM, and continuous wave lasing up to 85° C.



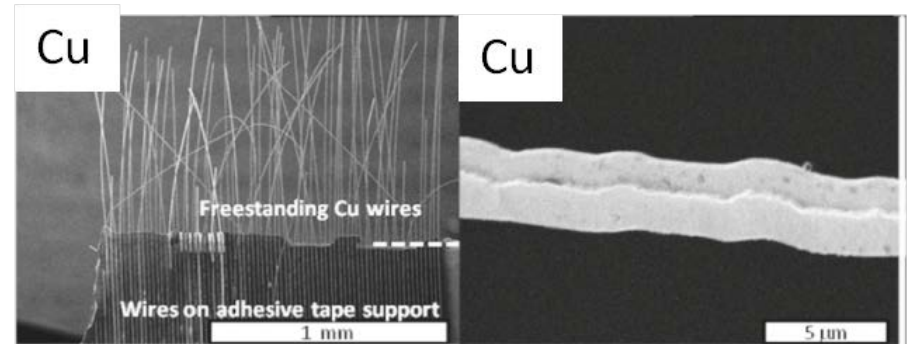
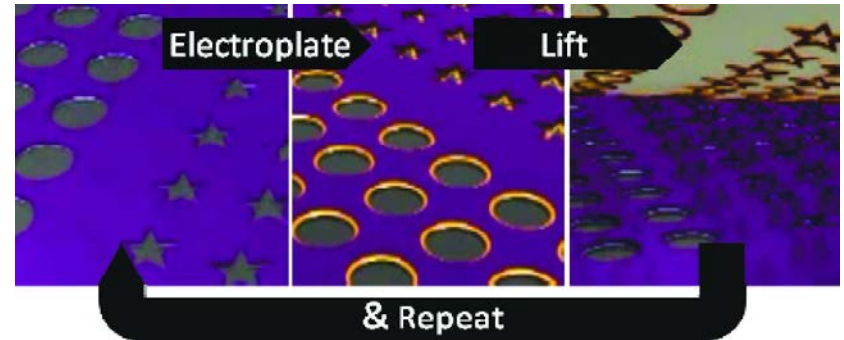
*Matthew Dummer, Klein Johnson, William Hogan, Mary Hibbs-Brenner, Vixar LLC
Work performed at University of Minnesota
Nanofabrication Center*



Electroplate-and-Lift (E&L) Lithography

The Electroplate-and-Lift Lithography Project involves a novel technique for mass production of micro- and nano-wires of any electroplatable material. The technique employs a reusable template of lithography patterned ultrananocrystalline diamond (UNCD). Wires initially nucleate on the edge of a 50nm thick conductive layer (nitrogen incorporated-UNCD). Wire growth continues as long as voltage is applied, to the desired final diameter. Wires may be removed by applying an adhesive polymer, such as office tape, to regenerate the template for subsequent electrodepositions.

Wires have been produced with 26 distinct materials. Wire diameters have varied from <100nm to 10 μ m, solely by controlling electrodeposition time. The composition of alloy wires is controlled through the chemical composition of the electroplating solution. Lifted-off wires are self-supporting for lengths >100x their diameter.

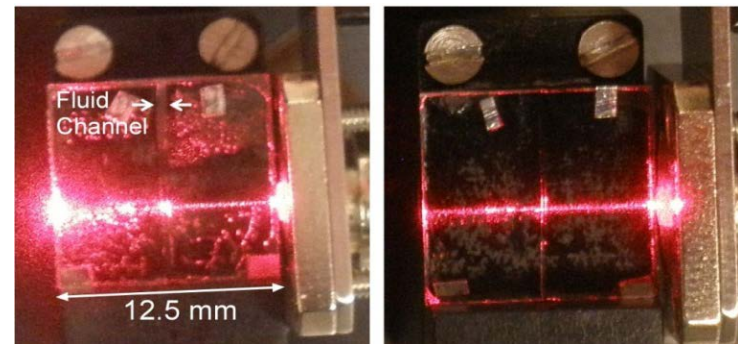
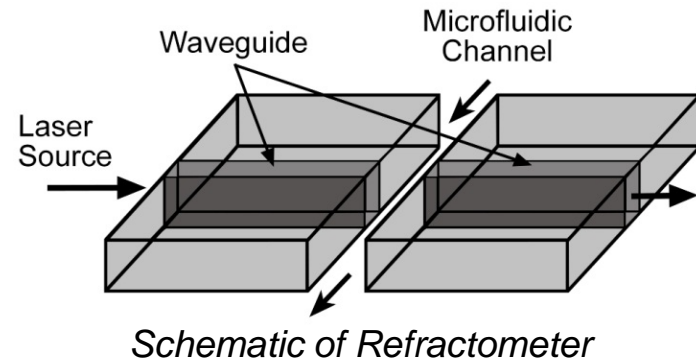


*Michael Zach and Lori Lepak, University of Wisconsin
Stevens Point, Department of Chemistry
Work performed at University of Minnesota
Nanofabrication Center*

Characterization of Holographic Photopolymer

In this work on holographic photopolymer characterization, the stiffness of the polymer is studied as a function of the exposure time and intensity. Fourier Transform-Infrared Spectroscopy is used to study the conversion rate of monomer to polymer.

It has been observed that the reaction rate depends on the exposure intensity, and that reaction starts (and stops) almost instantaneously when illumination is turned on (and off) once the threshold dose is reached.



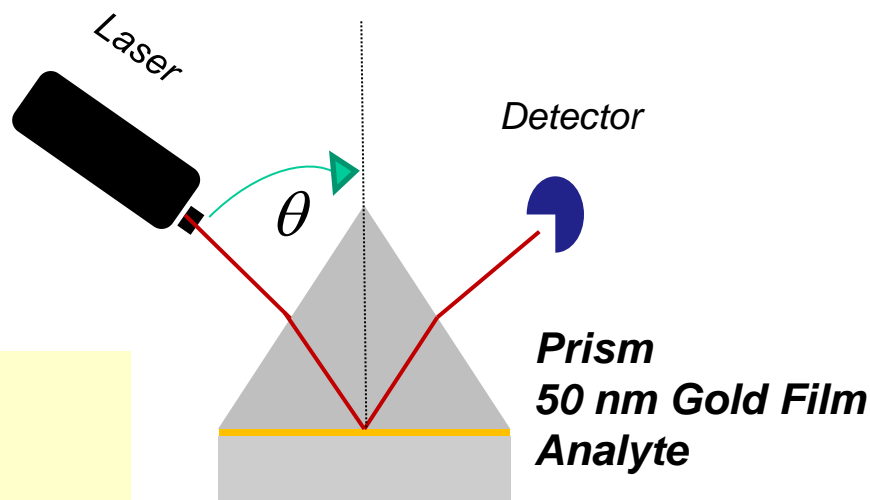
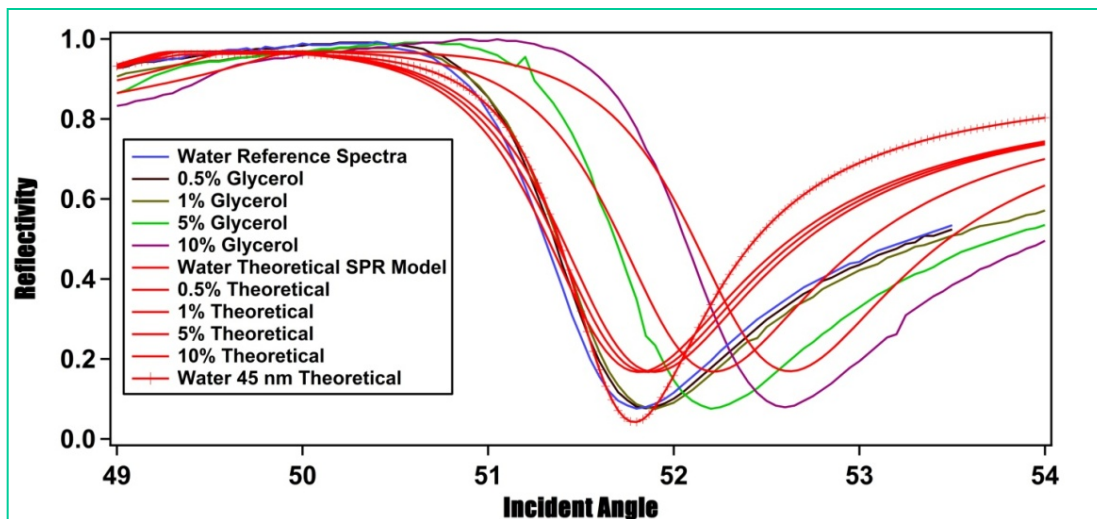
Refractometer without liquid (left) and with liquid (right) in the fluid channel realized using holographic photopolymer.

Martha Baylor and Lisa Plucinski, Carleton College
Work performed at University of Minnesota
Nanofabrication Center

Fabrication of Gold Films for Surface Plasmon Resonance (SPR) Measurements

The fabrication of gold films for SPR measurements employs 15 substrates fabricated by the University of Minnesota's Nanofabrication Center. A third of these substrates contain 50nm gold, 500nm silica; a third contain 50nm gold, 550nm silica; and a third contain 50nm gold, 600nm silica.

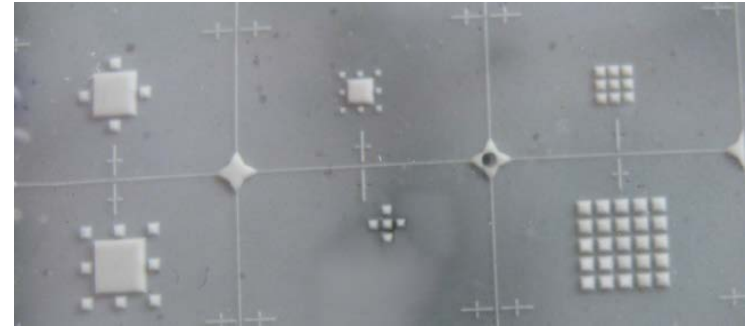
The films suitable for SPR measurements are those containing 60-64nm gold plus chromium and 523-555nm silica.



*Emily Smith, Kris McKee, Matthew Meyer,
Iowa State University, Department of Chemistry
Work performed at University of Minnesota
Nanofabrication Center*

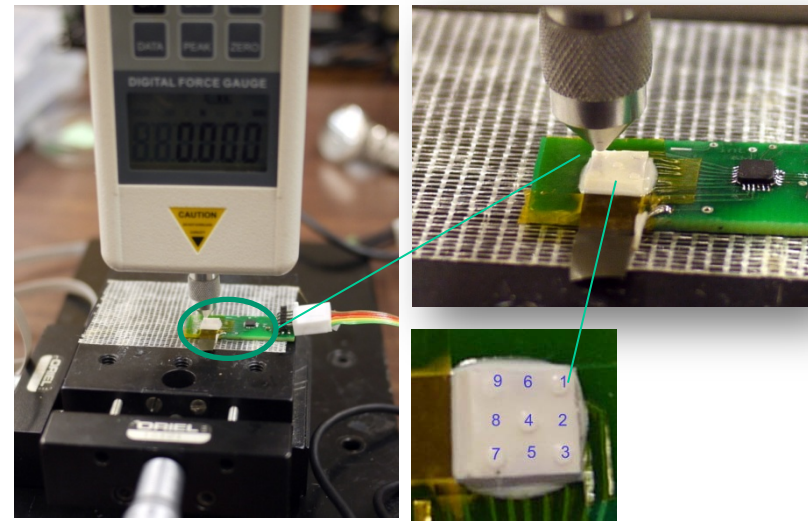
MEMS Sensors

The research group's work at the University of Minnesota's Nanofabrication Center involves investigations and fabrication of numerous sensor devices including tactile sensors, muscle force sensors for neuromuscular diseases, wireless carbon nanotube sensors for breath analysis in humans, and battery-less wireless MEMS sensors.



Polymer MEMS sensor nodes for capacitive tactile sensors

*Ahmet Serdar Sezen, Rajesh Rajamani, Peng Peng, Kalpesh Singal, Mahdi Ahmadi, Saint Cloud State University and University of Minnesota
Work performed at University of Minnesota Nanofabrication Center*



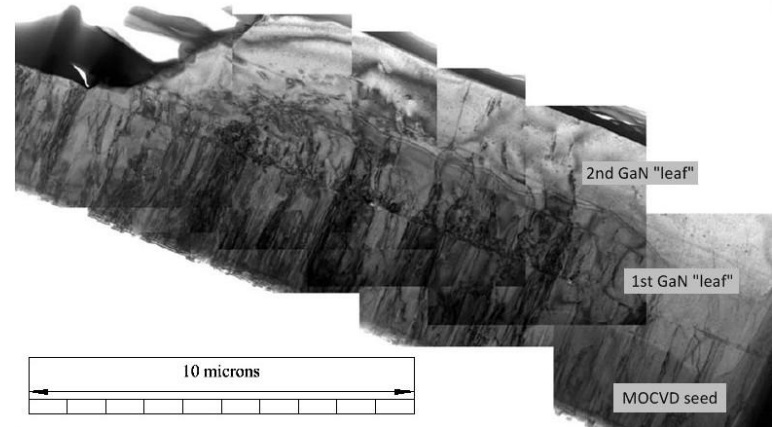
Capacitive Polymer MEMS Tactile Sensors for Minimally Invasive Applications

GaN Liquid Phase Epitaxy from Ca-Ga-N Solutions

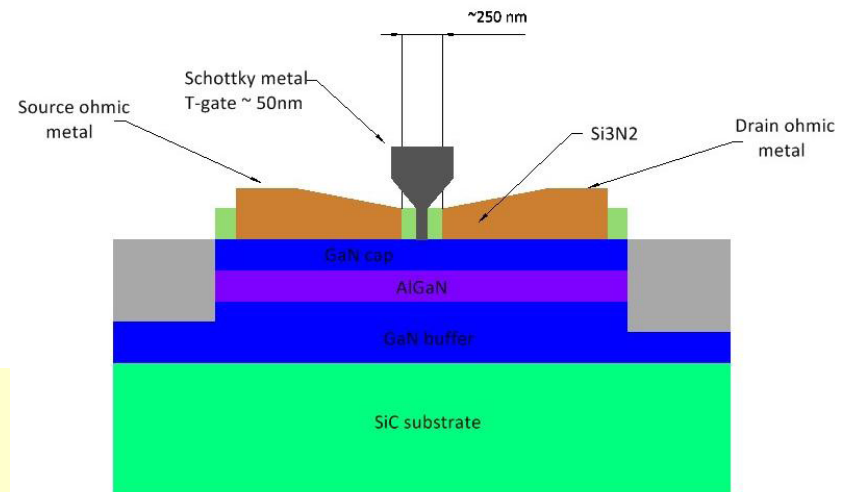
The IIAN Company has been conducting work at the Nanofabrication Center for a NASA sponsored Phase I SBIR project on GaN Liquid Phase Epitaxy from Ca-Ga-N solutions. Phase II has now been awarded and will rely heavily on use of the Vistec e-beam lithography tool for processing sub-micron gates for AlGaIn/GaN HEMTs.

E-beam lithography is used for “ultra-scaling” FET gates with lengths <50nm and source-drain spacing <200nm.

New III-nitride materials science work is a continuation of Phase I work with CaGaN for contact for reduction of parasitic resistances. The work also involves selective epitaxy for N+ GaN under contacts using LPE processes, high-k dielectrics for MISFET designs, and electric field engineering of source-drain region.



Gallium nitride epi-structure of LPE films (above), and 50nm t-gate (below)



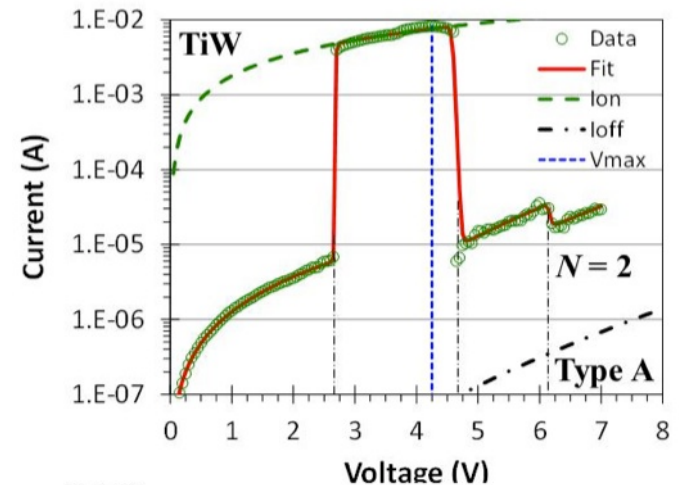
Jody Klaassen, The IIAN Company
Work performed at University of Minnesota
Nanofabrication Center

University of Texas

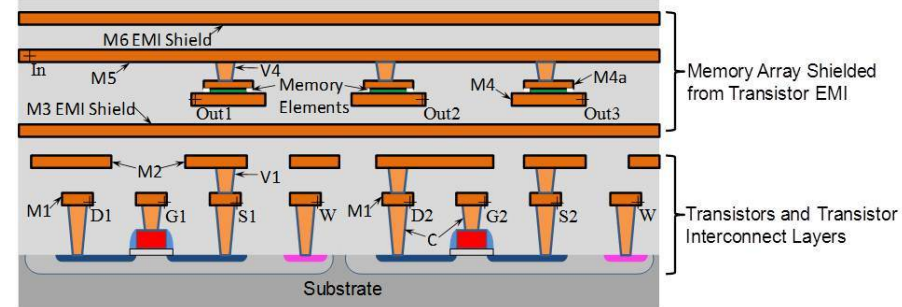
Low-Cost Radiation-Hard Nonvolatile Random-Access Memory

PrivaTran is developing advanced memristor-based architectures for nonvolatile random access memory (RAM). The requirements for proper memory element isolation, programming voltage drive and current sense circuitry will be determined by circuit analysis. Memristor circuit models will be developed and used to trade different memristor types and optimize performance to the technical program objectives. Viable circuit topologies will be identified that enable high-density data storage solutions for aerospace and defense applications. Phase II prototype fabrication and commercialization work plans will be developed including a manufacturability analysis addressing materials compatibility and integration methods for insertion into current CMOS and BJT platforms as well as scaling the technology to the 10nm technology node and beyond.

PrivaTran - Glenn Mortland
Air Force SBIR AF112-087
Work performed at University of Texas
Microelectronics Research Center



Memristor I-V Response and Model (red line)



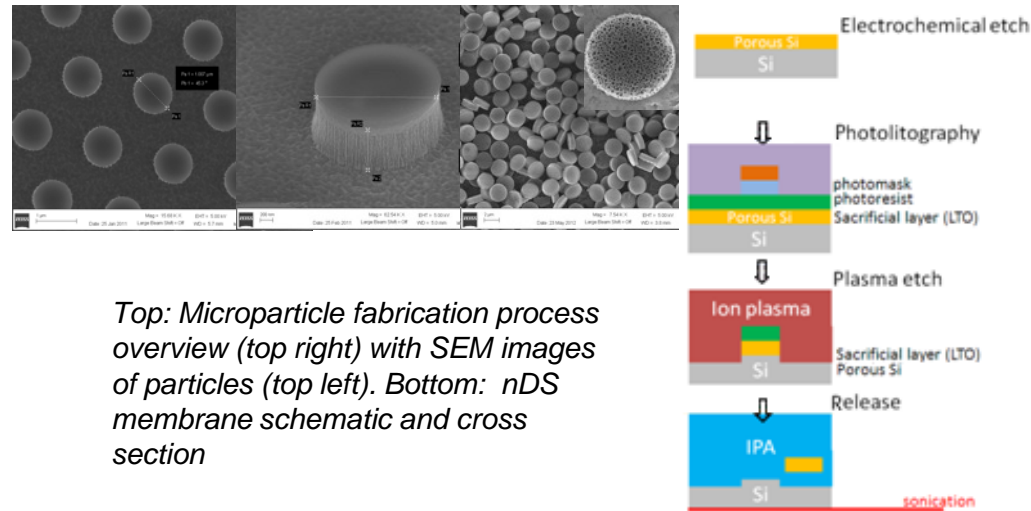
Memristor Integration Approach for 3D Architectures

Silicon fabrication of microparticles and nanochannels

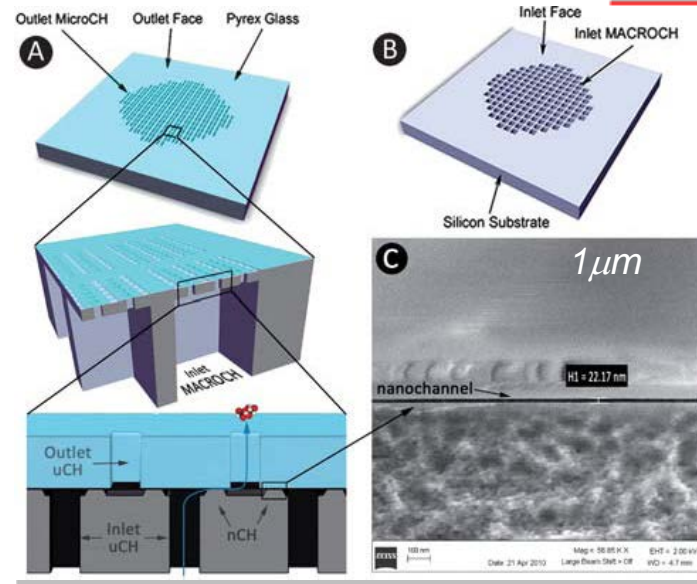
Silicon is utilized in the fabrication of microparticles and nanochannels to provide new strategies for delivery of pharmaceutical agents that maximize therapeutic efficacy while minimizing side effects.

Porous microparticles act as a first-stage vector for the intravenous delivery of therapeutics. Nanoscale drugs or imaging agents can be loaded into the pores and are delivered to the target site, avoiding sequential bio-barriers. Zero order release kinetics is observed allowing sustained therapy over long time periods. Microparticles are fabricated by patterning an electrochemically (EC) etched silicon substrate, where pore size, morphology, diameter and aspect ratio are controlled along the process.

The nanochannel delivery system (nDS) is capable of tunable long-term zero-order release of therapeutics for clinical applications. A silicon membrane inside the system, with nanochannels as small as 5 nm, allows for the independent control of both dosage and mechanical strength through the integration of high-density short nanochannels parallel to the membrane surface with perpendicular micro- and macrochannels for interfacing with the ambient solutions. These nanofluidic membranes are created using precision silicon fabrication techniques on silicon-on-insulator substrates enabling exquisite control over the monodispersed nanochannel dimensions and surface roughness. Zero-order release of analytes is achieved by exploiting molecule to surface interactions which dominate diffusive transport when fluids are confined to the nanoscale.



Top: Microparticle fabrication process overview (top right) with SEM images of particles (top left). Bottom: nDS membrane schematic and cross section

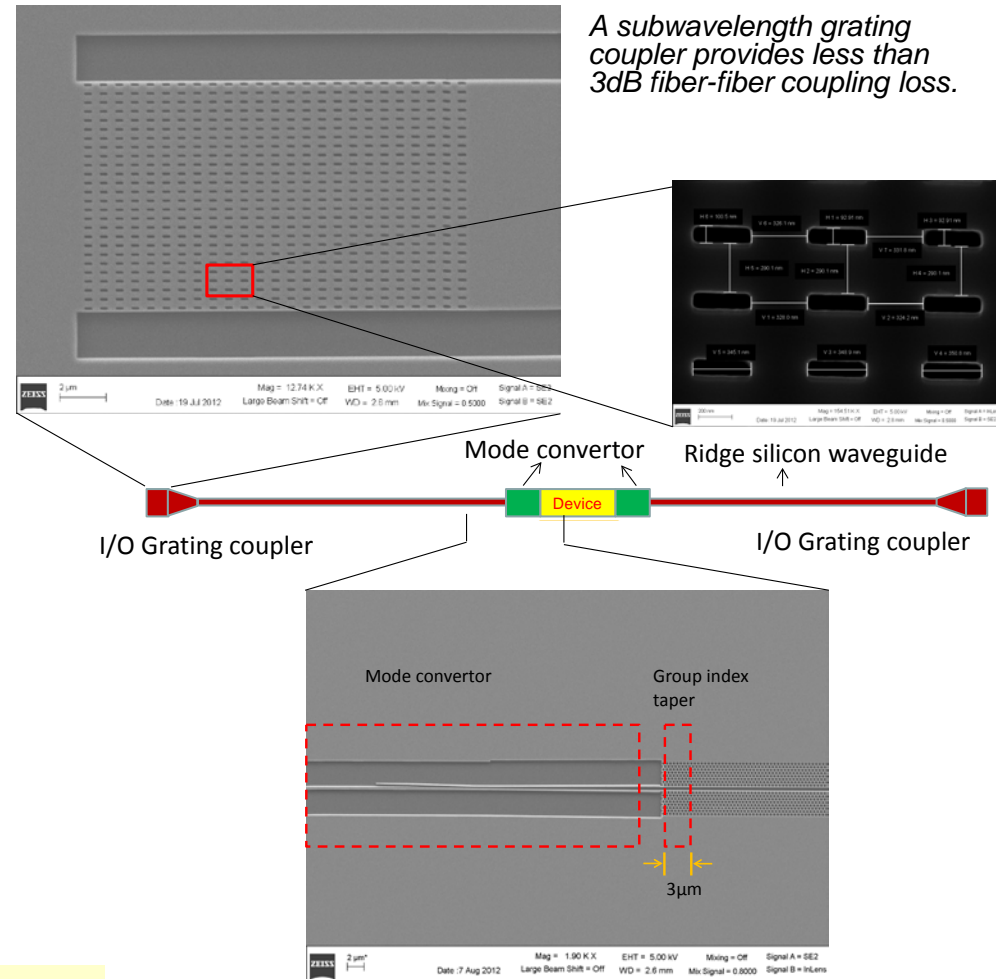


The Methodist Hospital Research Institute – Department of Nanomedicine (M Ferrari). Work performed at MRC UT-Austin

Sub-100 μm Electro-optic Polymer Modulator

Example---- Mach-Zehnder optical modulators provide both phase and amplitude modulations over a large working spectrum, however with a distinctive challenge of long device footprint (a few millimeters) compared to ring resonators and electro-absorption modulators. The purpose of this program is to achieve Error free (bit error rate $< 10^{-9}$), high speed operation (40GHz), and low insertion loss (10dB) on a hybrid Electro-Optic polymer and silicon platform. The slow light effect in silicon photonic crystal structure is exploited together with a high efficiency Electro-optical coefficient ($r_{33}=150\text{pm/V}$) and concentration of high energy photons in a photonic crystal slot waveguide region to realize the required phase shifts.

Amir Hosseini, Omega Optics Inc.
Work performed at UT Austin, Microelectronics Research Center facilities.



A photonic crystal waveguide phase modulator with phase-shifter length less than 100 μm . Electro-optic polymer with $r_{33}=150\text{pm/V}$ refills the slot waveguides and serves as the active material.

Enhanced Cooling using Nanofluids & Nanosensor Arrays in Microchannels containing Nanofins

Efficacy of coolants can be enhanced by *doping with nanoparticles at low concentrations (“nanofluids”)* and *during flow in microchannel which contain nano-sized pillars (or “nanofins”)*. *Nanofluid coolants and nanofins in microchannels augment the effective surface area in contact with the hot surface. Cooling efficacy is monitored using hi-speed & hi-resolution temperature nanosensors (Thin Film Thermocouples, “TFT”) arrays in microchannel. Nanofins also enhanced phase change (e.g., boiling, condensation).*

MRC facilities are used for making *nanosensors (TFT) and nanofins* using: *Step & Flash Imprint nanolithography (SFIL, IMPRIO 100), Deep Reactive Ion Etching (DRIE/ RIE, Plasma Therm #2), Atomic Force Microscopy/ Electron Microscopy (AFM/ SEM), and Physical Vapor Deposition (PVD, CHA #1).*

Sponsors: National Science Foundation (USA), '12-'14

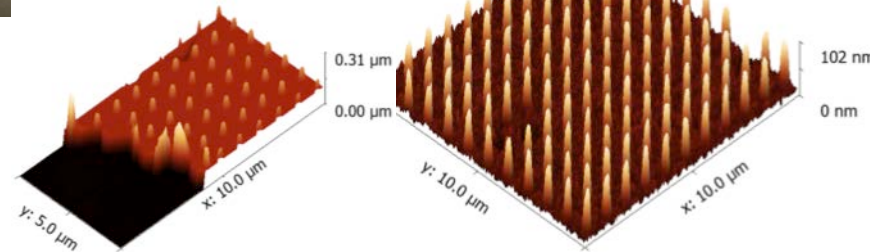
PI: D. Banerjee - Texas A&M Univ.

Qatar National Research Foundation, '09-'12. PI: D. Banerjee (US) and Dr. R. Sadr (Qatar)

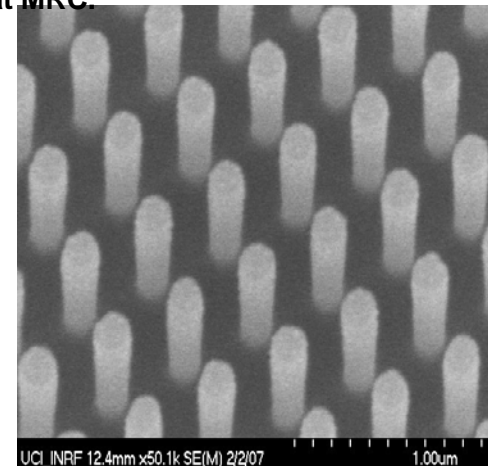
Work performed at the MRC (Univ. of Texas, Austin)



High-speed & high-resolution temperature nanosensors (Thin Film Thermocouples “TFT”). TFT are fabricated in a dense array using E-beam evaporation and the “lift-off” process. The TFT are ~200–500 nm thick and have response speed of ~5–10 MHz.



Dense array of nanofins with 200 nm diameter, 10-600 nm height and 800 nm pitch before etching (AFM top left) and after etching (AFM top right /SEM below). The nanofins are made by SFIL at MRC.



UCI_INRF 12.4mm x50.1k SE(M) 2/2/07

1.00um

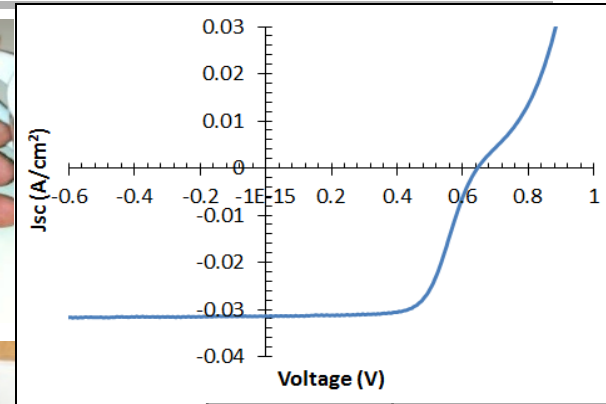
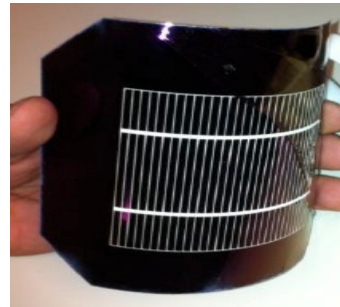
AstroWatt—Thin Crystalline SOM (Semiconductor on Metal) PhotoVoltaic (PV) and CMOS applications

Thin crystalline foils have been exfoliated to demonstrate large area PV cells and CMOS devices. Thin materials allow costs to be substantially reduced and enable new form factor applications. 8" wafers were exfoliated for the first time and large area processing completed on these foils.

Thin crystalline CMOS cells can be used in the emerging TSV(Thru-Silicon Via) and 3D integrated products as well as flexible electronics.

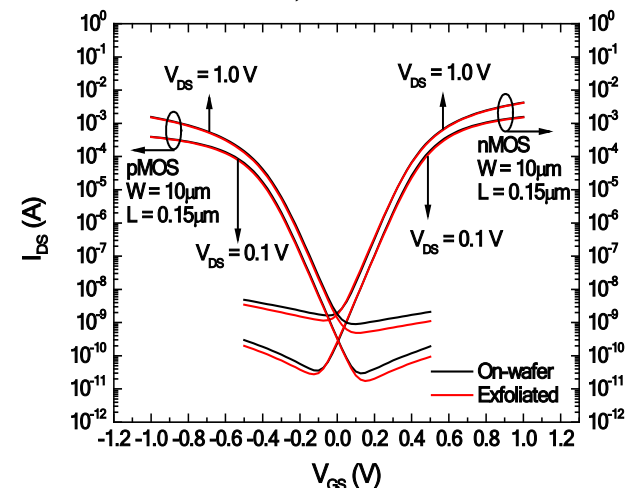
Thin crystalline silicon allows the highest efficiency solar cells by using the optimal silicon thickness to eliminate bulk losses, reduce cost and fabricate modules with traditional and new curved form factors. RPCVD (Remote Plasma-CVD) was used to complete these PV cells and very high Voc was demonstrated.

AstroWatt Inc.: Work Performed at UT-Austin NNIN – Microelectronics Research Center. by L Mathew et



Voc	645 mV
Jsc	31.5 mA/cm ²
FF	66.2%
Efficiency	13.4%

Thin Crystalline Silicon PV cells, less than 30um thick cells



Large Area Flexible thin crystalline Silicon CMOS.

NanoMembrane Silicon Photonics Project

The purpose of the nanomembrane photonics project is to develop photonic components based on patterned semiconductor crystalline nanomembranes transferred onto foreign rigid or flexible plastic substrates. Photonic crystal patterning and fabrication process was carried out at NNIN-UT Austin MRC site. High quality flexible photonic filters, ultra-compact membrane reflectors on Si have been fabricated based on membrane printing transfer processes, carried out at both University of Wisconsin-Madison (in collaboration with Prof. Zhenqiang Ma) and at University of Texas at Arlington NanoFAB center.

Prof. Weidong Zhou, University of Texas at Arlington
Prof. Zhenqiang (Jack) Ma, University of Wisconsin-Madison
Work Supported by AFOSR MURI, ARO and AFOSR STTR projects (PM: Gernot Pomrenke)
Fabrication support, partially at NNIN UT Austin MRC

References:

- *H. Yang et al., IEEE Photon. Tech. Lett. 24, 346 (2012).*
- *Z. Qiang et al., IEEE Photon. Tech. Lett. 22, 1108 (2010).*
- *W. Zhou et al., J. Phys. D. 42, 234007 (2009).*

Ultra-compact single layer photonic crystal Fano resonance broadband reflectors on silicon and on glass.

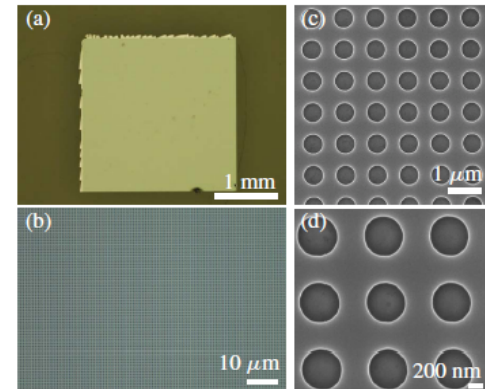


Fig. 2. (a) and (b) Optical microscope images. (c) and (d) Scanning electron microscope (SEM) images of transferred Si NM on glass.

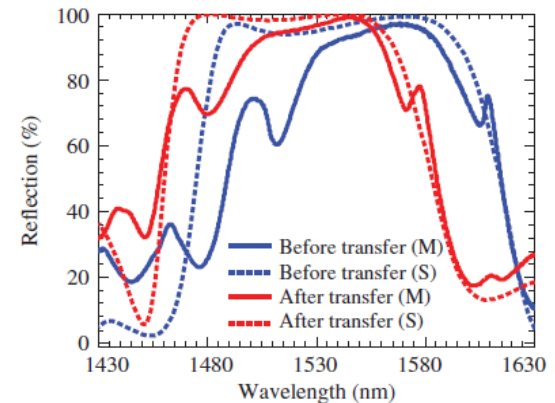
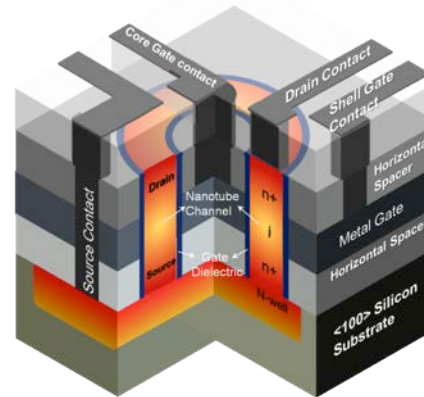


Fig. 3. Measured ("M") and simulated ("S") Si NM membrane reflector reflection spectra on SOI (before transfer) and on glass substrate (after transfer).

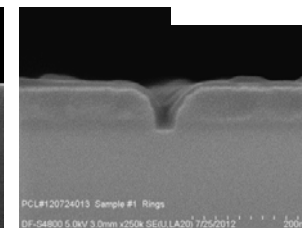
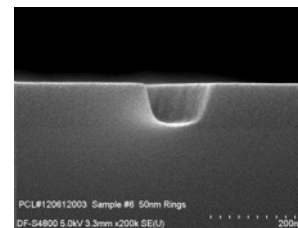
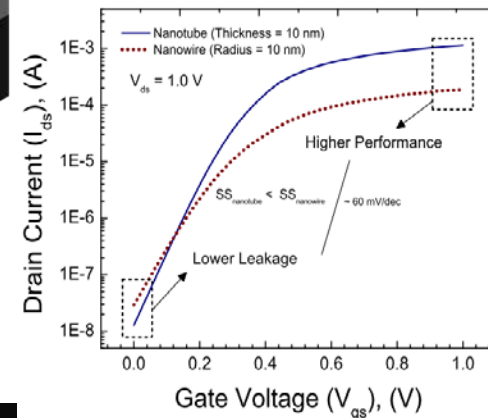
Si Nanotube Field Effect Transistors

The goal of this project is to demonstrate the capability of vertical nanotube transistors using conventional silicon based channel materials for hybrid high performance and low power operation. These devices are controlled by dual inner/outer core/shell gate stacks to invert the entire volume of the nanotube channel similar to gate-all-around nanowires, leading to low leakage and near ideal sub-threshold swings. Unlike nanowires, these devices are capable of higher performance than a stacked array of nanowires while occupying minimal chip area. Process advantages such as selective epitaxy, deposition controlled gate length definition and steep in-situ graded doping enable these devices for ballistic charge transport study in ultra short channel devices and extension to beyond-Si platforms such as III-V based nanotubes. Films for the gate stacks were deposited using low pressure CVD furnaces. Patterns were defined using electron beam lithography and reactive ion etching. Selective epitaxy and in-situ doping were achieved using a rapid thermal CVD reactor.



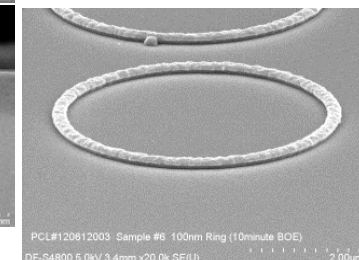
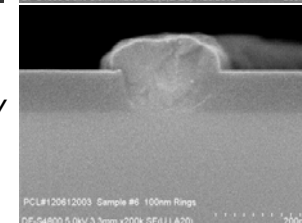
3D illustration of silicon based nanotube FET

Simulated advantage of a nanotube over a nanowire architecture



Gate stack definition

Selective silicon epitaxy



Hossain Fahad, Muhammad Hussain, KAUST
Work performed at Microelectronic Research Center,
UT Austin

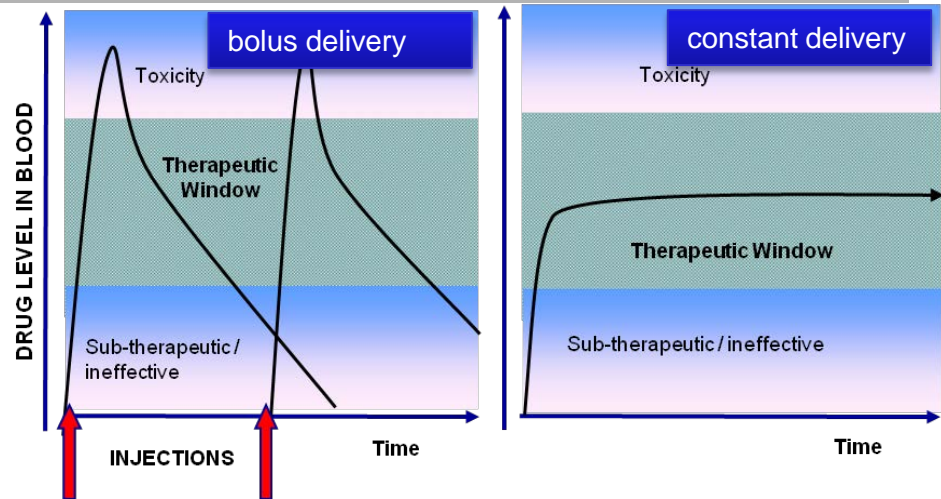
Long-term implantable drug-delivery devices

NanoMedical Systems, fabricated medical device that used silicon chip embedded in a capsule. The silicon chip formed by nanochannels filled with pharmaceutical drug are implanted under the skin to provide constant drug release over an extended period of time.

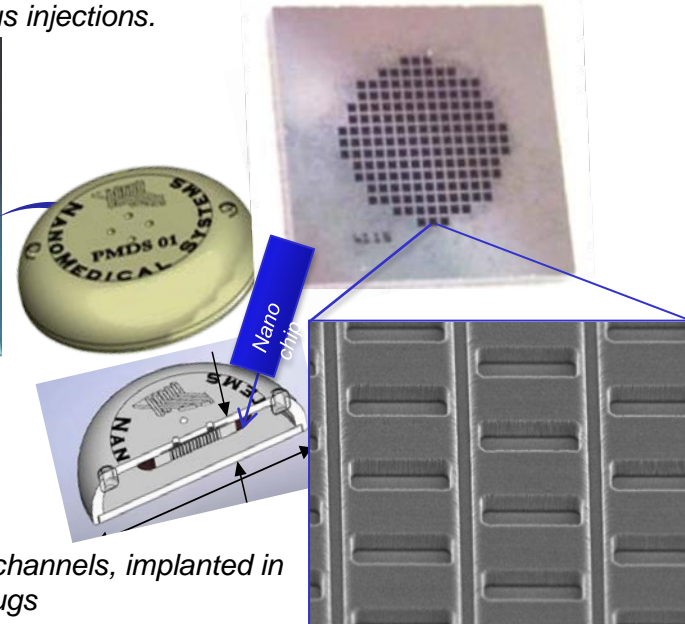
Nanochannels near the size of drug molecules (2nm – 300nm high) are fabricated in silicon based devices at the wafer level using advanced semiconductor processes. Further the wafers are diced into individual devices.

At the UT-MRC, sacrificial materials are the stripped off and the chips are cleaned with various chemical solutions. Precise structural dimensions and surface quality are characterized using the SEM.

The chips are then inspected, packaged, and tested for in-vitro and in-vivo drug release characteristics.

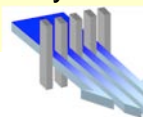


A constant drug dosing in the therapeutic window is desirable compared to bolus injections.



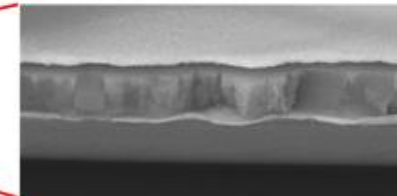
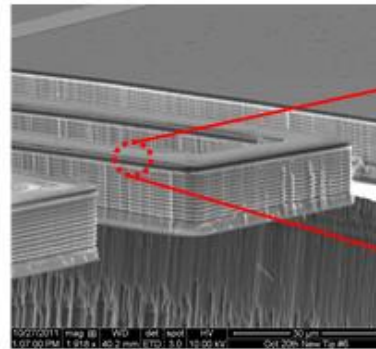
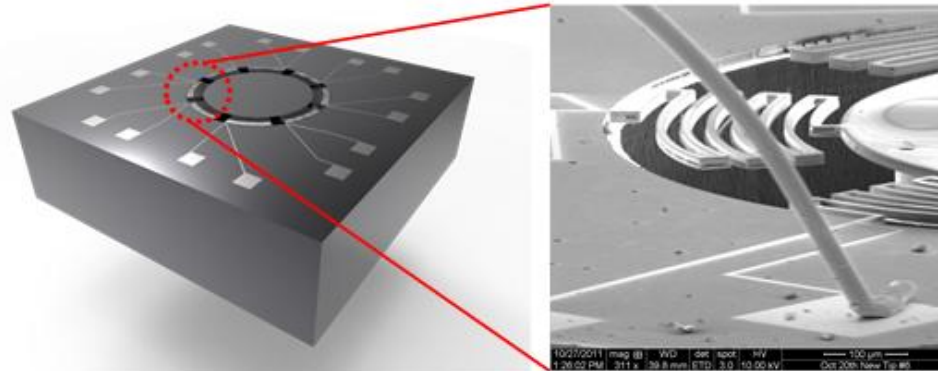
Nano chip with nanochannels, implanted in capsule filled with drugs

Kunal Raghuwansi et al. at NanoMedical Systems
Work performed at MRC UT-Austin



Micromachined Seismometers with Piezoelectric Sensing and Actuation

Seismometers utilizing piezoelectric materials for sensing and actuation of a proof mass provides both low noise acceleration measurements + ultra-high dynamic range and linearity. These sensors can be made small, cheap, disposable, and with low acceleration and velocity noise floors. This seismic sensor can be used for the monitoring of explosions, oil and gas exploration, civil infrastructure monitoring, and scientific instrumentation applications. Prototypes have been successfully fabricated at UT-MRC.



- ← Top Electrode (Ti/Pt)
- ← PZT (1 μm)
- ← Bottom Electrode (TiO_x/Pt)
- ← Thermal SiO₂ (1 μm)

(PI) Neal A. Hall , U. Texas Austin
Work sponsored by DOE NNSA

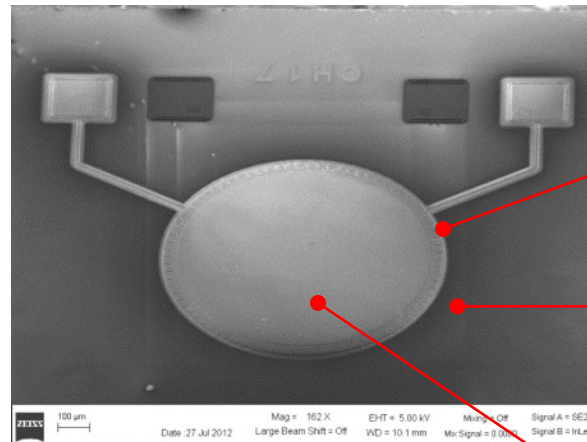
Top: CAD image of a 3mm x 3mm MEMS Seismometer and an SEM of prototype showing the active springs and an electrical wirebond to a piezoelectric electrode. Bottom: zoomed-in images of a spring illustrating the piezoelectric films on top.

High Performance MEMS Microphones for Hearing Aids

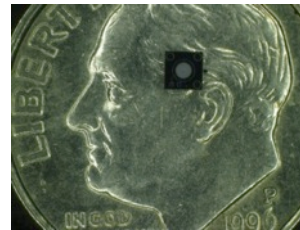
The purpose of this project is to introduce the first commercialized optical-based MEMS microphone. Semiconductor lasers and diffractive optics enable a robust micro-interferometer, which in turn is used to resolve acoustic waves with 20dB improvement in SNR as compared to conventional miniature microphones. High fidelity MEMS microphones will improve hearing aid performance and the quality of life for those with hearing-impairments.

The ability to apply internal forces to the microphone diaphragm via piezoelectric materials empowers the device with a “self-calibration” feature. Processing of these piezoelectric materials is being developed at Microelectronics Research Center at The University of Texas at Austin.

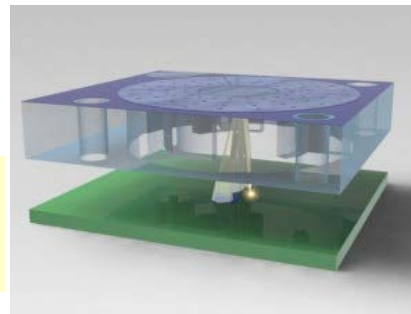
Neal A. Hall and Arjang Hassibi (PIs at UT-Austin), and Silicon Audio, Inc.
Work sponsored by NIH



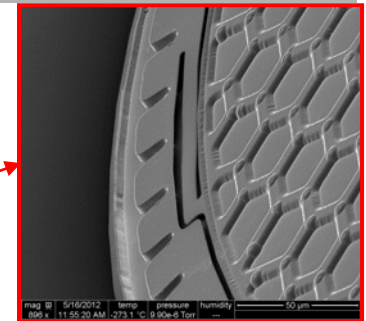
A MEMS microphone structure fabricated on silicon.



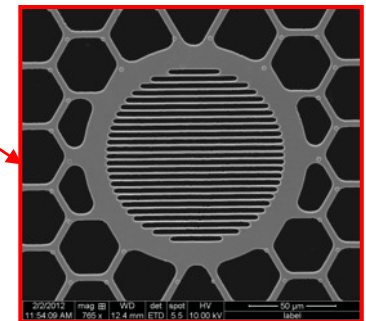
Relative size comparison between MEMS microphone and a US dime



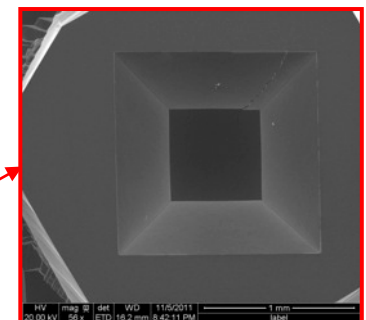
Schematic illustrating optical readout of the microphone diaphragm.



Spring connecting the diaphragm to the anchor



Underneath the diaphragm resides a back-plate consisting of a diffraction grating etched into polysilicon



Backside cavity of the MEMS microphone, fabricated by KOH etching.

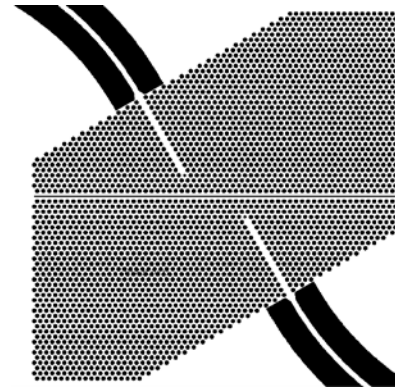
University of Washington

Optical Trapping in a Photonic Crystal Microcavity: Chip Based Cavity QED

The objective of this project is to study the interaction of single metal and semiconductor nanoparticles with single photons: cavity quantum electrodynamics. This is to be done on a wafer-scale, using silicon-on-insulator optical circuits to excite and probe the interaction region, defined by a photonic-crystal-based optical microcavity. The microcavity is based on a slot-waveguide geometry which supports modes localized primarily outside of the silicon. By operating the circuit in a solvent (such as hexane), containing metal and/or semiconductor nanocrystals, efficient optical trapping of the nanoparticles at the antinode of the cavity is expected.

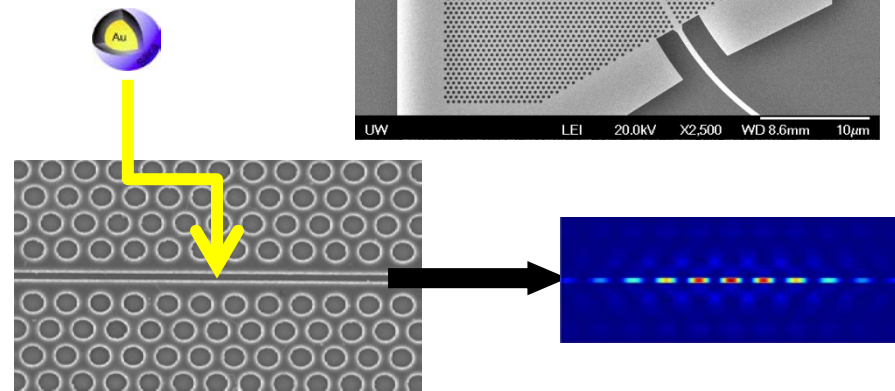
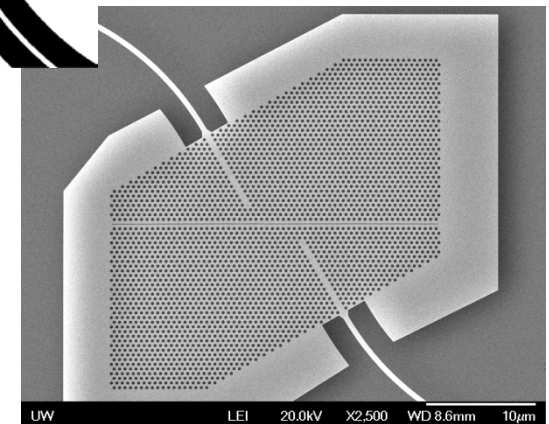


Jeff Young,
University of British Columbia, Vancouver, Canada
Work performed at U. Washington.



Left: Layout, holes represent photonic crystal and lines represent 1D defects (grating couplers not shown).

Below: SEM micrograph of the fabricated photonic crystal microcavity.

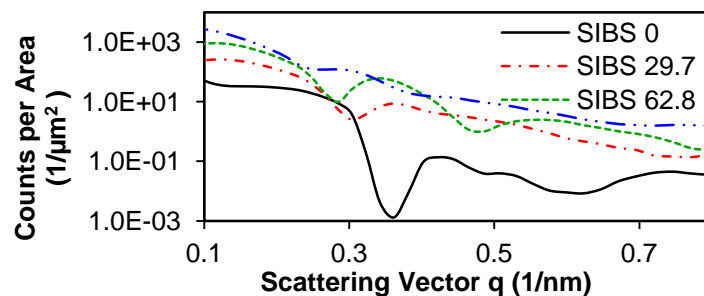
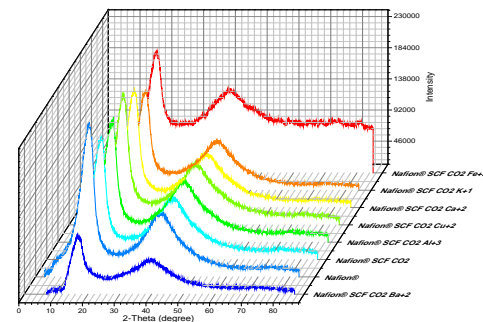


Nanoparticle will be "self-aligned" in cavity via optical trapping

Morphology of Block Copolymer Ionomer Thin Films for Micro Fuel Cell Devices

The purpose of this investigation is to develop selective and efficient block copolymer ionomers for direct methanol micro-fuel cell (μ DMFC) applications. The study evaluated changes in the morphology and nanostructure of Nafion® and poly(styrene-isobutylene-styrene) (SIBS) with changes in: sulfonation level, counter-ion substitution, hydration effect and even substrate type. The results show significant variations in crystallinity upon supercritical fluid processing of Nafion®, and changes in the morphology as well as the interconnected ionic distance with sulfonation for SIBS membranes.

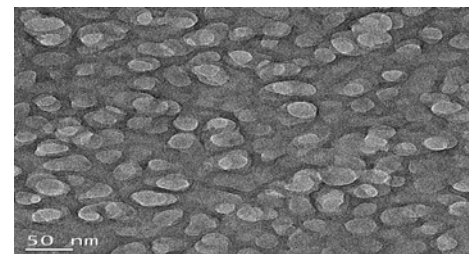
XRD results showing changes in the crystallinity of Nafion® upon Supercritical Fluid CO₂ Processing with Counter-Ion Substitution.



SAXS results for poly(styrene-isobutylene-styrene) showing changes in morphology and interstitial ionic distance



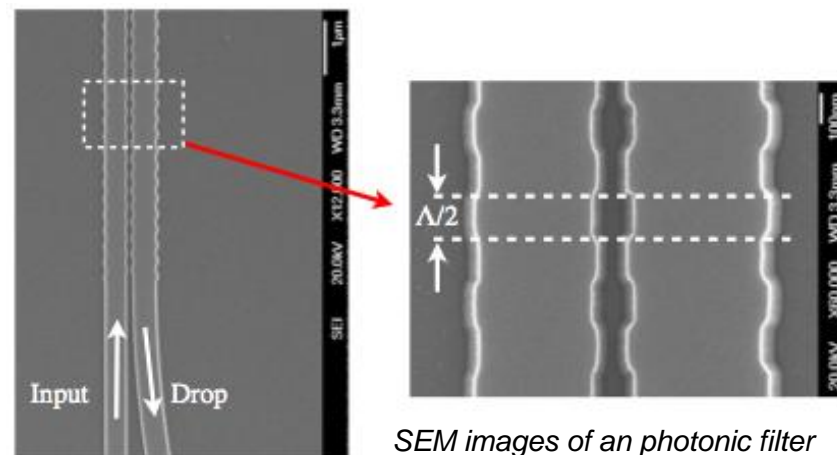
TEM image of sulfonated poly(styrene-isobutylene-styrene)



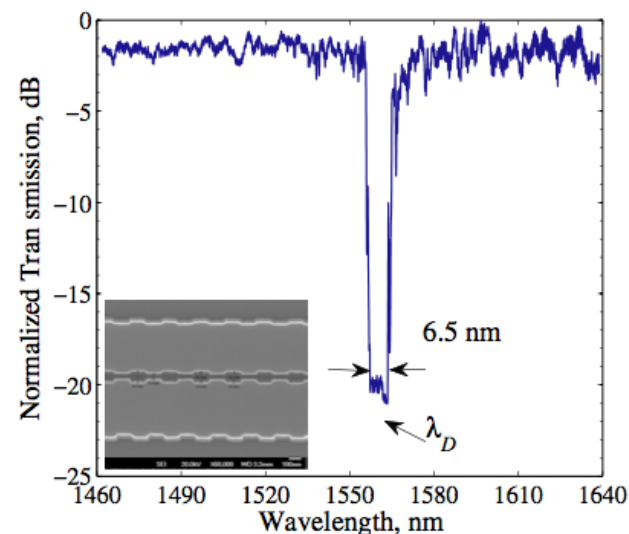
David Suleiman, Universidad de Puerto Rico
Mayaguez, PR
Work performed at U. Washington

Wavelength-Division Multiplexing Networks for On-Chip Optical Interconnects

Chrostowski's group develops low-power, low-cost on-chip wavelength-division multiplexing (WDM) systems for high-speed optical interconnects in order to eliminate the communication bottleneck between and within microchips. The fabricated devices are essential photonic filtering components in the proposed system, which are designed to overcome the main issues facing silicon photonics (such as high-temperature sensitivity and wafer non-uniformity) and enable athermal, high-performance wavelength multiplexer and demultiplexers. The devices were fabricated using e-beam lithography and plasma etch for the required fabrication accuracy and in-time verification of the design concept.



SEM images of an photonic filter using grating-assisted, contra-directional couplers.



Measured transmission spectrum of an add-drop photonic filter.



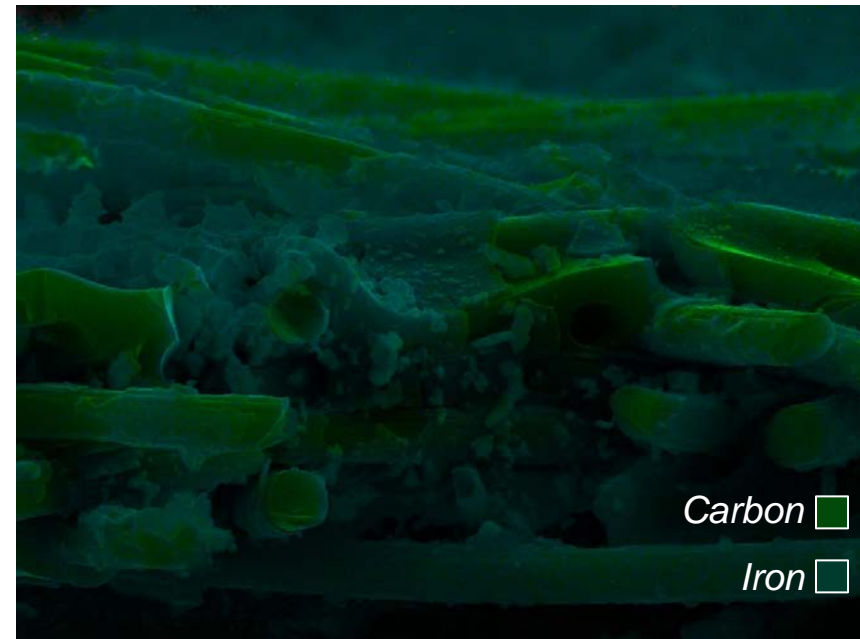
Lukas Chrostowski, The University of British Columbia,
Vancouver, Canada
Work performed at U. Washington

Iron Nanoelectrodes for Powerful Air Batteries

The objective of this project is to develop iron electrodes for metal-air batteries that charge and discharge more quickly than conventional metal-air batteries (i.e., have greater power densities). We deposit iron oxides as continuous nanoparticle coatings onto porous carbon nanomaterials, and use SEM-EDS mapping to visualize the degree that FeO_x coats the pore walls of the carbon scaffold. The resulting electrodes are electrochemically reduced into metallic iron, and their normalized discharge capacity is compared to that of planar iron electrodes as current densities are increased.



Justin Lytle, Pacific Lutheran University, Tacoma, WA
Work performed U. Washington



SEM-EDS map of FeO_x -coated carbon nanofoam electrodes

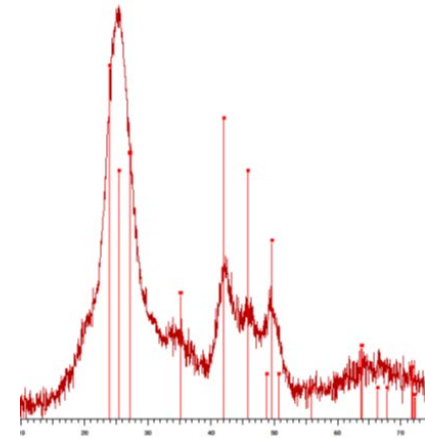
Comparing Surface Ligand Effects on Nanocrystal Spheres and Belts

The purpose of this project is to compare the effects of a variety of surface ligands on the photoluminescence of nanocrystals with different shapes. For example, pyridine is known to quench CdSe nanocrystal sphere photoluminescence. We examine whether pyridine also quenches CdSe nanobelt photoluminescence.

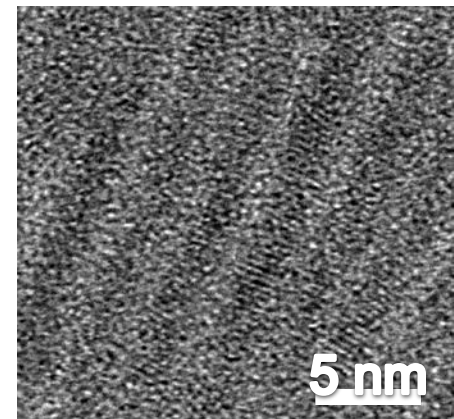
Munro's group uses the UW-NNIN facilities to study the synthesized nanocrystals in order to confirm their size, shape, and crystallinity. The imaging is also used to determine the size and shape distributions in each batch of nanocrystals.



Andrea Munro, Pacific Lutheran University, Tacoma, WA
Work performed at U. Washington



XRD of spherical CdSe nanocrystals



HR-TEM image of CdSe nanobelts

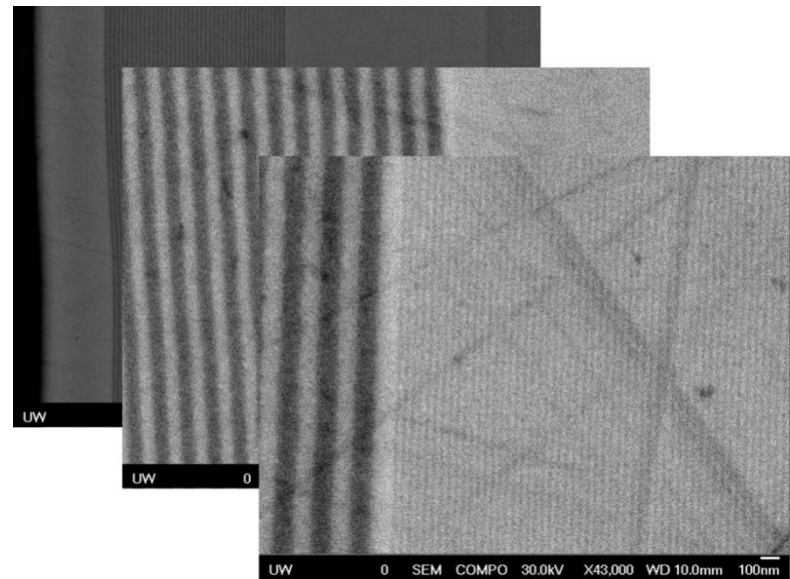
Nanolaminated Material Characterization

Modumetal is creating a revolutionary new class of nanolaminated materials. Modumetal is based on the interaction of different materials at their interfaces. By laminating metals, Modumetal creates a new way to influence material properties. By growing metal using low-cost electrochemistry, Modumetal enables a whole new class of applications of these materials.

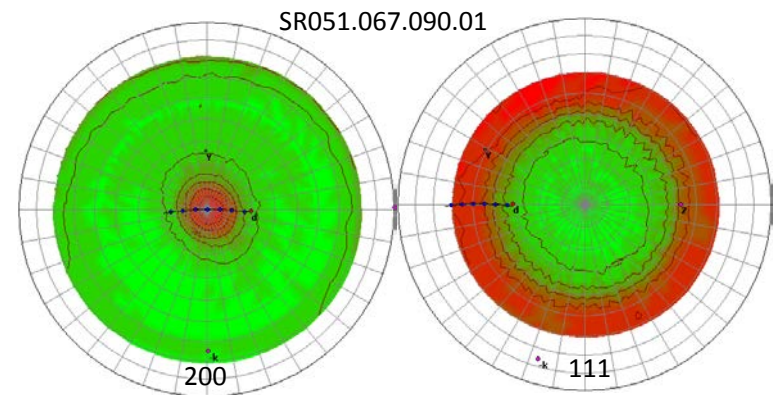
Today, Modumetal is poised to revolutionize metal performance as we know it by controlling material interfaces at the nanoscale. Modumetal manufacturing is based on a "green" approach which reduces the carbon footprint of conventional metals manufacturing, and it redefines the approach to materials engineering.



Modumetal, Seattle, WA
Work performed at U. Washington



Multiscale Lamination



Pole figure obtained using Bruker D8 Discover with GADDS

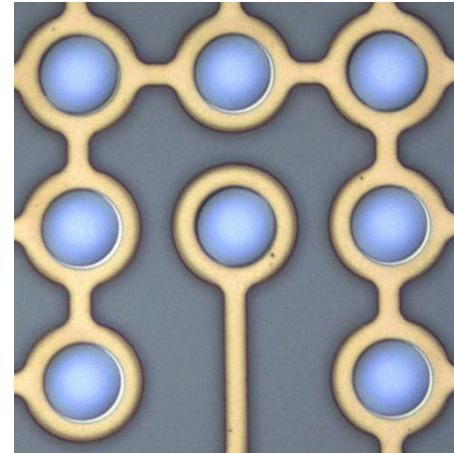
Electronic Molecular Detection

3D nanochannels in silicon for electronic molecular detection enable a wide range of capabilities, including 3rd Generation Nucleic Acid sequencing. The technology will greatly decrease the time and cost for genome-scale sequencing, as well as enable new form factors, molecular detection modes and markets.

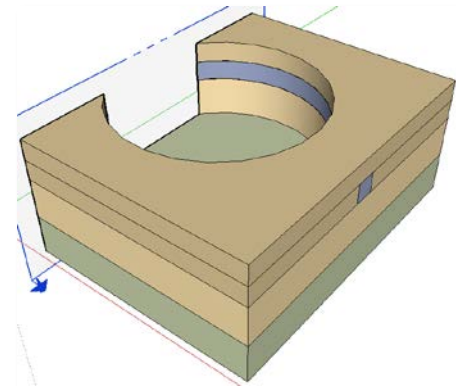
The components of this system fabricated at UW-NNIN include 3D structures and integrated electrodes. The structures are fabricated using a 'stack' of dielectrics holding electrodes on top of a silicon substrate.



NorthShore Bio
Work performed at U. Washington



Top view, 3D nanochannels in silicon



3D nano-channels in silicon

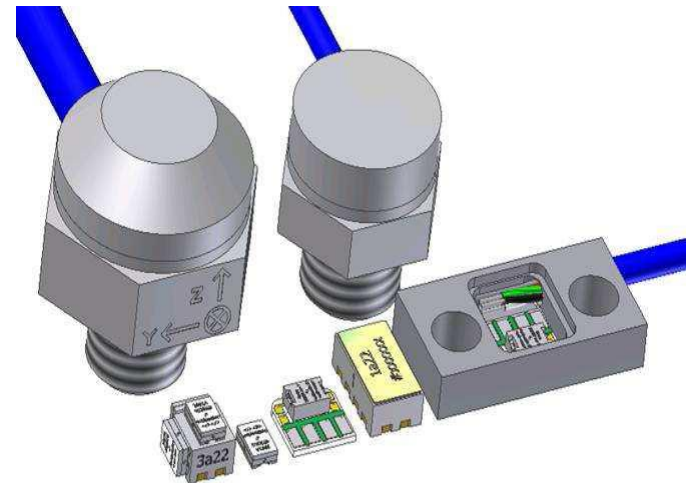
Car Crash Shock Sensor

PCB Piezotronics develops and fabricates high performance, reusable sensors for car crash testing. The component of this system fabricated at UW-NNIN site is the chip around which the remaining components of the sensor are assembled. SOI (silicon on insulator) wafers provide the sensing element. The base and lid wafers are fabricated, and the three wafers bonded and diced using UW-NNIN facilities.

High G sensors for ballistics testing, oil drilling, and pyroshock applications are also made here.



Chips are packaged in a variety of ways for different customers.

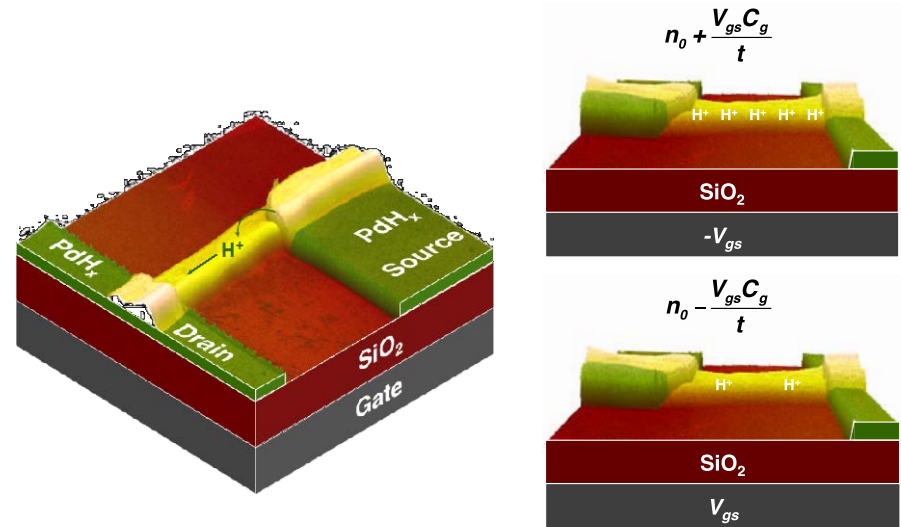


PCB PIEZOTRONICS™

PCB Piezotronics
Work performed at U. Washington

Bioprotonic Field Effect Transistor

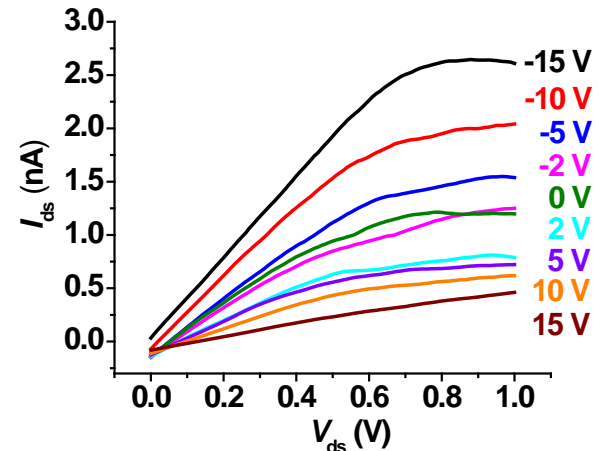
In nature, protonic (H^+) and ionic, rather than electronic currents are used to communicate information across cell membranes. The Rolandi lab has demonstrated the first biopolymer field effect transistor using protons as charge carriers. In a maleic chitosan nanofibers, protons hop along the hydrated nanofiber hydrogen bond network following the Grotthuss mechanism. The H^+ flow is measured with PdH_x proton transparent contacts, and this flow is turned on or off by an electrostatic potential applied to a gate electrode. This work was highlighted on the New York Times, EnGadget, Popular Science, MRS 360, IEEE Spectrum, Materials Views, and over 100 sites.



Schematic of a protonic FET and gating mechanism



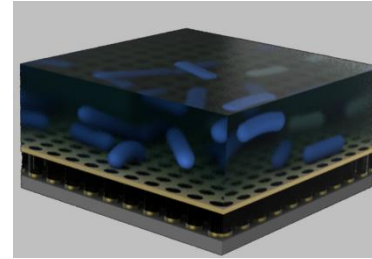
Chao Zhong, Yingxin Deng, and Marco Rolandi, UW MSE, M. Anantram, UW EE, and A. Raudsari, U. Waterloo, ON, Canada
Work performed at U. Washington



Transfer characteristics of a protonic FET

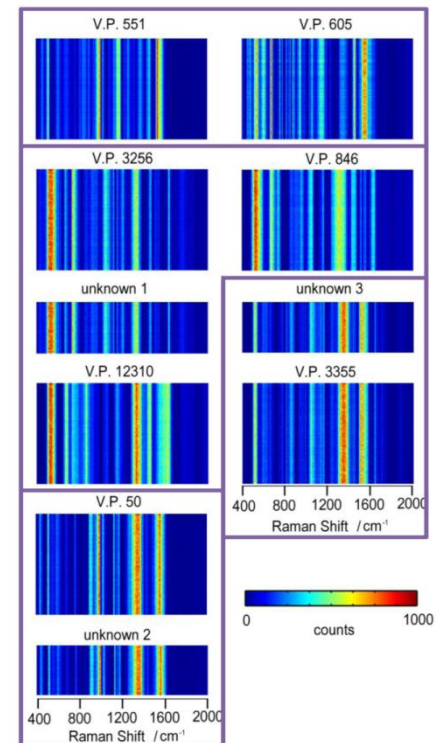
SERS Barcoding for Rapid Identification of Bacteria

A new biosensing technique for rapid identification of marine pathogenic bacteria based on surface-enhanced Raman scattering (SERS) is being developed. This technique employs the unique quasi-3D plasmonic nanostructure arrays (Q3D-PNAs) composed of a gold thin film with subwavelength nanoholes on top and gold nanodiscs at the bottom. Using finite-difference time-domain (FDTD) method, Q3D-PNAs were designed with strong local electric field at the top gold nanoholes, enabling the sensitive and reproducible detection of large analytes like bacteria. SERS barcodings were generated for each strains and the unknown samples can be rapidly identified by simply comparing the SERS barcodings.



Quasi-3D plasmonic nanostructure arrays are specifically designed for sensitive and reproducible detection of bacteria using SERS.

SERS barcodings, which carry the molecular specificity embedded in cell outer membranes, are generated for different strains of marine bacteria. The unknown samples can be rapidly identified by simply comparing the SERS barcodings.

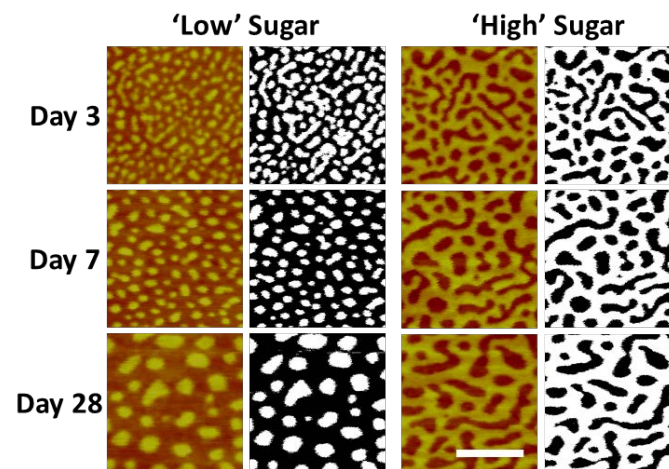
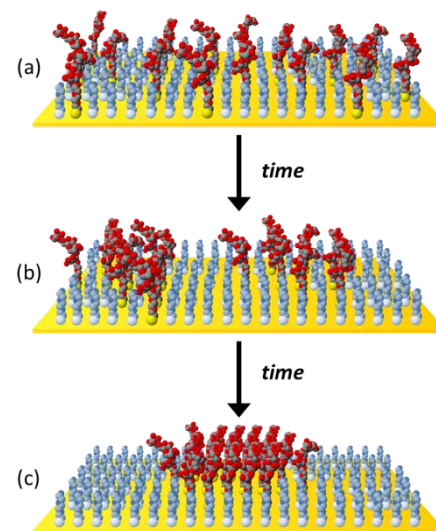


Mark Wells, Mark Strom, Vera Trainer and Qiuming Yu,
U. Maine, NOAA and UW
Work performed at U. Washington

Nanoscale Clustering of Carbohydrate Thiols

Time-dependent nanoscale clustering of self-assembled monolayers of sugar-thiol and OEG-thiol (oligo-ethylene-glycol) on gold substrates was investigated. We analyzed composition and surface morphologic changes in the monolayers analyzed by X-ray photoelectron spectroscopy (XPS) and atomic force microscopy (AFM), respectively. Evidence was found that the observed clustering is consistent with a phase separation process in which surface-bound glycans self-associate to form dense glycoclusters within the monolayer. These observations may have significant implications for the construction of mixed glycoSAMs for use in biosensing and glycomics applications.

Proposed time-dependent clustering in mixed SAMs of sugar (red) and OEG thiols (blue) based on AFM observations at UW-NNIN.



Domain coverage analysis for two different sugar-thiol/OEG-thiol ratios using binarized AFM images (black/white).

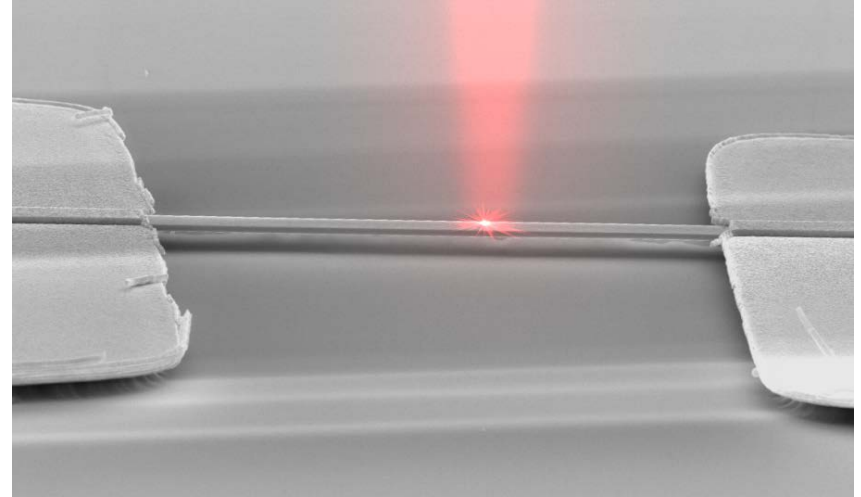


Dirk N. Weiss, Washington Technology Center, and
Daniel M. Ratner, UW BioE
Work performed at U. Washington

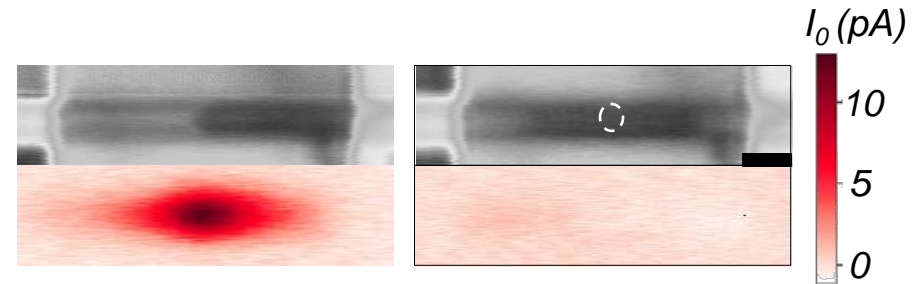
Strongly Correlated Optoelectronics

The objective of this project is to understand the fundamental optoelectronic response of strongly correlated electronic systems for developing novel optoelectronic and photonic devices. We fabricated suspended VO_2 nanobeam transistors. VO_2 is an exemplary strongly correlated material known for its dramatic metal-insulator transition (MIT) at $T_C \approx 68^\circ\text{C}$. The nanobeams were first grown on SiO_2/Si substrate. Once selecting the nanobeams, we applied photolithography, e-beam metal evaporation, and metal lift-off to fabricate gold electrodes on top of nanobeams. Nanobeams were suspended by etching away SiO_2 . It was determined that photo-thermoelectric effect dominates photocurrent generation in VO_2 . Results are reported in *Nature Nanotechnology*.

Xiaodong Xu and David Cobden, UW Physics
Work performed at U. Washington

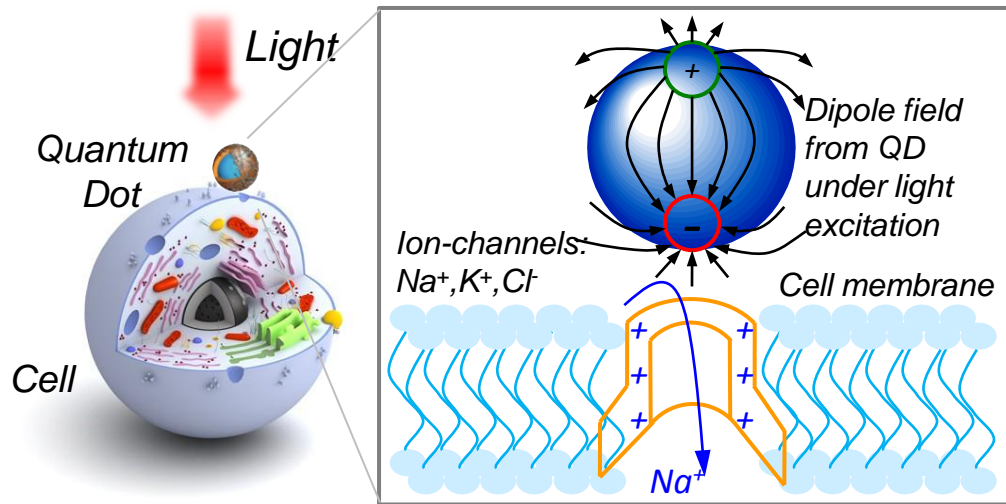


A focused laser is depicted superimposed on a SEM image of a VO_2 nanobeam suspended between gold electrical contacts.



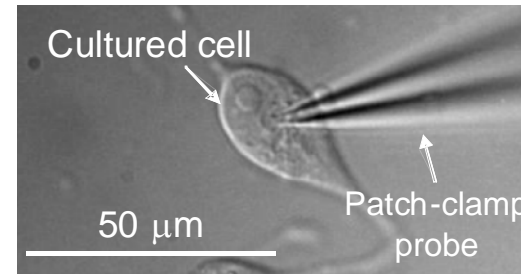
Reflection (top) and photocurrent (bottom) images of a suspended VO_2 device at 70°C using $1\ \mu\text{W}$ CW laser at $800\ \text{nm}$. In the reflection images, the light (dark) gray represents insulating (metallic) phase. The bottom left image shows pronounced photocurrent response at M/I interface. By applying a second laser ($2.4\ \mu\text{W}$) focused at the location of the dashed circle in the top right image, the metallic bubble is pulled to the center of the beam and photocurrent vanishes, (bottom right image).

Quantum Dot (QD) Neurophotronics



Optical activation of cells and neurons through quantum dots

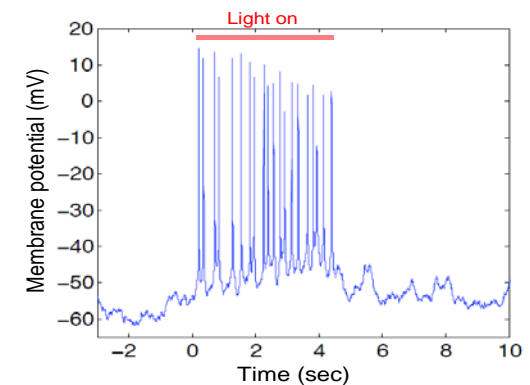
This research explores stimulating cells to trigger signaling in neural networks using QDs, an approach that combines the advantage of semiconductors, namely high sensitivity, fast response, and high design flexibility, with the advantage of photosensitive proteins, namely small size and cell-specific targeting. An optically excited QD exhibits an electric dipole moment. When placed close to a cell membrane, this light-stimulated dipole is polarized by the membrane potential. The dipole field can be detected by the voltage sensor of a voltage-gated ion channel in the proximity of the QD, leading to channel activation. One future potential applications for this technology is simple and effective retinal prosthetics using QDs to replace deteriorated rods and cones.



Cell cultured on a quantum-dot film under patch-clamp recording



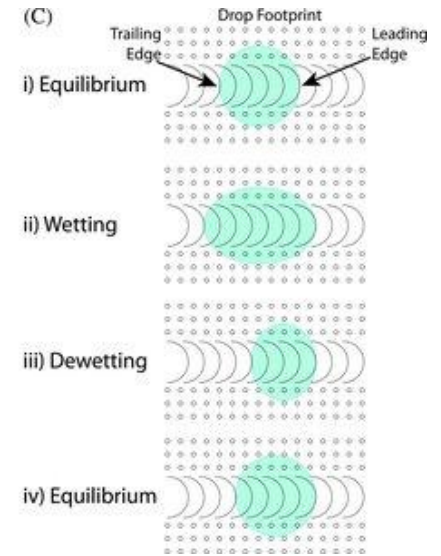
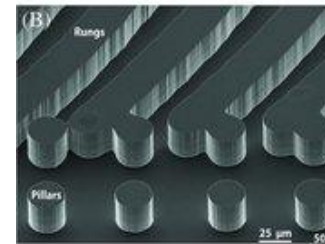
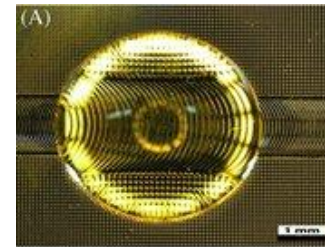
Fluorescent silicon quantum dots for future in vivo applications



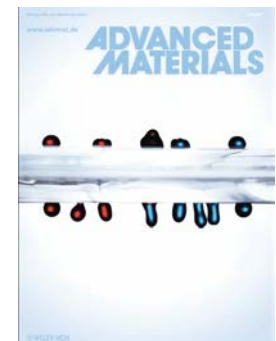
Neuron firing action potentials upon optical activation through quantum dots

Microfluidics: Controlling liquid drops with texture ratchets

A texture ratchet is a surface region whose microstructured, asymmetric features propel drops when vibrated. Drop motion can persist over long distances, along circular paths, up- or down-hill. Specific drop volumes resonate at specific frequencies, providing a means to separately control the motion of different-sized drops. We analyze the physical mechanism responsible for drop transport and reveal the relationship between design parameters such as microscale geometry and surface wettability, operation parameters such as drop volume and viscosity, vibration frequency and amplitude, and performance parameters such as drop velocity. Experiments demonstrate water drop transport on silicon and elastomer substrates. Texture ratchets can move liquid samples without electric fields, pressure gradients or gravity, making them an attractive low-cost platform for lab-on-chip applications.



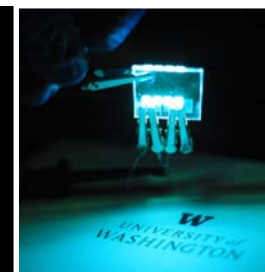
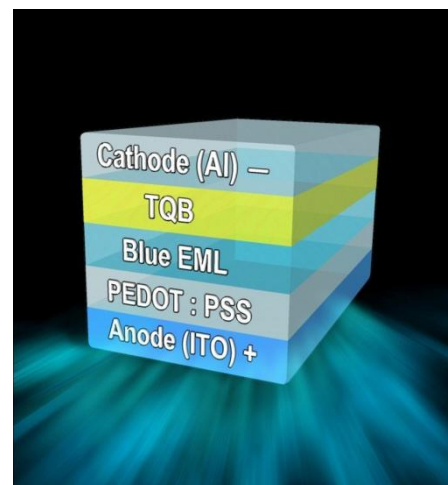
A texture ratchet is etched in silicon and coated with fluoro-octyl-trichloro-silane (FOTS), or molded in elastomers.



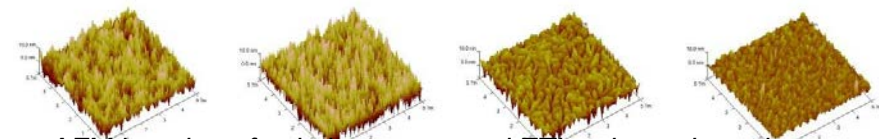
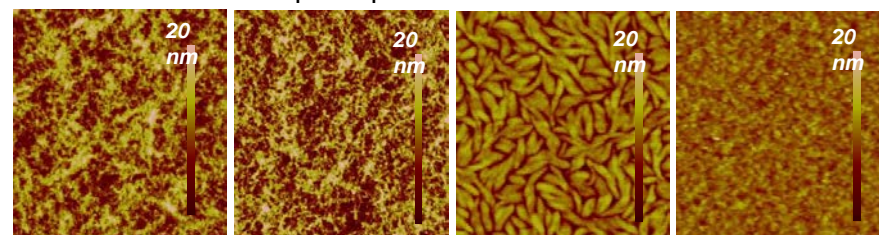
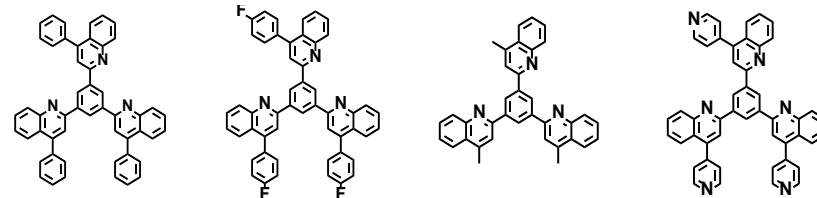
Karl Bohringer, UW EE
Work performed at U. Washington

High Performance Solution-Processed PhOLEDs enabled by New ETMs

Phosphorescent organic light-emitting diodes (PhOLEDs) are of great interest in research and industrial applications for next-generation full-color display panels, flexible displays, and solid-state lighting. However, high-performance PhOLEDs are currently made by expensive vacuum-deposition processes. Highly efficient polymer-based blue PhOLEDs were fabricated by a novel, low-cost, solution-processing method and new solution-processable electron-transport materials (ETMs). Atomic force microscopy (AFM) imaging shows that the solution-deposited oligoquinoline ETMs form vertically oriented nanopillars and rough surfaces that enable good electron-transport layer (ETL) / cathode contacts, eliminating the need for cathode interfacial materials.



High-performance multilayered blue PhOLEDs fabricated by novel solution-processing method.

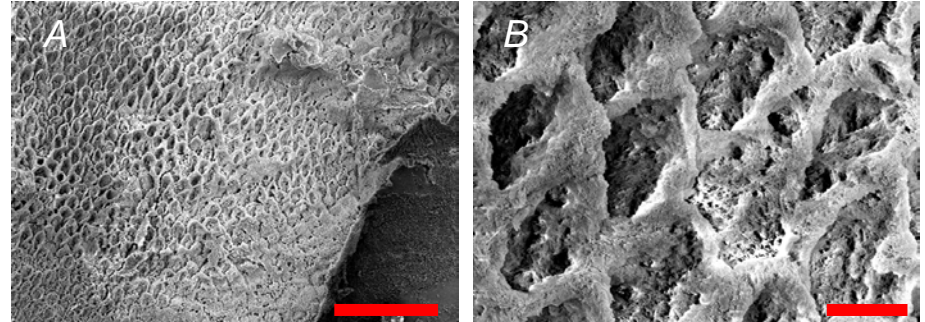


AFM imaging of solution-processed ETLs showed rough surface morphologies that enabled good ETL/cathode interface for efficient charge injection.

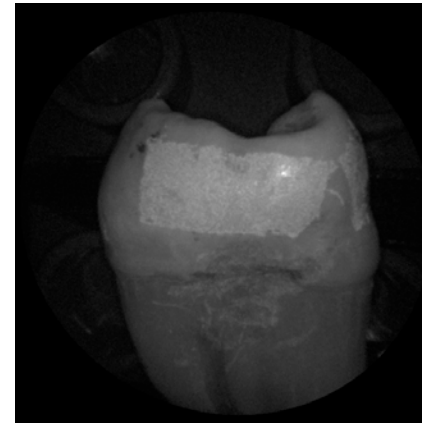
Samson A. Jenekhe, UW ChemE
Work performed at U. Washington

Multimodal Detection of Early Childhood Caries using a Scanning Fiber Endoscope

Early childhood caries is among the most common diseases throughout the world, yet there remains a lack of early diagnostic detection techniques. The purpose of this project is to develop a multimodal optical detection device to detect dental caries at a stage where remineralization is possible and surgical intervention is not required. UW-NNIN tools were used to characterize both natural caries and artificially demineralized enamel. Understanding the morphology of demineralized enamel is crucial to the development of the diagnostic optical technology used in this project.



A) Scanning electron microscopy (SEM) images of demineralized enamel. Scale bar is 50 μm B) Zoomed in view reveals porous enamel structure indicative of structural damage. Scale bar is 5 μm .



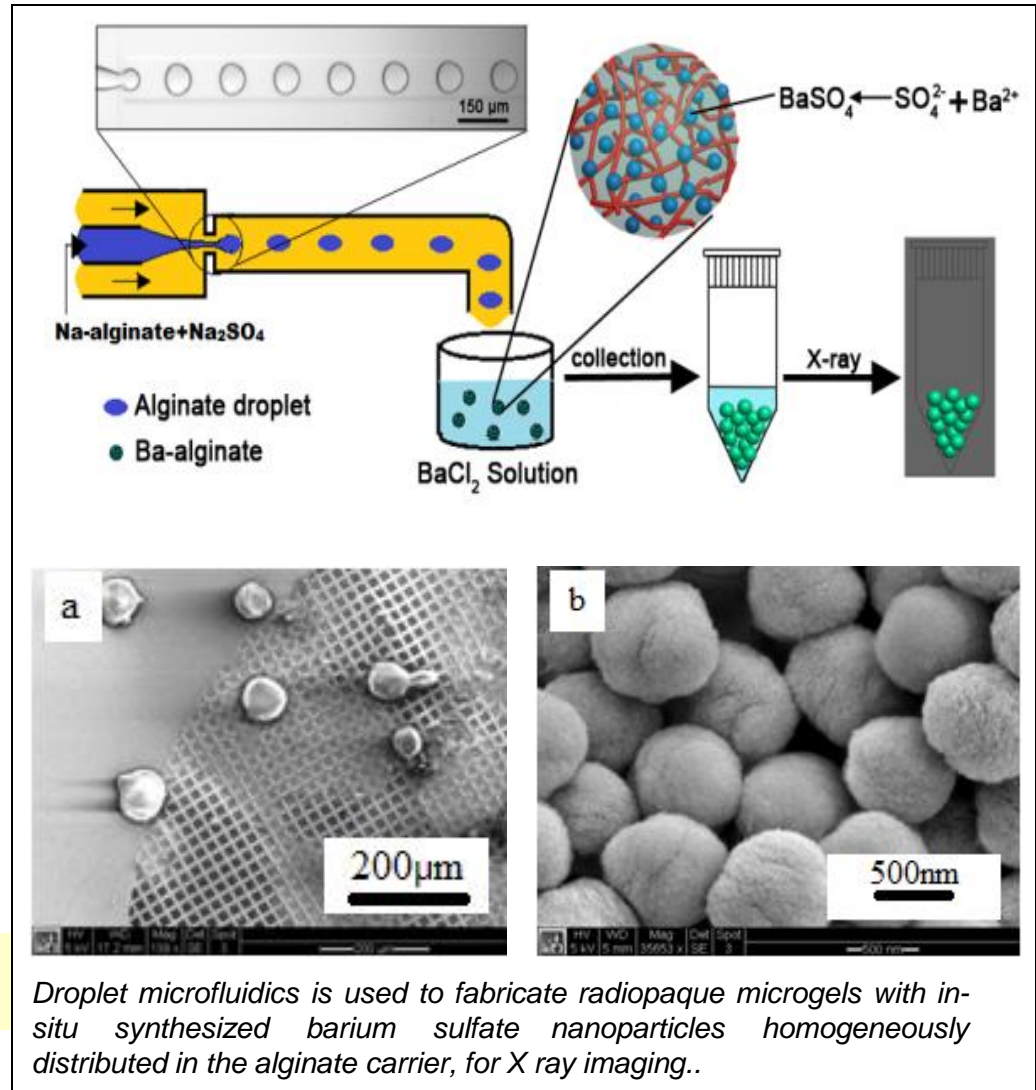
A scanning fiber endoscope image obtained using 405 nm illumination. The white band is demineralized enamel. Due to the structure of the demineralized enamel, as seen in the SEM images, 405 nm was determined to be the optimal illuminating wavelength.

Eric Seibel, UW Mechanical Eng.
Work performed at U. Washington

Microfluidic one-step fabrication of radiopaque alginate microgels for diagnostic imaging

This work presents a new strategy to fabricate monodispersed radiopaque alginate (Ba–alginate) microgels by a one-step microfluidic method. Alginate droplets containing sulfate ions are first formed by a flow focusing microfluidics setup. These alginate droplets are subsequently solidified by barium ions in a collection bath. During the solidification process, excessive barium ions in the collection bath also react with sulfate ions in the alginate droplet, resulting in barium sulfate (BaSO_4) nanoparticles in-situ synthesized within the Ba–alginate microgels. The Ba–alginate microgels are also visible under X-ray irradiation. This facile route to fabricate alginate microgels as radiopaque embolic materials is of particular importance for endovascular embolization and localized diagnostic imaging applications.

Amy Q. Shen, UW Mechanical Eng.
Work performed at U. Washington



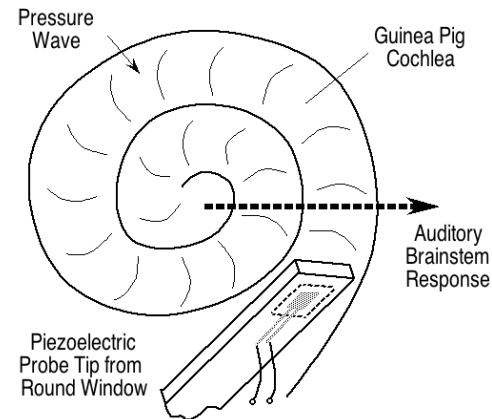
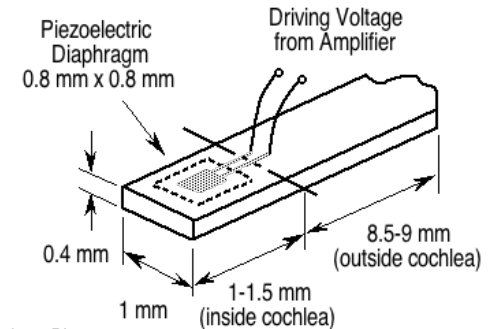
Droplet microfluidics is used to fabricate radiopaque microgels with in-situ synthesized barium sulfate nanoparticles homogeneously distributed in the alginate carrier, for X ray imaging..

Hybrid Cochlear Implant Project

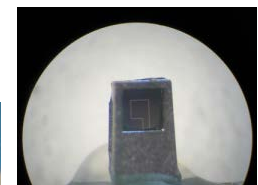
The objective of this research is to study novel small-scale piezoelectric Lead-Zirconium-Titanium oxide (PZT) thin-film micro-actuators to be implanted in the inner ear. The PZT micro-actuator will generate a pressure wave directly stimulating perilymph in the cochlea to provide acoustic stimulation. Together with a shortened electrode, the PZT micro-actuator could enable combined electric and acoustic stimulation (CEAS) of the inner ear via an integrated device. Specifically, we have developed an actuator probe with 1 mm wide, 10 mm long, and 0.4 mm thick. At the tip of the probe, there is a piezoelectric diaphragm serving as an acoustic actuator. The entire actuator is packaged with parylene of 2- thick together with lead wires for bottom and top electrodes of the piezoelectric diaphragm

I. Y. Steve Shen, G. Z. Cao
UW Mechanical Eng., MSE and Otolaryngology
Work performed at U. Washington

At the tip of the actuator probe, there is a PZT diaphragm that vibrates to generate acoustic stimulation.



The tip of the actuator probe can be implanted in the basilar region of cochlea to generate acoustic stimulation.



An implantable piezoelectric thin-film acoustic micro-actuator probe to enhance hearing and speech recognition

Washington University St. Louis

Magnetomotive Enhanced Thrombolysis

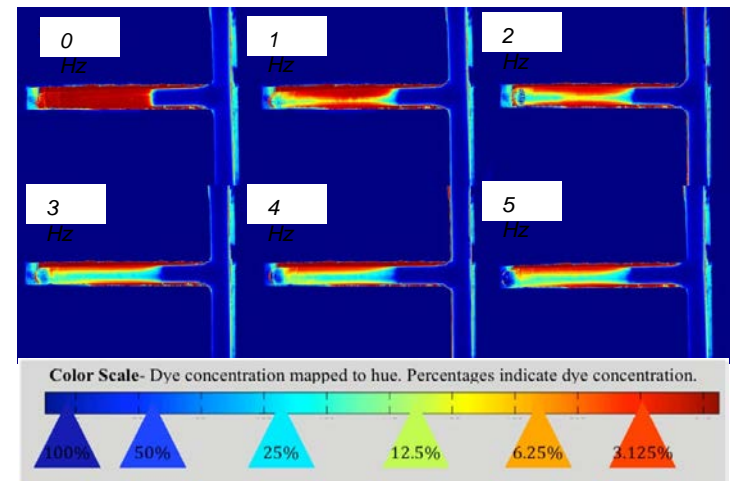
In the past year, Pulse Therapeutics Inc. has begun its first clinical trial in Australia. This trial is focused on using magnetomotive enhanced thrombolysis in patients suffering an ischemic stroke. Pre-clinical testing of the sub-micron magnetite particles was conducted during this period using the facilities at NRF. An Australian news report on the clinical trial can be viewed at <http://www.youtube.com/watch?v=bJIDAcTQNrc&feature>.

Given the successful *in vivo* results thus far, Pulse has begun looking into the technology for other applications including enhanced diffusion in capillary beds. The NRF facility constructed two microfluidic phantoms for use in our initial testing. In an effort to further quantify the effects of our diffusion mechanism, samples processed by NRF allowed Pulse to correlate diffusion rates with the amount of particles that were collected at various frequencies of operation.

Michael Sabo, Senior Director of R&D, Pulse Therapeutics Inc.
Work performed at Washington University in St. Louis
Nano Research Facility



Clinical trials of magnetomotive enhanced thrombolysis using magnetic nanoparticles.

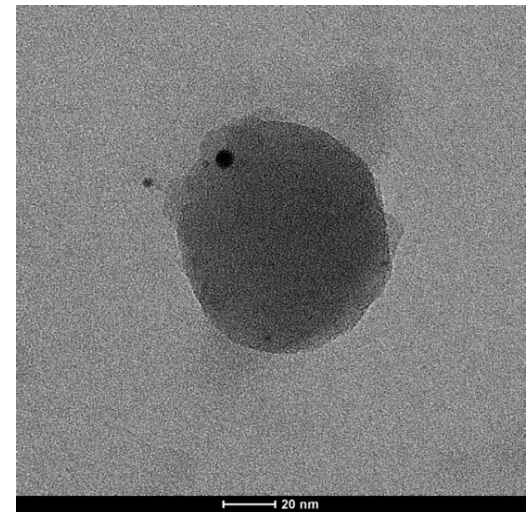
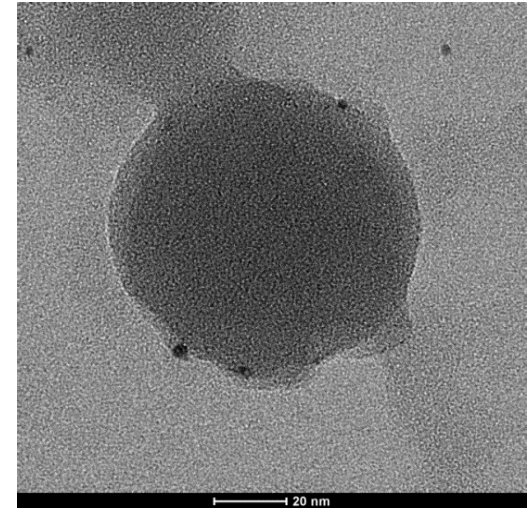


Diffusion of magnetic nanoparticles (conjugated with blue dye) from a flow channel (vertical) into a stagnant channel representative of a blood vessel branch with a distal clot under influence of the magnetomotive device at operation frequencies from 0Hz to 5Hz.

Formation of Metal Nanoparticles in Hollow Polymer Nanocapsules

Usually fabrication and handling of metal nanoparticles requires use of surfactant molecules for stabilization and prevention of aggregation. The downside is that the surface of the nanoparticles is completely covered by surfactant molecules. We use polymer nanocapsules as a physical barrier between nanoparticles. Since no surfactants are needed the surface of the metal nanoparticles is “naked”, which is advantageous in catalysis.

In the current project we study formation of metal nanoparticles in hollow polymer nanocapsules. Polymer nanocapsules have pores in their ultrathin shells that allow fast transfer of small molecules and ions while bigger molecules can not enter or escape nanocapsules. Using this approach we entrapped relatively large organic molecules capable of reducing metal ions. Thus we can selectively synthesize gold nanoparticles inside the polymer nanocapsules for use as Surface Enhanced Raman Scattering based sensors for detection of organic molecules, catalysis, and medical imaging agents..



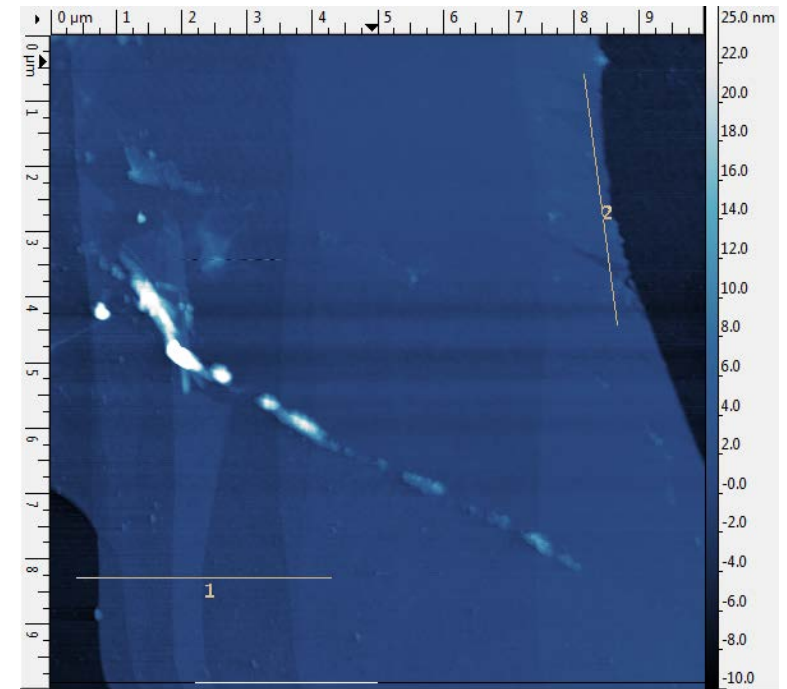
Gold nanoparticles (black dots) inside polymer hollow nanocapsules.

Sergey Shmakov and Dr. Eugene Pinkhassik, Saint Louis University
Particle characterization performed at Washington University in St. Louis Nano Research Facility

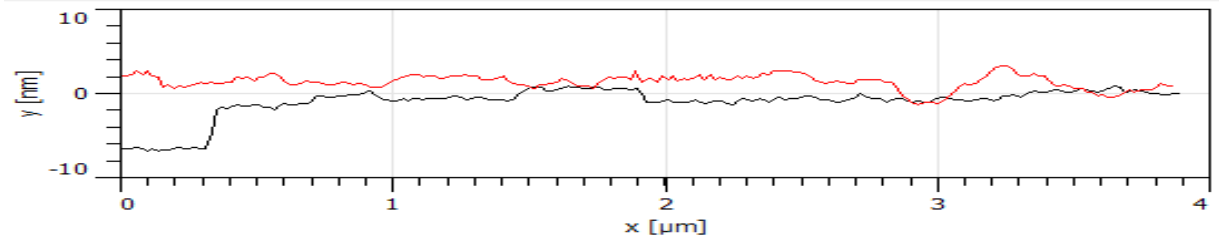
SPM studies of Electromagnetic Properties of Graphene

Graphene is a 2-dimensional atomically flat hexagonal lattice of carbon that has excellent mechanical electrical and optical properties, however it's unique bandstructure makes it impractical for certain applications. Therefore, it is sometimes necessary to modify graphene properties in a controllable manner. One method of modification to enhance the properties of graphene is to pattern the surface of the graphene.

In this study graphene flakes are prepared by mechanical exfoliation on Si/SiO₂ substrates are characterized using scanning probe microscopy tools. Selected samples are studied before and after modification by Scanning Probe Microscopy tools and optical microscopy or spectroscopy. Single, double, and triple layered graphene samples were tested. Topological features of the graphene and their electromagnetic properties were tested via atomic force microscopy Methods at the NRF.



Topographical image of Graphene.



Two line profiles show steps representing additional graphene layers. Black line corresponds to line 1 in topographical image. Red line corresponds to line 2 in topographical image.

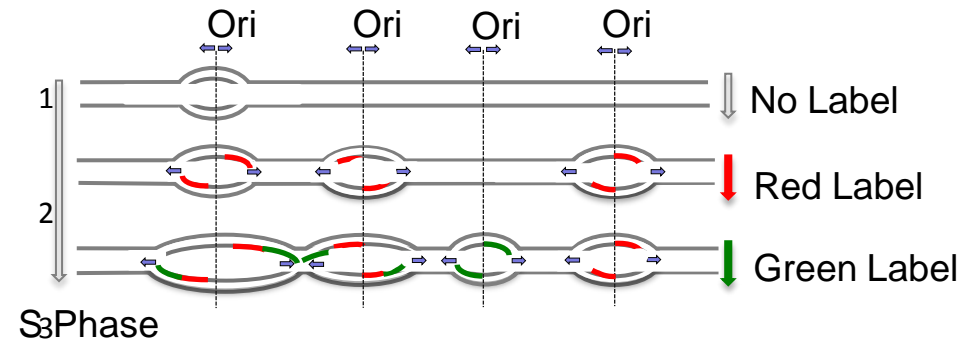
John Cavin and Dr. Irma Kuljanishvili, Saint Louis University

Work performed at Washington University in St. Louis Nano Research Facility

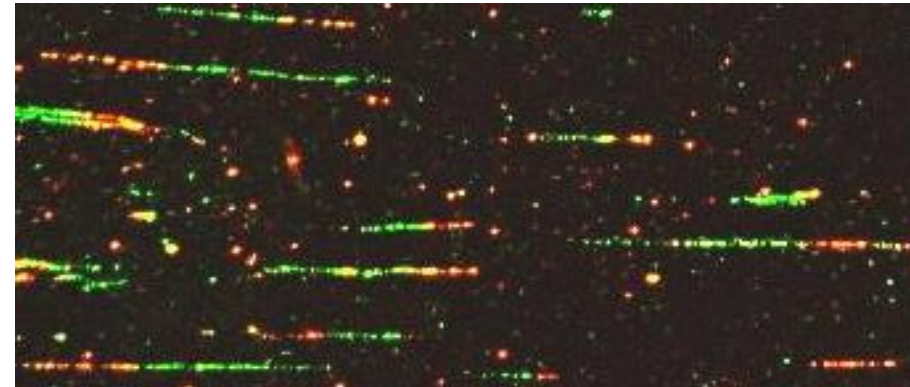
Genome wide single molecule analysis of human DNA replication dynamics in RECQ1 depleted cells

Topoisomerase1 (Top1) poisons are an important class of anticancer drugs. The discovery that Top1 poisons induce replication fork slowing and reversal in a PARP1 dependent process provided the important piece of information about the existence of accumulated reversed forks during this process. However, the factors required to push the reversed fork back to normal, once the lesion has been repaired, are still unknown.

Microfluidic capillary channels fabricated at the NRF were used to stretch these labeled DNA molecules and later immunostained for replication analysis. Our studies point to a new exciting genetic dependency for this process. Using a unique combination of proteomic, biochemical, single molecule DNA fiber assay and electron microscopy approaches, we show that the human RECQ1 helicase interacts with PARP1 and is a key cellular mediator required to restore an active replication fork after Top1 cleavage complex repair. These studies provide a fresh view of the complex mechanism that regulates replication stress response upon Top1 poisoning.



Model for label incorporation profile during DNA replication.



Confocal microscope image of DNA fiber tracts.

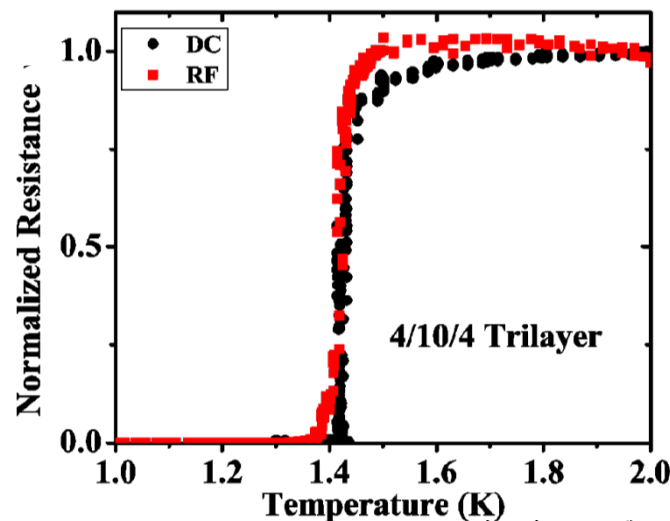
Saravanabhavan Thangavel, Saint Louis University
Work performed at Washington University in St. Louis Nano Research Facility

NNIN is supported by NSF ECCS-0335765

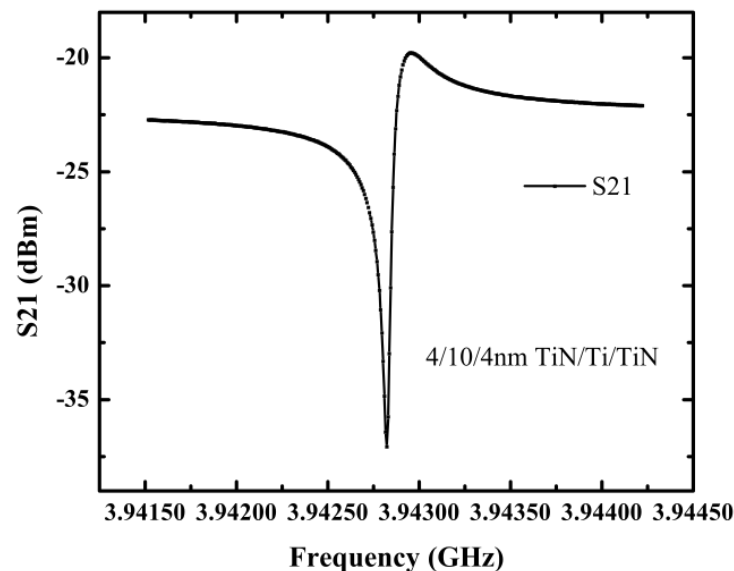
Improving Materials in Quantum Information Devices

High quality factor (Q) microwave resonators fabricated from a variety of superconducting metals and substrates can be used to study new materials for quantum information and to improve the design of superconducting circuits. This project involves the microfabrication of superconducting microwave resonators and quantum bits for the purpose of studying dielectric loss in new materials for quantum information.

These devices are Microwave Kinetic Inductance Detectors (MKID) composed titanium nitride (TiN) and titanium. Reactive ion etching at the NRF is used to pattern the superconducting thin films (100-300 nm) on Si(100) substrates. When a photon is absorbed by the MKID, a change in the kinetic inductance occurs. This change in kinetic inductance causes a shift in the resonance frequency of the LC resonator which is then detected. These devices have applications in both quantum computing and astronomy.



The superconducting transition temperature of a trilayer (TiN/Ti/TiN) device using DC (black) and RF (red) measurements.



A dip in the scattering parameter S21 at the resonance frequency of the MKID..

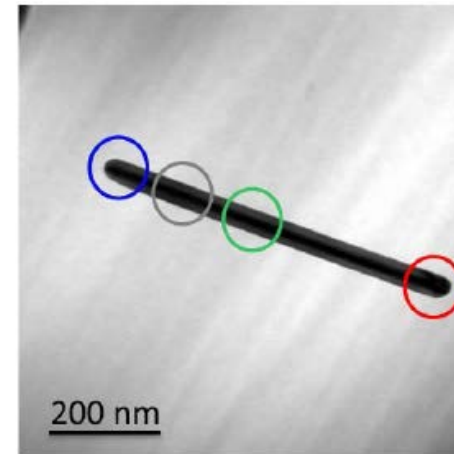
Dr. David Wisbey, Saint Louis University
Work performed at Washington University in St. Louis
Nano Research Facility

Surface Plasmon Modes of a Silver Nanorod

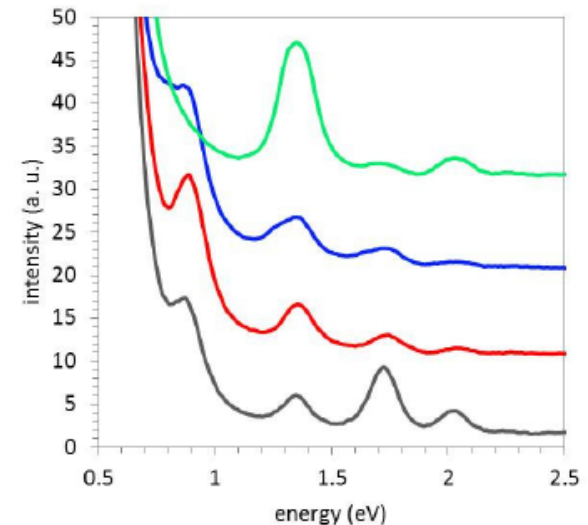
Many of the remarkable optical properties of metallic nanoparticles (NPs) arise because of the excitation of surface plasmon resonances. The variety of surface plasmon resonant modes seen in metallic NPs is brought about by the dependence of surface plasmon excitation with the NP shape, size, composition and environment. Most applications of these properties, such as biochemical sensing and surface enhanced raman spectroscopy, are dependent on sub-wavelength spatial variations of the surface plasmons induced in the metal NPs..

In this study electron energy loss is characterized using energy filtered TEM of spatially resolved surface plasmon excitations on a silver nanorod supported on a silicon nitride substrate. Our results show that the excitation is quantized as resonant modes whose intensity maxima vary along the nanorod's length and whose wavelength becomes compressed towards the ends of the nanorod. Theoretical calculations modeling the surface plasmon response of the silver nanorod - silicon nitride system show the importance of including retardation and substrate effects in order to describe accurately the energy dispersion of the resonant modes.

Olivia Nicoletti, Martijn Wubs, N. Asger Mortensen, Wilfried Sigle, Peter A. van Aken, and Paul A. Midgley, University of Cambridge, Technical University of Denmark, and Max Planck Institute for Intelligent Systems Silver nanorods synthesized at Washington University in St. Louis Nano Research Facility



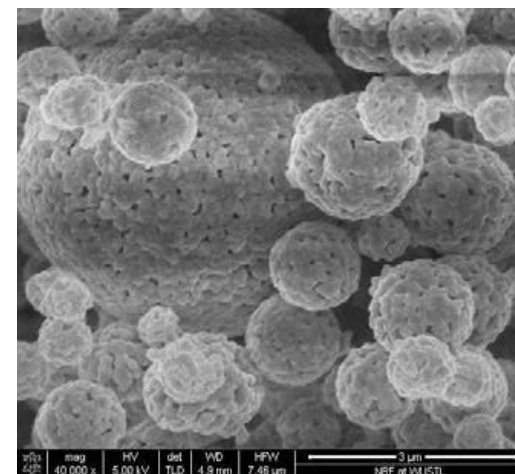
Bright-field (BF) zero-loss image of a 666 ± 3 nm long silver nanorod, with 47 ± 3 nm diameter.



Electron energy-loss spectra (unprocessed) acquired at the positions marked in the bright-field image of matching color. Spectra have been obtained using a selected-area approach and shown displaced on the intensity axis for clarity.

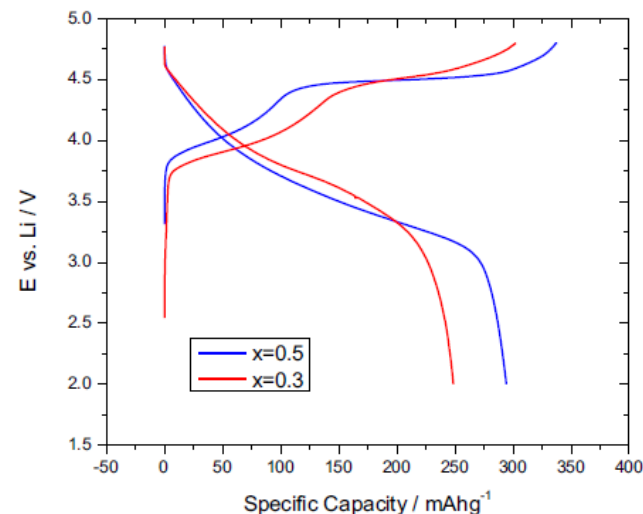
Lithium ion battery cathode material development

Materials with layered structures of the form $x\text{Li}_2\text{MnO}_3 \cdot (1-x)\text{LiMO}_2$ ($M = \text{Mn, Ni, Co}$) have received attention as high-capacity, low cost, and safer cathode materials for lithium-ion batteries. These compounds are considered as an integration of two layered components: Li_2MnO_3 (C2/m) and $\text{Li}[\text{MnNiCo}]_{1/3}\text{O}_2$ (R-3m), forming a composite. Conventional synthesis methods of these materials are primarily co-precipitation processes involving the preparation of transition metal carbonates or hydroxides and a post-lithiation step. While promising, the co-precipitation method has challenges associated with scale-up and the electrochemical performance of these composite materials is highly dependent on their chemistry and morphology.



Morphology of the $0.3\text{Li}_2\text{MnO}_3 \cdot 0.7\text{Li}[\text{NiMnCo}]_{1/3}\text{O}_2$ powder.

To address this, a spray pyrolysis synthesis method has been developed as a method for producing submicron-size Li- and Mn-rich cathode materials with porous morphologies. The composite materials display high rate capability and capacities, but a capacity loss is observed over cycles for the materials. To improve the cycling performance and capacity of these materials, cobalt has been doped in the materials to stabilize their structure. Preliminary results indicate stabilization of the structure due to cobalt addition.



Voltage vs. capacity of a $\text{Li}/0.3\text{Li}_2\text{MnO}_3 \cdot 0.7\text{Li}[\text{NiMnCo}]_{1/3}\text{O}_2$ cell compared to a $\text{Li}/0.5\text{Li}_2\text{MnO}_3 \cdot 0.5\text{Li}[\text{NiMnCo}]_{1/3}\text{O}_2$ cell between 2.0 and 4.8 V, tested at room temperature.

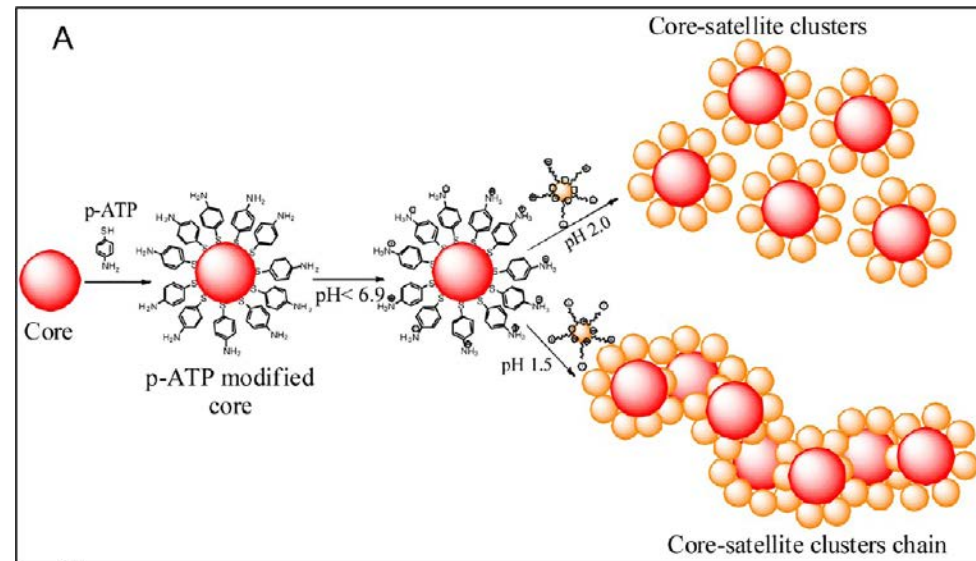
X-tend Energy LLC. and Miklos Lengyel, Xiaofeng Zhang, and Dr. Richard Axelbaum, Washington University in St. Louis

Material characterization performed at Washington University in St. Louis Nano Research Facility

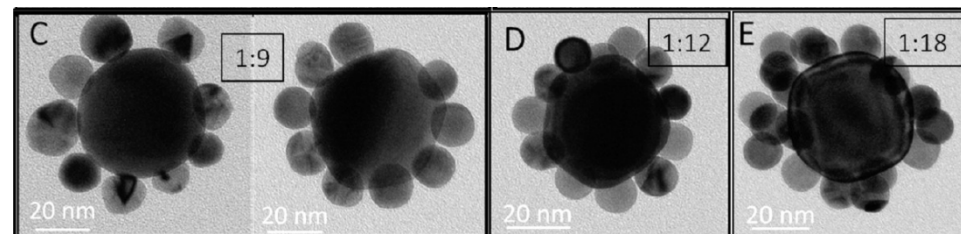
Plasmonic Planet–Satellite Analogues: Hierarchical Self-Assembly of Gold Nanostructures

In the past few years, remarkable progress has been made in unveiling novel and unique optical properties of strongly coupled plasmonic nanostructures, known as plasmonic molecules. However, realization of such plasmonic molecules using nonlithographic approaches remains challenging largely due to the lack of facile and robust assembly methods.

We demonstrate that core–satellite structures comprised of shape-controlled plasmonic nanostructures can be achieved through self-assembly using simple molecular cross-linkers. Prevention of self conjugation and promotion of cross-conjugation among cores and satellites plays a key role in the formation of core–satellite heteroassemblies. The in-built electromagnetic hot-spots and Raman reporters of core–satellite structures make them excellent candidates for surface-enhanced Raman scattering probes.



Schematic illustrating the steps involved in the self-assembly of nanostructures into core–satellite clusters highlighting the changes in the surface charge state of the nanoparticles, which determines the assembly.



Average number of satellites on each core can be controlled by manipulating the volume of satellite solution added to the core solution. Representative TEM images for core–satellite ratio of (C) 1:9, (D) 1:12, and (E) 1:18.

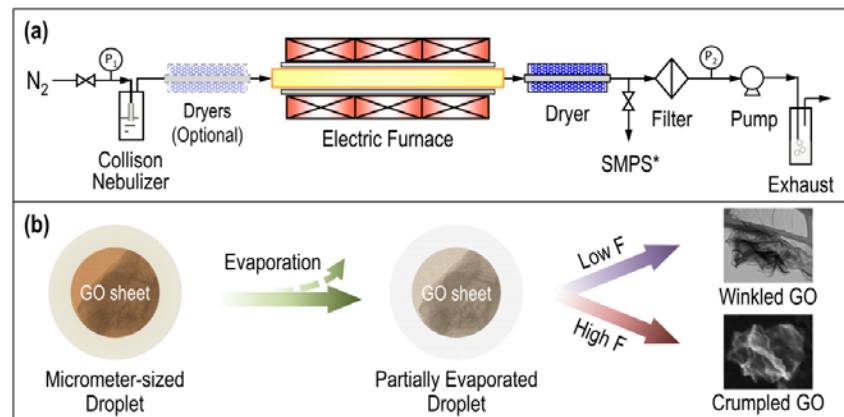
Dr. Naveen Gandra and Dr. Srikanth Singamaneni, Washington University in St. Louis
Work performed at Washington University in St. Louis Nano Research Facility

Facile Development of Crumpled Graphene Nanoballs for Energy & Environmental Applications

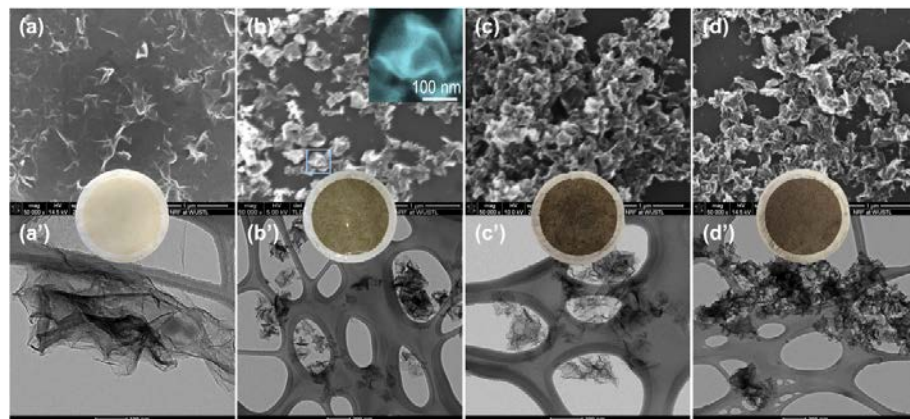
Evaporation-induced crumpling of two dimensional nanosheets, such as graphene oxide (GO), is an important phenomenon, which is attracting increasing attention. However, a fundamental understanding of the process is still lacking. In this project, the correlations between the confinement force and various parameters, such as evaporation rate, droplet size, and precursor concentration, were investigated systematically.

The morphology and size evolution of crumpled GO particles synthesized by a furnace aerosol reactor method were analyzed by both in-line and off-line methods, including scanning mobility particle sizer, aerodynamic particle sizer, dynamic light scattering, and electron microscopy (TEM & SEM). A universal equation of confinement force was derived, from which the evaporation rate and temperature are important factors to be considered. These crumpled nanosheets show high flexibility during applications, enabling the possibility of encapsulation for drug delivery, photocatalysis, solar cells, and electrical energy storage systems.

Wei-Ning Wang, Yi Jiang and Dr. Pratim Biswas,
Washington University in St. Louis
Work performed at Washington University in St. Louis Nano
Research Facility



Experimental Setup. (a) Schematic diagram of a furnace aerosol reactor (FuAR) and (b) the possible formation mechanism of crumpled graphene oxide. SMPS indicates the scanning mobility particle sizer, which is an in-line particle size measurement system.



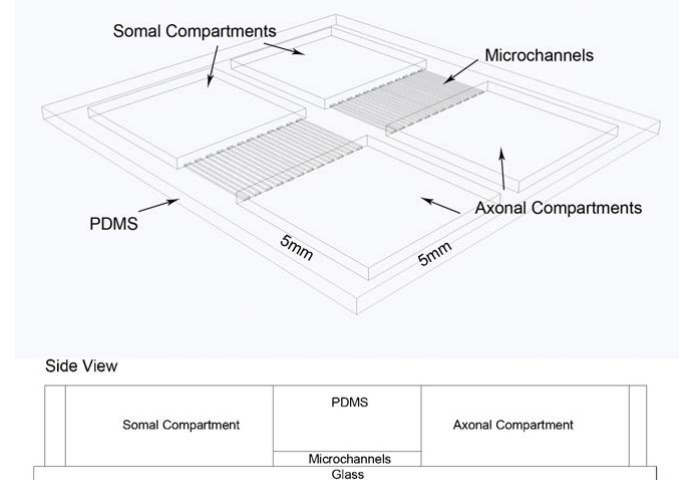
Morphology evolution of graphene oxide particles as a function of synthesis temperature. (a) to (d) are FE-SEM images and (a') to (d') are corresponding TEM images. (a)/(a') 200 ° C, (b)/(b') 400 ° C, (c)/(c') 800 ° C, and (d)/(d') 1000 ° C. The inset at each condition is the corresponding photo of graphene oxide collected on a filter.

A microdevice platform for visualizing mitochondrial transport in aligned dopaminergic axons

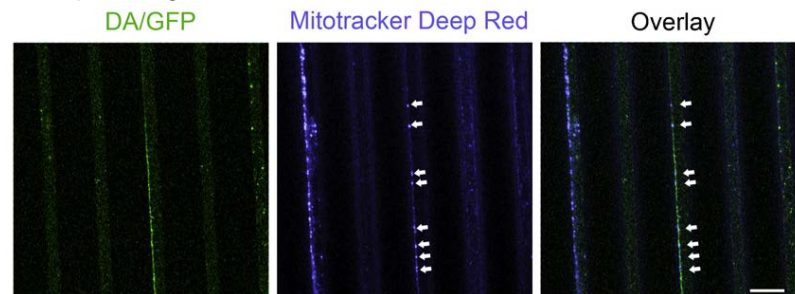
Experimental evidence points to the importance of mitochondrial transport defects in contributing to major neurodegenerative diseases, such as Parkinson's disease (PD). Studies of mitochondrial transport along single axons are difficult with traditional dissociated culture systems and the fragility of the midbrain dopaminergic cultures precludes their survival in previously developed microfluidic devices with an enclosed architecture.

Using soft lithography, we generated a microdevice from polydimethylsiloxane (PDMS) for the purpose of studying the transport of mitochondria along single dopaminergic axons. The device comprises two large open culture chambers connected by a parallel array of microchannels that achieves fluidic separation of axons from the soma and allows the tracking of mitochondrial movement along oriented axons.. We have found that the parkinsonism drug, 6-hydroxydopamine or 6-OHDA, disrupts mitochondria transport prior to disruptions of mitochondria membrane potential and microtubules structural stability. We are investigating whether 6-OHDA affects transport of other organelles, cargos, or protein clearance processes.

Xi Lu and Dr. Shelly Sakiyama-Elbert, Washington University in St. Louis
Work performed at Washington University in St. Louis Nano Research Facility



Schematic of "open" compartment microdevice and visually tracking axonal mitochondria within the microdevice. (A) Two compartments (5 mm x 5 mm) are connected by a parallel array of microchannels, which are 5 μ m high, 10 μ m wide, and 900 μ m long.



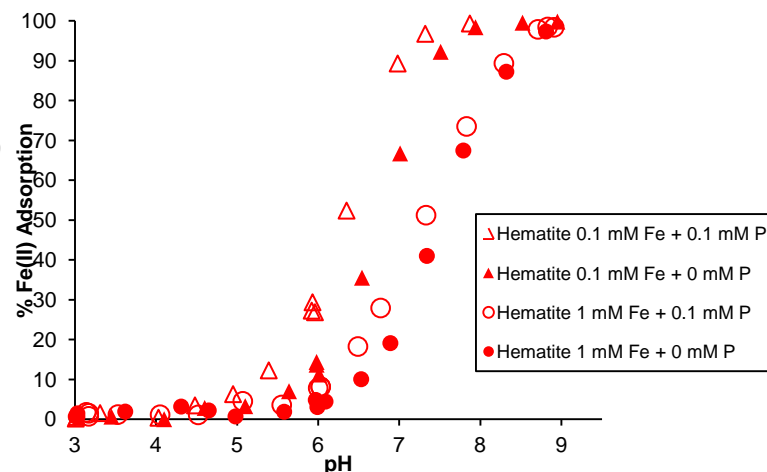
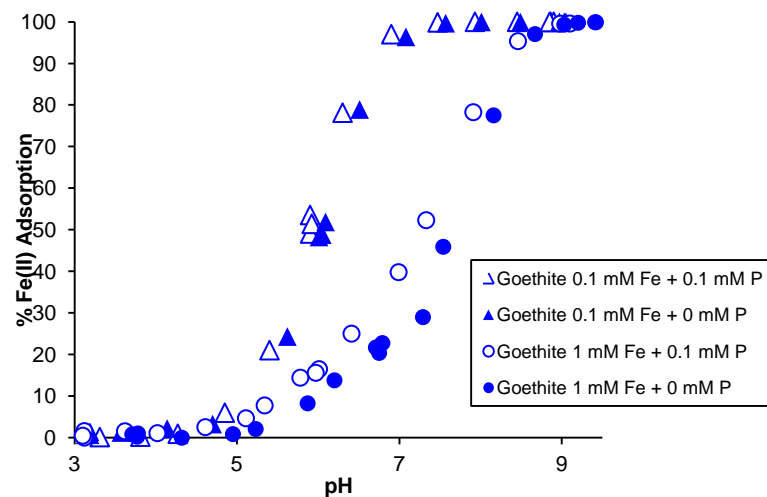
Mitochondria from both dopaminergic (arrows) and non-dopaminergic axons can also be tracked within the microchannels using Mitotracker Deep Red. The direction of transport can be clearly distinguished as the axons grow from the soma to the axonal compartment (top to bottom). Dye adsorbs into the microchannels and causes them to fluoresce. This generates background noise that can significantly reduce the signal to noise ratio. Scale bar indicates 40 μ m.

Interactions of phosphate and sulfate with Fe(II) on Fe(III) oxide mineral surfaces

Biogeochemical iron cycling involves the reductive dissolution and oxidative precipitation of iron oxides and activates interfacial electron transfer and atom exchange (ETAE) reactions between aqueous Fe(II) and solid Fe(III) oxide minerals. These ETAE processes cause mineral recrystallization, which in turn results in the incorporation of divalent metal adsorbates (e.g. Ni(II)) into the mineral and the release of preincorporated divalent metal ions to solution.

In this research, we probe the effect of aqueous Fe(II) on the adsorption of phosphate and sulfate, oxoanions common in aqueous systems, and the effect of phosphate and sulfate on Fe(II) adsorption onto Fe(III) oxide minerals. We have observed that the pH dependent adsorption of Fe(II) onto hematite and goethite increases with increasing phosphate and sulfate concentrations. Both phosphate and sulfate adsorption onto Fe(III) oxides is enhanced in the presence of aqueous Fe(II). Attenuated total reflectance-Fourier transform infrared spectroscopy indicates that the enhanced co-adsorption of aqueous Fe(II) and sulfate is the result of purely electrostatic interactions, while enhanced co-adsorption of aqueous Fe(II) and phosphate may likely be the result of ternary complexation.

Margaret Anne Hinkle and Dr. Jeffery Catalano,
Washington University in St. Louis
Work performed at Washington University in St. Louis
Nano Research Facility



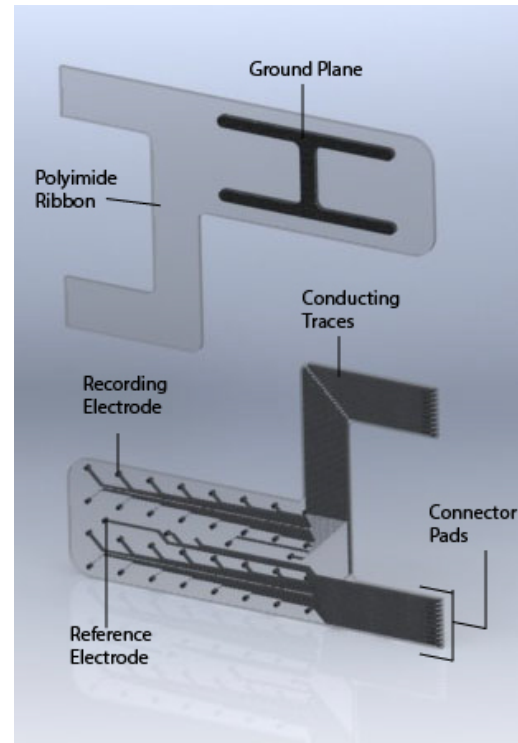
Effect of phosphate on Fe(II) adsorption onto goethite (blue) and hematite (red) at constant ionic strength (0.01 M NaCl) and constant mineral loading (4 g/L goethite or hematite), with 1mM Fe(II) (circles), or 0.1mM Fe(II) (triangles), and no phosphate (solid) or 0.1mM phosphate (hollow).

Microfabrication of microelectrocortigraphy (μ ECoG) electrode grids

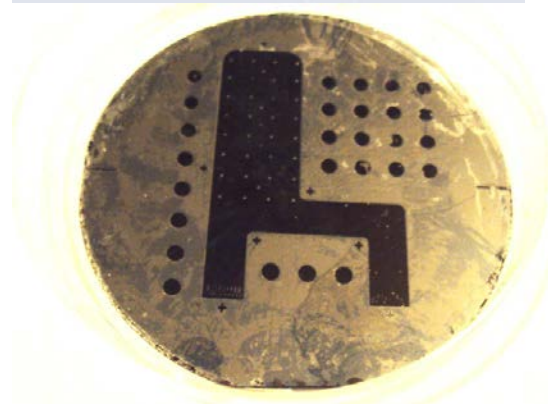
The utility of electrode arrays and electrocortigraphy (ECoG) based neural recordings in clinical medicine and basic neuroscience research has been shown to be incredibly valuable for brain computer interface research and a variety of neuroengineering applications. While the ECoG modality has been greatly accepted in the neuroscience community, only marginal engineering design and process development has gone into fabricating the electrode arrays that are responsible for making these recording possible.

This project asserts a frame for the introduction of MEMS technology into the fabrication and design optimization of microelectrocortigraphy (μ ECoG) electrode grids. The μ ECoG electrode grids are designed in conjunction with Nano Research Facility staff and are fabricated using standard photolithography, deposition, and reactive ion etching techniques.

Juan Pardo and Dr. Daniel Moran, Washington University in St. Louis
Work performed at Washington University in St. Louis Nano Research Facility



Solidworks rendition of the microelectrocortigraphy electrode grid final product and concept.

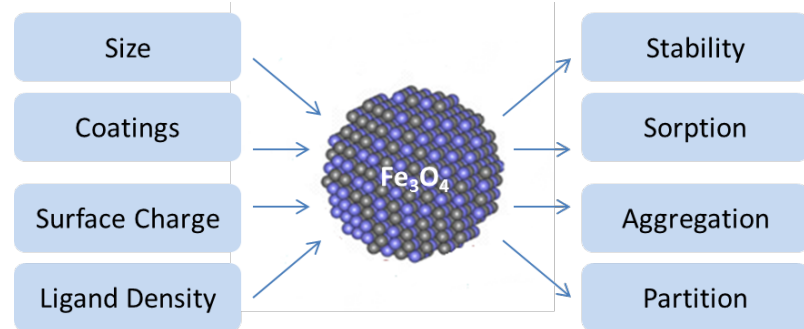


Microelectrocortigraphy electrode grid after lift-off showing electrode sites and connector plates.

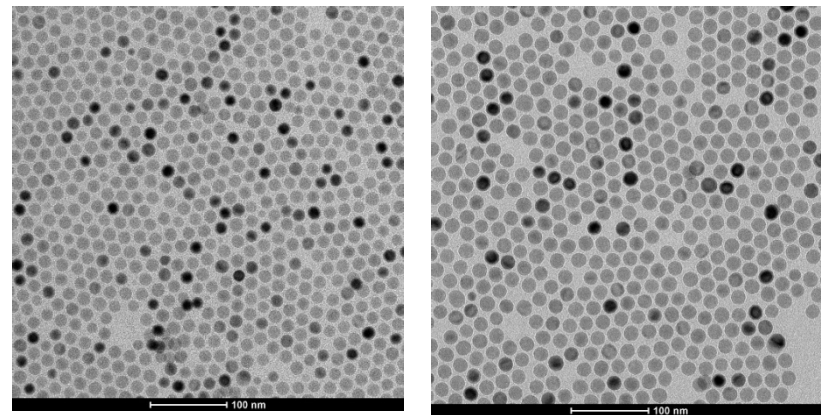
Engineered nanoscale iron oxide for environmental sensing and remediation

Engineered magnetite nanocrystals have high potential as platform materials for environmental sensing and remediation due to their unique size and physicochemical properties. Size control and surface chemistry of magnetite nanocrystals are crucial for application, especially in saturated, porous (media) matrixes. This project investigates both size and surface control of monodispersed magnetite nanocrystals, examining a range of 8 to 30 nm (discreet) particle suspensions.

The magnetite nanocrystals can be transferred into water through a variety of surface modifications, including a tailored series of surfactants, varying in charge and hydrophobicity, and/or simple organic acids. Once stabilized, interfacial surface interactions are quantitatively investigated with a quartz crystal microbalance with dissipation monitoring (QCM-D) using both hydrophilic (SiO₂) and hydrophobic (polystyrene) sensor surfaces. Changing the water chemistry and/or the type of organic coating(s) on the nanocrystal surface directly influences both the surface density and viscoelastic properties of (surface) sorbed particles.



Available surface modifications of magnetite nanocrystals and associated characteristics affecting surface interaction.



Monodispersed magnetite nanocrystals with a diameter of 14 ± 1.0 nm (left) and 16.8 ± 0.7 nm (right).

Wenlu Li and Dr. John Fortner, Washington University
in St. Louis
Work performed at Washington University in St. Louis
Nano Research Facility

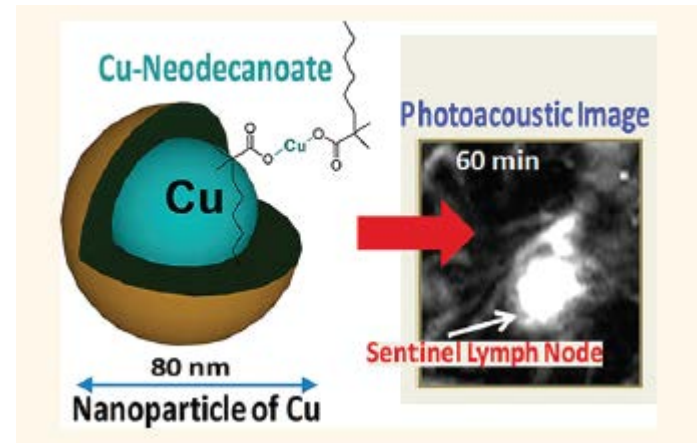
Photoacoustic Sentinel Lymph Node Imaging with Copper Neodecanoate Nanoparticles

Photoacoustic tomography (PAT) is emerging as a novel, hybrid, and non-ionizing imaging modality because of its satisfactory spatial resolution and high soft tissue contrast. PAT combines the advantages of both optical and ultrasonic imaging methods. It opens up the possibilities for noninvasive staging of breast cancer and may replace sentinel lymph node (SLN) biopsy in clinic in the near future.

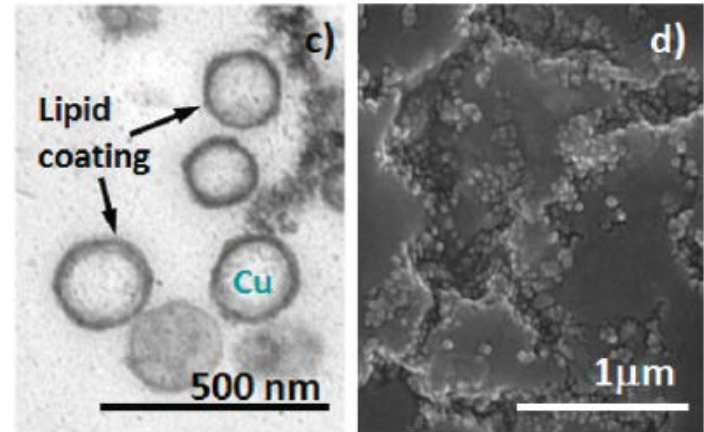
In this work, we demonstrate for the first time that copper can be used as a contrast metal for near-infrared detection of SLN using PAT. A unique strategy is adopted to encapsulate multiple copies of Cu as organically soluble small molecule complexes within a phospholipid-entrapped nanoparticle. The nanoparticles assumed a size of 80-90 nm, which is the optimum hydrodynamic diameter for its distribution throughout the lymphatic systems. These particles provided at least 6-fold higher signal sensitivity in comparison to blood, which is a natural absorber of light. We also demonstrated that high SLN detection sensitivity with PAT can be achieved in a rodent model. This work clearly demonstrates for the first time the potential use of copper as an optical contrast agent.

Xin Cai, Ceren Yalaz, Dr. Dipanjan Pan, Dr. Samuel Wickline, Dr. Gregory Lanza, and Dr. Lihong Wang, Washington University in St. Louis

Work performed at Washington University in St. Louis Nano Research Facility



Schematic of copper nanoparticle structure and photoacoustic image of a mouse lymph node utilizing the nanoparticles as a contrast agent.



Anhydrous state TEM image (c) and SEM image (d) of the copper nanoparticles.

The End

For additional information on the National
Nanotechnology Infrastructure Network please visit
<http://www.nnin.org> or call (607)-254-4872